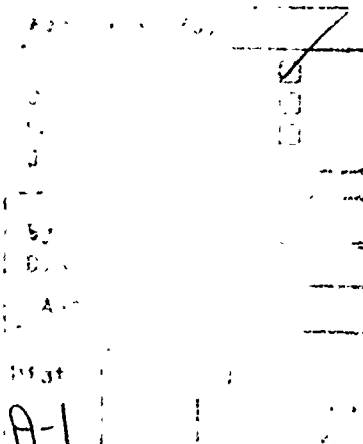


AD-A234 733

DOCUMENTATION PAGE

Form Approved
OMB No. 0704-0188

ion is estimated to average 1 hour per response, including the time for reviewing instructions, searching existing data sources, gathering and reviewing the collection of information, sending comments regarding this burden estimate or any other aspect of this burdening this burden, to Washington Headquarters Services, Directorate for Information Operations and Reports, 1215 Jefferson and to the Office of Management and Budget, Paperwork Reduction Project (0704-0188), Washington, DC 20503.

1. AGENCY USE ONLY (Leave blank)		2. REPORT DATE 13 Mar 1991	3. REPORT TYPE AND DATES COVERED Final Report/1 Apr 90-31 Dec 90	
4. TITLE AND SUBTITLE Experimental Testing of Corpuscular Radiation Detectors			5. FUNDING NUMBERS 61102F/2301/A1	
6. AUTHOR(S) Robert T. Wangemann				
7. PERFORMING ORGANIZATION NAME(S) AND ADDRESS(ES) Institute of Electrical and Electronics Engineers, Inc. Conference Management PO Box 1331/445 Hoes Lane AFOSR-TR.			8. PERFORMING ORGANIZATION REPORT NUMBER 91 0273	
9. SPONSORING/MONITORING AGENCY NAME(S) AND ADDRESS(ES) AFOSR/NP Bk 410 Bolling AFB DC 20332-6448			10. SPONSORING/MONITORING AGENCY REPORT NUMBER AFOSR-90-0197	
11. SUPPLEMENTARY NOTES				
12a. DISTRIBUTION/AVAILABILITY STATEMENT Approved for public release; distribution is unlimited.			12b. DISTRIBUTION CODE	
13. ABSTRACT (Maximum 200 words) The Nonlinear Optics: Materials, Phenomena, and Devices Conference was held as planned. 				
14. SUBJECT TERMS			15. NUMBER OF PAGES 182	
			16. PRICE CODE	
17. SECURITY CLASSIFICATION OF REPORT UNCLASSIFIED	18. SECURITY CLASSIFICATION OF THIS PAGE UNCLASSIFIED	19. SECURITY CLASSIFICATION OF ABSTRACT UNCLASSIFIED	20. LIMITATION OF ABSTRACT SAR	

GENERAL INSTRUCTIONS FOR COMPLETING SF 298

The Report Documentation Page (RDP) is used in announcing and cataloging reports. It is important that this information be consistent with the rest of the report, particularly the cover and title page. Instructions for filling in each block of the form follow. It is important to *stay within the lines* to meet optical scanning requirements.

Block 1. Agency Use Only (Leave blank)

Block 2. Report Date. Full publication date including day, month, and year, if available (e.g. 1 Jan 88). Must cite at least the year.

Block 3. Type of Report and Dates Covered. State whether report is interim, final, etc. If applicable, enter inclusive report dates (e.g. 10 Jun 87 - 30 Jun 88).

Block 4. Title and Subtitle. A title is taken from the part of the report that provides the most meaningful and complete information. When a report is prepared in more than one volume, repeat the primary title, add volume number, and include subtitle for the specific volume. On classified documents enter the title classification in parentheses.

Block 5. Funding Numbers. To include contract and grant numbers; may include program element number(s), project number(s), task number(s), and work unit number(s). Use the following labels:

C - Contract	PR - Project
G - Grant	TA - Task
PE - Program Element	WU - Work Unit Accession No.

Block 6. Author(s). Name(s) of person(s) responsible for writing the report, performing the research, or credited with the content of the report. If editor or compiler, this should follow the name(s).

Block 7. Performing Organization Name(s) and Address(es). Self-explanatory.

Block 8. Performing Organization Report Number. Enter the unique alphanumeric report number(s) assigned by the organization performing the report.

Block 9. Sponsoring/Monitoring Agency Name(s) and Address(es). Self-explanatory.

Block 10. Sponsoring/Monitoring Agency Report Number. (If known)

Block 11. Supplementary Notes. Enter information not included elsewhere such as. Prepared in cooperation with..., Trans of ..., To be published in.... When a report is revised, include a statement whether the new report supersedes or supplements the older report.

Block 12a. Distribution/Availability Statement. Denotes public availability or limitations. Cite any availability to the public. Enter additional limitations or special markings in all capitals (e.g. NOFORN, REL, ITAR).

DOD - See DoDD 5230.24, "Distribution Statements on Technical Documents."

DOE - See authorities.

NASA - See Handbook NHB 2200.2.

NTIS - Leave blank.

Block 12b. Distribution Code.

DOD - Leave blank.

DOE - Enter DOE distribution categories from the Standard Distribution for Unclassified Scientific and Technical Reports.

NASA - Leave blank.

NTIS - Leave blank.

Block 13. Abstract. Include a brief (Maximum 200 words) factual summary of the most significant information contained in the report.

Block 14. Subject Terms. Keywords or phrases identifying major subjects in the report.

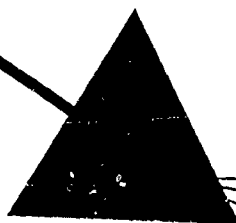
Block 15. Number of Pages. Enter the total number of pages.

Block 16. Price Code. Enter appropriate price code (NTIS only).

Blocks 17. - 19. Security Classifications. Self-explanatory. Enter U.S. Security Classification in accordance with U.S. Security Regulations (i.e., UNCLASSIFIED). If form contains classified information, stamp classification on the top and bottom of the page.

Block 20. Limitation of Abstract. This block must be completed to assign a limitation to the abstract. Enter either UL (unlimited) or SAR (same as report). An entry in this block is necessary if the abstract is to be limited. If blank, the abstract is assumed to be unlimited.

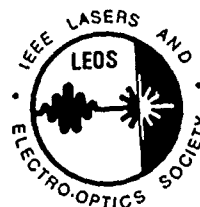
AFOSR 90-0197
NLO'90



NONLINEAR OPTICS:
Materials, Phenomena and Devices

DIGEST

Stouffer Waiohai Beach
Kauai, Hawaii
July 16-20, 1990



Sponsored by
IEEE Lasers and Electro-Optics Society
In Cooperation with
the Optical Society of America

91 4 16 069

AFDSR90-0197

ATCHB

**PREREGISTERED ATTENDEES
LIST**

**NONLINEAR OPTICS:
Materials, Phenomena
and
Devices**

Kauai, Hawaii
July 16 - 20, 1990

NLO'90 PREREGISTERED ATTENDEES LIST

Lastname.....	FIRSTNAME.....	MINIT	AFFNAME.....	AFFADD.....	STREET.....	CITY.....	State	ZIP-CODE..	COUNTRY.....
Agarwal	Girish	S.	University of Hydera	School of Physics	Central University P	Hyderabad - 500 134	IA	52242	INDIA
Andersen	David	R.	The University of Io	4400 Engineering Bui		Iowa City	IA	52242	USA
Anderson	Dana		University of Colora	J1LA CB-440		Boulder	CO	80309	USA
Awaj	George		Fiberstars, Inc.	47456 Fremont Blvd.		Fremont	CA	94538	USA
Bachor	Hans		Australian National	Physics, Faculty	GPO Box 4	Canberra Act 2601			Australia
Baldwin	Kenneth		Australian Nat'l Uni	GPO Box 4		Canberra Act. 2601			Australia
Ballagh	Robert		University of Otago	PO Box 56		Dunedin	NY	13244	New Zealand
Banerjee	Partha		Syracuse University	310 Link Hall, Dept.		Syracuse	NY	13244	USA
Barnes	Norman		NASA Langley Researc	Mail Stop 474		Hampton	VA	23665-5225	USA
Bashaw	Matthew		Dept. Applied Physic	PO Box 2157 Yale Sta		New Haven	CT	06520-2157	USA
Benitez	Alexander		The MITRE Corporatio	7525 Colshire Drive		McLean	VA	22102	USA
Bjorklund	Gary		IBM Almaden Research	650 Harry Road	Dept. K95/801	San Jose	CA	95120	USA
Bloembergen	Nicolaas		Harvard University	231 Pierce Hall Das		Cambridge	MA	02138	USA
Blum	Olga		University of Califo	197 M. Cory Hall		Berkeley	CA	94720	USA
Boyd	Robert		University of Roches	College of Engr. & A		Rochester	NY	14627	USA
Brueck	Steven	W.	University of New Me	Cntr for High Techno		Albuquerque	NM	87131	USA
Burland	Donald		IBM Almaden Research	650 Harry Rd.	K95/801	San Jose	CA	95120-6099	USA
Carlsten	John		Montana State Univer	Physics AJM106		Bozeman	MT	59717	USA
Chi	Sien		National Chiao Tung	Institute of Electro	Engineering - Chiao	Hsinchi, Taiwan			REP. OF CHIN
Chiou	Arthur		Rockwell Internation	Science Center	1049 Camino Dos Rios	Thousand Oaks	CA	91358	USA
Cho	Kikuo		Osaka University	1-1, Machikaneyama		Toyonaka 560			Japan
Christensen	Douglas		University of Utah	Dept. of Elec. Engr.	MEB	Salt Lake City	UT	84112	USA
Coldren	Larry		University of Califo	ECE Dept.		Santa Barbara	CA	93106	USA
Combscot	M.		Universite Paris VII	de L'Ecole Normale S	Tour 23, 2 place Jus	75251 Paris, Cedex 0			France
Corvo	Antonio		Sandia National Lab	ORG 1128, PO Box 580		Albuquerque	NM	87185	USA
Dagenais	Mario		University of Maryla	Dept. of Elec. Engr.		College Park	MD	20742	USA
Deacon	David		Deacon Research	2440 Embarcadero Way		Palo Alto	CA	94303	USA
Ding	Yujie	J.	The Johns Hopkins Un	34th & Charles Stree		Baltimore	MD	21218	USA
Ducloy	M.		Universite Paris-Mor	Laboratoire de Physi	Lasers	93430 Villeteaneuse			France
Dunning	Gilmore		Hughes Research Labo	3011 Malibu Canyon R		Malibu	CA	90265	USA
Egami	Chikara		Muroran Institute of	Dept. of Mathematics,	& Engineering	27-1 Mizumoto Murora		050	JAPAN
Eichler	Haus	J.	Technische Universit	Strape des 17 Juni 1		Berlin 12			GERMANY
Ema	Kazuhiro		University of Tokyo	Dept. of Applied Phy	7-3-1 Hongou Bunkyo-	Tokyo 113			Japan
Eubank	Mark		Rockwell Science Cen	1049 Camino Dos Rios		Thousand Oaks	CA	91360	USA
Ewart	Paul		University of Oxford	Clarendon Laboratory	Parks Rd.	Oxford OX13PU			United Kingd
Farrow	Roger	L.	Sandia National Labo	PO Box 969	Div. 8354	Livermore	CA	94551-0969	USA
Feinberg	Jack		Univ. of So. Califor	Dept. of Physics		Los Angeles	CA	90089-0484	USA
Fejer	Martin		Stanford University	Ginzton Laboratory		Stanford	CA	94305	USA
Fischer	Baruch		Israel Institute of	Technion	Electrical Engineeri	Haifa 32000			Israel
Frey	Robert		Ecole Polytechnique	Lab d'Optique Quanti		Palaiseau 91128			France
Gaeta	Celestino		Hughes Research Labo	3011 Malibu Canyon R		Malibu	CA	90265	USA

NLG'90 PREREGISTERED ATTENDEES LIST

Lastname.....	FIRSTNAME.....	MINIT	AFFNAME.....	AFFADD.....	STREET.....	CITY.....	State	ZIP-CODE..	COUNTRY.....
Gamo	Hideya		University of Califo	Dept. of Elec. & Com		Irvine	CA	92717	USA
Garito	Anthony		University of Pennsy	Dept. of Physics		Philadelphia	PA	19104	USA
Garmire	Elsa		University of Southe	California	University Park MC 1	Los Angeles	CA	90089-1112	USA
Giancarlo	Righini					Rome			Italy
Gibbs	Hyatt		University of Arizon	Optical Sciences		Tucson	AZ	85721	USA
Gierulski	Alfred		BASF APR Tsukuba	2-1-6 Sengen D-9	Tsukuba	Ibaraki 305			Japan
Grimes	Craig		Lockheed-Advanced Te	3251 Hanover G91-60		Palo Alto	CA	94304-1191	USA
Grischkowsky	Daniel		IBM, TJ Watson Resea	PO Box 218		Yorktown Heights	NY	10598	USA
Grynberg	Gilbert		Univ. Pierre et Mari	Tour 12 E01		Paris 05		75252	France
Gustafson	Ture Kenneth		University of Califo			Berkeley	CA	94720	USA
Haddad	George		University of Michig	EECS Dept. 2228 EECS		Ann Arbor	MI	48109-2122	USA
Haga	Hiroshi		Osaka University - F	Engineering Scienc	1-1, Machikaneyama	Toyonaka, Osaka 560			JAPAN
Hagan	David		CREOL	University of Centra		Orlando	FL	32826	USA
Hanamura	Eiichi		University of Tokyo	Department of Applie	7-3-1 Hongo, Bunkyo-	Tokyo 113			JAPAN
Harris	Stephen		Stanford University	Ginzton Laboratory	Room 4	Stanford	CA	94035	USA
Harvey	Albert		National Science Fou	1800 G Street, NW	Room 1151	Washington	DC	20550	USA
Harvey	John	D.	University of Auckla	Physics Dept.	Private Bag	Auckland			New Zealand
Hasenber	Thomas		Hughes Research Lab	3011 Malibu Canyon		Malibu	CA	90265	USA
Hashizume	Naoki		University of Tokyo	Dept. of Applied Phy	7-3-1 Hongo, Bunkyo-	Tokyo 113			Japan
Haufl	Thomas		Universitaet Kaisers	P. O. Box 3049, Univ	Kaiserlautern	Kaiserslautern			WEST GERMANY
Heckenberg	Norman		University of Queens	Physics Department		Brisbane, Q 4067			Australia
Henneberger	Fritz		Humboldt Universitat	Sektion Physik	Bereich 05-Halbleite	Berlin 1040			West Germany
Hermann	John	A.	DSTO/Surveillance Re	Box 1650, Salisbury		Adelaide, South Aust			AUSTRALIA
Hermann	Mark		Lawrence Livermore N	Laboratory	P. O. Box 808 L-495	Livermore	CA	94550	USA
Hulin	D.		Ecole Polytechnique	Lab d'Optique Appliq	Batterie de l'Yvette	91120 Palaiseau			France
Ichiro	Akai		Osaka City Universit	3-3-138 Sugimoto	Sumiyoshi-ku	Osaka 558			Japan
Ikura	Katsuyata		Nippon Soda Co., Ltd	Odawara Research Cen	345 Takada	Odawara 250-02			USA
Izutsu	Masayuki		Osaka University	Machikaneyama		Toyonaka, Osaka 560			Japan
Jahoda	Franz		Los Alamos National	PO Box 1663		Los Alamos	NM	87545	USA
Johnson	Kristina	M.	University of Colora	Campus Box 525		Boulder	CO	80309-0525	USA
Joshi	Chan		UCLA	Elec. Engr. Dept.	7731 Boelter Hall, 4	Los Angeles	CA	90024-1594	USA
Kalibjian	Ralph		Lawrence Livermore N	PO Box 808, PO Box L		Livermore	CA	94550	USA
Kawaguchi	Hitoshi		Yanagata University	8-3-16, Jonan	Yonezawa	Yanagata 992			Japan
Khitrava	Galina		University of Arizon	Optical Sciences		Tucson	AZ	85721	USA
Khoo	I.	C.	Penn State Universit	Elec. Engr. Dept.		University Park	PA	16802	USA
Khurgin	Jacob	B.	The Johns Hopkins Un	34th & Charles Stree		Baltimore	MD	21218	USA
Kim	Inho		University of Califo	1034 9th St., #47		Albany	CA	94710	USA
Kitazawa	Manabu		Ajinomoto Co., Inc.	1-1 Suzuki-cho, Kawa		Kanagawa 210			Japan
Kobayashi	Takayoshi		University of Tokyo	Department of Physic	Hongo 7-3-1, Bunkyo-	Tokyo			Japan
Kondo	Takashi		University of Tokyo	7-3-1 Hongo, Bunkyo-	Dept. of Applied Phy	Tokyo 113			Japan
Kost	Alan		Univ. of So. Califor	Dept. of Elec. Engr.		Los Angeles	CA	90089-1112	USA

NLO-90 PREREGISTERED ATTENDEES LIST

Lastname.....	FIRSTNAME.....	MINIT	AFFADT.....	STREET.....	CITY.....	State	ZIP-CODE..	COUNTRY.....
Kukhtarev	Nicolai		Institute of Physics	Prospect Nauki 26	252650 Kiev			USSR
Kulander	Kenneth		Lawrence Livermore N	PO Box 808, L-438	Livermore	CA	94550	USA
Kuwata-Gonokami	Makoto		University of Tokyo	Dept. of Applied Phy	Tokyo 113			Japan
Lam	Juan		Hughes Research Labo	3011 Malibu Canyon R	Malibu	CA	90265	USA
Lansdon	Robert		ABN Holographics Cre	80 E. Sir Francis Dr	Larkspur	CA	94939	USA
Law	Kwok-Keung		University of Califo	Elec. Engr. Dept.	Santa Barbara	CA	93107	USA
Leith	Emmett	N.	University of Michig	Dept. of EECS	Ann Arbor	MI	48109-2122	USA
Levenson	Marc		IBM Almaden Research	M/S K32/802D	San Jose	CA	95120-6099	USA
Levine	Alfred		Staten Island/Cuny	130 Stuyvesant Place	Staten Island	NY	10301	USA
Leyva	Victor		Caltech	128-95 Watson Lab	Pasadena	CA	91125	USA
Li	Guifang		University of Wiscon	Dept. of ECE	Madison	WI	53706-1691	USA
Lind	Richard		Hughes Research Labo	3011 Malibu Canyon R	Malibu	CA	90265	USA
Liu	J.	Y.	University of Boulde	Campus Box 525	Boulder	CO	80309-0425	USA
Lopresti	Peter		Pennsylvania State U	121 Electrical Engr.	University Park	PA	16803	USA
Lotshaw	William		General Electric Res	PO Box 8, Room KWD27	Schenectady	NY	12301	USA
Loy	Michael		IBM - T. J. Watson R	Center	Yorktown Heights	NY	10598	USA
Lucht	Robert		Sandia National Labo	Combustion Research	Livermore	CA	94583	USA
Luther-Davies	Barry		Australian Nat'l Uni	GPO Box 4	Canberra Act 2601			Australia
Lytel	Richard		Lockheed	D9701, B201	Palo Alto	CA	94304	USA
MacCormack	Stuart		University of Southa	Optoelectronics Rese	Southampton S09 SN4			United Kingd
Mace	David		British Telecom Rese	Rt 2461 Martlesham H	Suffolk IP5 7RE			United Kingd
Matsumoto	Keisuke		Osaka University	1-1 Machikaneyamacyo	Toyonaka 560			Japan
McMichael	Ian		Rockwell Science Cen	1049 Camino Dos Rios	Thousand Oaks	CA	91360	USA
Miki	Kojiro		Osaka University	1-1 Machikaneyamacho	Toyonaka 560			Japan
Miller	David		AT&T Bell Laboratori	Crawfords Corner Rd.	Holmdel	NJ	07733	USA
Misra	Raj		Syracuse University	111 Link Hall	Syracuse	NY	13244	USA
Mitchell	Phillip		Hughes Research Labo	3011 Malibu Canyon R	Malibu	CA	90265	USA
Miyata	Seizo		Tokyo University of	Koganei	Tokyo 184			Japan
Morita	Ryuji		University of Tokyo	Dept. of Applied Phy	Tokyo 113			Japan
Morita	Tetsuya		University of Califo	Elec. Engr. Dept.	Davis	CA	95616	USA
Mueller	George		Naval Research Labor	4555 Overlook Ave.,	Washington	DC	20375-5000	USA
Mullen	Ruth Ann		Hughes Research Cent	3011 Malibu Canyon R	Malibu	CA	90265	USA
Murata	Hiroshi		Osaka University	1-1 Machikaneyamacho	Osaka 560			Japan
Nakagawa	Kazuo		Muroran Institute of	Dept. of Mathematics	27-1 Mizumoto Murora		050	JAPAN
Nakanishi	Hachiro		Research Inst for Po	& Textiles	Ibaraki 305			Japan
Nguyen	Khanh		University of Califo	1734 Blake St., #K	Berkeley	CA	94703	USA
Noda	Susumu		Kyoto University	Yoshida-Hormachi	Kyoto 606			Japan
O'Brien	Stephen		The MITRE Corporatio	7525 Colshire Drive	McLean	VA	22102	USA
Olbright	Greg		Sandia National Labo	Division 1164	Livermore	CA	94550	USA
Osborne	Robert		Technical University	ARCISSTR.21	8000 Muenchen 2	WM	87185-5300	West Germany
Osugi	Minoru		Toda Kogyo Corp.	4-1-2, Funairi-Minam	Hiroshima 730			Japan

NLO'90 PREREGISTERED ATTENDEES LIST

Lastname.....	FIRSTNAME.....	MINIT	AFFNAME.....	AFFADD.....	STREET.....	CITY.....	State	ZIP-CODE..	COUNTRY.....
Oudar	Jean-Louis		CNET-Laboratoire de	196 av. Henri Ravera		Bagneux F-92220			France
Owyoung	Adelbert		Sandia National Labo	Dept. 1160		Albuquerque	NM	87185-5800	USA
Pan	Janet			350 Memorial Drive		Cambridge	MA	02139-4304	USA
Parshall	Elaine		Tufts University	Electro-Optics Court	PO Box 113	Medford	MA	02153	USA
Partanen	Jovni		Univ. of So. Califor	Phys. Dept.	SSC 303	Los Angeles	CA	90089-0484	USA
Paulson	Ronald		EDO Corp./Barnes Eng	88 Long Hill Cross R		Shelton	CT	06484	USA
Pegg	David		Griffith University	Div. of Sc. & Tech.		Brisbane Q 4111			Australia
Pepper	David		Hughes Research Labs	3011 Malibu Canyon R		Malibu	CA	90265	USA
Perry	Joseph		Jet Propulsion Labor	M/S 67-201		Pasadena	CA	91109	USA
Peterson	Phillip		US Air Force	WL/AR-N		Albuquerque	NM	87117-6008	USA
Petrovic	Mark		Oklahoma State Univ	413 Noble Research C		Stillwater	OK	74078	USA
Potasek	M.		Columbia University	Dept. of Applied Phy		New York	NY	10027	USA
Potter, Jr.	Barrett	S.	University of Florid	AMRC	1 Progress Blvd #11	Alachua	FL	32615	USA
Rakestraw	David		Sandia National Labo	Division 8362		Livermore	CA	94551	USA
Ralph	Stephen		AT&T Bell Laboratori	600 Mountain Ave.		Murray Hill	NJ	07974	USA
Rikken	Geert		Philips Research Lab	PO Box 80000		Eindhoven 5600 JA			Netherlands
Saar	Amir		Caltech	125 So. Hollister Av		Pasadena	CA	91105	USA
Sakuma	Jun		Univ. of So. Califor	1727 W. 158th St.		Gardena	CA	90247	USA
Savage	Craig		Australian National	Physics, Faculty	GPO Box 4	Canberra Act 2601			Australia
Schiek	Roland		Technical Univ of Mu	Arcisstr.21		D8000 Munich			West Germany
Schroeder	Andreas		University of Iowa	180 AMRF Oakdale Cam		Iowa City	IA	52242	USA
Schrof	Wolfgang		BASF Aktiengesellsch	Kunststofflaboratori		Ludwigshafen D-6700			West Germany
Seppen	Ans C. J. E.		Philips Research Lab	PO Box 80000		Eindhoven 5600 JA			The Netherla
Shapiro	Jeffrey		MIT	Room 38-401		Cambridge	MA	02139	USA
Sharp	Edward	J.	CECOM Center for Nig	& Electro-Optics	ANSEL-RD-NV-LRT	Ft. Belvoir	VA	22066-5677	USA
Shen	Tsae-Pyng		Rockwell Science Cen	1049 Camino Dos Rios		Thousand Oaks	CA	91360	USA
Shen	Y.	R.	University of Califo	Physics Dept.		Berkeley	CA	94720	USA
Simmons	Catherine	J.	University of Florid	1 Progress Boulevard		Alachua	FL	32615	USA
Simmons	Joseph	H.	University of Florid	4642 NW 12th Place		Gainesville	FL	32603	USA
Simmons	Kelly		University of Arizon	Optical Sciences Dep		Tucson	AZ	85704	USA
Simoni	Francesco		University di Napoli	Dipartimento di Scie		80-80125 Napoli			Italy
Skinner	Steven		University of Iowa	Dept. of ECE	4400 EB	Iowa City	IA	52242	USA
Soileau	Marion		CREOL	University of Centra		Orlando	FL	32826	USA
Spoonhower	John		Eastman Kodak	BLD8 81 Research Lab		Rochester	NY	14650	USA
Statman	David		US Air Force	Weapons Laboratory	WL/ARDJ Advanced Con	Kirtland AFB	NM	87117-6008	USA
Steel	Duncan		University of Michig	Dept. of Physics		Ann Arbor	MI	48109	USA
Stegeman	George		University of Arizon	Optical Science Cent		Tucson	AZ	85721	USA
Steier	William		University of So. Ca	M/C 0483		Los Angeles	CA	90089-0483	USA
Stepanov	Sergei	I.	A.F. Ioffe Physico-T	Academy of Sciences		Leningrad K-21			USSR
Summers	Christopher		Georgia Tech. Resear	Physical Sciences Di		Atlanta	GA	30332	USA
Suzuki	Hideo		Hamamatsu Photonics	Hamakita Research Pa		Hamakita 434			Japan

NLO'90 PREREGISTERED ATTENDEES LIST

Lastname.....	FIRSTNAME.....	MINIT	AFFNAME.....	AFFADD.....	STREET.....	CITY.....	State	ZIP-CODE..	COUNTRY.....
Swartzlander	Grover		University of Maryland	Baltimore County	Elec. Engr. Dept.	Baltimore	MD	21228	USA
Szabo	Alex		National Research Co	Bldg M-50, Montreal		Ottawa, Ont. K1A 0R6			Canada
Ticktin	Anton		BASF AG, Applied Pol	APR Japan	09, 2-1-6 Sengen	Tsukuba 305			Japan
Tomiyama	Hironitsu		Hodogaya Chemical Co.	7-6, 3-chome, Kamiya	Kitaku	Tokyo 115			Japan
Toshio	Fukumi		Govt. Ind. Res. Inst	1-8-31 Midorigaoka		Ikeda, Osaka 563			Japan
Trebino	Rick		Sandia National Labs	Combustion Research		Livermore	CA	94551	USA
Tutt	Lee		Hughes Aircraft Co.	3011 Malibu Canyon R	M/S RL92	Malibu	CA	90265	USA
Ulrich	Bruno		CNRS	5 rue de l'universit		Strasbourg F-67084			France
Van Eck	Timothy		Lockheed	3251 Hanover St.	0-9720 B-202	Palo Alto	CA	94304	USA
Van Stryland	Eric		CREOL	University of Centra	12424 Research Parkw	Orlando	FL	32826	USA
Vanherzeele	Herman		E. I. Du Pont de Nem	PO Box 80356		Wilmingon	DE	19880-0356	USA
Vesperinas	Manuel	J.	Instituto de Optica	Serrano 121		Madrid 28006			Spain
Vickers	Deborah		General Motors Resea	7631 Reseda Blvd., #		Reseda	CA	91335	USA
Walls	Daniel		University of Auckla	Physics Dept.		Auckland			New Zealand
Weidman	David		Corning Incorporated	SP-FR-1-7		Corning	NY	14831	USA
Winful	Herbert		University of Michig	EECS Dept.		Ann Arbor	MI	48109-2122	USA
Wood	Gary	L.	CZNEVO - U. S. ARMY	AMSEL-NV-RD-LRT		Fort Belvoir	VA	22060-5677	USA
Wu	Ming Hsien		Hamamatsu Corp.	360 Foothill Rd.		Bridgewater	NJ	08807	USA
Yamashita	Ken		Nippon Sheet Glass C	5-4 Tokodai,		Ibaraki 300-26			Japan
Yasuda	Hiroaki		University of Tokyo	Dept. of Applied Phy		Tokyo 113			Japan
Ye	Peixian		Inst of Physics Acad			Beijing 100080	CA	91360	China
Yeh	Pochi		Rockwell Internation	1049 Camino Dos Rios		Thousand Oaks	CA	94035-4085	USA
Young	James		Stanford University	Ginzton Laboratory		Stanford			USA
Zhang	He-Yi		Peking University	Physics Dept.		Beijing 100080			PR China
Zhu	Qiang		MacQuarie University	Centre for Lasers &		Sydney N. S. W. 2109			Australia
Ziari	Mehrdad		University of So. Ca	University Park		Los Angeles	CA	90089-0483	USA
Zozulya	A.	A.	P.N. Lebedev Physica	Academy of Sciences	Leninsky pr. 53	Moscow			USSR

Approved for public release; distribution unlimited.

NLO'90

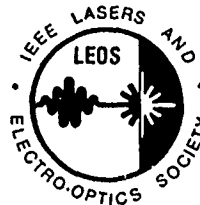
NONLINEAR OPTICS:

Materials, Phenomena and Devices

DIGEST

Stouffer Waiohai Beach
Kauai, Hawaii
July 16-20, 1990

IEEE Catalog Number: 90CH2905-8
IEEE Library of Congress Number: 90-82545



Sponsored by
IEEE Lasers and Electro-Optics Society
In Cooperation with
the Optical Society of America

IEEE (APSO)
is
20-02

The papers in this book comprise the digest of the meeting mentioned on the cover and title page. They reflect the author's opinions and are published as presented and without change, in the interests of timely dissemination. Their inclusion in this publication does not necessarily constitute endorsement by the editors, the Institute of Electrical and Electronics Engineers, Inc.

Copyright and Reprint Permissions: Abstracting is permitted with credit to the source. Libraries are permitted to photocopy beyond the limits of U.S. copyright law for private use of patrons those articles in this volume that carry a code at the bottom of the first page, provided the per-copy fee indicated in the code is paid through the Copyright Clearance Center, 29 Congress Street, Salem, MA 01970. Instructors are permitted to photocopy isolated articles for noncommercial classroom use without fee. For other copying, reprint or republication permission, write to Director, Publishing Services, IEEE, 345 E. 47th., New York, NY 10017. All rights reserved. Copyright © 1990 by The Institute of Electrical and Electronics Engineers, Inc.





FOREWORD

Program Co-Chairs:

Hyatt M. Gibbs
University of Arizona

Duncan G. Steel
University of Michigan

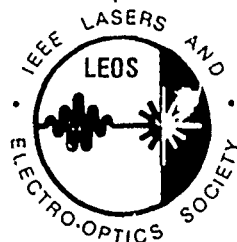
Juan F. Lam
Hughes Research Labs

Pochi Yeh
Rockwell International

Welcome to NLO'90, the First International Meeting on Nonlinear Optics organized by the Lasers and Electro-Optics Society of IEEE and in cooperation with the Optical Society of America. NLO'90 is being managed by LEOS, with subsequent meetings to alternate between OSA and LEOS.

The goal of NLO'90 is to provide a relaxed forum for interactions among researchers interested in recent progresses in nonlinear optical materials, phenomena, and devices. Areas to be covered include Fundamental Phenomena, Laser Spectroscopy, Liquid Crystals, Organics, Fibers, Waveguides/Couplers, Phase Conjugation, Applications of Nonlinear Semiconductor, Photorefractives, Semiconductors, Organic NLO and Devices, Photorefractive Applications, Semiconductor Lasers and Interfaces. Highlights of the program include plenary sessions with talks given by leaders of the field. Nonlinear Optics has become a diverse field with hundreds of practitioners. We are proud of the enthusiastic response to our Call for Papers. To preserve the workshop atmosphere of the meeting and to stimulate technical discussion, all contributed papers will be presented in an open-ended poster format. There will be no parallel sessions, so everyone can hear all oral presentations and discussions. We hope you will take full advantage of the free time in the afternoons to enjoy Hawaii and to discuss Nonlinear Optics.

We would like to thank all who have contributed to this exciting program especially Conference Co-Chairs I.C. Khoo and M. Dagenais, Members of our Advisory Committee, P.F. Liao, D.S. Chemla and Y.R. Shen, the International Chairs and Program Committee Members, authors and members of LEOS Executive Office. We hope you find the meeting an exciting and enjoyable forum for expanding the field of Nonlinear Optics.



CONFERENCE COMMITTEE

Conference Co-chairs ▲▲▲▲

Iam-Choon Khoo, Penn State University, University Park, PA
Mario Dagenais, University of Maryland, College Park, MD

Advisory Committee ▲▲▲▲

Paul F. Liao, Bellcore, Red Bank, NJ
Daniel S. Chemla, AT&T Bell Labs, Holmdel, NJ
Yuen Ron Shen, University of California, Berkeley, CA

Program Co-Chairs ▲▲▲▲

Hyatt M. Gibbs, University of Arizona, Tucson, AZ
Juan F. Lam, Hughes Research Labs, Malibu, CA
Pochi Yeh, Rockwell International, Thousand Oaks, CA
Duncan G. Steel, University of Michigan, Ann Arbor, MI

International Chairs ▲▲▲▲

M. Adams, British Telecom, Ipswich, UK
H. Eichler, Berlin Technical University, Berlin, West Germany
J. Hermann, Australian SRL, Salisbury, Australia
C.F. Li, Harbin Institute of Technology PRC, Harbin, PRC China
T. Kobayashi, University of Tokyo, Tokyo, Japan
R. Normandin, Canada NRC, Ottawa, Ontario, Canada
B. Ya. Zeldovich, USSR Academy of Sciences, Chelyabinsk, USSR
J. Zyss, CNET, Bagneux, France

Program Committee ▲▲▲▲

G. Bjorklund, IBM Almaden Research Center, San Jose, CA
C.M. Bowden, U.S. Army Missile Command, Huntsville, AL
S.R.J. Brueck, University of New Mexico, Albuquerque, NM
C.M. Clayton, Air Force Weapons Lab, Kirtland AFB, NM
L. Coldren, UC Santa Barbara, Santa Barbara, CA
J.H. Eberly, University of Rochester, Rochester, NY
L.S. Goldberg, NSF, Washington, D.C.
R.D. Guenther, Army Research Office, Research Triangle Park, NC
T. Ken Gustafson, University of California, Berkeley, CA
J.W. Haus, Rensselaer Polytechnic Institute, Troy, NY
R.W. Hellwarth, University of Southern California, Los Angeles, CA
R.S. Lytel, Lockheed, Palo Alto, CA
H. Pilloff, ONR, Arlington, VA
E. Sharp, Night Vision and Electro-Optics Lab, Ft. Belvoir, VA
C. Tang, Cornell University, Ithaca, NY



MEMORIAL

Farres P. Mattar
12/21/47 - 11/8/89

Farres Mattar died on 8 November, 1989, of cardiac arrest. His loss comes as a shock to the laser physics community. Farres had recently rejoined New York University as a Senior Research Scientist and was optimistic about establishing a strong research effort at New York University in computational laser physics.

Farres had a distinguished career and was recognized internationally for his contributions to laser physics and quantum optics. He obtained a BS degree in Electrical Engineering from Ain Shams University in Cairo in 1969, an MS degree in Electrical Engineering from the Polytechnic Institute of New York in 1970, and the PhD in Electrical Engineering and Electrophysics from the Polytechnic Institute of New York in 1975. Since that time, Farres held positions at the University of Rochester, University of Montreal, Polytechnic Institute of New York, University of Paris, Massachusetts Institute of Technology, University of Essen, Center for Nuclear Studies – Saclay, New York University, and the City University of New York. He had collaborations in all parts of the world and his list of coauthors includes a major representative sample of the laser physics community.

Farres' thesis research with M.C. Newstein resulted in a comprehensive computer code that could be used to model laser pulse propagation in active media. Farres was one of the first to appreciate the way in which transverse effects modify pulse dynamics. His thesis research resulted in the prediction of a new phenomenon, on-resonance self-focusing, which was subsequently verified experimentally. Farres then turned his attention to the roles of quantum fluctuations and transverse effects in superfluorescence, again achieving an impressive agreement with experiments carried out in Cs. His research program and computer codes were expanded to treat "three-level" atoms interacting with two laser fields. Using fully three-dimensional codes, he was able to study a multitude of problems relating to propagation effects in Raman scattering. Among problems considered were the control of light by light, three-level superfluorescence, pump-probe energy exchange, generation of Rabi sidebands, and the generation of Raman solitons. His recent work is the first to demonstrate the existence of stimulated Raman solitons in the presence of self-focusing and defocusing. Farres developed efficient computer codes and graphics for analyzing these extremely complex problems – access to his computer codes was sought by numerous research groups in attempts to compare their experimental data with theory.

Those of us who knew Farres saw a man whose life was dedicated to physics, his family and friends. He could be found in the physics building or computer center at almost any time of the day or night and was always enthusiastically willing to discuss his latest output plots. He showed a child-like excitement over the latest graphics acquisition at the computer center. Existing side by side with this dedication to science was a generosity and compassion beyond measure. Farres was always willing to give his time freely to students who wished to ask him questions. In particular, he enjoyed working with young people and recently supervised the research of a student who became a finalist in the Westinghouse Talent Search. Farres looked out for the welfare of his friends and colleagues and often presented them with gifts from his frequent travel.

To have known Farres was to have been touched by him, his passing leaves a void that is immediately apparent. Farres is survived by his wife Eliana, son Ken, sisters Jeanine, Mary and Nadia, and a brother Tony.

"The family and friends of Farres have established the Farres P. Mattar Scholarship at New York University. Those wishing to contribute to this endowed scholarship can send (tax-deductible) contributions to New York University, Attn. Muriel Mantel, Office of the Treasurer, Kimball Hall, New York, NY 10003. Indicate on the check that this donation is for the Farres Mattar Scholarship Fund."

MEMORIAL



Frederic A. Hopf
3/6/42 - 4/11/89

Frederic A. Hopf, Professor of Optical Sciences and Adjunct Professor of Ecology and Evolutionary Biology at the University of Arizona, passed away April 11, 1989. Fred obtained his PhD at Yale in 1968, graduating in the top 1% of his class in spite of taking the most difficult science courses, and came to the Optical Sciences Center in 1970. During his career, Fred's research stressed interdepartmental and international collaboration. His work took him from the Math, Physics, Chemistry, Astronomy, and Biology departments to as far away as the Max Planck Institute in Garching, West Germany (for experimental laser research), CSIRO, in Australia (for nonlinear optics research), and the University of Hungary (for optical chaos).

Fred Hopf made scientific advances in topics ranging from nonlinear optics and lasers, to chaos, to Darwin's theory of evolution. His pioneering experiments demonstrating chaos in optical systems led to his work in chaos and organization in evolution. Fred believed that Charles Darwin's explanation of missing links in evolution of species could be improved upon by making a direct analogy between the underlying processes in selection and competition phenomena found in laser physics.

When the famous Hahn-McCall self-induced transparency paper appeared, Fred's reaction was, "It's all wrong, and I'll be back tomorrow with the proof that it's wrong!" The next day he returned a very neat alternative derivation of the area theorem. He then went on to make many seminal contributions to the problem of coherent pulse propagation through attenuating and amplifying media, such as zero π pulse propagation, multiple echoes, and Brewer's coherent transient spectroscopy.

Fred also felt that the Heisenberg picture was the natural picture for quantum field theory and developed a very pretty treatment of pulse propagation and superradiance, building from quantum noise in the Heisenberg picture.

When in the mid 1970s the free-electron laser was first reported by Madey and coworkers at Stanford, it was originally thought to be a device that is inherently quantum mechanical in nature. That is, it was thought that the quantum nature of the electron and the electromagnetic field were essential to understand the free-electron laser. Working with colleagues at the University of Arizona, Fred was instrumental in publishing the first classical theory of the free-electron laser. In later work he applied the concept of laser lethargy (which was developed by Hopf and coworkers at Arizona in the context of the x-ray laser) to the free-electron laser problem and explained data that had been puzzling previously.

In the eighties, tenured and otherwise uncommitted, Fred struck out on his own, applying his brilliance to far-out problems. He studied the route to chaos of a hybrid electronic-optical system with delayed feedback. He demonstrated order in chaos, discovered periodic windows in chaos, and developed techniques for distinguishing noise from chaos. For these major contributions, and for endearing personal traits that need not be recounted for those who knew him, Fred became known as Captain Chaos.

Throughout this time Fred was immersed in southwestern culture. He became an expert in cactus and plant life in the southwest. The story is often repeated of Fred's calling a guest at 2.00 in the morning announcing that his night-blooming cereus were in bloom and the guest should get over to his house from the hotel as quickly as possible. The guest reports that it was indeed worth the trip!

Fred was a globetrotting birdwatcher, with a lifelist of about 2700 species, and a US list of 635 (out of about 700!) He had fantastic skill as a fisherman; he could think like a fish and catch his limit even when there were no fish around. He loved music and sang in the St. Michael and All Angels church choir, and was active in the Tucson Gilbert & Sullivan Society, at various times singing lead roles in productions and acting as President for almost five years.

Whatever Fred decided to do, he did with undivided attention, either he was with you completely, or he simply did not realize that his trail of coffee drops had just passed you by. He was typically convinced that he was right about whatever, and consequently stated his opinions as fact rather than as opinions. Naturally, some of the time, the premises upon which his conclusions were based were incorrect or incomplete, and hence the conclusions were wrong. However, right or wrong, his ideas were inevitably worth listening to. He was stimulating and thought provoking.

One colleague recounts the following. "I fondly remember sitting on a cactus and quickly assuming an upright position with approximately 10^6 (or so it felt) saguaro cactus spines in the derriere. Fred's typical attitude was 'Hush up and bend over, I've got my pliers.' This was our friend Fred at his best, taking command of the situation and getting right to the heart of the problem. We will all miss him, but we must at the same time rejoice that Fred was able to accomplish so much in his shortened career."

Frederic A. Hopf 3/6/42-4/11/89

Chaos – The behavior of a system whose final state depends so sensitively on the system's precise initial state that the behavior is in effect unpredictable and cannot be distinguished from a random process, even though it is strictly determinate in a mathematical sense
–McGraw-Hill Dictionary of Scientific and Technical Terms, Fourth Edition

TABLE OF CONTENTS

MONDAY, July 16, 1990

Session: Fundamental Phenomena in Nonlinear Optics I

MI1	Chaos in Nonlinear Optics, R.W. Boyd	
MI2	Optical Squeezing and Phase, D.T. Pegg	2
MI3	Quantum Noise Reduction in Optical Fields, D.F. Walls, M.J. Collett, A.S. Lone, and R.B. Levien	3
MI4	Theory and New Experiments on Physical Effects in Optical Fields with Nonzero Average Cube, B. Ya Zeldovich	N/A

Session: Liquid Crystals, Organics and Other Materials I

MI5	Quadratic Optical Properties of a New Organic Crystal: N-Methoxymethyl-4-nitro-aniline (MMNA), S. Miyata, H. Yamamoto, S. Katogi, and T. Hosomi	5
MI6	Laser-Induced Reorientation and Ultrasound Generation in the Liquid Crystal SCB Induced by Picosecond Laser Pulses, L.B. Au, H.J. Eichler, R. Macdonald, and L. Solymar	6
MI7	Nonlinear Optics of PLZT Thin Films, S.R.J. Brueck, A. Mukherjee and A.Y. Wu	N/A
MI8	Novel Polydiacetylenes for Nonlinear Optics, H. Nakanishi, H. Matsuda, S. Okada, A. Masaki, M. Ohsugi, and S. Takaragi	10

Session: Laser Spectroscopy

MI9	Femtosecond Laser Desorption of Molecules from Surfaces, M.M.T. Loy	N/A
MI10	Materials Studies with TeraH _z Beams, D. Grischkowsky	11
MI11	Subharmonic Resonances in Nonlinear Spectroscopy, G.S. Agarwal	13
MI12	Nonlinear Laser Spectroscopy of Solids and Applications to Computers, A. Szabo	14

POSTER SESSION:

Fundamental Studies I

MP1	Spontaneous Trapping in a Three-Level Atom, D.A. Cardimona, M.P. Sharma	16
MP2	Lasing Without Inversion, V.R. Blok, and G.M. Krochik	18
MP3	Laser Cooling with Two Wave Mixing, Y. Shevy	19
MP4	Novel Fluorescent Spectra From an Atom Strongly Coupled to a Driven Cavity, C. M. Savage	20
MP5	Second Harmonic Generation due to Photon-Photon Scattering in Magnetized Vacuum, Y.J. Ding and E.E. Kaplan	22
MP6	Signal Suppression in the Phenomenon of Long-Lived Photon Echo, N.N. Akhmediev	24
MP7	The Origin of Third Order Nonlinear Optical Effects in Polysilanes, D.M. Burland, C. Walsh, and R.D. Miller	26
MP8	Search for CHAMPS by Two-Photon Spectroscopy in Hydrogen, G. Grynberg, P. Verkerk, P. Fayette, M. Spiro, and S. Zylberajch	28
MP9	Fourier Theory, Number-Ket Causality, and Rational Phase States, J.H. Shapiro, S.R. Shepard, and N.C. Wong	30

MP10	Spatial and Temporal Contributions to Non-Observation of Laser Induced Continuum Structure in Sodium, K.G.H. Baldwin, P.B. Chapple, H.A. Bachor, J. Zhang and P. Lambropoulos	32
MP11	Optical Ramsey Fringes in Diamond, D.A. Redman, S.W. Brown, and S.C. Rand	Withdrawn
MP12	Nonlinear Spectroscopy in Substituted Polysilanes, F.M. Schellenberg, R.L. Byer, and R.D. Miller	34
MP13	Observation of Dark Solitary Stripes and Grids, G.A. Swartzlander Jr., D.R. Andersen, and A.E. Kaplan	36

Session: Fibers/Waveguides & Couplers

MP14	Nonlinear Waveguides with Liquid Crystalline Cores, S.K. Lo, L.M. Galarneau, D.J. Rogers, and S.R. Flom	37
MP15	A Generalized Scalar Formulation of Nonlinear Pulse Propagation in Single-Mode Fibers, R. Osborne	40
MP16	Time Resolved Switching Characteristic of the Nonlinear Directional Coupler Under Consideration of Susceptibility Dispersion, R. Schiek	43
MP17	Two-Photon Absorption in High-Nonlinearity Fibers, D.L. Weidman, J.C. Lapp, and M.A. Newhouse	45
MP18	Broadband Complete Optical Switching in a Polarization-Maintaining Fiber, H. Vanherzeele, and B.K. Nayar	47
MP19	Semiconductor Nonlinear Directional Coupler With Gain, M.J. Adams, D.A.H. Mace, J. Singh and M.A. Fisher	49
MP20	Energy Redistribution at the Interaction Between Two Femtosecond-Solitons in Optical Fibers, C.C. Yang, and B.J. Hong	51
MP21	Femtosecond Raman Scattering in Birefringent Fibers, S. Trillo and S. Wabnitz	53

Session: Fundamental Studies on Organic Nonlinear Materials

MP22	Nonlinear Optical Properties of Platinum Poly-ynes, S. Guha, K. Kang, P. Porter, C.C. Frazier, E. Chauchard and D. Beekman, and J. Falk, X. Hua and S.H. Park	55
MP23	Nonlinear Optical Properties of Organometallic Compounds in Solids and Solutions, L.W. Tutt, S.W. McCahon and M.B. Klein	57
MP24	Optical Nonlinearities in Crystalline Organic Multiple Quantum Wells, J.F. Lam, G.L. Tangonan, and S.R. Forrest	59
MP25	Excited State Absorption and Optical Nonlinearities of Metallophthalocyanines and Naphthalocyanines In Solution, J.W. Perry, L.R. Khundkar, D.R. Coulter, T.H. Wei, E.W. Van Stryland and D.J. Hagan	61
MP26	All-Optical Switching in New Nonlinear X-Junctions, H. Murata, M. Izutsu and T. Sueta	63
MP27	Saturation of the Hyperpolarizability of Oligothiophenes, G.L.J.A. Rikken, H. Thienpont, W. ten Hoeve, H. Wynberg, and E.W. Meijer	65

TUESDAY, JULY 17

Session: Phase Conjugation I

TI1	Phase-Conjugate Interferometry, I. McMichael	68
TI2	Four-Wave Mixing Oscillators, G. Grynberg	70
TI3	Degenerate Four Wave Mixing with Pulsed Lasers: Theory and Applications, P. Ewart	72
TI4	Three-Dimensional Analysis of Four-Wave Mixing Configurations, A.A. Zozulya	N/A

Session: Liquid Crystals, Organics and Other Materials

TI5	Nonlinear Optical Processes in Polymers, A.F. Garito, J.R. Heflin, N.Q. Wang and Y.M. Cai	73
TI6	Ultrafast Relaxation in Polymers with Large Optical Nonlinearity, T. Kobayashi and M. Yoshizawa	75
TI7	Polymer Dispersed Liquid Crystals - New Materials for Nonlinear Optics, F. Simoni, G. Cipparrone, D. Duca, C. Umeton, and I.C. Khoo	77
TI8	Nonlinear Optics of Nematic, Smectic and Cholesteric Liquid Crystals, N.V. Tabiryan and I.C. Khoo	78

Session: Applications of Nonlinear Semiconductor II

TI9	Optical Functional Devices Using Semiconductor Laser Nonlinearity, H. Kawaguchi	79
TI10	Application of Nonlinear Semiconductor Laser Amplifiers, R.P. Webb	81
TI11	Low Power Optical Switching in GaAs Epitaxial Etalons, J.L. Oudar, R. Kuszelewicz, and B. Sfez	83
TI12	Quantum Well Devices for Digital Optics, D.A.B. Miller	85

Plenary Session

Historical Reminiscences About Nonlinear Optical Materials, N. Bloembergen	87
--	----

POSTER SESSION:

Fundamental Studies II

TP1	Greater Than 90% Conversion Efficiency by Stimulated Rotational Raman Scattering in Hydrogen (H_2), E. Gregor, D.W. Mordaunt, and K.V. Strahm	90
TP2	The Permittivity of Polycrystalline Electromagnetic Materials: Extension of Current Method for Spectra Calculation, C.A. Grimes and E.L. Hixson	92
TP3	Room Temperature $1.06 \sim 0.53 \mu m$ Second Harmonic Generation with $MgO:LiNbO_3$, J.Q. Yao, J.E. Millerd, E. Garmire, M. Birnbaum, W.Q. Shi, and G.F. Xu	93
TP4	Molecular Orientation in Monolayers from Variation of Nonlinear Optical Generation with Incident Angle, Q. Zhu and P. Browne	95
TP5	Beam Reshaping Effects in Saturable Media, R.J. Ballagh and A.W. McCord	96
TP6	A Unified Theory of Spontaneous and Stimulated Rotational Raman Scattering, M.R. Hermann, D.H. Chambers, S. Dixit, and T.J. Karr	97
TP7	Polarization Dependence on High-Order Rotational Raman Frequency Conversion, M.R. Hermann, S. Dixit, and T.J. Karr	99
TP8	Third Harmonic Generation in SiO_2-TiO_2 SOL-GEL Films, W.E. Torruellas, L.A. Weller-Brophy, R. Zanoni, G.I. Stegeman, Z. Osborne, and B.J.J. Zelinski	101
TP9	Spatial Polarization Separation in An Absorptive Medium, D.E. McClelland, J.C. Wang and H.A. Bachor	103
TP33	Theoretical Study of Optical Second-Harmonic Generation From A Nonlinear Medium of Finite Cross-Section, R. Morita, N. Ogasawara, S. Umegaki, and R. Ito	105

Session III-V Quantum Wells

TP10	Carrier Cooling in Strained $In_xGa_{1-x}As/GaAs$ Single Quantum Well, Z. Yu, W. Peng, Q. Li, S. Yuan and S. Qian	107
TP11	Coulomb Enhancement of Ultrafast Nonlinearities in Quantum Well Structures, J. Khurgin	109

TP12	Nonlinear Absorption In a Strained InGaAs/GaAs MQW/n-i-p-i Structure, T.E. Van Eck, K.P. Aron, G.A. Hansen, R.S. Lytel, S. Niki, W.S.C. Chang, and H.H. Wider	111
TP13	Infrared Second Harmonic Generation by Intersubband Transitions in AlGaAs/GaAs Quantum Well Structures, A. Sa'ar, I. Grave, N. Kuze, and A. Yariv	113
TP14	Optical Properties of Asymmetric Triangular Quantum Wells for Self Electro-Optic Effect Devices, R.A. Puechner, D.S. Gerber, D.A. Johnson, R. Droopad, and G.N. Maracas	115
TP15	Self-Electro-optic Effect Device Based on an Asymmetric Fabry-Perot Modulator Using Wannier-Stark Localization in Superlattice, K.K. Law, R.H. Yan, L.A. Coldren, and J.L. Merz	117
TP16	Transient Optical Nonlinearities in Asymmetric Superlattices, S.E. Ralph, F. Capasso and R.J. Malik	119
TP17	Precision Nonlinear Laser Spectroscopy of Exciton Dynamics in GaAs/AlGaAs Multiple Quantum Well Structures, D.G. Steel, M. Jiang, H.Wang, and J.T. Remillard	121
TP18	Optical Properties of Strained-Layer InAs/GaAs Quantum Wells in Hetero n-i-p-i Structures, T. Hasenberg, A. Kost and E. Garmire	122
TP19	Nonlinear Optical Absorption Caused by Interaction Between Interband - and Intraband-Resonant Lights in Multiple Quantum Well Structure, S. Noda, T. Uemura, and A. Sasaki	124

Session: Parametric Processes and Stimulated Brillouin Scattering

TP20	A Novel Single Mode Oscillator Incorporating an Internal Multi-mode Optical Fibre and Phase Conjugate Reflector, B. Luther-Davies, A. Liebman, A. Maddever	126
TP21	Astigmatic Stimulated Brillouin Scattering Thresholds with Applications to Nuclear-pumped Gas Lasers, A. Corvo, C.A. Huguley, C.M. Clayton, and A. Gavrielides	128
TP22	Transfer Function Characteristics of Optical Parametric Amplification, C.J. Wetterer, P.A. Laferriere, and D. A. Cardimona	130
TP23	Stability of Three-dimensional States of a Parametric Ring SBS Oscillator, V.V. Eliseev, V.T. Tikhonchuk, A.A. Zozulya	132
TP24	An Infrared - Visible - Ultraviolet Tunable Optical Parametric Generation System, L. Huang, Y.-C. Yao, G. Li, and B.-L. Yin	134
TP25	Tunable Mid-Infrared Source Using AgGaSe ₂ , N.P. Barnes	136
TP26	Growth, Characterization, and Applications of Beta-Barium Metaborate and Lithium Triborate, C.L. Tang, W.R. Bosenberg, T. Ukachia, W.S. Pelouch, and R. Lane	137
TP27	Characteristics of Optical Parametric Oscillation Using β -BaB ₂ O ₄ Crystal, H. Suzuki, Y. Ohbayashi, and M. Takahashi	139
TP28	Stimulated Brillouin Scattering Revisited, P. Yeh and X. Gu	141
TP29	Phase Conjugate Oscillation In a Kerr Medium In the Presence of Pump Depletion, S. Guha and P. Conner	143
TP30	Picosecond Laser-Induced Reorientation, Density, Temperature, and Flow Effects In the Mesophases of Liquid Crystals, I.C. Khoo, R.R. Michael, R.G. Lindquist, R.J. Mansfield, and P. LoPresti	145
TP31	Second Harmonic Generation in Guided Wave Ferroelectric Liquid Crystal Structures, M.G. Robinson, J. Liu, K.M. Johnson, D. Walba, and D. Doroski	147
TP32	Time-Dependent Dynamical Reorientation Induced by CW Laser Beam In a Nematic Liquid Crystal Film, E. Santamato, C. Abbate, P. Maddalena, L. Marrucci, and Y.R. She	149

WEDNESDAY, JULY 18

Session: Photorefractives I

WI1	Photorefractive Materials and Devices, J. Feinberg	152
WI2	BaTiO ₃ Developments: 1) Seeded Stimulated Photorefractive Scattering, and 2) Photoluminescence. R.A. Mullen, K.L. Schumacher, D. Vickers, and D.M. Pepper	153
WI3	Enhancing Photorefractive Properties for Specific Applications, G.L. Wood, W.W. Clark, III, G.J. Salamo, and E.J. Sharp	155
WI4	Recent Progress in Photorefractive Nonlinear Wave Mixing, B. Fischer	157

Session: Semiconductors I

WI5	Exciton Coherency, Its Superradiant Decay and Enhanced Optical Nonlinearity, E. Hanamura	158
WI6	Femtosecond Excitonic Nonlinearities Under Resonant and Non Resonant Excitation, D. Hulin, A. Migus, M. Joffre, and A. Antonetti	160
WI7	Optical Stark Effect of the Exciton, M. Combescot	161
WI8	Large Nonlinear Susceptibilities Due to Intersubband Transitions in AlGaAs Quantum Wells, M. Fejer	N/A

Session: Fundamental Phenomena in NLO II

WI9	Using (As Opposed to Studying) X ⁽³⁾ , M.D. Levenson	162
WI10	Nonlinear Optical Processes with Incoherent Light and Their Applications for Studies of Ultrafast Dephasing Processes, P. Ye	164
WI11	Nonlinear Guided Wave Grating Phenomena, G.I. Stegeman, J.E. Ehrlich and G. Assanto	166
WI12	Ring Resonator Stability, A. Gavrielides, P.R. Peterson	N/A

Plenary Session:

	Photorefractive Crystals for Nonlinear Optical Applications, A. Yariv	N/A
--	---	-----

Poster Session: Fundamental Studies III

WP1	Simultaneous Measurement of Vibrational Spectra and Dynamics Through Femtosecond Fourier-Transform Nonlinear-Optical Spectroscopy, W.T. Lotshaw, and D. McMorro	170
WP2	Coherence and Chaos in a Quantum Optical System, G.J. Milburn	172
WP3	Second-Order Phase Transition at the Critical Point of Optical Bistability Due to Nonlinear Absorption, O. Fa	174
WP4	N-Color Ferroelectric Binary Processor, K.L. Block, and K.S. Redus	183
WP5	Nonperturbative Calculation of Nearly Degenerate Multi-Wave-Mixing Spectra, R.P. Lucht, R. Trebino, and L.A. Rahn	185
WP6	On the Interpretation of n ₂ Measurements Using an Externally Focussed Gaussian Beam, R.M. Mishra, P.P. Banerjee, and A. Korpel	187

WP7	Scaling Behavior of Optical Bistability in Nonlinear Medium, Y.H. Kao and C.S. Wang	188
WP8	Exploration of Optical Propagation in a Nonlinear Dispersive Medium Based on An Incommensurate Spectral Formalism, P.P. Banerjee, and M.R. Chatterjee	190
WP9	Liouville Operator Theory of Nonlinear Optical Susceptibilities, P.L. Kelley, J.P. Taran, O. Blum, I. Kim, and T.K. Gustafson	191
WP10	Size Dependence of $X^{(3)}$ for Frenkel Excitons in a Periodic Chain, H. Ishihara and K. Cho	193
WP32	Resonant Degenerate Four-Wave Mixing for Imaging and Temperature Measurements of Molecules in Combustion, R.L. Farrow, and D.J. Rakestraw (originally paper #THP19)	194

Session: Organic NLO Materials & Devices

WP11	Nonlinear Optical Waveguide Using Polymer Film Doped with 2-Methyl-4-Nitroaniline, H. Haga and S. Yamamoto	196
WP12	Second-Harmonic Generation with Laser Diodes and Organic Channel Waveguides, T. Kondo, N. Hashizume, S. Miyoshi, R. Morita, N. Ogasawara, R. Ito, and S. Umegaki	198
WP13	Selective Poling of Polymers by Laser-Heating, J.F. Valley and A.J. Ticknor	200
WP14	Poling Studies on Composition Modulated Nonlinear Polymeric Thin Films, T. Morita, B.G. Higgins, and A. Knoesen and S.T. Kowel	202
WP15	Poled Polymer for Frequency Doubling of Diode Lasers, G.L.J.A. Rikken, C.J.E. Seppen, S. Nijhuis, and E.W. Meijer	204
WP16	Progress in Crosslinked Nonlinear Optical Polymers, D. Jungbauer, G.C. Bjorklund, B. Reck, R.J. Twieg, J.D. Swalen, C.G. Willson, and D.Y. Yoon	206

Session: Photorefractive Applications

WP17	Observation of Extended-Lifetime Holograms in Photorefractive $\text{Bi}_{12}\text{SiO}_{20}$ at 785 nm, M.C. Bashaw, T.P. Ma, R.C. Barker, S. Mroczkowski, and R.R. Dube	208
WP18	Real-Time Pulse Shaping Using a Dynamic Grating, K. Ema and F. Shimizu	210
WP19	Large Photorefractive Beam-Coupling Gain Using the Franz-Keldysh Electrorefractive Effect in Temperature-Stabilized InP:Fe , A. Partovi, J. Millerd and E. Garmire	212
WP20	Self-Aligning Optical Heterodyne with Four-Wave Mixing, K. Nguyen, T.K. Gustafson, S. Yee, and R. Neurgaonkar	214
WP21	Color Holographic Storage in LiNbO_3 , F.T.S. Yu, S. Wu, A. Mayers and S. Rajan	215
WP22	High Power Diode Laser Array Beam Combination Via Injection Locking and Photorefractive Beam Coupling, S. MacCormack, R.W. Eason, and S.W. James	216
WP23	Dynamic Range Compression Using Incoherent Erasure in Photorefractive Two-Beam Coupling, A. Chiou	217

Session: SC Lasers & Interfaces

WP24	Anisotropy of Second Harmonic Generation from Magnetized Surfaces, R. Pan, H.D. Wei, and T.J. Watson Yang	219
WP25	Optical Second-Harmonic Generation at the Interface Between Silver Thin Film and LiNbO_3 , T. Kakano, Y. Inoue, K. Yano, T. Tokumaru, and Y. Okada	220
WP26	Surface Magnetoplasmon-Polariton Solitons on Semiconductors: Voigt Geometry, T.P. Shen, D. Rogovin, and A.D. Boardman	222
WP27	Soliton Interaction and Spectral Laser Linewidth in Wavelength Multiplexing Transmission Systems, T. Hauff, and W. Heinlein	224
WP28	Fundamental Dark Surface Waves at a Nonlinear Interface, S.R. Skinner and D.R. Andersen	226
WP29	Million Fold Enhancement of Surface Emitting Harmonic Generation in Semiconductor Waveguides, R. Normandin, F. Chatenoud and R.L. Williams	228
WP30	Demonstration of Cascadability and Spectral Bistability in Bistable Diode Laser Amplifiers, Z. Pan, T.-N. Ding and M. Dagenais	230

WP31	Optical Bistability and Switching by Nonlinear Waveguiding in Semiconductor Lasers and Laser Amplifiers, J.G. McInerney, L. Yuan, T.C. Salvi, and D.M. Heffernan	232
------	--	-----

THURSDAY, JULY 19

Session: Semiconductors II

THI1	Quantum-Confined Franz-Keldysh Effect in CdTe Quantum Dots in Glass, G. Khitrova, V. Esch, H.M. Gibbs, J.Xu, L. Liu, and S. Risbud	N/A
THI2	Nonlinear Optical Effects in GaAs/AlAs Type-II Heterostructures, G.R. Olbright, and J.F. Klem	236
THI3	Two-Color, Ultrafast, Anisotropic Transient Grating Separation of Photorefractive, Bound-Electronic and Free-Carrier Grating Dynamics in Zincblende Semiconductors, A.L. Smirl, W.A. Schroeder, M.D. Dawson, T.S. Stark and T.F. Boggess	238
THI4	Nonlinear Optical Effects in Visible-Band-Gap Semiconductors and Microcrystallites, F. Henneberger	239

Session: Phase Conjugation II

THI5	Degenerate Resonant Four Wave Mixing of Laser Radiation in a Plasma, C. Joshi	240
THI6	Resonant Wave Mixing Processes in Vapors, M. Ducloy, M. Oria, M. Chevrollier, D. Block, and M. Fichet	241
THI7	Depletion, Diffraction and Partial Coherence in Non-Linear Optical Mixing, M. Nieto-Vesperinas	243
THI8	Efficient Phase Conjugation and Optical Oscillators Via Four-wave Mixing in Photorefractive BTO Crystals, S.I. Stepanov and S.L. Sochava	N/A

Session: Fundamental Phenomena in NLO III

THI9	Effects of Quantum Fluctuations of Raman Soliton Formation, J.L. Carlsten	245
THI10	Solitons and Raman Scattering in Optical Fibers, S. Chi	247
THI11	Relativistic Nonlinear Optics, A.E. Kaplan	248
THI12	Nonlinear Faraday Rotation in Diluted Magnetic Semiconductors, R. Frey, J. Frey, and C. Flytzanis	250

Plenary Session

Surface Nonlinear Optics for Material Studies, Y.R. Shen	251
--	-----

POSTER SESSION:

Photorefractive Materials

THP1	Four Wave Mixing in Doped and Un-doped KNSBN Crystals, W. Peng, R. Zhu, W. She, Q.Li, Z. Yu, H.-C. Chen, Q.L. Zhang, Y. Xu and D.- R. Zhu	254
THP2	Photorefractive Properties of CdTe:V at 1.5 μ m, M.Ziari, W.H. Steier, A. Partovi, J. Millerd, E. Garmire, S. Trivedi, and M. Klein	255
THP3	Electrooptic Properties of Lead Barium Niobate (PBN) Single Crystals, R. Guo, D.A. McHenry, A.S. Bhalla, and L.E. Cross	257
THP4	Growth of Single Crystal Fibers for Optical Applications, J.K. Yamamoto, and A.S. Bhalla	258

THP5	Investigation of the Microscopic Parameters Governing the Photorefractive Effect in $\text{KTa}_{1-x}\text{Nb}_x\text{O}_3\text{:Cu,V}$, V. Leyva, A. Agranat, and A. Yariv	259
THP6	Direct Determination of the Electron Mobility in Photorefractive $\text{Bi}_{12}\text{SiO}_{20}$ by a Holographic Technique, J.P. Partanen, J.M.C. Jonathan, and R.W. Hellwarth	261

Session: Semiconductors

THP7	Picosecond Nonlinear Optical Phenomena in Undoped Cadmium Telluride, M.S. Petrovic, A. Suchochi, R.C. Powell, G.C. Valley, and G. Cantwell, and J. Aldridge	263
THP8	Excitonic Nonlinearities in ZnSe/ZnS Multiple Quantum Wells, C. Li, Y. Liu, and D. Shen, X. Fan	264
THP9	Optical Nonlinearities of the Metal-Oxide Semiconductor Particles, H. Fei, J. Zhao, L. Han, B. Zhou, L. Xiao, and T. Li	266
THP10	Temporal Behavior of the Optical Stark Effects on the Stacking Fault Exciton States in Bi_2 , I. Akai, T. Karasawa, and T. Komatsu	268
THP11	Nonlinear Optical Properties of Phenyl-Capped CdS Molecular Particle Doped Organic Polymer, T. Fukumi, T. Sakaguchi, M. Miya, S. Yanagida, T. Enokida, H. Mori, and H. Fujita	270
THP12	Clockwise Bistable Photocurrent and Inverse Franz Keldysh Effect of Thin CdS Films, C. Bouchenaki, B. Ullrich, and J.P. Zielinger	272
THP13	Preparation and Third-Order Optical Nonlinearities of CuCl Microcrystallite-Doped Glasses, N. Sugimoto, T. Manabe, S. Ito, T. Tokizaki, T. Kataoka, and A. Nakamura.	274
THP14	Biexciton Phonon Interaction Studied by Two-Photon Polarization Spectroscopy, M. Kuwata-Gonokami, J. Iwamatsu, R. Shimano, and H. Akiyama	276
THP15	The Beam Propagation Method Applied to Nonlinear Optical Microstructures, I. Kim, P.J. Harshman, and T.K. Gustafson	278

Session: Phase Conjugation

THP16	Chirp and Self-Phase Modulation in Induced-Grating Autocorrelation Measurements of Ultrashort Pulses, R. Trebino, C.C. Hayden, A.M. Johnson and A.M. Levine	279
THP17	Phase Conjugate Interferometry for Thin Film Analysis, E.R. Parshall, and M. Cronin-Golomb	281
THP18	Coherence Effects in a Laser Phase-Locking Geometry, M.T. Gruneisen, E.D. Seeberger, and J.F. Mileski	283
THP19	Resonant Degenerate Four-Wave Mixing for Imaging and Temperature Measurements of Molecules in Combustion, R.L. Farrow, D.J. Rakestraw, and T. Dreier See paper WP32	194
THP20	Cross-Talk in Self-Pumped Photorefractive Phase Conjugation, F.C. Jahoda, P.R. Forman, and B.L. Mason	285
THP21	Nonlinear Optics with an Argon Laser, J.D. Harvey	288
THP22	Self-Pumped Optical Phase Conjugation In Cesium Vapor, C.J. Gaeta, and J.F. Lam	290
THP23	Dual-Port Optical Neural Network Using A Mutually Pumped Phase Conjugate Mirror, G.J. Dunning, Y. Owechko, and B.H. Soffer	291
THP24	Beam Steering Using Phase Conjugation, A.M. Scott, K.D. Ridley, and G. Cook	293
THP25	Linear Stability of Photorefractive Phase Conjugation, J.A. Tataronis and B.E.A. Saleh	294
THP26	Optical and Structural Characterization of Semiconductor-doped Glasses, L. Baldassarre, C. DeBlasi, V. Degiorgio, G. Fagherazzi, M. Ferrara, M. Lugara, S. Pelli, and G.C. Righini	296
THP27	New Phenomena on Laser-Induced Photorefractive Effect in $\text{LiNbO}_3\text{:Fe}$, Q. Li, X. Huang, A. Zhong and Z. Yu	298

FRIDAY, JULY 19

Session: Phase Conjugation III

FI1	Application of Phase Conjugation to Communications Systems, D.M. Pepper, C.J. Gaeta, M. Minden, R.A. Mullen and P.V. Mitchel	N/A
FI2	Nonlinear Methods in Image Formation, E.N. Leith and A. Cunha	302
FI3	A CO ₂ Laser with a Nonlinear Mirror, N.R. Heckenberg, R. McDuff, and A. Smith	303
FI4	Coherent Lidars Based on Laser Systems with Brillouin Cells, G.A. Pasmanik, N.F. Andreev, O.V. Kulagin, E.A. Khazanov, and A.A. Shilov	Withdrawn

Session: Photorefractives II

FI5	Wave Mixing in the Photorefractive Crystals, N. Kukhtarev and A. Volyar	305
FI6	Photorefractive Phase Conjugators, M.D. Ewbank	306
FI7	Competitive and Cooperative Dynamics in Photorefractive Optical Systems, D.Z. Anderson, C. Benkert and A. Hermanns	307
FI8	Internal and External Ring Cavity Self-Pumped Phase Conjugators and Their Dynamic Processes in Different Photorefractive Crystals, H. Zhang, H.X. Hua and T.S. Hai	309

Session: Semiconductors III

FI9	Diode Laser Scaling Using Optical Phase Conjugation, R.C. Lind, R.R. Stephens, W.J. Gignac and D.L. Persechini	N/A
FI10	Semiconductor Nonlinearities for Optical Limiting, E.W. Van Stryland, D.J. Hagan, M. Sheik-Bahae, and M.J. Soileau	311
FI11	Nonlinearities of Gallium Arsenide Doping Superlattices, M.S. Tobin, G.J. Simonis, and J.D. Bruno	313
FI12	Enhanced Carrier Transport Nonlinearities, E. Garmire	315

Session: Special Topics

ST1	Nonlinear Optical Processes Using Electromagnetically Induced Transparency, S.E. Harris, J.E. Field, and A. Imamoglu	317
ST2	High-Order Harmonic Generation in Gases, K.C. Kulander, Bruce W. Shore, and A. I'Huillier	319
ST3	Deterministic Beam Position Noise in Laser Arrays, H.G. Winful	320
ST4	Organic Nonlinear Optical Materials and Their Device Applications, D.M. Burland, S. Duchame, W.W. Fleming, R.D. Miller, W.E. Moerner, W.P. Risk, R.J. Twieg, and C.A. Walsh	322

Author Index	324
--------------	-----

MONDAY, JULY 16
ORAL PRESENTATIONS

D.T.Pegg

Division of Science and Technology, Griffith University, Nathan, Brisbane 4111, Australia.

A squeezed state of light is usually taken to mean a state in which the fluctuations of one of the quadratures are below the level associated with a coherent or vacuum state. These squeezed fluctuations are phase sensitive in the sense that they vary periodically as the field evolves, but the relationship between squeezing and phase fluctuations is not trivial. While squeezed states can exhibit an arbitrarily low level of phase fluctuations [1], the phase states, which are eigenstates of the Hermitian optical phase operator [2] are not themselves quadrature squeezed [3]. A phase-squeezed state is one with a lower level of phase fluctuations than a coherent state with the same mean photon number. Phase squeezing is fundamentally different from quadrature squeezing in much the same way that sub-Poissonian photon statistics is different. For this reason optimally squeezed states and states with minimum phase noise will be distinct. We derive the form of the states which minimum phase noise for a given intensity. These have an Airy function behavior for the photon number probability distribution. These phase squeezed states have a far better phase resolution than coherent states of similar intensity, but do not seem to offer a significant reduction of phase fluctuations compared with conventional squeezed states.

- [1] J.A.Vaccaro and D.T.Pegg, *Opt. Commun.* **70**, 529 (1989).
- [2] D.T.Pegg and S.M.Barnett, *Europhys. Lett.* **6**, 483 (1988); S.M.Barnett and D.T.Pegg, *J. Mod. Opt.* **36**, 7 (1989); D.T.Pegg and S.M.Barnett, *Phys. Rev. A* **39**, 1665 (1989).
- [3] S.M.Barnett and D.T.Pegg, *Phys. Rev. A* (submitted).

D.F. Walls, M.J. Collett, A.S. Lane and R.B. Levien
 Department of Physics
 University of Auckland
 Auckland
 New Zealand

Current laser systems have phase and amplitude fluctuations which are partially quantum in origin. The amplitude fluctuations of a highly stabilized laser are shot noise limited, that is they have quantum fluctuations due to the Poissonian fluctuations of photons in a coherent state. These photon number fluctuations have been shown to have an origin in the incoherent pumping mechanism used for standard lasers. It has recently been demonstrated experimentally that by suppressing the amplitude fluctuations of the pump a laser output with reduced amplitude fluctuations is possible. The phase fluctuations in a laser are due to phase diffusion and are substantially above the quantum limit. Techniques to reduce the laser phase fluctuations have been proposed making use of correlated spontaneous emission.

In this paper we wish to study the possibility of reducing the noise in the laser output field by using intracavity nonlinear elements to provide an internal stabilization.¹ We first consider intracavity second harmonic generation. This results in a reduction of amplitude fluctuations in the output field at the second harmonic 50% below the shot noise. The explanation for this noise reduction is as follows. The laser is producing photons at the fundamental frequency with a Poissonian distribution ($V(I_1) = I_1$). In a regime where the second harmonic conversion efficiency is very high and the output photons are nearly all at the second harmonic $I_2^{\text{out}} = \frac{I_1}{2}$. The variance in the output at the second harmonic is $V(I_2^{\text{out}}) = \left(\frac{1}{2}\right)^2 V(I_1) = \frac{1}{2} \langle I_2^{\text{out}} \rangle$ that is, 50% below the shot noise.

In order to achieve the condition for near total output at the second harmonic without a very high SHG efficiency, it is useful to employ an injected signal at the fundamental. The input light reflected from the cavity mirror interferes with the light emerging from the cavity at the fundamental giving $(I_1^{\text{out}}) \approx 0$. This enables the amplitude noise reduction in the second harmonic to be achieved with lower SHG efficiencies.

A small injected signal (I_2^{in}) at the second harmonic results in the maximum noise reduction in the second harmonic occurring in a sideband frequency $\omega_c \sim \sqrt{I_2^{\text{in}}}$. A large injected signal at the second harmonic will produce good phase squeezing at the fundamental. In contrast to passive subharmonic generation below threshold, this squeezing occurs in a field with a finite amplitude.

Finally we consider intracavity subharmonic generation with a small injected signal at the laser frequency. Under conditions where the laser gain balances linear cavity losses at the fundamental good phase squeezing may be obtained in the subharmonic field.

References

1. For related work see:

Y.M. Golubev, Sov.Phys. JETP **66**, 265 (1987)

V.N. Gorbachev and E.S. Polzik, Sov.Phys. JETP **69** (1989)

H. Ritsch (to be published)

P. Garcia Fernandez, L. Lugiato, F.J. Bermejo and P. Galatola (to be published)

MI5 Quadratic Nonlinear Optical Properties of a New Organic Crystal: N-Methoxymethyl-4-nitroaniline (MMNA)

Seizo Miyata, Hironobu Yamamoto,
Shigeki Katogi and Takeshi Hosomi.

Tokyo University of Agriculture and Technology.
Koganei, Tokyo 184, Japan.

It is well known that p-nitroaniline (p-NA) shows no quadratic optical nonlinearity because of the centrosymmetry in the crystal, although it has large hyperpolarizability, β . If p-NA is chemically modified without decreasing its β value so as to form noncentrosymmetric crystals, it will change into strong quadratic nonlinear optical materials.

We found that N-methoxymethyl-4-nitro-aniline(MMNA), prepared simply by reacting p-NA, formaldehyde and methanol with sodium hydroxide at room temperature, exhibited strong SHG activity. MMNA yielded large single crystals; 5-6 cm in length, 1 cm in width and 0.5 cm in thickness, when crystallized in tetrahydrofuran solution for a few days. The crystal structure of MMNA evaluated by x-ray methods indicates that the crystal belongs to orthorhombic space group $P2_12_12_1$. The crystal data are $a=11.236\text{\AA}$, $b=17.550\text{\AA}$, $c=4.573\text{\AA}$, and $Z=4$. The calculated density of the crystal is 1.34 g/cm^3 and the melting point is 115°C . The refractive indexes at $1.06\text{ }\mu\text{m}$ and $0.53\text{ }\mu\text{m}$ are $n_a^w=1.748$, $n_b^w=1.602$ and $n_c^{2w}=1.635$ respectively.

Phase-matching in MMNA is obtained by illuminating laser beam with 3 incident angle to the crystallographic $[110]$ direction, where the (110) plane is natural crystal growth surface. The d_{eff} obtained experimentally is 15 pm/V by comparing the phased-matched SH light with those of KTP and quartz. This value agrees well with the calculated one by using crystallographic data according to the theory of oriented gas model developed by Zyss.

Since MMNA possesses various merits such as ease of preparation from p-NA, fast crystal growth rate, and high quadratic optical nonlinearity, it seems very promising for the future opto-electronic technology.

Laser-Induced reorientation and Ultrasound Generation in the Liquid Crystal SCB Induced by Picosecond Laser Pulses

L. B. Au^{*}
H.J. Eichler
R. Macdonald
L. Solymar^{*}

Optisches Institut
Technische Universität
D-1000 Berlin 12, FR Germany

^{*} on leave of absence from Dept. Eng. Science, University of Oxford, UK

Abstract

Dynamics of picosecond laser-induced molecular reorientation phenomena and ultrasound-generation in the liquid crystal SCB are investigated in transient grating experiments. It is shown that the reorientation process is still increasing after the pump-pulse leaves the sample and relaxes exponentially later. Further a coupling between reorientation effects and the excitation of sound-waves has been observed.

Introduction

Liquid crystals are fluids with strong correlations between the constituting molecules showing anisotropic physical properties in general. This behaviour results not only in strong electro-optical and magneto-optical¹ but also in remarkable opto-optical effects. Optical field-induced reorientation of nematic liquid crystals has been investigated with low power cw-lasers^{2, 4} and with short laser pulses^{3, 6} and the related optical nonlinearity is of some interest to applications like phaseconjugation, photonic switching and processing of light or optical bistability.

All recent studies of field-induced molecular reorientation in nematics show that the static and dynamic properties of molecular motion obey the Erickson-Leslie theory³ which describes the collective reorientation phenomena by the deformation of a so called director, the average molecular orientation. In the present paper it is shown that the Erickson-Leslie theory is also applicable if ultrashort laser pulses of less than 100ps duration and strong optical fields as high as 10^7 V/m are used for excitation. For the first time we have observed effects which give evidence that an inertial moment has to be considered in this case. Further we have observed a nonthermal ultrasound-generation mechanism in these experiments, where the acoustic waves are excited by the molecular reorientation process due to inverse flow-orientation coupling.

Experiments and Results

In our experiments we used a wave-mixing arrangement, which is schematically shown in Fig. 1a. Two pump-pulses of 80 ps duration (FWHM) obtained from a frequency-doubled mode-locked Nd:YAG laser with a single-pulse extraction are focussed to an e^{-2} -diameter of 800 μm on a thin film ($d = 25 \mu\text{m}$) of a homeotropically aligned nematic liquid crystal SCB (4'-n-pentyl-4-cyanobiphenyl). The two pump beams are linearly polarized, their polarizations either parallel or perpendicular to each other, producing an intensity- or polarization-grating in the sample. The resulting optical field-fringes modulate the alignment of the molecules and change the optical properties of the birefringent liquid crystal by rotating the director and the optical axis. The center of the induced phase-grating (grating

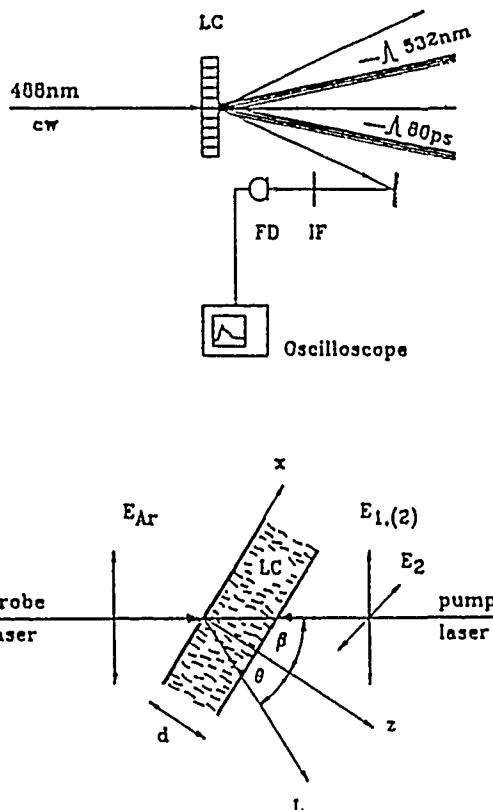


Fig. 1: Experimental setup (a): LC-Liquid crystal; FD-fast photodiode; IF-interference filter. Experimental geometry (b): E_1 , E_2 - optical pump fields; E_{Ar} - optical probe field; β -initial alignment angle (22.5 deg); θ - reorientation angle.

period $\Lambda = 30 \mu\text{m}$) is probed by a weak argon cw-laser (488 nm) with a spot size of $100 \mu\text{m}$ diameter. The first order diffracted intensity of the probe-beam is measured, with a fast photodiode and a fast real-time oscilloscope. The oscilloscope-traces are recorded and processed with a digitizing video-camera system. The time resolution is limited by a rise-time of about 400 ps and a decay-time of less than 4 ns with the PIN-diode used so far.

The experimental geometry is shown in Fig. 1b. The unperturbed director and the optical fields E_{Ar} and E_1 are in the x-z plane while the second pump field E_2 is chosen parallel or perpendicular to E_1 . If $E_1 \parallel E_2$ the two beams interfere to give an intensity-grating and field-dependent as well as intensity-dependent effects will be excited in a periodic structure leading to diffraction of the probe-beam. If however $E_1 \perp E_2$, the two beams will not interfere and intensity-dependent effects (e.g. thermal heating) will not occur in a grating and are not detected. But the optical fields still add together vectorially to form a polarization-grating. The liquid crystal will respond to a polarization-grating with a periodic reorientation structure which is detected by the probe beam diffraction without any additional intensity-dependent effects⁷. Fig. 2 displays typical oscilloscope-traces of the diffracted probe-beam intensity during the first 500 nanoseconds after the ps-excitation pulse for the two types of excitation gratings.

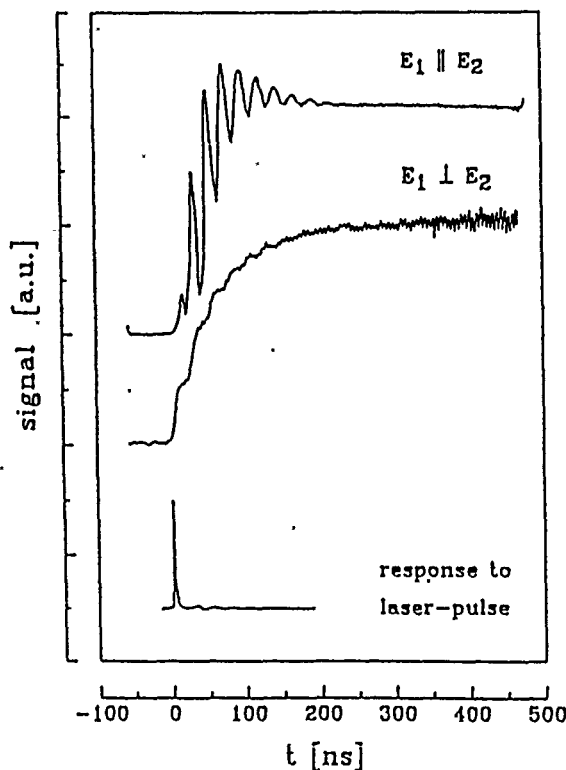


Fig. 2: Diffracted probe-beam intensity vs. time after ps grating-excitation. Pump energy $W_p = 0.25 \text{ mJ}$. The response of the detector system to a single pump-pulse is shown for comparison.

In both cases the signal is still increasing long after the pump-pulse (which can be approximated as a δ -peak at $t=0$ on the graph) leaves the sample, showing strong additional oscillations in the case $E_1 \parallel E_2$. These oscillations occur due to laser-induced ultrasonic standing-waves and diffraction at the resulting density modulations (forced Brillouin-scattering), which will be enhanced mainly by thermal heating, if an intensity-grating is used. The trace $E_1 \perp E_2$ shows the effect of an almost pure reorientation-grating. If however the pump energy is increased strong oscillations will also occur for a polarization-grating as shown in Fig. 3. This can be explained by generation of ultrasound due to the reorientation process itself and the related molecular motions.

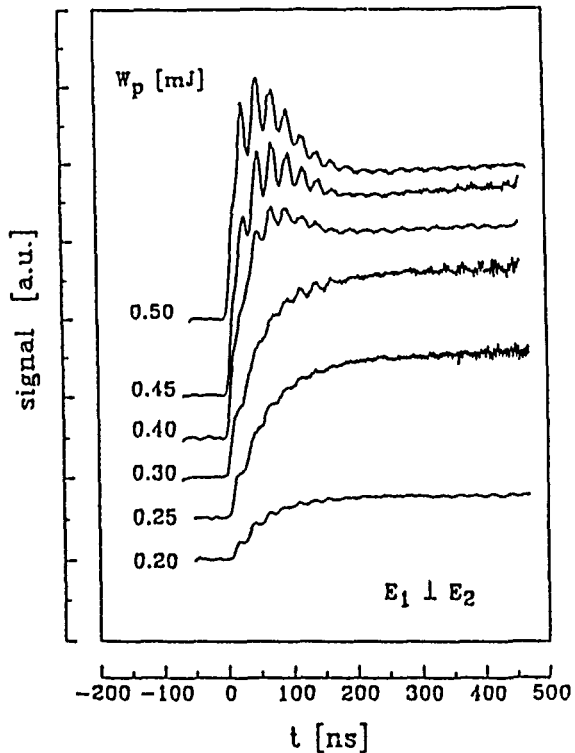


Fig. 3: Diffracted probe-beam intensity after ps polarization-grating excitation at different pump energies W_p . The sample is nematic SCB at $T = 25^\circ\text{C}$, $d = 25 \mu\text{m}$.

The slower increase of the signal at low pump-energies is of the type $(1 - \exp(-t/\tau_R))$ showing rise-times τ_R between 20 and 50 ns depending on excitation-energy (see Fig. 4). Much later the signal will decrease and the grating decay can be fitted well by a single exponential law as is shown in Fig. 5. The evaluated decay times are in the millisecond-range, depending on sample temperature as is depicted in Fig. 6.

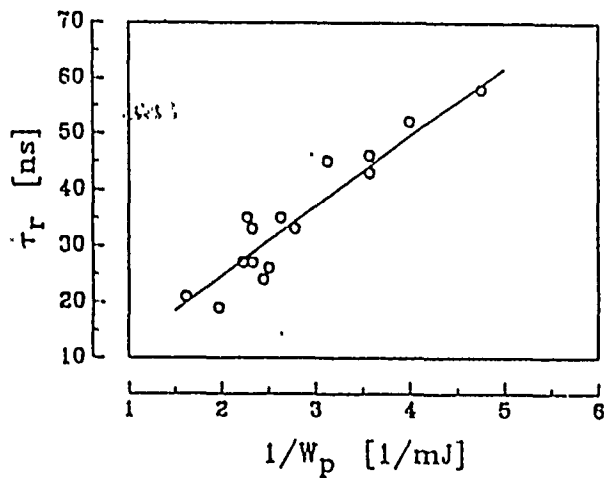


Fig. 4: Observed rise-times vs. reciprocal pump-energy.

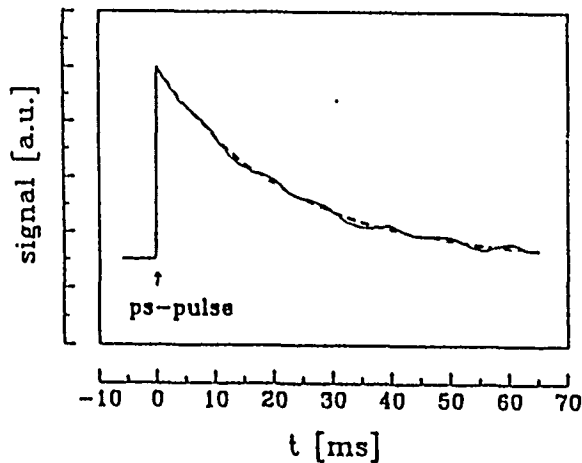


Fig. 5: Reorientation relaxation after ps excitation.

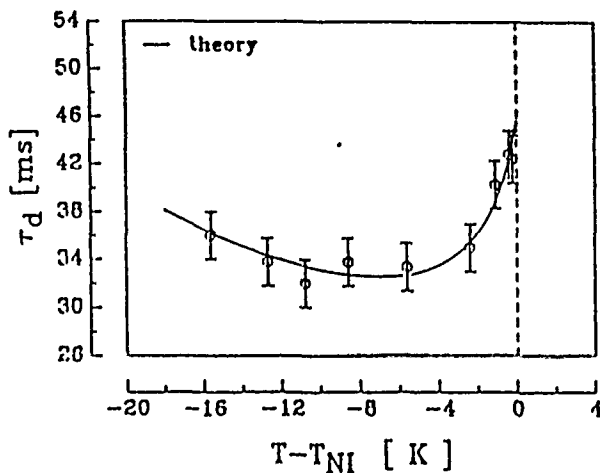


Fig. 6: Reorientation relaxation-times as function of the reduced sample temperature. T_{NI} is the nematic-isotropic phase transition temperature.

Theory and Discussion

The observed dynamics at low pump-energies can be described by the Erickson-Leslie continuum theory for calculation of the optical nonlinearity in combination with a dynamic grating diffraction model⁶. Considering a polarisation grating on a homotropic aligned nematic film the optical field-fringes will modulate the reorientation of the director and the refractive-index to form a phase-grating. Refractive-index changes established by molecular reorientation are given by

$$\delta n = n_e (\Theta + \beta) - n_e (\beta) \quad (1)$$

where

$$n_e(\theta) = n_{\perp} n_{\parallel} (n_{\parallel}^2 \cos^2 \theta + n_{\perp}^2 \sin^2 \theta)^{-1/2} \quad (2)$$

with $\theta = \Theta + \beta$ and $\theta = \beta$ respectively. n_{\perp} and n_{\parallel} are the refractive-indices perpendicular and parallel to the director. In an plane wave approximation the director motion can be described by a single reorientation angle Θ which is obtained by a torque balance

$$\mu \frac{\partial^2 \Theta}{\partial z^2} + \gamma \frac{\partial \Theta}{\partial t} - K \Delta \Theta - \frac{1}{2} \epsilon_0 \epsilon_a E^2 \sin 2(\Theta + \beta) = 0 \quad (3)$$

where K is the elastic constant (in a one constant approximation), γ the rotational viscosity, μ the inertial moment, $\epsilon_a = \epsilon_{\parallel} - \epsilon_{\perp}$ and E the optical field. Flow-orientation coupling has been neglected.

It may be shown that

$$\Theta = \Theta_m(t) \cos(qy) \sin(\pi z/d) \quad (4)$$

is an approximate solution of the linearized eq. 3 under hard boundary conditions $\Theta(z=0) = \Theta(z=d) = 0$ where q is the wave-number of the grating and Θ_m obeys the equation

$$\mu \frac{\partial^2 \Theta_m}{\partial t^2} + \gamma \frac{\partial \Theta_m}{\partial t} + D \Theta_m = F \quad (5)$$

with $D = K(q^2 + \pi^2/d^2) - \epsilon_0 \epsilon_a E^2 \cos 2\beta$ and $F = \frac{1}{2} \epsilon_0 \epsilon_a E^2 \sin 2\beta$. Eq. 5 describes the dynamics of an over-damped oscillator typical material parameters and experimental data like $\gamma = 0.01$ kg/ms, $K = 10^{-12}$ N, $d = 25$ μ m, $q = 0.2$ μ m⁻¹ and $\mu \leq 10^{-4}$ kg/m are used. This upper limit of the inertial moment corresponds to the motion of correlated molecules within a volume of $l \leq 300$ μ m radius which is much more than the correlation length.

In the time scale of our experiments the pump-pulse can be taken as a Delta-peak $E^2(t) = E_0^2 \delta(t)$ and the approximate solution of eq. 5 is given by

$$\Theta_m = \frac{F_0 \pi^2 R}{\mu} (\exp(-t/\tau_D) - \exp(-t/\tau_R)) \quad (6)$$

where

$$\tau_R = \frac{\mu}{\gamma} \quad (7a)$$

$$\tau_D = \frac{\gamma}{K(q^2 + \pi^2/d^2)} \quad (7b)$$

and τ_p is the length of the pulse.

The rise-time is given by the inertial moment and viscosity while the decay-time depends mainly on viscosity and the elastic forces as in simple relaxation models.⁵ If we take $\gamma = 0.015$ kg/ms, $K = 7 \cdot 10^{-12}$ N we get $\tau_p = 36$ ms (at $T = 25^\circ\text{C}$) in good agreement with experimental data. The observed temperature dependence of the relaxation time can be explained¹ by the well-known temperature dependence of the viscosity γ and the elastic constant K .

A response-time of e.g. $\tau_R = 40$ ns can be explained with $\mu = 6 \cdot 10^{-10}$ kg/m. This corresponds to a volume of $l = 800$ nm radius. Compared to the usual definition of a correlation length $l_k = (K/\epsilon_0 \epsilon_a E_0^2)^{1/2}$ which is $l_k = 40$ nm during the laser-pulse and $l_k = 8$ μm without optical field (at $t \rightarrow \infty$ after excitation) the assumed value l lies well between these two extreme cases. The observed dependence of the rise-time τ_R on the pump-energy W_p also suggests that $\mu \sim l_k^2$ or $l \sim l_k$ respectively.

During the laser-pulse however the correlation length is in the order of some ten nanometers resulting in much faster rise-times of some picoseconds which is comparable to the pulse-length. This can explain the occurrence of fast reorientation-effects and related refractive-index changes even when the picosecond pump-pulses are still in the sample as has been demonstrated in self diffraction experiments recently⁶.

The observed oscillations in the MHz frequency range cannot be explained with the simple reorientation model and show the limits of the approximations which have been introduced. At higher pulse-energies the flow-orientation coupling and the inverse process can obviously not be neglected any longer. We explain the observed nonthermal excitation of ultrasonics with the fast and impulsive reorientation and rotation of molecules.

If the sound waves are excited by a grating one gets two counterpropagating wave-packets which results in a standing wave at the excitation region, leading to the observed oscillations⁸. The period of the acoustic oscillations is given by

$$T_{ac} = \Lambda / v_s \quad (8)$$

where Λ is the grating period and v_s the speed of sound in the liquid. The damping of the oscillations is determined not by the acoustic attenuation but by the beam profile.

Similar results have been obtained in the isotropic phase of SCB where the optical Kerr-effect can be expected to be a very effective mechanism for the generation of ultrasonic waves.

Conclusion

In the present paper we report on investigations of the dynamics of molecular reorientation phenomena and ultrasound generation in a nematic liquid crystal using picosecond excitation pulses and dynamic grating diffraction. We have observed an increase of the director deformation for times much longer than pump-pulse duration. The observed rise-times are in the order of 20 to 50 ns depending on pump-energy. The reorientation is later decaying exponentially with time-constants of 30 to 40 ms depending on sample temperature. The observed dynamics can be described by the Ericksen-Leslie theory considering an inertial moment term. The inertial moment of the director motions has been assumed to be in the order of $\mu = 10^{-10}$ kg/m to explain the observed rise-times. This corresponds to an averaged correlation length of some hundred nanometers.

The observed oscillations of the diffraction signal are explained by a nonthermal generation of ultrasound and additional acoustic gratings driven by the reorientation-process.

Financial support from the Deutsche Forschungsgemeinschaft is gratefully acknowledged.

References

1. P.G. de Gennes "The Physics of Liquid Crystals", Clarendon Oxford (1974)
2. I.C. Khoo, Y. R. Shen, Opt. Eng., Vol. 24, p. 579 (1985)
3. A.S. Zolot'ko et al., JETP Lett., Vol. 32, p. 155 (1980)
4. H.J. Eichler, R. Macdonald, C. Dettmann, Mol. Cryst. Liq. Cryst. Vol. 174, p. 153 (1989)
5. H. Hsiung, L. P. Shi, Y.R. Shen, Phys. Rev. A, Vol. 30, p. 1453 (1984)
6. H.J. Eichler, R. Macdonald, Proc. Int. Conf. Lasers 88, p. 511 (1989)
7. G. Eyrling, M.D. Fayer, J. Chem. Phys., Vol. 81, p. 4314 (1984)
8. H.J. Eichler, D. Günter, D.W. Pohl, "Laser-Induced Dynamic Gratings", Springer Berlin (1986)

H. Nakanishi, H. Matsuda, S. Okada, A. Masaki,
M. Ohsugi* and S. Takaragi*

Research Institute for Polymers and Textiles, 1-1-4 Higashi,
Tsukuba 305, Japan * Toda Kogyo Co., Funairi, Naka-ku,
Hiroshima 730, Japan

Polydiacetylenes (PDAs) are peculiar conjugated polymers which can be obtained as single crystals by the solid-state polymerization, and PDAs are known to have superior nonlinear optical properties in the nonresonant region. Their third order susceptibilities ($\chi^{(3)}$), say $\sim 10^{-9}$ esu of PTS polymer, however, are not large enough for semiconductor-laser device application. Here we present our synthetic approaches to the novel PDAs with enlarged $\chi^{(3)}$ briefly and describe newly tried thin-film fabrication method for them in more detail.

At the molecular level, PDAs with increased numbers of π -electrons per repeating units such as those having aromatic rings or acetylenic groups directly bound to the main chain must be better candidates for enlarged $\chi^{(3)}$. In a series of synthetic studies based on the crystal engineering to have aromatic-ring-substituted diacetylenes crystallized in a solid-state polymerizable stack, we have demonstrated five times enlarged $\chi^{(3)}$ for the polymer of bis-(4-n-butyltetrafluorophenyl)butadiyne (BTFP), and ca. ten times of enlargement for that of 1-(3-(methylamino)phenyl)-4-(3,5-bis(trifluoromethyl)phenyl)-1,3-butadiyne (MADF). In the next series of studies on PDAs with acetylenic substituents, we have found that PDAs from amphiphilic tri-ynes and dialkyltera-ynes give more elongated π -conjugation: The absorption maxima at the longest wavelength are around 660~670nm for tri-yne polymers and 700~710nm for tetra-yne polymers, whereas ~630nm for the corresponding di-yne polymers. Interestingly, structural analysis of the tetra-yne polymers reveals the possibility to attain novel π -conjugation structure.

Through the synthetic studies, more than hundred of new PDAs have been obtained. However, only a few of them gave thin-films with the optical quality sufficient for $\chi^{(3)}$ evaluation, either by a microtome cutting technique or via crystallization of monomers from molten state or vapor phase; in other words, most of the PDAs remains un-assessed. Thus, aiming at the better optical quality, fabrication of thin films composed of matrix polymers and PDA crystallites has been investigated. By spin-coating of monomer solutions including matrix polymers such as PMMA, poly-urethane and poly-carbonate, transparent thin films of about μm thick were prepared and when subjected to UV- or thermal polymerization, colored but transparent thin films of PDA crystallites were obtained. It should be noted that even at the volume ratio of PDA and matrix polymer as high as 9 : 1, sufficient optical quality was achieved, whereas pure monomer solutions gave only inhomogeneous and turbid films.

D. Grischkowsky

IBM Watson Research Center, P.O. Box 218, Yorktown Heights, NY 10598
Telephone (914)-945-2057

Recently a new THz-beam system has become available for spectroscopic studies in the range from 0.1-2 THz (1-6). This system is based on the optoelectronic generation and reception of a beam of sub-picosecond THz pulses. By inserting a sample in the beam and comparing the shape of the original sub-picosecond THz pulses with the shapes of pulses that have propagated through the sample, one is able to deduce the frequency-dependent absorption and dispersion.

The combination of the above time-domain spectroscopy (TDS) technique with teraHz beams has some powerful advantages compared to traditional c.w. spectroscopy. Firstly, the detection of the far-infrared radiation is extremely sensitive. Although the energy per THz pulse is very low (0.1 femtoJoule), the 100 MHz repetition rate and the coherent detection allow one to measure the electric field of the propagated pulse with a signal-to-noise ratio of about 10,000 for an integration time of 125 msec (5). In terms of average power this sensitivity exceeds that of liquid helium cooled bolometers (7), by more than 1000 times. Secondly, because of the gated and coherent detection, the thermal background, which plagues traditional measurements in this frequency range (7), is observationally absent.

In this paper some examples are presented of far-infrared time-domain spectroscopy of the dielectrics, crystalline sapphire and quartz, and fused silica and the semiconductors, silicon, gallium arsenide and germanium (4). These measurements fill an important gap in the available data. Previous measurements with Fourier transform spectroscopy extend down in frequency to about 0.6 THz, where the data is relatively imprecise (8). Our results, on the other hand, extend from 0.2 to 2 THz and thereby cover this previously neglected frequency range. For sapphire and quartz, the measured absorptions are consistent with the earlier work below 0.5 THz. Above 1 THz we measure significantly more absorption for sapphire, while for quartz our values are in reasonable agreement. Our results on high-purity fused silica are consistent with the most transparent fused silica measured to date. With respect to the semiconductors, for GaAs our measurements extend the precision of the previous work, and we have resolved two weak absorption features at 0.4 and 0.7 THz. Our measurements on germanium demonstrate the dominant role of intrinsic carriers; the measured absorption and dispersion are well fit by the simple Drude theory. In contrast, for silicon there is strong disagreement with the earlier work. In the THz frequency range the absorption is extremely sensitive to carrier density. From our measurements on highly-resistive (10 k Ω -cm), float-zone silicon, we conclude that many of the previous measurements in the THz frequency range were dominated by impurities. Our measurements for silicon give absorptions of approximately 1/10 that of some of the earlier measurements. As a consequence, we find that intrinsic silicon is an exceptional THz optical material, more transparent than crystalline quartz.

Another described example is the TDS measurement of the absorption and dispersion due to carriers in doped silicon (3). The samples were N- and P-type silicon, with resistivities of 0.1, 1 and 10 Ω -cm. From the transmission measurements performed at room temperature and at 80 K, the absorption and dispersion, and concomitantly the full complex conductivity, of the doped silicon could be obtained. The results provide an accurate view on the dynamics of the electrons and the holes. Although the simple Drude model, with an energy-independent relaxation time, gives a surprisingly accurate description of the observed carrier dynamics, the measurements do show that some refinements are needed.

The final TDS example is the characterization (6) of three dielectric substrates used with high Tc coplanar transmission lines, magnesium oxide (9), yttria-stabilized zirconia YSZ (10) and lanthanum aluminate (11). These materials were measured at both low temperature (85K) and room temperature. From our measurements, YSZ is seen to be unsuitable due to its unusually high absorption at THz frequencies. MgO is dielectrically a good material with a relatively low value of the static dielectric constant and at 85K sufficiently low loss to allow for the extended propagation of subpssec electromagnetic pulses. However, epitaxial high Tc films of the quality required for high-bandwidth, transmission lines have not yet been grown on MgO. The new substrate lanthanum aluminate allows good film growth for transmission lines, but has a relatively high value of the static dielectric constant, and significant loss at THz frequencies. Consequently, the optimal substrate for high Tc high-bandwidth transmission lines remains to be discovered.

References

1. Ch. Fattering and D. Grischkowsky, Appl. Phys. Lett. Vol.53, 1480 (1988); Vol. 54, 490 (1989).
2. Martin van Exter, Ch. Fattering and D. Grischkowsky, Optics Lett., Vol. 14, 1128 (1989).
3. Martin van Exter and D. Grischkowsky, to be published in Phys. Rev. B15.
4. D. Grischkowsky, S. Keiding, M. van Exter, and Ch. Fattering, to be published in JOSA-B.
5. Martin van Exter and D. Grischkowsky, to be published in IEEE Trans. Microwave Theory Tech.
6. D. Grischkowsky and S. Keiding, submitted to Appl. Phys. Lett.
7. C. Johnson, F. J. Low and A. W. Davidson, Optical Engr., Vol. 19, 255 (1980).
8. "American Institute of Physics Handbook", Third Edition, Edited by D. E. Gray, McGraw-Hill Book Company (New York), reissued and published 1982.
9. A.A. Valenzuela and P. Russer, Appl. Phys. Lett., Vol.55, 1029 (1989).
10. D.R. Dykaar, R. Sobolewski, J.M. Chwalek, J.F. Whitaker, T.Y. Hsiang, G.A. Mourou, D.K. Lathrop, S.E. Russek, and R.A. Buhrman, Appl. Phys. Lett. Vol.52, 1444 (1988).
11. M.C. Nuss and K.W. Goossen, IEEE J. Quantum Elect., Vol.QE-25, 2596 (1989).

SUBHARMONIC RESONANCES IN NONLINEAR SPECTROSCOPY

G.S. Agarwal
School of Physics,
University of Hyderabad - 500 134, India.

Most experiments in nonlinear spectroscopy are characterized in terms of the third order susceptibilities which exhibit a resonant character when the pump and probe frequencies ω_p, ω_s differ by the Raman frequency ω_R . Thus the scan of the four wave mixing signal as a function of ω_s yields the Raman resonance $\omega - \omega_s = \omega_R$ with a line width R . The situation could be different if the intensities of the pump and probe start becoming large. In such a case higher order nonlinearities $X^{(5)}, X^{(7)}$ etc. become important. Consideration of these can lead to the fractional Raman resonances $^{1,2} \omega_p - \omega_s = \omega_R/n$ with a width r_R/n , where n is an integer. I demonstrate almost universal existence² of such Raman resonances in nonlinear mixing experiments in any type of the medium. I consider several models which are typically used to describe vibrational Raman effect, electronic Raman effect. I give results for the nonlinearly generated signals which explicitly show the subharmonic Raman resonances.

For understanding subharmonic Raman resonances at still higher intensities I develop nonperturbative models for the calculation of the signals. A fully quantized treatment of such resonances will be given. The transient³ growth of the nonlinear signal in the region of subharmonic Raman resonances will also be discussed.

I further demonstrate that odd subharmonics like $\omega_{R/3}$ can be understood in terms of Stokes-antiStokes coupling. For this purpose I consider⁴ an effective two-level model and account for both Stokes and antiStokes processes. I obtain an effective Hamiltonian and show the odd subharmonics both from analytical and numerical considerations.

I also examine the question whether the spontaneous generation of radiation at subharmonics like $\omega, \pm \omega_{R/2}$ is possible. Finally I consider the collisional mixing of various Raman transitions. I develop⁵ the appropriate higher order nonlinear susceptibilities so that one can study how the subharmonic resonances are affected by the collisional mixing.

1. R. Trebino and L.A. Rahn, Opt. Lett. 12, 912 (1987); D. Debarre, M. Lefevre and M. Pealat, Opt. Commun. 69, 362 (1989).
2. G.S. Agarwal, Opt. Lett. 13 482 (1988).
3. N.C. Kothari and G.S. Agarwal, Phys. Rev. A, in press.
4. G.S. Agarwal, to be published.
5. N.C. Kothari and G.S. Agarwal, Opt. Commun. 74, 342 (1990).

Nonlinear Laser Spectroscopy of Solids and Applications to Computers

Alex Szabo
National Research Council
Ottawa, Ontario, Canada, K1A 0R6

Address: Bldg. M-50, Montreal Road
Phone: (613) 993-1122

Summary

Following a brief introduction to the physics of optical homogeneous linewidths in low-temperature solids, two recent experimental studies in our lab will be described. These experiments are aimed at spin flip rate measurements, since it appears that the main factors determining linewidths (dephasing times) are the spin flips of the host and/or dopant ions. In ruby these are the Al and Cr ions respectively. Using the Raman heterodyne technique we have observed Al nuclear dephasing in the frozen core and verified the concept proposed by Bloembergen some 40 years ago. An important realization is that such observations provide a new method for measurements of the Cr spin flip rate. The concentration dependence of this rate has been studied and found to agree with theory. In the second experiment, a pump-probe method has been used to study hole-burning in the frequency domain with ~ 1 kHz resolution. By varying the pump-probe delay, we have observed spectral diffusion which occurs in a time scale of ~ 100 usec for 0.0034 Wt % Cr_2O_3 ruby. This time is much shorter than the Cr-Cr spin flip time and suggests that Al-Al flips are responsible for the diffusion. Finally applications of hole-burning to optical processing and storage in the time and frequency domains will be discussed.

MONDAY, JULY 16
POSTER PRESENTATIONS

Spontaneous Trapping in a Three-Level Atom

D.A. Cardimona and M. P. Sharma

Air Force Center for Nonlinear Optics
Quantum Optics Branch

WL/AROM

Kirtland AFB, NM 87117-6008
(505)844-0475

For a 3-level atom in the "V-configuration" (two excited states $|1\rangle$ and $|2\rangle$ each dipole-coupled to a common ground state $|g\rangle$) interacting with a quantized field, we have found a set of initial atomic state amplitudes for which the usual time-dependent oscillations, collapses, and revivals vanish. Preparing the atom initially in this special way forces the atomic population to remain coherently trapped in this configuration. The dressed-state energy of this particular linear combination of bare-atom states is zero, so that $e^{iEt} = 1$ and the population remains constant in time - as long as the applied field remains on.

It turns out that this initial preparation step is not required. The linear combination of bare-atom states described above is actually a dressed-state that is decoupled from all field modes [see D. A. Cardimona, M. G. Raymer, and C. R. Stroud, Jr., J. Phys. B 15, 55 (1982)]. The dipole transition rates into this state are non-zero, while the rates out are zero. Therefore, no matter how the atom is initially prepared, spontaneous decay redistributes the atomic-state amplitudes into the desired configuration. Population decays out of all other configurations into the special one, and then remains coherently trapped there. The two figures demonstrate this phenomenon for an atom initially in the ground state. Figure 1 shows the normal collapse and revival dynamics for our 3-level atom when spontaneous emission is forbidden. In Figure 2, a spontaneous damping constant of $.3\omega_{21}$ is included in the calculation of the inversion. The dynamics begin with the usual collapses and revivals. Then as the atom reconfigures itself into the special dressed state, the time-dependent dynamics disappear.

The existence of this decoupled dressed state depends on the tuning of the dressing laser field, which in turn depends on the bare-atom excited state dipole moments and energy level separation. For a general three-level problem, there will be three energy eigenvalues possible. If we tune the applied field to a special frequency (ω_L) between the two excited states

such that $\Delta = \omega_L - \omega_{1g} = \omega_{21}d_1^2/(d_1^2 + d_2^2)$, where d_j is the dipole moment for the $|g\rangle$ to $|j\rangle$ transition, then one of these energies will be zero. It is the appearance of the zero eigenvalue that allows the coherent trapping and spontaneous reorientation of the population to occur. If we tune away from this special value, the population trapping and subsequent loss of time-dependent dynamics are less evident. If we tune within a power-broadened width of the special detuning, the collapse to time-independent dynamics prevails.

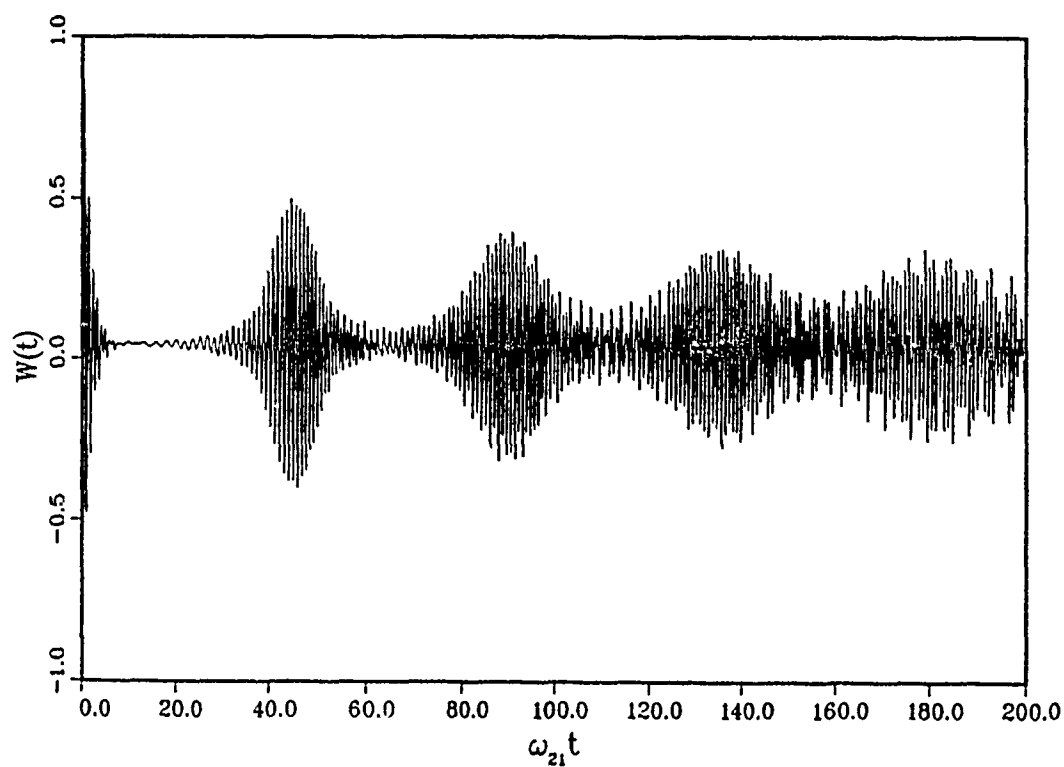


Figure 1: Inversion vs. time with the atom initially in the ground state and spontaneous emission not allowed.

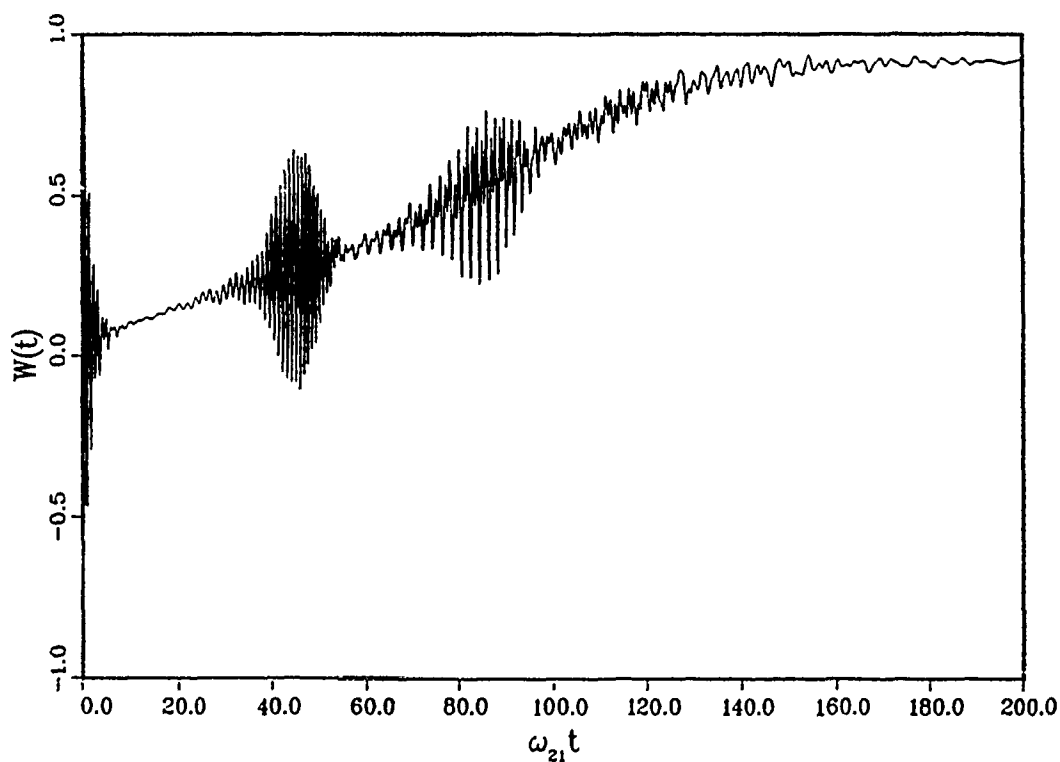


Figure 2: As in Fig. 1, but now we allow spontaneous reorientation of the population into the time-independent special dressed state.

Victor R. Blok, and Gennady M. Krochik

*Applied Science Research Laboratory, 106-3C Twin Willow Ct.,
Owings Mills, MD 21117-2729*

We present the first self-consistent theory of lasing without inversion in the system with split laser levels taking into account phase considerations in the framework of standard for laser theory, density matrix formalism. Although we applied this approach to the case of lasing in the system with a split upper laser level, it can also be applied to the case of split lower laser level or to more complicated multi-level systems, which may be promising for lasing without inverted population. We formulate general condition of lasing without inversion in the systems with split laser levels: the rate of coupling of split laser levels should to be much greater then the line-widths of split transitions as well as the frequency detuning of laser field from the resonances.

We consider the standard four-level laser system for the case when the upper laser level is split. The laser field interacts with quasi-degenerate transitions $1 \rightarrow 2$ and $1 \rightarrow 3$ simultaneously. For the coherent mixing of levels 2 and 3 we analyze two opportunities: (i) levels 2 and 3 are coupling by an electromagnetic low-frequency (microwave, millimeter-wave) field with a frequency $\omega_0 = \omega_{32}$ and (ii) they interact with each other through level 5.

Two different situation were considered. a) Laser gain may be provided due to the asymmetry in radiative characteristics of quasi-degenerate transitions and can be attributed to the interference of absorption ($\omega = \omega_{ij}$) and "hyper-Raman scattering" ($\omega + \omega_0 - \omega_0 = \omega_{ij}$), where ω_0 is the frequency of the field or effective process through auxiliary level 5, that coherently mixes the quasi-degenerate levels. This case is similar to the case of split autoionizing states first considered by *S. E. Harris*, however we show that there are not any requirements for strong asymmetry in radiative characteristics of quasi-degenerate transitions if the rate of coupling of quasi-degenerate levels is high enough. b) In the second situation the effect may be attributed to the interference of absorption ($\omega = \omega_{ij}$) and "Raman scattering" ($\omega - \omega_0 = \omega_{ij}$). The feasibility of lasing now depends on the sign or, in a more general case, on the phase of the complex dipole or multipole moment of transition between upper quasi-degenerative levels (phase-transfer mechanism). Since phase-transfer mechanism can provide amplification only for definite phase, it can be used for generation of short pulses (for example, pico- and femtosecond pulses).

Lasing without inversion may be realized in free atoms, molecules, or ions if they contain two levels that are quasi-degenerate with respect to magnetic quantum number or angular moment, and if they exchange very fast with third level that is random degenerate with these two ones. Another widely spread possibility is when these two levels are embedded in continuum and exchange energy with it. Such systems on hydrogen-like ions may serve as an example of a promising laser medium for vacuum ultraviolet and soft X-ray regions.

There is also an opportunity for constructing lasers without inversion on solid-state materials, which are in general more rich for the realization of different energetic level configurations. For example, when two narrow quasi-degenerate levels are embedded in quasi-free states (low-density state conduction band), the rate of coherent exchange between these levels with continuum may be very high, that provides the sufficient rate of mixing of quasi-degenerate levels.

Y. Shevy

California Institute of Technology 128-95.

Pasadena, CA-91125.

The process of laser cooling in a quasi resonant standing laser wave is one of the principal techniques of laser cooling of free atoms. It will be shown that the nonlinear interaction between the counter propagating waves in a standing wave have a profound affect on the mechanical manifestations of the light on the atoms. This can be understood simply by noting that in the Two Wave Mixing (TWM) process, a momentum kick of $2\hbar k$ is transferred to the atom, as a photon is absorbed from one wave and emitted into the counter propagating wave.

This process is in fact responsible for the so called "Dipole force" Or "Stimulated Molasses" and has been verified experimentally¹. However, since the TWM process requires high laser intensity under normal conditions it does not usually lead to lower equilibrium temperatures. Nevertheless, It has been shown that the TWM process can be modified when the normal decay rates of the atom are altered. This modification can give rise to the appearance of the TWM at lower intensity and can even change its lineshape. This in turn have an important implications on the laser cooling process in a standing wave. Among the important effects: (i) The appearance of the stimulated force at lower intensity when the dipole decay rate is increased by dephasing events. (ii) The appearance of a narrow resonance characterized by the ground state decay in an open system.² (iii) The modification of the stimulated force when the quantum fluctuations of the vacuum field are modified by quadrature squeezing³.

Processes (ii) and (iii) can change the sign of the stimulated force from a heating force to a cooling force at the red side of the atomic resonance and give additional cooling force much larger than the radiation pressure force.

References:

- 1) A. Aspect *et-al*, Phys. Rev. Lett, 57, 1688 (1986).
- 2) Y. Shevy, Phys. Rev. A, in review.
- 3) Y. Shevy, Phys. Rev. Lett., in review.

Novel Fluorescent Spectra From an Atom Strongly Coupled to a Driven Cavity

Craig. M. Savage,

Department of Physics and Theoretical Physics, Australian National University, Canberra,
ACT 2601, Australia.

Recently there has been both theoretical [1-3] and experimental [4] interest in atoms strongly coupled to single mode optical cavities. Strong coupling means that the energy level splitting due to a single quantum of excitation is comparable to the dissipative linewidth of the system. Single quantum frequency splitting has been observed for as few as 20 atoms strongly coupled to a cavity [4].

We are concerned with the resonance fluorescence spectrum of a single two-level atom strongly coupled to a driven cavity. When driven by coherent light the sidebands of the usual Mollow triplet have been predicted to be broadened by the strong coupling [5]. In certain limits the sideband width is then proportional to the width of the dressed state population distribution. For strong driving fields this population distribution is approximately the same as the empty cavity photon number distribution, whose width depends on the photon statistics of the driving field. An antibunched, or in-phase squeezed, driving field has a photon number distribution narrower than that of a coherent state and hence the fluorescent sidebands are expected to be narrower. Similarly a driving field which is bunched, or quadrature squeezed, has a broader photon number distribution and should have broader sidebands. Unlike previously reported effects the entire electromagnetic vacuum seen by the atom does not have to be squeezed for optimum effect [6,7]. A single squeezed mode driving the cavity is sufficient.

The figure shows the incoherent fluorescent spectra calculated for a 90% squeezed driving field and with the dissipation much smaller than the atom-cavity coupling ($\gamma/g=\kappa/g=0.2$). The coherently scattered Rayleigh peak at the resonance frequency ω_0 has been suppressed. The three spectra correspond to no squeezing, in-phase squeezing, and quadrature squeezing. The width of the sideband for quadrature squeezing is four times that for in-phase squeezing. These spectra can be understood in terms of the energy level structure of the coupled atom-cavity system.

Although single atom and high resolution spectroscopy experiments are difficult there appears to be no fundamental obstacle to realizing the described effect.

References

- [1] Rice P R and Carmichael H J 1988 *IEEE J. Quantum Electron.* **24** 1351
- [2] Savage C M and Carmichael H J 1988 *IEEE J. Quantum Electron.* **24** 1495
- [3] Savage C M 1988 *Phys. Rev. Lett.* **60** 1829
- [4] Raizen M G, Thompson R J, Brecha R J, Kimble H J and Carmichael H J 1989 *Phys. Rev. Lett.* **63** 240
- [5] Savage C M 1989 *Phys. Rev. Lett.* **63** 1376
- [6] Gardiner C W 1986 *Phys. Rev. Lett.* **56** 1917
- [7] Carmichael H J, Lane A S and Walls D F 1987 *Phys. Rev. Lett.* **58** 2539;
J. Mod. Optics **34** 821.

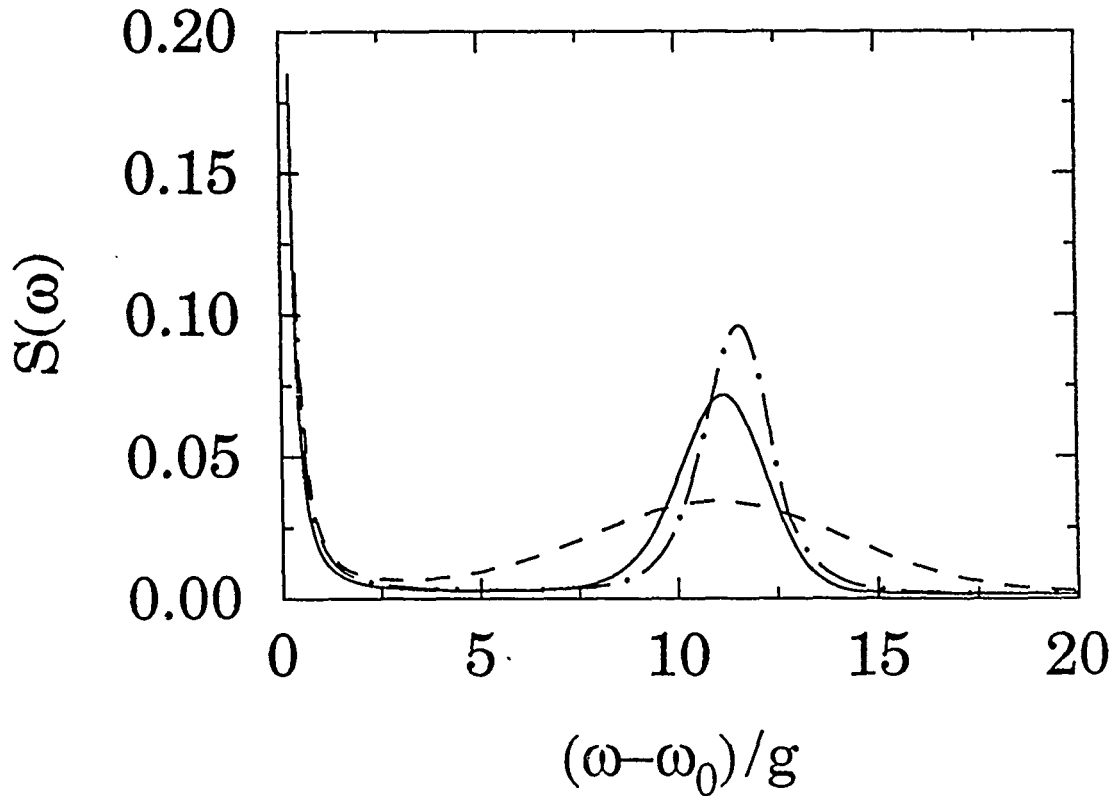


Figure 1. (a) Incoherent spontaneous emission spectra $S(\omega)$ versus frequency ω , in units of the dipole coupling strength, g . The solid line is for a coherent state driving field; the dash-dot line is for in phase squeezing; and the dashed line for quadrature squeezing. The spectra are symmetric about $\omega=\omega_0$ and have been normalized so that the maximum of $S(\omega)$ is one for each spectrum. For clarity of the sidebands the resonant peak has been truncated in height.

MP5 Second Harmonic Generation due to Photon-Photon Scattering in Magnetized Vacuum

Y. J. Ding and A. E. Kaplan

Department of Electrical and Computer Engineering,
The Johns Hopkins University, Baltimore, MD 21218

Photon-photon scattering in a vacuum [1] is perhaps one of the most fundamental mechanisms giving rise to nonlinear optical effects. Although the significance of experimental observation of the phenomena for fundamental physics as a nonlinear optical test of QED is obvious, no experimental observation of this phenomenon has been done. This is basically due to the fact that too large intensities of optical field are required for the effects proposed so far, such as the birefringence of the refractive index for a probe field in a dc magnetic (or electric) field [2] or intense laser field [3], and multi-wave mixing processes [4]. Recently, we have demonstrated the feasibility of new nonlinear magneto-optical effects in a vacuum that gives rise to optical second harmonic generation (SHG) of the fundamental wave under the action of both strong dc magnetic field and high intensity optical laser radiation using available high-power laser systems [5]. Since only a second-order effect for the optical field is involved, the laser power required to observe SHG is much lower than in previously proposed effects [2-4]. The SHG can also be measured at a frequency different from the fundamental frequency injected into the system, which may result in higher sensitivity.

Here we review practical aspects of possible experiment on the SHG in vacuum. In contrast to conventional nonlinear optics, a single monochromatic plane wave acting upon vacuum nonlinearity does not exhibit any nonlinear effects. This "degeneracy" of the nonlinearity is broken if a strong dc magnetic field (\vec{H}_0) is present, which gives rise to second-order nonlinear optical effects. Because of the spatial anisotropy imposed by \vec{H}_0 , SHG depends upon the propagation direction and the polarization of the fundamental optical wave with respect to \vec{H}_0 . If the fundamental wave propagates along the direction of \vec{H}_0 , the nonlinear effects are suppressed. The strongest interaction occurs when the laser radiation propagates in a direction normal to \vec{H}_0 and is linearly polarized. The SHG wave at frequency $\omega_2 = 2\omega_1$ after passing through the interaction length L is also linearly polarized and its amplitude is [5]:

$$E_2 = (2\pi/\lambda_1) L \xi H_0 E_1^2 (33\cos^2\theta_1 + 16)^{1/2}, \quad (1)$$

where $\xi = \alpha/45\pi H_{cr}^2 = 2.6 \times 10^{-32} \text{ Gauss}^{-2}$ is a nonlinear interaction constant in the vacuum with $\alpha = e^2/\hbar c = 1/137$ the fine structure constant and $H_{cr} \equiv m_0^2 c^3 / e\hbar = 4.4 \times 10^{13} \text{ Gauss}$ the QED critical field, λ_1 is the wavelength of the fundamental wave, and θ_1 is the angle between \vec{H}_0 and direction of polarization of the fundamental wave \vec{E}_1 . The ratio of maximum intensity of the second harmonic (which occurs at $\theta_1 = 0$) to minimum intensity (at $\theta_1 = \pi/2$) is $(7/4)^2 \simeq 3$, which can be directly measured in an experiment. The SH can never be polarized along the direction of the dc magnetic field, i.e. there is a prohibited sector for the SH polarization. These polarization properties can be used in a future experiment to rule out all nonvacuum nonlinear mechanisms.

The state-of-the-art photon counting systems provide a dark photon count rate $r_{\text{dark}} \sim 10$ photons/s and a typical quantum efficiency $\eta \sim 0.25$. For the ideal instrumental arrangement [5], stipulating that signal-to-noise ratio (SNR) is sufficiently high, e.g., $\geq 10^2$, considering the minimal SH photon output ($\theta_1 = \pi/2$), using pulsed magnetic field $H_0 \sim 8 \times 10^6 \text{ Gauss}$, $L \sim 2.8 \text{ cm}$, and the laser focal area $A \sim \lambda_1 L/2$, one can obtain the least laser intensity of $I_1 \simeq 10^{14} \text{ W/cm}^2$, which can readily be achieved even by using commercial laser systems. In fact, in the most powerful laser systems available, the intensity reaches $10^{15} - 10^{18} \text{ W/cm}^2$. In these systems, the averaged number of detected photons per pulse nears unity, i.e.

$\langle n_{\text{det}} \rangle = \eta \langle n_{\text{SHG}} \rangle \lesssim 1$ (where n_{SHG} is the number of SHG photons generated per pulse). One can use also averaging of photon counts over a few laser beam lines for a single pulse or/and over many pulses of laser. A high power pulsed Nd:Glass laser with either $\lambda_1 \sim 0.35 \mu\text{m}$ (NOVA) or $\lambda_1 \sim 0.53 \mu\text{m}$ (GEKKO XII), $\tau_p \sim 10^{-9}$ sec, can provide the laser energy of 6-10 KJ/pulse in each of 10-12 beam lines. If all the beam lines are used, the probability of not observing any SHG photons within N laser pulses is $p = \exp(-N \langle n_{\text{det}} \rangle)$, which can be as low as $\sim 10^{-6} - 10^{-4}$. Using picosecond Excimer and Nd:Glass lasers with high repetition rates (1-10 Hz) and stipulating that the probability p is $\leq 10^{-2}$, the required number of pulses to observe the effect is $N \sim 10^6 - 10^7$. Our estimates show that the SHG from the plasma of the ionized residual gas becomes negligible compared with vacuum contribution when the vacuum pressure is $\lesssim 10^{-5}$ torr.

This research is supported by AFOSR.

- [1] H. Euler, *Ann. D. Phys.* 26, 398 (1936); W. Heisenberg and H. Euler, *Zs. f. Phys.* 98, 714 (1936).
- [2] Z. Bialynicka-Birula and I. Bialynicki-Birula, *Phys. Rev. D* 2, 2341 (1970); S. L. Adler, J. N. Bahcall, C. G. Callan, and M. N. Rosenbluth, *Phys. Rev. Lett.* 25, 1061 (1970).
- [3] E. B. Aleksandrov, A. A. Ansol'm, and A. N. Moskalev, *Sov. Phys. JETP* 62, 680 (1985).
- [4] R. L. Dewar, *Phys. Rev. A* 10, 2107 (1974).
- [5] Y. J. Ding and A. E. Kaplan, *Phys. Rev. Lett.* 63, 2725 (1989).

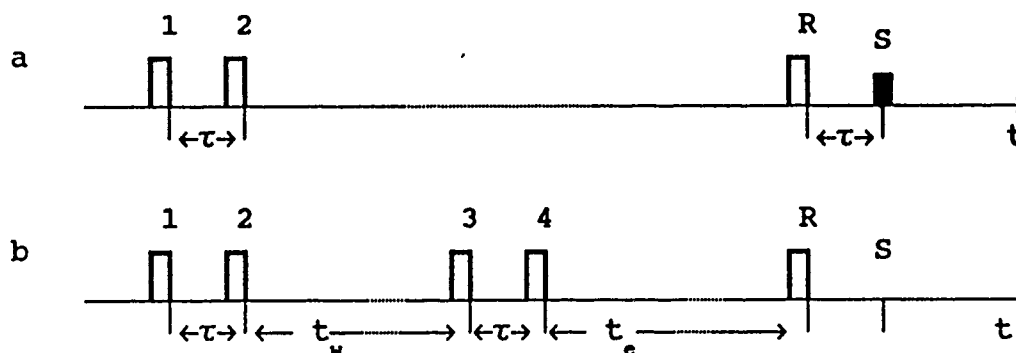
MP6 Signal Suppression in the Phenomenon of Long-Lived Photon Echo

N.N.Akhmediev

Institute of Physical Problems, Moscow 103460, USSR

The phenomenon of long-lived photon echo (LPE) has attracted much recent attention [1-6]. This interest stems from the possible application of this phenomenon in high-capacity optical memory devices (OMD) [7-8]. At present many fundamental problems crucial to the construction of an operating device are solved. The possibility of multiple information read out without refresh is shown theoretically [9] and experimentally [5,10]. Resonant media with storage times of the order of tens of hours and more have been investigated [4,5]. Nevertheless, up to now it has not been clear whether it is possible to selectively erase information in an arbitrary memory cell of OMD. It was pointed out for the first time in Ref. [11] that it is in principle possible to erase information with random access using LPE signal suppression. We investigate the effect of LPE signal suppression in this work in more detail, and propose a simple technique for random access information erasing.

It is known, that after the illumination of the resonant medium by two pulses 1 and 2 with the time interval τ between them (see fig.a) the population of the ground state is frequency and spatially modulated. This grating is stored during a time periods less than the relaxation times of some long-lived levels or sublevels [3] and leads to generation of an echo-signal [3] after illumination of the medium by a third (read out) pulse (designated by R).



The method of echo-signal suppression we proposed is to write new information with a phase of frequency modulated population opposite to that of the existing information, hence superimposing two frequency population modulation which have opposite phase such that the full modulation disappears. Suppose that the radiation of a new pair of pulses 3 and 4 identical to the first one (see fig.b) but with a phase difference $\Delta\phi$ of carriers differed from the phase difference of carriers of writing pulses by π impinges on same spatial memory cell. It can

be shown that the influence of this pair and the optical relaxation after the pulses is equivalent to the "painting over" the information written previously. Thus, by irradiating the given memory cell by a pair of pulses identical to the writing pair but with a phase difference of π we can suppress the LPE signal totally.

It is occurred that for large relaxation times between sublevels of the ground state it is possible to write and erase information in a particular memory cell limited number of times. The number of cycles depend on the relation between relaxation times and on the areas of the writing and erasing pulses. By choosing the most suitable resonance molecules and optimizing the pulse parameters we can obtain the number of write-erase cycles up to 10^5 or more. Hence, the described erasing process can be used quite well in OMD.

REFERENCES

1. Chen Y.C., Chiang K., Hartmann S.R. Opt.Common. 29, 181, (1979).
2. Morsink J.B.W., Wiersma D.A., Chem.Phys.Lett., 65, 105, (1979)
3. Morsink J.B.W., Hesselink W.H., Wiersma D.A., Chem.Phys., 71, 289, (1982).
4. Kim M.K., Kachru R., J.Opt., Soc.Am., 4, 305, (1987); Opt. Lett., 12, 593, (1987); Opt.Lett., 14, 423, (1989).
5. Babbitt W.R., Mossberg T.W., Opt.commun., 65, 185, (1988).
6. Akhmediev N.N., Mel'nikov I.V. Zhurn.Tech.Fiz., 58, 942, (1988). [Sov.Phys.Tech., 33, No 5, (1988)].
7. Friedlander M.A., Meth S.Z. US Patent No 4.479.199, (1984).
8. Akhmediev N.N., Borisov B.S., Kokin A.A., Samartsev V.V. Elektronnaia Promyshlennost (USSR), No 9(137), 56 (1984).
9. Akhmediev N.N., Borisov B.S. Pis'ma Zhurn.Tech.Fiz., 11, 533, (1985). [Sov.Tech.Phys.Lett., 11, 222, (1985)].
10. Akhmediev N.N., Borisov B.S., Zuikov V.A., Samartsev V.V., Stel'makh M.F., Usmanov R.G., Fomichev A.A., Yakshin M.A.- Pis'ma Zh. Exp.Teor.Fiz., 48, 585, (1988). [JETP Lett., 48, 634, (1988)].
11. Akhmediev N.N., Mel'nikov I.V., Kvantovaja Elektronika, 15, 2522, (1988). [Sov.J.Quant.Electr., 18, (1988)].

MP7 The Origin of Third Order Nonlinear Optical Effects in Polysilanes

C. Walsh, D.M. Burland and R.D. Miller
IBM Almaden Research Center
650 Harry Road
San Jose, CA 95120

The polysilanes constitute a class of polymers whose backbone consists entirely of Si atoms. One of the unexpected features of these polymers is that the excitation is delocalized along the polymer backbone, much as it is in polyenes and polydiacetylenes. Because of the nature of the molecular orbitals involved in this delocalization, the resulting electronic transition is shifted into the near ultraviolet. In this respect the polysilanes represent an interesting class of compounds that should give rise to a substantial third order susceptibility and yet have little or no absorption throughout the visible.

Third order susceptibilities have been measured [1] and are on the order of 10^{-11} esu. In this paper we discuss the origins of the third order susceptibility in the lowest excited singlet state of the polysilanes. In particular we have examined singlet-singlet, singlet-triplet absorption, fluorescence and phosphorescence spectra of poly(di-n-hexylsilane). The spectra are consistent with an assignment of the lowest excited singlet state to an exciton like state of a linear chain. Figure 1 shows a calculated absorption spectrum assuming a linear chain of Si backbone atoms of an average length of 15 atoms. Figure 2 is the experimentally observed absorption spectrum at 1.5K in a 3-methylpentane glass matrix. The energy axis for the calculate spectrum is normalized to the half-width of the exciton band. By comparison of simulated and experimental absorption spectra, one can conclude that the experimental results agree with what would be expected from absorption to an excitonic state.

Photochemical hole-burning experiments have also been performed in this system. The changes in the absorption spectra induced by photochemistry are also consistent with an excitonic lowest singlet state. The photochemistry has been modelled by assuming that it results in random chain scissions. Thus as photochemistry progresses, the average chain length begins to decrease. This results in a general shift of the spectrum to the blue. We also observe photochemical induced structure in the absorption spectrum. This structure is consistent with the excitonic nature of the lowest singlet state, arising from structure in the expected absorption of excitons restricted to short chains (less than 10 atoms).

A pronounced decrease in the third order susceptibility is observed upon heating the sample above 42C [1]. At this temperature the hexyl-side chains go from an ordered low temperature phase to a disordered state. This results in a significant shift of the absorption maximum to the blue as the backbone conjugation length decreases due to the disorder. The change in susceptibility is consistent with the breaking up of the exciton chain at higher temperatures.

1. F. Kazjar, J. Messier and C. Rosilio, *J. Appl. Phys.* **60**, 3040 (1986); J.C. Baumert, G.C. Bjorklund, D.H. Jundt, H. Looser, R.D. Miller, J. Rabolt, R. Sooriyakumaran, J.D. Swalen and R.J. Twieg, *Appl. Phys. Lett.* **53**, 1147 (1988).

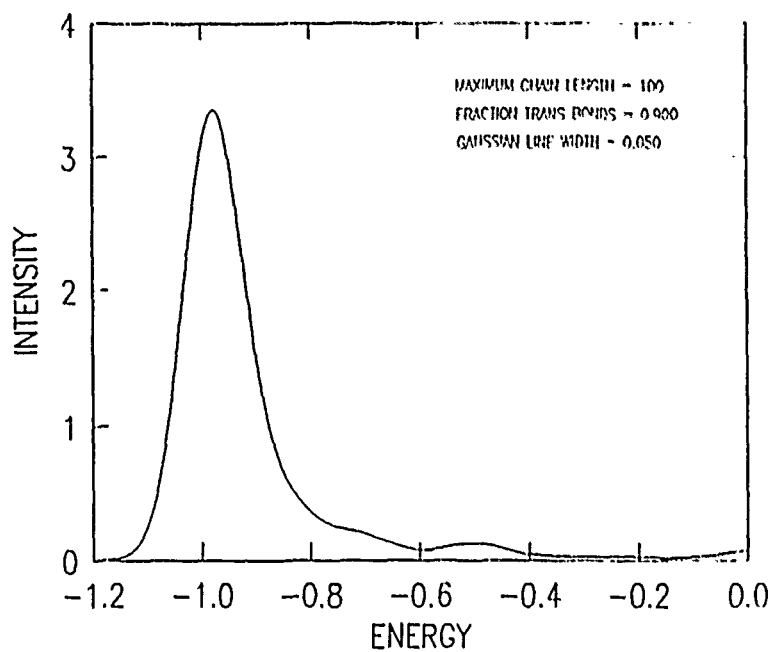


Figure 1. Simulated absorption spectrum assuming lowest excited state is a one-dimensional exciton. The energy is normalized to the exciton bandwidth 2.

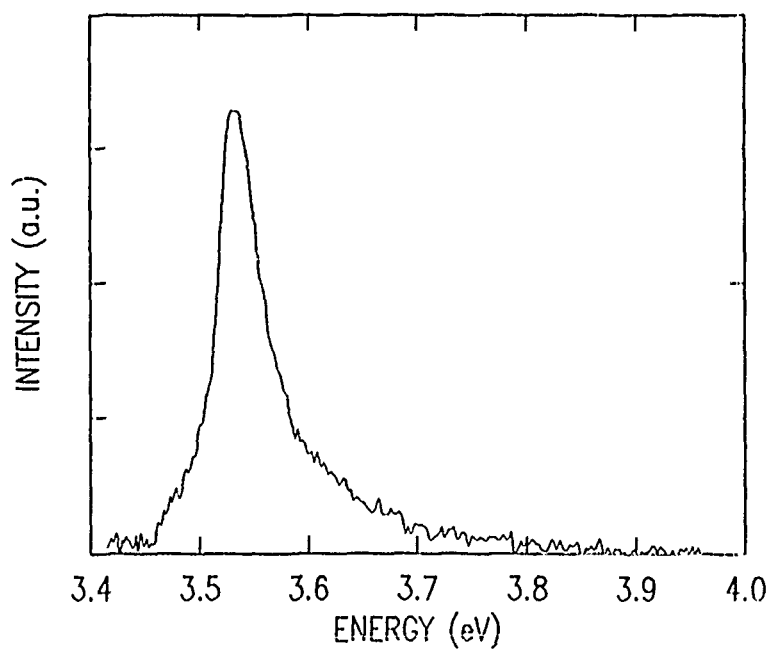


Figure 2. Fluorescence excitation spectrum of polysilane in 3-methylpentane at 1.5K.

MP8 Search for CHAMPS by Two-Photon Spectroscopy in Hydrogen

G. Grynberg*, P. Verkerk*, P. Fayet**, M. Spiro⁺, S. Zylberajch⁺

* Laboratoire de Spectroscopie Hertzienne de l'Ecole Normale Supérieure - Université Pierre et Marie Curie, Tour 12 - E01, 75252 Paris Cedex 05, France

** Laboratoire de Physique Théorique, Ecole Normale Supérieure, 75231 Paris Cedex 05, France.

⁺ D Ph PE, CEN Saclay, 91191 Gif sur Yvette Cedex, France.

In a recent paper, A. de Rujula, S.L. Glashow and Uri Sarid [1] have shown that dark matter halos could be made of charged particles C^+ and C^- (CHAMPS) provided that the mass of these particles is sufficiently high (> 20 TeV) to avoid the primordial collapse during galaxy formation, and not too high (< 1000 TeV) to get enough primordial annihilation in order not to overclose the universe. Most of the positively charged particles should appear in form of superheavy hydrogen (C^+e^-).

If they exist, these particles should be found on earth because earth is submitted to a flux of dark matter particles. If we assume that the positive CHAMPS captured during the last 10^7 years are found in oceans, an abundance of the order of 10^{-14} is predicted. It should be noticed that in spite of their mass, it is not expected that these particles should sediment at the bottom of the ocean. Indeed their fall speed limit ($5 \cdot 10^{-7}$ cm sec⁻¹ for $M = 1000$ TeV) is substantially smaller than the typical vertical currents which are of the order of 10^{-5} sec⁻¹. Thus these particles should remain in the sea water.

In order to set a limit on the abundance of these particles, we have done a laser spectroscopy experiment in hydrogen. The detail of the experimental apparatus has been described previously [2]. We use a powerful narrow band light source around 205 nm to induce a Doppler-free two-photon transition between the levels $n=1$ and $n=3$ of the hydrogen atom. The excitation is detected by monitoring the fluorescence on the Balmer α transition at 656 nm. Because of the large mass of the superheavy hydrogen, its excitation energy differs from that of deuterium by 26 cm⁻¹ (isotopic mass shift). We have scanned the range of frequency corresponding to hydrogen, deuterium and superheavy hydrogen. From the noise level recorded near the excitation energy of the superheavy hydrogen, we deduce

that the abundance of C^+ relative to deuterium is $N_{C^+}/N_D < 5.10^{-7}$. Since deuterium is less abundant than hydrogen by a factor 6.10^3 we deduce that $N_{C^+}/N_H < 10^{-10}$. This result has been obtained in several samples of hydrogen. In particular, one experiment has been done with hydrogen originating from the reduction of a sea water sample where the number of heavy particles has been initially enriched by a factor 2.10^4 by centrifugation. We can thus conclude that the relative abundance of C^+ compared to protons is less than 5.10^{-15} .

This result seems to exclude the scenario of De Rujula, Glashow and Sarid. However, one should be very cautious with the interpretation of this experiment. In particular, there is certainly a relatively large uncertainty about how long a C^+ stays in the ocean before disappearing and it will be probably necessary to improve the present experimental precision by a factor of the order of 20 to have an unambiguous answer to the model of Glashow et al. More generally, this type of experiment shows how laser spectroscopy can be useful in other areas of physics.

[1] A. de Rujula, S.L. Glashow and Uri Sarid. Preprint HUTP 89/A001 and CERN-TH-5214/89.

[2] P. Verkerk, M. Pinard, F. Biraben and G. Grynberg, Opt. Commun. 72, 202 (1989).

MP9 Fourier Theory, Number-Ket Causality, and Rational Phase States

Jeffrey H. Shapiro, Scott R. Shepard, and Ngai C. Wong
Massachusetts Institute of Technology
Research Laboratory of Electronics
Room 38-409
Cambridge, MA 02139
Phone: (617) 253-4607

The problem of phase in quantum mechanics is an old one, but one that has received increasing attention of late. For a single-mode radiation field with annihilation operator \hat{a} there have been two recent formulations for its quantum phase. Pegg and Barnett [1] have created an Hermitian phase operator $\hat{\phi}_S$ by truncating the state space associated with \hat{a} to the subspace spanned by the number kets $\{|n\rangle : 0 \leq n \leq S\}$. Phase-measurement statistics are then calculated on this subspace via the usual procedure for observables, and then the limit $S \rightarrow \infty$ is taken. Shapiro, Shepard, and Wong [2] have introduced phase-measurement statistics through the route of quantum estimation theory. They have shown that the maximum-likelihood phase estimator employs the probability operator measure (POM) generated by the phase eigenkets of the Susskind-Glogower (SG) phase operator, $(\hat{a}\hat{a}^\dagger)^{-1/2}\hat{a}$. The POM description—akin to a similar well-known development for optical heterodyne detection [3]—corresponds to ideal measurement of a pair of noncommuting observables on the state space of \hat{a} , or, equivalently, ordinary measurement of a pair of commuting observables on an enlarged, signal \times apparatus, state space. Both theories yield proper phase-measurement statistics and identical number-phase uncertainty principles [1,4]. Indeed, it is a simple Fourier theory calculation [5] to demonstrate that these two formalisms are alternative paths to *identical* phase-measurement statistics for arbitrary quantum states. In this paper we extend the Fourier theory development by establishing an analogy between the non-negative index set of the number kets and that of causal discrete-time waveforms.

The SG POM is founded on the number-representation, phase-representation Fourier transform relation for a ket $|\psi\rangle$,

$$\psi_n \equiv \langle n|\psi\rangle \xleftrightarrow{\mathcal{F}} \Psi(e^{i\phi}) \equiv \langle e^{i\phi}|\psi\rangle, \quad (1)$$

wherein the number-measurement probability mass function is

$$\Pr(n | |\psi\rangle) = |\psi_n|^2, \quad \text{for } n = 0, 1, 2, \dots, \quad (2)$$

and the phase-measurement probability density function (pdf) is

$$p(\phi | |\psi\rangle) = \frac{1}{2\pi} |\Psi(e^{i\phi})|^2, \quad \text{for } -\pi < \phi \leq \pi. \quad (3)$$

Because $\psi_n \equiv 0$ for $n < 0$ —a condition we call number-ket causality—the Paley-Wiener theorem implies that a phase-measurement pdf is achievable *if and only if* it obeys

$$\int_{-\pi}^{\pi} d\phi |\ln[p(\phi | |\psi\rangle)]| < \infty. \quad (4)$$

Hilbert transform theory then shows that there is a minimum average-energy state for realizing each achievable phase pdf. These concepts will be illustrated for the case of rational phase states, viz. states whose number representations have rational z -transforms,

$$\Psi(z) \equiv \sum_{n=0}^{\infty} \psi_n z^{-n} = \frac{\mathcal{N}(z)}{\mathcal{D}(z)}, \quad \text{for } z \in \mathcal{Z} \subset \mathcal{C}, \quad (5)$$

where \mathcal{N} and \mathcal{D} are polynomials, \mathcal{Z} is a region of convergence that includes $\{z : |z| \geq 1\}$, and \mathcal{C} is the set of complex numbers. The coherent phase states and the squeezed phase states [6] are the simplest examples of rational phase states, the former having a single-pole z -transform and the latter a two-pole z -transform.

References

- [1] D.T. Pegg and S.M. Barnett, Phys. Rev. A **39**, 1665 (1989).
- [2] J.H. Shapiro, S.R. Shepard, and N.C. Wong, Phys. Rev. Lett. **62**, 2377 (1989).
- [3] H.P. Yuen and J.H. Shapiro, IEEE Trans. Inform. Theory **IT-26**, 78 (1980).
- [4] J.H. Shapiro, S.R. Shepard, and N.C. Wong, "A New Number-Phase Uncertainty Principle," in *Coherence and Quantum Optics VI*, L. Mandel, E. Wolf, and J.H. Eberly, eds. (Plenum, New York, 1989).
- [5] J.H. Shapiro, S.R. Shepard, and N.C. Wong, "Fourier Theory, Uncertainty Relations, and Quantum Phase," to be presented at IQEC'90.
- [6] J.H. Shapiro, S.R. Shepard, and N.C. Wong, "Coherent Phase States and Squeezed Phase States," in *Coherence and Quantum Optics VI*, L. Mandel, E. Wolf, and J.H. Eberly, eds. (Plenum, New York, 1989).

Spatial and Temporal Contributions to Non-Observation of Laser Induced Continuum Structure in Sodium

K.G.H. Baldwin, P. B. Chapple and H.-A. Bachor

Laser Physics Centre, Australian National University,

GPO Box 4, Canberra, A.C.T., AUSTRALIA

and

J. Zhang and P. Lambropoulos

University of Southern California, Los Angeles, CA., U.S.A.

Structure in the continuum of an atomic system attributed to the coupling of a bound state by a strong laser field has been reported elsewhere (1-3). Such experiments have employed a second laser to probe the continuum from the ground state by measuring polarization rotation (1), third harmonic generation (2) or three photon ionization (3). We report here an experiment similar to reference 2 using two photon resonant, third harmonic generation in sodium, perturbed by a second laser which couples the 5s state to the continuum. Under no conditions was any laser induced continuum structure (LICS) observed in these experiments, in contrast to the results reported elsewhere (2).

The present experiment was carried out over a range of laser intensities ($10^7 - 10^{11}$ W/cm²) to ensure complete coverage of the intensities used in reference 2 ($\sim 2 \times 10^9$ W/cm²). The significant differences between the earlier and the present experiment are:

- (i) the higher ($\times 5 - \times 25$) sodium density used previously
- (ii) the probe laser detuning from two photon resonance (3nm vs. 0 - 1.5 nm)
- (iii) the shorter (2ns vs. 25 ns) pulse duration used previously
- (iv) the focal geometries of the laser in the sodium cell.

However, in a similar experiment (4) here, radiation in the same ultraviolet wavelength region (~ 190 nm) was generated in a four wave mixing process using the same sodium cell, and the same two lasers. This result indicates that substantial spatial overlap of the two lasers was achieved in both the present experiments. The four wave mixing experiment demonstrated quantum mechanical interference as the result of competition between two separate four wave mixing pathways distinguished by different intermediate two-photon resonances.

To determine the cause of the non-observation of LICS, a theoretical calculation was carried out based on the solution of the time-dependent density matrix equations of the four level atomic system (with accurately determined atomic parameters) in interaction with gaussian-like laser pulses. It was found that at the two photon resonance, with high peak laser intensities, there was saturation of ionization in the focal region. As a result, the relative intensities (figure 1), spatial distribution and pulse duration of the two laser beams seriously affected the enhancement of the third harmonic generation and the observability of LICS.

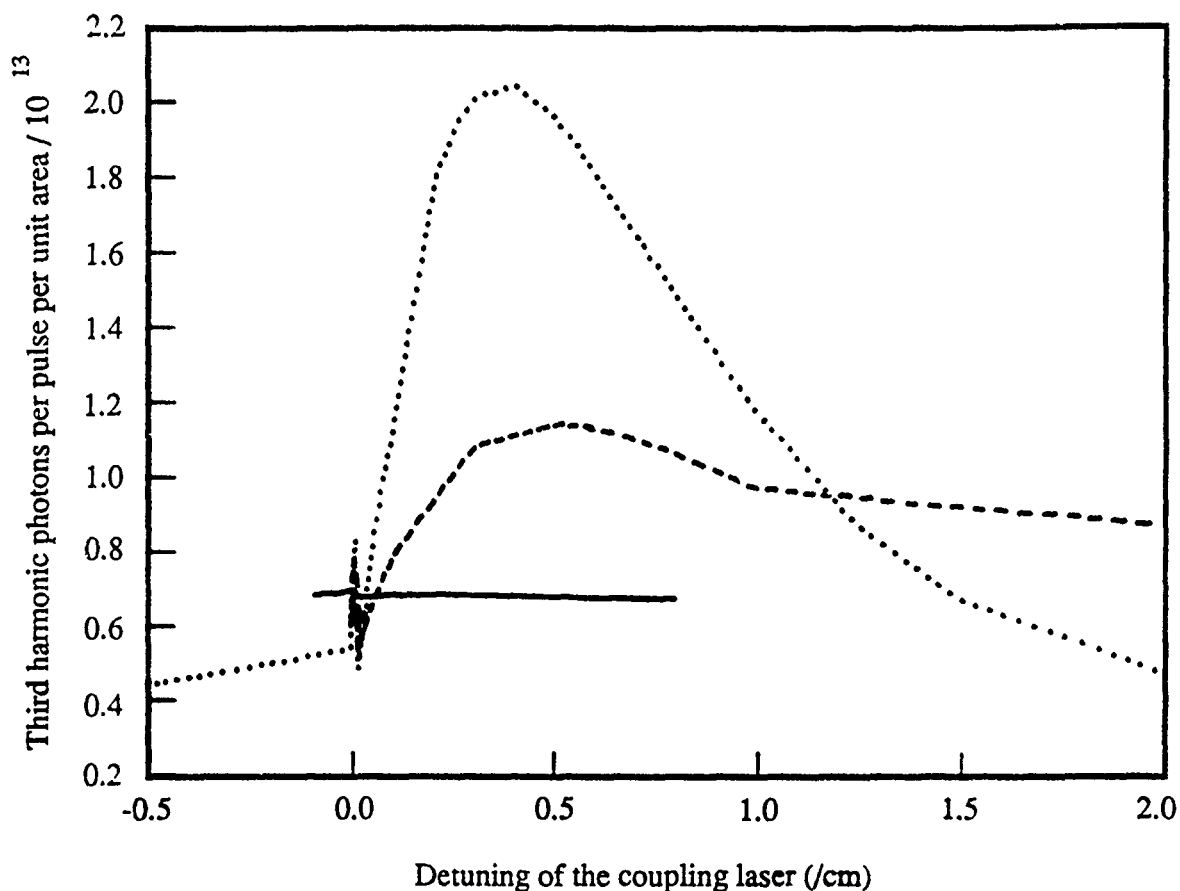


Figure 1: Enhancement of the third harmonic signal as a function of detuning of the coupling laser from the two photon resonant, three photon energy in the continuum, using various coupling laser intensities (i) solid line - 10^9 W/cm² (ii) dashed line - 10^{10} W/cm² (iii) dotted line 2.2×10^{10} W/cm². Pulse duration 25 ns, probe laser 2.2×10^{10} W/cm².

REFERENCES

1. Yu I. Heller, V.F. Lukinykh, A.K. Popov, and V.V. Slabko, Phys. Lett. 82A, 4 (1981).
2. S.S. Dimov, L.I. Pavlov, K.V Stamenov, Yu I. Heller and A.K. Popov, Appl. Phys. B30, 35 (1983).
3. M.H.R. Hutchinson and K.M.M. Ness, Phys. Rev. Lett. 60 (2), 105 (1988).
4. P.B. Chapple, K.G.H. Baldwin and H.-A. Bachor, J.O.S.A. B 6, 180 (1989).

MP12 Nonlinear Spectroscopy in Substituted Polysilanes

F.M. Schellenberg, R.L. Byer
E.L. Ginzton Lab Stanford University Stanford, CA 94305

R.D. Miller
IBM Almaden Research Lab 650 Harry Rd. San Jose, CA 95120

Polysilane polymers consist of a long catenated silicon backbone with two sidegroups attached to each Si atom in the backbone chain. Delocalization of electrons along the σ -bonded backbone results in very large oscillator strengths for UV transitions. Excitation by UV photons decays either by UV fluorescence or scission of the polymer backbone, making these materials useful as deep UV photoresists for microlithography. The large oscillator strengths also give rise to large optical nonlinear susceptibilities, and the ease of forming patterned waveguides by conventional spin coating and UV lithographic techniques make these materials interesting candidates for applications in nonlinear integrated optics.

We have, however, observed an extremely large, resonant two-photon absorption for poly(di-*n*-hexylsilane) which restricts the utility of these materials for nonlinear optical switches to the red or near infrared [1]. The spectrum, measured by two-photon induced backbone scission, consists of a broad band and a sharp spike, as shown in fig. 1. The maximum two-photon absorption coefficient on resonance is $\beta \approx 1.5$ cm./MW (corresponding to $\chi^{(3)} \approx 1 \times 10^{-9}$ esu). This contrasts with the lower off-resonance values (typically $\chi^{(3)} \approx 10^{-11}$ esu at $1.06 \mu\text{m}$) previously measured for third order nonlinear processes [2]. We have also found that polarized two-photon exposure retains the memory of the exposing laser polarization, making fabrication of unique waveguide devices by birefringent lithography possible [3].

The highest occupied molecular orbital of polysilane polymers has been conclusively determined to involve the delocalized σ -bonded conjugated backbone. Mintmire [4] has successfully modelled these polymers as one-dimensional semiconductors, predicting the overall lineshape and shifts in energy correctly for several polymer conformations. The similar linewidth of the broad feature in the two-photon spectrum suggests that a similar band-to-band absorption may be involved, but the origin of the sharp feature remains unexplained. We have, however, recently observed that spectroscopic features similar to those found in the two-photon spectrum (i.e. a broad band with a lower energy sharp spike) can be produced in the UV spectrum as well by rapid quenching of amorphous polymer on dry ice, as shown in fig. 2. This suggests that the low energy states are due to the formation of conformational defects in the polymer chain, and hence would not be predicted by the simple infinite chain model.

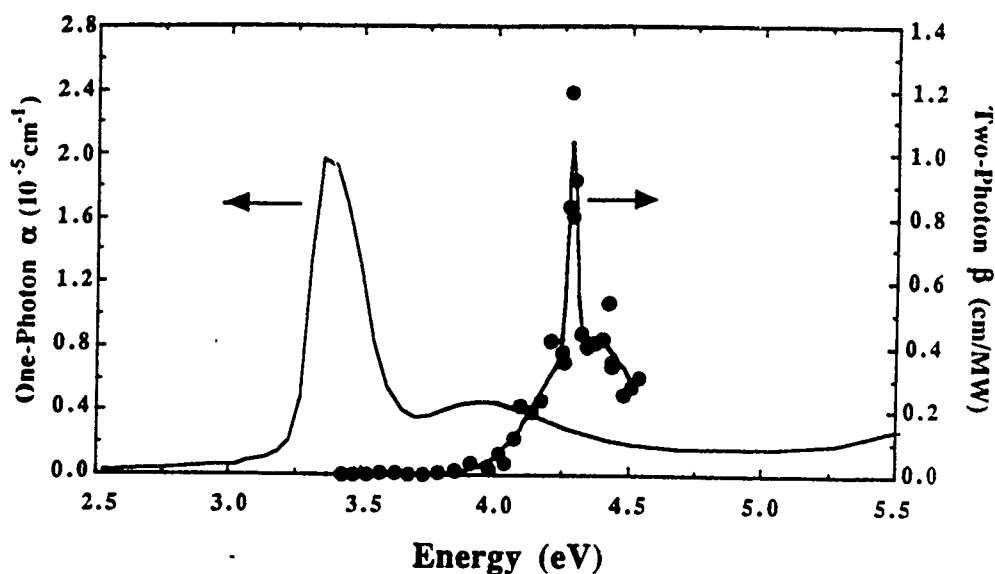


Figure 1: One- and two-photon absorption for a high molecular weight ($MW \approx 2 \times 10^6$) film of poly(di-*n*-hexylsilane).

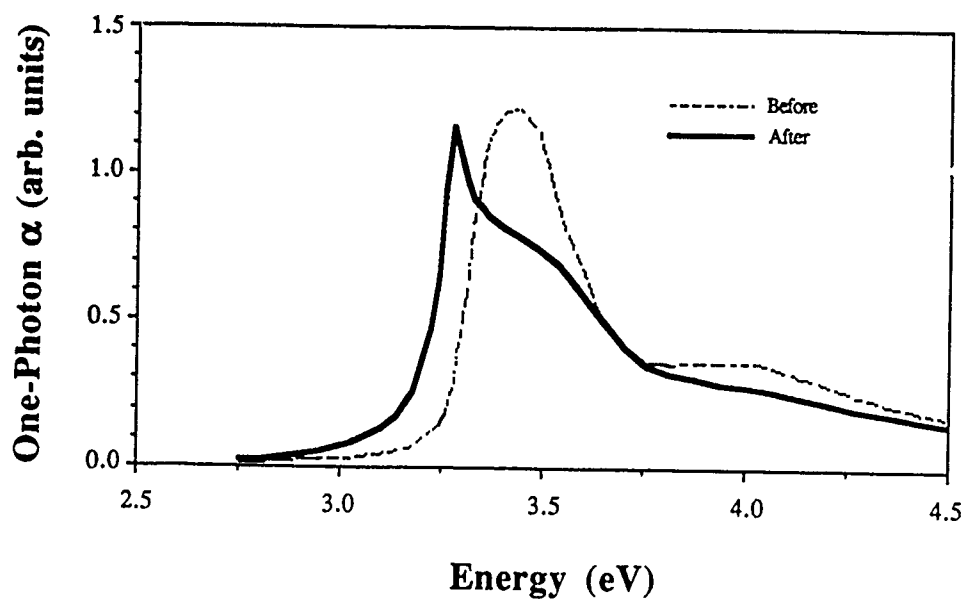


Figure 2: One-photon absorption for a film of poly(di-*n*-hexylsilane) before and after recrystallization

- [1] F.M. Schellenberg, R.L. Byer, J. Zavislan, and R.D. Miller, in *Nonlinear Optics of Organics and Semiconductors*, T. Kobayashi, ed. (Springer Verlag, New York, 1989), pp. 192-196.
- [2] F. Kajar, J. Messier, and C. Rosilio, *J. Appl. Phys.* **60**, 3040 (1986)
- [3] F.M. Schellenberg, R.L. Byer, and R.D. Miller, *Opt. Lett.* **15**, 242 (1990)
- [4] J.W. Mintmire, *Phys. Rev. B* **39**, 11028 (1989)

MP13 Observation of Dark Solitary Stripes and Grids

G. A. Swartzlander Jr.¹, D. R. Andersen²,
and A. E. Kaplan³

¹ Department of Electrical Engineering
The University of Maryland, Baltimore County
Baltimore, MD 21228

² Department of Electrical and Computer Engineering
The University of Iowa
Iowa City, IA 52242

³ Department of Electrical and Computer Engineering
The Johns Hopkins University
Baltimore, MD 21218

Although dark solitons are well-known solutions of the two-dimensional non-linear Schrodinger equation (NSE), three-dimensional (or "2+1") dark solitary phenomena have been elusive. However, we believe that we have made the first observations of inherently three-dimensional dark solitons which were formed when a laser beam propagated through a mask and into a self-defocusing nonlinear ($n_2 < 0$) medium. In particular, two rectilinear groups of dark solitary stripes appeared in the cross-section of a laser beam. In our initial experiment, a laser beam (100 mW) was passed through a mask (an 80-mesh wire screen) which was imaged at the input face of the nonlinear medium (sodium vapor, $n_2 = -10^{-7} \text{ cm}^2/\text{W}$). As the nonlinear refractive index, $|n_2 I|$, was increased above zero, the Fraunhofer diffraction pattern of the mask underwent beautiful transformations, indicating that self-reorganization was occurring under nonlinear propagation. This experiment was repeated in materials with larger (thermal) nonlinearities using only a few mW of power, and the same qualitative results were observed. In addition, numerical solutions of the NSE confirmed our belief that dark solitons had indeed formed, propagating at constant angles with respect to the optical axis, and remaining stable after collisions with other solitons of either group. Because of the limited beam size, the background on which these dark solitons exist diminishes adiabatically, and thus, these nonlinear waves are solitons in a weak sense. We have found that spatial dark solitons can be easily formed and detected (unlike temporal dark solitons), and may therefore find uses in a variety of applications such as optical computing and inter-connecting.

This work was supported by AFOSR and the National Science Foundation. Computations were performed at the National Center for Supercomputing Applications and the Pittsburgh Supercomputing Center.

MP14 Nonlinear Waveguides with Liquid Crystalline Cores

S.K. Lo, L.M. Galarneau, D.J. Rogers, S.R. Flom
Honeywell Systems and Research Center
3660 Technology Drive
Minneapolis, Minnesota 55418

Summary

We have succeeded in making low loss liquid crystal core waveguides, with losses less than 1.3 dB/cm over a 3 cm length using a *smectic* liquid crystal 4-cyano-4'-octylbiphenyl (8 CB). The losses measured agree well with the previous measurements on a planar *smectic* liquid crystal waveguide.¹ Our waveguide structures are cylindrical glass capillaries of inner diameters from 50 to 150 μm , filled with homeotropically aligned liquid crystals. Optical glass fibers of slightly smaller diameters are inserted at both ends and in optical contact with the liquid crystals. Most of the measured loss is associated with the coupling into and out of the liquid crystal waveguide via the optical fibers. In contrast to the *nematic* liquid crystals, we did not observe any Rayleigh scattering in the *smectic* liquid crystal filled waveguide (Figure 1). We believe the 8 CB is aligned homeotropically with its director perpendicular to the wall of the guided structure, except near the axis of the cylindrical guide. Presumably, near the center of the guide, either the director orients parallel to the axis of the guide or, if its free energy is high enough, it results in a small isotropic core region. The index profile of such a guide is being measured which will help to determine the orientation of the core region.

Under a high power microscope, we observed light scattered along the waveguide with a homeotropically aligned *nematic* liquid crystals, MBBA, showing highly polarized propagation modes (Figure 2). Very interesting propagation modes with a nodal spacing of 200-300 μm were observed in the 150 μm diameter guide. These features are absent from the unaligned liquid crystal waveguide. The nodal characteristics are puzzling since the predicted radial refractive index profile of the guide is higher at the wall than at the center, therefore propagation of the light should bend towards the wall instead of towards the center as it travels through the guide, which we observed.

Due to the low light scattering from the *smectic* liquid crystal waveguide we were not able to see the light propagation characteristics.

High scattering losses in liquid crystal waveguides had previously prevented the exploitation of their nonlinearities in the waveguide structure for optical modulation applications.^{2,3} With the low loss liquid crystal waveguide constructed, we have observed nonlinear transmittance through the waveguide under high input intensity, probably due to induced optical scattering (Figure 3). With an optimized device structure, we believe this type of novel waveguide has promise as an effective optical switch.

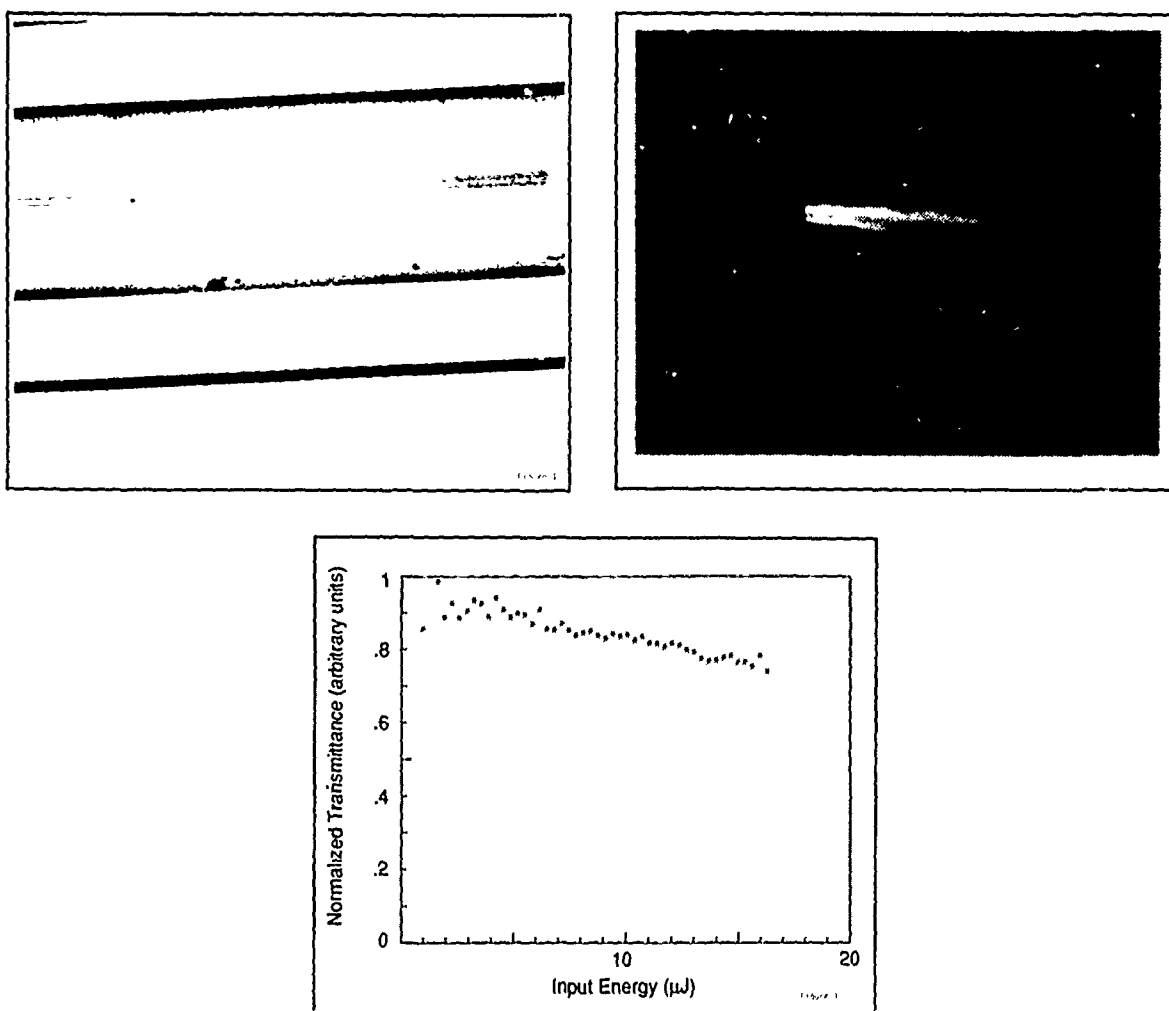
References

1. T.G. Giallorenzi, J.A. Weiss, and J.P. Sheridan, "Light Scattering from Smectic Liquid-Crystal Waveguides" J. of Appl. Phys. 47: 1820 (1976).
2. C. Hu and J.R. Whinnery, "Losses of a Nematic Liquid Crystal Optical Waveguide" J. of Opt. Soc. Amer. 64:1424 (1974).
3. J.R. Whinnery, C. Hu, and Y.S. Kwon, "Liquid Crystal Waveguides for Integrated Optics" IEEE J. of Quan. Electron. QE-13:262 (1977).

Figure 1. Optical Micrograph of a Smectic Liquid Crystal Filled Cylindrical Waveguide with Inner Diameter of 150 μm

Figure 2 Light Propagation Through a Homeotropically Aligned Nematic Liquid Crystal Waveguide (Analyzer Perpendicular to Propagation Axis)

Figure 3 Normalized Transmittance Through a Smectic Liquid Crystal Waveguide (With Fiber Coupled Input and Output) as a Function of Input Laser Energy



A Generalized Scalar Formulation of Nonlinear Pulse Propagation in Single-Mode Fibers

R. Osborne

Technische Universität München, Lehrstuhl für Hochfrequenztechnik,
Arcisstrasse 21, 8000 München 2, Federal Republic of Germany

Recently, increased importance has been attached to the inclusion of higher order terms in the nonlinear Schroedinger equation with the goal of more adequately describing the influence of material nonlinearity on pulse propagation in fiber waveguides[1]. This has been motivated, in part, by the observation of new nonlinear effects, such as the soliton self-frequency shift[2], where consideration of the large signal bandwidth and the frequency dependence of the nonlinear susceptibility becomes important.

Here, we present a generalized scalar evolution equation for the electric field in a nonlinear, weakly guiding, non-polarization preserving fiber incorporating the full wavelength dependence of the third order isotropic susceptibility $\chi^{(3)}$, fiber dispersion and fiber attenuation. We employ the resulting equation to numerically simulate pulse propagation under the combined actions of phase modulation, modulation instability, self-frequency shifting, Raman scattering and waveguide dispersion to third order.

By treating the fiber nonlinearity as a perturbation, one obtains for the evolution of a spectral component of the peak transverse electric field

$$\frac{\partial E(\omega)}{\partial z} - i\beta(\omega)E(\omega) - i\frac{c\omega\mu_0}{4n(\omega)}P^{nl}(\omega) = 0 \quad (1)$$

where P^{nl} denotes the nonlinear polarization, β is the frequency dependent propagation constant which may include fiber attenuation and n is the effective fiber refractive index. Under the assumption that the nonlinear susceptibility is constant except near the Raman resonance and that coupling to third harmonic terms can be neglected, P^{nl} can be written as

$$P^{nl}(\omega) = 3/4\epsilon_0\chi^{(3)}(\omega;\omega_1,-\omega_2,\omega_3)E(\omega_1)E^*(\omega_2)E(\omega_3) \quad (2)$$

and the third order susceptibility expressed in the symmetrized form

$$\chi^{(3)}(\omega;\omega_1,-\omega_2,\omega_3) = \{\bar{\chi}(\omega_1-\omega_2) + \bar{\chi}(\omega_3-\omega_2)\}/2. \quad (3)$$

This last equation defines the susceptibility $\bar{\chi}$ and allows one to write, consistent with the Born-Oppenheimer approximation[3],

$$P^{nl}(t) = 3/4\epsilon_0E(t)\mathcal{F}^{-1}\{\mathcal{F}\{|E(t)|^2\} \times \bar{\chi}(\omega)\} \quad (4)$$

where \mathcal{F} represents the Fourier transform. An expansion of $\bar{\chi}$ to first order in ω about $\omega=0$ recovers the terms describing the effect of the nonlinear refractive index n_2 and the self frequency shift, as employed in previous studies[4, 5].

The results of a numerical simulation based on Eqs. (1) and (4) are shown in Fig. 1 for a 1 psec gaussian pulse with a peak power of 600 W after propagation over 11 m of fiber in the negative dispersion region at 1.32 μ . For comparison, the peak power of the fundamental soliton of equal duration is 4.3 W. Self-phase modulation rapidly increases the pulse bandwidth to a value comparable to the Raman shift of 450 cm^{-1} at maximum gain at which point intra-pulse Raman conversion becomes significant. The time domain signal (Fig. 2) is marked by the fragmentation of the initial pulse and the formation of a compressed frequency-shifted pulse, containing a large fraction of the total energy, which

rapidly separates from the initial pulse due to group-velocity dispersion.

As in the present example, the use of the generalized formulation enables an accurate and unified treatment of nonlinear interactions spanning a broad spectral range.

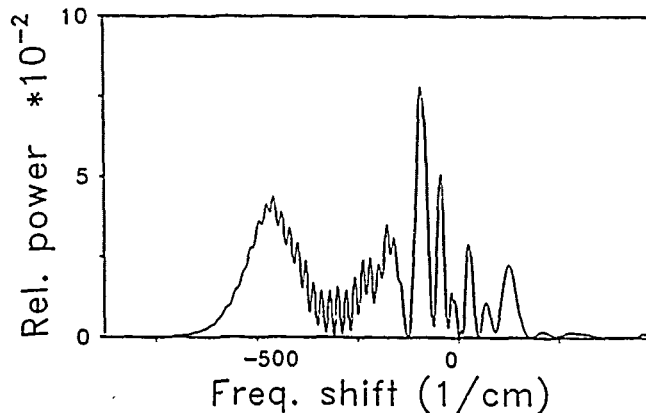


Fig. 1 Pulse power spectrum, normalized to the initial peak power, after 11 m of propagation.

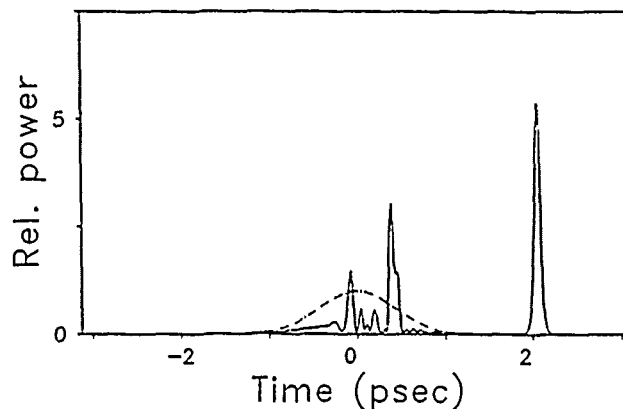


Fig. 2 Signal corresponding to Fig.1. The initial pulse (broken line) has fragmented, producing a sub-picosecond, frequency-shifted pulse (corresponding to the spectral feature at -500 cm^{-1}) which, under the action of group velocity dispersion, has walked off by 2 psec.

ACKNOWLEDGMENT

This work was supported by the Deutsche Forschungsgemeinschaft.

REFERENCES

- 1 Y. Kodama, A. Hasegawa, "Nonlinear pulse propagation in a monomode dielectric guide", IEEE J. Quantum Electron. QE-23, 510-524 (1987)
- 2 J. Gordon, "Theory of the soliton self-frequency shift", Opt. Lett. 11, 662-664 (1986)
- 3 R. Hellwarth, "Third-order Optical Susceptibilities of Liquids and Solids" in Progress in Quantum Electronics, Vol. 5, J. Saunders and S. Stenholm, Editors, Pergamon Press, N. Y., 1977
- 4 E. Bourkoff, W. Zhao, R. Joseph, D. Christodoulides, "Intensity-dependent spectra of pulses propagating in optical fibers", Opt. Commun. 62, 284-288 (1987)
- 5 B. Beaud, W. Hodel, B. Zysset, H. Weber, "Ultrashort pulse propagation, pulse breakup, and fundamental soliton formation in a single-mode optical fiber", J. Quantum Electron. QE-23, 1938-1946 (1987)

Fig. 1 Pulse power spectrum, normalized to the initial peak power, after 11 m of propagation.

Fig. 2 Signal corresponding to Fig.1. The initial pulse (broken line) has fragmented, producing a sub-picosecond, frequency-shifted pulse (corresponding to the spectral feature at -500 cm^{-1}) which, under the action of group velocity dispersion, has walked off by 2 psec.

MP16 Time Resolved Switching Characteristic of the Nonlinear Directional Coupler Under Consideration of Susceptibility Dispersion

Roland Schiek, Technische Universität München
Lehrstuhl fuer Technische Elektrophysik, Arcisstrasse 21, D-8000 München 2

The nonlinear directional coupler in either of its two forms, as fiber coupler [3] or integrated optic coupler [4], has assumed increased importance as an ultrafast optical switch in recent years. Most of the theoretical investigations are based on the stationary usual nonlinear coupled-mode theory introduced by Jensen [1]. But the temporal switching characteristics of the nonlinear coupler are determined by self-phase modulation, and waveguide and susceptibility dispersion. That is why we introduce for the computation of the temporal behaviour of the switching process from the limits of stationary through quasistationary [3] up to ultrafast excitations [2] a system of nonlinear coupled equations for the basis mode amplitudes in the frequency domain.

First we employ the modes of the isolated coupler branches as basis functions in the nonlinear coupled-mode theory. It is important, that one cannot neglect the lack of their orthogonality in the nonlinear theory. It is well known that the coupling length is incorrectly predicted by usual linear coupling theory if the coupling becomes strong. The error committed is even under weaker coupling conditions so strongly magnified in the nonlinear case that the usual nonlinear theory leads to qualitatively incorrect, and therefore to unusable results in integrated optics. The nonorthogonality of the modes causes a renormalization of the couple integrals in the evolution equations for the Fourier transform of the pulse envelopes:

$$\frac{da_1(\omega - \omega_0)}{dz} = \frac{-j\omega}{N_{11}^2 - N_{12}^2} \left[a_1(\omega - \omega_0)\epsilon_0 J_6 + a_2(\omega - \omega_0)\epsilon_0 J_7 + \iint df_1 df_2 \chi^{(3)}(\omega_1, \omega_2, -\omega_3) \cdot \right. \\ \left. (J_1 a_1(\omega_1 - \omega_0) a_1(\omega_2 - \omega_0) a_1^*(-\omega_3 - \omega_0) \exp(-j(\beta_1(\omega_1) + \beta_1(\omega_2) - \beta_1(\omega_3) - \beta_1(\omega))z) + \right. \\ \left. + J_2 a_1(\omega_1 - \omega_0) a_1(\omega_2 - \omega_0) a_2^*(-\omega_3 - \omega_0) \exp(-j(\beta_1(\omega_1) + \beta_1(\omega_2) - \beta_2(\omega_3) - \beta_1(\omega))z) + \right. \\ \left. + 2J_2 a_1(\omega_1 - \omega_0) a_2(\omega_2 - \omega_0) a_1^*(-\omega_3 - \omega_0) \exp(-j(\beta_1(\omega_1) + \beta_2(\omega_2) - \beta_1(\omega_3) - \beta_1(\omega))z) + \right. \\ \left. + 2J_3 a_1(\omega_1 - \omega_0) a_2(\omega_2 - \omega_0) a_2^*(-\omega_3 - \omega_0) \exp(-j(\beta_1(\omega_1) + \beta_2(\omega_2) - \beta_2(\omega_3) - \beta_1(\omega))z) + \right. \\ \left. + J_3 a_2(\omega_1 - \omega_0) a_2(\omega_2 - \omega_0) a_1^*(-\omega_3 - \omega_0) \exp(-j(\beta_2(\omega_1) + \beta_2(\omega_2) - \beta_1(\omega_3) - \beta_1(\omega))z) + \right. \\ \left. + J_4 a_2(\omega_1 - \omega_0) a_2(\omega_2 - \omega_0) a_2^*(-\omega_3 - \omega_0) \exp(-j(\beta_2(\omega_1) + \beta_2(\omega_2) - \beta_2(\omega_3) - \beta_1(\omega))z) \right] \\ J_i = I_i N_{11} - I_{i+1} N_{12} \quad (1)$$

Here, the I_i are the mode overlap integrals and

$$N_{ij} = \int dx dy (\vec{e}_{it} \times \vec{h}_{jt}^* + \vec{e}_{jt}^* \times \vec{h}_{it}) \cdot \vec{e}_z$$

are the mode normalization integrals. We find a corresponding equation for the Fourier amplitude $a_2(\omega - \omega_0)$.

A second selection of a truly orthogonal basis function set, consisting of the first even and the first odd supermode of the linear coupler, leads to more simple evolution equations:

$$\frac{da_1(\omega - \omega_0)}{dz} = \frac{-j\omega}{4W/m} \iint df_1 df_2 \chi^{(3)}(\omega_1, \omega_2, -\omega_3) \cdot \\ [I_1 a_1(\omega_1 - \omega_0) a_1(\omega_2 - \omega_0) a_1^*(-\omega_3 - \omega_0) \exp(-j(\beta_1(\omega_1) + \beta_1(\omega_2) - \beta_1(\omega_3) - \beta_1(\omega))z) + \\ + 2I_3 a_1(\omega_1 - \omega_0) a_2(\omega_2 - \omega_0) a_2^*(-\omega_3 - \omega_0) \exp(-j(\beta_1(\omega_1) + \beta_2(\omega_2) - \beta_2(\omega_3) - \beta_1(\omega))z) + \\ + I_3 a_2(\omega_1 - \omega_0) a_2(\omega_2 - \omega_0) a_1^*(-\omega_3 - \omega_0) \exp(-j(\beta_2(\omega_1) + \beta_2(\omega_2) - \beta_1(\omega_3) - \beta_1(\omega))z)] \quad (2)$$

The equation for a_2 has a corresponding form.

Shown in Fig. (1) is the evolution of the intensity in two strongly coupled film waveguides determined by the solutions of Eqs. (1) and (2) for a stationary excitation with Dirac distributions as ansatz for the Fourier transforms a_1 and a_2 . The couple lengths computed by both methods deviate slightly since the spatial excitation of the input waveguide cannot be identically represented with only two basis functions. For a weaker coupling the deviation of the superposition of the two basis functions in the two cases becomes insignificant and the results of both methods become identical. A comparison of the mode couple results with the results of a finite difference simulation confirms the validity of the theory, so that the approach can be used for the investigation of the temporal switching characteristic.

The time-dependent pulse evolution can be calculated by solving the integro-differential system (1) or (2). As initial conditions we take the Fourier transform of the input pulse envelope. As shown in Fig. (2) we can confirm the experimental result that up to relatively long pulses of a few picoseconds the pulse wings switch incompletely in contrast to the pulse center [3].

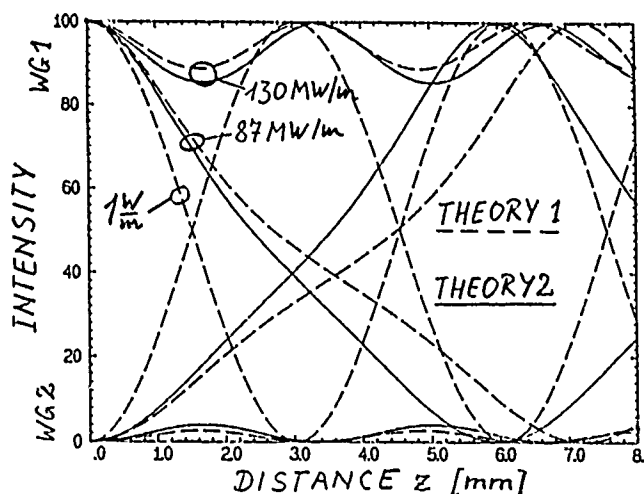


FIG.1: INTENSITY IN TWO COUPLED WG's

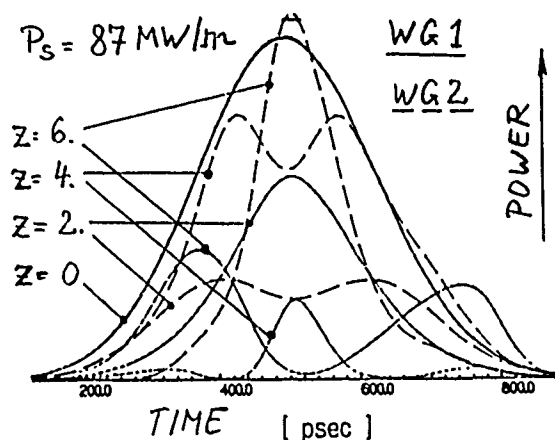


FIG.2: PULS EVOLUTION

The coupling behaviour of pulses with a further reduced length is principally determined by the difference in the group velocities of the basis functions and the degree of nonlinear mixing between the components of the Fourier amplitudes of the puls. We investigate under which conditions the predicted soliton switching in integrated optic couplers is possible [2] and how the nonnegligible frequency dependence of the couple integrals and of the phonon contribution to the third order susceptibility affect the switching characteristics.

[1] Jensen, S.M.: IEEE QE-18 (1982), p.1580.

[2] Trillo, S.; Wabnitz, S.; Wright, E.M.; Stegeman, G.I.: Optics Lett., 13 (1988), p.672.

[3] Friberg, S.R.; Silberberg, Y.; Oliver, M.K. u.a.: Appl. Phys. Lett., 51 (1987), p.1135.

[4] Li Kam Wa, P.; Sitch, J.E.; Mason, N.J. u.a.: Electronics Lett., 21 (1985), p.26.

MP17 Two-Photon Absorption in High-Nonlinearity Fibers

D. L. Weidman, J. C. Lapp, and M. A. Newhouse
Corning Incorporated, Corning, NY 14831

High-nonlinearity glass fibers may offer optimum performance in all-optical pipeline switching applications because of their combination of moderate nonlinearity with potentially very low loss.^{1,2,3} We have previously identified a number of glass compositions in which highly polarizable heavy metal cations increase the switching nonlinearity by up to 50× as compared to silica,⁴ and have reported the fabrication of a single-mode lead-silicate fiber (40 cation% heavy metal) with a nonlinearity 9× larger than silica.⁵ Here, we report the fabrication of a multimode lead-bismuth-gallate composition fiber. Two-photon absorption (TPA) measurement results at a number of wavelengths in both fibers are given.

Bulk samples of the lead-bismuth-gallate glass denoted RN (75 cation% heavy metals) were found to have a nonlinearity $\gamma = 125 \times 10^{-20} \text{ m}^2/\text{W}$, where γ is defined by $n = n_0 + \gamma I$, n_0 being the linear index and I the optical intensity.⁴ This nonlinearity is 50× larger than in silica. We fabricated a fiber of similar composition which had a core diameter of 10 μm , a core-clad index $\Delta = 2.5\%$, and a loss at 1.06 μm of 15 dB/m.

Results for measured transmission vs. incident power for both fibers are shown in Figure 1. Included are fits to the standard TPA transmission model.⁵ The TPA coefficients, β , obtained from these fits are plotted against photon energy in Figure 2. Also shown are data from Reference 6 on a multimode fiber of composition close to that of our lead-silicate fiber. Their data deviate about an order of magnitude from our results, pointing to the possibility that effects such as glass processing or optical history may significantly influence the nonlinear optical properties.

A criterion for insignificant TPA-induced degradation of all-optical switching is $2\beta\lambda/\gamma < 1$.⁶ For the silicate composition $2\beta\lambda/\gamma = 0.07$ at 1.06 μm , and for the gallate composition, $2\beta\lambda/\gamma < 0.1$ at 1.06 μm , indicating insignificant switching degradation in both compositions. Note that at 1.06 μm both the switching nonlinearity γ and the TPA nonlinearity β scale approximately equally, maintaining the same ratio. One might expect, in the absence of any significant single-photon resonance and in amorphous glass systems where symmetry selection rules are broken by the disorder, that the density of states for TPA measured at frequency ω should scale with the density of states for linear absorption at 2ω , i.e. $\beta(\omega) \propto \alpha(2\omega)$. The solid curves in Figure 2 are a scaling of the measured glass absorption curves with Urbach-behavior extrapolation to high energies. Additional work is needed to more fully understand the dispersion of the nonlinearities in these materials.

References

1. S. R. Friberg and P. W. Smith, *IEEE J. Quantum Electron.* **QE-23**, 2089 (1987).
2. G. I. Stegeman and R. H. Stolen, *J. Opt. Soc. Am. B* **6**, 652 (1989).
3. D. L. Weidman, M. A. Newhouse, and D. W. Hall, *Topical Meeting on Nonlinear Optical Properties of Materials*, Troy, NY, August 1988.

4. D. W. Hall, M. A. Newhouse, N. F. Borrelli, W. H. Dumbaugh, and D. L. Weidman, *Appl. Phys. Lett.* **54**, 1293 (1989).
5. M. A. Newhouse, D. L. Weidman, and D. W. Hall, *Conf. on Lasers and Electro-Optics*, Baltimore, MD, 1989 and submitted to *Optics Letters*.
6. V. Mizrahi, K. W. DeLong, G. I. Stegeman, M. A. Saifi, and M. J. Andrejco, *Opt. Lett.* **14**, 1140 (1989).

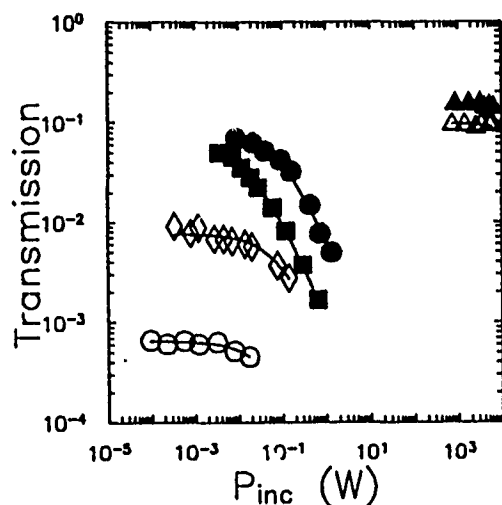


Figure 1 Transmission as a function of incident power for the lead-silicate fiber at 488 (■), 515 (●), and 1064 nm (▲) and for the lead-bismuth-gallate fiber at 515 (○), 647 (◇), and 1064 nm (△).

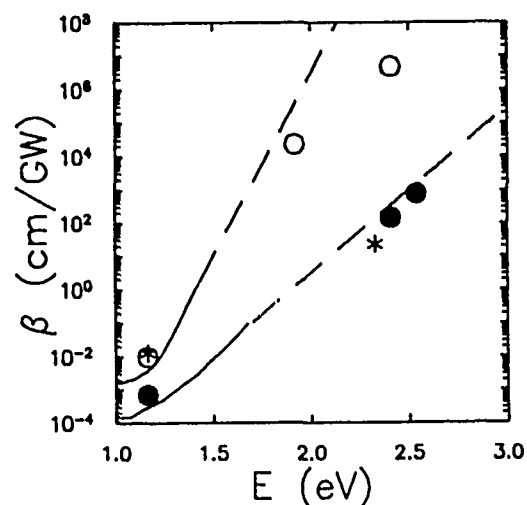


Figure 2 Two-photon absorption for several photon energies in the lead-silicate (●) and lead-bismuth-gallate (○) fibers. The solid lines are scaled from measured absorption data and are extrapolated to high energies (dashed lines) using the Urbach approximation. Also shown are data from a lead-silicate fiber reported in Reference 6 (*).

MP18 Broadband Complete Optical Switching in a Polarization-Maintaining Fiber

H. Vanherzeele

E.I. Du Pont De Nemours & Company, CR&D Department, P.O. Box 80356, Wilmington,
DE 19880-0356.

and

B. K. Nayar

British Telecom Research Laboratories, Martlesham Heath, Ipswich IP5 7RE, UK.

Ultrafast all-optical switching has been demonstrated in various optical fiber interferometric devices using the optical Kerr effect [1-4]. The ultrafast nonlinearity of silica results in incomplete optical switching with non-square pulses. Complete pulse switching can be achieved using soliton-like pulses [5]. In many applications it is not possible to be in the soliton regime. For these applications we have demonstrated complete optical switching of a signal pulse by a high power control pulse in a polarization-maintaining fiber. The signal pulse experiences a uniform phase change if the two pulses are temporally overlapping. However, when the two pulses are of different wavelengths they will walk off due to the group velocity dispersion (GVD). In this case complete optical switching can still take place for a range of temporal delays as long as the signal pulse can walk through the control pulse (or vice versa), regardless the signal wavelength and the ratio of the pulse widths. When the fiber length does not exceed the walk-off length, a minimum switching power results for an initial temporal offset equal to one-half of the relative group delay.

For the experimental work we used a broadly tunable 100 MHz source, described elsewhere [6]. The control pulses are derived from a Nd:YLF laser producing 52 ps (FWHM) pulses at 1053 nm and the signal pulses are generated by a synchronously mode locked tunable dye laser capable of giving either broad (30-50 ps) or short (2-5 ps) FWHM pulses. The basic experimental arrangement is an optical Kerr modulator/switch and consists of a polarization-maintaining fiber and an analyser at the output. The signal and the control pulses are co-propagating and have their polarizations at 45° and along one of the fiber axes respectively. In the absence of the control pulse there is no signal transmission. The short dye laser pulses, have a polarization dispersion walk-off length of 2.2 m. In order to overcome this we used two approximately equal lengths (each 1.8 m) spliced such that the fiber axes were reversed at the splice and this resulted in a 100:1 polarization extinction ratio.

The switching characteristics of both the broad and short dye laser pulses were investigated for the dye laser wavelength range of 830 nm (higher mode cut-off) to 1000 nm. The optimum initial delay for a given wavelength was determined by measuring the signal switching ratio as a

function of the temporal delay for a given control power. The switching characteristics were then measured at the optimum delay settings for the above wavelengths using both the broad and short dye laser pulses : see Fig.1. The solid line is the theoretical fit. It can be seen that for the short pulses complete switching results. In addition, it is significant to note that even for the broad pulses (0.6 x control pulse width) nearly complete switching occurs. Over the 830-1000 nm wavelength range, the switching energy for the control pulses is 4.8 ± 0.5 nJ.

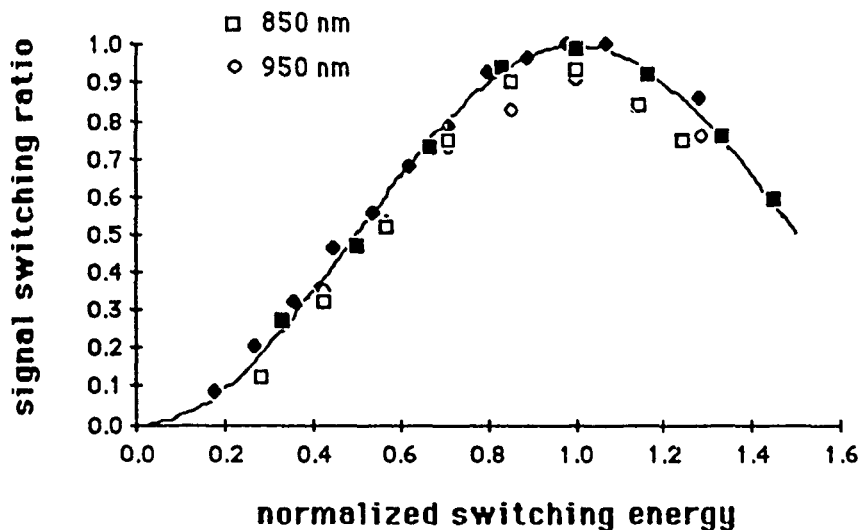


Fig.1 : Signal pulse switching ratio at 850 nm and 950 nm as a function of control pulse energy (normalized to 4.8 nJ) at 1053 nm. Open (filled) dots correspond to broad (short) signal pulses. The solid line is a theoretical fit.

In conclusion, broadband ultrafast complete pulse switching has been demonstrated using a pump-probe configuration. It is shown that the walk-off due to the GVD can be exploited to achieve complete switching. Our experiments demonstrate the feasibility of the use of a high power control laser at 1300 nm to switch signal pulses in the low loss fiber windows (1250-1350 nm and 1450-1550 nm).

REFERENCES:

1. J.M. Dziedzic, R.H. Stolen, and A. Ashkin, Appl. Opt. **20**, 1403 (1981).
2. T. Morioka, M. Saruwatari, and A. Takada, Electron. Lett. **23**, 453 (1987).
3. M. J. LaGasse, D. Liu-Wong, J.G. Fujimoto, and H.A. Haus, Opt. Lett. **14**, 311 (1989).
4. S.R. Friberg, A.M. Weiner, Y. Silberberg, B.G. Sfez and P.W. Smith, Opt. Lett. **13**, 904 (1988).
5. K.J. Blow, N.J. Doran and B.K. Nayar, Opt. Lett. **14**, 754 (1989).
6. H. Vanherzeele, Opt. Lett. **14**, 728 (1989).

M J Adams, D A H Mace, J Singh and M A Fisher,
British Telecom Research Laboratories, Martlesham Heath, Ipswich, IP5 7RE, UK.

This paper presents theoretical predictions for optically induced switching in an active nonlinear directional coupler which includes feedback effects. These are confirmed by an experimental result of all-optical switching in a semiconductor twin-ridge amplifier driven close to threshold.

The active nonlinear directional coupler shown schematically in Fig. 1 consists of two parallel, $185\mu\text{m}$ long InGaAsP ridge laser amplifiers which are approximately $4\mu\text{m}$ apart. Current is injected into both the ridges and light is launched into ridge 1. The theoretical model, an extension of a recently developed theory for the twin-guide Fabry-Perot laser amplifier [1], calculates the optical transmission for both ridges as a function of the input optical power, and includes the effects of feedback from the end facets of the ridges. Increasing the injected optical power modifies the carrier concentration in the ridges, which in turn alters the transmission strongly for wavelengths close to the cavity resonances.

The results for this are summarised in Fig 2 where transmitted gain is plotted against normalised input power P_{lin}/P_s . P_s is the saturation intensity defined in the usual way [2]. At low powers the gain is higher for the through state (output from ridge 1) whilst the cross state (output from guide 2) dominates at high powers. The crossover occurs at $P_{\text{lin}}/P_s=0.001$, and for typical parameter values for $1.55\mu\text{m}$ InGaAsP amplifiers [2] this is expected to correspond to input power levels of order a few microwatts. This power is significantly lower than the power predicted for switching in a travelling wave amplifier [3] because of the effect of feedback from the end facets of the guides.

Figure 3 shows the experimentally measured optical power dependence of the gain when light is injected into ridge 1. At low powers the nonlinear directional coupler is in the through state with $> 8\text{dB}$ gain. As the power increases, the gains crossover and if the power rises to -22.5dBm ($5.6\mu\text{W}$), a cross state of the coupler is selected where the gain is 14.3dB . This demonstration confirms the theoretical predictions that all-optical switching with gain can be achieved in an active nonlinear directional coupler with optical power levels of order microwatts. This device may therefore be useful for future photonic switching applications.

[1] M J Adams, 1989, IEE Proc. J, vol 136, pp 287-292.

[2] M J Adams, H J Westlake, M J O'Mahony and I D Henning, 1985, IEEE J Quantum Electron, vol QE-21, pp 1498-1504.

[3] J M Liu and C Yeh, 1987, Appl Phys Lett, vol 50, pp 1625-1606.

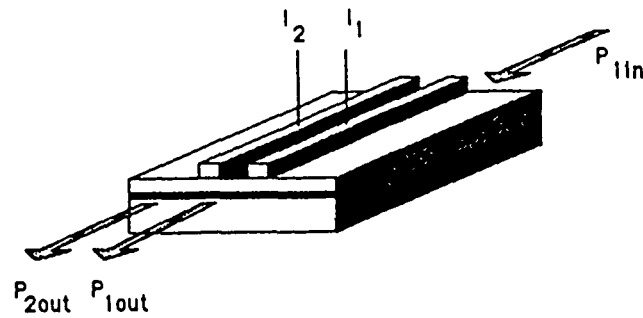


Fig. 1 Schematic illustration of the twin-ridge amplifier structure.

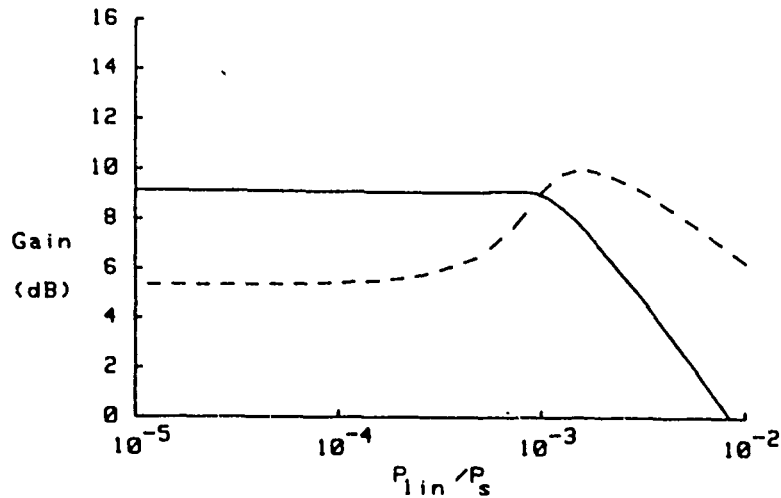


Fig 2 Calculated transmitted gains as a function of normalised input power. Solid line - ridge 1; broken line - ridge 2.

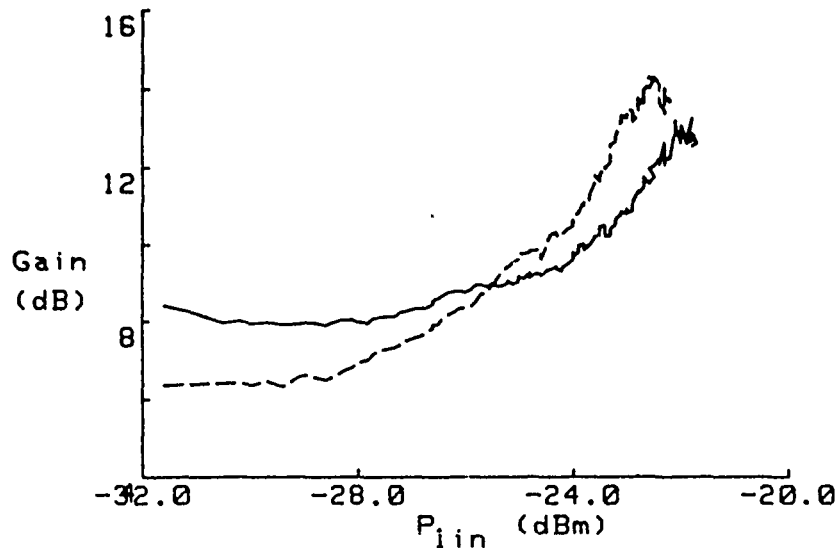


Fig. 3 Experimental results for transmitted gains versus optical input power. Solid line - ridge 1; broken line - ridge 2.

MP20 Energy Redistribution at the Interaction Between Two Femtosecond-Solitons in Optical Fibers

B. J. Hong and C. C. Yang
Department of Electrical Engineering
The Pennsylvania State University
121 Electrical Engineering East
University Park, PA 16802

It is well known that the collision between two solitons of picoseconds in width is elastic [1]. The two solitons are basically recovered after the collision because the effects of cross-phase modulation in the first half-crossing are cancelled by those in the second half. However, for solitons of femtoseconds in width, the collisions becomes inelastic due to the existence of higher-order dispersion, shock effect and Raman scattering. The Raman scattering includes the stimulated Raman scattering between the two solitons and the intrapulse Raman frequency shift. The latter is equivalent to the noninstantaneous Kerr effect [2,3]. It was experimentally measured that the peak gain of the Raman spectrum is at 440 cm^{-1} frequency shift which corresponds to a delay time of 75 fsec in the response function. Hence, any two femtosecond-pulses, separated by a time period smaller than or comparable to 75 fsec, Raman scattering would occur besides the well-known soliton-soliton interaction. During the process, the energy in the two pulses is redistributed. The redistribution ends up with the formation of two new solitons which can be completely separated. The intensities and central wavelengths of the two new solitons are different from each other and different from those of the initial solitons. In Fig. 1, the numerical results of the interaction between two identical solitons of 40 femtoseconds in width and $1.51\text{ }\mu\text{m}$ in center wavelength are shown. The initial pulse separation is 140 fsec. The dashed and solid curves depict the initial and final solitons, respectively. It has been observed that the energy redistribution in the interaction between two femtosecond-solitons depends on the initial soliton intensity, soliton separation, relative phase, and wavelength difference between the two solitons. In Fig. 2, the results of the collision between two solitons of the same width at 40 fsec but different central wavelengths at 1.5 and $1.51\text{ }\mu\text{m}$, respectively, are shown. Here, the dependence on initial relative phase can be seen. In this paper, the dependences of energy redistribution on several initial parameters will be presented. Meanwhile, the mechanism of energy redistribution during the interaction between two femtosecond-solitons will be discussed.

References:

- [1] L. F. Mollenauer, et. al., IEEE, J. Quantum Electron, QE-22, 157, (1986)
- [2] R. H. Stolen, et. al., J. Opt. Soc. Am. B, 1159 (1989)
- [3] K. J. Blow and D. Wood, IEEE J. Quantum Electron, QE-25, 2665, (1989)

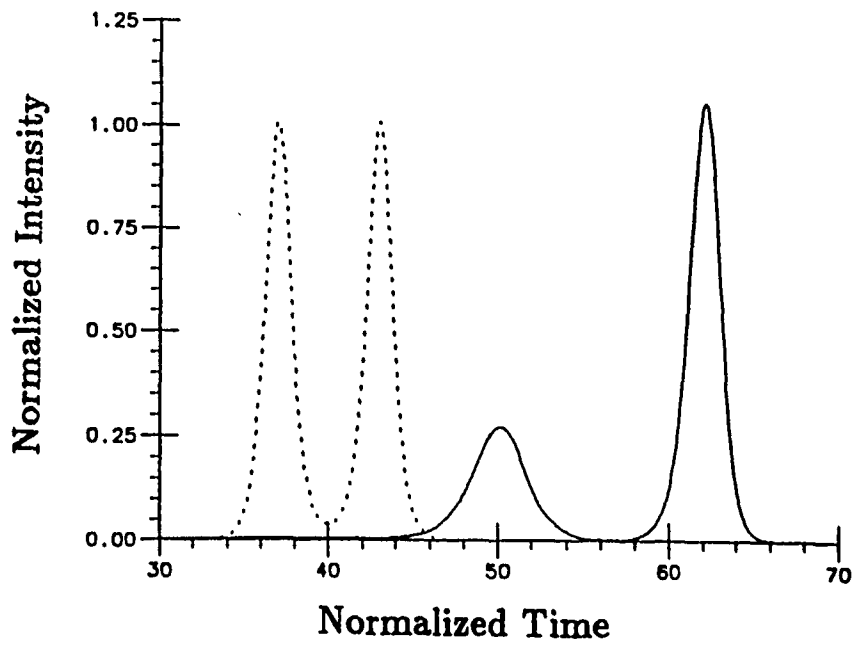


Figure 1 Dashed and solid curves depict the initial and final solitons, respectively.

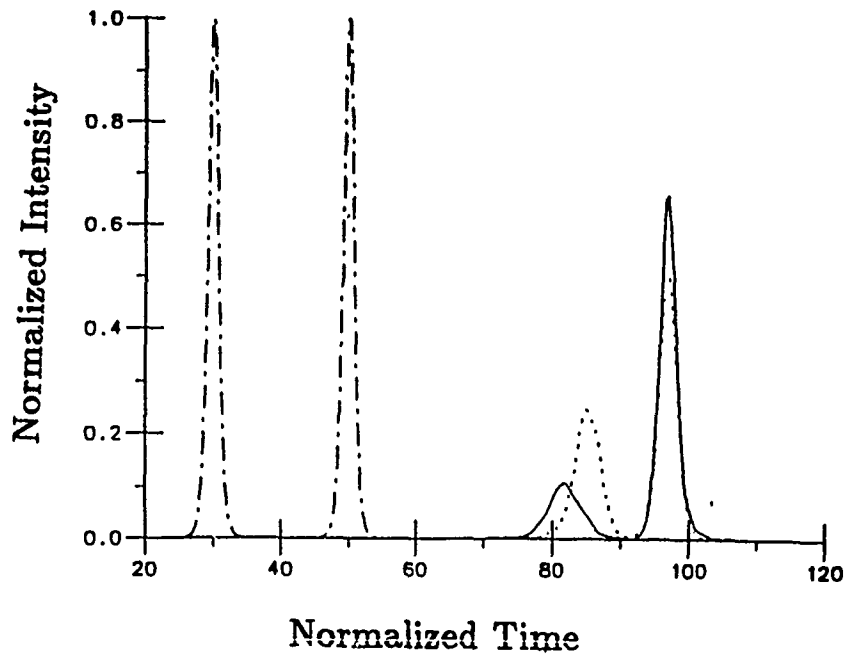


Figure 2 Dashed-dotted, solid and dashed curves represent the initial solitons, final solitons with zero initial phase, and final solitons with π initial phase, respectively.

MP21 Femtosecond Raman Scattering in Birefringent Fibers

S. Trillo and S. Wabnitz

Fondazione Ugo Bordoni, Via B. Castiglione 59, 00142 Rome, Italy

Tel.: +396-5480-3206

Summary

The effect of stimulated Raman scattering on the propagation of ultrashort optical pulses in silica fibers has been recently studied by means of the Schrödinger equation with a delayed contribution to the nonlinearity.¹ In this work we extend the analysis to deal with pulses of arbitrary polarization which propagate in the two orthogonal polarization modes of a birefringent fiber. This has important implications for femtosecond pulse compression experiments, where intensity-dependent polarization rotation may be used to eliminate the wings of a compressed pulse, and for all-optical switching devices employing the two polarization modes of a fiber.^{2,3}

Figure 1 shows examples of computed pulse envelopes emerging from the slow (1a) and the fast (1b) axis of a birefringent fiber of length $z = 0.25$ (in soliton units^{1,2}), respectively, whenever the input pulse is slightly misaligned with the slow axis. As can be seen, considerable polarization rotation occurs near the edges of the weak pulse component. Moreover, a temporal asymmetry is introduced by the noninstantaneous Raman contribution, in close agreement with recent pulse shaping measurements.⁴ A similar asymmetry also results in the spectral distributions. By simulating the passage of these pulses through a grating with anomalous dispersion, we have studied the effect of Raman-induced asymmetries on the choice of parameters for optimal pulse compression. Figure 2 illustrates the coupling between linear polarization modes which is predicted to occur in the anomalous dispersion regime for femtosecond solitons in a periodically twisted fiber filter.² The distance is given in terms of the linear coupling length of the polarization coupler. The input pulse is launched on the fast axis (fig. 2(a)): as can be seen, the pulse slowing down due to soliton self-frequency shift competes with the differential group delay and the linear coupling between the modes. The results of the calculations permit an optimal design of femtosecond soliton switching and wavelength demultiplexing experiments with birefringent fibers and filters, in the presence of self-stimulated Raman scattering.

References

- [1] R.H. Stolen, J.P. Gordon, W.J. Tomlinson, and H.A. Haus, *J. Opt. Soc. Am. B* **6**, 1159 (1989).
- [2] S. Trillo, S. Wabnitz, and G.I. Stegeman, *IEEE J. Quantum Electron.* **QE-25**, 1907 (1989).
- [3] M.N. Islam, *Opt. Lett.* **14**, 1257 (1989).
- [4] J.E. Rothenberg, and D. Grischkowsky, *Phys. Rev. Lett.* **62**, 531 (1989).

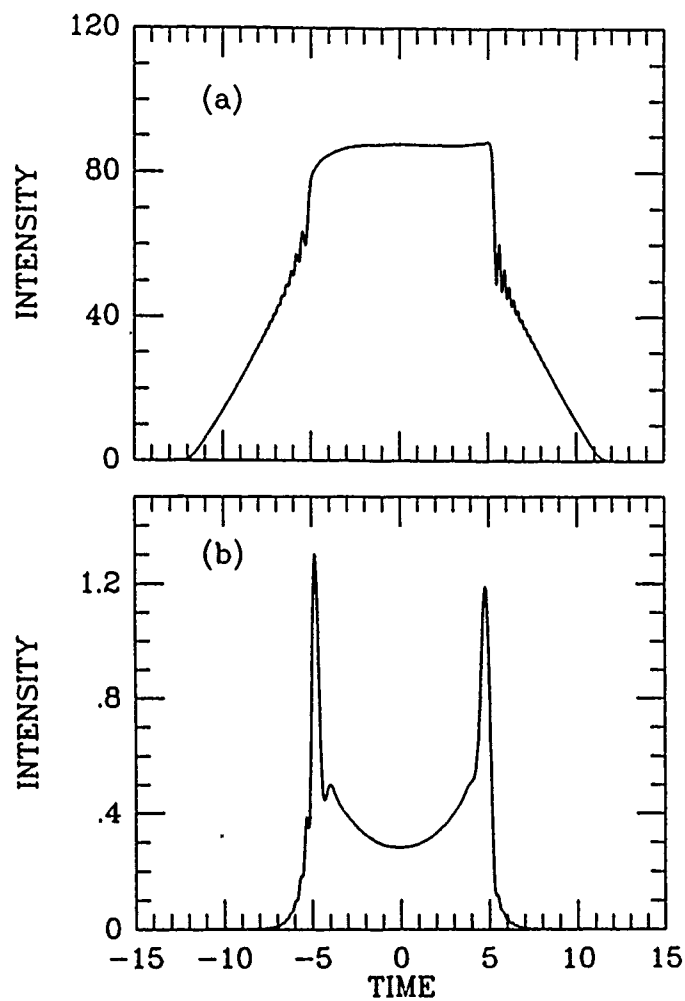


Figure 1: Pulses in slow (a) and fast (b) fiber axis at $z = 0.25$, normal dispersion.

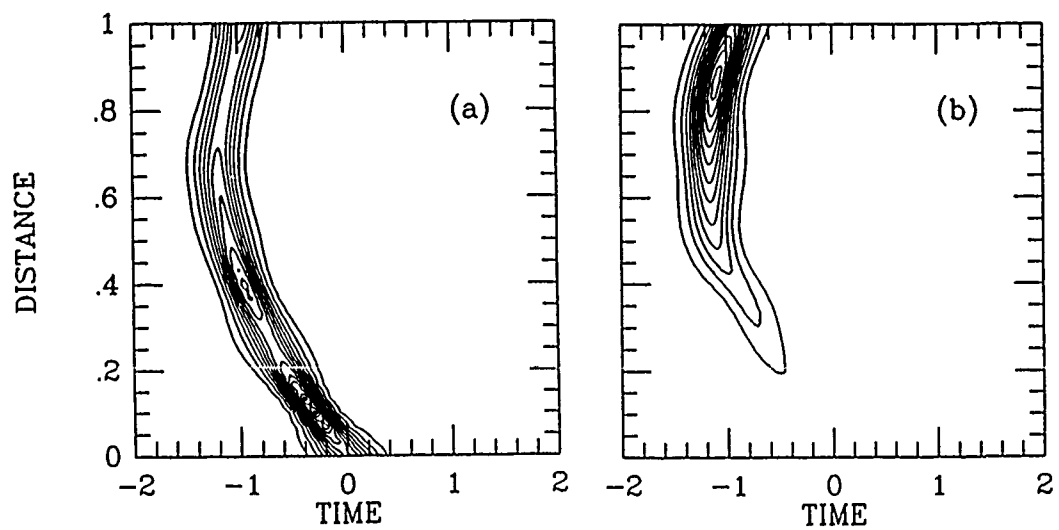


Figure 2: Pulses in fast (a) and slow (b) fiber axis at $z = L_C$, anomalous dispersion.

MP22 Nonlinear Optical Properties of Platinum Poly-ynes

Shekhar Guha, Keith Kang, Pam Porter, Claude C. Frazier,
Eve Chauchard and Dan Beekman
Martin Marietta Laboratories, 1450 S. Rolling Road, Baltimore, MD 21227

Joel Falk, Xuelei Hua and Seung-Han Park
Department of Electrical Engineering, University of Pittsburgh, Pittsburgh, PA 15261

SUMMARY

Transition metal-organic polymers have attracted considerable attention because of their potential applications to optoelectronic devices. Recently, we showed that platinum poly-ynes have large optical nonlinearities and low absorption in the visible and near infrared.¹ Here, we report measurements showing the separation of nuclear and electronic contributions to the third-order optical nonlinearities ($\chi^{(3)}$). We also describe measurements of strong two photon absorption in the platinum poly-ynes.

The nonlinearity of the platinum poly-ynes arises from both the electronic and nuclear contributions. The pt poly-ynes have an anisotropic polarizability and therefore the more polarizable axis of the molecule tends to align with the plane of polarization of the light. We have used polarization discrimination techniques^{2,3} to resolve the nuclear and electronic contributions to $\chi^{(3)}$. A phase conjugate output signal is monitored for a Nd:YAG laser probe beam polarized either perpendicular or parallel to a pumping laser beam. These measurements allow determination of both nuclear and electronic contributions to the nonlinear susceptibility. A ratio $\chi^{(3)}(\text{nuclear}) / \{\chi^{(3)}(\text{electronic}) + \chi^{(3)}(\text{nuclear})\} = 0.31 \pm 0.10$ was obtained at 1.064 μm . Third-harmonic generation, which is insensitive to the nuclear response, shows an electronic nonlinearity similar to that measured in the polarization discrimination experiments. We note that contributions to $\chi^{(3)}$ due to thermal gratings are insignificant since absorption in the platinum poly-ynes at 1.064 μm is minimal.

Strong nonlinear absorption and enhanced back-scattering are observed at 532 nm for pump intensities of above .5 MW/cm². Degenerate-four-wave mixing output signals show a fifth-order power dependence on the incident 532 nm pump intensity as shown in Fig. 1. We attribute this strong power dependence to the formation of a two-photon absorption-induced grating in the metal-organic polymers. The nonlinear absorption and strong backscattering lead to very efficient optical power limiting and optical switching. Potential applications of the observed nonlinearity are discussed.

REFERENCES

1. S. Guha, C.C. Frazier, P.L. Porter, K. Kang and S.E. Finberg, *Opt. Lett.* **14**, 952 (1989).
2. R.W. Hellwarth, A. Owyong and N. George, *Phy. Rev. A* **4**, 2342 (1971).
3. D.J. McGraw, A.E. Siegman, G.M. Wallraff and R.D. Miller, *Appl. Phys. Lett.* **54**, 1713 (1989).

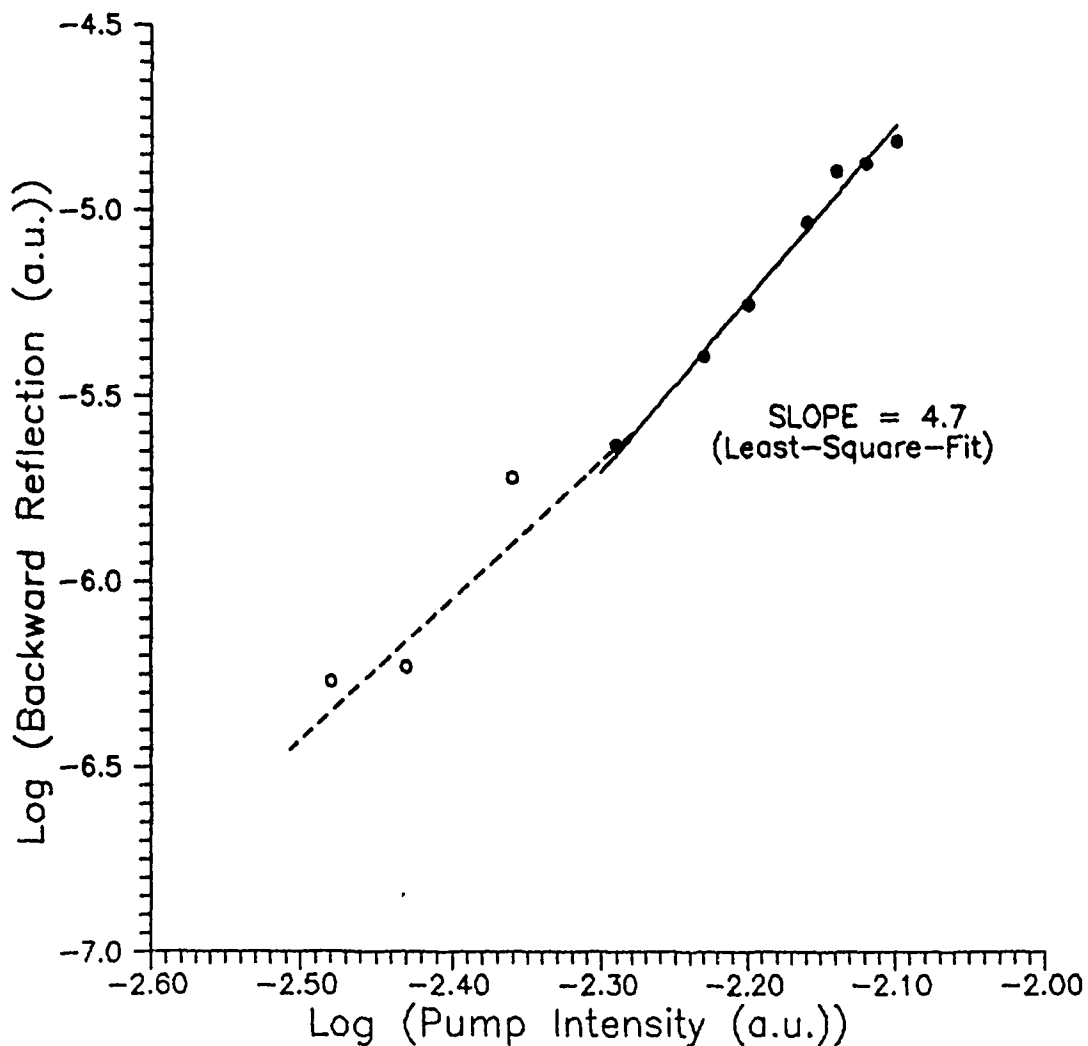


Figure 1. Backward reflected signal intensity versus incident pump intensity. The system prf is 10 Hz and the average intensities in the pump and signal beams are recorded. (The abscissa value of -2.3 corresponds to pump intensity of approximately .5 MW/cm².)

MP23 Nonlinear Optical Properties of Organometallic Compounds in Solids and Solutions

L.W. Tutt, S.W. McCahon and M.B. Klein
Hughes Research Laboratories
Malibu, Ca 90265
(213) 317-5834

SUMMARY

We have measured the excited state absorption spectra of a number of organometallic cluster compounds that have previously been shown to possess optical limiting properties. The two cluster compounds $\text{HFeCo}_3(\text{CO})_{10}(\text{PMe}_3)_2$ and $\text{HFeCo}_3(\text{CO})_{10}(\text{P}(\text{C}_6\text{H}_5)_3)_2$ exhibit very similar ground state absorption spectra throughout the visible spectrum, however, their excited state absorption spectra are quite different. This is consistent with an excited state absorption that heavily involves the electronic contributions of the ligand, while the ground state absorption depends only slightly on the electronic effects of the ligand. The lifetime of the excited state was measured for each compound and was observed to be ~ 115 ns for both, indicating a similar excited state. These results are consistent with an electronic transition from a metal d ground state to a metal-metal anti-bonding orbital followed by a metal-ligand charge transfer transition.

Metal atom substitution in the FeCo_3 tetrahedral core of the organometallic cluster compounds is known to cause a shift in the ground state absorption spectra indicating modification of the ground state transition. The effects of metal atom replacement on the optical limiting properties are presented and the results discussed in terms of metal-metal bond breaking followed by metal to ligand charge transfer.

Measurements of optical limiting properties, using a collimated optical beam, were conducted on three of the best reported optical limiting compounds to allow direct comparison of the optical limiting values. The three compounds are indanthrone, chloroaluminum phthalocyanine, and N-methylthioacridone. The optical fluence threshold for limiting, the degree of limiting, and the expected broadband limiting performance are compared to values measured using our organometallic cluster compounds.

Solutions of the organometallic cluster compounds in organic solvents have previously been shown by us to possess optical limiting properties. We now report the incorporation of these organometallic cluster compounds into polymer hosts such as polymethylmethacrylate. Optical

limiting based on reverse saturable absorption is again observed. The optical limiting properties of these organometallic cluster compounds are modified by incorporation in the solid polymer host material. Specifically, the operational dynamic range is reduced due to the breakdown of the polymer host. Use of a converging optical beam extends the dynamic range by moving the location of highest fluence from the air-polymer interface at the beam entrance into the bulk of the host where thermal dissipation and mechanical strength are higher.

Optical Nonlinearities in Crystalline Organic Multiple Quantum Wells

J.F. Lam*, S.R. Forrest**, and G.L. Tangonan*

* Hughes Research Laboratories
Malibu, California 90265

** University of Southern California
Dept. of Electrical Engineering and
Materials Science
Los Angeles, California 90089-0241

This paper reports new results arising from the studies of optical interaction in newly demonstrated crystalline organic multiple quantum wells. Recently, these novel materials have been grown by means of organic molecular beam epitaxy¹, and their excitonic energy levels have been shown to experience a blue shift as the spatial dimension of the well decreased. The constituent materials were 3,4,9,10 perylenetetracarboxylic dianhydride (PTCDA) as the well and 3,4,7,8 naphthalenetetracarboxylic dianhydride (NTCDA) as the barrier.

Using the Davydov Hamiltonian², modified by the spatial quantization, we analyzed the linear and nonlinear optical properties of these materials. The Davydov Hamiltonian takes into account the effect of the coupling between the charge transfer exciton with the phonons and the external applied fields.

The results of our analysis can be summarized as follows. First, the solution of the Heisenberg equation of motion gives the exciton optical coherence and yields the linear absorption coefficient. Figure 1 shows the quantitative comparison between the theoretical and experimental absorption coefficients of the S_0 and S_1 exciton line in PTCDA quantum wells. The energy separation is the Davydov splitting. And second, we found an exact analytical, nonlinear solution of the coupled exciton-phonon equations. It predicts the existence of intrinsic optical bistability which originates from the intensity dependence of exciton-phonon coupling. Figure 2 shows the two-wave mixing absorption of the weak wave as a function of the strong wave Rabi frequency to the second power. A transition to bistable behavior, with energy transfer (negative value of absorption) to the weak wave, is observed for increasing strong wave Rabi frequency.

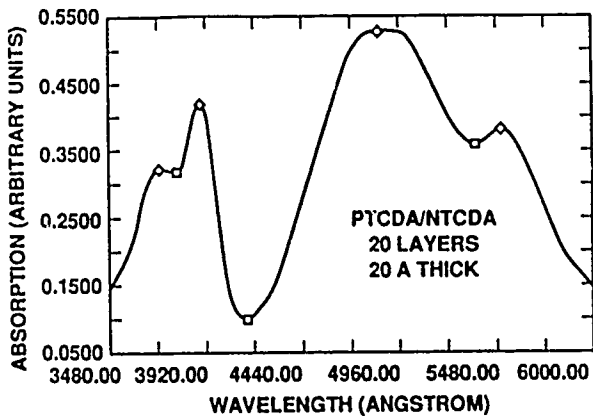
This work is supported by the Air Force Office of Scientific Research (Howard Schlossberg and Cole Litton), and we thank F.F. So for technical discussions.

1. F.F. So, S.R. Forrest, V.Q. Shi and W.H. Steier, Appl. Phys. Lett. 56, 674 (1990)
2. A.S. Davydov, THEORY OF MOLECULAR EXCITON, Plenum Press (1972)

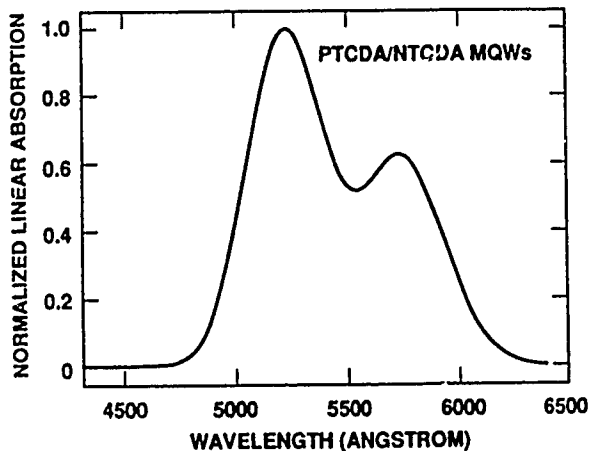
FIGURE CAPTIONS

Figure 1 Linear absorption spectra of PTCDA/NTCDA quantum wells. (a) experimental results showing both the NTCDA (left) and PTCDA (right). The layer thickness is 20 Å. (b) theoretical results for PTCDA showing the Davydov splitting

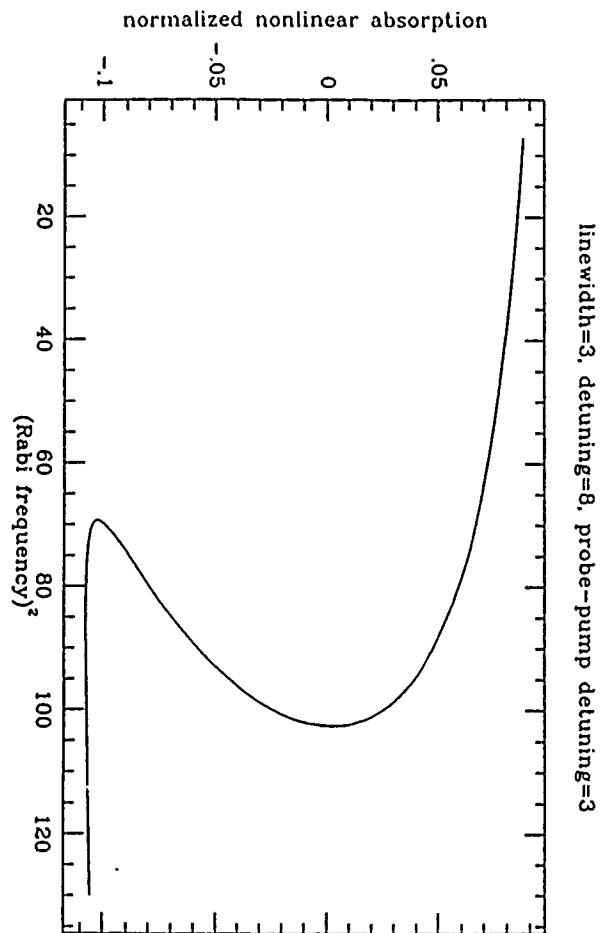
Figure 2 Nonlinear absorption coefficient of the weak wave as a function of the strong wave Rabi frequency to the second power. The linewidth of the exciton resonance and the laser detuning from it is normalized to $2\lambda^2/\omega_0$. λ and ω_0 are the exciton-phonon coupling constant and the phonon frequency.



(1a)



(1b)



Excited State Absorption and Optical Nonlinearities of Metallophthalocyanines and Naphthalocyanines In Solution

J. W. Perry, L. R. Khundkar, D. R. Coulter, T. H. Wei,[†]
E. W. Van Stryland[†] and D. J. Hagan[†]

Jet Propulsion Laboratory, California Institute of Technology
Pasadena, CA 91109

[†]Center for Research in Electro-Optics and Lasers and Department of Physics
University of Central Florida
Orlando, FL 32816

Abstract Picosecond and nanosecond studies of nonlinear absorption and refraction in solutions of phthalocyanines are presented. The importance of excited state absorption and the implications for optical limiters will be discussed.

Solutions of metallophthalocyanines and metallonaphthalocyanines are currently of interest in optical limiting applications. We have recently reported on the optical limiting of picosecond and nanosecond duration laser pulses by such solutions[1], as well as on the use of tandem combinations of these solutions and wide gap semiconductors as hybrid optical limiters[2]. In this paper, we will present some recent results on the study of the optical nonlinearities of solutions of chloroaluminumphthalocyanine (CAP) in methanol and a silicon naphthalocyanine (SiNc) derivative, SiNc(OSi(hexyl)₃)₂ or SiNc, dissolved in toluene using the "Z-scan" technique[3].

The "Z-scan" technique involves measurement of the transmission of a focussed laser beam through a material as a function of the position of the material relative to the beam waist. Measurements are made on the total transmitted energy (dependent on nonlinear absorption) as well as on the energy transmitted through an aperture (dependent on nonlinear absorption and refraction) located in the far field. Thus, the measurements allow isolation of the nonlinear refraction(magnitude and sign) and nonlinear absorption.

While CAP is well known as a saturable absorber at 694 nm[4], it was used early on as a passive Q-switch for ruby lasers, it also exhibits excited state absorption at shorter wavelengths in the range between the so called Q and B bands where the linear absorption is quite weak. Figure 1 illustrates the excited state absorption in CAP and SiNc solutions at 532 nm with a plot of total transmitted energy vs. input energy (expressed as fluence) measured using unfocussed nanosecond pulses. Since the dye concentrations and linear absorption were the same the results suggest stronger excited state absorption for SiNc. In the transient regime, the intensity dependent transmission depends on the energy level structure, absorption cross-sections and the various relaxation rates. For pulses short relative to the decay time of the intermediate level(first excited singlet state), relaxation out of the intermediate may be neglected and the analysis is simplified. Total energy Z-scan measurements using 30 psec (much shorter than the excited singlet state lifetimes of CAP and SiNc) 532 nm pulses have been performed and analyzed using a three-level sequential-absorption model. Excited state absorption cross-sections of $4 \times 10^{-17} \text{ cm}^2$ and $5 \times 10^{-17} \text{ cm}^2$ have been obtained for CAP and SiNc, respectively. Results obtained on CAP with a train of

about ten 30 psec pulses spaced by 10 nsec show a cumulative effect demonstrating the importance of triplet-triplet absorption at long times, see Figure 2. These results will be discussed in the context of a rate equation analysis.

Z-scan measurements with picosecond pulses in both CAP and SiNc show that the nonlinear refraction is self-focussing. For a solution concentration of 6×10^{-4} moles/liter we obtain n_2 values of 3.3×10^{-12} esu and 4×10^{-12} esu for CAP and SiNc, respectively. While the dyes are relatively dilute, these values are roughly an order of magnitude larger than those of the pure solvents, indicating large nonlinearities for the dyes.

1. D. R. Coulter et al., Proc. SPIE Vol. 1105, "Materials for Optical Switches, Isolators and Limiters (1989).
2. T. H. Wei et al., CLEO '90 Digest of Technical Papers, Anaheim (1990)
3. E. W. Van Stryland et al., *J. Opt. Soc. Am.*, **B5**, 1980 (1988).
4. W. E. K. Gibbs, *Appl. Phys. Lett.*, 11(4), 113 (1967); J. A. Armstrong, *J. Appl. Phys.*, 36, 471 (1965).

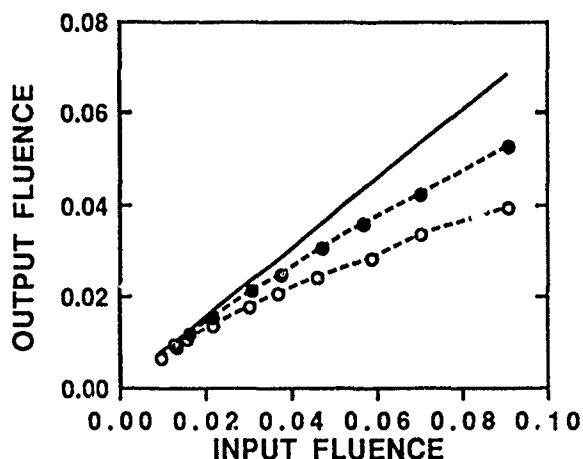


Figure 1. Nanosecond nonlinear absorption of CAP (filled circles) and SiNc solutions. Fluences are in J/cm^2 . Solid line corresponds to linear absorption ($T = 75\%$).

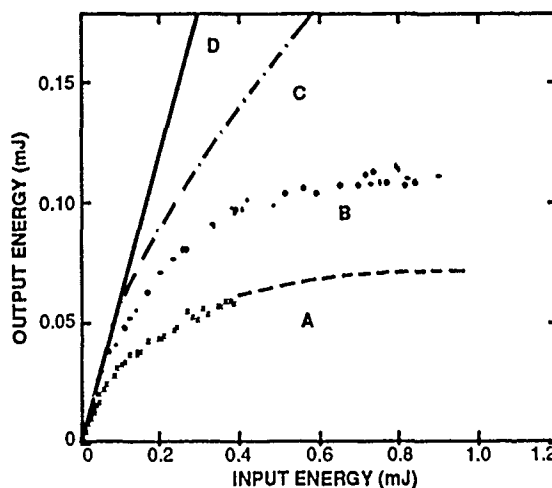


Figure 2. Picosecond nonlinear absorption of CAP solution. A) Data for single 30 psec pulses, B) Data for pulse train, C) Calculated pulse train response assuming response to each pulse is independent, D) Linear absorption ($T = 58\%$).

MP26 All-Optical Switching in New Nonlinear X-Junctions

Hiroshi MURATA, Masayuki IZUTSU and Tadasi SUETA

Faculty of Engineering Science
Osaka University
Toyonaka Osaka 560 Japan

We found numerically all-optical switching in novel nonlinear X-junctions, where one branch is made from Kerr like material, while the others from linear one. The output port of the signal light can be switched by the power of control light. The unbalance of nonlinearity between branches causes all-optical switching. Fig.1 shows the nonlinear X-junction we proposed. It consists of four single-mode branches with different width. The branch-3 has Kerr like nonlinearity. The signal light is launched to the branch-2 and control light to the branch-1.

In a sufficiently small branching angle range, a thin cross-section of the branching region can be regarded as a part of five-layer straight waveguide, so that the branching waveguides can be analyzed by using a concept of local normal mode. The signal light from branch-2 moves to an even local mode with propagation, and the control light from branch-1 to an odd local mode. We have calculated the normal modes of the five-layer system with localized nonlinearity. The field distribution of modes is described by a Jacobian elliptic function[1]. Transmission power of modes versus effective index is shown in Fig.2. There exist three different even modes for the same transmission power. Fig.3 shows examples of field distributions of these modes. An induced nonlinear index change for the mode-a is bigger than that for the mode-c. It is expected that the even mode can be switched from c to a if a controlling light beam of a certain intensity is provided.

We analyzed the characteristics of all-optical switching by BPM[2]. For simplicity, no correlation between signal and control light is assumed, for instance wavelength of two beams are different. Fig.4 is calculated examples of the intensity variation of signal light. The signal light from the branch-2 propagates to the branch-4 when the intensity of control light is low, while to the branch-3 with the high intensity. Fig.4 shows the signal transmission of each branch versus the normalized control power. All-optical switching is presented. For semiconductor doped glass waveguides[3], switching is achieved at several hundreds mW power range.

When the signal and the control lights are coherent, switching characteristics will be complicated because of the interference effect of two beams. Further details will be presented in the talk.

REFERENCES

- [1] A.D.Boardman and P.Egan, IEEE J.Quantum Electron., QE-22,2,319/324(1986). [2] J.van Roey, J.van der Donk and P.E.Lagasse, J. Opt.Soc.Am., 71,7,803/810(1981). [3] T.J.Cullen, C.N.Ironside, C.T.Seaton and G.J.Stegeman, Appl.Phys.Lett., 49,21,1403/1405(1986)

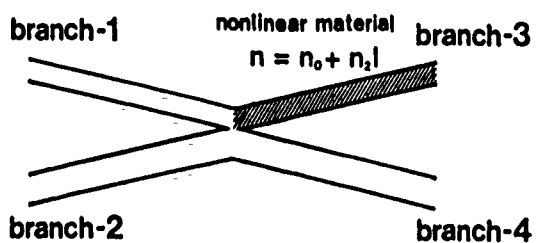


Fig.1. Nonlinear X-junction.

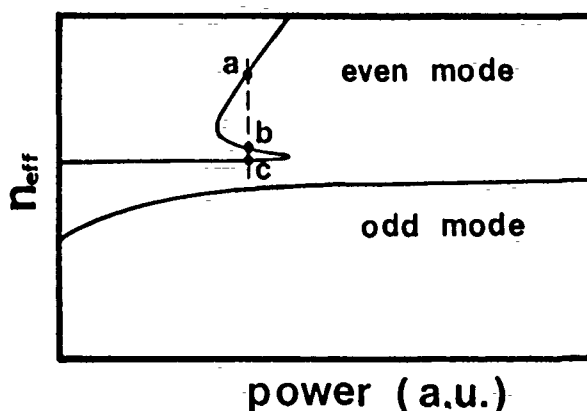


Fig.2. The effective index of local normal modes vs. transmission power.

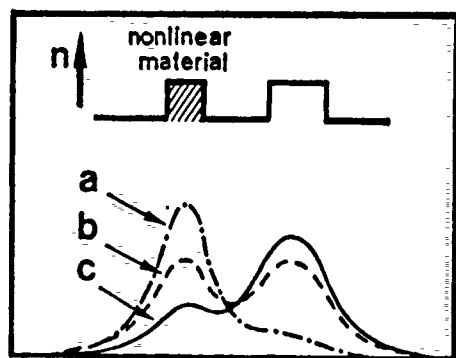


Fig.3. Field distributions of local normal mode with the same transmission power.

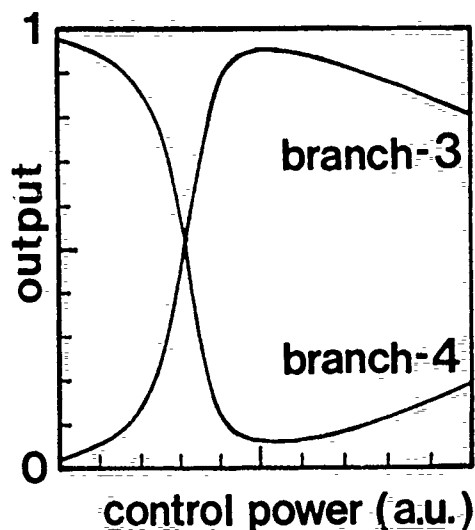


Fig.5. The signal transmission of each branch vs. control power.

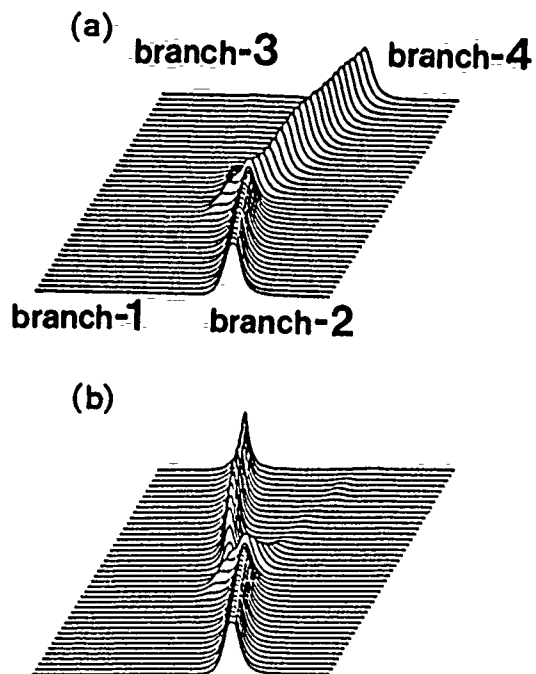


Fig.4. Intensity variations of the signal light at (a) low control power (b) high control power.

Saturation of the Hyperpolarizability of Oligothiophenes

H. Thienpont*, G.L.J.A. Rikken and E.W. Meijer**, Philips Research Laboratories, P.O. Box 80000, NL-5600 JA Eindhoven, The Netherlands.

W. ten Hoeve and H. Wynberg, Syncom BV, University of Groningen, P.O. Box 2253, NL-9704 CG Groningen, The Netherlands.

* Vrije Universiteit Brussel, Dienst Toegepaste Natuurkunde, Pleinlaan 2, B-1050 Brussel, Belgium.

** DSM Research, P.O. Box 18, NL-6160 MD Geleen, The Netherlands.

Conjugated organic molecules have attracted much attention for their nonlinear optical properties, both from a fundamental point of view and for their potential in optical data processing. Many theoretical studies on the length dependence of the second hyperpolarizability γ have been published, that all predict a strong increase of γ with chain length. Only at approximately 15 double bonds in polyacetylene, saturation of γ is predicted¹.

Recently, a systematic experimental study of α and γ was reported by Zhao et al² for a series of oligothiophenes, ranging in length from 1 to 6 repeat units, in which no saturation was observed. By using a new synthetic route, that will be published separately, we have made soluble thiophene oligomers with 3, 4, 5, 7, 9, and 11 repeat units (table 1). We here report on measurements of the bandgap, the polarizability α and the second hyperpolarizability γ of these well-defined molecules.

Thin film samples were prepared by introducing a few mass % oligothiophene in a PMMA matrix. The polarizabilities were determined from accurate refractive index measurements at 632.8 nm. Electric field induced second harmonic generation (EFISH) was used to determine the orientation averaged $\langle \gamma(-2\omega; \omega, \omega, 0) \rangle$ at room temperature at a fundamental wavelength of 1064 nm.

The results are visualized in the figures 1 and 2. As a linear behavior is typical for non-conjugated molecules, these observations show that for $N \geq 7$ the oligothiophenes can no longer be considered as fully conjugated. The saturation of γ can have an electronic or a conformational origin. For the polyenes many theoretical results, both *ab initio* and semi-empirical, are available. Fortunately, it is well established that the linear optical properties of the oligothiophenes are similar to those of the polyenes that would result from taking out the sulphur atom. Furthermore, Heflin et al³ have shown that the conformation of a polyene is not essential as long as it is planar, and that the calculated γ is determined by the geometrical length

of the molecule. Using this and the theoretical results of Beratan et al¹ for polyenes, saturation of the γ of *planar* oligothiophenes between 7 and 8 repeat units is predicted, in fair agreement with our experimental findings.

It is however not obvious that these molecules are fully planar; poly-3-alkyl-thiophenes show a strong solvatochromism and thermochromism, which are attributed to twisting of (groups of) rings around the connecting bond, disrupting the conjugation. We also observe solvatochromism and thermochromism for the longer oligothiophenes, albeit rather weak, which indicate that these molecules are not fully planar in a PMMA matrix at room temperature and that somewhat larger hyperpolarizabilities can be expected if the molecules could be planarized.

- 1) D.N. Beratan, J.N. Onuchic and J.W. Perry, J. Phys. Chem. 91, 2697 (1987).
- 2) M. Zhao, B.P. Singh and P.N. Prasad, J. Chem. Phys. 89, 5535 (1988).
- 3) J.R. Heflin, K.Y. Wong, O. Zamani-Khamiri and A.F. Garito. Phys. Rev B38, 1573 (1988).

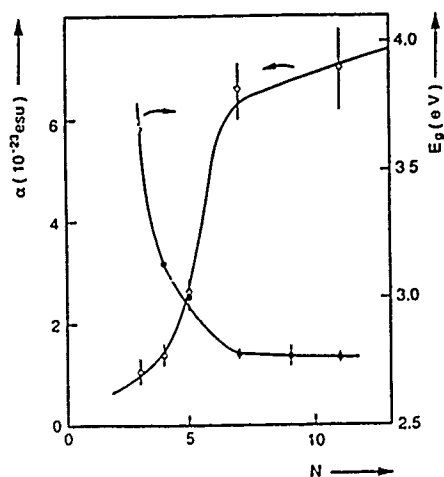
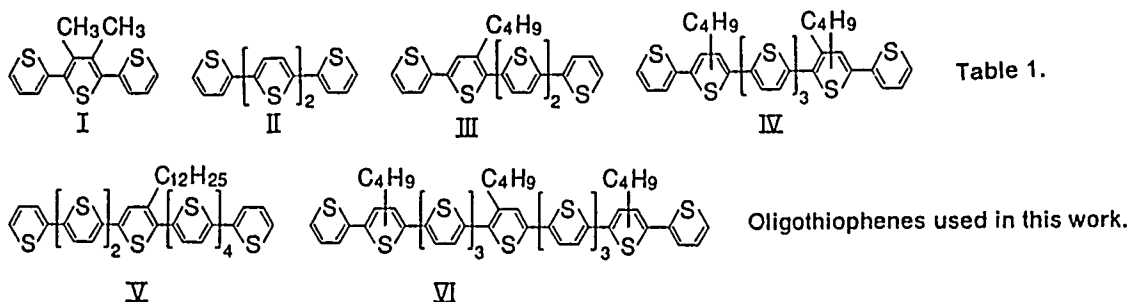


Figure 1. Polarizability and band gap versus the number of repeat units for oligothiophenes in PMMA.

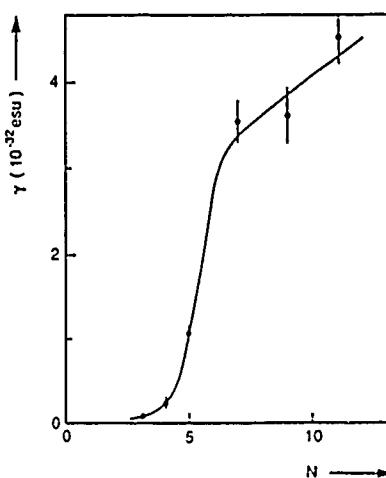


Figure 2. Second hyperpolarizability versus the number of repeat units for oligothiophenes in PMMA.

TUESDAY, JULY 17
ORAL PRESENTATIONS

Phase-Conjugate Interferometry

Ian McMichael
Rockwell International Science Center
1049 Camino Dos Rios
Thousand Oaks, CA 91360

Distortion correction by phase-conjugation as shown in Fig. 1 is probably more familiar than phase-conjugate interferometry as shown in Fig. 2. However, as the similarity of the figures indicates, these processes are closely related. In the process of distortion correction shown in Fig. 1, when an incident plane wave passes through a distorter, the resulting wavefront can be represented as a sum of many plane wave components. When retroreflected from a phase conjugate mirror, the relative phases of these plane wave components are such that when they "interferometrically" recombine at the distorter, they reproduce the incident plane wave. Phase conjugate interferometry, as shown in Fig. 2, is very similar, except that an incident plane wave, instead of being converted into many plane wave components by a distorter, is often split into two well defined beams by a beam splitter. As with the case of distortion correction, the relative phase of the retroreflected beams is such that they "add" in the direction counterpropagating to the incident wave, and "subtract" out the other port of the beam splitter.

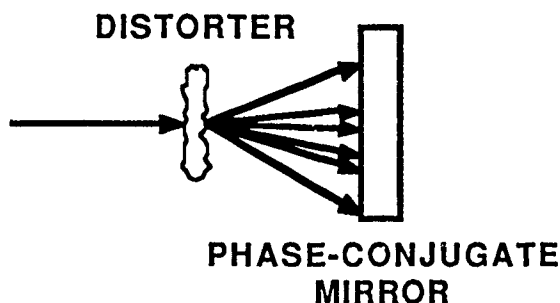


Fig. 1 Distortion correction by phase conjugation.

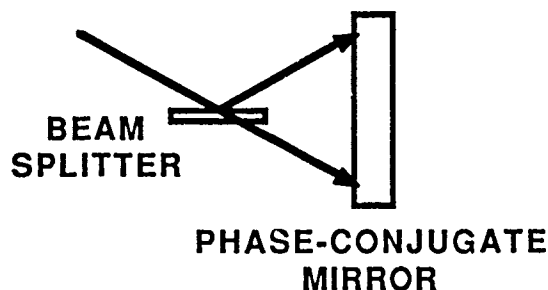


Fig. 2 Phase-conjugate interferometry.

The phase-conjugate interferometer shown in Fig. 2 is one example chosen to illustrate its relationship to distortion correction. A large number of phase-conjugate interferometers have been reported, and a sample of these is shown in Fig. 3. Perhaps the first demonstrated application of phase-conjugate interferometry was Basov's scheme for obtaining polarization-preserving phase conjugation shown in the upper right of Fig. 3. More recent and very interesting applications are in the area of image processing. They include image subtraction, novelty filters, and parallel optical computation. Other applications include gyros, hydrophones, interferometric holography, and measurements of phase shifts of phase-conjugate waves and photorefractive gratings.

These applications take advantage of the following unusual properties of phase-conjugate interferometers; real time distortion correction, self-referencing, self-biasing, wide field-of-view, and alignment insensitivity. The real time distortion correction of phase-conjugate interferometers allows them to use low cost multimode fibers while maintaining interferometric sensitivity. When the two arms of an interferometer are terminated on the same phase-conjugate mirror, as is the case in the upper three interferometers in Fig. 3, the beams reflected from the phase-conjugate mirror have the same relative phase relationship as the incident beams. This is a result of the holographic process that generates the conjugate waves, and we refer to this as self-referencing. If the phase-conjugate mirror is dynamic, then the self-referencing is also dynamic, and the

interferometer can operate even in the presence of environmental perturbations that would overwhelm the signal from conventional interferometers. Depending on the configuration and nonlinear material used in the phase-conjugate mirror, the output from a phase-conjugate interferometer can be a maxima, a minima, the point of maximum slope, or anything inbetween. This property can be exploited to make self-biased interferometers. Alignment of phase-conjugate interferometers is relatively easy; one merely needs to insure the incident beams overlap with the pumping beams in the nonlinear medium.

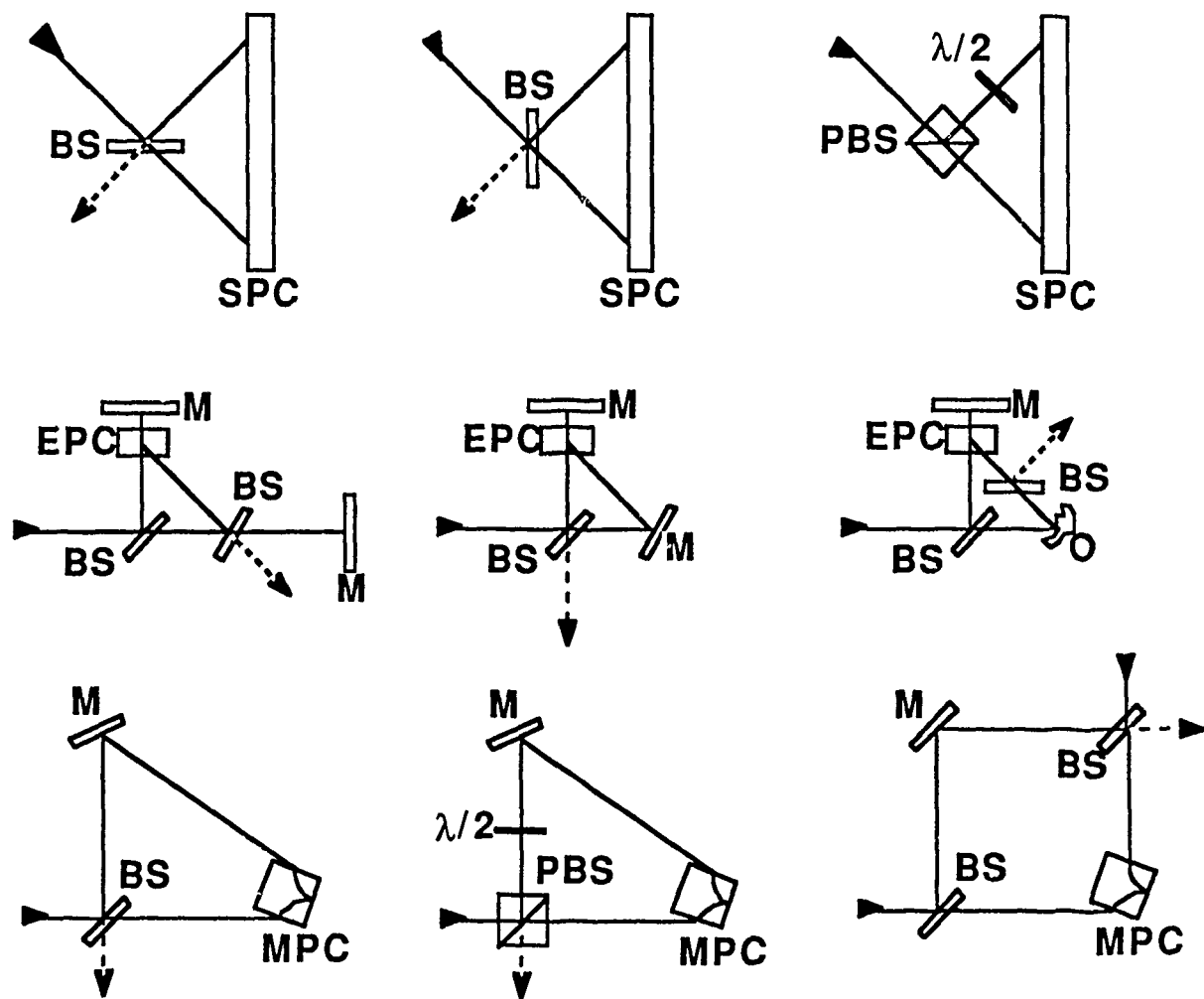


Fig. 3 A sampling of phase-conjugate interferometers reported in the literature. BS - beam splitter, SPC - self-pumped conjugator, PBS - polarizing beam splitter, $\lambda/2$ - half-wave retarder, M - mirror, EPC - externally pumped conjugator, O - object, MPC - mutually pumped conjugator.

In our talk, we will emphasize two applications of phase-conjugate interferometers; phase-conjugate fiber-optic gyros and measurements of the phase of phase-conjugate waves.

Partial support provided by the Office of Naval Research contract N0014-88-C-0230.

Gilbert Grynberg

Laboratoire de Spectroscopie Hertzienne de l'Ecole Normale Supérieure
 Université Pierre et Marie Curie - 75252 PARIS Cedex 05 - France

A non-linear medium interacting with two intense counterpropagating beams can give rise to a four-wave mixing gain for a probe wave [1]. This gain can be sufficient to observe oscillation when the medium is placed inside a cavity [2], or placed in front of a single mirror [3] or even in free space without any mirrors [4].

When the medium is enclosed inside a ring cavity (fig. 1), the intensities of the two beams emitted in the two counterrotating directions exhibit a strong correlation. It has been shown that the noise on the intensity difference ($I_1 - I_2$) is smaller than the shot-noise limit. An experimental observation done using sodium shows that a quantum noise reduction of 10% is obtained above threshold [5]. Furthermore a recent theoretical analysis [6] predicts that a larger reduction could be achieved.

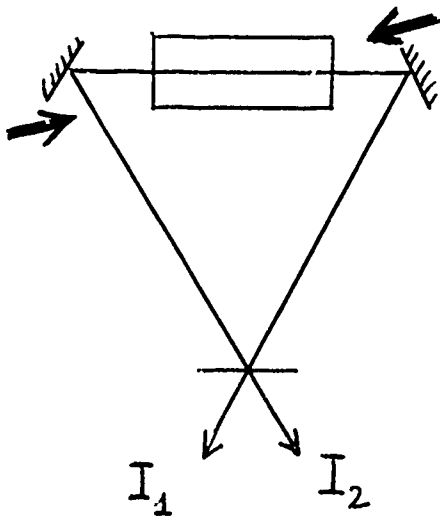


Figure 1 : Scheme of a ring four-wave mixing oscillator.

If the gain is sufficiently high (by using high density vapors and high intensity counterpropagating pump beams) the oscillation can be observed without any cavity [4]. The oscillation generally appears as a ring surrounding the pump beams (fig. 2). This ring is observed on the self-focusing side of the resonance. The light polarization in the ring can be either identical to the pump beam polarization or orthogonal to it depending on the experimental conditions. The different behaviours can be

understood from the analysis of the optical pumping.

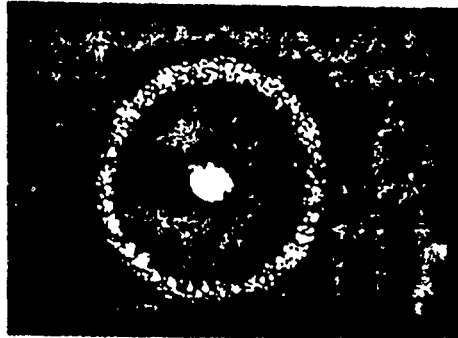


Fig. 2 : Conical emission in a standing wave (experiment done with sodium)

The preceeding effects are examples of the variety of physical phenomena involved in four-wave mixing oscillation.

- [1] A. Yariv and D.M. Pepper, Opt. Lett. 1, 16 (1977)
- [2] D. Grandclément, G. Grynberg and M. Pinard, Phys. Rev. Lett. 59, 44 (1987)
- [3] D.M. Bloom, P.F. Liao and N.P. Economou, Opt. Lett. 2, 58 (1978)
- [4] G. Grynberg, , E. Le Bihan, P. Verkerk, P. Simoneau, J.R.R. Leite, D. Bloch, S. Le Boiteux, and M. Ducloy, Opt. Commun. 67, 363 (1988) ; J. Pender and L. Hesselink, IEEE J. of Quantum El. 25, 395 (1989) ; D.J. Gauthier, M.S. Malcuit, A.L. Gaeta and R.W. Boyd, Phys. Rev. Lett. 64, 1721 (1990)
- [5] M. Vallet, M. Pinard and G. Grynberg, Europhys. Lett. 11, 739 (1990)
- [6] W. Zhang and D. Walls (private communication).

Degenerate Four Wave Mixing with Pulsed Lasers: Theory and Applications

P. Ewart

Clarendon Laboratory, University of Oxford, Parks Road, Oxford OX1 3PU, U.K.

Resonant Degenerate Four Wave Mixing, DFWM, is a nonlinear optical process arising from the third order susceptibility $\chi^{(3)}$. Resonance enhancement of $\chi^{(3)}$ in absorbing media makes the process useful for spectroscopic applications[1]. In many situations pulsed, high power lasers are used which have broad spectral bandwidths. The stochastic fluctuations of amplitude and phase associated with this bandwidth complicates the theoretical description in such cases. An averaging of the atom-field interaction is required simultaneously over the temporal and spatial variations of the fields. A solution has been found in the broad bandwidth limit which uses an appropriate decorrelation approximation. Theoretical and experimental results will be presented for the effects of laser bandwidth on the power dependence and temporal behaviour of resonant DFWM[2].

Time delayed FWM processes, closely related to transient grating methods, are often used to study ultra-fast relaxation phenomena[3]. Using incoherent (broad bandwidth) light a temporal resolution may be achieved which is limited only by the coherence time which may be much shorter than the pulse duration. Autocorrelation measurements may be made in such experiments which give information on relaxation rates in the medium or on the spectral structure of the laser light itself. Experiments of this type will be described giving evidence of the effects of radiation trapping on the nonlinear process of DFWM.

Resonant DFWM using tunable pulsed lasers is emerging as a potentially powerful tool for combustion diagnostics. The process shares the coherence properties of Coherent Anti-Stokes Raman Scattering (CARS) but has the sensitivity of Laser Induced Fluorescence (LIF) owing to the strongly resonant nature of the interaction. Species of combustion interest such as OH have been detected by this method[4] and the DFWM spectra used to make accurate temperature measurements in a flame[5]. A powerful feature of the technique is its ability to provide 2-dimensional maps of concentration distributions with a single laser shot giving high temporal and spatial resolution[6]. The *phase conjugate* property of the DFWM signals is exploited to enhance noise rejection for applications in highly luminous or scattering flames. Recent results of experiments giving 2-dimensional mapping of both temperature and concentration in flames will be reported. A further development - multiplex DFWM - which may yield single shot temperature measurements will be described.

References

- [1] *Optical Phase Conjugation*, R.A. Fisher, Ed. Academic Press, (1983)
- [2] J. Cooper, A. Charlton, D.R. Meacher, P. Ewart and G. Alber, Phys. Rev. A **40**, 5705, (1989); D.R. Meacher, A. Charlton, P. Ewart, J. Cooper and G. Alber, Phys. Rev. A (1990) *accepted for publication*.
- [3] *Laser Induced Dynamic Gratings*, H.J. Eichler, P. Gunter and D.W. Pohl, Springer-Verlag, (1986).
- [4] P. Ewart and S.V. O'Leary, Optics Lett., **11**, 279, (1986)
- [5] T. Dreier and D.J. Rakestraw, Optics Lett., **15**, 71, (1990)
- [6] P. Ewart, P. Snowden and I. Magnusson, Optics Lett. **14**, 563, (1989)

A. F. GARITO, J. R. HEFLIN, N. Q. WANG, and Y. M. CAI

Department of Physics

University of Pennsylvania

Philadelphia, PA 19104

In atoms and molecules, nonresonant second order and third order optical processes mediated by virtual electronic excitations are described by their microscopic second order $\beta_{ijk}(-\omega_3; \omega_1, \omega_2)$ and third order $\gamma_{ijkl}(-\omega_4; \omega_1, \omega_2, \omega_3)$ optical susceptibilities, respectively. In general, the real population of the initial state for the virtual electronic excitations of $\beta_{ijk}(-\omega_3; \omega_1, \omega_2)$ and $\gamma_{ijkl}(-\omega_4; \omega_1, \omega_2, \omega_3)$ can be either the usual singlet ground state S_0 , or an optically pumped excited state S_n . In a nonlinear optical medium consisting of quasi-one (1D) or two (2D) dimensional chain-like or disc-like conjugated structures, compared to the ground state, the nonresonant excited state $\beta_{ijk}^{S_n}(-\omega_3; \omega_1, \omega_2)$ or $\gamma_{ijkl}^{S_n}(-\omega_4; \omega_1, \omega_2, \omega_3)$ can markedly increase, or even change sign, when the first (S_1), or second (S_2), π -electron excited state is optically pumped and then populated for timescales sufficiently long to allow nonresonant measurements of $\beta_{ijk}^{S_n}(-\omega_3; \omega_1, \omega_2)$ or $\gamma_{ijkl}^{S_n}(-\omega_4; \omega_1, \omega_2, \omega_3)$.^[1] The principal reasons are the larger optical transition moments and smaller excitation energies between excited states, especially for highly charge correlated virtual excitations.

In recent experiments, two to three orders of magnitude enhancement was observed in the nonresonant third harmonic susceptibility $\gamma^{S_1}(-3\omega; \omega, \omega, \omega)$ when the S_1 π -electron excited state of a disc-like structure having a decay time of a few nanoseconds was populated by direct optical pumping at one frequency and then probed nonresonantly at a different frequency by time delayed picosecond pulses through the third harmonic process.^[2] Whereas the ground state $\gamma^{S_0}(-3\omega; \omega, \omega, \omega)$ is less than $\pm 50 \times 10^{-36}$ esu, the excited state $\gamma^{S_1}(-3\omega; \omega, \omega, \omega)$ is measured to be -18100×10^{-36} esu. As shown in Figure 1, in the limit of negligible S_0 ground state contribution to the macroscopic $\chi^{(3)}(-3\omega; \omega, \omega, \omega)$, $\chi_{S_1}^{(3)}(-3\omega; \omega, \omega, \omega)$ is directly proportional to the S_1 population and decays exponentially within the S_1 lifetime.

Thus, by optical pumping into a designated electronic state within an excited state manifold, second order and third order optical properties can be controllably selected to greatly enhance their magnitude, or change their sign. In turn, new material structures,

compositions, and phases can be developed to include enhanced nonlinear optical and electrooptical properties originating from real population of not only the ground state but also excited electronic states. Furthermore, the study of excited state nonlinear optical responses in this manner should prove a general method in the nonlinear optical spectroscopy of excited electronic states and their dynamics.

- [1]. J. R. Heflin, K. Y. Wong, O. Zamani-Khamiri, and A. F. Garito, Phys. Rev. B38, 1573 (1988); J. W. Wu, J. R. Heflin, R. A. Norwood, K. Y. Wong, O. Zamani-Khamiri, A. F. Garito, P. Kalyanaraman, and J. Sounik, J. Opt. Soc. Am. B 6, 707 (1989); A. F. Garito, OSA Annual Meeting 1989, Technical Digest Series, Vol. 18 (Optical Society of America, Washington, D. C., 1989) p. 22; and references therein.
- [2]. J. R. Heflin, N. Q. Wang, Y. M. Cai, and A. F. Garito, Phys. Rev. Lett. (submitted).

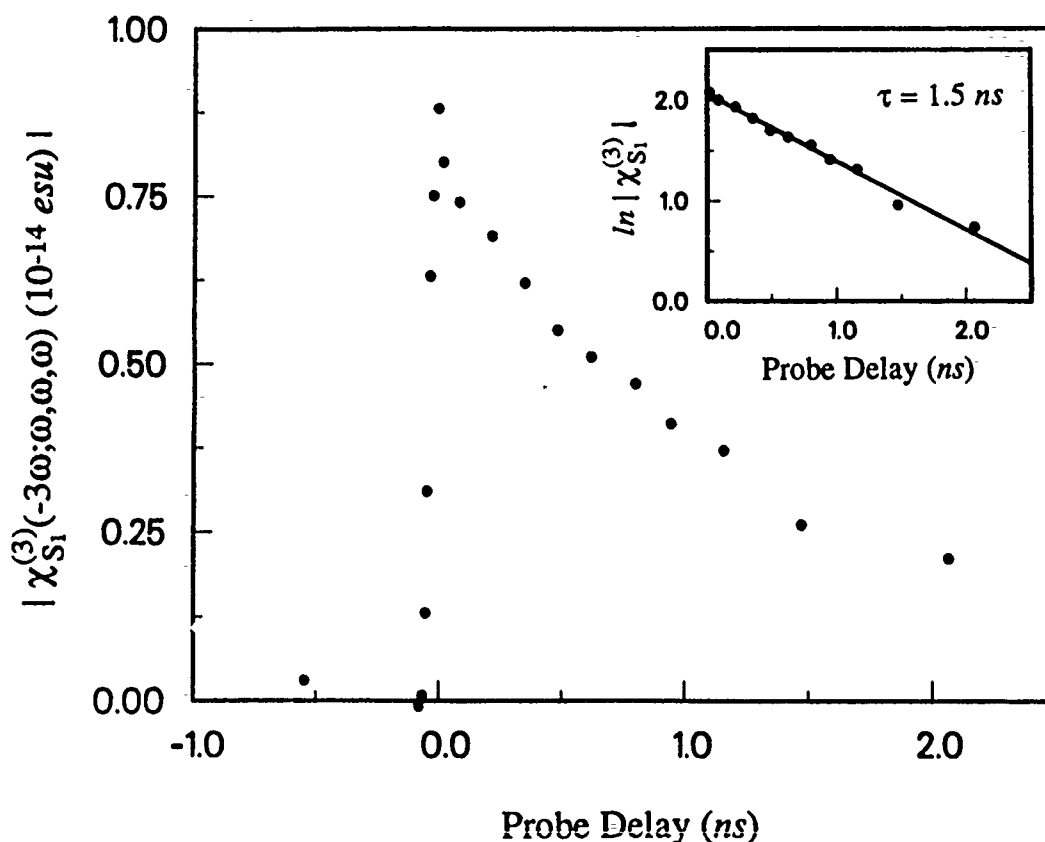


Figure 1. $\chi_{S1}^{(3)}(-3\omega; \omega, \omega, \omega)$ as a function of the time delay between the pump and probe beams. As shown in the inset, the data is well-fit by a decay $e^{-t/\tau}$ with an S_1 lifetime of $\tau = 1.50 \pm 0.05 \text{ ns}$.

Ultrafast Relaxation in Polymers with Large Optical Nonlinearity

Takayoshi Kobayashi and Masayuki Yoshizawa

Department of Physics, Faculty of Science, University of Tokyo,
7-3-1 Hongo, Bunkyo, Tokyo 113, Japan

In recent years, there has been great interest in optical and electrical properties of conjugated polymers because of their large and fast optical nonlinearities and their role as model compounds for quasi-one dimensional semiconductors. Recent progress in the field of high speed optoelectronics has encouraged the search for new materials with large third-order nonlinear optical susceptibilities. Conjugated polymers seem to be very promising candidates for future practical applications in nonlinear optical devices.

In the present study, time evolution in polydiacetylenes (PDA-3BCMU and PDA-4BCMU) and poly(3-methylthiophene) (P3MT) was investigated by absorption and luminescence spectroscopies from femtoseconds to microseconds.¹⁻³ The samples of PDA-3BCMU and PDA-4BCMU (butoxycarbonylmethylurethane) are cast films of about 100 nm thickness on glass substrates. About 1 μm -thick films of P3MT was prepared by electrochemical polymerization on glass substrates.

The transient photoinduced absorbance changes in P3MT are shown in Fig. 1. The bleaching due to ground-state depletion appears around 2.0 eV and broad-band absorption below the band-gap is due to self-trapped excitons. A small minimum at 1.8 eV can be explained in terms of Raman gain. The Raman shift is 1450 cm^{-1} and is assigned to the C=C stretching vibration. The absorbance changes due to several nonlinear optical processes, i.e. hole burning, Raman gain, resonant Kerr effect, and optical Stark effect were observed both in PDA and P3MT at the short delay times.

Figure 2 shows the time dependence of the absorbance change (ΔA) at 1.77 eV in PDA-3BCMU. The formation time of the self-trapped excitons is estimated from the rise time of ΔA as to be 150 ± 50 fs and 70 ± 50 fs in PDA-3BCMU and P3MT, respectively. The decay times of the self-trapped excitons at 10 K are 2.0 ± 0.1 ps, 3.0 ± 0.3 ps, and 800 ± 100 fs in PDA-3BCMU, PDA-4BCMU, and P3MT, respectively.

In conclusion, the relaxation from photoexcited free excitons to self-trapped excitons was observed in PDA-3BCMU and P3MT for the first time. The difference in the dynamics of excitons among PDA-3BCMU, PDA-4BCMU, and P3MT was compared and explained in terms of the differences in main chain structures and the size of the side groups. A model of relaxation dynamics of photoexcitations in conjugated polymers will be given to successfully explain all the experimental data taken by us and other groups.

1. M. Yoshizawa, M. Taiji, and T. Kobayashi, IEEE J. Quantum Electron. QE-25, (1989) 2532.
2. U. Stamm, M. Taiji, M. Yoshizawa, K. Yoshino, and T. Kobayashi, Mol. Cryst. Liq. Cryst. 182A (1990) 147.
3. T. Kobayashi, M. Yoshizawa, U. Stamm, M. Hasegawa, and M. Taiji, J. Opt. Soc. Am. B. (Special Issue on the Application of the Ultrafast Spectroscopy to Chemistry and Biology), to be published.

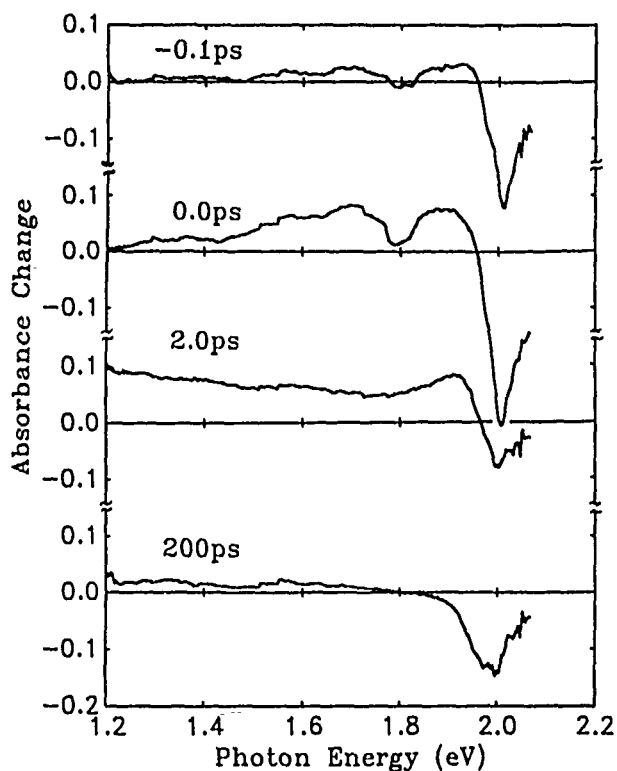


Fig. 1. Transient absorption spectra in P3MT at 10 K excited by 100-fs pump pulse. The pump photon energy is 1.97 eV.

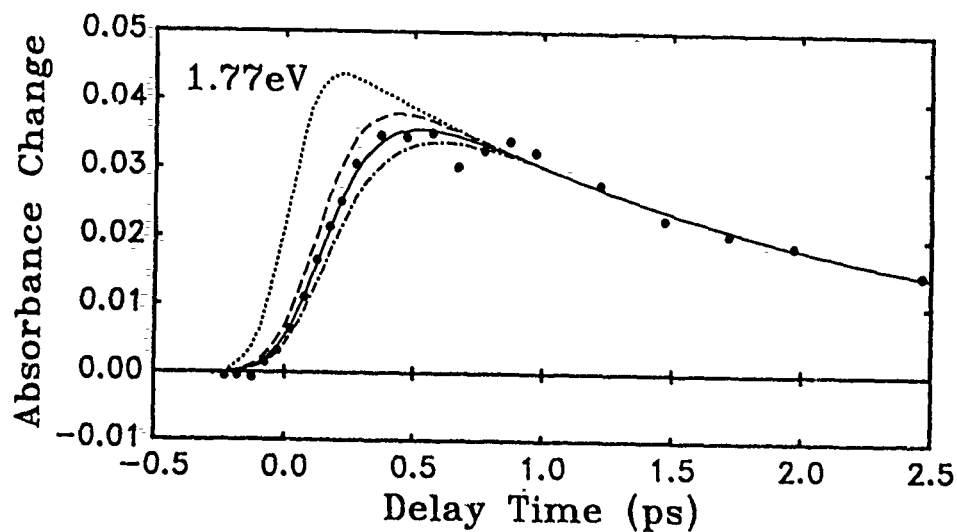


Fig. 2. Time dependence of the absorbance change at 1.77 eV in PDA-3ECMU at 10 K. Curves are the calculated transient absorbance changes with the formation time of 0 fs (dotted curve), 100 fs (dashed curve), 150 fs (solid curve), and 200 fs (dash-dotted curve). The decay time is estimated to be 2.0 ps from the absorbance changes at the delay times longer than 1.0 ps. The durations of pump and probe pulses are both 150 fs.

Polymer Dispersed Liquid Crystals - New Materials for Nonlinear Optics

F. Simoni

Dipartimento di Scienze Fisiche, Università di Napoli, Piazzale Tecchio 80,
80125 Napoli, Italy

G. Cipparrone, D. Duca, C. Umeton

Dipartimento di Fisica, Università della Calabria, 87036 Rende (CS), Italy

I.C. Khoo

Department of Electrical Engineering, Pennsylvania State University,
University Park, Pennsylvania 16802, USA

We present several nonlinear optical effects observed in dye doped Polymer Dispersed Liquid Crystals (PDLC). They are plastic polymeric matrices containing minodroplets of nematic liquid crystals, therefore their optical properties are affected by the strong light scattering induced by the droplets (size $\sim 0.1 \div 1 \mu\text{m}$).

The following features make PDLC very interesting for nonlinear optics:

- a) they are solid materials with optical properties strongly dependent on liquid crystal orientation.
- b) they are two-components media where light scattering may be easily controlled; therefore they are materials suitable to study nonlinear scattering.
- c) they allow to couple orientational and thermal properties of liquid crystals to produce nonlinear optical effects.

In the experiments which we present, we have used dye doped samples of PDLC in order to enhance the thermal nonlinearities induced by light absorption. In fact the light scattering depends on the indexes mismatch

$\delta = n_{\text{eff}}^2 - n_p^2$, where n_{eff} is the effective refractive index of the droplet and n_p is the refractive index of the polymeric matrix. The absorption of radiation by the dye molecules and subsequent thermalization process heats the PDLC sample, thus changing the quantity δ through the thermal indexing effect.

We have studied the nonlinear light scattering with the observation of self-transparency occurring when the liquid crystal droplets reach the transition temperature to the isotropic state and the indexes mismatch δ approaches zero.

In a second experiment thermal grating has been induced in PDLC. We have studied the nonlinear light diffraction which show a typical threshold behavior due to the mentioned self-transparency effect. Phase and amplitude gratings have been created under different experimental conditions.

Finally the coupling of the orientational and thermal properties of liquid crystals have been exploited to get all optical switching and bistability in PDLC. In this case the light scattering was suppressed by a bias voltage applied to the sample and the nonlinear optical behavior was given by the increasing light absorption of the dye molecules.

T18 Nonlinear Optics of Nematic, Smectic and Cholesteric Liquid Crystals

I.C.Khoo^x, N.V.Tabiryan⁺

^xDep. of Electr. Engineering. The Pennsylvania State Univ.,
University Park, PA 16802

⁺Inst. of Appl. Probl. of Phys., Armenian Academy of Sci.,
Str. Nersisyan 25, 375014 Yerevan, USSR

Recent advances in nonlinear optics of liquid crystals (LC) are related to optically induced collective molecular reorientation processes, which account for non-resonant but huge nonlinearities. Those processes exhibit such spectacular features as propagation-induced reorientation, self-oscillations, etc. Jumps and hysteresises of LC's orientational state with changing incidence angle and intensity of light provides new schemes for optical bistability and opto-optical modulation. In certain circumstances, direct orientational interaction may be conquered by absorption-induced effects. Among several mechanisms to transform the energy of absorbed light beam into molecular reorientation, the strongest one utilizes generation of hydrodynamic motions. In this way, e.g., infrared-visible modulation turns out to be possible at microwatt power level. Thermally induced reorientation in cholesteric LC (CLC), resulting in its helix pitch change, is able to lead to a new effect of light wave tunneling through CLC's Bragg reflection region. A nonlinear resonator can be designed with intensity dependent reflection coefficients of CLC-mirrors. Thermal indexing itself can have remarkable contribution to nonlinear optics of LC. It provides, in particular, the effect of stationary energy exchange between two equal-frequency light waves through media with local and instantaneous nonlinear response. Thus degenerate wave mixing and beam cleaning turns out to be possible with only two incidence beams.

Optical Functional Devices Using Semiconductor Laser Nonlinearity

Hitoshi Kawaguchi

Yamagata University
Yonezawa-shi, Yamagata 992, Japan

Various kinds of optical functional devices, are constructed based on the nonlinearities of semiconductor lasers as shown in Table 1. The most distinctive feature is that they have optical gain. Optical gain results in the following advantages : (1) low optical switching power, high ON-OFF ratio, and large fan-out in bistable devices, (2) low operating power in optical wavelength converters, and (3) narrow bandwidth in optical wavelength filters.

Bistable Optical Devices

Absorptive and dispersive bistable devices are obtained using inhomogeneously excited LDs and resonant type LD amplifiers, respectively. Various methods of set-reset operation of bistable LDs have been obtained by means of all-optical ways [1]. Switching time and switching energy have been very much improved in the last few years.

Optical-Wavelength Conversion Devices and Filters

A tunable optical-wavelength conversion device has been demonstrated using a tandem type DFB LD [2]. The device has two main functions, i.e., (1) the device emits coherent light only when light is injected and (2) output wavelength is continuously tuned by changing the driving current. The performance of the device has been improved gradually. The tuning range of 3.5 nm was achieved by using a bistable LD with a DBR section and a phase shifter section [3]. High speed operation at 1 Gbit/s has been also demonstrated with extremely low input power [4].

Frequency conversion with use of nearly-degenerate four-wave mixing in travelling wave LD amplifiers is also attractive from the view point that coherent optical signals can be transmitted [5].

Using a multielectrode DFB LD amplifier, a narrow spectrum selection with a frequency tunability was achieved while maintaining a constant gain and a constant gain bandwidth. The frequency tunability is obtained by changing LD amplifier bias current through the carrier density dependence of the active layer refractive index [6]. A tuning range was extended to 120 GHz by using a phase-shift-controlled DFB LD [7].

Applications

Many proposals and experiments on applications of such optical functional devices have been reported in the field of optical fiber communication and photonic switching. Examples are as follows : bistable LDs as optical memories in time-division switching and in broadband subscriber loop [9], self-pulsation LDs as clock generators and bistable LDs as AND gates in all-optical

regenerators [10], and optical-wavelength convertors and filters in wavelength-division switching [11]. Such optical functional devices will become much more attractive for Gbit/s all-optical signal processing in the near future by combining with technologies of ultra-low threshold LDs and surface emitting LDs.

Reference

- [1] For example, H.Kawaguchi, Tech.Dig. OEC'90, Makuhari, Japan. (to be publised)
- [2] H.Kawaguchi et al., IEEE J. Quantum Electron., QE-24(1988)2153.
- [3] S.Yamakoshi, Tech.Dig. IOOC'89, Kobe, 21A3-3.
- [4] K.Kondo et al., Tech.Dig. PS'90, Kobe, 13D-9.
- [5] G.Großkopf et al., Tech.Dig. PS'90, Kobe, 13D-6.
- [6] K.Magari et al., IEEE J. Quantum Electron., QE-24(1988)2178.
- [7] T.Numai et al., Appl.Phys.Lett., 54(1989)1859.
- [8] S.Suzuki et al., J.Lightwave Technol., LT-4(1986)894.
- [9] N.Fujimoto et al., Tech.Dig. PS'90, Kobe, 13C-15.
- [10] M.Jinnō et al., Electron.Lett., 25(1989)1332.
- [11] H.Kawaguchi et al., Tech.Dig. 46th DRC, Boulder, (1988) VI A-5.

Table 1. Optical Functional Devices Using Semiconductor Laser Nonlinearity

LD structure	Function	Application
Inhomogeneously excited LD	Bistability	Memory
	Pulsation	
Resonant type LD amplifier	Thresholding and Logic operation	Wavelength conversion
		Wavelength filter
Travelling wave LD amplifier	Wavelength selective amplification	Clock regeneration
	Four-wave mixing	Decision

TI10 Application of Nonlinear Semiconductor Laser Amplifiers

R. P. Webb, *British Telecom Research Laboratories,
Martlesham Heath, Ipswich IP5 7RE, UK.*

Nonlinear optics offers the potential for all-optical implementation of switching and logic functions required in communication and processing systems. But most of the devices fast enough to stand comparison with their electronic equivalents require optical power levels that would be prohibitively high in multi-element systems. Semiconductor laser amplifiers, however, show significant intensity-dependent dispersion, associated with the gain saturation, at μW power levels and on ns time scales. In wavelength-multiplexed transmission systems, this is a limitation because four-wave mixing causes intermodulation between channels that are too closely spaced;^{1,2} but the same nonlinear behaviour can be exploited to produce optical gates, bistables, switches and wavelength translators.³⁻⁶ Thus semiconductor amplifiers allow nonlinear optical devices to be demonstrated at low powers. Also, they are suited to monolithic integration with waveguides and electronic devices to form complex systems.

We demonstrated the first all-optical regeneration of a 140 Mbit/s data stream, using an amplifier operating as an optically clocked bistable (OCB).⁴ Since the OCB's operation was based on dispersive bistability in a Fabry-Perot amplifier (Fig. 1), it suffered from the practical disadvantage that its sensitivity to the incoming data stream was strongly wavelength dependent. In this paper, experimental results on a modified implementation which overcomes this limitation will be presented for the first time.

In general, to prevent the sensitivity to the data input being wavelength dependent requires that the optical field carrying the data signal should experience no resonance. The field carrying the clock signal, however, must resonate to obtain dispersive bistability and both fields must interact in the nonlinear gain medium in the resonant cavity for correct operation of the OCB. Data and clock fields must therefore be in orthogonal modes with only one coupled to a resonator, but both experiencing gain from the same population of excited electronic states, for example, by spatial overlap in the gain region (Fig. 2).

Our experimental system (Fig. 3) employs orthogonal polarisations to separate the clock and data fields. The TE mode can resonate between the uncoated amplifier facet and the external mirror, but the polarising beam splitter prevents the TM mode from doing so and provides a port for coupling to this mode. Measurements with a wavelength-swept source showed Fabry-Perot resonances for the TE mode (with asymmetry resulting from nonlinearity) and no resonance for the TM mode.

1. "Experimental confirmation of a laser amplifier intermodulation model", R. P. Webb and T. G. Hodgkinson, *Electron. Lett.*, 1989, **25**, pp. 491-493.
2. "Communications theory analysis of multichannel carrier density intermodulation distortion effects in a semiconductor optical amplifier", T. G. Hodgkinson and R. P. Webb, *IEEE Photonics Technology Letters*, 1990, **2**, pp. 69-71.
3. "High contrast 1.3 μm optical AND gate with gain", W. F. Sharfin and M. Dagenais, *Appl. Phys. Lett.*, 1986, **48**, p 1510.
4. "Error-rate measurements on an all-optically regenerated signal", R. P. Webb, *Optical and Quantum Electronics*, 1987, **19**, pp. S57-60.
5. "All-optical flip-flop operation in an optically bistable device using two lights of different frequencies", K. Inoue, *Opt. Lett.*, 1987, **12**, p 918.
6. "Optical frequency exchange utilizing semiconductor laser amplifiers and Mach-Zehnder filters", K. Inoue and N. Takato, *Conference on Lasers and Electro-Optics*, 1989, FM2.

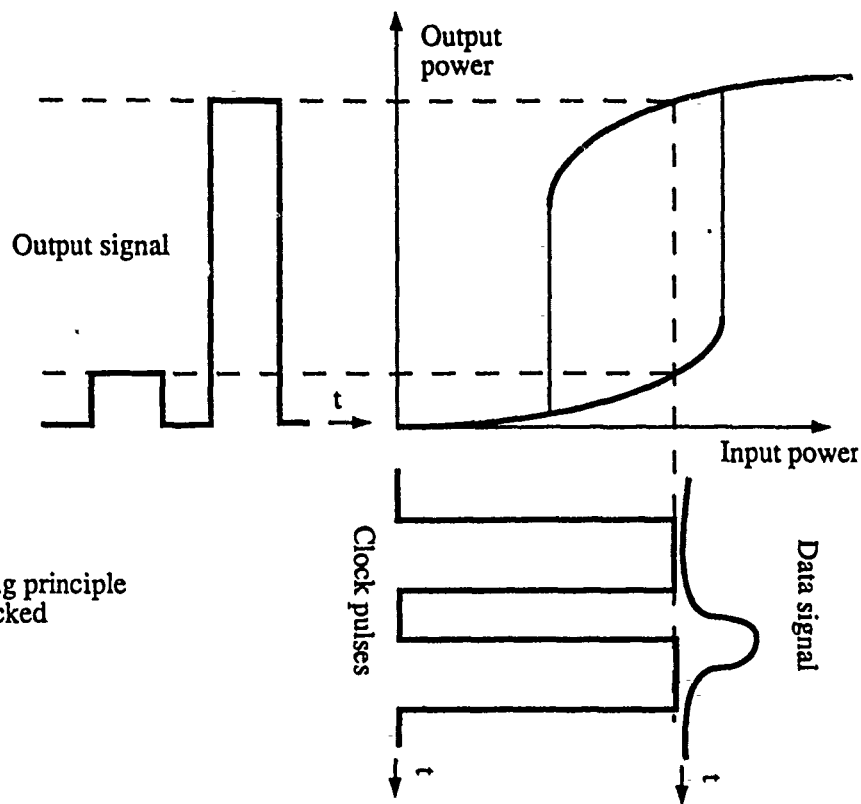


Fig. 1. Operating principle of optically clocked bistable.

Fig. 2. General configuration of OCB with clock and data in orthogonal modes allowing the clock field to resonate while the data field has broadband gain.

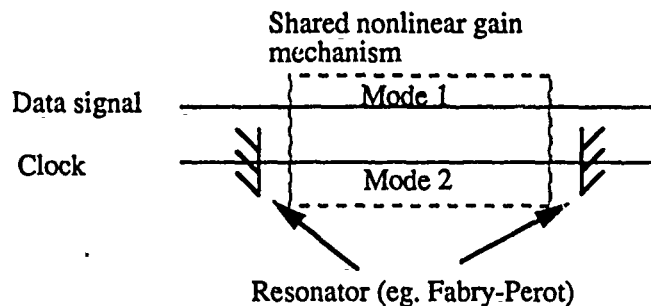
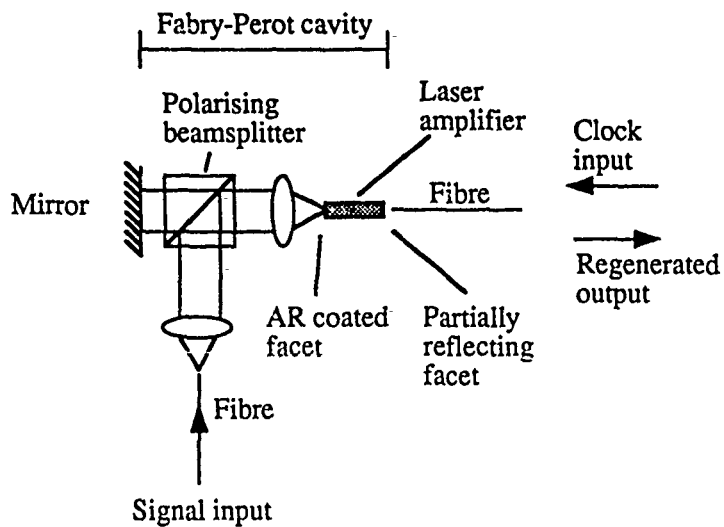


Fig. 3. Experimental system using orthogonal polarisations to separate clock and data fields.



TI11 Low Power Optical Switching in GaAs Epitaxial Etalons

J. L. Oudar, B. Sfez, and R. Kuszelewicz
C.N.E.T. - Laboratoire de Bagneux
196, Avenue Henri Ravera, 92220 Bagneux - France

Epitaxial methods allow the fabrication of nonlinear interferometric structures which include the mirrors and the nonlinear medium in a single crystal. Optical bistability is observed in these structures at mW optical power¹. The large excitonic and band-gap resonant nonlinearities of direct-gap semiconductors, such as bulk GaAs or Multiple Quantum Wells (MQW), allow to reach a substantial phase-shift (0.2-0.3 radian) over interaction lengths as small as a few wavelengths. This results in very compact nonlinear microcavities, with typically 5 μm overall thickness.

We review our latest experimental results on these structures, including the observation of high contrast switching in the reflection mode, the direct measurement of dispersive optical nonlinearities in MQW's, evidencing their saturation behavior at high intensities. We report external-beam switching experiments, which allow to assess the potential of these structures as all-optical gates. Finally we discuss the optical power reduction that can be expected from laterally restricted microresonators.

The sample linear and nonlinear behavior was studied at room temperature using a styryl-9M dye laser operating around 840 nm. The étalon was found to display a high finesse of 38, and a wide hysteresis loop, with a bistable threshold below 3 mW. The response time of the nonlinearity was due to carrier recombination and was below 10 ns. The dispersive optical nonlinearity of the active layer (a 10 nm/10 nm GaAs/Al_{0.3}Ga_{0.7}As MQW structure) was measured as a function of wavelength for different intensities of the laser beam. The wavelength shift of the reflectivity minimum was related to the nonlinear phase-shift of light during a cavity round-trip, providing a direct measurement of the active layer nonlinear refractive index, as a function of intracavity intensity. An original experimental technique was developed², to allow a quasi steady-state measurement of the electronic nonlinearity, which is free of any spurious thermal effect. A strong saturation behavior was clearly observed, which limits the nonlinear refractive index change to about 0.02 at the wavelength of interest. This shows that the usual n_2 approximation cannot be used to describe the étalon nonlinear characteristics. As a result there is a minimum cavity finesse for the observation of bistability³, and above this condition the width of the hysteresis loop does not increase indefinitely with the incident intensity or initial detuning, but rather goes through a maximum.

External beam switching was performed by maintaining the dye laser incident power within the hysteresis loop, providing a holding, or bias beam, and sending an additional beam coming from a 820 nm general purpose semiconductor laser. We observed both amplification (by a proximately a factor of 10) and memory effects. With our sample the memory effect lasted more than 100 μs for an input pulse of 100 ns. The memory was reset by a temporary decrease of the holding beam. We also performed experiments where both beams came from the same dye laser, but were of orthogonal polarization. In this case the set-up allows signal cascading in a simple way, since the input and output signals are at the same wavelength. The holding beam was strictly continuous and was set just below the lower bistability power threshold. An optical isolator was used to extract the output signal reflected from the device. Amplification with inversion contrast and some pulse reshaping was observed, as shown in Fig. 2.

REFERENCES

1. R. Kuszelewicz, J. L. Oudar, J. C. Michel, and R. Azoulay, *Appl. Phys. Lett.* **53**, 2138 (1988)
2. B. G. Sfez, J. L. Oudar, J. C. Michel, R. Kuszelewicz, and R. Azoulay, *Appl. Phys. Lett.* (to be published).
3. J. L. Oudar, B. G. Sfez, R. Kuszelewicz, J. C. Michel, and R. Azoulay (to be published in *Physica Status Solidi*, Proceedings of NOEKS II Workshop, Bad Stuer, Nov. 1989).

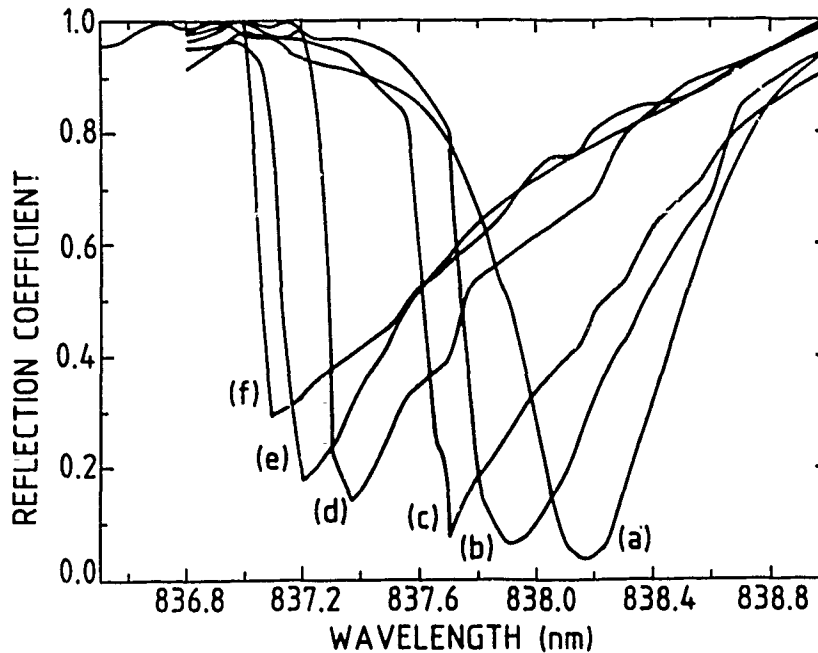


Fig.1: Reflection coefficient of the étalon as a function of wavelength for different incident powers: (a) 0.28 mW, (b) 1.12 mW, (c) 2.1 mW, (d) 4.2 mW, (e) 5.6 mW, (f) 8.4 mW

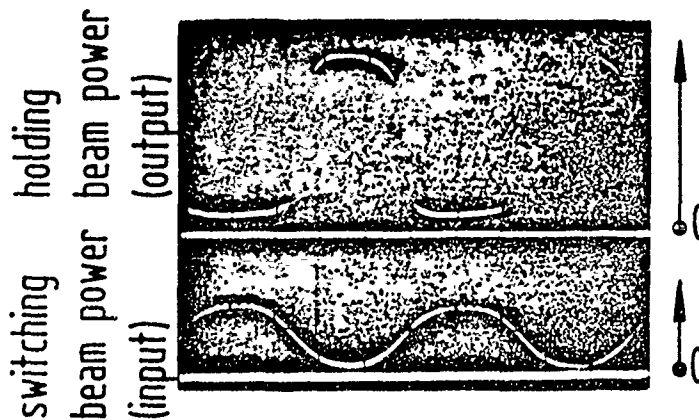


Fig.2: Signal amplification and reshaping observed in a 2-beam (single wavelength) experiment.

D. A. B. Miller,

AT&T Bell Laboratories,
Holmdel, NJ 07733
USA

Optics has many potential benefits in digital processors, especially in its ability to communicate information, both in fibers and, more speculatively, in "free space". Recent advances in devices have stimulated new interest in such "free space" digital optics¹, and have highlighted the critical device features for digital applications. This talk will discuss quantum well optoelectronic devices² for digital applications, especially self-electrooptic-effect devices (SEEDs), and put these in context with the requirements for future systems applications. Important trends in SEED work include not only larger two-dimensional arrays of smaller and faster devices, but also attempts to allow more complex logical functionality to improve their usefulness in systems.

Free space optics itself offers high bandwidth, ground-loop isolation, absence of clock skew, global interconnect patterns, and large numbers of interconnects through two-dimensional parallelism. To take advantage of such features, appropriate devices must first of all operate at sufficiently low energy so that they are usable in large two-dimensional arrays at reasonable clock rates, and must be integrable in large arrays with high yields. In addition, however, for digital systems of any size they must also have the mathematical properties of good input-output isolation, absence of critical biasing, cascability and logic level restoration. Unfortunately, these criteria taken together eliminate nearly all nonlinear optical devices and processes³. The symmetric SEED (S-SEED)⁴ satisfies all of the mathematical criteria, and is now being made in large arrays (e.g. 64×32).⁵ Energy densities are comparable to electronic devices, and scaling to small devices is promising⁶. Recent understanding⁷ of limiting physical processes has also improved device performance, including switching as fast as 33 ps (on or off)⁸. It has also recently been demonstrated that more complex logical functions can be performed with related devices⁹. The principles and operation of the many different SEED configurations have recently been reviewed extensively.¹⁰ The physics behind these devices is now relatively well understood.¹¹

A complementary approach to improving functionality is to integrate more electronics with the quantum well devices. Recent advances include integration of field effect transistors (F-SEED)¹², and successful modulators on Si substrates¹³. This raises the question of the trade-off between optics and electronics. Optical devices can have reasonable logic energies, although only simple functionalities. Importantly, the logic energy is also the communication energy because of the impedance transformation intrinsic to quantum processes¹⁴. Electronic devices can have good

logic energies and complex functionality, but have very high communication energies, a fact that is a considerable constraint on electronic systems. The technology to integrate optics and electronics to get the best of both worlds is still a challenge, but offers a major opportunity for digital system performance.

- [1] See, e.g., N. Streibl, K.-H. Brenner, A. Huang, J. Jahns, J. Jewell, A. W. Lohmann, D. A. B. Miller, M. Murdoch, M. E. Prise and T. Sizer, *Proc. IEEE*, **77**, 1954 (1989).
- [2] For a general discussion of quantum well optical devices, see D. A. B. Miller, *Optics and Photonics News*, **1**, 7 (Feb. 1990).
- [3] D. A. B. Miller, "Optical Switching Devices: Some Basic Concepts", *Proc. Summer School on Optical Computing*, ed. B. S. Wherrett, (SUSSP Publications, Univ. Edinburgh, UK, 1990)
- [4] A. L. Lentine, H. S. Hinton, D. A. B. Miller, J. E. Henry, J. E. Cunningham, and L. M. F. Chirovsky, *Appl. Phys. Lett.* **52**, 1419 (1988).
- [5] A. L. Lentine, F. B. McCormick, R. A. Novotny, L. M. F. Chirovsky, L. A. D'Asaro, R. F. Kopf, J. M. Kuo and G. D. Boyd, *IEEE Photonics Tech. Lett.*, **2**, 51 (1990).
- [6] A. L. Lentine, L. M. F. Chirovsky, L. A. D'Asaro, C. W. Tu, and D. A. B. Miller, *IEEE Photonics Tech. Lett.* **1**, 129 (1989)
- [7] G. Livescu, A. M. Fox, D. A. B. Miller, T. Sizer, W. H. Knox, A. C. Gossard, and J. H. English, *Phys. Rev. Lett.* **63**, 438 (1989); A. M. Fox, D. A. B. Miller, J. E. Cunningham, J. E. Henry, W. Y. Jan, and G. Livescu, Paper MB2, OSA Annual Meeting, Orlando, 1989
- [8] G. D. Boyd, A. M. Fox, U. Keller, D. A. B. Miller, L. M. F. Chirovsky, L. A. D'Asaro, J. M. Kuo, R. F. Kopf and A. L. Lentine, Conference on Lasers and Electro-Optics, Anaheim, May 1990, Postdeadline Paper CPDP4.
- [9] A. L. Lentine, D. A. B. Miller, J. E. Henry, J. E. Cunningham, L. M. F. Chirovsky and L. A. D'Asaro, Conference on Lasers and Electro-Optics, Paper CTUC1 (Anaheim, California, May 1990), (1990 Technical Digest Series, Vol. 7 (Optical Society of America, Washington, DC 1990), pp 66-7)
- [10] D. A. B. Miller, *Opt. Quantum Electron.*, (to be published) (1990).
- [11] S. Schmitt-Rink, D. S. Chemla and D. A. B. Miller, *Advances in Physics*, **38**, 89 (1989).
- [12] D. A. B. Miller, M. D. Feuer, T. Y. Chang, S. C. Shunk, J. E. Henry, D. J. Burrows, and D. S. Chemla, *IEEE Photonics Tech. Lett.* **1**, 61 (1989)
- [13] K. W. Goossen, G. D. Boyd, J. E. Cunningham, W. Y. Jan, D. A. B. Miller, D. S. Chemla and R. M. Lum, *IEEE Photonics Technol. Lett.*, **1**, 304 (1989).
- [14] D. A. B. Miller, *Optics Lett.* **14**, 146 (1989)

PLENARY TALK Historical Reminiscences about Nonlinear Optical Materials

N. Bloembergen

Pierce Hall, Harvard University, Cambridge, MA 02138

The birth of nonlinear optics is generally identified with the 1961 experiment of Peter Franken and coworkers on the second harmonic generation of light by passage of a ruby laser pulse through a quartz crystal. In quick succession, the ruby laser led to the discovery of many nonlinear optical phenomena.

The history of nonlinear optics during the years 1961-1963 will be reviewed. The significance of the early nonlinear optical materials will be illustrated with some personal anecdotes.

Attention will also be given to nonlinear optical phenomena before the year 1960. This prehistory of nonlinear optics includes the Pockels effect, the photo-electric effect and Kerr-cell light modulators and shutters, as well as many nonlinear precursors in the field of magnetic resonance.

TUESDAY, JULY 17
POSTER PRESENTATIONS

TP1 Greater Than 90% Conversion Efficiency by Stimulated Rotational Raman Scattering in Hydrogen (H₂),

by

E. Gregor, D. W. Mordaunt, and K. V. Strahm

Electro-Optics and Data Systems Group
Hughes Aircraft Company
P.O. Box 902
El Segundo, CA 90245
213/616-3955

Stimulated rotational Raman scattering (SRRS) has been used with a variety of pump lasers and Raman media to shift to longer wavelengths. In 1989 we reported on the efficient generation of SRRS in hydrogen using a phase conjugate, frequency doubled Nd:YAG laser.¹ We achieved a maximum SRRS conversion of 88% with the energy concentrated in the first three rotational Stokes lines. These results were obtained with a single focus geometry. A two cell dual focus configuration was reported later in 1989 by S. R. Bowman, et al, with enhanced rotational Raman conversion into the first rotational line.²

Our experimental work reported here was intended to obtain the highest possible conversion efficiency into the first five or six rotational lines of H₂ pumped by the frequency doubled Nd:YAG laser line of 532 nm, with 200 mJ of energy and 20 ns pulsewidth. The resulting rotational Raman Stokes lines of H₂ are 549, 567, 587, 608, 630, and 655 nm. We recorded the energy, the pulse shape of the pump laser and the energy, pulse shape and spectral distribution of the Raman converted output. The dual focus geometry of the gas cell was optimized to obtain the highest efficiency and largest shift to the higher order rotational Raman lines, as shown in Figure 1. We observe that there is less than 6% of energy remaining in the depleted laser pump beam. This exceptionally high conversion is also verified by observing the pulse shape of the depleted laser pump as compared to the input beam, as shown in Figure 2. The time evolution of the successive rotational Stokes orders is shown in Figure 3 and demonstrates the sequential nature of this process.

We demonstrated that the doubled output of a phase conjugated Nd:YAG laser which features good beam quality and good coherence can be efficiently converted into higher rotational Raman orders when a two-focus gas cell configuration is used.

1. E. Gregor, O. Kahan, and D. W. Mordaunt, in Technical Digest, Conference on Lasers and Electro-Optics (Optical Society of America, Washington, D. C., 1989), technical paper FD3.

2. S. R. Bowman, B. J. Feldman, J. M. McMahon, A. P. Bowman, and D. Scari, Technical Digest, Tunable Solid State Lasers Conference, May 1989, paper WB1.

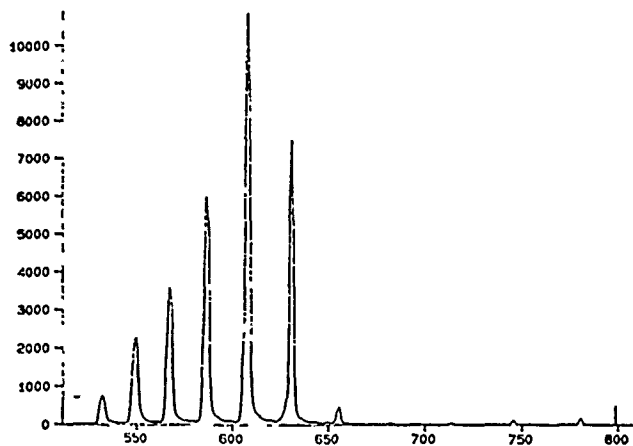


Figure 1. Spectral distribution of the rotational Raman output with the two H_2 gas cell configuration.

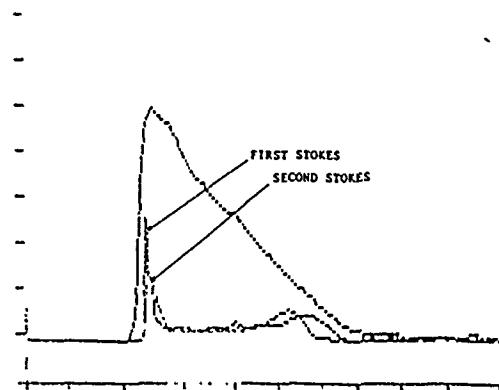


Figure 3a. Pulse shape of the first and second rotational Raman lines compared with the input pump (10 ns/Div).

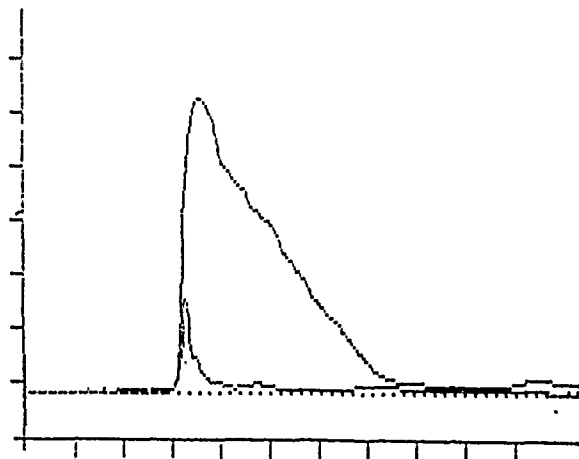


Figure 2. Pulse shape comparison of pump beam and depleted pump (10 ns/Div).

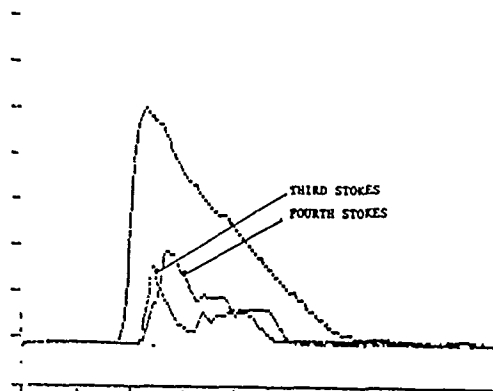


Figure 3b. Pulse shape of the third and fourth rotational Raman lines compared with the input pump (10 ns/Div).

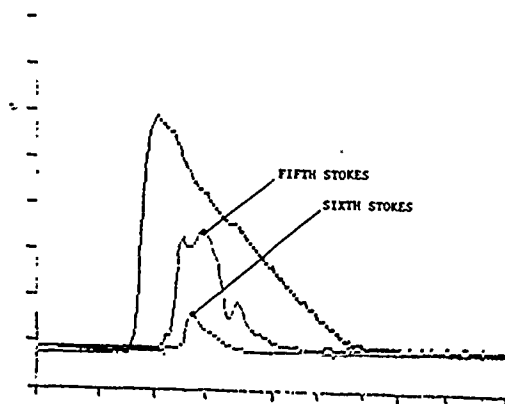


Figure 3c. Pulse shape of the fifth and sixth rotational Raman lines compared with the input pump (10 ns/Div).

TP2 The Permittivity of Polycrystalline Electromagnetic Materials: Extension of Current Method for Spectra Calculation

Craig A. Grimes¹ and Elmer L. Hixson

Department of Electrical and Computer Engineering,
The University of Texas at Austin, Austin, Texas 78712-1084
(512) 471 - 1294

¹ Current Address:

Lockheed Missiles & Space Company, Inc.
Advanced Systems Technology
3251 Hanover Street
Palo Alto, CA 94304-1191

SUMMARY

This work extends the present analytic technique for calculating the permittivity and permeability spectra of composite materials. It addresses the relationship between grain properties, their size-to-wavelength ratio, and the permeability and permittivity spectra of polycrystalline material.

The scattered multipolar fields about a single sphere are related to the polarizability of an ordered congregation of such spheres. Using the Clausius-Mossotti relation the effective permeability and permittivity spectra of a congregate polycrystalline material is determined for arbitrary size, permittivity, and permeability of individual, identical spheres making up the composite. Although we consider the spectra over a range where the product of the external wave vector and sphere radius is kept small, typically less than one-tenth, the product of the internal wavevector and sphere radius can be quite large.

The theory developed predicts many different spectra type, including complex nonlinear permittivity and permeability spectra that have been measured experimentally and explained either by including multiple sources or statistical weighing. The theory presented here predicts both the 'classical' and 'anomalous' spectra that have been experimentally measured, without employing multiple additive sources. Results suggest that the permeability and permittivity spectra of composite materials, considered as an ordered array of uniform spheres, can be simply explained as the manifestations of electromagnetic boundary conditions and dimensional effects of the size-to-wavelength ratio.

The theory also predicts certain more difficult, conglomerate spectra that have been measured and for which no theory has been put forth. Also predicted are certain chaotic type permittivity spectra.

TP3 Room Temperature 1.06 ~ 0.53 μm Second Harmonic Generation with $\text{MgO}:\text{LiNbO}_3$

J. Q. Yao¹, W. Q. Shi², J. E. Miller¹, G. F. Xu³, E. Garmire¹, and M. Birnbaum¹

¹ Center for Laser Studies, University of Southern California, Los Angeles, California 90089-1112

² Laser Research Center, Cedars-Sinai Medical Center, Los Angeles, California 90048

³ Southwest Institute of Technical Physics, Chengdu, China

LiNbO_3 is an important nonlinear optical crystal due to its large nonlinearity and the possibility of noncritical phase matching. However, the optically induced refractive index damage greatly reduces the conversion efficiency of second harmonic generation (SHG) processes and therefore restricts its applications. In the early 1980's, Zhong et al [1] reported that a 100-fold increase in the refractive index damage resistance of LiNbO_3 could be acquired by codoping LiNbO_3 with MgO . While the $\text{MgO}:\text{LiNbO}_3$ crystals can withstand higher incident power intensities, they have to be used at elevated temperatures [2] to achieve phase matching, which requires an additional temperature control unit.

We report here, for the first time to our knowledge, on the efficient 1.064 ~ 0.532 μm SHG with $\text{MgO}:\text{LiNbO}_3$ at room temperature. The crystal was supplied by the CSK Co. in Los Angeles. It was cut for Type I phase matching (PM) at 24°C with $\theta = 82.3^\circ$ and had a dimension of 5×5×12 mm. The Sellmeier equations of our $\text{MgO}:\text{LiNbO}_3$ were experimentally determined and were utilized to calculate the room temperature phase matching parameters as functions of the fundamental wavelength. These parameters include phase matching angle (θ_0), effective nonlinear coefficient (d_{eff}), acceptance angle-length ($\Delta\theta \cdot l$), acceptance temperature ($\Delta T \cdot l$), spectral acceptance ($\Delta\lambda \cdot l$), and walk-off angle (α). At $\lambda = 1.064 \mu\text{m}$, we found that $\theta_0 = 82.28^\circ$, $d_{eff} = 4.98$, $\Delta\theta \cdot l = 3.29 \text{ mrad}\cdot\text{cm}$, $\Delta T \cdot l = 1.13^\circ\text{C}\cdot\text{cm}$, $\Delta\lambda \cdot l = 0.3 \text{ nm}\cdot\text{cm}$, and $\alpha = 0.596^\circ$.

The energy conversion efficiency of our $\text{MgO}:\text{LiNbO}_3$ crystal was measured using a pulsed Q-switched (20 nsec, 10 Hz) and two mode-locked (30 psec, 5 Hz; and 100 psec, 76 MHz) Nd:YAG lasers. The conversion efficiency per unit crystal length for $\text{MgO}:\text{LiNbO}_3$ (circles) obtained with the Q-switched laser is shown in Fig. 1. A 37% conversion efficiency was observed for our 12 mm long $\text{MgO}:\text{LiNbO}_3$ at a fundamental peak power density of 38 MW/cm². Also included in Fig. 1 is the conversion efficiency data for a 6 mm KTP (Type II) and a 9 mm LBO (Type I) crystal obtained using the same laser. The difference in the SHG performance of the three crystals is due to the difference in their nonlinear coefficients. We have also measured the angular acceptance $\Delta\theta$ and acceptance temperature ΔT for $\text{MgO}:\text{LiNbO}_3$ by mounting the crystal on a rotation stage with a thermal electric device. Fig. 2 plots the SHG conversion efficiency as a function of angular phase mismatch $\Delta\theta$. It was found that $\Delta\theta \cdot l$ ($l = 12 \text{ mm}$) and $\Delta T \cdot l$ were 3.4 mrad·cm and 1.2°C·cm, respectively, in good agreement with the theoretical predictions.

A 45% SHG conversion efficiency was achieved with a 140 MW/cm² peak power density, pulsed mode-locked (30 psec, 5 Hz) Nd:YAG laser beam which was unfocused and had a beam size of 3 mm in diameter. Using a 2.8-W average power, CW mode-locked (100 psec, 76 MHz) Nd:YAG beam focused to a 6.1 MW/cm² peak power density, a 7.6% average power conversion efficiency was measured.

We gratefully acknowledge Prof. J. Feinberg, Dr. X. F. Cao and Mr. V. Dominold for their technical assistance in part of the experiments and CSK Co. for the MgO:LiNbO_3 crystal.

References

- [1] G. G. Zhong, J. Jian, and Z. K. Wu, 11th International Quantum Electronics Conference, IEEE Cat. No. 80 CH1561-0, June 1980, P.631.
- [2] W. J. Kozlousky, E. K. Gustafson, and R. L. Byer, Opt. Lett., Vol. 13, No. 12, 1102 (1988).

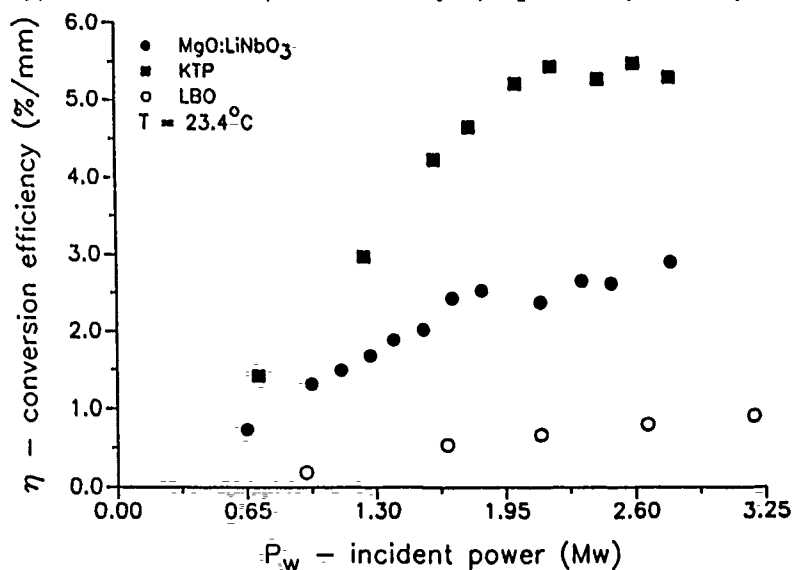


Fig. 1 Measured SHG conversion efficiencies of MgO:LiNbO_3 , KTP and LBO.

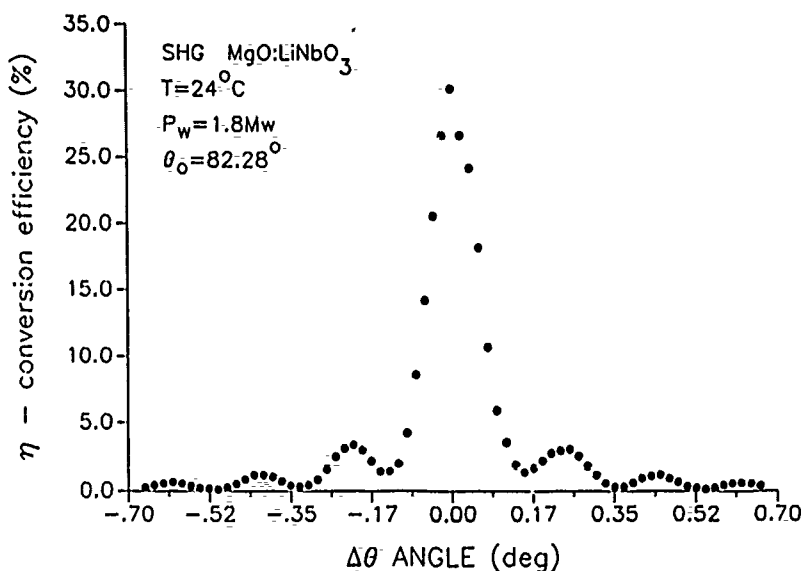


Fig. 2 SHG conversion efficiency of MgO:LiNbO_3 versus angular phase mismatch $\Delta\theta$.

TP4 Molecular Orientation in Monolayers from Variation of Nonlinear Optical Generation with Incident Angle

Qiang Zhu and Peter Browne

Centre for Lasers and Applications,
School of Mathematics, Physics, Computing and Electronics
Macquarie University, N.S.W 2109, Australia

Second harmonic generation (SHG) has been measured in transmission from a Langmuir-Blodgett monolayer of hemicyanine as the angle of incidence of the fundamental is varied. Attempts to match the observed behaviour of the SHG with predictions from the model of Dick et al¹, which assumes that the refractive index of the monolayer is the most important parameter, were not successful. We conclude that the refractive index of the monolayer is *not* the major factor in determining the form of the nonlinear signal vs incident angle. We have used an alternative analysis where orientation of the molecular dipoles in the monolayer is the most important parameter. Rotational invariance about the surface normal is assumed, and dispersion in the monolayer is ignored. With these assumptions, we obtain good agreement between the observed and calculated dependence of the SHG on the angle of incidence when the inclination angle of the hemicyanine molecular dipoles measured from the surface normal is $40^\circ \pm 5^\circ$.

When analysing third harmonic generation (THG) from monolayers of polydiacetylene, we consider the nonlinearity of the polydiacetylene repeating units to be dominated by one tensor component α_{zzzz} . However, to obtain a match between the calculated and measured THG as a function of the angle of incidence, we found that the orientation of the tensor component α_{zzzz} with respect to the surface normal had to be greater than 80° , i.e. almost in the plane of the monolayer. Thus the nonlinear dipole moment of the polydiacetylene is not along its molecular axis. From the structural point of view, the polarisation direction of the two large π bonds lies perpendicular to the molecular axis, in the direction that our experiments indicate is the direction of the molecular dipole. This differs from the assumption of Berkovic et al² that the dipole axis is along the molecular axis.

References:

1. B. Dick, A. Gierulski, G. Marowsky, and C. A. Reider, Appl.Phys.B 38, 107-116(1985).
2. G. Berkovic, R. Superfine, P. Guyot-Sionnest, Y. R. Shen and P. N. Prasad, J.Opt.Soc.Am B 5, 668-673(1988).

Beam Reshaping Effects in Saturable Media

R.J.Ballagh and A.W.McCord

Physics Department
University of Otago
Dunedin, New Zealand

The spatial beam profile reshaping that occurs when strong laser fields propagate in near resonant media may have important consequences in intensity sensitive experiments, and it is desirable that simple quantitative predictions of the scale and character of the reshaping can be made. In saturable media, the usual model of self focussing based on a $\chi^{(3)}$ nonlinear refractive index is often inappropriate, and a more accurate treatment of the medium is required. A homogeneously broadened two state transition, which displays saturable absorption and dispersion, is a more realistic choice of medium, but leads to a nontrivial propagation equation. For a strong laser field however, the essential physics is that an initial encoding in the saturation region at the edges of the beam gives rise to a diffraction dominated step, producing focussing. A model of this sequence is presented and in the regime where dispersive effects are dominant, is solved approximately to give simple analytic expressions for the position and magnitude of the first region of focussing. More complex transitions can lead to quite unexpected focussing behaviour. An example is given where a $J = \frac{1}{2} \leftrightarrow J = \frac{1}{2}$ transition couples the two circular polarized components of an elliptically polarized beam and gives rise, in combination with diffractive propagation, to a self induced spatial separation of the two polarizations. The physical mechanism can again be understood in terms of a modified initial encoding and subsequent diffraction dominated steps.

A Unified Theory of Spontaneous and Stimulated Rotational Raman Scattering

Mark R. Hermann, David H. Chambers, Sham Dixit, and Thomas J. Karr
Lawrence Livermore National Laboratory
P.O. Box 808, L-495
Livermore, CA. 94550
(415) 423-8672

SUMMARY

The dynamics governing the evolution of spontaneously generated random and unpolarized fields into coherent lightsources, which have deterministic macroscopic properties, has generated a great deal of attention in recent years. Quantum fluctuations, the statistical properties of Stokes fields and solitons produced by vibrational Raman scattering (VRS) have been measured experimentally and analyzed theoretically. In contrast, little experimental or theoretical effort has addressed the study of the statistical properties of spontaneous light generated by rotational Raman scattering (RRS) or its dependence on polarization, degeneracy and Stokes/anti-Stokes coupling. Knowledge of the dynamics governing spontaneous and stimulated Stokes and anti-Stokes fields is of practical interest in the design and operation of rotational Raman frequency convertors and oscillators and for characterizing parasitic depletion of high power lasers due to amplified spontaneous emission over long propagation distances. Studies in this area require a comprehensive and unified theoretical descriptions of spontaneous and stimulated RRS.

The theory presented here extends a previous description of spontaneous and stimulated VRS to include parametric coupling of the pump, Stokes and anti-Stokes fields with arbitrary polarization and the degeneracy of the rotational states. The importance of Stokes/anti-Stokes coupling, polarization, and rotational state degeneracy in RRS is well known experimentally and some of these effects have been included in previous steady-state and transient stimulated analytical theories. To our knowledge, however, this is the first theory presented to incorporate all these important effects into a single unified analytic theory of both spontaneous and stimulated RRS.

The theory predicts that a linearly polarized pump will generate no appreciable Stokes or anti-Stokes light, a circularly polarized pump will result in Stokes conversion but little anti-Stokes, and an elliptically polarized pump

can in principle generate nearly as much anti-Stokes as Stokes. The theory further predicts that the initial spontaneous fields are unpolarized and the initial growth is linear and independent of pump polarization. However, in the same low gain limit the statistical properties of the fields are sensitive to the pump polarization. In the high gain limit, the spontaneous Stokes and anti-Stokes fields have the same exponential gain and are both circular but oppositely polarized and the quantum induced fluctuations of both fields grow at the same rate as the mean intensity. Furthermore, in the same limit the Stokes field arising from stimulated amplification of a seed is always circularly polarized independent of the initial seed and pump polarization state. Comparison of spontaneous and stimulated Stokes intensities also indicates which process will dominate for a particular exponential gain, pump and Stokes polarization state and initial Stokes intensity. These predictions can easily be verified using current experimental techniques, and, it is hoped that this work will motivate further experimental investigation of the statistical properties of spontaneous and stimulated rotational Raman scattered light.

This research was performed under the auspices of the U.S. Department of Energy by the Lawrence Livermore National Laboratory under contract number W-7405-Eng-48.

TP7 Polarization Dependence on High-Order Rotational Raman Frequency Conversion

Mark R. Hermann, Sham Dixit, and Thomas J. Karr
Lawrence Livermore National Laboratory
P.O. 808, L-495
Livermore, CA. 94550
(415) 423-8672

SUMMARY

Rotational Raman frequency conversion for arbitrary input laser pump polarization is examined. Vibrational anti-Stokes Raman conversion has long been employed as a frequency convertor to shorter wavelengths. In this case the polarization of the pump laser is irrelevant. In contrast, Stokes/anti-Stokes conversion efficiencies are strongly dependent on polarization of the pump for rotational Raman scattering. Results of numerical calculations suggest that efficiencies as high as 20% conversion to 1st anti-Stokes and .1% conversion through 8th order anti-Stokes can easily be obtained for an appropriately polarized laser pump in H_2 . These calculations employ the recently developed multipole expansion formalism (1), which correctly describes the coupling of the molecular rotational states with the electric field polarization. The purpose of this work is twofold. First, the numerical results are compared with results from several analytic theories (2), which employ various simplifying approximations. Consequently, it is useful to verify the simple analytic predictions with results obtained from a more comprehensive theory and, furthermore, investigate regimes in which the analytic theories are no longer valid. Second, the numerical calculations reported here form a basis for design of experiments currently being performed.

Calculations were performed for circular, linear and various elliptically polarized input pump beams. Figures 1-3 show typical results of Stokes and anti-Stokes energy fractions for circular, elliptical, and linear polarized light as a function of propagation distance. The effects of varying the degree of elliptical polarization of the pump as well as the input Stokes seed intensity will also be presented.

This research was performed under the auspices of the U.S. Department of Energy by the Lawrence Livermore National Laboratory under contract number W-7405-Eng-48.

1. S. Dixit, M. Hermann, and T. Karr, Phys. Rev. A, submitted for publication
2. G.V.Venkin, Yu.A. Il'inskii, and G.M. Mikheev, Sov. J. Quantum Electron. 15, 395 (1985), and D.Eimerl, R.S. Hargrove, and J.A.Paisner, Phys. Rev. Lett. 46, 651 (1981)

Figure 1

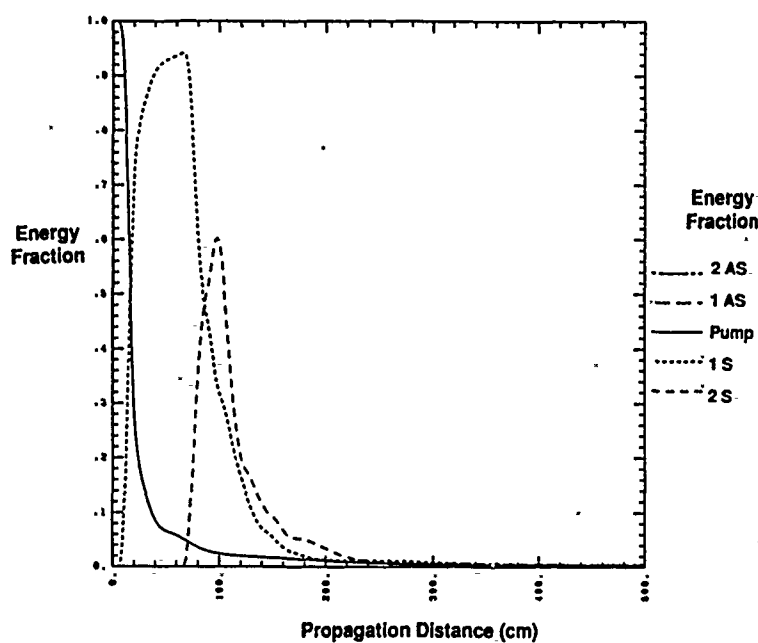


Figure 2

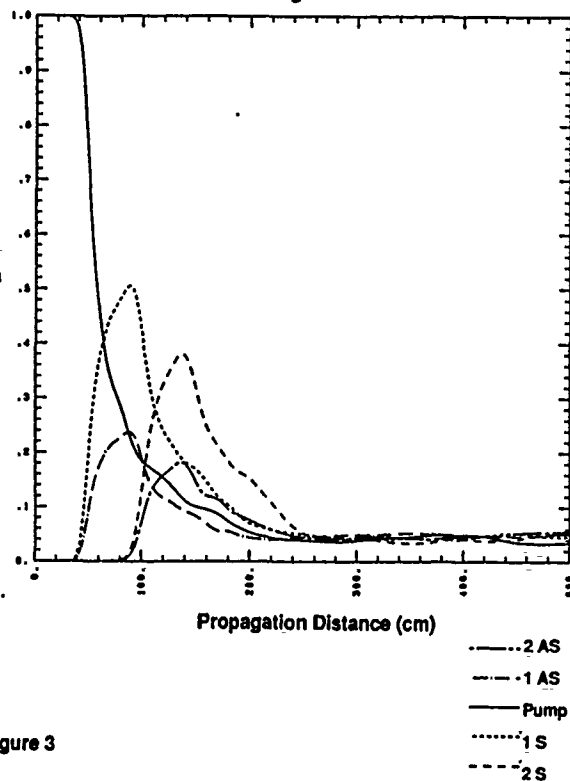
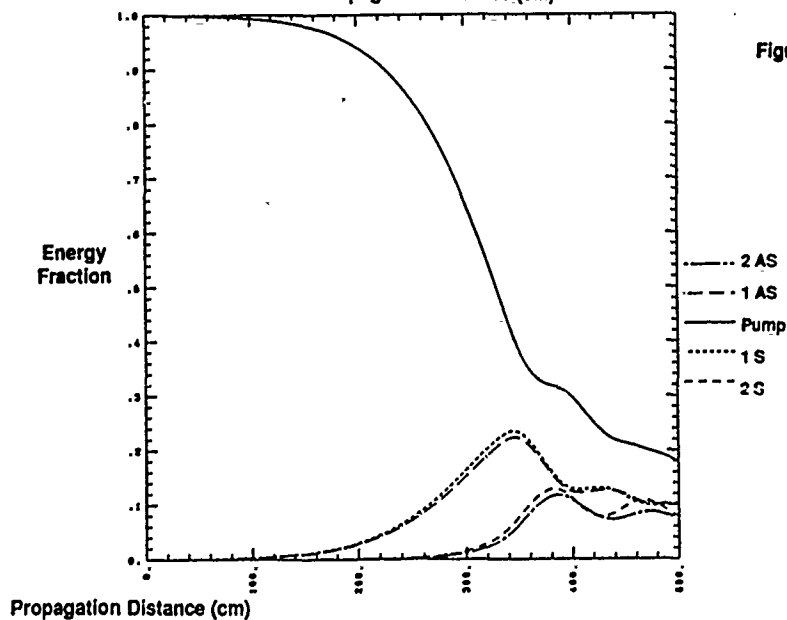


Figure 3



TP8 Third Harmonic Generation in $\text{SiO}_2\text{-TiO}_2$, SOL-GEL Films

W.E. Torruellas, L.A. Weller-Brophy, R. Zanoni, G.I. Stegeman

Optical Sciences Center
University of Arizona
Tucson, Arizona 85721
(602) 621-4684

Z. Osborne, B.J.J. Zelinski

Materials Sciences and Engineering Department
Arizona Materials Laboratory
University of Arizona
Tucson, Arizona 85721

To the best of our knowledge, this is the first time a Third-Harmonic-Generation, THG, experiment has been performed on a sol-gel thin film. THG has been shown to be an extremely powerful probe for measuring and comparing the third order nonlinearity, $\chi^{(3)}$, of very thin film conjugated organic polymers¹. Spin-coated sol-gel films of very good optical quality are attractive for integrated optics². In addition their composition as well as their stoichiometry can be easily changed. They allow us to study the influence of heavy-ions in the nonlinear properties of high-index glasses. Nonlinear experiments at only a single wavelength have been previously reported in order to measure the non-resonant $\chi^{(3)}$ of bulk glasses^{3,4,5}.

Multiple reflections as well as absorption at 3ω are taken into account in the Maker fringe model we used to fit the experimental data, fig.1. Under these conditions we have been able to evaluate both the magnitudes and phases of $\chi^{(3)}(3\omega)$ relative to SiO_2 at three different wavelengths, fig.2. At $0.953\mu\text{m}$ $\chi^{(3)}$ is resonantly enhanced, its sign is negative and has a considerable imaginary contribution. In comparison the magnitude and phase of $\chi^{(3)}$ at $1.064\mu\text{m}$ are close to the non-resonant ones at $1.579\mu\text{m}$. The magnitude of the non-resonant $\chi^{(3)}$ is one order of magnitude larger than that of pure SiO_2 , which is in good agreement with bulk D4WM measurements³. Preliminary results show an increase in $\chi^{(3)}$ with Ti concentration. A more complete study will be presented at the time of the conference.

1) F.Kajar, J.Messier, in Nonlinear Optical Properties of Organic Molecules and Crystals, Vol.2, Chap.3, 1987.

2) K.Tiefenthaler, V.Briquet, E.Buser, M.Horisberger, W.Lukosa, Proc. SPIE, vol.401, 165-173, Thin Film Technologies, April 1983.

3) D.W.Hall, M.A.Newhouse, N.F.Borrelli, W.H.Dumbaugh, D.L.Weidman, Appl.Phys.Lett.54(14), 1293-1295, April 1989.

4) R.Adair, L.L.Chase, S.A.Payne, J.Opt.Soc.Am.B, 4, (6), 875-881, June 1987.

5) H.Nasu, Y.Ibara, K.Kubodera, J. Non-Crys. Solids, 110(1989), 229-234.

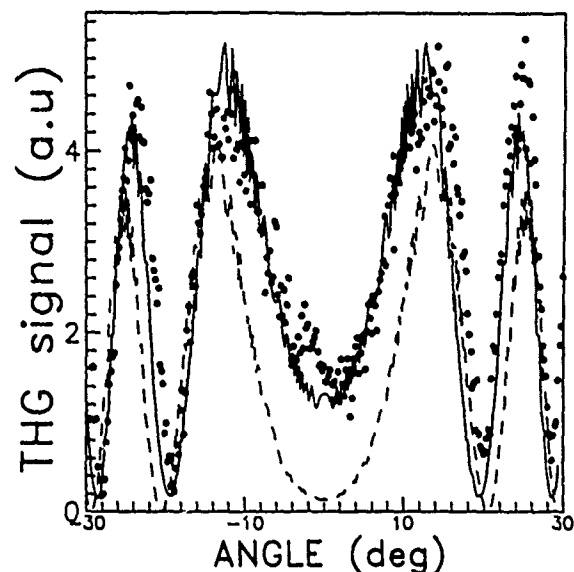


Figure1: THG at 1572nm of a 50:50 mole % SiO₂-TiO₂ 500nm thick sol-gel thin film. The dark dots are the experimental data points. The solid line is the best fit to the Maker fringe. The dashed-line represents the THG-Maker fringes for the clean substrate taken at the same location than the film+substrate.

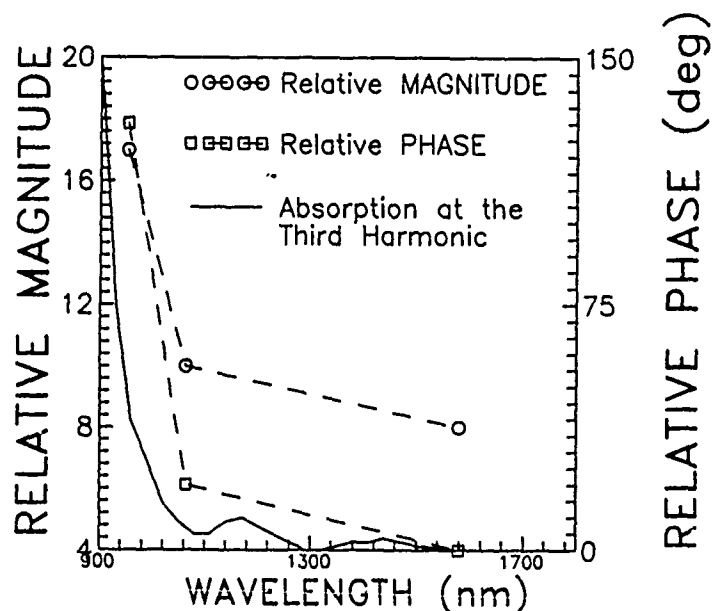


Figure 2: Both the relative magnitudes and phases of the third order susceptibility are plotted as a function of the fundamental wavelength. Absorbance of the 500nm thick, 50:50 SiO₂:TiO₂ films are also plotted for the the third harmonic frequencies.
 The absorbance at 317nm is 0.60
 at 355nm is 0.15
 at 526nm is 0.02.

TP9 Spatial Polarization Separation in An Absorptive Medium

D.E.McClelland, J.C.Wang and H.-A. Bachor

*Department of Physics and Theoretical Physics
Faculty of Science, The Australian National University
P.O.Box 4, Canberra , ACT 2601, AUSTRALIA
Tel. + 61 62 492747 Fax + 61 62 490741*

Summary

The phenomenon of dispersive self-focussing has been well studied since its prediction by Javan and Kelly [1] in 1966. Many types of media have exhibited such behaviour. The opposite process, self defocussing, along with self trapping, in which the tendency to focus is just balanced by spreading due to diffraction, has also been studied in detail both experimentally and theoretically. More recently Boshier and Sandle [2] have predicted from a numerical simulation, that a medium possessing an intensity dependent absorption can also self-focus. This phenomenon, known as absorptive self-focussing, occurs when the edges of a Gaussian beam are strongly absorbed during propagation whilst the more intense core suffers little attenuation due to the saturation of the medium, an effect first observed by Tai et. al.[3].

Recently McCord and Ballagh [4] have predicted, via numerical simulation, an exciting, potentially important new phenomenon - the possibility of controlling one polarisation component of a laser beam propagating through an absorptive medium with a beam of opposite polarisation. They showed that under suitable conditions, an elliptically polarised laser beam propagating through a $J=1/2$ to $J=1/2$ atomic system can separate into a central Gaussian core of circular polarisation surrounded by a ring of opposite circular polarisation. The two beams are spatially separated, the intensity distribution of one polarisation component depends on the strength of the other component.

Until now, no experimental evidence for this prediction has been presented. Only the formation of rings in a purely absorptive medium was reported by Sohrab and Lawandy [5] without giving any details of the polarisation state of the observed beams.

Here, we present the first experimental evidence for the polarisation separation. A laser beam was tuned to the centre of the pressure broadened D1 transition of atomic sodium and is focussed to a waist of $80\text{ }\mu\text{m}$ at the input face of a vapour cell. In the presence of 100 torr argon the homogeneous line width is approximately 1 GHz, sufficient to mix the $F=1$, $F=2$ hyperfine states. The $3S-3P$ transition then resembles a $J=1/2$ to $J=1/2$ transition. The input ellipticity is controlled by a polarisation rotator and a polariser. The beam leaving the cell was analysed using a Babinet Soleil compensator and polariser, allowing both the $\sigma+$ or $\sigma-$ component to be imaged onto a screen. The full 2 dimensional intensity distribution was recorded on video tape and later digitised for processing. The vapour density was determined from absorption scans at intensities below the onset of saturation. Typical line centre absorption coefficients were 1000 m^{-1} , with corresponding Fresnel numbers of 40.

An example of the observed intensity distributions for σ_+ and σ_- is given in Fig.1. With an input power of 120mW and an ellipticity of 0.2 the initially stronger σ_+ beam shows a ring structure after propagation through 0.03m of vapour. The σ_- beam is considerably narrowed to the size of the hole in the ring of the σ_+ beam. Notice that both profiles are recorded with similar but not identical intensity scales. The observed structure appears at the absorption line centre of the transition and can only be explained by the process proposed by McCord and Ballagh. The behaviour is in qualitative agreement with the numerical predictions for small propagation distances. Unfortunately we have not yet observed all the features of the numerical model. Our calculations suggest that we require twice the laser power in order to achieve complete separation of the polarisation components and to observe the self-guiding of the beams.

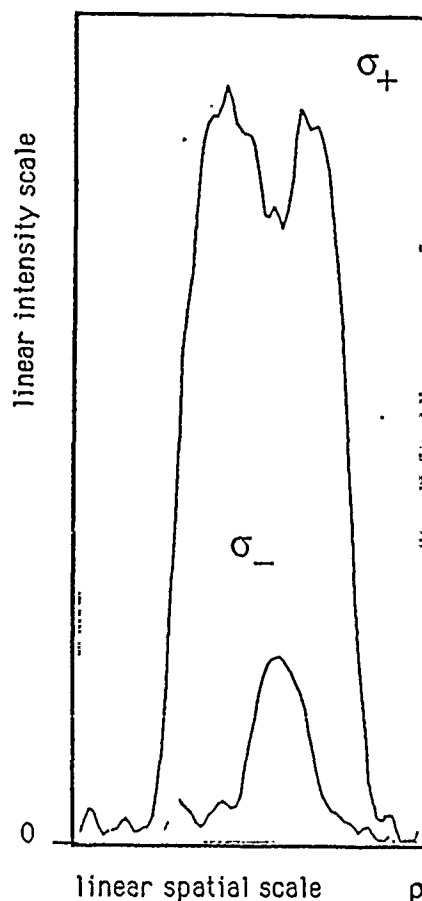
This experiment demonstrates the nonlinear coupling of the polarisation modes, in particular the exciting possibility of controlling the intensity of one of the modes by the other. This could form the k component for digital optical processing in a homogeneous medium.

References:

- [1] A. Javan, P.L.Kelly, IEEE J.Quant.Elect. 2 470 (1966)
- [2] M.G.Boshier, W.J.Sandle, Opt.Comm. 42, 371 (1982)
- [3] A.W.McCord R.J.Ballagh JOSA B January (1990)
- [4] R.Sohrab Afzal N.M.Lawandy Optics Letters 14, 794 (1989)
- [5] K.Tai, H.M.Gibbs, M.C.Rusford, N.Peyghambarian, J.S.Satchell, M.G.Boshier, R.L.Ballagh, W.J.Sandle, M.Leberré, E.Ressayre, A.Tallet, J.Teichmann, Y.Claude, F.P.Mattar, P.D.Drummond Opt.Lett. 9, 243 (1984)

Fig.1

Spatial intensity distributions of the two polarisation components σ_+ and σ_- after propagating through the absorptive medium. The input beam shows a Gaussian distribution with a width of the σ_+ component. The linear scale for both components is comparable.



**TP33 Theoretical Study of Optical Second-Harmonic
Generation from a Nonlinear Medium of Finite Cross-Section**

Ryuji MORITA, Nagaatsu OGASAWARA,
Shinsuke UMEGAKI[†] and Ryoichi ITO

*Department of Applied Physics, Faculty of Engineering, the University of Tokyo,
7-3-1, Hongo, Bunkyo-ku, Tokyo 113, Japan*

[†] *Department of Electronics, Faculty of Engineering, Tokyo Engineering University,
1404-1, Katakura-cho, Hachioji, Tokyo 192, Japan*

Optical second-harmonic generation from a nonlinear medium embedded in a linear medium was theoretically investigated. The electromagnetic radiation theory was used to obtain the general expression for the far-field radiation pattern and the integrated power of the second-harmonic wave generated from a nonlinear prism with a rectangular cross-section. The fundamental wave was taken to propagate as a plane wave; wave-guiding effects were not considered.

The the far-field radiation pattern is essentially determined by a product of two factors; one corresponds to the diffraction pattern of a rectangular aperture, and the other originates from the phase-matching condition in the direction parallel to the fundamental-wave propagation. As example of the second-harmonic far-field pattern, consistent with experiment, is shown in Fig. 1 for a Čerenkov-type phase matching condition.

Approximate analytic expressions were derived for the total second-harmonic power for the two limiting cases: the interaction length much larger (Case A) and much smaller (Case B) than the linear dimension of the cross-section of the nonlinear prism. In Case A, Čerenkov-type phase matching is possible, where the velocity of the nonlinear polarization wave exceeds that of the free second-harmonic wave. The second-harmonic power is emitted at a constant rate over the interaction length, resulting in the total

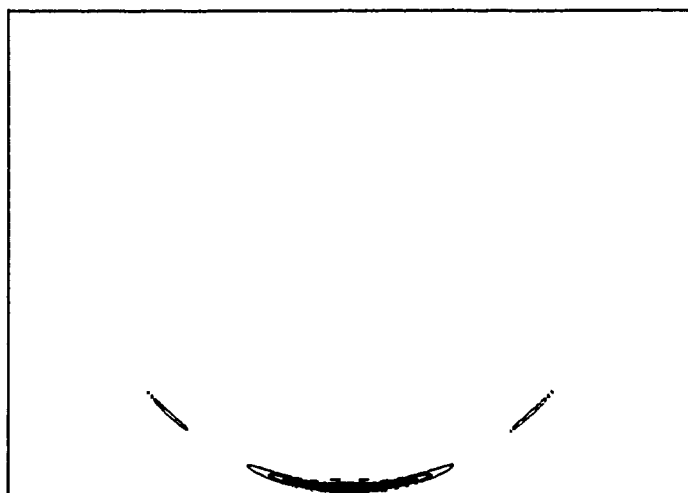


Fig. 1. Contour diagram of far-field pattern of Čerenkov-type second-harmonic wave from a nonlinear prism.

harmonic power that increases linearly with the length of the nonlinear prism. In case B, the diffraction condition restricts the phase matching only to the collinear one. The expression for the second-harmonic power is found to agree exactly with the formula obtained on the basis of the coupled-wave theory.¹⁾ Under the collinear phase-matching condition, the second-harmonic power exhibits a familiar quadratic dependence on the interaction length.

Result of numerical calculation will also be reported, and optimum-design conditions for the Čerenkov-type second-harmonic generation will be discussed in detail.

Reference

- 1) J. A. Armstrong, N. Bloembergen, J. Ducuing and P. S. Pershan: Phys. Rev. **127** (1962) 1918.

Carrier Cooling in Strained $\text{In}_x\text{Ga}_{1-x}\text{As}$ GaAs Single Quantum Well

Yu Zhenxin, Peng Wenji and Li Qingxing

Ultrafast Laser Spectroscopy Laboratory, Zhongshan University
Guangzhou 510275, P. R. China

Yuan Shu and Qian Shixiong

Physics Department, Fudan University, Shanghai 200433, P. R. China

summary

Recently, considerable interest has been developed in semiconductor quantum wells and heterostructures of the lattice-mismatched $\text{In}_x\text{Ga}_{1-x}\text{As}/\text{GaAs}$ system because of their potential for high speed and photoelectronic device applications. The recognition of the hot-electron properties in semiconductor microstructure is needed to develop small fast optoelectronic devices. We report the measurement of the carrier cooling behavior in the strained $\text{In}_x\text{Ga}_{1-x}\text{As}/\text{GaAs}$ single quantum well samples of different In content with the same well thickness $L_z = 50 \text{ \AA}$, which allows us to separate the influence of dimensionality and In content x on the carrier cooling.

The samples grown by MBE (molecular beam epitaxy) are excited with a synchronously pumped mode-locked dye (Rh6G) laser (Spectra-physics Inc. Series 3000) with a repetition rate of 4 MHz and a pulse duration of 6 ps. The photon energy of excitation beam is 2.13 eV. The photoluminescence of the sample is spectrally dispersed by a W2 monochromator and temporally resolved by a 2D Hamamatsu synchroscan streak camera (C1587 + M1955).

From the transient photoluminescence spectra of the transitions between the $n = 1$ electrons and heavy holes in the strained $\text{In}_x\text{Ga}_{1-x}\text{As}$ layer amounted at 1.45 eV with the k -coversion at various delay times after the maximum of the excitation pulse, we obtain the temporal behaviors of the carrier temperature T_e for two strained $\text{In}_x\text{Ga}_{1-x}\text{As}/\text{GaAs}$ SQW with two different In contents $x = 0.2$ and 0.1, which show that a rapid cooling during the first 100 ps from about 1000 K and 500 K to 300 K and 180 K respectively, followed by a considerably slower decrease of T_e in both samples at the same excitation level. Obviously carriers remain hot at delay times up to 500 ps (Fig. 1)

Our theoretical description of the cooling processes is based on Fermi-Dirac statistics for electrons and holes in the quazi- equilibrium states. The energy-loss mechanism for $T_e \geq 150 \text{ K}$ is given.

The authors gratefully acknowledge the Support of National Science Foundation of China and K. C. Wong Education Fundation, Hong Kong.

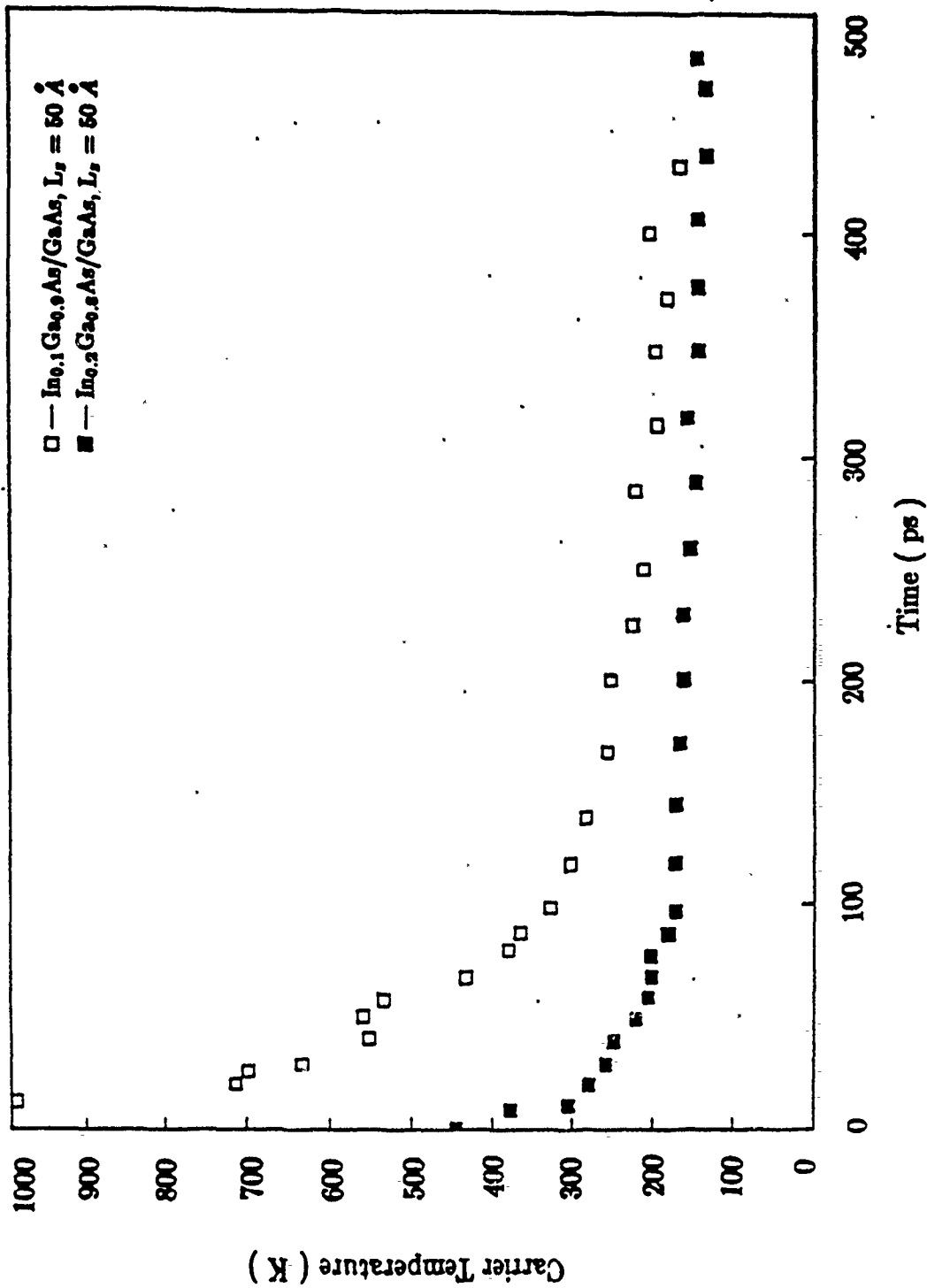


Fig. 1. Carrier cooling temporal processes of the two strained $\text{In}_x\text{Ga}_{1-x}\text{As}/\text{GaAs}$ SQW with different In content x for the excitation level of about $2 \times 10^{12} \text{ cm}^{-2}$ at 77 K.

Coulomb Enhancement of Ultrafast Nonlinearities in Quantum Well Structures

J. Khurgin

Department of Electrical and Computer Engineering
The Johns Hopkins University
Baltimore, MD 21218

Recent works in the area of ultrafast nonlinearities due to virtual carriers in semiconductor heterostructures have generated significant interest among researchers. It has been shown¹ that excitons in QW's behave very much like conventional two-level atoms, to the extent that exciton-exciton interaction can be neglected. Therefore, fast coherent phenomena usually associated with two-level system may occur in excitonic QW transitions. Indeed, dynamic (AC) Stark effect in QW's have been demonstrated^{2,3}. When semiconductor QW's were pumped below the absorption edge there were a strong "blue" shift of the exciton resonance, accompanied by a strong bleaching.

The effect of blue shift caused by the below absorption edge excitation can be understood very simply if one uses virtual carrier (or virtual exciton) concept⁴. The virtual carriers are excited by the nonresonant (below the bandedge) radiation. In the limit of long electric dipole relaxation time T_2 virtual carrier population pulsates with Rabi frequency $\Omega = \mu E / \hbar$ and amplitude proportional to the light intensity and inversely proportional to the square of detuning. Therefore, absorption is modulated with Rabi frequency, i.e. absorption sidebands appear at frequencies $\omega \pm \Omega$. This is called dynamic Stark effect⁵.

In this work we discuss influence of Coulomb carrier-carrier or exciton-exciton interaction on the ultrafast nonlinear optical properties of QW's. Due to large differences in effective masses of electron and hole in III-V QW's electron and hole wavefunctions can be separated from each other by relatively large (tens of \AA) distances, as, for example, in stepped QW (symmetric or asymmetric) shown in Fig.1a. In this situation, interaction between virtual carriers can be treated in Hartree approximation, and can be expressed in the form of Coulomb potential $V(t)$ (Fig.1d). Since the magnitude of this potential is proportional to the virtual population, it pulsates with the Rabi frequency Ω . When treated as perturbation, this pulsating Coulomb potential leads to synchronous pulsations of the energy levels (shown in dashed lines in Fig.1e). In other words, introduction of Coulomb carrier-carrier or exciton-exciton interaction into the description of pump-probe experiment, results in a following situation: *saturation of upper state (phase state filling) and increase of the energy difference between ground and excited levels occur simultaneously and in phase with each other at the same frequency Ω . As a result, dynamic Stark effect is enhanced.* Similar enhancement occurs for the case of intersubband transitions, where spatial separation between ground and excited electron levels can be made quite large.

We present the results of calculations of the Coulomb enhancement of dynamic Stark effect in the QW's of different geometries, for the cases of excitonic, band-to-band and intersubband transitions. It is shown that by proper design of QW's, the dynamic Stark effect can be enhanced by as much as factor of 5 and for the intersubband transitions by a factor of two to four depending on modulation doping density. An interesting situation occurs for the bandedge transitions, where Coulomb enhancement is insignificant at low temperatures, but at

room temperature it can be observable. We also consider potential applications of the effect in the ultrafast all-optical switching devices.

This work is supported by AFOSR.

References

- ¹ S. Schmitt-Rink and D. S. Chemla, Phys. Rev. Lett., **57**, 2752, (1986).
- ² A. Mysyrowicz, D. Hulin, A. Antonetti, and A. Migus, Phys. Rev. Lett., **58**, 2748, (1986).
- ³ A. Von Lehmen, D. S. Chemla, J. E. Zucker, and J. P. Heritage, Opt. Lett., **11**, 609, (1986).
- ⁴ E. Yablonovitch, J. P. Heritage, D. E. Aspnes, and Y. Yafet, Phys. Rev. Lett., **63**, 976, (1989).
- ⁵ R. W. Boyd and M. Sargent III, J. Opt. Soc. Am. B, **5**, 99, (1988).

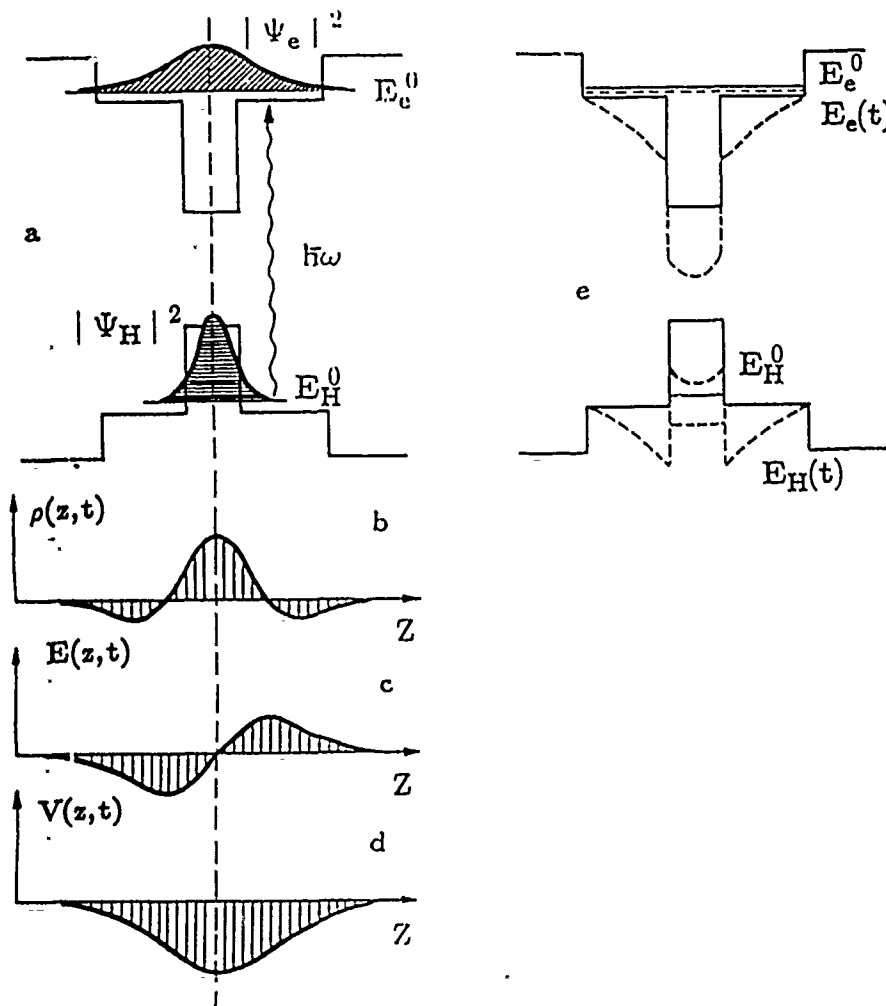


Fig.1. Coulomb-assisted energy level pulsations of excitonic transition in stepped quantum well.

- a. geometry of the QW and the ground states energies and wavefunctions for conduction and valence bands.
- b. pulsating virtual charge density $\rho(z,t) = \rho(z)e^{-i\Omega t}$
- c. pulsating electric field $E(z,t) = E(z)e^{-i\Omega t}$
- d. pulsating Coulomb potential $V(z,t) = V(z)e^{-i\Omega t}$
- e. pulsating energy levels for electron and hole $E_{e,h}(t) = E_{e,h}^0 + \delta E_{e,h}e^{-i\Omega t}$

Nonlinear Absorption In a Strained InGaAs/GaAs MQW/n-i-p-i Structure

T. E. Van Eck, K. P. Aron, G. A. Hansen, and R. S. Lytel
 Lockheed Palo Alto Research Laboratory
 3251 Hanover St., O/97-20, B/202
 Palo Alto, CA 94304

S. Niki, W. S. C. Chang, and H. H. Wieder
 University of California, San Diego
 Department of Electrical and Computer Engineering, R-007
 La Jolla, CA 92093

The quantum well/n-i-p-i structure combines the high sensitivity of a n-i-p-i structure with the relatively large modulation depth of a multiple quantum well (MQW) modulator.^{1,2} We report here the first demonstration of nonlinear absorption in a MQW/n-i-p-i structure in the InGaAs/GaAs material system, a lattice mismatched material system³ which features a transparent substrate and an isolated absorption peak. Both a two-beam pump-probe measurement and a one-beam nonlinear absorption measurement are reported. The low optical power suggests that operation of large arrays with moderate laser power may be feasible.

Our structure consists of 5 p-i-n structures of alternating polarity, with 10 quantum wells in each i region, and an internal electric field of 6 V/ μ m. The structures were grown on a strained superlattice buffer to isolate the quantum wells from dislocations caused by the lattice mismatch with the substrate. In the cw pump-probe measurement a 780 nm diode laser pump and a tungsten lamp probe were used. Figure 1 shows the transmittance spectrum near the absorption edge with and without the 1.4 W/cm² pump. Without the pump the absorption peak is red-shifted, weakened, and broadened by the internal electric field. The pump creates carriers in the quantum wells, which are swept out, reducing the electric field and blue-shifting the peak. Figure 2 shows the differential transmittance spectra for pump intensities from 5 mW/cm² to 1.4 W/cm². These intensities are several orders of magnitude less than those required for absorption saturation in unbiased quantum wells.

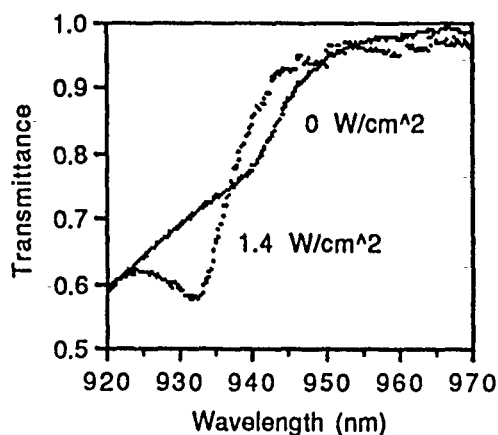


Figure 1. Probe transmittance with and without the 1.4 W/cm² pump.

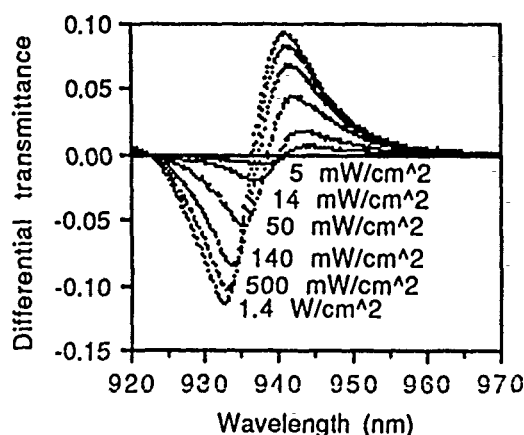


Figure 2. Differential probe transmittance as a function of pump intensity.

Using the differential transmittance data and the measured effect of electric field on the absorption peak, the recombination time and potential drop across the p-i-n diode are calculated for each value of pump intensity, and are shown in Figure 3. The dependence of the recombination time on the potential suggests that recombination is due to a tunneling, not thermal, mechanism.⁴

The nonlinear transmittance was measured using a single pulsed incident beam from a tunable Ti:sapphire laser with a pulse length of 50 nsec. The measured transmittance vs. intensity, presented in Figure 4, shows increasing transmittance at 942.5 nm and decreasing transmittance at 931.9 nm, in agreement with the cw pump-probe measurement. Since this is a nonequilibrium measurement the intensities are larger than in the cw measurement, but the transmission change as a function of photogenerated sheet charge density is consistent with the cw measurement.

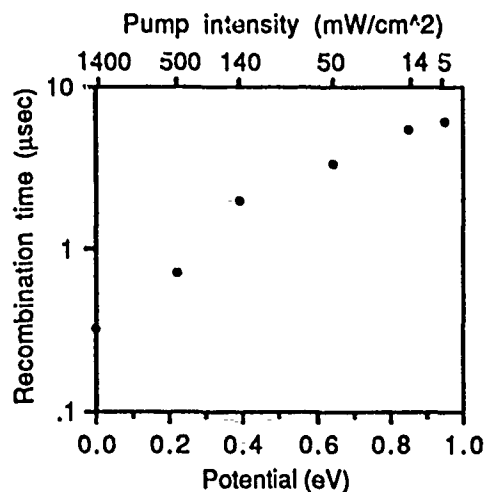


Figure 3. Calculated recombination time as a function of pump intensity and potential drop across the p-i-n diode.

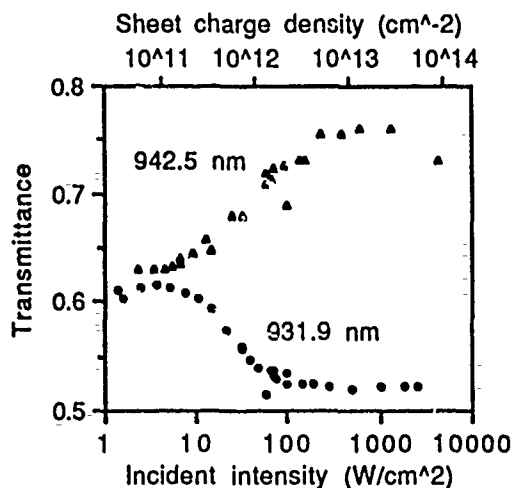


Figure 4. One-beam transmittance as a function of incident intensity and calculated sheet charge density.

References

1. A. Kost, E. Garmire, A. Danner, and P. D. Dapkus, *Appl. Phys. Lett.* **52**, p. 637 (1988).
2. H. Ando, H. Iwamura, H. Oohashi, and H. Kanbe, *IEEE J. Quantum Electron.* **25**, p. 2135 (1989).
3. T. E. Van Eck, P. Chu, W. S. C. Chang, and H. H. Wieder, *Appl. Phys. Lett.* **42**, 135 (1986).
4. G. H. Döhler, *IEEE J. Quantum Electron.* **22**, p. 1682 (1986).

TP13 Infrared Second Harmonic Generation by Intersubband Transitions in AlGaAs/GaAs Quantum Well Structure

A. Sa'ar, I. Grave, N. Kuze, and A. Yariv
California Institute of Technology (128-95)
Pasadena, CA 91125

Recent studies show that intersubband optical transitions in quantum wells (QW) exhibit large oscillator strength⁽¹⁾. Novel mid-infrared (8-14 μ m) devices such as detectors^(2,3) and modulators⁽⁴⁾, based on these transitions, have been proposed and demonstrated. Moreover, Fejer et. al.⁽⁵⁾ have shown recently that very large intersubband second order susceptibility (ISOS) can be obtained by electrically biasing a QW in a structure with a very short interaction length ($\sim 1\mu$ m).

In this work we report on second harmonic generation (SHG) obtained in an asymmetric QW⁽⁶⁾ with a very long interaction path length. We show that intersubband absorption and phase matching are the two dominant effects that limit the efficiency of SHG near resonance. We also point out that the SHG efficiency can be considerably enhanced far from resonance.

We have used an asymmetrically stepped QW (ASQW) structure, grown by MBE, consisting of a 60 \AA GaAs layer followed by 40 \AA Al_{0.1}Ga_{0.9}As inserted between 300 \AA Al_{0.4}Ga_{0.6}As barriers. The structure is designed so as to exhibit three confined levels with approximately equal energy spacings, $\hbar\Omega \cong E_{32} \cong E_{21} \cong 115$ meV (corresponding to 10.8 μ m transition wavelength). In this structure transitions between the first and third levels, which are forbidden in symmetric structures, are allowed due to the built-in asymmetry.

The ISOS in a QW is given by^(7,8)

$$d^{2\omega} = \frac{e^3 N}{\epsilon_0 \hbar^2} \frac{\langle z \rangle_{12} \langle z \rangle_{23} \langle z \rangle_{31}}{(\omega - \Omega - i\delta)(2\omega - 2\Omega - i\delta)} \quad [1]$$

where $\langle z \rangle_{ij} = \langle \psi_i | z | \psi_j \rangle$, $\delta \cong 7$ meV is the linewidth of the states⁽¹⁾ and N is the carrier density. The solid line in Fig. 1 shows the variation of $d^{2\omega}$ with frequency. The value of the ISOS at resonance was calculated to be $d_{res} \cong 10^{-6}$ m/v, three orders of magnitude larger than the value in bulk GaAs (shown by the dashed line, $d_{bulk} \cong 4 \times 10^{-10}$ m/v). Moreover, off resonance and at lower frequencies, the ISOS is still larger by more than an order of magnitude than that of bulk GaAs. Two additional factors have considerable effect on the efficiency of SHG, phase matching and absorption. Due to dispersion one has $\Delta k = k^{2\omega} - 2k^\omega = 2\omega/c [n(2\omega) - n(\omega)] \neq 0$. Hence, the effective contribution to SHG is limited to a somewhat short coherence length $L_c \cong 1/\Delta k$. To circumvent this limitation one can resort to quasi phase matching⁽⁹⁾ by taking advantage of the sensitivity of the ISOS to an external electric field. By applying a periodically alternating electric field along the direction of propagation one can spatially modulate $d^{2\omega}$ with a period Λ . By choosing $1/\Delta k \cong \Lambda$ we get quasi phase matching conditions, i.e., $\Delta k_{eff} = \Delta k - \Lambda \cong 0$.

The absorption of the pump and of the SHG also play an important role. In particular, near resonance the intersubband absorption of those fields is fairly large.⁽¹⁰⁾ Under most practical situations the oscillator strength for the 1 \rightarrow 2 transition is larger than the one for the 1 \rightarrow 3 transition. Thus, one can assume that $\alpha^\omega \gg \alpha^{2\omega}$. The expression for these absorption coefficients can be written as

$$\alpha_{1j}(\omega) = e^2 \sqrt{\frac{\mu_0}{\epsilon}} \left| \langle z \rangle_{1j} \right|^2 N \frac{\omega \delta}{(\Omega - \omega)^2 + \delta^2} \quad [2]$$

whereas we assume that the linewidth of the levels are approximately equal. In Fig. 1 we show the theoretical spectral dependence of the absorption coefficients. At resonance the absorption of the pump and SHG fields can be as large as $\alpha^\omega_{res} \cong 2000$ cm⁻¹ and $\alpha^{2\omega}_{res} \cong 100$ cm⁻¹ respectively. By taking into account these effects, the efficiency of the SHG can be approximated by

$$\frac{P^{2\omega}}{P^\omega} = 8 \left(\frac{\mu}{\epsilon_0} \right)^{3/2} \epsilon_0^2 \omega^2 \frac{(d^{2\omega})^2}{n^3} \left[\frac{P^\omega}{\text{area}} \right] \frac{e^{-\alpha^{2\omega} z}}{\Delta k^2 + (\alpha^\omega)^2} \quad [3]$$

In the regime where $\Delta k \ll \alpha^\omega$ one can see that a coherent contribution to the SHG is limited to an effective length $1/\alpha^\omega$, where the length of the device should not exceed $1/\alpha^{2\omega}$. As can be seen from Eq [3], the operating spectral range of the device should be near $\omega = \Omega/2$. In this case the values of the absorption coefficients can be reduced by two orders of magnitude while the ISOS is still larger than that of bulk GaAs. The limiting process turns out to be phase-matching through the availability of a periodic modulation of the ISOS.

The intensity of the SHG in our ASQW structure was measured by using a CO₂ laser chopped at 325 Hz, together with a mercury-cadmium-telluride detector in a standard lock-in detection scheme. A sapphire window was used to block the CO₂ laser wavelength while a second narrow band filter ensured that only SHG was detected. In Fig. 2(a) we show the intensity of the SHG as a function of the pump level for a sample 500 μm long. The quadratic dependence expected for second order effect is observed.

In Fig. 2(b) we show the intensity of the SHG as a function of sample length. The exponential dependence is an indication that absorption processes are dominant. From the experimental results we estimate the value of $\alpha^{2\omega}$ to be 92 cm^{-1} .

In conclusion we have shown that second harmonic generation due to intersubband transition can be obtained in a structure with long interaction length. The efficiency of SHG is found to be dominated by intersubband absorption and by phase matching. It is found that, in order to increase the overwhole SHG efficiency, the device should operate off resonance.

References:

1. L. C. West and S. J. English, Appl. Phys. Lett. **46**, 1156 (1985).
2. J. S. Smith, L. C. Chiu, S. Margalit, A. Yariv and Y. Cho, J. Vac. Sci Technol. B **1**, 376 (1983).
3. B. F. Levine, C. G. Bethea, G. Hashain, J. Walker, and R. J. Malik, Appl. Phys. Lett. **53**, 296 (1988).
4. M. J. Kane, M. T. Emeny, N. Apsley, C. R. Whitehouse, Electron. Letts. **25** 320 (1989).
5. M. M. Fejer, S. J. B. Yoo, R. L. Byer, A. Harwit and J. S. Harris, Phys. Rev. Lett. **62**, 1041 (1989).
6. E. Rosencher, P. Bois, J. Nagle and S. Delaitre, Electron. Letts. **25**, 1063 (1989).
7. A. Yariv, Quantum Electronics, (Wiley, N.Y. 1989).
8. Y. R. Shen, The Principles of Nonlinear Optics, (Wiley, N.Y. 1984).
9. S. Somekh and A. Yariv, Opt. Commun. **6**, 301 (1972).
10. D. Ahn and S-L. Chuang, IEEE J. Quant. Electron. **QE-23**, 2196 (1987).

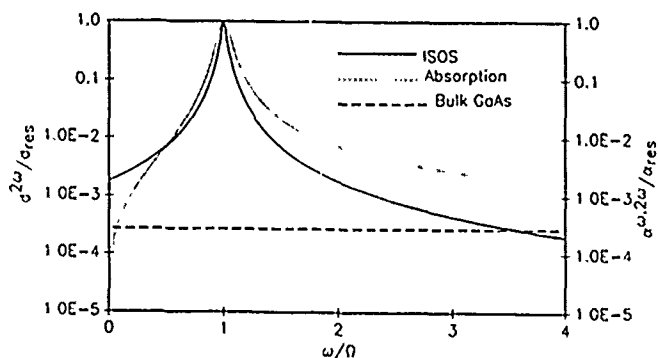
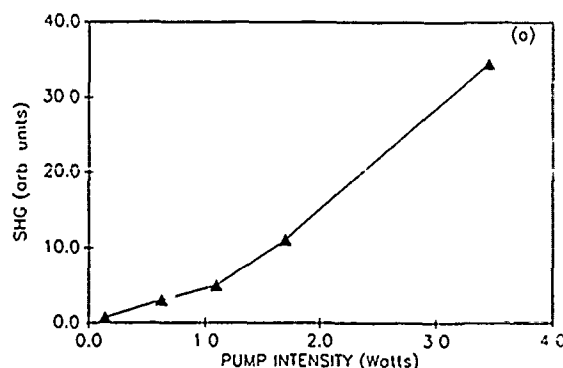
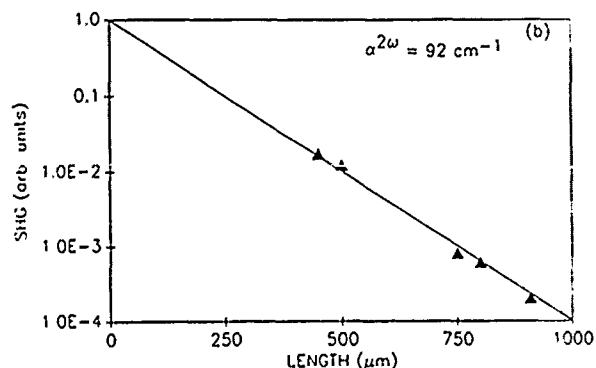


Fig. 1: Second order susceptibility (solid line) and the intersubband absorption (dashed line) as a function of the frequency.

Fig. 2: (a) SHG as a function of the pump level. The interaction length is 500 μm .
(b) SHG as a function of the interaction length. Pump Intensity is 3.5 Watts.



TP14 Optical Properties of Asymmetric Triangular Quantum Wells for Self Electro-Optic Effect Devices

R. A. Puechner, D. S. Gerber, D. A. Johnson, R. Droopad, G. N. Maracas

Center For Solid State Electronics Research, EEE 5706
Arizona State University
Tempe, AZ 85287
(602) 965-2551

We have grown by molecular beam epitaxy, asymmetric triangular quantum well self electro-optic effect device (SEED) structures and have characterized their optical properties. This is the first report of a SEED structure with nonrectangular quantum wells. The structure consists of a GaAs / AlGaAs p-i-n diode with a 10 period multi-quantum well (MQW) in the intrinsic region. Each quantum well is composed of multiple layers of GaAs and AlGaAs to approximate a linearly varying aluminum mole fraction in the well. The well is 200 Å wide with 500 Å $\text{Al}_{0.3}\text{Ga}_{0.7}\text{As}$ barriers in between. The 10 triangular quantum wells are then confined by one-micron-thick p- and n-AlGaAs regions. A mesa of 2 square millimeters is etched into the top of the structure to define the device. Ohmic contacts are made to the p- and n-AlGaAs regions for photocurrent measurements.

Both photoluminescence and photocurrent spectra show pronounced excitonic transitions in this structure due to confinement of carriers in the asymmetric triangular wells. Figure 1 shows room temperature photocurrent spectra as a function of applied reverse bias voltage. Several excitonic transitions are observed, most dominant of which are the $n=1$ light and heavy hole excitons. Transition energies are seen to shift and excitonic absorption efficiencies are seen to change with applied reverse bias. Some transitions are strengthened and others are weakened with increasing electric field. In Figure 2, the variation of the $n=1$ electron to light and heavy hole transitions with electric field are exhibited. Figure 3 shows the shift towards lower energy of these two peaks with applied voltage. A third transition in this energy range emerges with increasing electric field.

This represents the first of a series of experiments aimed at improving the performance of SEED devices by utilizing novel quantum well and superlattice structures.

Fig. 1 Photocurrent Spectra vs. Applied Bias for an Asymmetric Triangular MQW Modulator at 293K (curves shifted for clarity)

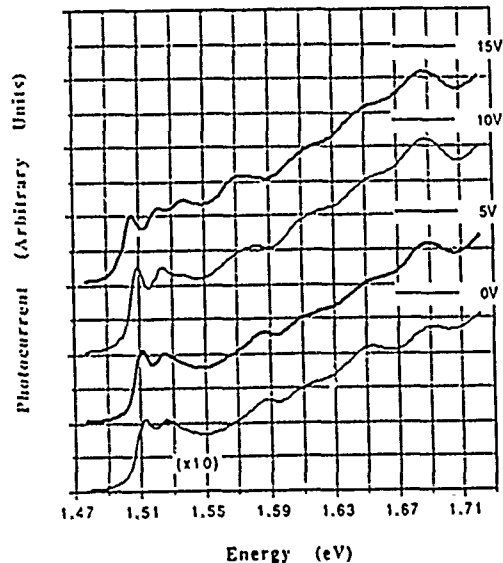


Fig. 3 The $n=1$ to heavy and light hole photocurrent peak shifts vs. applied voltage for the asymmetric triangular MQW modulator.

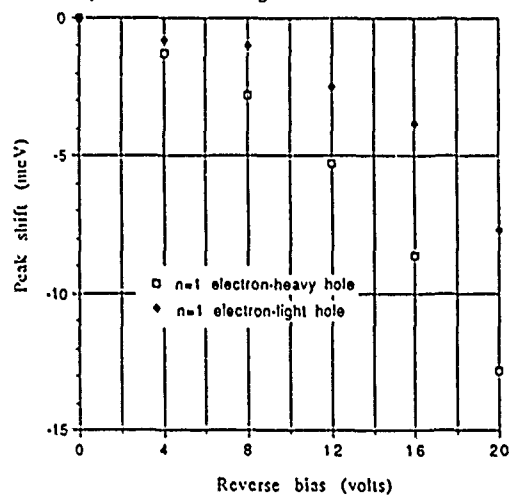
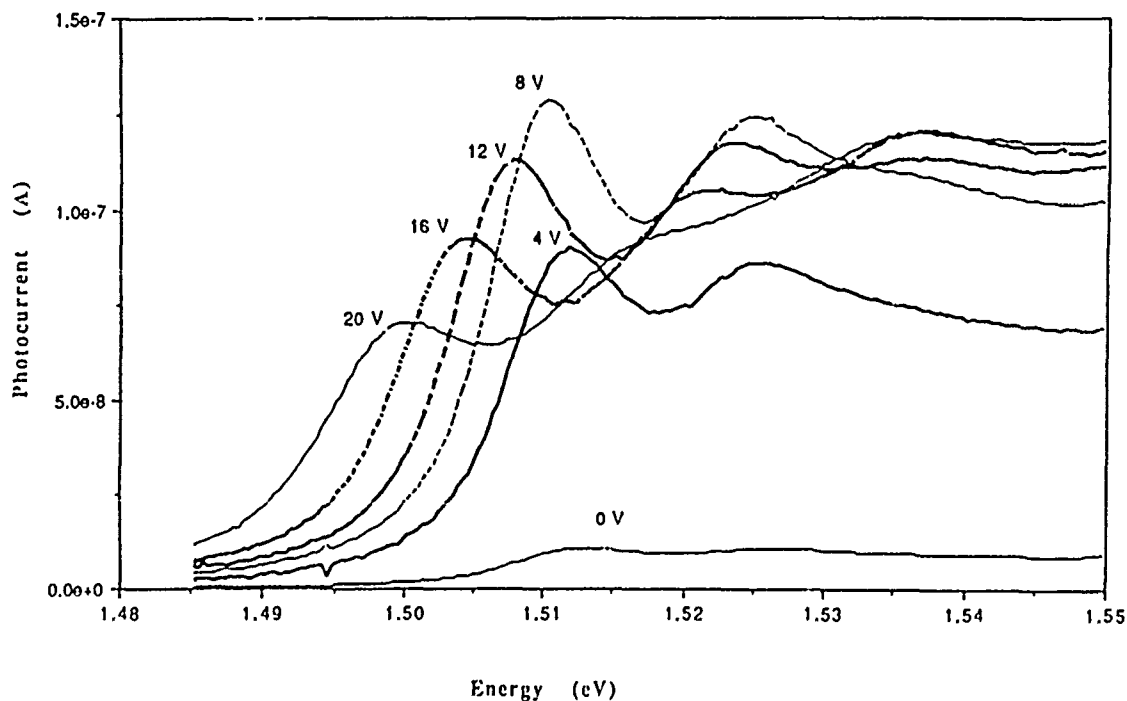


Fig. 2 Absolute Photocurrent Spectra of an Asymmetric Triangular Multiquantum Well Modulator at 293K Versus Applied Voltage



TP15 Self-Electro-optic Effect Device Based on an Asymmetric Fabry-Perot Modulator Using Wannier-Stark Localization in Superlattice

K-K. Law, R. H. Yan, L. A. Coldren, and J. L. Merz
Department of Electrical and Computer Engineering,
University of California, Santa Barbara,
Santa Barbara, CA 93106

Recently, superlattice asymmetric Fabry-Perot (SL-ASFP) reflection modulators using superlattice (SL) Wannier-Stark localization¹ have been demonstrated to achieve high contrast ratio at low voltage swings². Also, symmetric self-electro-optic effect devices (S-SEEDs) have been shown to have suitable characteristics for optical computing and information processing³. However, the on/off ratio of a normal quantum-well S-SEED is not large because it only relies on the nonlinearity of absorption coefficient that appears on the high energy side of excitonic peaks of the device's quantum wells. Since SL-ASFP is a modulator with high contrast ratio, it is expected to be a favorable candidate for a self-electro-optic effect device (SEED) with better performance. In this work, we connected the SL-ASFP in series with a silicon photodiode (Fig 1) to form a superlattice Fabry-Perot SEED (SL-FP-SEED) and report such device's potential of achieving higher on/off ratios than conventional SEED or S-SEED.

The normally-off SL-ASFP we employed for the SL-FP-SEED consists of a superlattice (100 and half periods of 30Å GaAs/30Å Al_{0.3}Ga_{0.7}As) inside a resonant cavity sandwiched between a less reflecting top mirror (an air-semiconductor interface) and a highly reflective bottom quarter-wave stack (15 and half periods of 618Å AlAs/535Å Al_{0.3}Ga_{0.7}As). The net Fabry-Perot reflection is turned on by reducing the cavity loss at resonance through the blue-shifted electro-absorption effect of Wannier-Stark localization in the superlattice¹. As shown in Fig 2 are the photocurrent measurements of the SL-ASFP at room temperature at various biases. The fraction of the incident light absorbed in the active region is to first order equal to one minus the reflectivity of the SL-ASFP, and in fact, the photocurrent spectra almost look like the mirror image of its reflectivity counterparts². Also, Fig 2 depicts that a negative differential resistance exists in a wide range of wavelengths (~7500Å to 7650Å) which is a necessary condition for SEED operation.

We connected the SL-ASFP in series with a 7 volt supply as shown in Fig 1. This is a circuit similar to that of a S-SEED in which the state of the SL-ASFP depends on the ratio of the incident light powers on the two diodes. We illuminated the SL-ASFP using a Ti:sapphire laser with a fixed input intensity ~1.5mW at wavelength ~7600Å where the modulator has high contrast ratio. We illuminated the photodiode with a GaAs laser diode and then ramped the incident power up and down. Shown in Fig 3 is the reflected power of the SL-ASFP vs the incident power onto the photodiode where optical bistability is clearly seen. The on/off ratio of this SL-FP-SEED is more than 5:1 and is higher than that of any SEED previously reported. This demonstrates the potential advantage of incorporating SL-ASFP into SEED designs.

REFERENCES

- [1] Mendez et al., Phys. Rev. Lett. 60, 2426 (1988).
- [2] Law et al., to be published in Appl. Phys. Lett.
- [3] Lentine et al., Appl. Phys. Lett. 52, 1419 (1988); Chirovsky et al., Paper ThD4-1, Photonic Switching, Salt Lake City Meeting '89

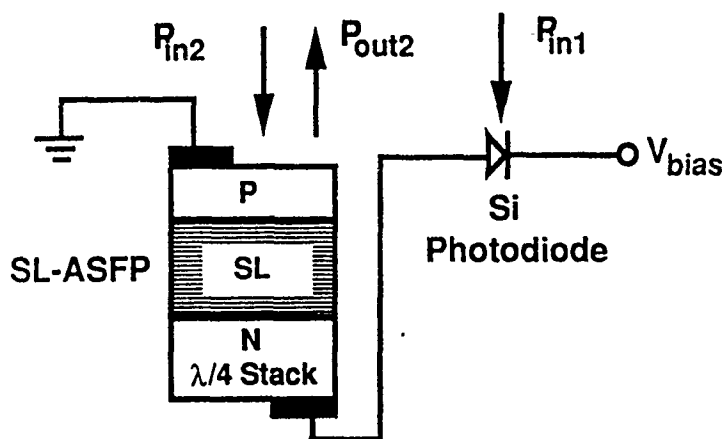


Fig 1. Schematic set-up of the SL-FP-SEED. P_{in1} and P_{in2} are the incident light powers of the Si photodiode and SL-ASFP respectively. P_{out2} is the reflected power from the SL-ASFP that can be switched by P_{in1} .

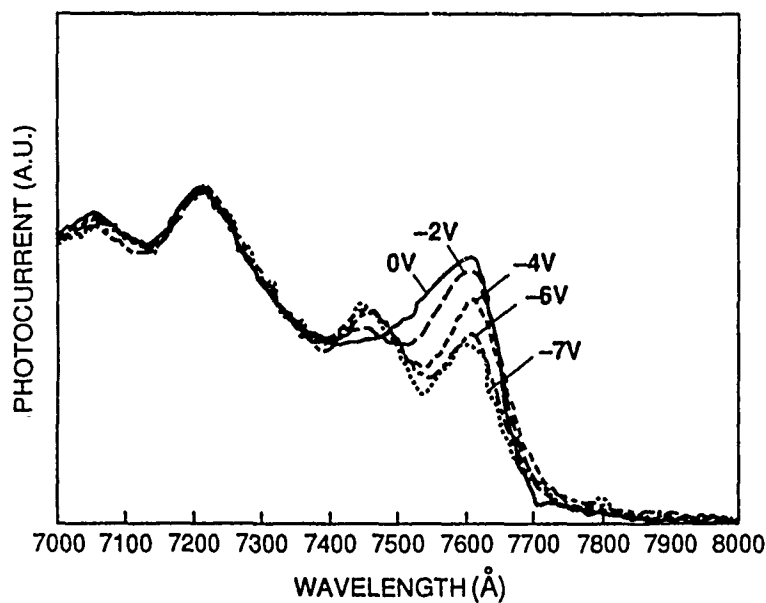


Fig 2. Photocurrent spectra of the SL-ASFP at various reverse biases. Negative differential resistance can be seen in a wide range of wavelengths.

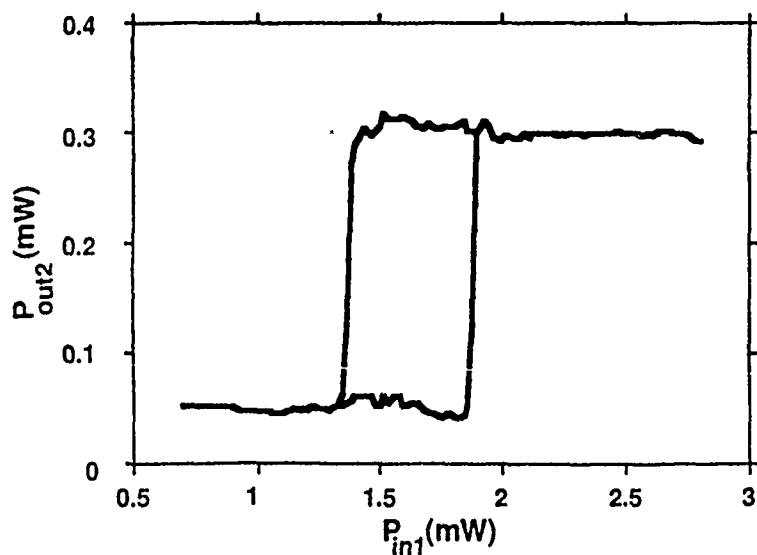


Fig 3. Optical power (P_{out2}) reflected from the SL-ASFP vs power incident onto the photodiode (P_{in1}) with P_{in2} held constant.

Transient Optical Nonlinearities in Asymmetric Superlattices

Stephen E. Ralph, Federico Capasso and Roger J. Malik
AT&T Bell Laboratories, Rm 6E-312
600 Mountain Avenue
Murray Hill, NJ 07974

Semiconductor structures which lack inversion symmetry as a result of asymmetric compositional or doping profiles have unique and potentially useful optical characteristics. We have observed significant photo-induced birefringence in asymmetric δ -doped structures using an electro-optical sampling technique. These effects result from the additive nature of the electro-optic effect ($\chi^{(2)}$) in these structures. Unlike resonant effects, this phenomena affects all optical wavelengths equally. The magnitude of the birefringence in the δ -doped structures is significantly larger than that observed in graded-gap superlattices.¹

Figure 1a depicts the doping profile of an asymmetric δ -doped superlattice in which thin layers of ionized dopants form sheets of charge, resulting in a well defined periodic modulation of the band structure (Fig. 1b). Because of the asymmetry of the structure, there is a net transport of photo-excited electrons and holes in opposite directions. This separation and accumulation of carriers results in a space charge field which opposes the field of the ionized dopants and produces a net photovoltage in addition to reducing the modulation of the band structure. The space charge field gives rise to a birefringence via the electro-optic effect. The temporal response of the birefringence and hence the space charge field is determined by measuring the difference signal between two orthogonal components of the transmitted probe beam as a function of delay between the pump and probe pulses.

The temporal response of the differential phase shift (birefringence) is shown in Fig. 2 for a range of pump intensities. At low carrier densities (Fig 2d) the photoinduced birefringence decays with a single time constant of 45ns. This is the rate of tunneling assisted recombination (path A in Fig. 1) for a nearly fully modulated (unscreened) structure. As the photo-excited carrier density increases, (Fig 2b and 2c) a fast decay component appears in addition to the longer decay time. This fast component results from increased direct band to band recombination (Fig. 1 path B) which accompanies the decreased spatial separation of electrons and holes. Further increases in pump intensity result in nearly complete screening of the dopants causing the fast decay component to become a larger percentage of the total signal.

For the highest pump intensity (a in Fig. 2) the space charge field is governed by a recombination time of $\tau = 750\text{ps}$ for times shorter than 1ns. This short decay time is followed by a longer decay of a 45ns as confirmed by absorption measurements. These times are much shorter than those typically found in symmetric nipi structures²

Since the decay times are longer than the pulse separation (10ns), the actual carrier densities are estimated from the known pump intensities and a simple rate equation. The average carrier density of the highest pump intensity shown in Fig. 2 is $6.6 \times 10^{17} \text{cm}^{-3}$, which results in $N^{\text{2D}} = 3.6 \times 10^{12} \text{cm}^{-3}$, or 72% of the doping density. This

sheet density is sufficient to cause significant screening of the impurities, and therefore the time dependent decay constant observed in Fig. 2 is expected to have a large pump intensity dependence. The carrier densities corresponding to the remaining birefringence data are b) $2.5 \times 10^{12} \text{cm}^{-2}$, c) $1.2 \times 10^{12} \text{cm}^{-2}$ and d) $1.2 \times 10^{11} \text{cm}^{-2}$.

The maximum birefringence observed was 3.8×10^{-4} with a pump fluence of $40 \text{fJ}/\mu\text{m}^2$. This implies a photo-induced space charge field of $70 \text{kV}/\text{cm}$ which correlates well with the field strength needed to sufficiently screen the dopant impurities and create a flat band condition. The index modulations observed here are comparable to those observed in resonant structures. However, the electro-optic effect demonstrated here is independent of wavelength, and therefore can be used equally well at wavelengths which have minimal absorption, $1.55 \mu\text{m}$ for example. The absorption associated with the index variations here will be limited by free carrier absorption which, for the carrier densities required, is less than 5cm^{-1} .

In conclusion, we have demonstrated a wavelength insensitive photo-induced birefringence effect which is unique to asymmetric structures. Using a picosecond electro-optic sampling technique the temporal dynamics of photo-excited carriers in δ -doped nipi superlattices were determined. The transition between the fast recombination associated with a near flat band condition and the much slower recombination of the modulated band structure was clearly observed. The peak change in the index of 3.8×10^{-4} is large enough to be useful in a variety of optical devices.

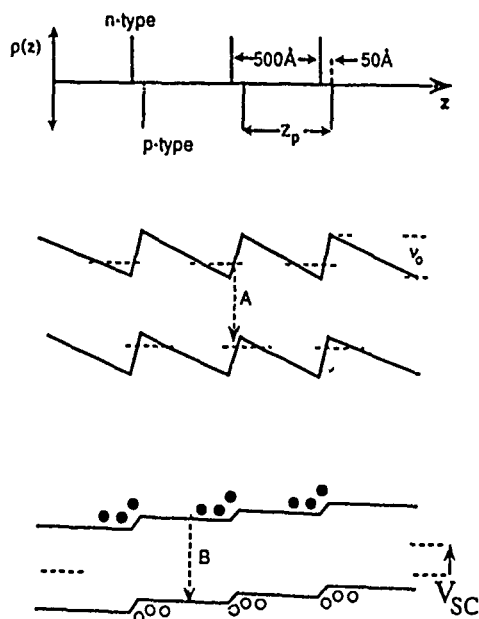


Figure 1. a) Doping profile of the δ -doped structure b) resulting modulation of the GaAs band structure c) band structure after illumination showing the space charge field.

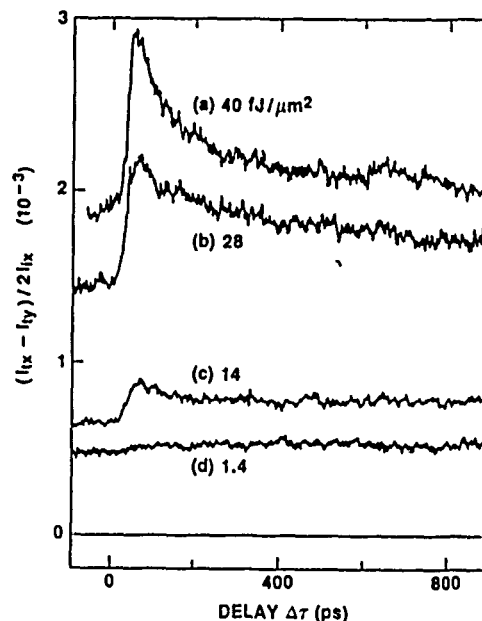


Fig. 2. Temporal response of the photo induced birefringence for decreasing pump intensities. The pump and probe wavelengths were 7000\AA and 9200\AA respectively

¹ S. E. Ralph, F. Capasso, R. J. Malik, Phys. Rev. Lett. 63, 2272 (1989).

² W. Rehm, P. Ruden, G. H. Dohler and K. Ploog, Phys. Rev. B. 28, 5937, (1983).

TP17 Precision Nonlinear Laser Spectroscopy of Exciton Dynamics in GaAs/AlGaAs Multiple Quantum Well Structures

H. Wang, J.T. Remillard, M. Jiang, and D.G. Steel
Randall Laboratory of Physics, University of Michigan, Ann Arbor, MI 48109

Frequency domain four wave mixing provides a unique method for studies of dynamics of excitations in solids. It can eliminate contributions from inhomogeneous broadening and provides a direct measurement of the homogeneous line shape of the excitation¹. The narrow optical band width (3 MHz) used in the measurement allows the measurement of excitation spectral diffusion as well as spatial diffusion at a given energy. In this paper, we discuss the use of these new nonlinear laser spectroscopy methods to studies of the lowest energy heavy hole exciton (HH1) in a GaAs/AlGaAs multiple quantum well structure (MQWS) at low temperature.

In the MQWS, interface roughness of one monolayer can result in a change in the exciton energy on the order of several meV. Consequently, heavy hole excitons at the low energy region of the HH1 absorption spectrum can be localized, while excitons at higher energy remain delocalized². Localization significantly changes exciton dynamics, and gives rise to such spectral diffusion behaviors as phonon assisted migration and thermal activation of localized excitons to delocalized states³.

The experimental configuration is based on backward four wave mixing, in which two counter-propagating pump beams interact in the sample with the probe beam through the third order nonlinear polarization producing a coherent signal beam¹. Information on the exciton homogeneous line shape is obtained by measuring the nonlinear response as a function of the backward pump frequency while fixing the frequencies of the forward pump and probe (designated the FWMb response). For excitons whose energy remains unchanged after creation, it follows from a simple hole burning picture that the FWMb response should be a symmetric function of forward pump and backward pump detuning. Our measurements at exciton energies below the absorption line center, however, show a strikingly asymmetric line shape, clearly indicating the presence of exciton spectral diffusion.

Exciton spectral diffusion is further examined by measuring the nonlinear response as a function of forward pump and probe detuning while fixing the frequencies of the backward pump and probe (designated the FWMf response). The FWMf response provides a measurement of the exciton relaxation rate at a given exciton energy. The dependence of this rate on the angle between the forward pump and probe also provides a measurement of exciton spatial diffusion coefficient. FWMf responses obtained below the exciton absorption line center show the absence of exciton spatial diffusion indicating excitons are localized in that energy region. Further measurements of the dependence of the exciton relaxation rate on the temperature shows that exciton dynamics is determined by phonon assisted migration up to a temperature of 15 K.

1. J.T. Remillard, H. Wang, D.G. Steel, J. Oh, J. Pamulapati, and P.K. Bhattacharya, Phys. Rev. Lett. **24**, 2861 (1989).
2. J. Hegarty, L. Goldner, and M.D. Sturge, Phys. Rev. B **30**, 7346 (1984).
3. T. Takagahara, Phys. Rev. B **32**, 7013 (1985).

Optical Properties of Strained-Layer InAs/GaAs Quantum Wells in Hetero n-i-p-i Structures

Tom Hasenberg

Hughes Research Laboratories,
3011 Malibu Canyon Road, Malibu, CA 90265

Alan Kost and Elsa Garmire

Center for Laser Studies, University of Southern California,
Los Angeles, CA 90089-1112

Semiconductor lasers with strained-layer InAs/GaAs active regions offer the possibility of low thresholds as well as lasing in the 900 nm - 1000 nm range. On the other hand, there have been very few studies of semiconductor materials that would be suitable as all-optical modulators for these lasers. Toward this end, we have performed the first studies of the optical properties of InAs/GaAs layers imbedded in a GaAs doping superlattice. We also demonstrate the usefulness of n-i-p-i structures for measurements of electroabsorption without the need to fabricate external contacts, in fact, without any material processing beyond the initial epitaxial growth. Furthermore, it is shown that electroabsorption is an extremely sensitive diagnostic which can be used to study the optical properties of new quantum structures.

Hetero n-i-p-i structures have been grown by conventional molecular beam epitaxy and by migration enhanced epitaxy. All structures are grown on GaAs substrates which are transparent at the wavelengths of interest. The i regions contain multiple quantum wells. The quantum well barriers are GaAs and the wells themselves are short period InAs/GaAs superlattices. The use of alternating InAs and GaAs layers to produce a region of smaller band-gap avoids the problem of alloy disordering arising from the use of an InGaAs ternary.

Figure 1 shows the low intensity transmission of a n-i-p-i containing 110 Å wide quantum wells. We attribute the pronounced dip near 978 nm and the slight depression near 957 nm to transitions involving excitons in the wells. Figure 2 displays the fractional change in the transmission of the n-i-p-i when illuminated by a HeNe laser. The laser light excites electron-hole pairs in the structure which partially cancel the built-in electric fields of the p-n junctions, so that the fields across the quantum wells become smaller. The oscillations centered at 978 nm and 957 nm in the resulting nonlinear spectrum are characteristic of blue shifts of the excitonic features. The oscillation centered at 957 nm very clearly shows the presence of an excitonic transition which is barely visible in the linear transmission.

We will discuss the effects of the superlattice structure on the nonlinear optical properties of the n-i-p-i's and present calculations of optical transition energies. The modulation amplitude in these n-i-p-i's is enhanced when they are excited with longer wavelength light, which is absorbed primarily by the quantum wells, and when reflective coatings are used.

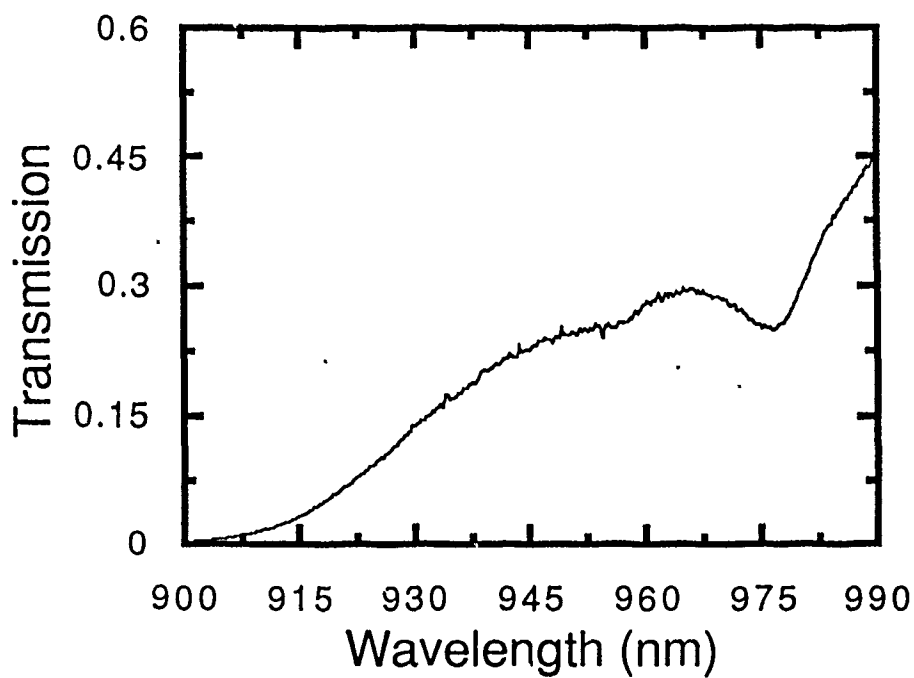


Figure 1. The low intensity, linear transmission of a strained-layer hetero n-i-p-i.

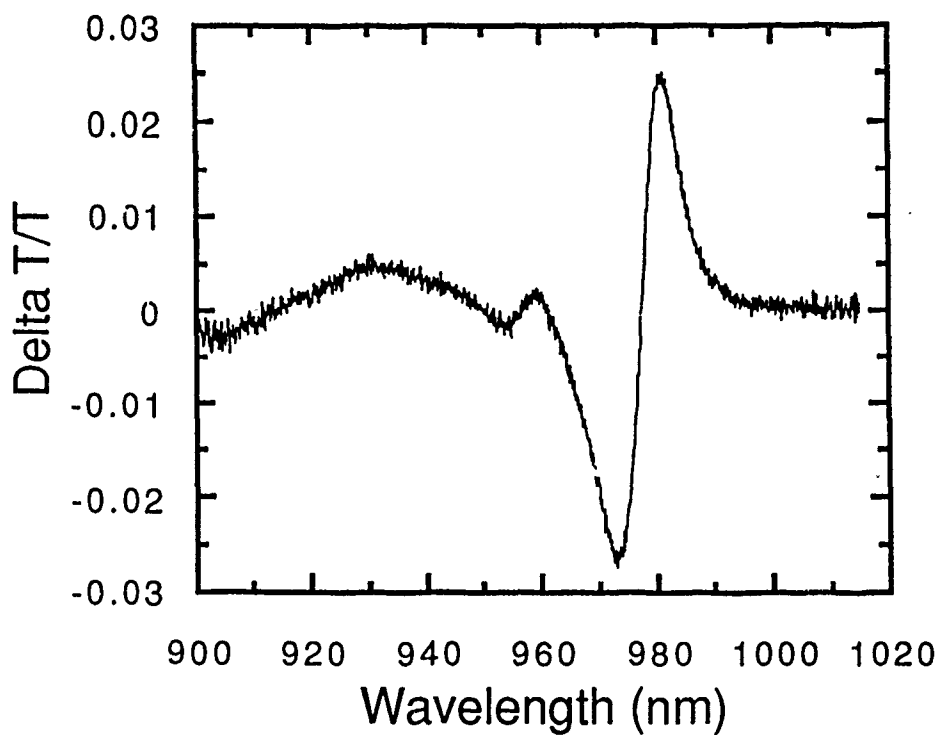


Figure 2. The nonlinear transmission of the same n-i-p-i illuminated with a HeNe laser.

TP19 Nonlinear Optical Absorption Caused by Interaction Between Interband - and Intraband-Resonant Lights in Multiple Quantum Well Structure

Susumu NODA, Tetsuya UEMURA, and Akio SASAKI

Department of Electrical Engineering, Kyoto University
Kyoto 606, Japan

There is a great interest in nonlinear optical phenomena in multiple quantum well (MQW) structure. However, the investigation has been focused on either interband or intraband transition. If the interband and intraband transitions are utilized simultaneously, new application fields such as light-controlled optical modulation can be expected. (Fig.1) In this paper, we investigate theoretically the nonlinear optical absorption of interband-resonant light in n-doped MQW structure, which is caused by the simultaneous incidence of intraband-resonant light. Here we use the transition from bound to extended states as the intraband transition.

The n-doped $\text{Al}_{0.3}\text{Ga}_{0.7}\text{As}/\text{GaAs}$ MQW structure was used for the analysis, where the widths of GaAs well and AlGaAs barrier are 40Å and 140Å, respectively, and the sheet carrier density in the well is $1.5 \times 10^{12} \text{ cm}^{-2}$.

First of all, we analyzed the optical absorption due to the transition from bound to extended states in the MQW structure, where the wavefunction in the extended state was obtained by using Kronig-Penny model. Figure 2 shows the calculated linear absorption spectrum for a single well. The discontinuous absorption curve reflects the forbidden energy band formed in the extended state energy level. This is the first report of the analysis for the bound to extended state optical absorption in MQW structure.

Then, using the density matrix formulation with the relaxation-time approximation, we analyzed the nonlinear optical absorption for interband-resonant light caused by the incidence of intraband-resonant light. The obtained absorption coefficient α for interband-resonant light is expressed as:

$$\alpha = \alpha_0 - a \cdot I_s + b \cdot I_c \quad (1)$$

where I_s and I_c are the optical powers of interband- and intraband-resonant lights, respectively. α_0 represents the linear absorption term, $-a \cdot I_s$ the absorption saturation term, and $b \cdot I_c$ the nonlinear absorption term caused by the interaction between interband- and intraband-resonant lights. Figure 3 shows the calculated α as a function of I_c , where the wavelengths of interband- and intraband resonant lights are taken to be $\lambda_s = 780 \text{ nm}$ and $\lambda_c = 7 \mu\text{m}$, respectively. The intraband relaxation time and the temperature were taken to be 0.2ps and 77K, respectively. From the figure, we can see that the large absorption coefficient change from 60 to 4180 cm^{-1} is obtained by changing I_c from 0 to 1 MW/cm^2 . This result indicates that the optical modulation for interband-resonant light can be realized by the incidence of intraband-resonant light as a controlled light. Detailed results such as wavelength, doping level, and MQW structure dependences of the absorption coefficient will be presented at the conference.

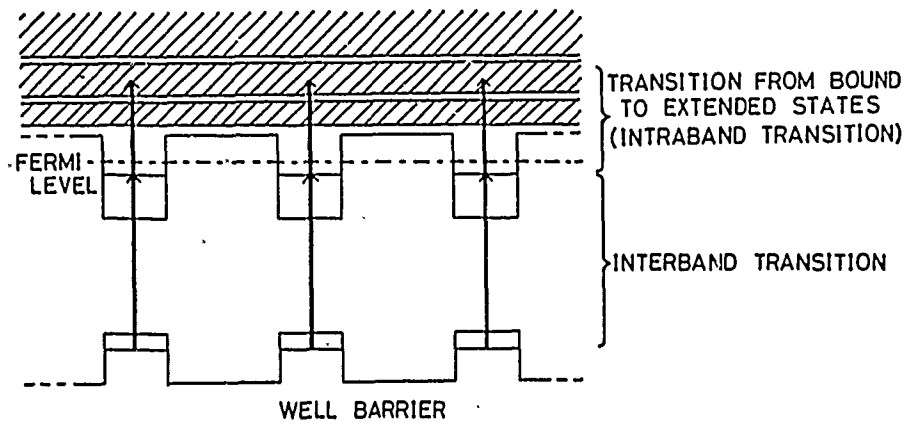


Fig.1 Schematic diagram to show simultaneous use of interband and intraband transitions in n-doped MQW structure. Where the transition from bound to extended states is used as the intraband transition, which is useful to obtain the large tolerance for the choice of wavelength.

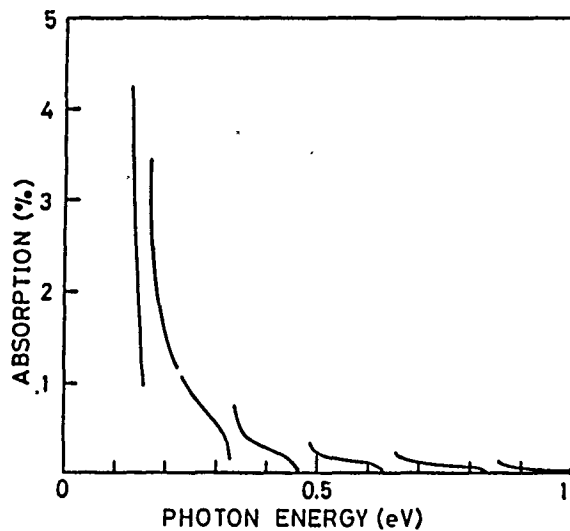


Fig.2 Absorption spectrum for a single well due to the transition from bound to extended states in n-doped MQW structure. The discontinuous absorption curve reflects the forbidden band formed in the extended energy level. The actual absorption curve, however, becomes smoother because the carrier relaxation broadening occurs.

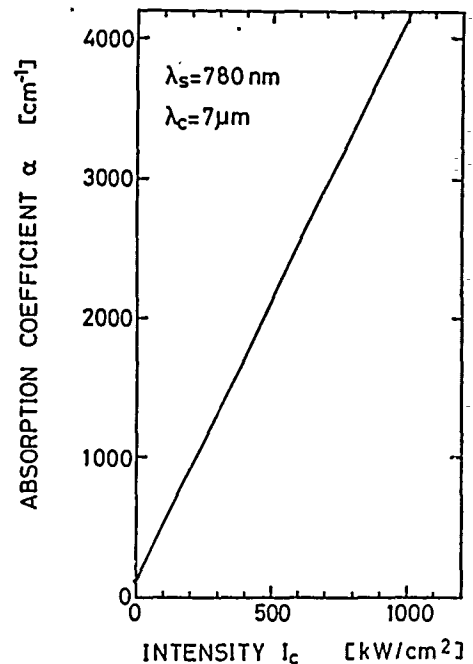


Fig.3 Absorption coefficient for interband-resonant light as a function of optical power of intraband-resonant light. A large absorption coefficient change is obtained by the interaction of both lights.

A Novel Single Mode Oscillator Incorporating an Internal Multi-mode Optical Fibre and Phase Conjugate Reflector

Barry Luther-Davies, Ariel Lieberman, Arthur Madzlever, Laser Physics Centre, Research School of Physical Sciences, Australian National University, Canberra ACT 2601

Phase conjugate mirrors can be used to correct for distortion introduced by optical elements inside laser resonators. A severe example of a phase distorting object is a multi-mode optical fibre. If a single-mode (TEM_{00}) laser beam is launched into such a fibre its energy becomes rapidly distributed amongst the large number of waveguide modes such that at the fibre output the emergent beam is spatially incoherent. During the process the inherent brightness of the laser radiation drops by typically 10^5 - 10^6 . This limits the usefulness of radiation to applications where brightness is not of importance. Obviously high brightness can be achieved if a single mode fibre can be employed but such fibres can transmit only a few kilowatts of peak power limiting their usefulness.

In this paper we describe a method of producing single mode output from multi-mode optical fibres, thereby potentially combining the high power transmission ability of those fibres with the high brightness characteristics of a single mode system. To achieve this it is necessary to include the multi-mode optical fibre within a laser resonator configured such that at the output of the fibre an ordinary dielectric mirror forms one of the resonator end mirrors so-arranged to selectively reflect only the lowest order mode back into the fibre. At the other end of the fibre a phase conjugate mirror reflects the multi-mode pattern generated from the reflected single mode light. The phase conjugate mirror thus launches a reflection that perfectly unscrambles the mode conversion on the return pass preserving the single mode radiation pattern at the output.

This paper describes the operation of a resonator of this type using a crystal of Barium Titanate pumped by a single mode (longitudinal and transverse) Argon ion laser as the phase conjugate reflector. The reflector itself was used as the gain medium in a resonator in a self-pumped geometry¹. The resonator layout is shown in figure 1. The mode pattern at the output was determined by the spacing, Δ , between the fibre and the ordinary mirror and single mode output was obtained for $\Delta \approx 1\text{mm}$. Once aligned the resonator could be flexed slowly demonstrating the feasibility of a high power beam delivery system based on this idea.

¹ J. Feinberg, *Self-pumped continuous wave phase-conjugator using internal reflection*, Optics Letters, 7, 486-488 (1982).

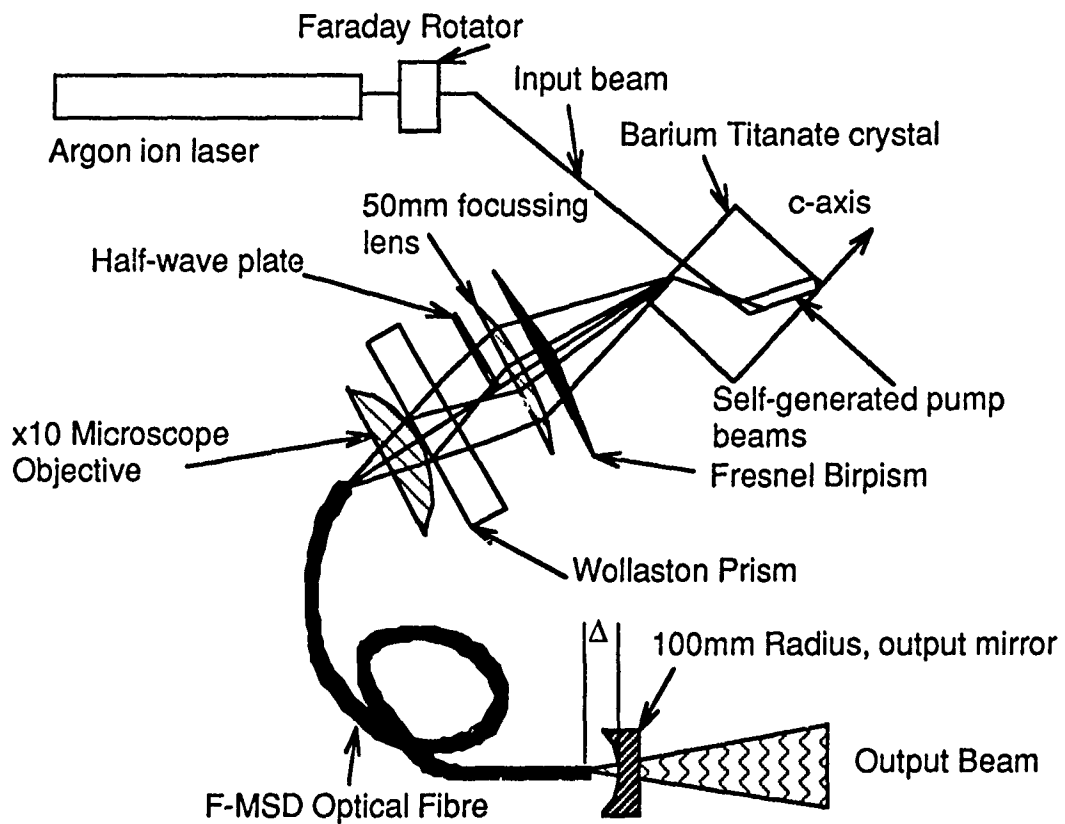


Figure 1: Experimental Apparatus. The Barium Titanate crystal was pumped with an input beam aligned at $\approx 75^\circ$ to the c-axis and the phase conjugate pair entered the crystal at about 65° to the c-axis. The self-generated counter-propagating pump beams align at about 85° to the c-axis.

Astigmatic Stimulated Brillouin Scattering Thresholds with Applications to Nuclear-pumped Gas Lasers

A. Corvo, Sandia National Laboratories, Div. 1128, Albuquerque NM; C.A. Huguley, C.M. Clayton, and A. Gavrielides, Center for NLO Research, Kirkland AFB, NM 87117

Nuclear-pumped gas lasers can exhibit strong density and refractive index gradients due to the deposition of fragment energy into the gas. This energy deposition results in heating of the gas and subsequently a focus effect in the direction of pumping that resembles an astigmatic aberration in an optical system. The use of Stimulated Brillouin Scattering (SBS) to correct for this aberration requires understanding various important parameters.

A method to estimate SBS thresholds for astigmatic aberrations relative to diffraction limited beams was introduced. The on-axis diffraction limited threshold power can be found for a gaussian beam from the equation

$$gI_p L = \frac{2\nu F z_{0g}}{\pi w_0^2} \int \frac{dz}{1 + (z/z_0)^2}$$

where, P is the pump beam power, z_0 the Rayleigh range, w_0 the beam waist at focus, g the SBS gain, and ν is a number of order 30 for steady state conditions or can include transient parameters. For astigmatic aberrations the focal lengths differ in the transverse directions to z and the equation above can be modified to

$$gI_p L = \frac{2\nu F z_{0g}}{\pi w_{0a} w_{0b}} \int d\zeta / \left\{ (1+\zeta^2) [1+(\alpha\zeta-\beta)^2] \right\}^{1/2}$$

where the subscript a denotes the respective values in the aberrating (pumped) direction, and $\zeta = z/z_{0a}$, $\alpha = z_{0b}/z_{0a}$, and $\beta = (f - f_b)/z_{0a}$. The astigmatic intensity has two maxima of respective heights $\approx \alpha$, and separated by a distance $\approx \beta$. The quantities f and f_b are the focal lengths in the diffraction limited and aberrated directions respectively. The ratio of astigmatic to diffraction limited threshold powers can be defined as the beam quality (BQ) and from the two equations above is given by

$$BQ = \frac{\pi(I\#)}{F(I\#)_b}$$

where the symbol f^* refers to the f number of the transverse directions, and F is the value of the astigmatic integral given above.

Calculation of the BQ compared to experimental results¹ using cylindrical lenses for aberrating media showed excellent agreement. The theory was extended to the case of a nuclear-pumped gas laser where the gas density is given by

$$\rho/\rho_0 = \beta_0 + \beta_2 \xi^2 + \dots$$

where ρ_0 is the density at $t=0$, β_n the time dependent n th Taylor expansion coefficient, and $\xi=x/L_x$ is the relative distance from the gas cell's optical axis to the wall. Although simple in appearance, calculating the density coefficients requires complicated calculations involving fragment range estimates. The gas's index of refraction, ray paths, and optical path differences were calculated based on the result of ρ .

Whereas cylindrical lenses typically used in experiments have only a few waves of error, requiring a threshold power a few times above threshold, the nuclear-pumped 1 atm (argon) gas modeled here had approximately 10 waves of error due solely to the heat generated by fragment pumping. This amount of error has been seen experimentally.² The BQ for this gas laser was calculated and it was found that at the end of pumping that the use of SBS would require approximately 35 times the diffraction limited power.

1. C. Hoefer, "Phase conjugation of astigmatic aberrations by stimulated Brillouin scattering", CLEO'89, M12, and private communications.

2. D.R. Neal, J.R. Torczynski, and W.C. Sweatt, Sandia National Laboratories, private communications.

Transfer Function Characteristics of Optical Parametric Amplification

Charles J. Wetterer, Paul A. Laferriere, David A. Cardimona
 Weapons Laboratory (AFSC), WL/AROM
 Kirtland Air Force Base, New Mexico 87117-6008
 (505) 844-0475

SUMMARY

Theoretical models¹ and experimental measurements² of the signal and idler transfer functions in optical parametric amplification (OPA) have been previously published. It was predicted that when a small negative phase-mismatch is induced, the optical transfer function's peak shifts to higher spatial frequencies and the passband of the transfer function narrows. The previously published theory of Ref. 1 is only valid for type I downconversion, which was subsequently studied in Ref. 2. This paper presents experimental observations on other types of phase-matching as well as an intuitive modification of the theory of Ref. 1 needed to extend its validity to cover the new results.

The experimental setup is shown in Fig. 1. A mode-locked Nd:YAG laser was used to provide light at 532 nm and 1064 nm in 100 ps pulses. The experiment consisted of rotating a D-KDP crystal about its y-axis and measuring the idler transfer function's peak spatial frequencies in the x direction, $p_{x\max}$. (The pump is along the z-axis and the crystal axis lies in the x-z plane at an angle θ_c from the z-axis.) Each type of upconversion and downconversion displayed qualitatively similar behavior to the type I case studied in Ref. 2. In the other cases, however, the center of the passband is at a non-zero spatial frequency. Figure 2 illustrates this passband behavior by plotting $p_{x\max}$ versus the external detuning angle, $d\theta$, for the different types of upconversion.

The values of Δk and δk in Ref. 1 were obtained using k_s , k_i , and k_p evaluated at θ_c , which are the correct values for the zero spatial frequency components of the signal and idler. Different spatial frequencies, however, correspond to different propagation directions within the crystal. For extraordinarily polarized light, these propagation directions will experience different indices of refraction, and the corresponding k-vectors will vary in length. The values of Δk , α , δk , and β in Ref. 1 can thus be thought of as functions of p . If these modified variables are used in the transfer function equations of Ref. 1, the agreement with these new experimental results is good. It should be noted that this modification of Ref. 1 can be shown to be equivalent (in the small off-axis regime) to modifying the paraxial wave equation by rotating the refractive index ellipses into the propagation direction, and then re-deriving the transfer functions.

1. A. Gavrielides, P. Peterson and D. Cardimona, J. Appl. Phys. 62, 2640 (1987).

2. P. Laferriere, C. Wetterer, L. Schelonka, and M. Kramer, J. Appl. Phys. 65, 3347 (1989).

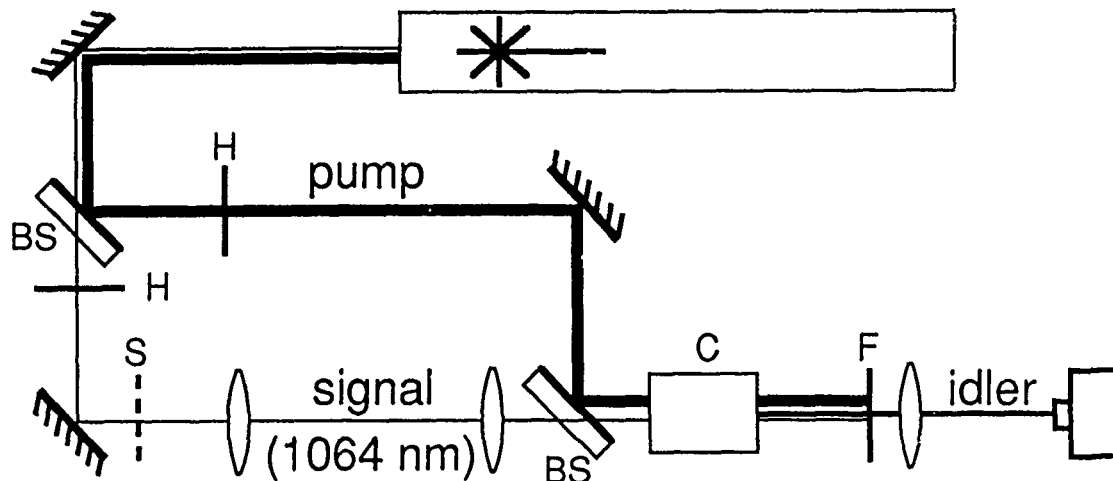


Figure 1. Experimental Setup. H: half-wave plates, S: scatter plate, C: D-KDP crystal, BS: beamsplitter, F: filter used to block pump frequency. In downconversion, the pump is at 532 nm and the idler is at 1064 nm. In upconversion, the pump is at 1064 nm and the idler is at 532 nm.

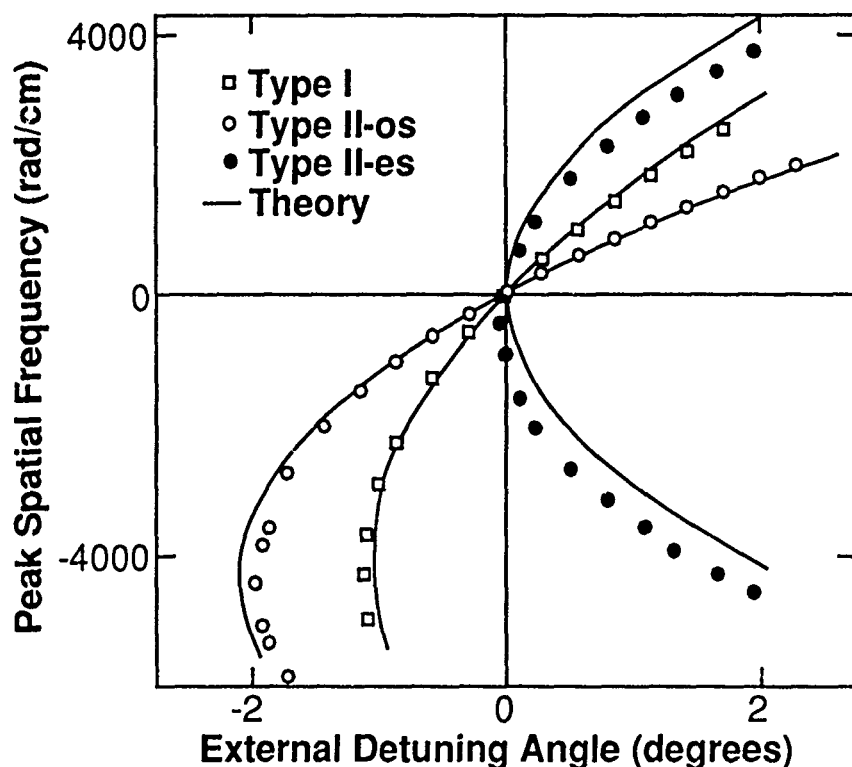


Figure 2. Peak spatial frequency of idler transfer function for each type of upconversion plotted against detuning angle. Type I: signal and pump ordinary. Type II-os: signal ordinary, pump extraordinary. Type II-es: signal extraordinary, pump ordinary. Idler is extraordinary in all types of upconversion.

TP23 Stability of Three-dimensional States of a Parametric Ring SBS Oscillator

V.V.Eliseev*, V.T.Tikhonchuk, A.A.Zozulya

P.N.Lebedev Physical Institute, Leninsky pr. 53,

Moscow, 117924, USSR. Tel. (095)135-7808.

*General Physics Institute of the Academy of Sciences of the USSR,

Vavilov st. 38, Moscow, 117942, USSR

Geometry of a parametric ring oscillator, based at four-wave mixing in a Brillouin-active medium is considered (Fig.1). This geometry is described by the following set of dynamical equations for the slowly-varying amplitudes of electromagnetic waves E_{ij} and the acoustic wave v :

$$\begin{aligned} \partial E_{0\pm 1} / \partial z &= -v E_{-1\pm 1}, \quad \partial E_{-1\pm 1}^* / \partial z = -v E_{0\pm 1}^* \\ (\tau \partial / \partial t + 1) v &= g (E_{01} E_{-11}^* + E_{0-1} E_{-1-1}^*) \end{aligned} \quad (1)$$

with the boundary conditions:

$$\begin{aligned} E_{01}(\rho, z=0; t) &= E_0(\rho), \quad E_{-11}(\rho, l; t) = 0 \\ E_{0-1}(\rho, 0; t) &= (r/\gamma) E_{01}(\rho/\gamma, l; t), \\ E_{-1-1}(\rho, l; t) &= r\gamma E_{-11}(\gamma\rho, 0; t) \end{aligned} \quad (2)$$

Here τ is the relaxation time, g - The SBS coupling coefficient, r - the reflection coefficient of the system of mirrors M , z - the longitudinal and $\rho=(x,y)$ - the transverse coordinates, $\gamma < 1$ is the transverse cross-section scale variation coefficient.

Nonlinear stationary three-dimensional solutions of system (1), (2) are found and their stability is investigated. For large

enough intensities of the input pumping beam $E_0(\rho)$ main stationary mode is shown to be unstable versus the excitation of both the amplitude perturbations of the interacting beams' spatial intensity distributions and versus the excitation of their wavefronts phase perturbations. Instability versus amplitude perturbations takes place for $r^2 < 1/3$, minimum instability threshold corresponds to the value of convective amplification coefficient $\kappa \sim 2\pi$ ($\kappa = g l |E(0)|^2$). Instability of the main stationary mode versus phase perturbations of the interacting beams' wavefronts takes place for any values of γ and r , minimum instability threshold corresponds to $\kappa \sim 4\pi$.

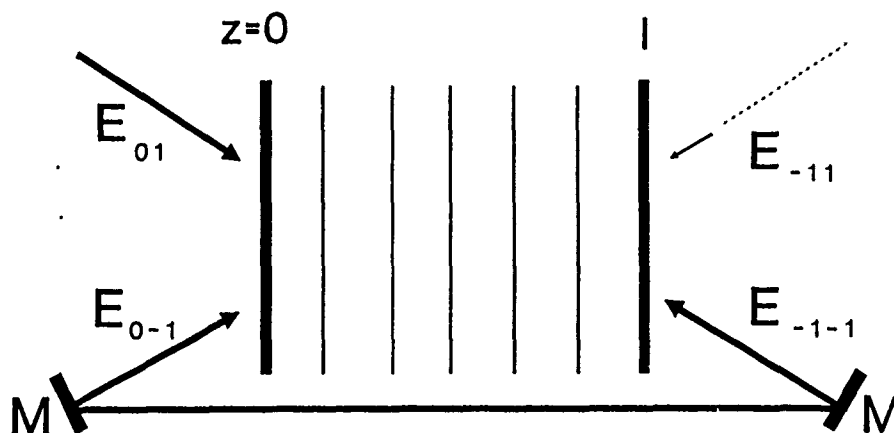


Fig.1. Geometry of a parametric ring SRS oscillator, $E_{0\pm 1}$ are the pumps, $E_{-1\pm 1}$ - the scattered waves, nonlinear medium is situated between $0 \leq z \leq 1$.

An Infrared - Visible - Ultraviolet Tunable Optical Parametric Generation System

Huang Lin, Yao Yu-chiu, Li Gang, Yin Bao-lu

Department of Applied Physics, Beijing Polytechnic University
Beijing 100022, P. R. China

Summary

A high stability, high power density active-passive mode locked Nd³⁺:YAG Laser with second harmonic, third harmonic generator is necessarily used as a pumping source to pump a BBO parametric crystal. The influences of the pumping parameters, the group velocity mismatching and the dispersion spread of the wave envelopes were analysed and calculated by computer. Based on this, the optimum curve of crystal length, phase-match and angle-tuned range respect to pumping energy were given. A BBO parametric crystal covering the range of 4032Å - 3μ and a BBO frequency mixing crystal covering the range of 2283Å - 3023Å were designed.

The detail theoretical analysis of optical parametric generator are given according to coupled-wave equations in the paper. The optical parametric conversion efficiency is about 32%.

The parametric conversion efficiency as a function of the pumping light intensity, the radial width, the divergence angle, the BBO crystal length and group velocity mismatch were shown below.

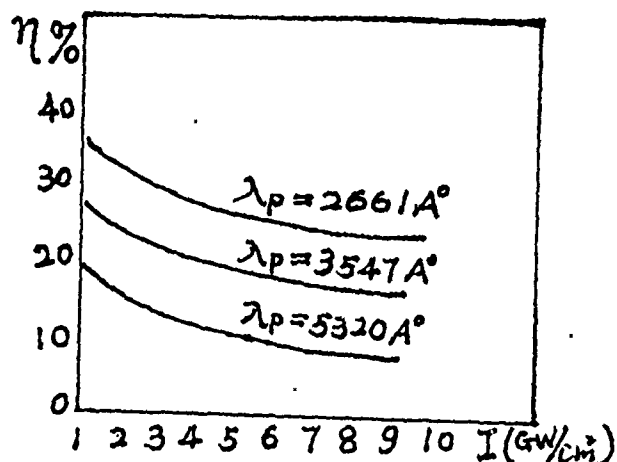


Fig.1 The higher of the pump light intensity, the lower of the parametric conversion efficiency.

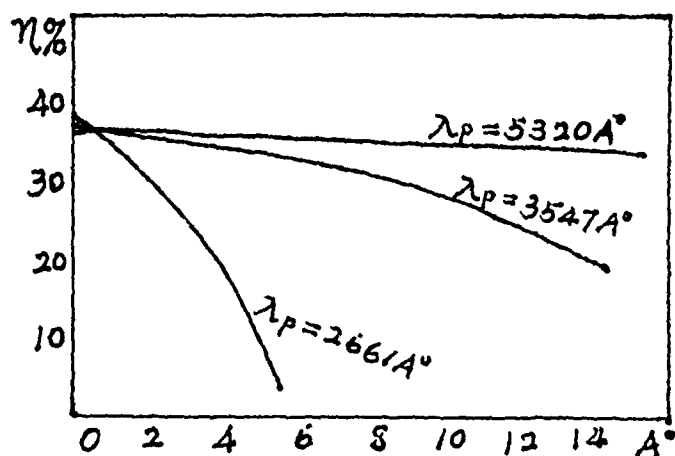


Fig.2 The larger of the radial width $\Delta\lambda$ the lower of the BBO parametric conversion efficiency.

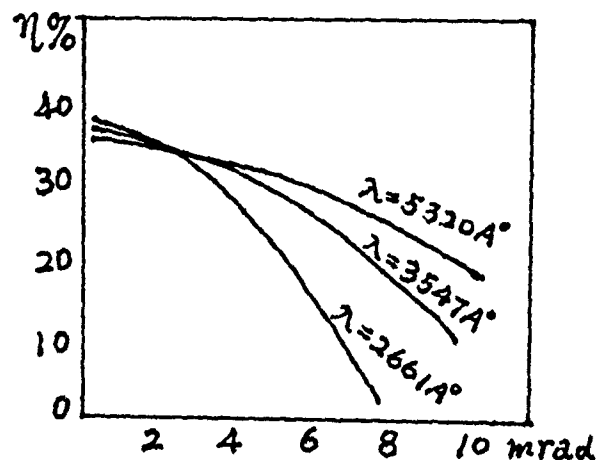


Fig.3 The wider of the divergence angle the lower of the parametric conversion efficiency.

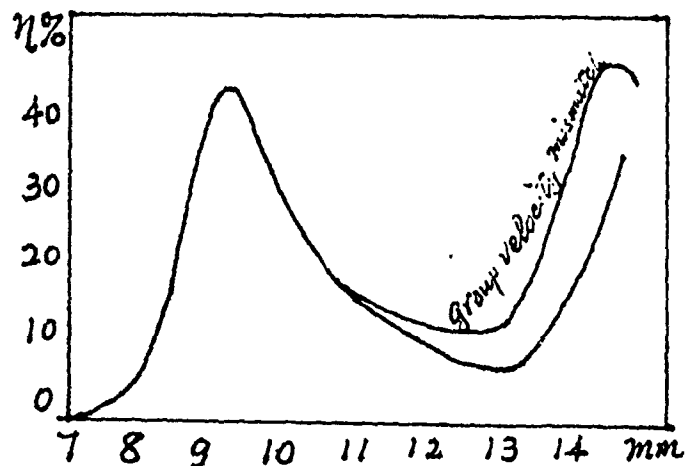


Fig.4 The parametric conversion efficiency as a function of the BBO crystal length and group velocity mismatch.

The results of the theoretical analysis, computer calculation and experimental confirmation were agreed.

Norman P. Barnes
NASA Langley Research Center
Hampton, Virginia 23665-5225
(804) 864-1630

Summary

Performance of both an AgGaSe_2 optical parametric oscillator and amplifier indicate that an efficient source, tunable over the mid-infrared, can be made. AgGaSe_2 is a very attractive nonlinear material because of its wide range of transparency, high nonlinear coefficient, and nearly ideal phase-matching characteristics. Using annealing techniques, the transmission between about 0.8 to 12.5 μm , can be improved dramatically. The nonlinear coefficient d_{36} is high, measured in amplifier experiments to be approximately $39 \cdot 10^{-12}$ m/V. Phase-matching calculations indicate that by using a 1.7 to 2.1 μm pump, the entire mid-infrared region can be covered with a single-nonlinear crystal. In addition, the birefringence is small enough that the birefringence angle is relatively small and the acceptance angle is relatively large.

Optical parametric amplification experiments have demonstrated a small signal gain in excess of 13 using a 20 mm crystal. An optical parametric amplifier, pumped by a 2.1 μm Ho:YAG laser, amplified at 3.39 μm HeNe. Both beam profiles were measured and found to closely approximate Gaussian beams. Gain was measured as a function of pump power and compared with theory. Plane-wave theory of optical parametric amplification was extended to cover the amplification involving Gaussian beams. Using the extended theory, the nonlinear coefficient was determined and found to agree well with other published values.

An optical parametric oscillator using an AgGaSe_2 crystal demonstrated a threshold of 3.6 mJ and a slope efficiency of 0.31. For these experiments, an Er:YLF laser, operating at 1.732 μm was used. Output energy was investigated as a function of pump energy and length of the optical parametric oscillator resonator. Decreasing the length of the resonator to 70 mm, the slope efficiency increased to 0.31. This can be compared with the ratio of photon energies of 0.46. Tuning over the range from 2.6 to 5.1 μm was achieved with a single set of mirrors. Details on the spectral bandwidth and beam profile will be given.

Calculation of the average power limit of the nonlinear interactions requires the variation of the refractive indices with temperature and the absorption coefficient. Variation of the refractive indices with temperature was measured as a function of temperature using a modified variation of the angle of deviation technique. Absorption coefficients were measured using both spectroscopic and calorimetric techniques. Results, as well as the ramifications on the average power limit will be presented.

Growth, Characterization, and Applications of Beta-Barium Metaborate and Lithium Triborate

C.L. Tang, W.R. Bosenberg, T. Ukachi ^{a)}, W.S. Pelouch, and R. Lane
Materials Science Center
Cornell University
Ithaca, New York 14853

Beta-barium metaborate (β -BaB₂O₄, BBO) and lithium triborate (LiB₃O₅, LBO) are two recently discovered nonlinear optical materials that have emerged as the materials of choice for many frequency conversion and electro-optic applications. Our laboratory has successfully grown, characterized, and used these two materials in suitable applications. Here, we report the results of our work.

Large single crystal boules of BBO (70 mm diameter, 15 mm thick) are routinely grown using the top-seeded-solution-growth (TSSG) technique with a Na₂O flux.^{1,2} Characterization measurements have determined that BBO has a broad transparency range (0.19-2.5 μ m),² a large birefringence ($\Delta n \cong 0.11$),³ a large nonlinear figure merit ($d_{22}=2.1$ pm/V),⁴ an exceptionally high bulk optical damage threshold (20-50 GW/cm²),⁵ and is mechanically hard and chemically stable.³ This fortuitous combination of optical, mechanical, chemical, and growth properties have made BBO the material of choice for visible/ultraviolet frequency conversion.

We exploit the strength of BBO as a frequency converter in the application of optical parametric oscillator devices pumped by the second, third, and fourth harmonics of a Nd:YAG laser. Optical parametric oscillators (OPOs) are broadly tunable, coherent radiation sources, and the BBO OPO devices in our laboratory have generated light over the range of 0.33-2.5 μ m,⁶⁻⁸ with conversion efficiencies up to 32%,⁸ and linewidths as narrow as 0.3 Å.⁸ The excellent performance of these radiation sources is in part due to the use of novel cavity configurations.^{7,8} Details on these new cavity designs and the BBO OPO as a radiation source will be given.

LBO is grown via the TSSG technique with a B₂O₃ self-flux at starting B₂O₃ composition of 94%. By inserting a seed into a slightly unsaturated solution and slowly cooling it, large boules, 30 x 30 x 10 mm³ in size, are obtained. Further details on the growth of LBO will be given.

The optical properties of LBO include: a large transparency range (0.16-2.6 μ m); a small birefringence ($\Delta n \cong 0.04$); a moderate nonlinear coefficient ($d_{23}=1.3$ pm/V); a very high surface optical damage threshold (25 GW/cm²).⁹ These properties coupled with LBO's mechanical hardness, chemical stability, and nondeliquescence make it an attractive material for frequency conversion. Experimental results of the use and characterization of LBO as an autocorrelator, and as a noncritically-phasematched, second harmonic generator of near infrared lasers (e.g. Nd:YAG) will be given.

References

- 1) A. Jiang, F. Cheng, Q. Lin, Z. Cheng, and Y. Zheng, J. Cryst. Growth **79**, 963 (1986).
- 2) L. K. Cheng, W. Bosenberg, and C. L. Tang, J. Cryst. Growth **89**, 553 (1988).
- 3) D. Eimerl, L. Davis, S. Velsko, E. K. Graham, and A. Zalkin, J. Appl. Phys. **62**, 1968 (1987).
- 4) Y. X. Fan, R. C. Eckardt, R. L. Byer, C. Chen, and A. Jiang, IEEE J. Quantum Electron. **QE-25**, 1196 (1989).
- 5) H. Nakatani, W. R. Bosenberg, L. K. Cheng, and C. L. Tang, Appl. Phys. Lett. **53**, 2587 (1988).
- 6) L. K. Cheng, W. R. Bosenberg, and C. L. Tang, Appl. Phys. Lett. **53**, 175 (1988).
- 7) W. R. Bosenberg, L. K. Cheng, and C. L. Tang, Appl. Phys. Lett. **54**, 13 (1989).
- 8) W. R. Bosenberg, W. S. Pelouch, and C. L. Tang, Appl. Phys. Lett. **55**, 1952 (1989).
- 9) C. Chen, Y. Wu, A. Jiang, B. Wu, G. You, R. Li, and S. Lin, J. Opt. Soc. Am. B **6**, 616 (1989).

Characteristics of Optical Parametric Oscillation Using β -BaB₂O₄ Crystal

H. Suzuki Y. Ohbayashi M. Takahashi
HAMAMATSU PHOTONICS K.K. CENTRAL RESEARCH LABORATORY
Hamakita Research Park
Hirakuchi Hamakita-City Shizuoka-Pref., JAPAN

Optical parametric oscillators (OPO) using beta barium borate (β -BaB₂O₄, BBO) pumped at 354.7nm to cover a broad tunable range of wavelengths from visible to near infrared have been reported^{1,2,3}. In order to assure practical applications, as a tunable coherent light source, it is essential to investigate and characterize the output power and wavelength resolution of an OPO in the tuning range.

Figure 1 shows a schematic diagram of an OPO used in this experiment for characterizations. The pump wavelength of 354.7nm was obtained from a Q-switched Nd-YAG laser (Spectra-Physics DCR-2(10)) with second and third harmonic generator under 10Hz repetition. The pump beam had the pulse width of 7-8ns. The beam after a harmonic separator was collimated by a telescope to increase its power density. Three BBO crystals with dimensions of 7x5x10.6mm³, respectively cut at the angle $\theta = 26.0^\circ$, 28.5° and 32.5° for Type-1 angle phase matching were employed in the measurements. These crystals were fabricated at the Fujian Institute of Research on the Structure of Matter in People's Republic of China⁴. The OPO cavity was formed by a pair of two flat mirrors M₁ and M₂. The oscillation wavelengths were tunable with proper rotations of the crystals. The pump beam was reflected out off the cavity through the mirror M. The total output power covering the visible and infrared wavelengths at a given angle of crystal rotation were first measured. The visible output power was further measured by filtering out the infrared power with hot mirrors.

This OPO oscillated in the wavelength range in 399.6nm-709.4nm for each of the above crystals. The infrared wavelengths were also oscillated simultaneously under the identical conditions. Figure 2 shows the measured output power in the tuning range at 42mJ of pump power. It is quite clear from the figure that for each of the crystals operated in conjunction with a pair of cavity mirrors, the output level is about 2mJ near 1000nm and slowly tapered to about 1mJ as the OPOs were tuned toward the vicinity of 2000nm. Sharp peaks of power occurred as the pump beam was incident perpendicularly to the crystal because of the state of minimum oscillation loss under such conditions. For example, the peak output power of 5.9mJ at 474.3nm and 2.6mJ at 1406.5nm was observed for the 28.5° cut crystal. The total conversion efficiencies for these wavelengths were nearly 20%.

The wavelength resolutions in the visible range were measured to be 0.3nm at 421.3nm, 0.4nm at 474.3nm, 0.5nm at

529.8nm, 1.2nm at 580.3nm, 4nm at 630.9nm and 11nm at 679nm respectively. The temporal pulse width was approximately 5ns for both 510.1nm and 1164.0nm.

- 1) L.K.Cheng, W.R.Bosenberg and C.L.Tang, Appl.Phys.Lett. 53 175(1988).
- 2) Y.X.Fan, R.C.Eckardt, R.L.Byer, J.Nolting and R.Wallenstein, Appl.Phys.Lett. 53 2014(1988).
- 3) H.Vanherzeele and C.T.Chen, Appl.Opt. 27 2634(1988).
- 4) A.Jiang, F.Cheng, Q.Lin, Z.Cheng and Y.Zheng, J.Cryst.Growth 79 963(1986).

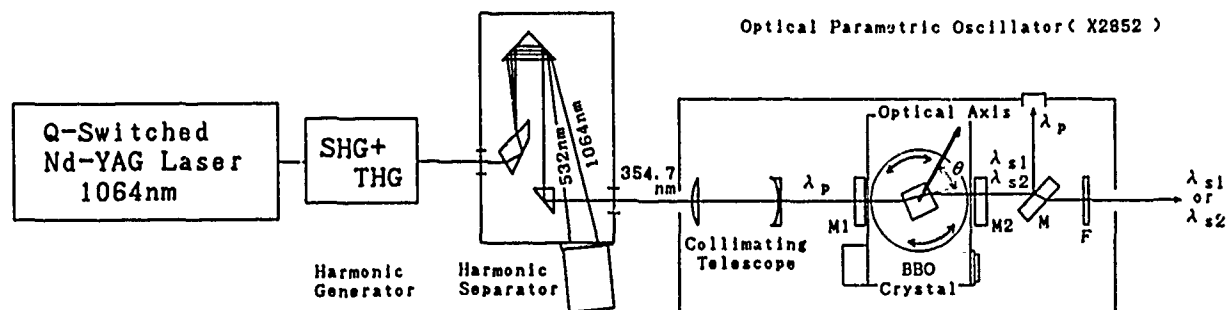


Fig.1 Schematic diagram of the OPO using BBO crystal. λ_p : pump beam wavelength(354.7nm). λ_{s1} , λ_{s2} : visible and infrared wavelengths, respectively. θ : angle between optical axis of BBO and the pump beam.

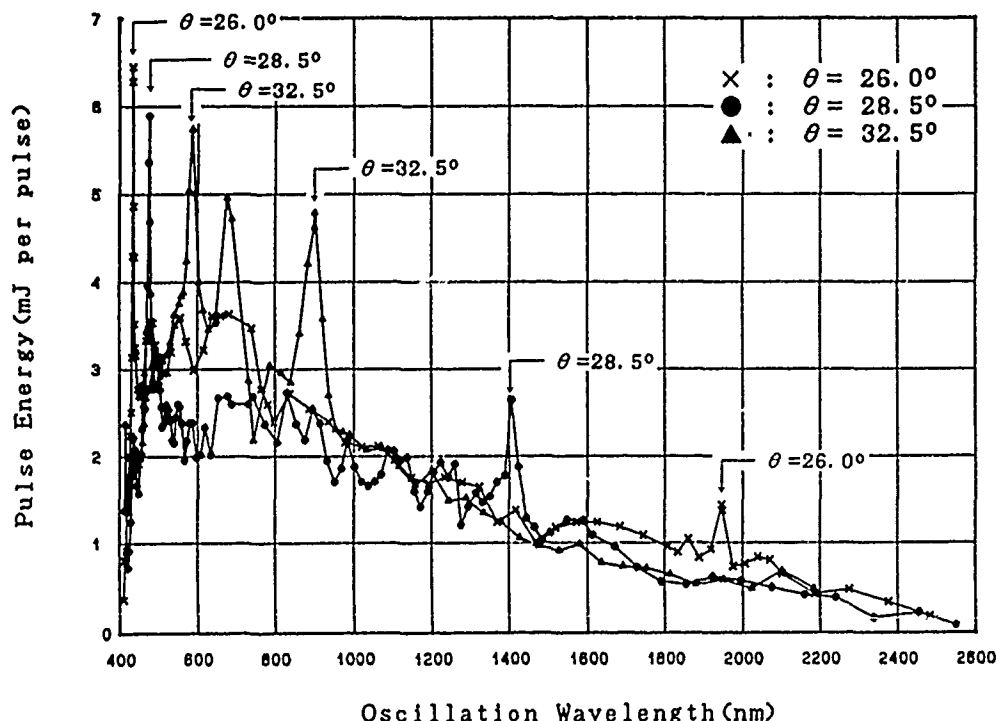


Fig.2 Output energy as a function of oscillation wavelength with pump energy of 42mJ at 354.7nm. Arrows indicate cases for perpendicular incident of the pump beam to each BBO crystal.

Pochi Yeh and Xiang-guang Gu

Rockwell International Science Center
 Thousand Oaks, CA 91360
 (805) 373-4138

It is known for sometime that Stimulated Brillouin Scattering is generated by scattering from phonons in liquids or solids. The Stokes light is first generated by a backward Bragg scattering from a moving index grating representing the phonon field. It is then amplified by the incident laser beam via a third order nonlinearity. In the coupled mode theory, the intensity of the beams are described by [1,2]

$$\frac{dI_1}{dz} = -gI_1I_2, \quad \frac{dI_2}{dz} = -gI_1I_2 \quad (1)$$

where I_1 is the intensity of the incident laser beam and I_2 is the intensity of the Stokes light, and g is the gain coefficient per unit intensity. We neglect the material absorption. According to these equations, a finite Brillouin intensity $I_2(0)$ at the input plane requires a finite $I_2(L)$ at $z = L$, where L is the interaction length. Eqs. (1) describe only the nonlinear coupling between the beams. The Bragg scattering due to the index gratings representing the phonon field is not included in the equations.

In this paper, we describe a nonlinear optical Bragg scattering in which a moving index grating representing the phonon field is present inside the medium. The coupled mode equations, including the contribution due to the phonon field, are given by

$$\frac{dI_1}{dz} = -gI_1I_2 - 2\kappa\sqrt{I_1I_2}, \quad \frac{dI_2}{dz} = -gI_1I_2 - 2\kappa\sqrt{I_1I_2} \quad (2)$$

where κ is the coupling coefficient between the beams due to the presence of the moving phonon field. These coupled equations can be integrated and the expressions for the beam intensities are obtained. In this model, a finite Brillouin intensity $I_2(0)$ at the input plane does not require a finite $I_2(L)$ at $z = L$. The diffraction efficiency, defined as $\eta = I_2(0) / I_1(0)$, is obtained in the following expression

$$\eta = \frac{\tanh^2(\kappa L \sqrt{1+b^2})}{[\sqrt{1+b^2} - b \tanh(\kappa L \sqrt{1+b^2})]^2} \quad (3)$$

with b given by

$$b = (1-\eta) \frac{gI_1(0)}{4\kappa} = (1-\eta) b_0 \quad (4)$$

where $I_1(0)$ is the incident intensity at $z = 0$.

Figure 1 shows the diffraction efficiency as a function of the input intensity. We note that the diffraction efficiency is an increasing function of the input intensity. Similar situation for the case of transmission grating was discussed by earlier workers[3]. Such a dependence can be explained in terms of the generation of phonons in Bragg scatterings. Consider the case of backward Bragg scattering with a down shift in frequency. For each photon scattered, a phonon is created and added to the phonon field. Thus, as the optical intensity increases more and more phonons are generated. These additional phonons strengthen the index gratings and increase the diffraction efficiency. Such a process leads to the build up of the Stimulated Brillouin scattering.

In summary, we treated the process of Stimulated Brillouin Scattering as a nonlinear optical Bragg scattering. A term representing the initial phonon field is included in the coupled equations. This leads to a finite Brillouin intensity even with a zero Stokes intensity at $z = L$. The diffraction efficiency is obtained as a function of the amplitude of the index grating representing the initial phonon field and the intensity of the incident beam.

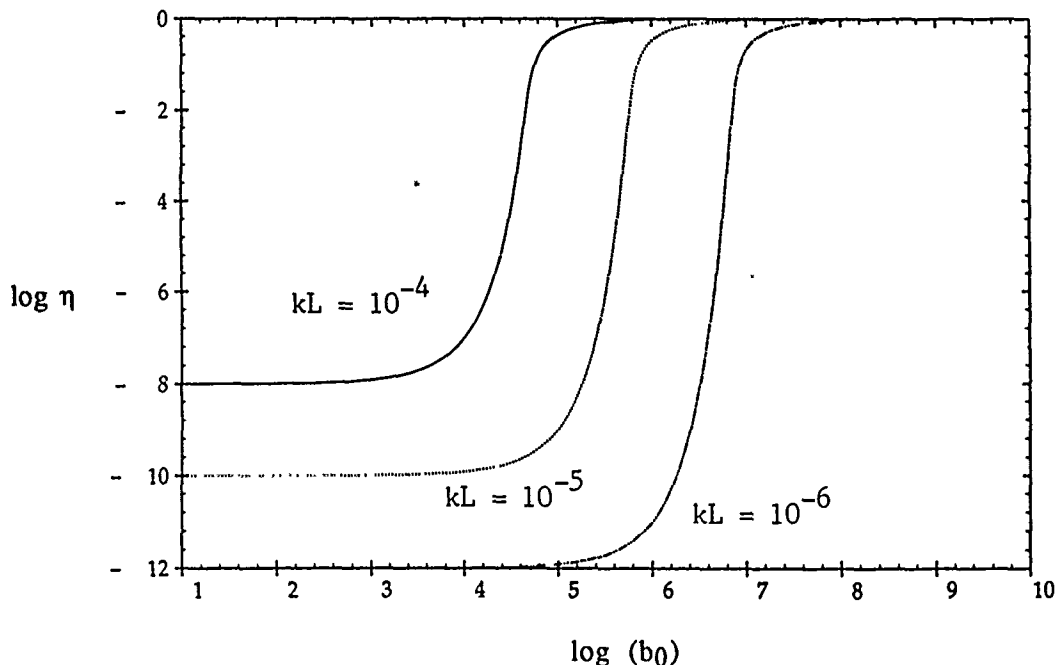


Fig. 1 Diffraction efficiency as a function of intensity for various values of κL .

References:

1. See, for example, Y.R. Shen, "Principles of Nonlinear Optics,"
2. See, for example, P. Yeh, "Two-Wave Mixing in Nonlinear Media," IEEE, JQE, 25, 484 (1989).
3. P. Yeh and M. Khoshnevisan, "Nonlinear Optical Bragg Scattering in Kerr Media," J. Opt. Soc. Am., B4, 1954 (1987).

Phase Conjugate Oscillation In a Kerr Medium In The Presence of Pump Depletion

S.Guha and P.Conner
 Martin Marietta Laboratories
 1450 South Rolling Road
 Baltimore, MD 21227

ABSTRACT

We extend the theory of phase conjugate oscillation in a Kerr medium⁽¹⁾ to include the effect of pump depletion. The oscillation condition is obtained in terms of elliptic integrals of the first and the third kind.

SUMMARY

A nonlinear medium placed inside a resonating cavity and pumped by a pair of counter-propagating beams (beams 1 and 2 in fig.1) may under certain conditions give rise to another pair of beams (beams 3 and 4 in fig.1) oscillating in the cavity. If the beams 1 and 2 are phase conjugates of each other, so will be the beams 3 and 4. The condition that the gain coefficient of the nonlinear medium must satisfy to give rise to such 'phase conjugate oscillation' has been deduced by Yeh¹ for the case in which the pump beams (1 and 2) are much stronger than the generated beams (3 and 4), i.e., when the pump depletion is small. Here, we present the oscillation condition for the case of significant pump depletion.

The nonlinear medium is assumed to be of thickness l , with its two faces placed at $z = 0$ and l . The reflectivities of the two mirrors are denoted by R_1 and R_2 . The intensities and phases of the four beams at $z = 0$ are denoted by I_{i0} and Q_{i0} respectively, and similarly the intensities and the phases of the four beams at $z = l$ are denoted by I_{il} and Q_{il} , where $i = 1 \dots 4$. We use two parameters, $q_1 \equiv I_{4l}/I_{10}$ and $q_2 \equiv I_{2l}/I_{10}$ to denote the probe ratio and the pump ratio respectively. For the case of no pump depletion, q_1 approaches zero. The coupling constant of the nonlinear medium is denoted by κ and the total phase shift when light travels from one mirror to the other is denoted by ϕ . Using the method suggested by Kessel and Musin², we solve the coupled four wave mixing equations to obtain the expression for the amplitudes and the phases of the four beams. Defining $Q_{34} \equiv (Q_{30} - Q_{3l}) - (Q_{40} - Q_{4l})$, we obtain from the Kessel and Musin solutions :

$$Q_{34} = \frac{\alpha_4 c}{2} \int_a^b \frac{dx}{x(\alpha_4 - x)\sqrt{P_4(x)}} \quad (1)$$

Here $a \equiv R_1(1 + R_2)/(R_2(1 + R_1))$, $b \equiv 1/R_2$ and c is a constant. $P_4(x)$ is a fourth order polynomial:

$$P_4(x) \equiv q_1^2(\alpha_1 - x)(x - \alpha_2)x(\alpha_4 - x) - c^2.$$

α_1 , α_2 and α_4 are defined as:

$$\alpha_1 \equiv a + 1/q_1$$

$$\alpha_2 \equiv b - q_2/q_1$$

and

$$\alpha_4 \equiv 1 + b.$$

The constant c is evaluated from the relationship:

$$2\kappa l = \int_a^b \frac{dx}{\sqrt{P_4(x)}} \quad (2)$$

and the oscillation condition is then given by

$$2\phi = Q_{34} \pm 2m\pi, \quad (3)$$

where m is an integer. When q_1 is zero, the integrals in equations 1 and 2 can be evaluated in terms of sine and cosine functions. Obtaining c from solution of eqn.2, substituting in eqn.1 to obtain Q_{34} and finally substituting Q_{34} in eqn.3, the oscillation condition deduced in ref.1 can be obtained. For q_1 non zero, the integrals in eqns. 1 and 2 can be expressed in terms of elliptical integrals of the third kind and the first kind respectively. The values of the elliptic integrals can be obtained from standard tables or by numerical integration and the oscillation condition can be determined.

We will present the results obtained for different values of q_1 and q_2 .

1. P.Yeh, J.Opt.Soc.Am., 2,727,1985.
2. A.R.Kessel and V.M.Musin, Opt.Comm., 44,133,1982.

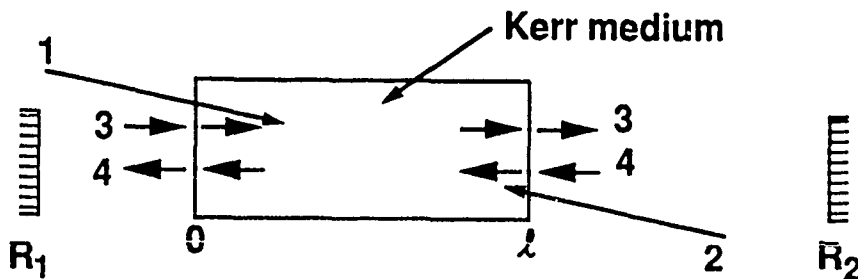


Fig.1. Schematic drawing of a phase conjugate oscillator. 1 and 2 denote the pump beams and 3 and 4 are the oscillating beams.

Picosecond Laser-Induced Reorientation, Density, Temperature, and flow Effects in the Mesophases of Liquid Crystals

I. C. Khoo, R. R. Michael, R. G. Lindquist, R. J. Mansfield,
and P. LoPresti, The Pennsylvania State University

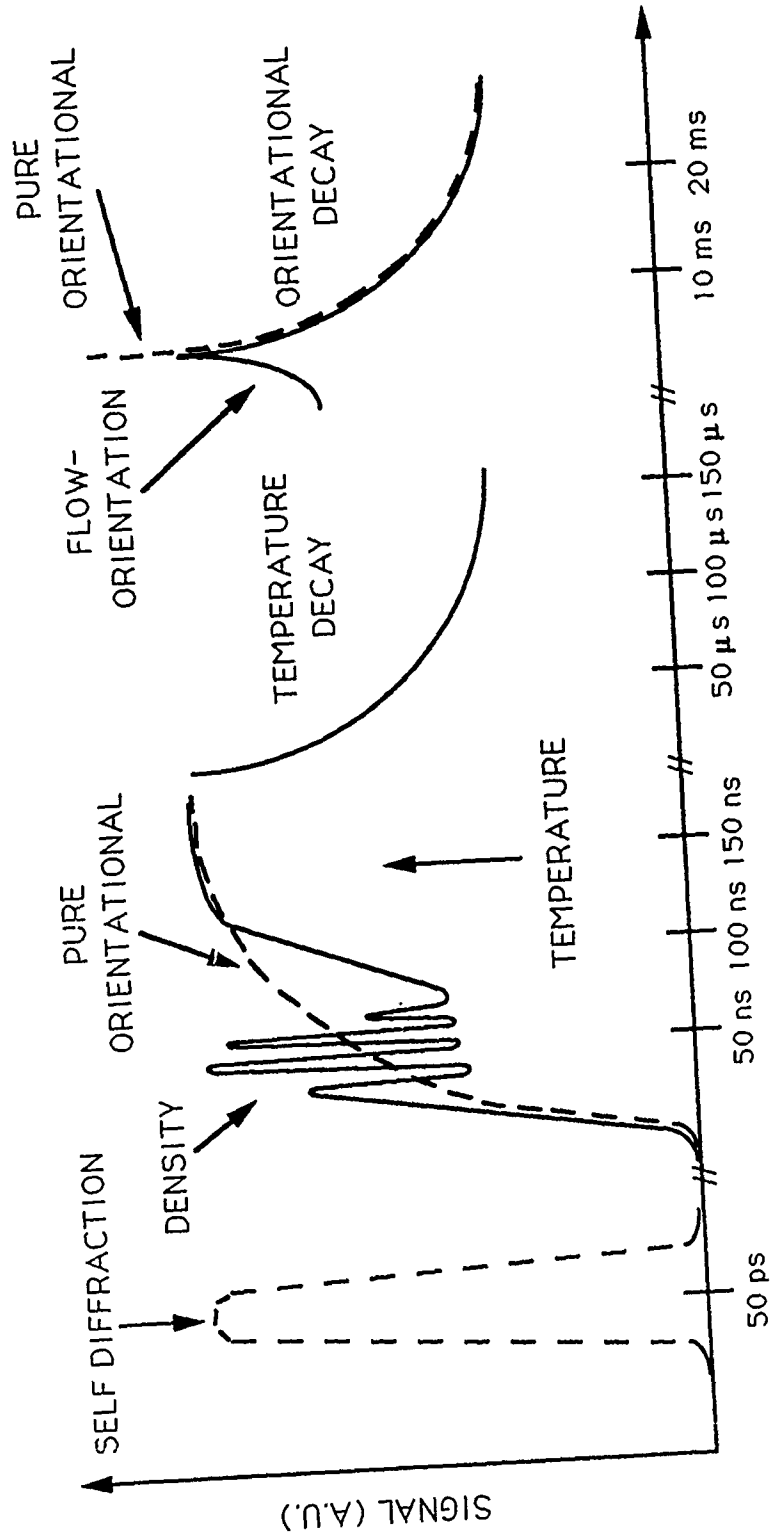
SUMMARY

Previous studies¹⁻³ of nonlinear light scatterings in the mesophases of liquid crystals with nanosecond laser pulses have demonstrated the possibility of inducing large refractive index changes associated with photo-induced fluctuations in density, temperature, and director-axis orientations. High frequency acoustic waves, with periods on the order of a few nanoseconds, have also been observed. In this paper, we report the results of a study where we employed picosecond laser pulses to unambiguously create and measure these nonlinear effects associated with thermoelastic, electrostrictive and dipolar interaction, and their dynamics. A quantitative theory based on solving the full hydrodynamically coupled equations for the density and temperature changes, an Erickson-Leslie type of equation for the laser-induced director-axis reorientation, and the hydrodynamic equation for the flow phenomenon, is also presented for the first time.

Figure 1 summarizes the nonlinear effects observed for the time scales spanning the picosecond to millisecond range following a single-shot 66 ps Nd:YAG second-harmonic laser pulse in a usual wave mixing pump-probe dynamic grating experiment². In the picosecond regime, "individual" molecular responses dominate (for the smectic, nematic, as well as isotropic phases). In the nanosecond-microsecond regime, we have observed laser-induced density, temperature, and director-axis reorientation. As a result of large density and temperature fluctuations, "flows" are observed. The density and temperature effect are characterized by relaxation times on the order of nanoseconds and microseconds, whereas the flows and reorientation effects relax in milliseconds. Quantitative theoretical estimates of the relative contribution from these mechanisms, their relaxation time constants, ultrasonic velocity and frequencies, and flow relaxations are in remarkable agreement with the experimental observations. These newly observed effects provide new avenues for fundamental liquid crystalline studies, as well as for "broadband" mechanisms for applications of liquid crystals in nonlinear optical switches and modulation devices.

REFERENCES: 1. H. Hsiung, L. P. Shi, and Y. R. Shen, *Phys. Rev. A*, Vol. 30, 1453 (1984). 2. I. C. Khoo and R. Normandin, *Opt. Lett.*, Vol. 9, 285 (1984); *IEEE J. Quantum Electron.*, Vol. 21, 329 (1985). 3. I. C. Khoo, R. R. Michael, and P. Y. Yan, *IEEE J. Quantum Electron.*, Vol. 23, 267 (1987).

Figure 1. Schematic diagram of the laser-induced nonlinear effects in liquid crystals.



Second Harmonic Generation in Guided Wave Ferroelectric Liquid Crystal Structures

Michael G. Robinson, Jian-Yu Liu, Kristina M. Johnson, Dave Walba, Dave Doroski
Optoelectronic Computing Systems Center, Department of Electrical and Computer Engineering,
University of Colorado, Boulder, Colorado 80309-0525

Previously, we reported phase matched second harmonic generation (SHG) in commercially available ferroelectric liquid crystals (FLC)¹. In this paper we present the experimental and theoretical results on a new class of specially synthesized FLC materials that have much higher non-linear coefficients than commercially available mixtures. The measured d_{eff} in our new FLC mixtures is an order of magnitude greater than the results of the commercial mixture SCE9¹, and is the most efficient frequency doubling FLC material reported to date.

However, the overall efficiency of SHG when propagating normal to the FLC cells is small due to short interaction lengths ($< 100 \mu\text{m}$) required for alignment. Using guided wave structures, we overcome this problem with interaction lengths typically $> 1\text{cm}$. For large interaction lengths, the phase matching angle becomes very critical and thus accurate information about the refractive indices of the FLC material is needed. These are obtained together with the waveguiding propagation characteristics using the prism coupling technique. The FLC refractive indices, n_e and n_o , are obtained by numerical solutions of the equations governing the evanescent prism coupling. The dispersion spectrum of the FLC is measured by using different laser sources. Materials with large chevron distorted structures² show the effect of field dependent mode shift. This electro-optic effect can be understood as the chevron tends to be straightened out with a larger applied field, the details of which will be presented.

We will present a direct comparison of the non-linear electro-optic coefficients of commercially available FLC materials and standard electro-optic crystals, such as Quartz and LiNbO_3 with our newly synthesized FLC

materials. In the waveguiding structures, efficient second harmonic generation is achieved, with the results presented here for commercially available and novel FLC materials.

1. J.Y. Liu, M.G. Robinson, K.M.Johnson, "Second harmonic generation in ferroelectric liquid crystal SCE9" will be published on Mar. 1990 Opt. Lett..
2. T.P.Rieker, N.A.Clark, G.S.Smith, D.S.Parmar, E.B.Sirota, and C.R.Safinya; "Chevron local layer structure in surface-stablized ferroelectric smectic-C cell" Phys. Rev. Lett. Vol.59, No.23, p.2658, 1987.

TP32 Time-Dependent Dynamical Reorientation Induced by CW Laser Beam In a Nematic Liquid Crystal Film

E.Santamato, G.Abbate, P.Maddalena, L.Marrucci
Dipartimento di Scienze Fisiche, Università di Napoli
Pad.20 - Mostra d'Oltremare, I-80125 Napoli, Italy
Tel. +39-81-7253308 Fax +39-81-614508

and

Y.R.Shen
Department of Physics, University of California
Berkeley, California, 94720, USA

Liquid crystals in their mesophases are attractive materials for nonlinear optical devices because of their huge response to optical fields and their capability of being easily inserted in optically integrated structures. From the macroscopic point of view, we may consider a nematic liquid crystal as a fluid endowed with internal orientational degrees of freedom. These additional degrees of freedom, absent in ordinary fluids, may be accounted for by the director field $\mathbf{n}(\mathbf{r})$, a unit vector field attached at each point \mathbf{r} in the medium. Unlike in the case of externally applied static fields, where \mathbf{n} couples with the external field directly, in the case of optical fields \mathbf{n} couples with the light polarization. As a consequence, \mathbf{n} is driven by exchange of angular momentum between the light beam and the medium. This yields the appearance of various new nonlinear optical phenomena having no analogue in the static-field case. For instance, the molecular director \mathbf{n} can be put into uniform precession about the beam propagation direction by transfer of intrinsic angular momentum (photon spin) from the beam to the liquid crystal¹. This effect can be observed only with circular polarization of the incident beam, for, in this case only, the deposition of angular momentum in the medium has a constant rate. With an elliptically polarized beam, the situation is far more intriguing. The main difference between circular and elliptical input polarization is that in the former case the molecular reorientation first breaks the azimuthal symmetry of the whole system (radiation + liquid crystal). This yields characteristic different results in the two cases: the elliptically polarized input can lead the system through various dynamic regimes: torsional oscillations, nonuniform precession, nutation of \mathbf{n} superimposed on precession, and others.

In this work, we present the first experimental quantitative study of the dynamical phenomena occurring when a nematic liquid crystal film is reoriented by an elliptically polarized laser beam at normal incidence. The experiment was carried out on a 75 μm homeotropic film of 4-cyano-4'-pentyl-biphenyl (5CB). An Ar⁺ laser beam, focussed to 120 μm and normally incident on the film was used as pump beam, and a counter-propagating He-Ne laser beam, mounted in a heterodyne interferometer/polarimeter scheme, was used to probe the induced molecular reorientation. An example of the observed oscillations of the molecular director \mathbf{n} is shown in Fig.1, where the angle ψ of the polarization axis of the probe beam beyond the sample is plotted as a function of time. We observed different laser-induced dynamical regimes,

¹ E.Santamato, B.Daino, M.Romagnoli, M.Settembre, and Y.R.Shen, Phys.Rev. Lett., 57, 2423 (1986)

depending on the input intensity and/or polarization ellipticity. The results are summarized in Fig.2, where the various distorted "dynamical phases" of the system are indicated in the intensity/ellipticity plane. In the figure U denotes undistorted regime, S steady-state distortion, O torsional oscillation, in which the oriented molecules librate, and R the precession/nutation regime, in which the molecules precess as well as nutate about the beam propagation direction. Squares, circles, and triangles are experimental data points in different regimes. Empty and filled symbols refer to observation with increasing and decreasing pump intensity, respectively. The dashed curve describes the boundary between R and O with decreasing pump intensity. Hysteresis between these two time-dependent regimes is clearly shown. Also, a theoretical model has been developed, consistent with total (radiation + medium) angular momentum conservation, whose results are in good agreement with the experimental observations.

Fig.1 Angle ψ of the polarization ellipses major axis of the probe beam beyond the sample as a function of time. In the figure, the pump intensity and ellipticity angle are indicated by I and χ , respectively. $I_{th}(0)$ denotes the threshold for the Optical Fréedericksz Transition with linear pump polarization.

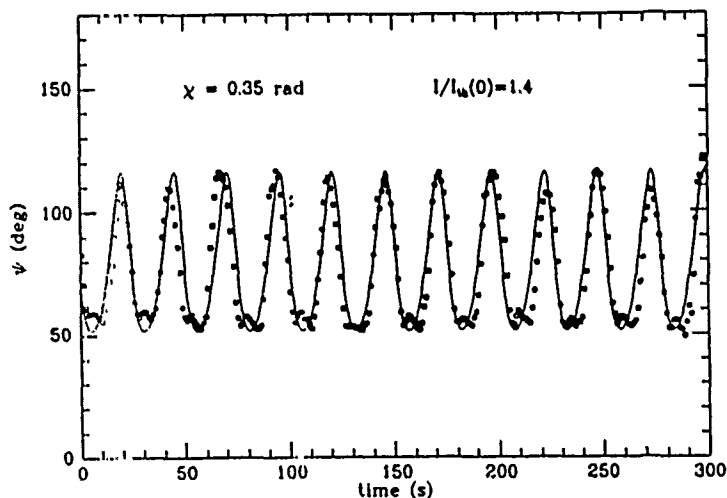
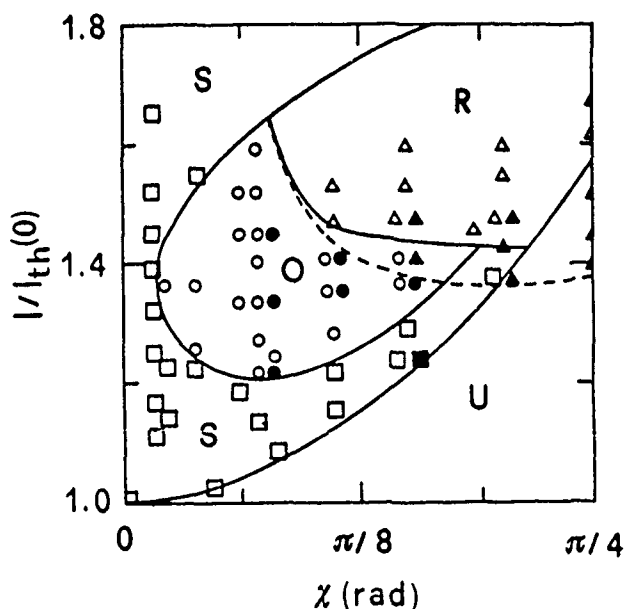


Fig.2 Zone diagram in the (χ, I) -plane for the observed dynamical regimes. $I_{th}(0)$ denotes the threshold for the Optical Fréedericksz Transition with linear pump polarization.



WEDNESDAY, JULY 18
ORAL PRESENTATIONS

Jack Feinberg

Departments of Physics and Electrical Engineering

University of Southern California

Los Angeles, CA 90089-0484

ABSTRACT

I will unravel some of the mysteries of photorefractive materials, and describe new optical devices that use these materials, including an electric-field autocorrelator and an optical switchboard.

SUMMARY

I will discuss some of our recent experiments to understand the photorefractive effect in BaTiO_3 crystals. These crystals show a marked variation in their photorefractive properties, even for samples grown under supposedly identical conditions. For example, some crystals can store a previously written photorefractive hologram for many days in the dark, while others can store such a hologram for only a few seconds. Also, in some BaTiO_3 crystals the speed of the photorefractive effect (i.e. the photoconductivity) scales almost linearly with the light intensity, while in other samples, the speed increases sublinearly with light. We present a simple model that explains the wide variation in the physical properties of BaTiO_3 crystals, and show data to support this model. I will also discuss a new technique for accurately measuring the effective density of charges in photorefractive crystals, and which avoids some of the problems associated with the usual beam-coupling techniques. This technique, based on absorption gratings, also lets us investigate the somewhat mysterious photovoltaic effect in photorefractive crystals. If time permits (which it probably won't), I will describe recent devices that use photorefractive crystals, including an autocorrelator for cw mode-locked picosecond laser pulses, and an optical switchboard using mutually-pumped phase conjugation.

BaTiO₃ Developments: 1) Seeded Stimulated Photorefractive Scattering, and 2) Photoluminescence

Ruth Ann Mullen, Kimberly L. Schumacher*,
Deborah J. Vickers**, and David M. Pepper

Hughes Research Labs
3011 Malibu Canyon Road
Malibu, CA 90265

Optical phase conjugation via stimulated scattering has been previously demonstrated in Brillouin, Raman, and photorefractive media. In Brillouin and in Raman media, the mechanism for the optical non-linearity is well-understood¹, while in photorefractive media, the details of the charge transport mechanism are largely unknown. Photoluminescence and the wavelength dependence of steady-state and transient phase-conjugate reflectivities in variously-doped and undoped crystals can be used to discriminate between photorefractively active and inactive impurity and defect centers.

Photoluminescence excitation and emission spectra, such as are shown in the figures², indicate that the rare earths are common contaminants in both Hughes-grown and Sanders-grown BaTiO₃ crystals. The Sanders-grown crystal was from boule #69, and the Hughes-grown crystals included both nominally-undoped crystals and crystals purposely doped with Co, Fe, Mn, and Eu. The BaTiO₃:Eu spectra, Figure 3, contained Eu emission lines as well.

What role, if any, do these rare earth contaminants play in photorefractive charge transport? To find the answer to this question, we have performed measurements of the steady-state and transient phase-conjugate reflectivity of both back-seeded and internally seeded, self-pumped SPS conjugators as a function of wavelength. A Ti:Al₂O₃ laser, tuned from 730 nm to 930 nm, was used as the pump laser.

The results of these experiments, as well as recent developments in externally-seeded³ stimulated photorefractive scattering phase conjugators, will be discussed.

REFERENCES

1. Y.R. Shen, Principles of Nonlinear Optics, (John Wiley and Sons, New York, 1984).
2. R.A. Mullen, K.L. Schumacher, B.A. Wechsler, and M.B. Klein, "Photoluminescence spectroscopy of doped and undoped BaTiO₃," OSA-SFO Topical Meeting on Photorefractive Materials, Effects, and Devices, Aussois, France, January 17-19, 1990.

3. R.A. Mullen, D.J. Vickers, and D.M. Pepper, "Stimulated photorefractive scattering phase-conjugators back-seeded with retro-reflector arrays," Conference on Lasers and Electro-Optics, Anaheim, California, May 21-25, 1990.

* Cavendish Laboratory, Cambridge University, Cambridge, England.

** General Motors Research Laboratories, Warren, Michigan

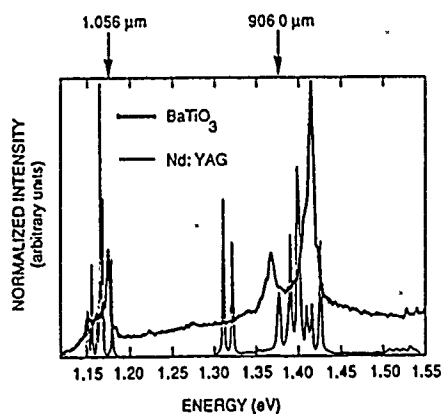


Figure 1 - Emission spectra of BaTiO₃ (thick line) superimposed on that of Nd:YAG (thin line). Both samples were excited with the 457.9 nm line of an argon ion laser, and a spectrometer was tuned from 500 to 1200 nm.

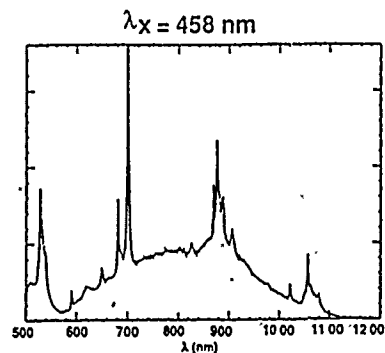


Figure 2 - The emission lines of BaTiO₃:Eu include peaks attributable to the following three rare earth elements: Nd, Eu, and Pr. The samples were excited with the 457.9 nm line of an argon ion laser.

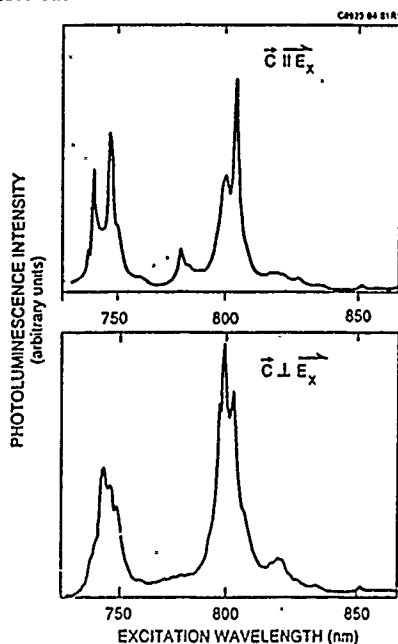


Figure 3 - Excitation spectra of Hughes-grown undoped BaTiO₃, for excitation polarization aligned parallel (top) and perpendicular (bottom) to the crystal's c-axis. The spectrometer was set to 875.3 nm, and a Ti:Al₂O₃ laser tuned from 730 to 883 nm was used to excite the sample. The excitation spectra of the 906.0 nm and 1.06 μm emission lines were almost identical to the spectrum illustrated. These excitation peaks line up closely with the absorption peaks of Nd:YAG. Note that the horizontal scales in these figures (from the micrometer drive positions on the Ti:Al₂O₃ laser's birefringent filter) are not linear in wavelength.

Enhancing Photorefractive Properties for Specific Applications

Gary L. Wood, William W. Clark III, Gregory J. Salamo*, and
Edward J. Sharp

CECOM Center for Night Vision and Electro-Optics
Fort Belvoir, Va. 22060-5677
(703) 664-1431

SUMMARY

Photorefractive materials have the ability to form dynamic gratings with large diffraction efficiencies. In addition, these materials exhibit the property of energy exchange. These unique properties have many potential applications. For applications where the minimum or maximum coupled energy density (fluence) is required the photorefractive material can be characterized by the optical gain and the photorefractive time response. Such applications include optical limiting and image amplification.

For two-beam coupling the throughput for the strong beam is given as

$$F_{th} = \int_0^t dt' \frac{(1 + m') I_0^- e^{-\alpha L}}{1 + m' \exp[\Gamma L (1 - e^{-t'/\sigma})]}$$

where $m' = m/(1 + I_d/I_0)$ and m is the modulation ratio, I_d is the dark contribution to the grating decay, I_0 is the total incident intensity of the two incident beams (one weak in intensity and the other strong), Γ is the optical gain coefficient, L is the length in the photorefractive material where the two beams overlap, I_0^- is the incident intensity of the strong beam to be depleted through energy exchange, σ is the photorefractive time response, and F_{th} is the throughput fluence. For effective reduction in the throughput fluence it is necessary for $t/\sigma \gg 1$ (for an incident square pulse of width t). If the photorefractive material is assumed to have a time dependence of the form, $\sigma = A/I^x$ where A is a time constant and $x \sim 1$ then the above condition becomes, with F_{in} the incident fluence given as $F_{in} = I_0 t$, $F_{in}/A \gg 1$, or more accurately $e^{-F_{in}/A} \ll 1.0$. With this condition for F_{in} the throughput fluence is reduced to

$$F_{th} = F_{in} e^{-\alpha L} / (1 + m' e^{\Gamma L}) = \Phi A e^{-\alpha L} / (1 + m' e^{\Gamma L})$$

where $F_{in} = \Phi A$ and $\Phi \geq 5$. As can be seen, Φ represents a dimensionless incident fluence.

The photorefractive gain and time constant can be altered through the dopant concentration. Increasing the dopant concentration increases the gain but increases the time constant. To achieve small throughput fluences it is desirable to have a small time constant and a large gain as can be seen from the above equation. Therefore, there is some optimum dopant concentration that will allow a compromise resulting in a minimum throughput fluence. In order guarantee some transmission through the photorefractive material without coupling it is necessary to have, $T = e^{-\alpha L} \leq \beta$, where β is some minimum acceptable transmission.

Expressing the absorption, the gain, and the time response in terms of the dopant level we find the minimum throughput fluence and corresponding dopant level. These calculations assume a two level model of electron donor sites, N_D , and electron acceptor sites, N_A . Optimum photorefractive performance can be calculated assuming infinite mobility, large electro-optic coefficients, a small static dielectric constant, and no dark contribution.

 * Dept. of Physics, University of Arkansas, Fayetteville,
 AR 72701.

Recent Progress in Photorefractive Nonlinear Wave Mixing

Baruch Fischer
Department of Electrical Engineering
Technion — Israel Institute of Technology
Haifa 32000, Israel

We describe recent results which show the hyper-adaptive behavior of nonlinear photorefractive wave mixing: The first one is a passive transverse mode-locking effect. It is demonstrated for oscillations in a cavity formed by two phase conjugate mirrors which contains a saturable absorber. It gives a collapse of the cross section of the oscillating beam near the absorber. In a second experiment, a cavity extension of laser diode arrays is used for an active mode-locking and frequency tuning of the laser.

Passive mode-locking of lasers is based on the insertion of a saturable absorber into the laser cavity. The saturable absorber encourages oscillation in short pulses, where the light intensity is large and the loss in the absorber is minimized. We could consider, however, another way for obtaining energy compression by using the transverse dimension of the oscillating beam in the cavity rather than the longitudinal one. We show that such a process is obtainable with a special resonator formed by two photorefractive phase conjugate mirrors⁽¹⁾. Such a phase conjugate resonator can support a large number of transverse modes. The saturable absorber was a film of bacteriorhodopsin in a polymer matrix⁽²⁾. Its low saturation intensity of (10 - 100) mWatts/cm² is compatible with typical beam intensities used in photorefractive oscillators.

The second experiment is of an active mode locking of an extended cavity laser which uses a GaAlAs laser array gain medium and a self-aligned, spatially matched external feedback from a phase conjugate mirror. We demonstrate 92 ps wide pulses, frequency tunability over 7 nm and single longitudinal mode operation under cw conditions⁽³⁾.

References

1. B. Fischer, S. Sternklar and S. Weiss, IEEE J. Quant. Electr. 25, 550, (1989).
2. O. Werner, B. Fischer, A. Lewis and I. Nebenzahl, submitted for publication in Opt. Lett..
3. M. Segev, Y. Ophir, B. Fischer and G. Eisenstein, submitted for publication in Appl. Phys. Lett.

Exciton Coherency, Its Superradiant Decay and Enhanced Optical Nonlinearity

Eiichi Hanamura

Department of Applied Physics

University of Tokyo

7-3-1 Hongo, Bunkyo-ku, Tokyo 113, Japan

Telephone 3-812-2111 ext. 6805

Faximile 3-816-7805

An exciton, a collective excitation in a crystal, is made by superposing coherently atomic or molecular excitation in each unit-cell over whole the crystal. Therefore the exciton in an ideal large crystal has macroscopic transition dipolemoment and the exciton-polariton is formed due to the strong resonant interaction between the exciton and the radiation field (photon) and the translational symmetry of the system in the 3-dimensional crystal.

In low-dimensional crystals such as semiconductor microcrystallites, as well as in real crystals, the coherent length of the exciton is limited to the mesoscopic size. Although the enhancement of the transition dipolemoment is restricted to a mesoscopic size, the exciton can show first a superradiative decay[1], e.g., in an order of 100ps in CuCl microcrystallites embedded in NaCl[2] and glasses[3]. Second we can show that the third-order optical susceptibility $\chi^{(3)}(2\omega_1 - \omega_2; -\omega_1, \omega_2, -\omega_1)$ is enhanced by the mesoscopic or macroscopic transition dipolemoment of the excitons[4,5] with associations of the exciton-exciton interaction working in the microcrystallites[6,7] and the relaxation and decay processes of the excitons.

In this paper, first we check again three conditions which were already discussed in [6] to get the enhancement of optical nonlinearities in

real systems such as microcrystallites, and natural or artificial quantum wells. Second, we discuss the effects of the exciton-trapped states on the dynamical and nonlinear optical responses, and third the effects of Bose-condensation[8], weak localization[9] and Kosterlitz-Thouless transition[10] of excitons on the optical nonlinearities.

[References]

- [1] E. Hanamura : Phys. Rev. **B38** (1988) 1228.
- [2] T. Itoh, F. Jin and T. Ikehara : in *Nonlinear Optics of Organics and Semiconductors*, ed. T. Kobayashi, Proc. in Phys. **36** (Springer-Verlag, Berlin, 1989) p.76.
- [3] A. Nakamura, H. Yamada and T. Tokizaki : Phys. Rev. **B40** (1989) 8585.
- [4] E. Hanamura : Phys. Rev. **B37** (1988) 1273.
- [5] E. Hanamura, M. Kuwata-Gonokami and H. Ezaki : Solid State Commun. **73** (1990) 551.
- [6] Y. Masumoto, M. Yamazaki and H. Sugawara : Appl. Phys. Lett. **53** (1988) 1527.
- [7] A. Nakamura et al. presented at Japan Phys. Soc. Meeting (1990).
- [8] A. Mysyrowicz, D. W. Snoke and J. P. Wolfe : to appear in Phys. Stat. Sol.
- [9] E. Hanamura : Phys. Rev. **B39** (1989) 1152.
- [10] T. Fukuzawa, E. E. Mendez and J. M. Hong : private communications.

Femtosecond Excitonic Nonlinearities Under Resonant and Non Resonant Excitation

D. Hulin, A. Migus, M. Joffre and A. Antonetti

Laboratoire d'Optique Appliquée

ENSTA - Ecole Polytechnique

Batterie de l'Yvette, 91120 Palaiseau, France

Since its first experimental evidence [1,2], the Optical Stark effect in semiconductors has raised a large number of experimental and theoretical studies. It corresponds to the coupling of the material energy levels with a below-gap light beam. It is often described as the creation of virtual excitons, i.e. particles whose ultrashort lifetime is inversely proportional to the detuning between the pump photon energy and the exciton level. The major characteristic of this effect is that light is not absorbed, implying no real creation of particles in the semiconductor and insuring therefore an ultrafast response time, a feature which can be promising for possible applications.

Experimentally the optical Stark effect has been evidenced as a blue-shift of the exciton absorption lines, lasting as long as the pump pulse is present in the sample. However it has been recently predicted that the direction of the shift may change in semiconductors in which the biexciton is stable with a sizeable binding energy. We have performed femtosecond experiments in such a semiconductor, CuCl, and we indeed find that the blue shift turns into a red shift when the excitation crosses the biexciton level. Such a modification can be interpreted as the effect of virtual biexcitons becoming more important than virtual excitons.

The situation is even more complex when now the excitation wavelength is tuned at the exciton resonance instead of staying inside the spectral transparency region. For a two-level system, one expects a splitting of the absorption line but a semiconductor at the absorption edge cannot be described in this simple framework. The problem has already been addressed in GaSe [4]; however these experimental results are not fully conclusive since the absorption spectra are completely bleached very rapidly by the excited particles. We have performed pump-probe experiments in the femtosecond regime in materials where the situation is more favorable. Whereas the total absorption strength still decreases in a significant manner during the excitation, we are able to follow the complete evolution of the line spectral position. Experimental results will be presented showing that the coupling of light with the energy levels cannot be ignored when studying the dynamics of the resonant creation of excitons.

1- A. Mysyrowicz, D. Hulin, A. Antonetti, A. Migus, W.T. Masselink and H. Morkoç, Phys. Rev. Lett. 56, 2748 (1986)

2- A. Von Lehmen, D.S. Chemla, J.E. Zucker and J.P. Heritage, Optics Lett. 11, 609 (1986)

3- M. Combescot, Sol. St. Comm. 68, 471 (1988)

4- C. Hirlimann, J.F. Morhange, M.A. Kanehisa, A. Chevy and C.H. Brito Cruz, Appl. Phys. Lett. 55, 2307 (1989)

Optical Stark Effect of the Exciton

Monique Combescot

G.P.S., Tour 23, Université Pierre et Marie Curie, 2 place Jussieu
75005 Paris

and

L.O.A., E.N.S.T.A. Ecole Polytechnique, 91120 Palaiseau.

When a semiconductor is irradiated by below gap photons, the exciton line blue-shifts. We show that this so-called exciton Optical Stark effect is due to a coupling between the exciton and all (bound and unbound) biexcitonic states. More precisely this effect measures the interactions between the two electrons and the two holes forming the biexcitonic states.

At large detuning, the Fermi (statistical) interaction dominates and the exciton shift is nothing but the dressed-atom shift. At small detuning, the Coulomb interaction dominates and, in materials having a well-bound biexcitonic molecule, transforms the large detuning blue-shift into a red shift, just below the exciton-biexciton resonance.

The exciton optical Stark effect theory can be seen as an expansion in Coulomb interaction, the corresponding reduced parameter being the exciton Rydberg divided by the detuning. We show that all theories based on an Hartree-Fock treatment, can give exact only the lowest order correction to the (dressed-atom) large detuning shift.

The exciton optical Stark effect is basically a dressed-exciton effect. It is however more complex than a simple two-level dressed-atom due to interactions between excited states. These interactions induce corrections to the large detuning shift ; they also induce a space dimension dependance of the absorption strength , which does not exist for dressed atom. The dressed exciton problem is also more complex due to the semiconductor band structure, which induces an exciton splitting linked to light polarizations. We show that the $(4 \times 2 = 8)$ fold exciton, built from a 4-fold ($J=3/2$) valence band and a 2-fold conduction band, has exactly the shifts of a $(4+2 = 6)$ level atom at large detuning. This is a strong support to the existence of a close relation between dressed exciton and dressed atom.

Although in the well-known polariton effect, excitons appear as non interacting bosons and in the exciton optical Stark effect, they only appear as formed of interacting fermions, we show how these two effects are closely related.

Using (As Opposed to Studying) $\chi^{(3)}$

M.D. Levenson, IBM Research Division
Almaden Research Center K32/802D
650 Harry Road
San Jose, CA 95120

The ultimate goal of science is to use knowledge to manipulate nature. In nonlinear optics, the phenomenon of nature we wish to manipulate is light. The second order nonlinear susceptibility - $\chi^{(2)}$ - has shown great promise in this regard. The situation with the third order nonlinear susceptibility is more problematical. In 1990, technology can provide field strengths sufficient to make processes of any order as strong as those of lowest order. Why is it then that the third order nonlinear susceptibility remains largely a laboratory curiosity?

One must admit that third order effects were once considerably more troublesome than mere "laboratory curiosities." Self-focussing, for example, complicated the explanation of many other phenomena and led to optical damage to many early laser systems. Today we look to $\chi^{(3)}$ for potential technological opportunity, not embarrassment.

Many of the effects that one might think could be best done using $\chi^{(3)}$ (such as third harmonic generation or optical switching) can also be accomplished using successive $\chi^{(2)}$ processes. Only when $\chi^{(3)}$ media possess unique technological advantages (as for example for third harmonic generation in the ultraviolet) does the third order nonlinearity prove better than lower order processes. These areas of advantage divide themselves into two categories: those where a small optical signal due to the nonlinear effect is sufficient and those where essentially the entire input amplitude must be processed in some way by the nonlinearity.

Of the small signal processes, probably the most useful is saturation, which allows the accurate determination of the center frequency of an optical transition. When the saturation occurs in the gain medium of a laser or in a weakly absorbing medium placed inside a laser cavity, the resulting normal or inverted Lamb dip marks the location of the transition frequency with a precision that is not affected by line broadening due to the Doppler effect [1]. When the laser frequency is locked to the center of such a dip, the laser wavelength (and frequency) may be determined accurately enough to be recognized internationally as a valid secondary standard. However, few applications require the full precision of an internationally recognized standard wavelength and no laser manufacturer currently offers a laser stabilized by this elegant $\chi^{(3)}$ technique. The stable lasers - that one can buy - lock the laser frequency to some location within the laser gain band - that is they rely on the $\chi^{(1)}$ process of gain to provide frequency stability.

When the nonlinearity is "strong" at least one of the many optical amplitudes is greatly modified by the process. Formally, this requires that

$$4\pi^2\chi^{(3)} E^2 L / \lambda \approx 1 \quad (1)$$

where $\chi^{(3)}$ is the desired third-order nonlinearity, E is the field, L the interaction length and λ the wavelength. This condition can be achieved in a number of ways, including buying a big enough laser so that the E^2 factor compensates for anything small. In that case, other unwanted nonlinear effects can be strong enough to - for example - destroy the medium whenever the desired nonlinear effect becomes operative.

The third order nonlinear susceptibility is generally weak, and this is the over-riding difficulty. In cgs units, typical values of $\chi^{(3)}$ are in the range of 10^{-13} cm³/erg [1]. To achieve the condition of equation (1), it is desirable to use a nonlinearity that is enhanced by a resonant process, or to employ very long nonlinear media. Both of these means of strengthening the interaction imply increasing in the time over which it operates. In the resonant case, the time-scale is set by the linewidth of the resonance, or the detuning of the exciting frequency from the resonance. Typical resonantly enhanced nonlinearities have a response time on the order of one picosecond - fast from an electronic point of view but slow from the perspective of today's femtosecond optics [1].

Only two $\chi^{(3)}$ media are widely used (as opposed to studied) in the strong interaction regime: Raman gain and Raman-resonant four wave mixing interactions in hydrogen are used to shift the wavelength of pump beams into more desirable spectral regions [1]. Raman amplification can also be used to combine the powers of low beam quality excimer lasers into an output beam with a more useful time and space profile. The Kerr and wave-mixing nonlinearities of fused silica optical fiber give rise to soliton pulses useful for communications and to self phase modulation which is now widely used for pulse compression [2]. While the nonlinearity involved in these processes is intrinsically very fast and the pulses very short, relatively large sample lengths are required to produce useful effects. In optical computing, this large sample length implies a long cycle time.

Many other strong effects (such as phase conjugation in BaTiO₃) which appear to result from $\chi^{(3)}$ actually result from successive $\chi^{(2)}$ processes. Perhaps materials scientists will be able to develop other useful $\chi^{(3)}$ materials by building on the virtues of the two that are useful today. But then again, perhaps not.

References:

- 1.) M.D. Levenson and S.S. Kano, "Introduction to Nonlinear Laser Spectroscopy", Academic Press, Boston, 1988.
- 2.) W.J. Tomlinson, R.H. Stolen and C.V. Shank, J. Opt. Soc. Am. B, 1, 139-149 (1984) and references therein.

WI10 Nonlinear Optical Processes with Incoherent Light and Their Applications for Studies of Ultrafast Dephasing

Peixian YE

Institute of Physics, Chinese Academy of Sciences,
P.O. Box 603, Beijing, 100080, China

SUMMARY

In recent years, a series of nonlinear optical processes with incoherent light, such as time-delay four-wave mixing,^{1,2} optical Kerr effect³ and coherent Stokes Raman scattering,⁴ were developed and attracted much attention. It has been demonstrated that these processes can be used to measure the ultrafast dephasing times of excitations (shorter than 1 psec.) with nanosecond pulse lasers or even CW lasers. In this talk, after a short review of the works done by others previously theoretical and experimental investigations in this field in my laboratory are presented.

In the first part, experimental studies of time-delay four-wave mixing with incoherent light (TDFWM-IL) are presented for the absorption band 4T_2 of ruby at temperatures from 20K to 300K, also for the absorption bands of Oxazine and Cresyl Violet in PMMA or in solution from 80K to 300K. Dephasing times have been obtained formally by analysing the experimental data on the basis of two-level theory at different conditions for different materials. The conclusion is that the two-level theory fails in the interpretation of the results since the dephasing time (T_2) does not depend on temperature in a wide range of 80 - 300K for all cases. Then, our multi-level theory of TDFWM - IL both in the cases of homogeneous and inhomogeneous broadening is described and applied successfully to explain the results. It is shown also that T_2 determined on the basis of two-level theory is not the ordinary dephasing time of individual transitions but an effective one which reflects the behavior of the total absorption spectrum of the band. A modulation structure observed in the delay-time dependence of signal intensity at the zero-phonon line of ruby at 20K is reported and demonstrates further the correctness of our multilevel theory.

In the second part, experimental studies in the Kerr shutter configuration using incoherent light are presented both for the absorption bands of Oxazine and Cresyl Violet in PMMA film at temperatures from 80K to 300K. A multilevel theory of Kerr shutter with incoherent light is developed for absorption bands that consist of a series of vibrational transitions. It is demonstrated

that in order to explain the experimental results this multilevel theory is needed.

In the last part, Raman enhanced nondegenerate four-wave mixing with incoherent light (RENFWM-IL) is proposed to be a new method to measure ultrafast dephasing processes of the Raman modes in Raman active media. Experimental studies in benzene and in dimethylsulfoxide (DMSO) are presented. A comparison between RENFWM-IL and coherent Stokes Raman scattering with incoherent light has also been made.

This talk is based on the works to which a lot of contribution was made also by Xin Mi, Ruihua Zhang, Haitian Zhou and Qian Jiang.

ACKNOWLEDGMENT

This research is supported by the National Natural Science Foundation of China.

1. N. Morita and T. Yajima, Phys. Rev. A30, 2525(1984)
2. S. Asaka, H. Nakatsuka, M. Fujiwara, and M. Matsuoka, Phys. Rev. A29, 2286 (1984)
3. K. Misawa, T. Hattori, and T. Kobayashi, Opt. Lett. 14, 453(1989)
4. T. Hattori, A. Terasaki, and T. Kobayashi, Phys. Rev. A35, 715(1987)

George I. Stegeman, Jeff Ehrlich and Gaetano Assanto
Optical Sciences Center, University of Arizona
Tucson, AZ 85721, USA

Summary:

The periodicity associated with gratings can be used to wavevector match various interactions between guided waves, and between guided waves and radiation fields. We have investigated such interactions in nonlinear waveguides containing gratings for coupling radiation into and out of waveguides, and distributed feedback gratings for retro-reflecting guided waves. Because the waveguides consist of materials with an intensity-dependent refractive index, the wavevector matching becomes intensity-dependent leading to all-optical functions such as bistability and switching. The geometries studied are all contained in Fig. 1. The waveguides were MBE grown InSb on GaAs substrates, and exhibited a thermo-optic nonlinearity at CO₂ laser wavelengths.

Using just an input grating coupler, optical limiting and bistability were observed and found to agree well with a theory for the coupling process which includes nonlinearities that diffuse in space. Under special conditions, butterfly bistability was also observed when the radiation was coupled out with a second grating.

Various CO₂ laser lines were used to map out the linear and nonlinear spectral response of distributed feedback gratings (DFBG). The wavelength associated with the peak grating reflectivity shifted with increasing power. As a result, when power is increased at a specific wavelength, the grating reflection and transmission coefficients vary leading to all-optical switching.

The presence of a DFBG, feeding back power into the input grating coupler region, enhances the bistable response of the input coupler. The DFBG is tuned so that its reflection coefficient increases with the power incident onto it. We have observed that such a nonlinear feedback leads to a large decrease in the power required for bistability (Fig. 2) in such a nonlinearly coupled input grating coupler-DFBG system.

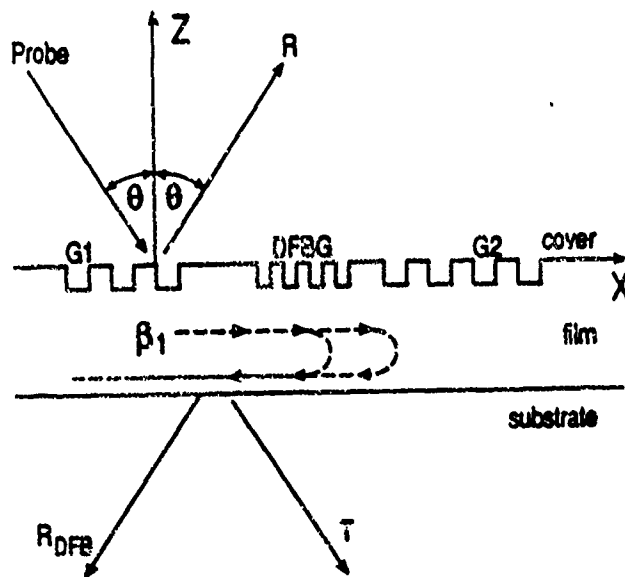


Figure 1 The most general sample geometry studied which includes an input grating coupler, a distributed feedback grating and an output coupling grating.

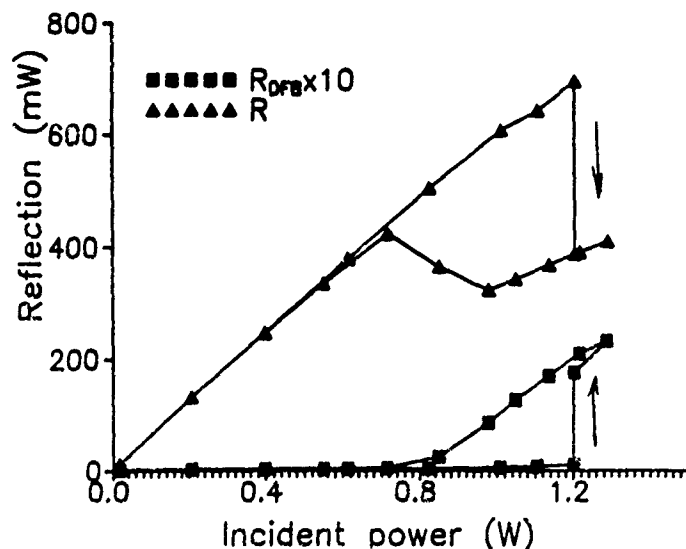


Figure 2 The bistability signal obtained on specular (R) and DFBG (R_{DFB}) reflection versus incident power. Without the feedback grating, no bistability is obtained for these conditions for input powers up to 4 W.

**WEDNESDAY, JULY 18
POSTER PRESENTATIONS**

WP1 Simultaneous Measurement of Vibrational Spectra and Dynamics Through Femtosecond Fourier-Transform Nonlinear-Optical Spectroscopy

William T. Lotshaw

G.E. Research and Development Ctr., P.O. Box 8, Rm. KWD-270, Schenectady, NY 12301
(518) 387-5163

Dale McMorro

Naval Research Laboratory, code 4613, Washington, D.C. 20375 (202) 767-3939

The spectral content present in femtosecond optical pulses produced with modelocked lasers may overlap multiple spectroscopic transitions in a material. When the center frequency of the optical pulse is far from any electronic resonance (*e.g.*, the medium is "transparent"), the Raman-active material resonances (lattice, intermolecular, intramolecular, *ect.*) accessible to the difference frequency spectrum of the pulse may be resonantly and coherently excited through four-wave-mixing processes involving different Fourier components of the pulse.¹ Therefore, it is essential that the Fourier composition of the pulse be explicitly accounted for whenever the interaction of femtosecond laser pulses with materials is considered.

We have developed a novel Fourier-transform (FT) technique for the analysis of time-resolved data obtained from various nonlinear-optical (NLO) spectroscopies which simultaneously 1) reveals the complex, frequency-dependent NLO susceptibility to ultrashort optical pulses, 2) separates uniquely and determines the relative amplitudes of the purely electronic and vibrational contributions to the nonlinear-optical susceptibility, and 3) determines directly the relevant kinetic rate constants. The information acquired through this technique can subsequently be used to correctly account for the material response produced by ultrashort optical pulses of arbitrary shape and duration. The principal constraint on the analysis is that the experimental signal must scale as the product of the "pump" and

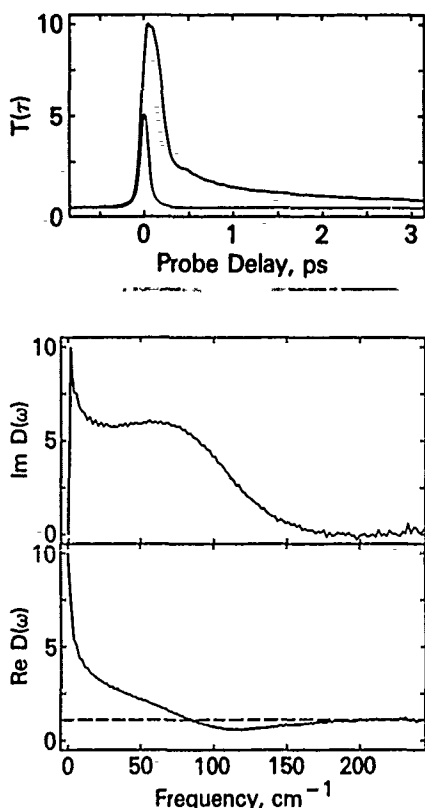
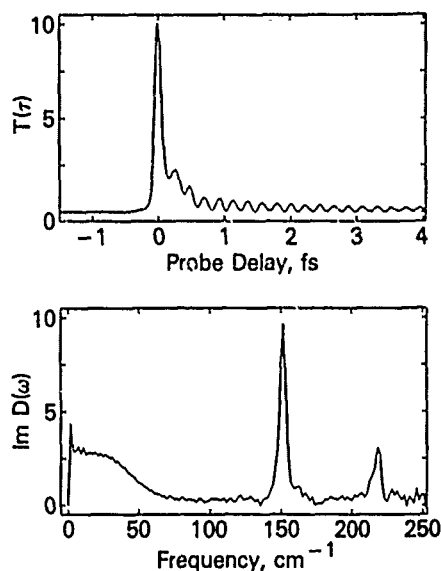


Figure 1. (upper) Femtosecond optically-heterodyne detected optical Kerr effect transient measured for liquid pyridine using 65 fs optical pulses with the zero-background laser pulse intensity autocorrelation function scaled to approximately represent the amplitude of the non-resonant electronic hyperpolarizability; (middle) Imaginary and (lower) real parts of the frequency response of the material obtained from the femtosecond OKE data illustrating the significance of lattice-like intermolecular vibrational motions and the separation of electronic and nuclear contributions to the OKE. In the lower two spectra the effects of the finite-duration are completely removed.

Figure 2. (upper) Femtosecond OHD OKE data for bromoform (CHBr_3) liquid illustrating a large instantaneous electronic contribution and the coherent vibrational motion of the intramolecular Raman resonances below 9 THz; (lower) Imaginary part of the NLO susceptibility exhibiting a clear separation in frequency space of the different nuclear contributions to the dynamical waveform free from interference of the nonresonant electronic hyperpolarizability.



"probe" pulse intensities, and hence possess an effective instrument function that can be represented by a second order (pump-probe) correlation function. The technique is thus applicable to both $\chi^{(2)}$ and optical-heterodyne-detected (OHD) $\chi^{(3)}$ spectroscopies. The OHD- $\chi^{(3)}$ spectroscopies of particular interest include the optical Kerr effect (OKE), the various transient-grating techniques, and coherent Raman spectroscopies.

We have investigated the ultrafast responses for numerous organic materials using the time-resolved OHD OKE. This experimental configuration meets the constraints noted above, allowing us to extract the frequency-dependent NLO susceptibility, $D(\omega)$, directly from the experimentally measured signal, $T(\tau)$, with no approximations or models [$D(\omega)$ is the FT of the NLO impulse response function of the medium, $R(t)$]. As an example, figure 1 gives the measured OHD OKE transient for pyridine liquid, together with the real and imaginary parts of $\bar{D}(\omega)$. The spectrum $\text{Im } D(\omega)$ contains all the information on the nuclear contribution to the dynamical response, and clearly reveals a broad resonance associated with lattice-like intermolecular vibrational motions of the liquid. $\text{Re } D(\omega)$ contains contributions from both the nuclear and non-resonant electronic signal contributions, with the latter appearing as a constant background indicated by the dashed line. Figure 2 gives the Kerr data and the $\text{Im } D(\omega)$ spectrum for liquid bromoform, indicating clearly the lower frequency intermolecular vibrational contributions and the sharp, higher-frequency intramolecular resonances.

In this paper we will present details of the method leading to the spectra of figures 1 and 2, and will discuss the application and significance of these considerations to non-OKE spectroscopies. We will describe the general utility of the deduced frequency-dependent susceptibilities for the interrogation of vibrational line broadening mechanisms, and the prediction of the material response under arbitrary pulsewidth and pulse-sequence excitation.

References

1. D. McMorro, W.T. Lotshaw, and G.A. Kenney-Wallace, IEEE J. Quant. Elect., 24, 443 (1988).

G.J.Milburn
Department of Physics
University of Queensland
St Lucia 4067
Australia

Summary.

The quantum dynamics of periodically kicked hamiltonian systems can reflect the classical dynamics be it regular or chaotic. However in quantum systems the classical chaotic diffusion of one phase space variable is suppressed due to irregular recurrences in the quantum state. This aspect of quantum nonlinear dynamics should be accessible to experimental test and recent results on the microwave ionization of hydrogen would seem to confirm it.

In this paper I will consider a single mode field interacting with an intensity dependent refractive index and periodically 'kicked' by a degenerate parametric amplifier interaction. The system could be a cavity containing both a Kerr nonlinearity and a parametric amplifier with the amplifier driven by a pulsed pump field. The dynamics is directly modelled by a nonlinear map, in fact a perturbed twist map, and exhibits the typical scenario of regular KAM surfaces which break up into island chains and regions of chaos.

The quantum dynamics may be studied by monitoring the mean photon number in the cavity. In the case that the origin of the classical phase space is surrounded by nonchaotic orbits the mean photon number for an initial vacuum state exhibits regular collapse and revival. However if there is a large region of chaos near the origin the mean photon number does not diffuse but exhibits irregular recurrences. This system should provide a direct experimental test of the quantum suppression of chaotic diffusion in an optical context. A study of photon number and quadrature phase statistics also show interesting behavior including large squeezing.

The experimental realization of the system requires a third order susceptibility of about 10^{-10} to 10^{-12} esu and a parametric gain of 1.2 to 1.5. Damping can be kept low by using lossless cavities and monitoring pump absorption instead of photon number directly. Of course thermal fluctuations are not important at optical frequencies. It would then seem that a practical test of quantum limited chaotic diffusion is possible in this system.

We also include dissipation and show that regions of chaos can still be found.

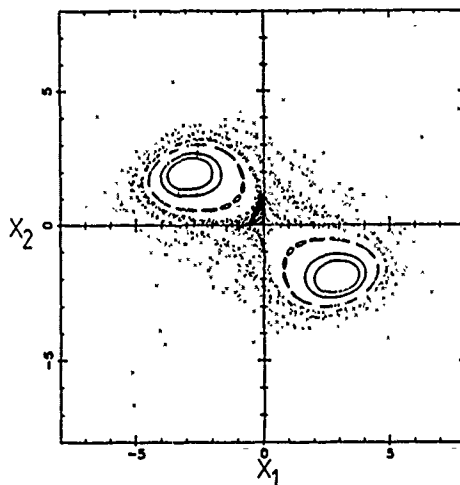


Fig. 1 A plot of typical orbits versus quadrature phase amplitudes. The parametric gain is 1.5 and the nonlinear phase shift is $0.03 \text{ rad photon}^{-1}$.

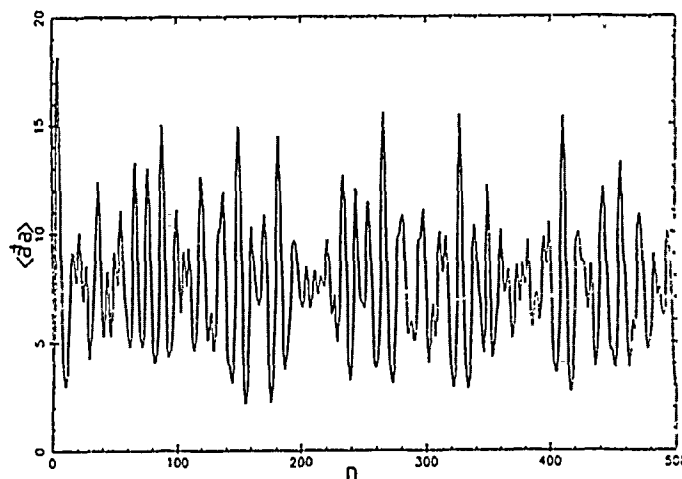


Fig. 2 Mean photon number versus time for an initial vacuum state and for the same parameters as figure one.

SECOND-ORDER PHASE TRANSITION AT THE CRITICAL POINT OF OPTICAL BISTABILITY DUE TO NONLINEAR ABSORPTION

Ou Fa

Physics Department

South China Institute of Technology,

Guangzhou, 510641, P.R. of China.

Critical phenomena in optical bistability (OB) are studied in details. Theoretical analyses, mainly based on the steady solution of the "thermodynamic" Fokker-Plank equation^[6] for absorptive OB, show that the critical phenomena in OB also can be brought into the framework of Landau's theory of second-order phase transitions, and the relations between different kinds of critical index numbers obey the scaling laws.

1. Introduction

Phase transition developing from equilibrium to nonequilibrium is always a fascinating problem. It has been found that although the equilibrium phase transitions may be different in mechanism of the interaction, but some common features exist among themselves. Ones reveal the analogy between equilibrium and far from equilibrium phase transition just for the purpose of finding the commonness in the more extent. Now, we would like to discuss this topic in quantum optics. In fact, the atoms coupled with optical (electromagnetic) field form an open system which exhibits phenomena analogous to phase transitions but far from thermodynamic equilibrium. The switching effect in optical bistability (OB) appears similar to first-order phase transition,^[1] as well as the threshold behavior of laser is similar to second-order phase transition.^{[2][3]} The first-order-like phase transition is shown also by other dissipative systems in quantum optics, for instance, the laser with saturable absorber, the dye laser, sub/second harmonic generation and the bidirectional ring laser.^{[4][5]} However, some authors (1984, 1982),^{[4][1]} famous in theory of OB, think "the characteristic features of optical bistability is that it occurs in a purely passive system and that it never exhibits a second-order transition." The critical phenomena studied in this paper is just the OB critical phenomena which occurs in the passive cavity. As we know, the two phase coexistence line of the first order transition in equilibrium system has a terminal point -- critical point, and the critical point in equilibrium transition is just the second-order transition (continuous transition) point. Although it is difficult to establish the concept of two-phase coexistence concerning OB, the similar critical point exists also. Let I_i , I_u and I_d represent the input light intensity and its jumping up and falling down threshold respectively; I_t -- output (transmitted) light intensity of system; C -- some control parameter. On the I_i - C plane, one can always draw $I_u \sim C$ and $I_d \sim C$ curves experimentally or theoretically (see Fig. 1a and b). These two curves divide the I_i - C plane into the single-stable region of higher branch, bistable region and the single-stable region of lower branch. And, these two curves intersect in one point and end in this point. This point is completely similar to the end point of the two-phase coexistence line, thus, it is also a critical point -- the critical point of OB system. Can't this critical point in OB respond to one kind of continuous transitions (second-order phase transitions)? This question will be answered in the following process of investigating into the critical phenomena in OB.

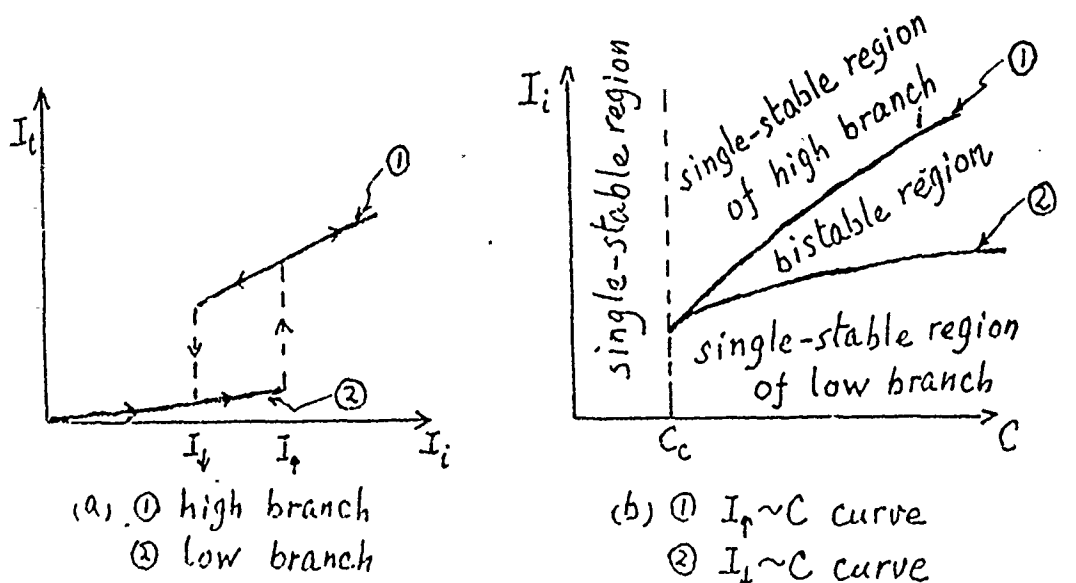


Fig. 1

II. Generalized Thermodynamic Potential, Order Parameter, Equivalent External Field

The Fokker-Plank equation of OB or laser is one kind of quantum statistical theories of non-equilibrium open system. From this equation the steady distribution $P_{st}(x)$ can be solved in an exponential form:

$$P_{st}(x) = \mathcal{N} \exp[-\tilde{G}(x)/q] \quad (1)$$

where \mathcal{N} is the normalized factor, q is the fluctuation parameter; the variable x is the normalized transmitted field, while function $\tilde{G}(x)$ is called the general thermodynamics potential which determines directly the properties of the steady statistical distribution of the system. In the case of neglecting quantum fluctuation, the $\tilde{G}(x)$ due to pure absorptive OB (AOB) can be written as following simple form [6][7]:

$$\tilde{G}(x) = 1/2 x^2 - xy + C \ln(1 + x^2), \quad (2)$$

where y is the normalized incident field, C is cooperative parameter (control parameter). If some internal factor of the system causes a small fluctuation of x to be δx , the corresponding change of $\tilde{G}(x)$ is $\Delta\tilde{G}(x)$ (y and C remain unchanged):

$$\Delta\tilde{G} = \frac{\partial\tilde{G}}{\partial x} \delta x + \frac{\partial^2\tilde{G}}{\partial x^2} (\delta x)^2 \quad (3)$$

$\frac{\partial\tilde{G}}{\partial x} = 0$ is the condition that \tilde{G} takes extreme value, it also gives the macroscopic state equation:

$$y = x \left(1 + \frac{2C}{1+x^2} \right), \quad (4)$$

$\frac{\partial^2\tilde{G}}{\partial x^2} > 0$ (i.e. $\frac{dy}{dx} > 0$) is the condition that \tilde{G} takes minimum; it is also a stability condition of macroscopic steady state. Thus, $\tilde{G}(x)$ is equivalent to the Gibbs free energy in equilibrium thermodynamics. This problem was discussed in detail in reference [6].

When $y = 0$ in equation [4], which means no inject signal, we have

$$x \left(1 + \frac{2C}{1+x^2} \right) = 0. \quad (5)$$

It can be taken as the laser state equation near threshold while the parameter C in this equation plays a role of pumping and $C < 0$. Of course, this paper considers chiefly the OB critical phenomena that others have not studied carefully. However, the threshold behavior of laser will be included naturally in our later discussion.

It is easy to find the values of (x, y, C) in critical point (x_c, y_c, C_c) by working out $\frac{dy}{dx} = 0$ and $\frac{d^2y}{dx^2} = 0$ according to eq. (4):

$$(x_c, y_c, C_c) = (\sqrt{3}, \sqrt{3}, 4). \quad (6)$$

for laser, it can be deduced from eq. (5), that is

$$(x_c, y_c, C_c) = (0, 0, -1/2). \quad (7)$$

The start point that we consider the OB critical behavior is the general thermodynamics potential $\tilde{G}(x)$, which reflects the statistical properties of AOB steady state and is shown in eq. (2). Just for the purpose of considering the critical behavior, we expand function $\tilde{G}(x)$ about the critical point $x = x_c$, let

$$x = x_c + \eta, \text{ and } \eta \ll x_c. \quad (8)$$

Then Taylor series of \tilde{G} may be expressed in terms of the deviation η :

$$\tilde{G}(\eta) = G_0 + G_1\eta + G_2\eta^2 + G_3\eta^3 + G_4\eta^4, \quad (9)$$

where η can be considered as an order parameter of OB system. Later, we would see that it is equivalent to the magnetization of the ferromagnetics, to the wave function of the electron pairs in superconductor, or to the difference between the gas density and liquid density at the gas -- liquid coexistence state. (Strictly speaking, is equivalent to the deviation of the gas or liquid density from its critical value). In order to compare with the Landau's transition theory conveniently, the series of \tilde{G} has been interrupted before the fifth power of η . In the advantage of eq. (2) it is easy to obtain the expansion coefficients

$$G_n (= \frac{1}{n!} (\frac{\partial}{\partial \eta})^n \tilde{G} \Big|_{\eta=0}, \quad n=0, 1, 2, 3, 4)$$

as follows:

$$G_0 = \frac{1}{2}x_c^2 - x_c y + C_c(1-t)\ln(1+x_c^2), \quad t = 1 - \frac{C}{C_c}, \quad (9a)$$

(for laser, $x_c = 0$, then $G_0 = 0$);

$$G_1 = -y + x_c \left(1 + \frac{2C}{1+x_c^2}\right) \equiv -\tilde{H} \quad (9b)$$

(for laser, $y = 0$, $x_c = 0$, then $H = 0$);

$$G_2 = \frac{t}{2}, \quad (\text{for laser, the same}); \quad (9c)$$

$$G_3 = \frac{C}{3!} \frac{4x_c^3 - 12x_c}{(1+x_c^2)^3} = 0 \quad (9d)$$

(for AOB, $x_c = \sqrt{3}$; for laser, $x_c = 0$);

$$G_4 = b(1-t), \quad (9e)$$

(for AOB, $b = 1/C_c^2 = 1/4$; for laser, $b = C_c^2 = 1/4$).

It worths to note that the quantity \tilde{H} , defined in eq.(9b), may be called "equivalent external field," because it is fairly similar to the external magnetic field in ferromagnetics. Let the incident field y operate in a special value y_{sp} , which means

$$y = y_{sp} = x_c \left(1 + \frac{2C}{1+x_c^2}\right) \quad (10)$$

the corresponding equivalent external field \tilde{H} will be zero, i.e.

$$H = 0. \quad (11)$$

Such as y_{op} is corresponding to the values of y with the same $x = x_c(\eta=0)$ in the equal C curves (see Fig. 2). Inserting eqs.(9a-e) into eq.(9), we have the expression of general thermodynamic potential of AOB near the critical point:

$$\begin{aligned} \widetilde{G}(\eta) = & \frac{1}{2} x_c^2 - x_c y + C_c (1-t) \ln(1+x_c^2) \\ & - \widetilde{H} \eta + \frac{t}{2} \eta^2 + b(1-t) \eta^4. \end{aligned} \quad (12)$$

In fact, obtaining this equation has laid the foundation to bring the OB critical phenomena in passive cavity ($C > 0$) into Landau's second-order phase transition theory.

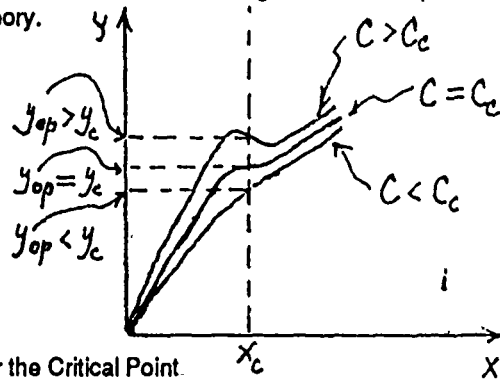


Fig. 2

III. The State Equation near the Critical Point.

From $\frac{\partial \widetilde{G}}{\partial \eta} = 0$, we obtain the state equation near the critical point:

$$\widetilde{H} = t\eta + 4b(1-t)\eta^3. \quad (13)$$

If we set the incident field y to be the y_{op} shown in equation (10), which means $H = 0$, we have

$$\eta [t + 4b(1-t)\eta^2] = 0. \quad (14)$$

The solutions of this equation are as follows:

$$\eta = 0, \quad \eta = \eta_{\pm} = \pm \frac{1}{2\sqrt{b}} (-t)^{1/2}. \quad (15)$$

The above results represent the bifurcation of one stable node into two stable nodes in OB critical phenomenon: When $t > 0$ ($C < C_c$), only solution $\eta = 0$ is stable, since $\frac{\partial^2 \widetilde{G}}{\partial \eta^2} \Big|_{\eta=0} = t > 0$. As soon as $t < 0$ ($C > C_c$), solution $\eta = 0$ becomes unstable, and instead of it, two solutions $\eta = \eta_{\pm}$ are stable, since $\frac{\partial^2 \widetilde{G}}{\partial \eta^2} \Big|_{\eta=\eta_{\pm}} = -2t > 0$. These three solutions meet in the critical point $t = 0$ with $\eta = 0$ which is critically unstable. $\eta = \eta_{+} > 0$ is corresponding to higher transmission branch; $\eta = \eta_{-} < 0$ - lower transmission branch. Because the equivalent external field $\widetilde{H} = 0$ in the given case η_{+} and η_{-} are completely similar to two opposite spontaneous magnetizations in ferromagnetics. In summary:

$$\begin{aligned} t > 0 \quad (C < C_c), \quad \eta = 0 & \text{ -- stable, no OB;} \\ t = 0 \quad (C = C_c), \quad \eta = 0 & \text{ -- critically unstable;} \\ t < 0 \quad (C > C_c), \quad \eta = \eta_{\pm} = \pm (-t)^{1/2} / 2\sqrt{b}, \\ \beta = 1/2, & \text{ -- OB occurs.} \end{aligned} \quad (16)$$

Now, let us consider the case of $\tilde{H} = y - x_c (1 + \frac{2C}{1+x_c^2}) \neq 0$ ($x_c = \sqrt{3}$).

When C equals the critical value, $C_c = 4$, i.e. $t = 0$, from eq. (13), we have

$$\eta = (\tilde{H}/4b)^{1/3}, \quad \gamma = 3. \quad (17)$$

This result indicates that, though C equals the critical value $C_c = 4$, the incident field y doesn't equal to the corresponding operating value, i.e., $y \neq y_{cp} = y_c = 3\sqrt{3}$.

It is obvious that $x \neq x_c$, i.e., $h \neq 0$. This h is equivalent to the magnetization of ferromagnetics under the effect of external magnetic field at the critical temperature. From eq. (13) "the equivalent susceptibility" χ in the vicinity of critical point of AOB can be also defined as follows:

$$\chi \equiv \frac{\partial \eta}{\partial \tilde{H}} = \left(\frac{\partial \tilde{H}}{\partial \eta} \right)^{-1} = |t|^{-1}, \quad \gamma = 1 \quad (18)$$

We continue to discuss the solutions of order parameter when the equivalent external field $\tilde{H} \neq 0$. For this purpose, reform the eq. (13) as the following typical form of third order algebraic equation:

$$\eta^3 + t'\eta + \tilde{H}' = 0 \quad (19)$$

$$\text{where } t' = \frac{t}{4b}, \quad \tilde{H}' = -\frac{\tilde{H}}{4b} = \frac{y - y_{cp}}{4b} \quad (20)$$

The discriminant of the solution of eq. (19) is [6]:

$$\Delta = (\tilde{H}'/2)^2 + (t'/3)^3 \quad (21)$$

When $\Delta > 0$, the h has only one real root which includes two situations: 1) C below the critical value C_c , i.e. $t' > 0$, it is absolutely single-stable, no matter what incident field y is taken; 2) $t' > 0$, but C insufficient- above C_c for the given y , deviated from y_{cp} ($\tilde{H} \neq 0$) the single real root of h means a single-stable state in high branch or in low branch, i.e., beyond the bistable region. When $\Delta < 0$, the h has two real roots which means that not only C above C_c ($t' \leq 0$), but also the Y has ever been biased into the bistable region. The above discussion shows that above critical point, $\tilde{H} = 0$ ensures the incident y hold always in the bistable region. Taking $\tilde{H} = 0$ would be more clear to demonstrate the characteristic features of OB critical phenomena.

So far, the OB critical features, revealed by us, are completely similar to ferromagnetics, while the critical phenomena of ferromagnetics are a prototype of second-order transition.

IV. Second-Order Transition and Scaling Rule

In order to demonstrate further that the OB critical phenomena accord with the general definition of second-order transition (Ehrenfest definition), we refer to the formal entropy \tilde{S} , introduced in reference [6]. \tilde{S} is just the first order derivation of \tilde{G} , i.e. $\tilde{S} = \frac{\partial \tilde{G}}{\partial C}$. First, we consider the case of the generalized thermodynamic potential \tilde{G} with $\tilde{H} \neq 0$. Referring to eqs. (2), (9a) and (9b), we have [6]

$$\begin{aligned} \tilde{S} &= \left(\frac{\partial \tilde{G}}{\partial C} \right)_h = \ln(1 + x_c^2) - \frac{\partial \tilde{H}}{\partial C} h - \frac{h^2}{2C_c} \\ \frac{\partial \tilde{H}}{\partial C} &= \frac{2x_c}{1+x_c^2}, \quad (h^2 \text{ being neglected}). \end{aligned} \quad (22)$$

It is just the approximate series expansion of \tilde{S} , formulated in reference [6] as follows:

$$\tilde{S} (= \ln(1+x^2)) = \ln[1+(x_c + \eta)^2]. \quad (23)$$

The advantage of the formal entropy \tilde{S} formulated as eq. (22) is that it includes the terms of first power of η . The OBS switching up or down, i.e., altering the sign of η , and then the formal entropy \tilde{S} is changed discontinuously. This shows evidently the character of first-order transitions. However, in order to demonstrate the second-order transition of OB we would prefer using the $\tilde{G}(\eta)$ with $\tilde{H} = 0$ to derive the formal entropy \tilde{S} , the result of which are in the following:

$$\tilde{S} = -\frac{\partial \tilde{G}}{\partial C} = \ln(1+x_c^2) - \frac{\eta^2}{2C_c} \quad (24)$$

Substituting the solution of η , expressed by eqs. (16) with $\tilde{H} = 0$, into this equation, we have

$$\left. \begin{aligned} t > 0 \quad (C < C_c), \quad \tilde{S}_0 &= \ln(1+x_c^2) \\ t < 0 \quad (C > C_c), \quad \tilde{S} &= \ln(1+x_c^2) + \frac{t}{2} \end{aligned} \right\} \quad (25)$$

Therefore, when the system passes the critical point, the formal entropy \tilde{S} , i.e., the first order derivation is continuous. Because of the cooperative parameter C is equivalent to the temperature in equilibrium thermodynamics, the formal specific heat \tilde{c} can be defined by the following fashion: [3][6]

$$\tilde{c} = C \frac{\partial \tilde{S}}{\partial C} = -\frac{C}{C_c} \frac{\partial \tilde{S}}{\partial t} \quad (26)$$

According to eq. (25), we have

$$\left. \begin{aligned} t > 0, \quad \tilde{c} &= -\frac{C}{C_c} \frac{\partial \tilde{S}}{\partial t} = 0 \\ t < 0, \quad \tilde{c} &= -\frac{C}{C_c} \frac{\partial \tilde{S}}{\partial t} = -\frac{C}{2C_c} \end{aligned} \right\} \quad (27a)$$

Thus, when the system passes the critical point, the formal specific heat \tilde{c} -- the second-order derivation of \tilde{G} -- changes discontinuously. This indicates rather clearly that the OB critical phenomena are a second order transition.

At the OB critical point formal specific heat \tilde{c} has a definite jump (see eq. (27a)), that is

$$\tilde{c}(t \rightarrow 0^+) - \tilde{c}(t \rightarrow 0^-) = \frac{1}{2} \quad (27b)$$

This singularity of the "specific heat" \tilde{c} may be expressed as follows [9]:

$$\tilde{c} \sim |t|^{-\alpha} + \text{non-singular parts}, \quad \alpha = 0. \quad (28)$$

Combining the critical indexes $(\beta = \frac{1}{2}, \delta = 3, \gamma = 1 \text{ and } \alpha = 0)$

in eqs. (16), (17), (18) and (28), we find that they are just the same as the critical indexes of ferromagnetics [9], and they obey scaling rules as follows [9]:

$$\left. \begin{aligned} \alpha + 2\beta + \gamma &= 2, \\ \alpha + \beta(\delta + 1) &= 2. \end{aligned} \right\} \quad (29)$$

V. Fluctuations and Correlations

In order to demonstrate the character of OB critical fluctuations and correlations, we would like to use the related results

calculated by H. Carmichael (1986) in reference [10]:

1. Field - field correlation, for example,

$$\langle \Delta \bar{a}^+ \Delta \bar{a} \rangle = N^{-1} x^2 \lambda \quad (30)$$

2. Atom-field correlation, for example,

$$\langle \Delta \bar{a} \Delta \bar{J}_+ \rangle = N^{-1} (2C)^{-1} x^2 \lambda \quad (31)$$

3. Atom-atom correlation, for example,

$$\langle \Delta \bar{J}_+ \Delta \bar{J}_- \rangle = N^{-1} x^2 (1 + x^2)^{-2} + N^{-1} (2C)^{-2} x^2 \lambda \quad (32)$$

All of above correlations represent correlated fluctuations of AOB in steady state, \bar{a} and \bar{J}_{\pm} stands for field operators of creation and annihilation, and atom operators of polarization respectively. $\langle \Delta (\dots) \rangle$ represents the average perturbations of above variables from the steady state. N - the total number of atoms, and

$$\lambda = f(x) \left(-\frac{dy}{dx} \right)^{-1} \quad (33)$$

in which the expression of function $f(x)$ can be seen in eq. (5.32) of reference [10]. The factor λ in the vicinity of critical point can always be expressed as

$$\lambda \left[= A \left(-\frac{dy}{dx} \right)^{-1} = A \left(-\frac{d\tilde{H}}{d\tilde{h}} \right)^{-1} \right] = A |t|^{-1}, \quad (A--\text{constant}). \quad (34)$$

Referring to eqs. (30) -- (34), it is evident that when the system approaches to the critical point, the fluctuations increases unnormally. It is worth to note that, according to reference [10], the first term in eq. (32) represents the self-correlative fluctuations of the same atom (direct fluctuations), while the second term that contains factor represents the correlations between different atoms (indirect fluctuations). Obviously, this kind of indirect fluctuations is just the correlated fluctuation of the atoms in different distance. Thus one can introduce some average correlation distance (length) to measure this indirect fluctuation. When the system approaches to the critical point, $\lambda \rightarrow \infty$, it means that the average correlation length tends to be infinite. Thus, for OB, when system approaches to critical point, the correlation distance increases unnormally and it leads to the fluctuation increasing unnormally. According to the above qualitative discussion, the OB critical fluctuation accords with the general rule of critical phenomena.^[9]

Vi. Conclusions

Summarizing the above discussion on OB critical phenomena, we would like to make following conclusions:

1. The optical bistability is not only an example of the first-order transition, but plays also the role of a prototype of the second-order transition.
2. OB critical phenomena can be brought into the framework of Landau phase transition theory, at least for the case of AOB.
3. The relations between the critical indexes of AOB obey the scaling rules as shown in eqs. (29).
4. Although the purpose of this paper is to consider the OB critical phenomena, after comparing this paper both with the work of Degiorgio and Scully (1970) (analogy between laser and ferromagnetics)^[2] and with the work of Graham and Haken (1970) (analogy between laser and super-conductor)^[3], it is easy to find that the discussion of this paper has included the laser threshold behavior with injected signal^[2] ($y \neq 0$, $H \neq 0$) or/and without injected signal^[3] ($y = 0$, $H = 0$, since for laser, $x_c = 0$). Thus, this paper would be a development and synthesis of the related works of above authors.
5. Basically, the discussion on OB critical behavior in this paper is a statistical theory, because the starting point of the discussion is the generalized thermodynamic potential G that represents the statistical properties of AOB. Certainly, the works

of the authors mentioned above are the same.

6. The generalized potential \bar{G} , related to our discussion, is a particular form as eq.(2) which satisfies the principle of detailed balance^[6]. Therefore, in the given case, the foundation of analogy between equilibrium and far from equilibrium phase transition would be still the detailed balance.

7. The fluctuations and correlations in the vicinity of OB critical point obey basically the general rule of critical phenomena. Approaching to the critical point, the fluctuations of OB increases unnormally, which would also come from the long range correlations.

Acknowledgement

I wish to thank Mr. Deng Wenji for helpful discussion. This work was supported in part by the Science and Engineering Research Section of SCIT (Guangzhou, China).

References

- [1] R. Bonifacio and L.A. Lugiato, in Dissipative systems in quantum optics, ed. R. Bonifacio, Springer-Verlag (1982), pp.61,64,84
- [2] (a) V. Degiorgio and M.O. Scully, Phys. Rev. A2, 1170 (1970);
(b) M. Sargent III, M. O. Scully, in Laser Handbook, Vol.I, eds. F.T. Arrechi, E.O. Schultz-Dubois, North-Holland (1972)
- [3] (a) R. Graham, H. Haken, Z. Phys. 237,31 (1970)
(b) H. Haiken, same as [2](b)
- [4] L.A. Lugiato, in Progress in Optics XXI, ed. E. Wolf, Elsevier Science Pub. (1984) PP.71, 188
- [5] C.R. Willis, in Optical Bistability, eds. C.M. Bowden et.al. Plenum Press (1981), p. 431
- [6] Ou Fa and Qin Zixiong, Optics Communications, 65,6, 455, (1988)
- [7] R. Bonifacio, M. Gronchi and L.A. Lugiato, Phys. Rev. A 18 2266 (1978)
- [8] Any kinds of mathematics handbook
- [9] S.K. Ma, Modern Theory of Critical Phenomena, W.A. Benjamin, Inc. (1976)
- [10] H.J. Carmichael, in Frontiers in Quantum Optics, eds. E.R. Pike and Sarkar, Adam Hilger (1986), pp. 120, 168-171

Supplement

Second-order Phase Transition in Increasing Absorption Optical Bistability (IAOB)

This supplement will offer another example to illustrate the character of the second-order phase transition at critical point of the optical bistability (OB). The present example is related to the OB due to increasing absorption, while the previous case – due to saturated absorption.

Recently, it has been found that a set of coupled dynamical equations below may be employed in describing the behaviors of IAOB:^[15]

$$\dot{e} = -\gamma_1 [e - a^{-1}(y-x)] \quad (s1)$$

$$\dot{x} = -\gamma_2 [x - e(2C - ex)], \quad (s2)$$

where e is a kind of matter variables, such as the density of excitons, temperature rise and so forth, excited by the light in the medium, C stands for a control parameter also, γ_1, γ_2 – decay rates and a – constant. Eliminating the matter variable e from eqn. (s2) one obtains the dynamic equation with single variable x (output)

$$\gamma_2^{-1} \dot{x} = -\{x - a^{-1}(y-x) [2C - a^{-1}(y-x)x]\} \quad (s3)$$

Put

$$a^2 \gamma_2^{-1} \dot{x} = -\frac{\partial G}{\partial x} \quad (s4)$$

It would be the simplest approach to introduce the generalized potential G for the given optical dynamical system and then we

have

$$G = \frac{1}{4}x^4 - \frac{2}{3}yx^3 + \frac{1}{2}(y^2 + 2aC + a^2)x^2 - 2aCyx \quad (s5)$$

and $\frac{\partial G}{\partial x} = 0 \quad (s6)$

corresponds to the steady state in which the values (C, x, y) of the critical point (C_c, x_c, y_c) are as follows.

$$C_c = 4a, \quad x_c = 2a\sqrt{2}, \quad y_c = 3a\sqrt{3} \quad (s7)$$

According to the same procedure, developed in the context, it can be proved that this potential G in the vicinity of the critical point may also be written approximately as in the following:

$$G(\eta) = G_o + 2t\eta^2 + \frac{1}{4a^2}\eta^4 \quad (s8)$$

where

$$t = 1 - C/C_c, \quad C_c = 4a \quad (s9)$$

$$\eta = x - x_c, \quad x_c = 2a\sqrt{2} \quad (s10)$$

The expression (s8) shows that the critical point of IAOB, as well as the saturated absorption OB, exhibits the feature of the second-order phase transition.

Reference

[1s] Fa Ou, Tingwan Wu, Yuchang Zhou, Coupled Dynamical Equations of the Increasing Absorption Optical Bistability, to be published.

N-Color Ferroelectric Binary Processor

K. L. Block

S. Systems Corporation
2501 Yale Blvd. SE
Albuquerque, NM 87106

K. S. Redus

LSR Research Corporation
203 Wellesley Dr. SE, Suite A
Albuquerque, NM 87106

Introduction

Spatial light modulators are being utilized in a variety of fields within photonics. Specifically, nonlinear ferroelectric liquid crystal (FLC) modulators have recently received attention in the field of optical computing¹. An increase in binary processor throughput may be achieved by advancing display technology in the areas of pixel size and quantity, framing speed, and pixel addressing schemes.

Here, a binary processor is introduced which exploits the visible transmission band of a modified commercial FLC display, both to increase the quantity of parallel processed information and to add a dimension of versatility to this processing. This technique uses current commercial hardware yet its applicability will scale directly as display technology advances.

Processor Device

Identically sized arrays of "on" and "off" pixels are binary inputs to the processor. A set of n distinct collimated sources and matched precision notch filters (narrowband high reflectors with low reflectance sidebands) are used to direct these intensity encoded information sets. The sets are coaligned through a linear polarizer and are incident upon a modified FLC. The FLC, with polarizers and backplate removed for transmission, is oriented such that full pixel modulation achieves a 90 degree polarization rotation of the linearly polarized light while an unmodulated pixel performs no such rotation. If each binary input set reaches the FLC within the same time period (being small compared with the framing rate), an identical operation is simultaneously performed upon each of the n sets. A polarizing beamsplitter and notch filters direct the resulting output to distinct ports, as a function of wavelength and modulation performed. Figure 1 contains a functional diagram of the processor device.

Some undesired noise will be introduced into output pixels through diffraction, small misalignments, and inefficient FLC polarization rotation. This noise will most noticeably affect the "off" pixels by introducing false output and may be reduced by setting a minimum pixel detection threshold at the output planes.

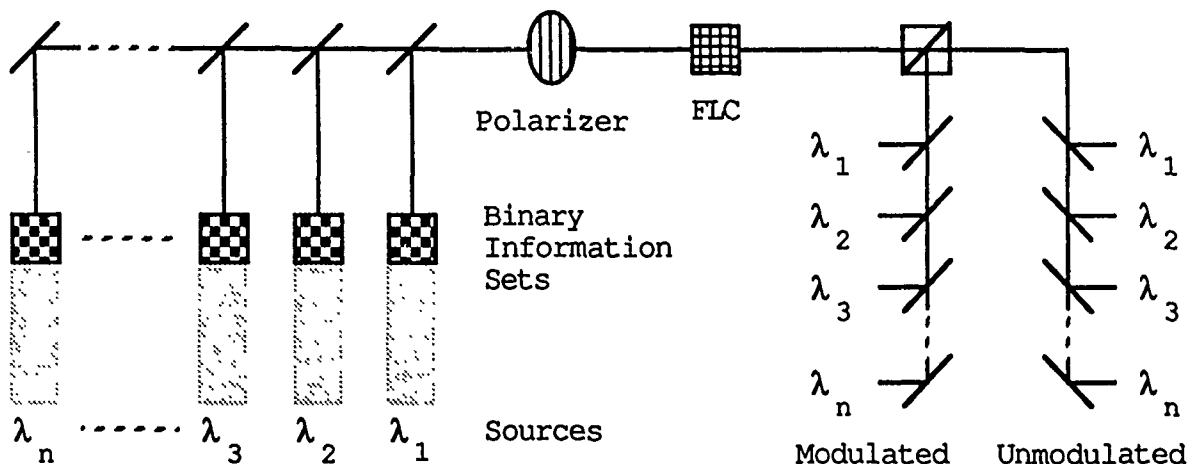


Figure 1. Functional Configuration.

The quantity of information processed per pixel will be limited by the optical bandwidth overall and of the individual notch filters combined. In addition, the overall optical transmittance will affect detection probability at the output planes.

Operation

Due to the binary input and processing nature of this device, the FLC driver is simplistic in its operation. A compact Seiko FLC is operated at a 32 Hz framing rate and has an active area of approximately 16 mm². Each of the (100 x 100) pixels is nearly square with dimensions approximately 160 x 168 μm.

This processor will therefore have as its theoretical limit the capability to perform 10⁴ simultaneous binary operations on n sets per frame, or $2 \cdot n \cdot 10^4$ operations per mm² per second, with twice as many output bits (both modulated and unmodulated). For a proof of concept experiment, maxpixels of much larger dimensions and two wavelength sources ($n=2$) are used for greater simplicity.

Applications

In addition to binary processing for boolean logic and neural networks, the spectral characteristics of this processor introduce potential in such areas as multicolor pattern recognition, n -scene image processing, multiple target tracking, and shared aperture devices. Modification of the technique presented here is underway to begin addressing these additional applications.

Reference

1. K. Johnson and G. Model, "Motivations for using ferroelectric liquid crystal spatial light modulators in neurocomputing," Appl. Opt. 28, 4888 (1989).

Nonperturbative Calculation of Nearly Degenerate Multi-Wave-Mixing Spectra

Robert P. Lucht, Rick Trebino, and Larry A. Rahn

Combustion Research Facility, Sandia National Laboratories, Livermore, CA 94551

Trebino and Rahn¹ observed subharmonic resonances in high-order wave-mixing spectra of the sodium atom in flames. They used two pulse-amplified, single-mode dye lasers to generate two nearly degenerate pump beams at 590 nm. The pump beams were tuned 2 cm^{-1} away from the sodium D_1 line resonance. At low laser intensity resonances at the hyperfine splitting $\omega_{\text{hfs}} = 0.06\text{ cm}^{-1}$ and at zero frequency difference were clearly visible. At higher intensities the hyperfine resonances broadened and a subharmonic resonance at $1/2\ \omega_{\text{hfs}}$ appeared. Trebino and Rahn¹ also used higher order wave mixing geometries to observe subharmonic resonances at $1/3$, $1/4$, and $1/5\ \omega_{\text{hfs}}$. Trebino and Rahn² have used diagrammatic perturbation theory to calculate high-order wave-mixing spectra.

In this study we have solved numerically the time-dependent density matrix equations for a three-level system consisting of two ground levels, split by 0.06 cm^{-1} , and an excited level. The three-level system is pumped by nearly degenerate laser beams at frequencies ω_1 and ω_2 , tuned 2 cm^{-1} from electronic resonance. The laser beams are assumed to be Fourier-transform-limited with Gaussian pulse shapes. The density matrix equations are integrated numerically using a variable-order Adams code to determine the time-dependence of the level populations and the off-diagonal matrix elements during the 15-nsec laser pulses. The off-diagonal matrix elements are Fourier analyzed to give N-wave mixing intensities, where $N = 4, 6, \dots, 14$. Multi-wave-mixing spectra are calculated by solving the density matrix equations as the frequency difference of the two pump beams was varied.

Calculated eight-wave mixing spectra are shown in Fig. 1. At low intensity, only the subharmonic resonance at $1/3\ \omega_{\text{hfs}}$ is noticeable. As the laser intensities are increased, the subharmonic resonance at $1/2\ \omega_{\text{hfs}}$ also appears. The relative intensities of the eight-wave-mixing resonances at $1/3\ \omega_{\text{hfs}}$ and $1/2\ \omega_{\text{hfs}}$ are very sensitive to the ratio of the dipole matrix elements. Spectra similar to the highest intensity spectrum in Fig. 1 were observed experimentally.¹

The computer analysis allows us to examine the time behavior of the level populations and the off-diagonal density matrix elements. For example, as shown in Fig. 2, when the laser detuning is $1/2 \omega_{\text{hfs}}$, the ground level populations oscillate at the laser difference frequency, but are also modulated at twice the laser difference frequency. The frequency modulations of the level populations and the off-diagonal elements are coupled and give rise to dramatic changes in the wave-mixing spectra.

1. R. Trebino and L. A. Rahn, "Subharmonic resonances in higher-order collision-enhanced wave mixing in a sodium-seeded flame," *Opt. Lett.* **12**, 912-914 (1987).
2. R. Trebino and L. A. Rahn, "Calculation of higher-order wave-mixing spectra," *Opt. Lett.*, accepted for publication (1990).

*Work supported by U. S. Department of Energy, Office of Basic Energy Sciences, Division of Chemical Sciences.

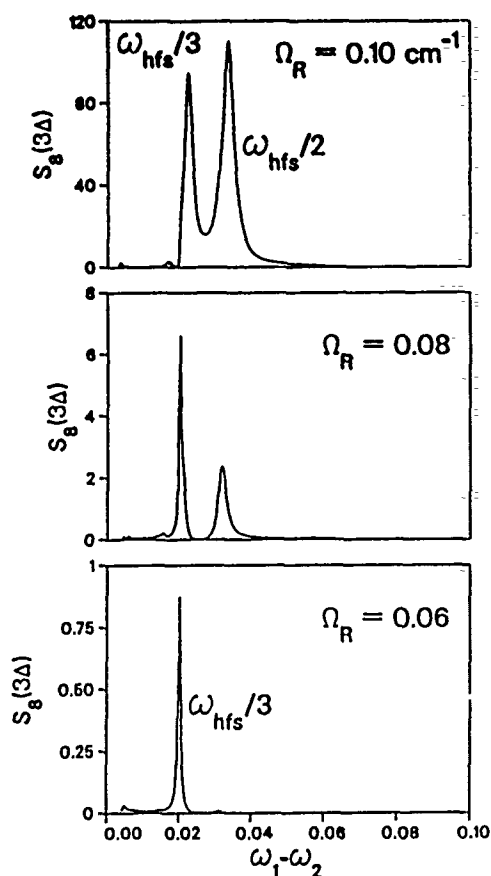


Fig. 1. Eight wave mixing spectra for Rabi frequencies of 0.06, 0.08, and 0.10 cm^{-1} .

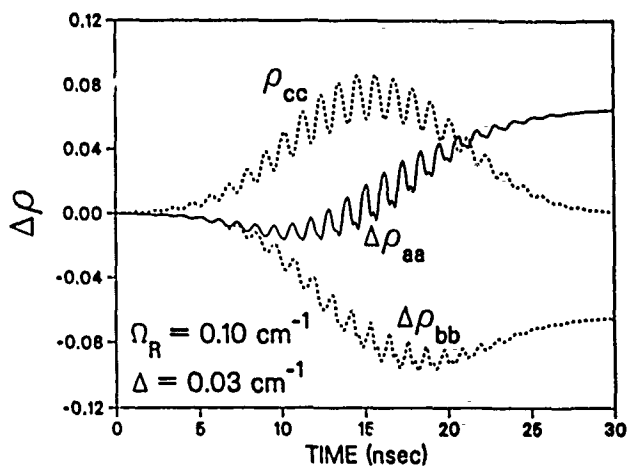


Fig. 2. Time dependence of the ground and excited level populations. The ground level populations are 0.5 initially; the change in ground level populations is shown in the figure. Levels a and b are the ground levels, and c is the excited level. The laser Rabi frequency is 0.10 cm^{-1} and the frequency difference $\omega_1 - \omega_2 = 1/2 \omega_{\text{hfs}}$.

On the Interpretation of n_2 Measurements Using an Externally Focussed Gaussian Beam

R.M. Mishra, P.P. Banerjee and A. Korpel

Extensive experimental and theoretical studies of laser beam self-focussing and defocussing arising due to an intensity dependent refractive index in various materials have been reported [see, for instance, Dabby et al IEEE-QE, 5, 516 (1969); Sheik-Bahae et al Opt. Lett., 14, 955 (1989)]. Relative contributions of the Kerr, electrostrictive and thermal effects to the above have been studied, and various experimental techniques for estimating n_2 of a material have been suggested and used. The majority of the techniques involve a measurement of the change in beam divergence over its diffraction-limited value, due to the nonlinear medium lying in the path of the beam. The medium is taken in the form of a "thin" sample within which the beam width is assumed constant and the sample is modelled as thin lens whose focal length is a function of the material characteristics and the beam parameters. However, it has been reported that for strongly focussed beams the effects of diffraction and nonlinearity in modifying the beam width within the sample cannot be ignored.

In this paper, we reexamine the technique for estimating the sign and magnitude of n_2 of a material based on the measurement of the far-field width of a focussed CW laser beam passing through a finite sample of the material. Beam width change within the sample due to both diffraction and nonlinearity is taken into account by analytically tracking the q-parameter of the beam in a way reminiscent of the split-step angular plane wave spectral technique. Hence the restriction to a thin sample is no longer necessary. The results are compared with previously published work. The experimental results for a chlorophyll solution in ethanol and a resulting estimate of n_2 based on the data and the theory proposed is reported.

Scaling Behavior of Optical Bistability in Nonlinear Medium

Yao-Huang Kao
 Department of Communication Engineering,
 Ching-Sheu Wang
 Institute of Optical-Electronics,
 National Chiao-Tung University,
 Hsin-Chu, Taiwan, R.O.C.

Optical bistability in nonlinear media is potentially useful because of its fast transition speed for all-optical logic operation [1-3]. The dynamics of these mirrorless systems have been described by a anharmonic Duffing oscillator [1-4]. After normalization the equation of motion is described by

$$\ddot{x} + k\dot{x} + x - f(x) = F \sin \omega t, \quad (1)$$

where k is the damping factor, F is the driving amplitude, ω is the driving frequency and $f(x)$ is a nonlinear function of x . Such a model predicts the existence of bistability under appropriate conditions [3]. It would be particularly important for this system to be tuned to some situation in order to efficiently generate these nonlinear phenomena. In this summary we would provide a globe picture of possible dynamic behaviours in Eq.(1), which can be used as a guide line in real experiment.

In the following the dynamics with $f(x) = gx^2$ and gx^3 are investigated, where g is the coefficient. The instability boundaries are searched by numerical calculation with Runge-Kutta fourth-order algorithm. Fig.1-a shows the possible instability boundaries in controlled parameter-space (F, ω) with $f(x) = 0.1x^2$ and $k = 0.1$, which is referred as state diagram. The transition boundaries in the state diagram appear as a swallow tail in each resonant region. The bistability (or hysteresis) can occur at each resonant region with driving frequency below the cusp frequency. It is noted that the cusp point with (F_t, ω_t) can act as a guiding post, from which the control parameters can be easily evaluated. Here, we focus on the fundamental resonant region. We found that for a fixed damping coefficient k the frequency ω_t is fixed and the magnitude of driving amplitude F_t is inverse proportional to g (i.e. $F_t g = \text{constant}$). For convenience, the dependence of frequency ω_t and driving amplitude F_t on damping factor k is shown in Fig.2.

Here an interesting phenomenon worth being mentioned is that a subharmonic suddenly emerges during the hysteresis jump at subharmonic resonant region with ω near 2. This behavior is referred as subcritical bifurcation [5]. After hysteresis two distinctive features are observed. One is that a large difference between the output levels of corresponding hysteresis loop is obtained. And the other is the subharmonic is dominant with strength larger than that of fundamental mode. It deserves us to pay more attention in the application to subharmonic generator.

As for the case with $f(x) = x^3$ the state diagram, shown in Fig.1-b, is similar to the above mentioned one but without subcritical bifurcation. This is because the system has symmetric property, which as usual is defined with solution satisfying the transformation $x(t+\pi/\omega) = -x(t)$. Besides that the driving amplitude F_t and coefficient g follow the scaling relation $F_t^2 g = \text{constant}$.

In conclusion, we present an extensive study of Duffing oscillator and predict the cusp frequency of the optical bistability in each resonant region. And a novel feature with generation of both hysteresis and subharmonic generation (subcritical bifurcation) is also indicated. This deserves us to pay more attention in the future.

REFERENCE:

1. C. Flytzanis and C. L. Tang, Phys. Rev. Lett., 45, 441(1980).

2. J. A. Goldstone and E. Garmire, Phys. Rev. Lett., 53, 91—(1984).
3. B. Ritchie and C. M. Bowden, Phys. Rev. A, 32, 2293(1985).
4. A. Yariv, Introduction to Optical Electronics, (3rd Ed. Holt, Rinehart and Winston, New York, 1985) Chap. 8.
5. J. C. Huang, Y. H. Kao, C. S. Wang, Y. S. Gou, Phys. Lett. A, 136, 131(1989).

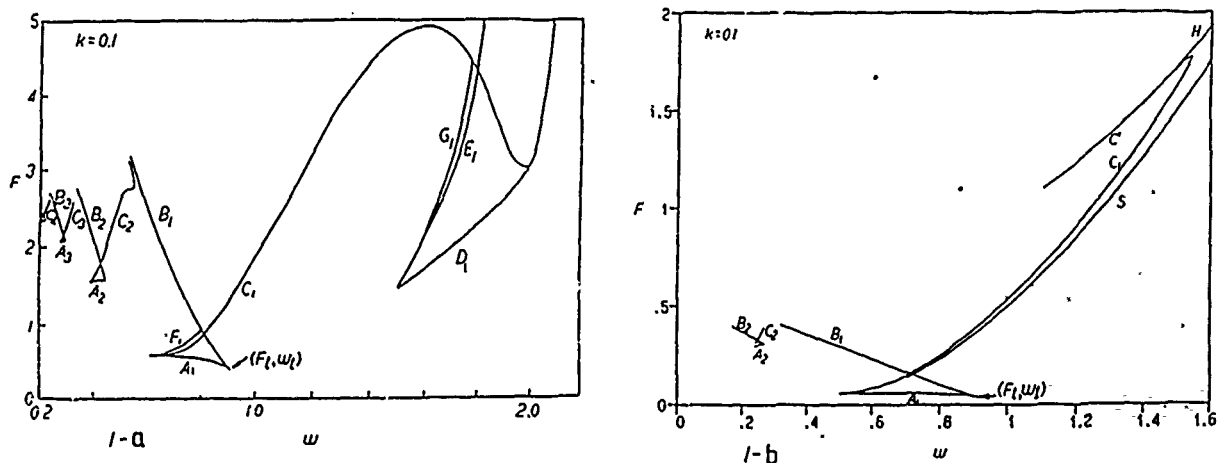


Fig. 1-a) The state diagram with $f(x)=0.1x^2$. Curves A_i , B_i , and D_i are the boundaries of hysteresis jump, curves C_i and E_i are the boundaries of the period doubling bifurcation, and curves F_i and G_i are the boundaries of destructive crisis, where $i=1, 2, 3, 4$. 1-b) The state diagram with $f(x)=x^3$. Curves A_1 , B_1 , A_2 and B_2 are boundaries of hysteresis jump. Curves C_1 , C_2 and C_3 are boundaries of period doubling. Curve S is the boundary of symmetry breaking. And Curve H is the boundary of escaping.

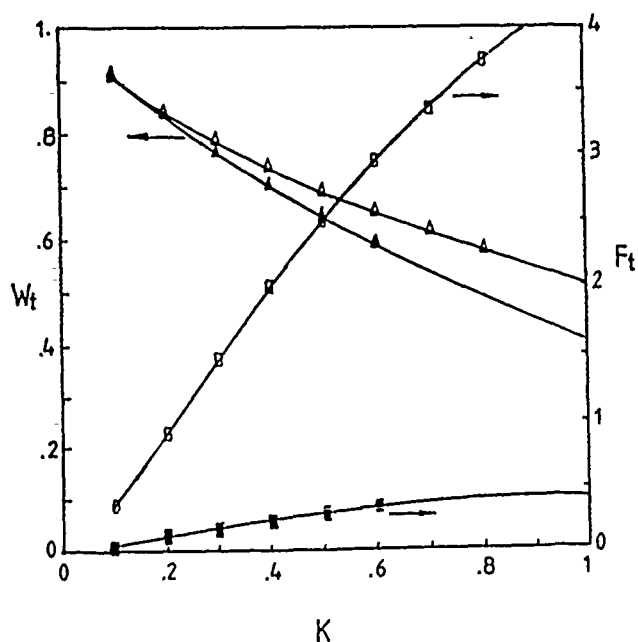


Fig. 2 The dependence of cusp frequency ω_t and driving amplitude F_t on damping factor K . Curves with blank mark Δ are for $F(x)=0.1x^2$ and Curves with solid mark Δ are for $f(x)=x^3$.

WP8 Exploration of Optical Propagation in a Nonlinear Dispersive Medium Based on An Incommensurate Spectral Formalism

P.P. Banerjee, Syracuse University, Syracuse, NY, and M.R. Chatterjee, SUNY at Binghamton, Binghamton, NY

A recent study involving the propagation of optical signals across a linear/nonlinear interface introduced a formalism based on *incommensurate* discrete sidebands around a carrier [Banerjee *et al*, JOSA B 7, 21 (1990)] in order to simplify the analysis of the coupled sideband amplitudes. This approach was shown to be fairly effective not only in the derivation of steady-state transmitted and/or reflected sideband amplitudes for the case of N incommensurate sidebands around an undepleted carrier, but also in the non-steady-state analysis based on a perturbation hierarchy. The first-order perturbation analysis indicated a spatial beating between the upper and lower sidebands with a spatial beat period inversely proportional to the frequency deviation of the pair. In the limit of a pulse where the number of incommensurate pairs is made to approach infinity, and the frequency deviation made to approach zero, the transmitted optical signal in response to an AM pulse was found to contain not only an AM burst, but a narrowband FM "packet" as well (assuming an undepleted carrier and weak nonlinearity). These transmitted "packets" were shown to propagate with distinct phase velocities, resulting in an infinite spatial separation in the asymptotic limit.

The above nonlinear problem is conventionally found to be considerably more complicated when the nonlinear medium is also made dispersive. Most approaches are bogged down in formidable coupled equations involving amplitudes and phase angles. The work reported in this paper is aimed at applying the *incommensurate* formalism mentioned above to the case of a nonlinear, dispersive medium in the hope of finding a more tractable analytical solution method. In particular, the medium is first characterized in terms of its linear cut-off frequency. The resulting linear dispersion relation is thereafter modified to incorporate the effect of a weak nonlinearity. By invoking the formalism of incommensurate sidebands, an analysis is then carried out for the transmitted sideband amplitudes using appropriate and reasonable approximations along the way. Among other results, the effect of the strength and sign of the (cubic) nonlinearity in modifying the linear cut-off is investigated in sufficient detail. It is shown that, for certain signs and strengths of the nonlinearity, nonpropagating sidebands corresponding to the linear case may be partially transmitted (i.e. the effective cut-off may be lowered), while for certain other signs and strengths, sidebands propagating in the linear case may be partially attenuated (i.e. the effective cut-off may be raised).

Liouville Operator Theory of Nonlinear Optical Susceptibilities

P. L. Kelley

Lincoln Laboratory

Massachusetts Institute of Technology

Lexington, Massachusetts 02173

Tel: 617-276-6731

J. P. Taran

Office National d'Études et de Recherches Aéronautiques

92320 Châtillon, France

Tel: 011-33-14-657-1160 (ext. 2454)

Olga Blum, Inho Kim, and T.K. Gustafson

*Department of Electrical Engineering and Computer Sciences
and*

The Electronics Research Laboratory

183M Cory Hall

University of California, Berkeley, CA 94720

Tel: 415-642-3139

Summary

Expressions for the n -th order nonlinear susceptibility, $\chi^{(n)}$, are given using Liouville operators. When damping is included, the n -th order susceptibility operator is expressed as a product of propagators, the output polarization dipole operator, and n input dipole Liouville operators operating on the unperturbed density operator with a sum performed over the input frequency permutations. When damping can be neglected, the susceptibility can be reexpressed as a product of propagators, the $n+1$ dipole operators, and the unperturbed density operator with the sum performed over the permutations of the input frequencies and the output frequency.

These expressions for the susceptibility can immediately be related to a diagrammatic analysis¹ for a particular nonlinear optical process and the form of the expressions used to deduce the number of diagrams.

When damping is important, double-sided diagrams are necessary. The number of possible diagrams consists of three factors, a frequency permutation factorial factor² relating to the number of possible distinct input frequencies that can be assigned to each of the input interaction vertices, a commutation factor² (2^n) relating to the possible interaction vertex assignments on the two sides of the diagram, and a state counting factor relating to the number of diagrams generated from an enumeration of specific material state assignments between interaction vertices.

When damping is neglected, single-sided diagrams can be used. In this case, the commutator factor does not appear; however, the outgoing frequency must be included in the factorial factor for the frequency permutations. The difference terms between the complete set of double-sided terms including collisions and the single-sided terms which reduce, in the absence of collisions, to the single-sided collisionless terms have been shown to give rise to the collisionally induced *extra resonances*.³

We will discuss the application of these results to several situations of interest including second harmonic generation, degenerate four-wave mixing, and resonant CARS (coherent anti-Stokes Raman scattering) in a four-level system.

The Lincoln Laboratory portion of this work was sponsored by the Department of the Air Force. The work was also supported in part by the Direction des Recherches, Études et Techniques and the Air Force Office of Scientific Research.

References

1. T. K. Yee and T. K. Gustafson, Phys. Rev. **A18**, 1597 (1978).
2. R. Trebino, Phys. Rev. **A38**, 2921 (1988).
3. Y. Prior, IEEE J. Quant. Electron. **QE-20**, 37 (1984).

WP10 Size Dependence of $\chi^{(3)}$ for Frenkel Excitons in a Periodic Chain

H. Ishihara and K. Cho

Faculty of Engineering Science, Osaka University, 560 Toyonaka, Japan

Summary

In order to study the size dependence of $\chi^{(3)}$ for a confined electronic system, we have investigated a system of non-interacting Frenkel excitons in a periodic (N -atom) linear chain, which allows us an exact treatment of $\chi^{(3)}$ in nonlocal form for arbitrary frequencies of external fields. The nonlinearity of this system arises from the Pauli exclusion principle which forbids two excitons to sit on a same site. The analytic expression of $\chi^{(3)}$, obtained for arbitrary N after the summation over the internal quantum number for two-exciton states, shows the absence of N as a multiplication factor. This is due to the cancellation of the terms which, in the long wavelength approximation, give rise to factors proportional to N . The N -dependence, described differently for even and odd N , is contained in factors which tend to be unity for large N . A numerical study for a particular case of pump-probe type nonlinear effect in a long wavelength approximation shows the following result:

- [1] $\text{Im}[\chi^{(3)}]$ contains a size enhancement for a limited region of N ,
- [2] the range of such N is determined by the magnitudes of exciton transfer energy and the relaxation times.

In comparison with the local 2-level system, the exciton transfer effect brings about a remarkable change in $\chi^{(3)}$, both in its spectral shape and magnitude.

WP32 Resonant Degenerate Four-Wave Mixing for Imaging and Temperature Measurements of Molecules in Combustion

R. L. Farrow and D. J. Rakestraw

Combustion Research Facility, Sandia National Laboratories, Livermore, CA 94550 USA

T. Dreier

Physikalisch Chemisches Institut, Im Neuenheimer Feld 253, 6900 Heidelberg, FRG

The potential of resonant degenerate four-wave mixing (DFWM) as a diagnostic technique in combustion has been demonstrated for atomic species.^{1,2} However, molecular DFWM has not been widely studied in this context. Molecules offer the additional capability for thermometry, but also pose new experimental and theoretical challenges: the existence of many populated levels reduces signal intensities, and theory must properly relate ro-vibrational line intensities to level populations. Ewart and O'Leary³ recently demonstrated the detection of OH in a laboratory flame with DFWM. We have obtained extensive spectra of OH and NH in flames and analyzed these to obtain rotational temperatures.⁴

In this paper, we describe two-dimensional imaging of OH using DFWM. Images of high signal intensity were obtained from a variety of flames, using in most cases a single laser pulse. For such measurements, the advantages of a technique with a coherent signal beam include ease of optical access to the sample and efficient discrimination against background light.

In the phase-conjugate geometry used here, two counter-propagating pump beams are collimated into thin sheets and intersected with an expanded probe beam at an angle of 20° . The resulting signal beam is the phase-conjugate of the probe beam, but the intensity profile of the former reflects the spatial distribution of resonant species. Figure 1 shows an



Fig. 1. Image of OH intensities produced by degenerate four-wave mixing in an axisymmetric methane/air diffusion flame. The frequency-doubled laser was tuned to 311.88 nm, corresponding to the $P_2(8)$ transition. The image results from OH distributions intersecting a flat laser sheet 300 μm in thickness.

*Work supported by the U.S. Department of Energy, Office of Basic Energy Sciences, Chemical Sciences Division, and the Energy Conversion and Utilization Technologies Program, and by the Deutsche Forschungsgemeinschaft, grant Az. Dr195/1-1.

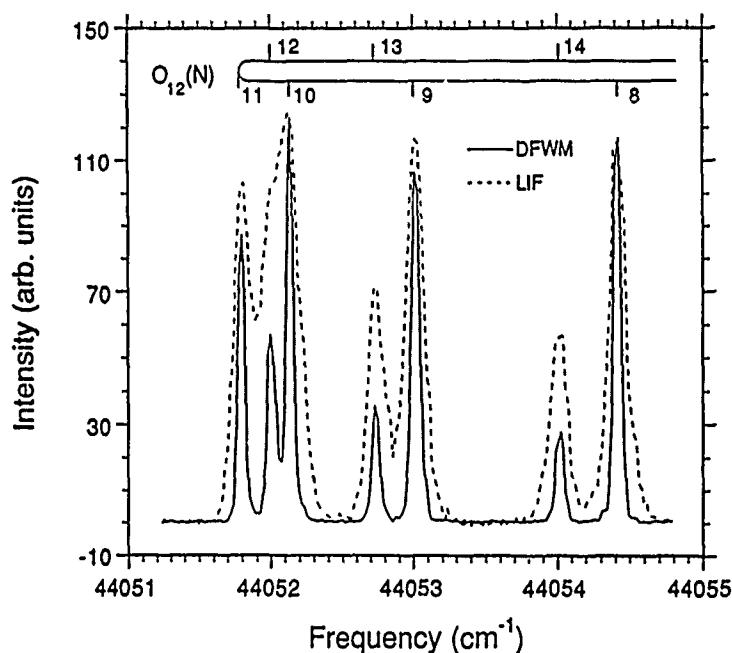


Fig. 2. Comparison of experimental DFWM (solid line) and LIF-excitation (broken line) spectra of the O_{12} branch of NO, obtained using 10 laser pulses per frequency step. The DFWM line intensity ratios are seen to vary approximately as the square of the corresponding LIF ratios, which are proportional to absorption. Note that the Doppler-free DFWM linewidths are limited by the laser bandwidth (0.05 cm^{-1} , FWHM).

example of a single-pulse image of OH intensities from a small methane/air diffusion flame. This intense image consisted of $\sim 5 \times 10^6$ signal photons incident on the CCD detector, and the image was mapped using $\sim 2 \times 10^4$ independent pixels.

We also present the first DFWM spectroscopy of NO, to our knowledge. NO is ideal for investigating collisional effects on molecular DFWM since NO has well known electronic quenching and rotational relaxation rates⁵ and can be studied in a gas cell under well defined environmental conditions.

We are currently investigating the use of DFWM for measuring concentrations and rotational temperatures of NO. Using a tripled dye laser tuned through one-photon transitions in the $A^2\Sigma^+ \leftarrow X^2\Pi$ system, we obtain high-quality, Doppler-free spectra from as little as 20 mTorr of pure NO at room temperature (see Fig. 2). Assuming $I_{\text{sig}} \propto (n_J S_J)^2$, where I_{sig} is the integrated line intensity, n_J the ground-state rotational level population and S_J the line strength, rotational populations analyzed from the O_{12} -branch are found to quantitatively agree with the gas temperature. With incremental additions of N₂ buffer gas from 2 to 155 Torr, we observed that line intensities exhibited a pressure dependence described by $I_{\text{sig}} \propto p_{\text{buff}}^{-0.67}$. This dependence is significantly weaker than expected from a simple two-level model that neglects laser bandwidth and molecular motion.

References

1. J. Pender and L. Hesselink, *Opt. Lett.* **10**, 264 (1985).
2. P. Ewart, P. Snowdon, and I. Magnusson, *Opt. Lett.* **14**, 563 (1989).
3. P. Ewart and S. V. O'Leary, *Opt. Lett.* **11**, 279 (1986).
4. T. Dreier and D. J. Rakestraw, *Opt. Lett.* **15**, 72 (1990).
5. See, for example, H. P. Broida and T. Carrington, *J. Chem. Phys.* **38**, 136 (1962).

Nonlinear Optical Waveguide Using Polymer Film Doped with 2-Methyl-4-Nitroaniline

Hiroshi Haga and Sadahiko Yamamoto

Department of Electrical Engineering,
Faculty of Engineering Science, Osaka University

1-1, Machikaneyama, Toyonaka, Osaka 560, Japan

Summary

Nonlinear optical devices based on integrated optics or guided-wave technology are very attractive because of their advantages such as phase matching by means of mode dispersion and large light intensity due to small cross-section of waveguides. Although certain organic materials have large nonlinear optical susceptibilities, organic crystals are too fragile to make a waveguide. On the other hand, poled polymer films, which can be coated and patterned photolithographically, are useful material to make guided-wave devices.

We used nonlinear optical organic molecules 2-methyl-4-nitroaniline(MNA) doped at 25% in poly-methyl-methacrylate(PMMA) with solvent methyl-iso-butyl-ketone(MIBK). Fabrication process is shown in Fig.1. The solution was spin-coated on Tempax glass plate with chrome planar electrodes for electric-field poling. Electrode gap is 1mm. After being removed the solvent, the film was heated to 80 degrees centigrade and applied an electric field for 20 minutes. Then, the film was cooled to ambient temperature before the electric field was removed. Several samples were poled by electric fields of different value ranging from 10 to 24kV/mm. The value was limited by the dielectric breakdown strength of polymer film.

When the refractive index of the film is larger than that of substrate glass, these samples can be used as slab optical waveguides. Prisms(SFS-1 glass) were used to confirm the function as waveguides and to measure the refractive indices of the films. Measured refractive indices were 1.52, 1.51, and 1.50 for wavelengths of 0.53, 0.63, and 1.06 μ m, respectively. Those values obtained from TE modes were equal to those from TM modes. Furthermore, there is no detectable dependence on the value of poling electric field in the range of our experiments.

We confirmed the polar orientation of the film by investigating the dependence of second harmonic power on the polarization of incident fundamental light from a pulsed Nd:YAG laser of 1.06 μ m wavelength. In Fig.2, two curves represent second harmonic outputs whose polarization are parallel and perpendicular to the poling electric field direction. Generation of each power are attributed to nonlinear coefficients d_{zz} and d_{yy} for the coordinate system shown in Fig.2.

Nonlinear coefficients were measured by comparing second harmonic outputs between samples and y-cut lithium niobate plate of 360 μ m thickness. Coherent length of reference crystal ob-

tained by Maker fringe was $3.6\mu\text{m}$. On the other hand, that of films was calculated to be $13\mu\text{m}$ from measured refractive indices data since the thickness ($4.3\mu\text{m}$) of films were too small to get Maker fringe. Figure 3 shows the poling-field dependence of the nonlinear coefficient d_{zz} . Maximum coefficient of the film was 18% of the largest coefficient d_{33} of lithium niobate crystal.

The second order nonlinear susceptibility from this experiment agrees with the value obtained from electro-optic coefficient reported previously[1]. This means that the nonlinear process of this film is due to electronic polarization in the material.

Reference

[1] H.Haga and S.Yamamoto, "Waveguide Electro-Optic Modulator using Poled Polymer film," IOOC'89, 20A2-3, Kobe, July 18-21, 1989.

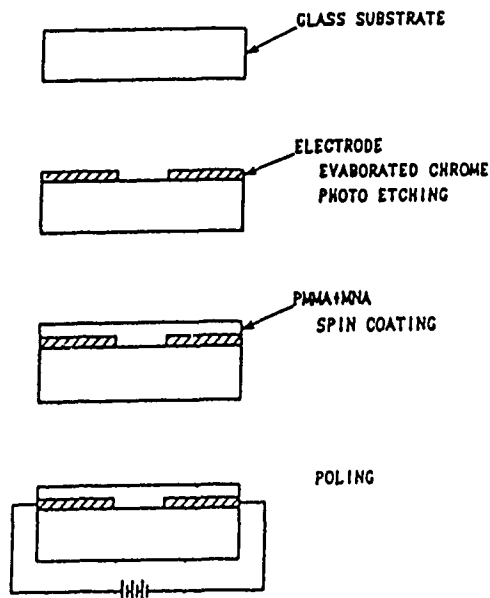


Fig.1 Fabrication process

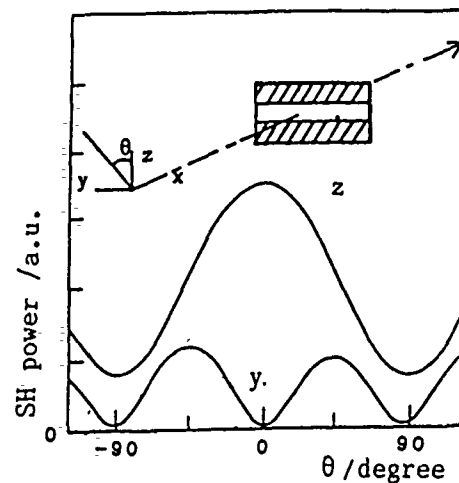
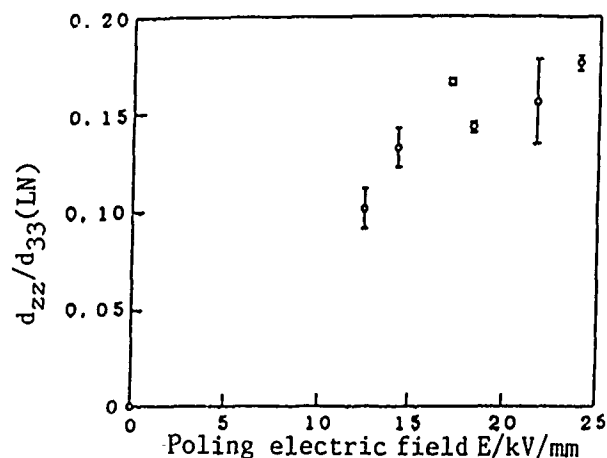


Fig.2 Polarization dependence of SH output

Fig.3 Poling electric field dependance of SHG coefficient



WP12 **Second-Harmonic Generation with Laser Diodes and Organic Channel Waveguides**

Takashi KONDO, Naoki HASHIZUME, Seiro MIYOSHI, Ryuji MORITA,
Nagaatsu OGASAWARA, Shinsuke UMEGAKI[†] and Ryoichi ITO

*Department of Applied Physics, Faculty of Engineering, University of Tokyo,
7-3-1, Hongo, Bunkyo-ku, Tokyo 113, Japan*

[†] *Department of Electronics, Faculty of Engineering, Tokyo Engineering University,
1404-1, Katakura-cho, Hachioji, Tokyo 192, Japan*

Frequency doubling of laser diode light in organic channel waveguides will be reported. (-)-2-(α -Methylbenzylamino)-5-nitropyridine (MBANP)¹⁻³⁾ crystal was used as a nonlinear medium. Blue light was obtained by second-harmonic generation (SHG) in the form of Čerenkov radiation⁴⁾ using a laser diode source.

MBANP is one of the most efficient nonlinear optical organic crystals. The nonlinear optical coefficient $d_{22} = 60$ pm/V is the largest component of the d tensor of this material.¹⁾

In order to realize efficient SHG devices, we have fabricated MBANP channel waveguides using glass substrates. Channels were defined on the glass substrates by photolithography and chemical etching. MBANP crystal was grown between the etched substrate and the flat glass substrate by slow evaporation of an acetone solution of MBANP. The structure of the waveguide is shown in Fig. 1. The orientation of the grown crystal (b axis is parallel to a side of the substrate) is the most suitable for SHG, because the d_{22} can be fully utilized. The typical dimension of the channel waveguide is 5 mm long (along c), 5 μ m wide (along b), and 1 μ m thick (along a). In order to satisfy the Čerenkov condition, we used appropriate high-index substrates.

The light source used was an AlGaAs/GaAs CSP laser oscillating at $\lambda = 870$ nm with the output power of 20 mW. The fundamental light was guided as a TE wave and 6 nW of blue light, which was slightly in the absorption band of the material, was generated in the form of Čerenkov radiation. Although the second-harmonic power was not so high,

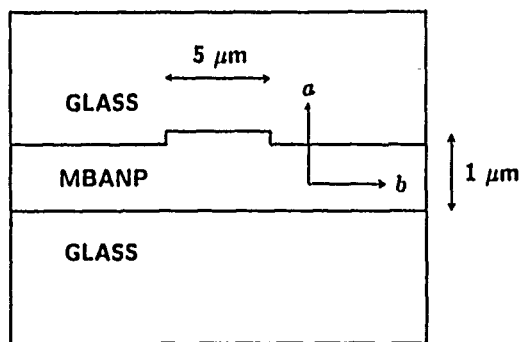


Fig. 1. Schematic cross section of the organic channel waveguide.
Crystal orientation is also shown.

second-harmonic light was radiated in the crescent shape as shown in Fig. 2, indicating that the fundamental light was two-dimensionally confined.

The low conversion efficiency is attributed mainly to the extremely low coupling efficiency of fundamental light into the channel waveguide and to the large propagating loss. It seems that some absorption also has a great influence on the conversion efficiency.

Experiments are now in progress to optimize processing methods and waveguide parameters to improve the performance of the device.



Fig. 2 Far-field pattern of the generated blue light.

References

- 1) T. Kondo, R. Morita, N. Ogasawara, S. Umegaki and R. Ito : Jpn. J. Appl. Phys. **28** (1989) 1622.
- 2) R. Twieg, A. Azema, K. Jain and Y. Y. Cheng : Chem. Phys. Lett. **92** (1982) 208.
- 3) R. T. Bailey, F. R. Cruickshank, S. M. G. Guthrie, B. J. McArdle, H. Morrison, D. Pugh, E. A. Shepherd, J. N. Sherwood, C. S. Yoon, R. Kashyap, B. K. Nayar and K. I. White : Opt. Commun. **65** (1988) 229.
- 4) P. K. Tien, R. Ulrich and R. J. Martin : Appl. Phys. Lett. **17** (1970) 447.

WP13 Selective Poling of Polymers by Laser-Heating

J. F. Valley and A. J. Ticknor

O/9720 B/202

Lockheed Palo Alto Research Laboratories

3251 Hanover St.

Palo Alto, CA USA 94304

Several techniques have been demonstrated to fabricate electrooptic (EO) waveguide devices in poled polymer thin films¹. Most of these procedures produce lateral variations in the film composition to provide the index structure necessary for lateral waveguiding. One technique, selective poling, utilizes localized poling electric fields to induce lateral variations of the birefringence in the film to form waveguide channels². Though all the methods require poling the active polymer to induce an electrooptic response, the selective poling procedure is distinguished by the fact that lateral waveguides are formed as a consequence of the poling and no modification of the composition of the film is required. Poling generally entails heating the entire polymer slab to temperatures near or above its glass transition temperature, T_g , and applying an electric field between electrodes disposed to either side of the film while the film poles and cools. Typically all structures of the electrode are connected to a common point and thus all poled regions are poled identically and simultaneously. We propose and demonstrate a new technique for forming channel waveguides in a single-composition film. This technique produces a structured poling pattern by heating the polymer only in selected regions using a laser beam. By selectively heating the polymer, the poling process can be both spatially resolved and temporally resolved. The temporal aspect of the laser poling allows different regions between the same poling electrodes to be poled under the influence of different electric fields. Novel device structures that require variable degrees and orientations of poling are thus possible without requiring complicated poling electrode geometries. Also, selective heating of the polymer film in the presence of a uniform field produces a uniform orientation of the birefringence over the poled region, whereas the electric fields produced by patterned electrodes induce rotations of the birefringence at the electrode edges. Other exciting possible uses of laser-heating include clean-up poling of selectively poled slabs that have flaws (component trimming) and depoling of regions near patterned reflective poling electrodes.

The experiment consists of a diode laser heterodyne Mach-Zender interferometer to monitor the EO response of the polymer sample in-situ (i.e., as a mirror or window in one arm of the interferometer) and a 514 nm argon laser beam for heating (see Fig. 1). The sample temperature is biased above room temperature using a slightly modified Mettler FP82 hot stage. To laser pole the sample a DC field, typically of the order of 50 volts per micron, is applied while the argon laser beam locally heats the active polymer. We control the intensity of the heating beam by using the first diffracted order of a digital acousto-optic modulator at duty cycles of 50% or less. Although we have damaged samples permanently by over exposure to the heating beam, the parameter range for nondestructive heating is quite broad.

Figure 2 is the power spectra for both a poled region (sidebands present) and an adjacent laser depoled region (no sidebands) from the heterodyne Mach-Zender interferometer detector. In order to facilitate this measurement a large-waisted ($w = 2$ mm) heating beam is used so that the overlap with the EO monitor beam is not a problem. The laser depoled region for this sample remained visibly darker than the surrounding poled regions, probably due to thin film interference effects amplifying the small index change due to poling. No visible spreading of the depoled region occurred over several days after which we reheated the sample to depole the entire slab. The region which had been laser depoled was no longer visibly distinguishable from the rest of the sample and was subsequently poled to confirm that no material damage occurred.

¹ D. Haas et. al. SPIE Proc. 1147, 222 (1989)

² J. I. Thackara et. al. ,Appl. Phys. Lett., 52, 1031 (1988)

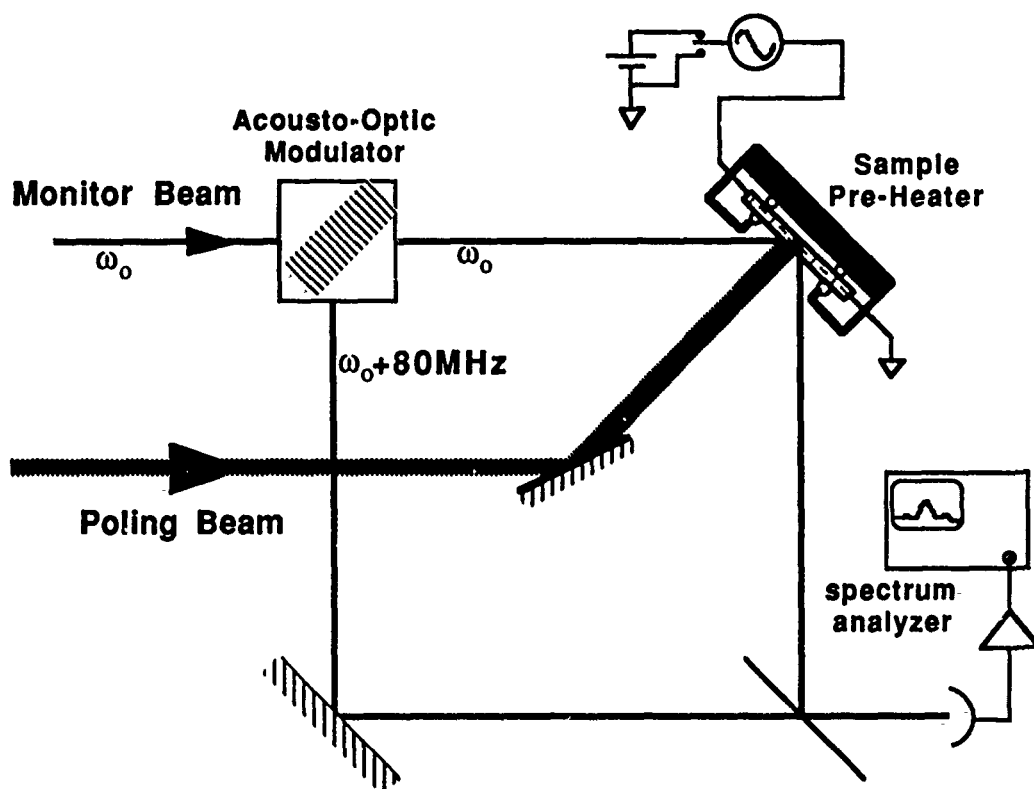


Fig. 1. Schematic diagram of the experimental arrangement.
The Bragg angle is greatly exaggerated.

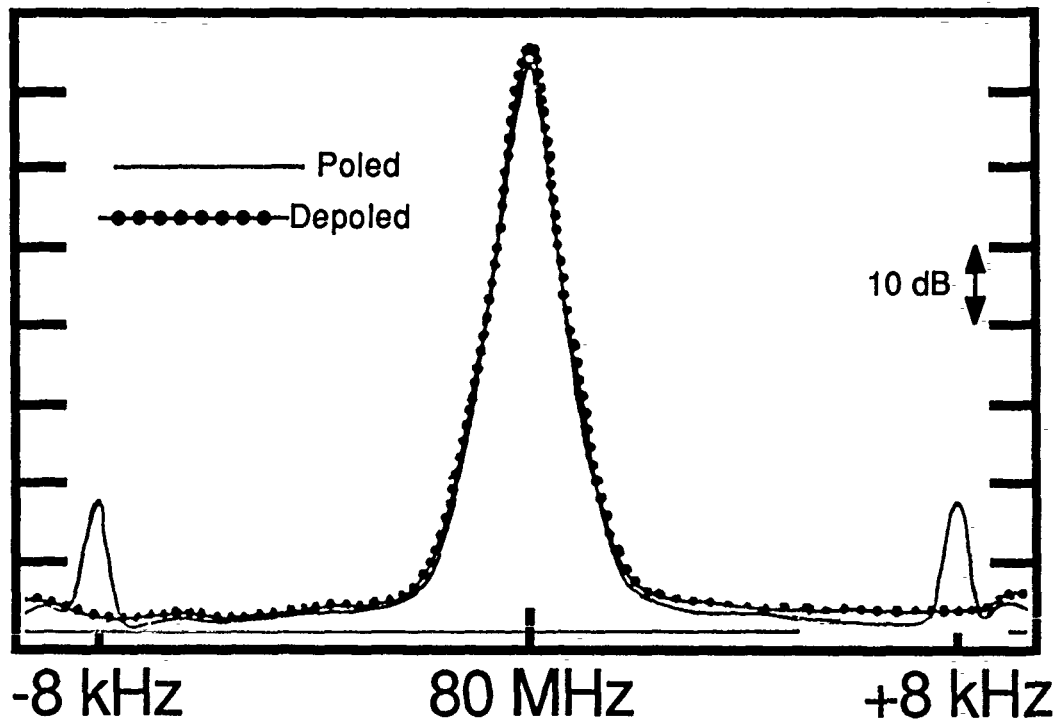


Fig. 2. Log power spectra of electrooptic response in poled and laser-depoled regions taken at room temperature with zero volts DC applied.

Poling Studies on Composition Modulated Nonlinear Polymeric Thin Films

T. Morita*, B. G. Higgins, A. Knoesen† and S. T. Kowel

Organized Research Program on Polymeric Ultrathin Films

University of California, Davis

Summary

Electric field poling has been used previously to obtain large macroscopic second-order nonlinear optical (NLO) properties of polymer films¹⁻⁴. The chromophores can be dopants in the polymer matrix or covalently attached to the polymer chain. Ordinarily the polymer film is prepared by spin coating a polymer solution. Films prepared in this manner are generally homogeneous in composition. Of interest in this study is to determine whether the film microstructure prior to poling, i.e. the spatial distribution of the constituents, effects the alignment induced by poling, and subsequent relaxation of the chromophore orientation through changes in polymer free volume.

The microstructure of the film can be controlled by depositing alternating layers of material of known thickness and composition. Artificial multilayers of this type are often referred to as composition modulated materials. In this paper, the NLO-polymer layer was alternated with an optically inert fatty acid or glassy polymer. The thickness and composition of the spacer layer were then varied systematically to study the effect of film microstructure on the magnitude and stability of the second order NLO properties.

A coumarin dye substituted polymer, poly(methylmethacrylate-coumaromethacrylate) (PMMA-CMMA) was used as a nonlinear material (Fig. 1). The optically inactive spacer material, was either behenic acid or PMMA. Composition modulated films were prepared by a variant on the Langmuir-Blodgett technique. Second order nonlinear properties were induced in the films by corona-onset poling⁵⁻⁶ at an elevated temperature. Optical properties were measured with UV-VIS spectroscopy and second harmonic generation (SHG).

PMMA-CMMA formed a stable monolayer at the air-water interface with no preferred orientation of the

chromophore and was deposited on BK7 glass substrate at a surface pressure of 10 mN/m with a transfer ratio of approximately unity. In the first attempt to fabricate a composition modulated film, the NLO monolayers were interleaved with behenic acid. The maximum number of NLO monolayers deposited was 20. The use of PMMA as an interleaving layer is currently under investigation. The absorption peak of PMMA-CMMA at 400 nm increased linearly with increasing number of PMMA-CMMA monolayers. After poling, the absorption peak decreased, suggesting an improvement in the average dipole orientation. Preliminary results show that poled composition modulated films and poled spun-on PMMA-CMMA of comparable thicknesses exhibit comparable order parameters.

The SHG intensities of the unpoled composition modulated films are comparable to the surface-SHG from the glass substrate, see Fig. 2. After poling the SHG intensities increased sharply. The result was consistent with the absorption order parameter measurements, i.e. an improvement in the orientation of the nonlinear chromophore. The SHG intensity fringes observed in all measurements resulted from interference of SHG from the deposited film and that from the glass substrate, and was verified experimentally. Quadratic enhancement of SHG intensities with thickness was observed for both composition modulated films and spin coated films, see Fig. 3. Because of scattering losses (attributed to polycrystallization of behenic acid during poling) the SHG intensity from a composition modulated film was less than that from a spin coated film of equivalent optical density. The use of PMMA as an interleaving layer is expected to reduce scattering losses. Stability of the NLO properties of composition modulated films will be discussed.

Acknowledgments: The authors thank Dr. G. A. Lindsay, Naval Weapons Center, China Lake, for providing the nonlinear polymeric material, and Dr. M. A. Mortazavi for experimental assistance.

References:

- [1] K. D. Singer, J. E. Sohn and S. J. Lalama, *Appl. Phys. Lett.* 49, 248-250 (1986).

* On leave from Sony Corporation. † To whom correspondence should be addressed: University of California Davis, Department of Electrical Engineering and Computer Science, Davis CA 95616.

- [2] D. J. Williams, *Nonlinear Optical Properties of Organic Molecules and Crystals*, vol. 1, D. S. Chemla and J. Zyss, eds. (Academic Press, 1987), p. 405.
- [3] M. Eich, H. Looser, D. Y. Yoon, R. Twieg, G. Bjorklund, and J. C. Baumert, *J. Opt. Soc. Am. B.*, 6, pp. 1590 - 1597, (1989).
- [4] H. L. Hampsch, J. Yang, G. K. Wong, and J. M. Torkelson, *Macromol.*, 21, 526-528, (1988).
- [5] A. Knoesen, M. A. Mortazavi, S. T. Kowel and A. Dienes, *Nonlinear Optical Properties of Materials*, (Optical Society of America, Washington, D.C., 1988), p. 244.
- [6] M. A. Mortazavi, A. Knoesen, S. T. Kowel, B. G. Higgins, A. Dienes, *J. Opt. Soc. Am. B.*, 6, 733-741, (1989).

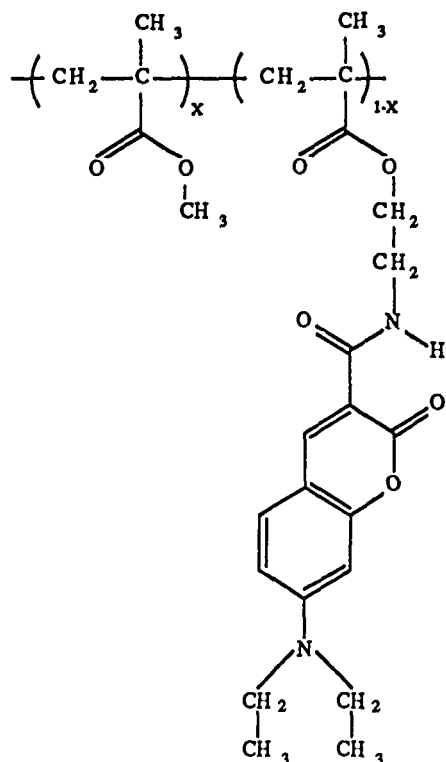
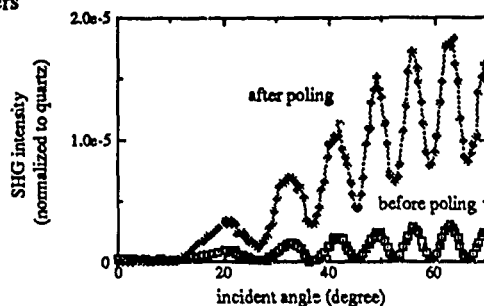
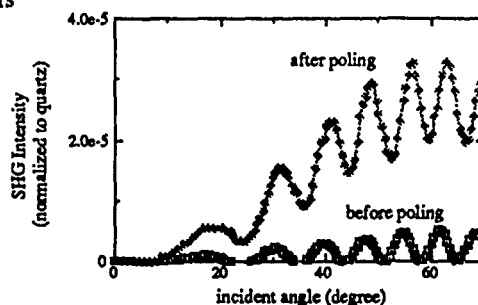


FIG. 1 The molecular structure of nonlinear material, poly(methylmethacrylate-coumaromethacrylate).

5 dye layers



9 dye layers



20 dye layers

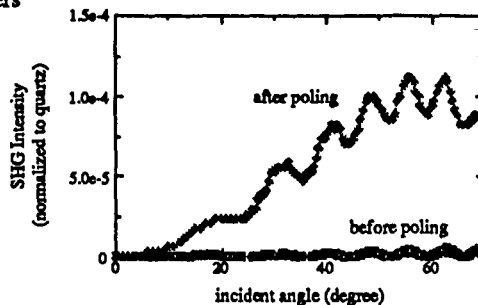


FIG. 2 SHG intensity before and after poling versus incident angle. The fringe pattern is a result of the interference between SHG from the deposited film and that from the glass surface.

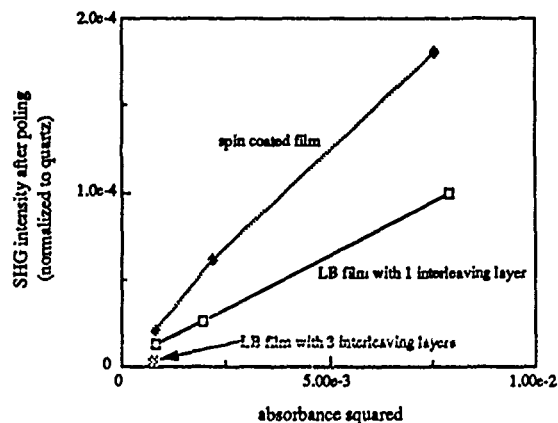


FIG. 3 SHG enhancement for composition modulated and spin coated films with absorbance. Quadratic enhancement of SHG with absorbance is observed for both composition modulated and spin coated films.

WP15 Poled Polymer for Frequency Doubling of Diode Lasers

G.L.J.A. Rikken, C.J.E. Seppen, S. Nijhuis and E.W. Meijer*, Philips Research Laboratories, P.O. Box 80000, NL-5600 JA Eindhoven, The Netherlands.

*: DSM Research, P.O. Box 18, NL-6160 MD Geleen, The Netherlands.

Aligning polar moieties in a polymer matrix by means of an electric field makes these materials suitable for second order nonlinear optical (NLO) effects, like electro-optical modulation and second harmonic generation. Especially for this last purpose, polymeric materials are very promising, as they can easily be applied in optical waveguide geometries, thereby transforming low powers like those emitted by diode lasers into high intensities and consequently giving high conversion efficiencies. However, up to now no poled polymer has been reported that can be used to frequency double the common AlGaAs-GaAs laser diodes ($\lambda \sim 820$ nm). In this contribution we will describe a polymer that was specifically designed for this purpose, with all its linear and nonlinear optical properties that affect its performance in such an application.

The major requirements for the NLO moiety are a high first order hyperpolarizability $\beta(-2\omega;\omega,\omega)$ and transparency at both the fundamental and the second harmonic wavelength. After having screened a large number of molecules¹, we have selected 4-alkoxy 4'-alkylsulfone stilbene compounds as favourable candidates. Methacrylate side-chain copolymers were synthesized², with various concentrations of the NLO moiety. The side-chain concentration was limited by the occurrence of crystallinity to about 25 to 50 mass %. Figure 1 shows the absorption spectrum of such a polymer. The refractive indices were determined using quasi-waveguide techniques at several wavelengths and fitted to a Sellmeier dispersion formula. From this, the coherence length $l_c = \lambda/4(n_{2\omega} - n_\omega)$ can be easily determined.

Thin film samples were prepared by spin-coating onto indium-tin oxide (ITO) covered glass. The electric field for poling was applied with a corona discharge at a temperature of 370 K ($T_g \simeq 390$ K). The nonlinearity shows the expected strong dependence on wavelength (fig. 2) and a linear dependence on NLO chromophore concentration. The temporal stability of the nonlinearity was fairly good, as shown in fig. 3, if the sample was stored in a dry environment. We found that poling introduced a birefringence $\Delta n \sim 1.10^{-3}$, which is too small for phase-matching purposes. Phase-matching may be obtained by periodic spatial modulation of the nonlinearity. This can be achieved in these poled polymers by periodically bleaching the NLO moiety with UV radiation (fig. 1).

- 1) L.T. Cheng, W. Tam, G.R. Meredith, G.L.J.A. Rikken and E.W. Meijer,
SPIE Proc. 1047, 61 (1989).
- 2) S. Nijhuis, G.L.J.A. Rikken, E.E. Havinga, W. ten Hoeve, H. Wynberg and E.W.
Meijer, to be published.

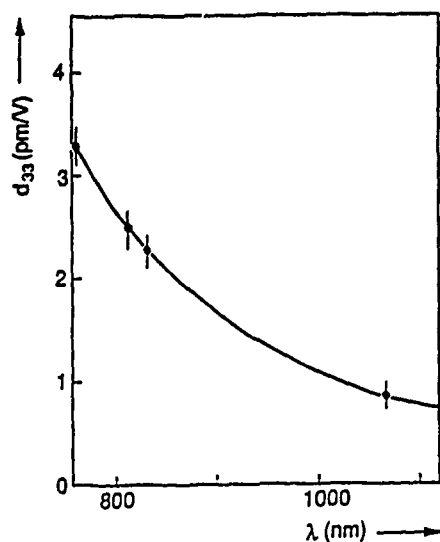
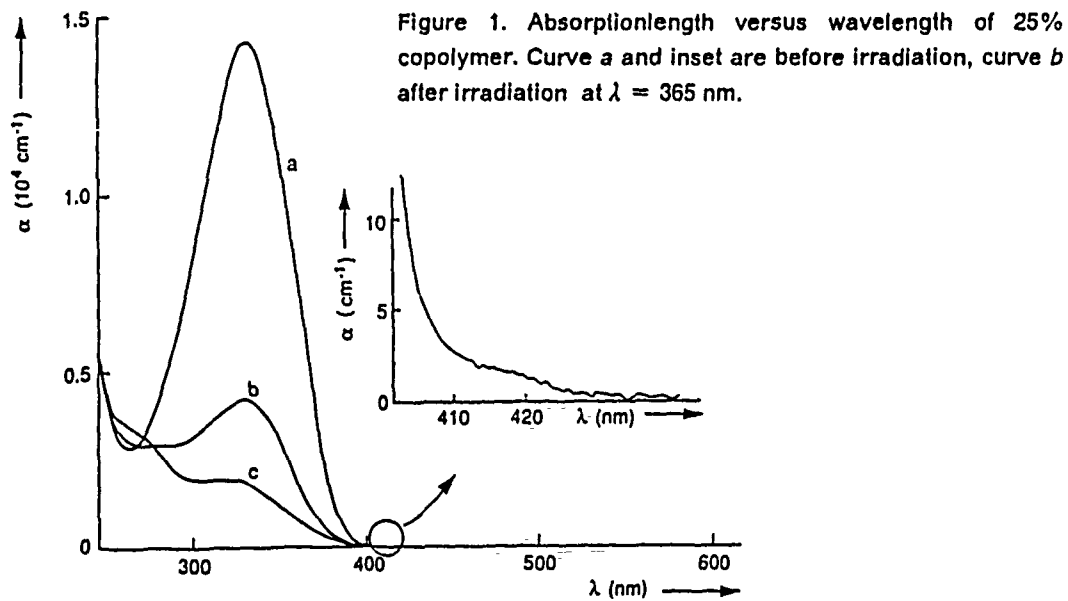


Figure 2. First order hyperpolarizability versus fundamental wavelength of 25% copolymer shortly after poling at 1.2 MV/cm.

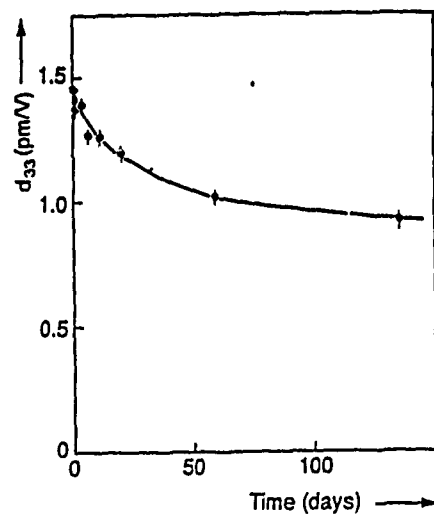


Figure 3. First order hyperpolarizability versus time at 1064 nm fundamental wavelength of 25% copolymer after poling at 1.2 MV/cm.

Progress in Crosslinked Nonlinear Optical Polymers

Dietmar Jungbauer, Gary C. Bjorklund, Bernd Reck, Robert J. Twieg,
Jerome D. Swalen, C. Grant Willson, and Do Y. Yoon

IBM Almaden Research Center
Dept K95/801, 650 Harry Road
San Jose, CA 95120
(408) 927-2424

SUMMARY

Nonlinear optical (NLO) waveguide devices based on currently available inorganic second order NLO crystals such as lithium niobate are playing an increasingly important role in modern optoelectronics technology, particularly when high speed modulation or switching is required {1}. Newly emerging polymeric second order NLO materials have the potential to supplant inorganic crystals as the materials of choice for these applications due to their intrinsic high figures of merit, compatibility with large low cost substrates, and tremendous advantages for fabrication of complicated structures.

In order for NLO polymers to fulfill this potential, materials must be found that have a poling-induced nonlinearity that is comparable to the best inorganic materials and that is stable for years at ambient temperature. In the last few years, high nonlinearity values have been achieved for polymers consisting of linear backbones to which NLO chromophores are covalently attached as sidegroups {2}. This approach allows very high concentrations of NLO chromophores to be obtained without phase separation. However these materials still suffer from a decay of the poling induced nonlinearity even at room temperature. Recently, it has been shown that covalent attachment of NLO chromophores by multiple chemical linkages to crosslinked polymer networks produces polymers with no apparent decay of nonlinearity, but at the expense of reduced concentration of NLO chromophores {3}.

In this paper, we report a better approach - attaching the NLO chromophores by a single chemical bond to the crosslinked polymer network - that yields stable NLO polymers with high concentrations of NLO chromophores. The specific NLO polymer we prepared and characterized was produced from the monomeric starting materials bifunctional N,N-(diglycidyl)-4-nitroaniline (a) and trifunctional N-(2-aminophenyl)-4-nitroaniline (b) shown in Figure 1. It is important to note that both of these monomers contain the NLO active para-nitroaniline type moiety. In fact, the finished polymer was composed ca. 63% by weight of this moiety.

The two monomers were heated and stirred to obtain a soluble prepolymer that was then spin-coated onto indium-tin-oxide coated glass substrates to produce thin film samples about 2 μm thick. After a precuring step, the samples were cured and poled step by step

Increasing the temperature to 120°C under a corona discharge and then cooling to room temperature under the corona field.

Values for the second harmonic nonlinear coefficients d_{33} and d_{31} were obtained using the Maker-fringe method with 1064nm fundamental radiation. Immediately after curing/poling, $d_{33} \approx 50$ pm/V and $d_{31} \approx 16$ pm/V were obtained. (For reference, LiNbO_3 has $d_{33} = 30$ pm/V.) The stability of the poling induced nonlinearity was tested by mounting the sample at a fixed angle while heating and annealing at 80°C. During the first 15 minutes, a partial decay of the second harmonic signal was observed, but after this initial quick decay, the signal was observed to be stable. After cooling to room temperature, the annealed sample had $d_{33} \approx 42$ pm/V and $d_{31} \approx 14$ pm/V.

The electro-optical coefficient of the annealed sample was directly measured at 530.9 nm using a Mach-Zehnder interferometer and a value $r_{13} = 6.5$ pm/V obtained. This compares well with an estimated value of $r_{13} = 8.3$ pm/V calculated from the measured d_{31} value using the procedure of Singer et al. {4}. The sample was then annealed for an additional 50h at 80°C and no measurable decay in r_{13} was observed. In addition, measurements of the poling induced birefringence showed no decay after 14 days of additional annealing at 80°C, confirming the essential stability of the poling induced nonlinearity. Experiments are in progress to apply this new approach to produce stable NLO polymers incorporating NLO chromophores with larger molecular hyperpolarizabilities.

1. R.C. Alferness, IEEE J. of Quant. Electron. **QE-17**, 946 (1981); R.C. Alferness, IEEE J. Sol. Ar. Comm. **6**, 1117 (1988).
2. M. Eich, A. Sen, H. Looser, G.C. Bjorklund, J.D. Swalen, R. Twieg, and D.Y. Yoon, J. Appl. Phys., **66**, 2559 (1989).
3. M. Eich, B. Reck, D.Y. Yoon, C.G. Willson, and G.C. Bjorklund, J. Appl. Phys., **66**, 3241 (1989).
4. K.D. Singer, M.G. Kuzyk, and J.E. Sohn, J. Opt. Soc. Am., **B 4**, 968 (1987).

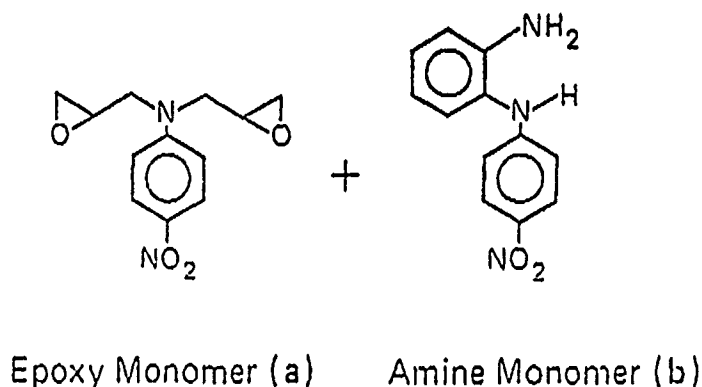


Figure 1. Schematics of the monomers composing the new crosslinked NLO polymer.

WP17 Observation of Extended-Lifetime Holograms in Photorefractive $\text{Bi}_{12}\text{SiO}_{20}$ at 785 nm

M.C. Bashaw, T.-P. Ma, R.C. Barker, and S. Mroczkowski
Department of Applied Physics and Department of Electrical Engineering,
Yale University, New Haven, Connecticut 06520-2157

R.R. Dube

IBM Research Division, T.J. Watson Research Center, Yorktown Heights, New York 10598

Abstract

Normal and extended-lifetime holograms have been observed in $\text{Bi}_{12}\text{SiO}_{20}$ at 785 nm. The extended-lifetime hologram has a decay rate approximately 150 times slower than the normal hologram's. This occurrence is explained by two-level electron-hole transport.

Summary

For a typical hologram-writing experimental setup, the holographic grating period is $\Lambda = 10 \mu\text{m}$, and normal photorefractive behavior is observed in $\text{Bi}_{12}\text{SiO}_{20}$ at 785-nm light wavelength. Write beam intensities are $665 \mu\text{W}/\text{cm}^2$ and $490 \mu\text{W}/\text{cm}^2$, and the erase intensity is $665 \mu\text{W}/\text{cm}^2$. Figure 1 shows a write/erase event. The response rate is 25 times slower than that at 514.5 nm. If, however, the BSO crystal is exposed to the write beams for time periods much longer than the normal response time, extended-lifetime holograms are generated, with a decay rate approximately 150 times slower than the normal holograms'.

An extended-lifetime hologram may be generated by one of two different methods. Using the first method, the hologram is written by exposing the crystal to the write beams with a high electric field (5 kV/cm) applied in the direction of the grating. The hologram is then simultaneously read and erased by one of the write beams. During this step, the hologram first fades, and then partially recovers, as shown in Fig. 2. The initial decay occurs at the same rate as erasure of a normal hologram, and the recovered hologram decays at a rate ~ 150 times more slowly.

Using the second method, the hologram is written by exposing the crystal to the write beams with no electric field applied. Because of the large grating period, the initial hologram is weak and is not detected with the current system. The write beams are turned off, a high electric field of (5 kV/cm) is applied, and the hologram is then probed by one of the write beams. During this step, the hologram is revealed at the same rate as normal decay, and then decays at a rate ~ 150 times more slowly, as shown in Fig. 3.

These effects can be explained by a simple two-level electron-hole transport model [1], shown in Fig. 4. The

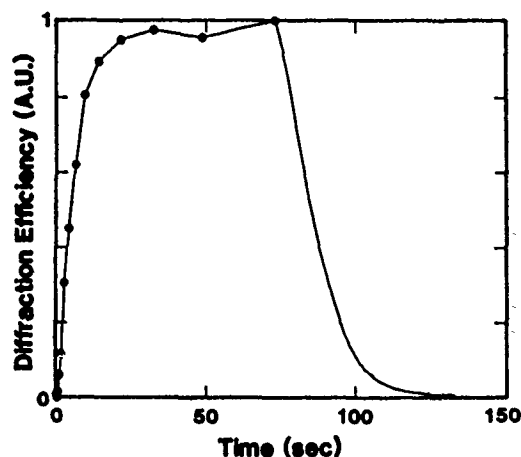


Figure 1: Write and erase evolution of diffraction efficiency. $E = 5 \text{ kV/cm}$. For the write portion of the curve, the points are assembled from different write events. The erase portion is taken from one erasure.

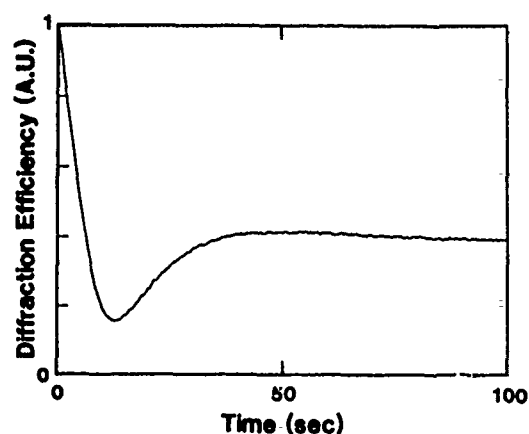


Figure 2: Typical decay of the diffraction efficiency for write periods several times longer than the grating time constant. $E = 5 \text{ kV/cm}$. The grating initially decays with approximately the same time constant, then partially recovers. The recovered grating decay rate is ~ 150 times slower than the normal grating decay rate.

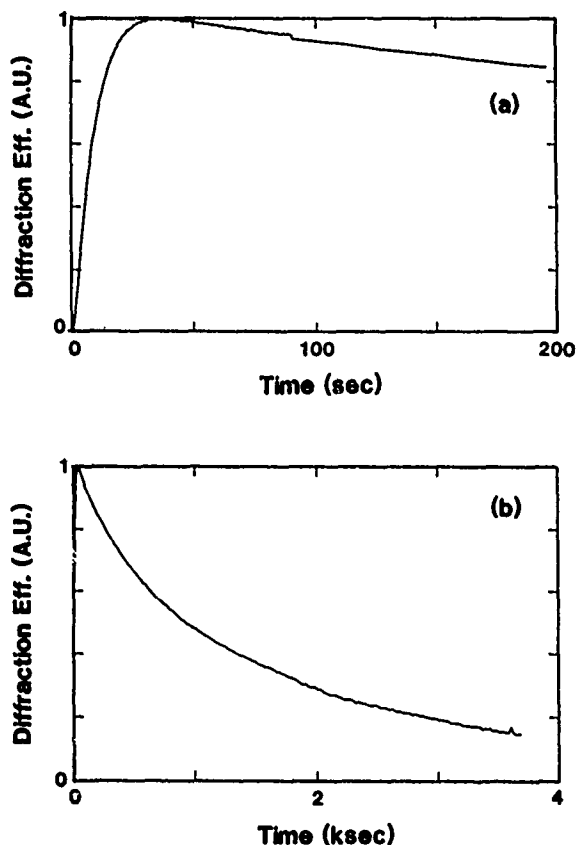


Figure 3: (a) Revelation sequence for extended-lifetime holograms. The zero-field write time was 640 s. The revelation rate ($E = 5$ kV/cm) is approximately the same as the grating write-erase rate. (b) Decay of residual grating. $E = 5$ kV/cm. This decay rate is ~ 150 times slower than the revelation rate.

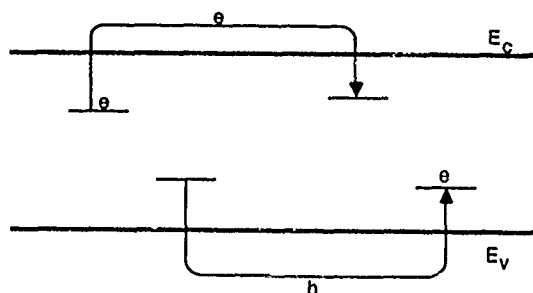


Figure 4: Electron-hole transport model utilizing two sets of levels in the energy band gap.

initial grating is established by electron transport and ordinary photorefractive behavior. With this grating in place, holes then migrate at a slower rate, generating a complementary grating. At the same time, electrons continue to migrate at the same rate as the holes in order to maintain the strength of the grating.

During the erasure sequence in both methods, the electron-formed grating is first erased, leaving the hole-formed grating, which decays more slowly. In the first method, the electron-formed grating is larger than the hole-formed grating, and thus an initial hologram is observed before the extended-lifetime hologram. In the second, the electron- and hole-formed gratings are approximately equal, and thus the extended-lifetime grating is revealed from an original grating of essentially zero net value.

Reference

- [1] G.C. Valley, *J. Appl. Phys.* 59, 3363 (1986).

WP18 Real-Time Pulse Shaping Using a Dynamic Grating

Kazuhiro Ema and Fujio Shimizu

Department of Applied Physics, University of Tokyo
7-3-1 Hongou Bunkyo-ku, Tokyo, Japan

summary

The technique for the arbitrary shaping of ultrafast pulses is recently progressed¹⁻³⁾. We demonstrated the picosecond pulse shaping technique using a non-dispersive grating pair and a static Fourier-transformed hologram³⁾. In this poster we report a real-time pulse shaping technique using a photorefractive $\text{Bi}_{12}\text{SiO}_{22}$ (BSO) crystal instead of a static hologram. The basic procedure of this technique is same as that of the Fourier pulse shaping. Our pulse shaping system, shown in Fig.1, consists of gratings (2400 line/mm), cylindrical lenses ($f=300\text{mm}$), an amplitude mask and the BSO crystal with an external applied electric field of 6 kV/cm. A synchronously pumped dye laser provides the 5-ps, 590-nm input pulse for the experiment. The first grating and lens spatially disperse the Fourier components of the input pulse on the BSO. The Fourier transformation of the mask pattern is recorded on the BSO at the same time using cw-Ar laser. The Fourier components of the input pulse is manipulated on amplitude and phase by the BSO, and the second lens and grating recombine them into the temporal shape of the output pulse. The output pulse shape is the convolution of the mask pattern with the input pulse.

Figure 2 shows the experimental results we obtained for two mask patterns; (a) double slits and (b) a single slit with movable transverse position. In both figure the left side is transmission pattern of the mask and the right side shows the output pulse shape, which is measured by the amplitude of the fringe obtained from the field-cross-correlation using a part of the input pulse as the probe. The reproduction of the mask pattern is excellent, considering that the observed pulse shape is the convolution of the mask pattern with the input pulse shape. The pulse position modulation is achieved by varying the 1-mm slit position, with the dispersion of 8.6 ps/mm agreeing with the theoretical calculation.

The diffraction efficiency and response time of the Fourier manipulation (BSO) are currently 0.1% and 1ms, respectively. By using an improved material this technique can be applied for the parallel-serial conversion of optical signals in psecond region.

references

- 1) A.M.Weiner, J.P.Heritage and J.A.Salehi, Opt.Lett., 13, 300(1988)
- 2) A.M.Weiner, D.E.Leaird, J.S.Patel and J.R.Wullert, Opt.Lett., submit for publication.
- 3) K.Ema and F.Shimizu, submit for publication.

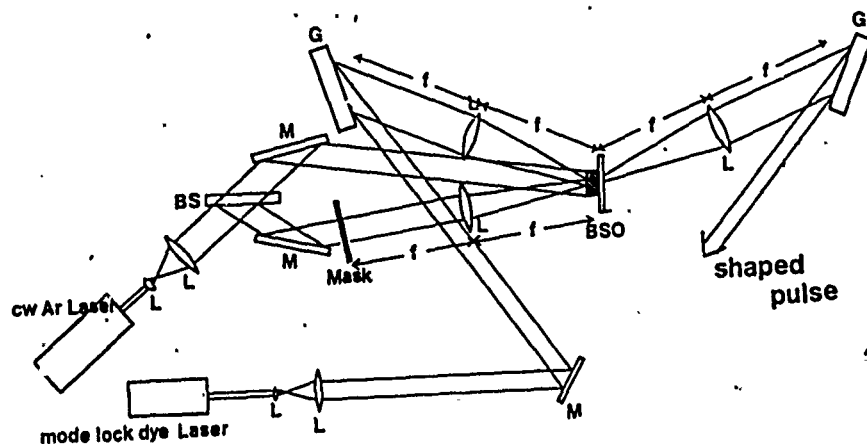
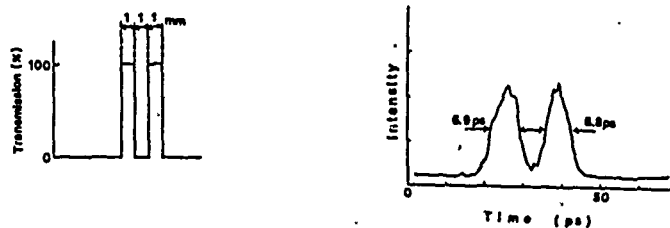


Fig.1 Experimental setup of the real-time pulse shaping.

(a)



(b)

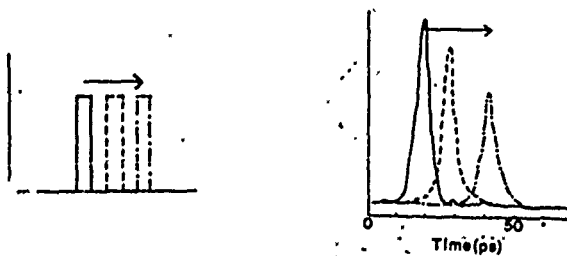


Fig.2 Experimental results of the pulse shaping. Mask patterns and shapes of the output pulses.

Large Photorefractive Beam-Coupling Gain Using the Franz-Keldysh Electrorefractive Effect in Temperature-Stabilized InP:Fe

Afshin Partovi, James Millerd and Elsa Garmire

Center for Laser Studies
University of Southern California
Los Angeles, CA 90089-1112

We have recently shown that at photon energies close to the band-edge of GaAs, large photorefractive beam-coupling gain coefficients ($\Gamma = 16.3 \text{ cm}^{-1}$) can be obtained using the moving grating technique [1]. However, the complexity of this technique is not desirable for many applications. Here we present results on obtaining large gain coefficients in InP:Fe ($\Gamma = 8.5 \text{ cm}^{-1}$) near the band-edge by controlling the temperature of the sample with a thermoelectric cooler. By combining the electrorefractive grating with the conventional electrooptic grating, we expect to achieve gain coefficients in the order of 20 cm^{-1} .

Formation of Franz-Keldysh electrorefractive photorefractive (ERPR) grating is shown in Figure 1. Intersection of a strong pump beam and a weaker signal beam in the crystal forms a sinusoidal space-charge field (E_{sc}) through the drift and diffusion of carriers. Figure 1a shows the corresponding total electric field $E_{tot} = E_{dc} + E_{sc}$ for two directions of applied field ($E_{dc} = +E_0$, and $E_{dc} = -E_0$) and the diffusion case ($E_{dc} = 0$). Only the 90° phase shifted grating is shown because this is the component that contributes to energy transfer. The electrorefractive change in the index of refraction is typically a quadratic function of the electric field. The refractive index change Δn_{ER} due to the fields shown in Fig. 1b are shown in Fig. 1c. The phase shift between Δn_{ER} and E_{sc} changes from $+90^\circ$ to -90° when the direction of the electric field is reversed. This results in a reversal of the direction of beam-coupling energy transfer. Without application of a field, the refractive index change has twice the spatial frequency of the space-charge field and can not transfer energy.

By using a crystal orientation for signal beam gain through conventional electrooptic photorefractive (EOPR) energy transfer and orienting the external field direction for ERPR energy transfer, the two effects can add to result in larger gain coefficients.

To achieve even larger gain coefficients, techniques that can enhance the photorefractive space-charge field can be employed. Two techniques have been previously used successfully to this end: The moving grating technique [2] and temperature stabilization [3]. We have previously used the moving grating technique to achieve large gain coefficients near the band-edge in GaAs [1]. Here we have investigated the photorefractive effect near the band-edge in temperature stabilized InP:Fe.

In order for a temperature-dependent resonance in the photorefractive space-charge field to occur, the carriers responsible for photoconductivity and dark conductivity must be of opposite sign [3]. It has been shown [3] that in InP:Fe, the

majority photoexcited carriers are holes for $\lambda = 1.06 \mu\text{m}$ illumination while dark conductivity is dominated by electrons. The photoionization cross sections for electrons and holes in InP:Fe [4] increase proportionally as the wavelength decreases from $\lambda = 1.06 \mu\text{m}$ towards the band-edge. The dominant photocarrier species near the band-edge is therefore also holes. It is therefore possible to apply the temperature stabilization technique near the band-edge.

We have performed preliminary beam-coupling experiments with a tunable dye laser in a crystal geometry that rules out an EOPR grating. We have obtained gain coefficients as high as 8.5 cm^{-1} for $\lambda = 960 \text{ nm}$, $E_{dc} = 10 \text{ kV/cm}$, $T = 290^\circ \text{ K}$, $\Lambda = 10 \mu\text{m}$, $\beta = 500$. Λ is the grating spacing and β is the pump to signal intensity ratio. Picoli et al. [3] have demonstrated gain coefficients as high as 11.4 cm^{-1} using the conventional EOPR beam-coupling. We can therefore expect gains in the order of 20 cm^{-1} by combining the EOPR and ERPR effects. These results are important because they present a simple way of obtaining very large gain coefficients in semiconductors.

REFERENCES

1. "Band-Edge Photorefractive Effect in Semiconductors", A. Partovi, A. Kost, E. Garmire, G. Valley, and M. Klein, To be published in Appl. Phys. Lett., March 1990.
2. B. Imbert, H. Rajbenbach, S. Mallick, J.P. Herriau, and J.P. Huignard, Opt. Lett., 13, 327 (1988).
3. G. Picoli, P. Gravey, C. Ozkul, and V. Vieux, J. Appl. Phys. 66, 3798 (1989) and references therein.
4. G. Bremond, A. Nouailhat, G. Guillot, and B. Cockayne, Sol. St. Commun. 41, 477 (1982).

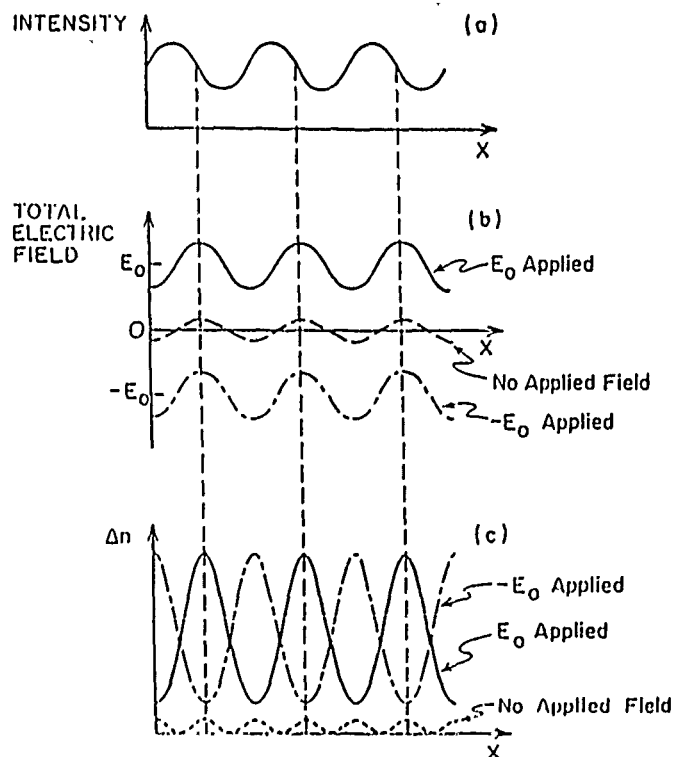


Figure 1. Formation of ERPR grating.

Self-Aligning Optical Heterodyne with Four-Wave Mixing

K. Nguyen, T.K. Gustafson
University of California, Berkeley, CA,
S. Yee, Lockheed Corp., Sunnyvale, CA,
and R. Neurgaonkar

Rockwell International Science Center, Tousand Oaks, CA

Summary

We have demonstrated self-aligning optical heterodyning with a large acceptance angle, using four-wave mixing in a photorefractive crystal.

The experiment was carried out in a 5 mm x 5 mm x 5 mm Ce-doped SBN crystal, grown at the Rockwell Science Center. It is a nonlinear optical central processing unit, utilizing three input beams to produce an output. The inputs are the local oscillator, and two collinear information beams, one a frequency probe beam, degenerate in frequency with the local oscillator, and the other a frequency-shifted information carrier. The unshifted beam and the local oscillator produce a grating in the crystal through the photorefractive effect. This grating diffracts the information carrier in the direction of the local oscillator, and aligns the two beams automatically for heterodyning in a detector. The electrical output, in the form of the beat signal between the carrier and the local oscillator can be easily detected and displayed.

Detailed investigation of the sensitivity, and robustness of the receiver in a noisy environment is under progress.

Color Holographic Storage in LiNbO_3

Frances T.S. Yu, Shudong Wu, Andy Mayers, and Sumail Rajan

Penn State University, University Park, PA

Summary

Previously, color holograms recorded in film had low angular and wavelength selectivities due to the thin photographic emulsion. Multiple color holographic storage is impossible with holographic films. Due to the increased thickness available in photorefractive materials, multiple color holographic storage can be realized. In addition, photorefractive materials can record holograms in real-time, avoiding the tedious chemical processing and emulsion shrinking problems encountered in using films. The setup geometry for recording multiple color holograms is based on the requirements set forth to obtain the wavelength selectivity, the angular selectivity and the dispersion of the holograms are discussed. The color holograms were recorded in LiNbO_3 using a "white light" Ar-Kr laser and could be reconstructed by incoherent white light source. The recorded color holograms may be addressed with a spatial light modulator. When the wavelength selectivity is not sufficient, we found cascading spatial grating beating phenomenon and observed as high as 5th order beating frequency. An analysis of wavelength cross talk is also presented.

High Power Diode Laser Array Beam Combination Via Injection Locking and Photorefractive Beam Coupling

S. MacCormack, R.W. Eason and S.W. James

*Department of Physics
Optoelectronic Research Centre
University of Southampton
Southampton
SO9 5NH
U.K.*

Tel: 0703-592098

Fax: 0703-585813

The attainment of a high power, diffraction limited output from semiconductor laser arrays is currently a subject of great interest for many applications such as increasing optical fiber launch efficiency and improvement of solid state laser pumping. The output from a single stripe, single mode semiconductor laser is essentially diffraction limited but power output from these devices is limited due to problems with dissipation of heat from the lasing region, the current highest cw operating power being 100 mW. Diode laser arrays and bars present a solution to the problem of higher output powers but their output is generally far from diffraction limited.

In this paper we demonstrate a technique for obtaining high power (in excess of 100 mW) diffraction limited beams from diode laser array(s) via an injection locking and photorefractive beam combining technique in BaTiO_3 .

Photorefractive two-wave mixing results in the non-reciprocal transfer of energy between two coherent beams which cross with a suitable geometry within a photorefractive crystal. In this case the pump and signal beams are the outputs from a high power array and a single stripe laser respectively, phase-locking between these lasers being provided by means of a conventional injection locking set up¹. Experimental and theoretical evidence² show that there is no phase cross talk between pump and signal beams so the nature of the single stripe output is preserved. The technique can be extended to the phase locking and combination of multiple laser arrays, the only limiting factor being the amount of injecting power available in the master laser.

Using this technique we have demonstrated a pump transfer efficiency of 45%, corresponding to diffraction limited, circular profile beams with powers well in excess of 100 mW from a single locked laser array. In addition, experimental results of the extension of this work to the locking and combining of multiple diode arrays will be presented.

References

- 1) "Injection locking of coupled stripe diode laser arrays" L. Goldberg, H.F. Taylor, J.F. Weller, D.R. Scrifres. *App. Phys. Lett.* 46 p. 236.
- 2) "Laser beam cleanup using photorefractive two-wave mixing and optical phase conjugation." A.E. Chiou and P.Yeh. *Opt. Lett.* 11 p. 461.

Dynamic Range Compression Using Incoherent Erasure in Photorefractive Two-Beam Coupling

Arthur Chiou
Rockwell International Science Center
1049 Camino Dos Rios
Thousand Oaks, CA 91360
(805) 373-4464

SUMMARY

Dynamic Range Compression (DRC) is an important preprocessing step required in any system where input range is larger than the dynamic range (DR) of the sensor(s) or detector(s) of the system. Two schemes for DRC using photorefractive two-beam coupling had been reported [1,2]. One, based on reduction in photorefractive coupling constant due to dark conductivity effect [Fig.1(a)], is limited to very low input intensity of the order of a few mW/cm^2 [1]. It also suffers from the major drawback that the range over which the compression occurs is very narrow (about one and a half decades). The other, based on gain saturation due to pump depletion [Fig.1(b)], is also rather limited in range [2]. Another method, similar in principle to the first, is to use non-degenerate two-wave mixing [Fig.1(c)]. Here, the intensity-dependent gain associated with the intensity-dependent response time provides the required nonlinearity. Theoretical results showing the output vs input intensities for these approaches are shown in Fig.2(a), (b), and (c).

In this paper, a new scheme based on incoherent erasure in photorefractive two-beam coupling, similar to the photorefractive incoherent-to-coherent optical converter [3], is proposed and demonstrated for dynamic range compression. In this approach, the input beam is used to (partially) erase the photorefractive grating written by two coherent write-beams, designated as the pump beam $I_p(o)$ and the probe beam $I_s(o)$ in Fig.1(d). The photorefractive crystal is oriented so that the energy is transferred from the pump to the probe beams. DRC is achieved, since the intensity range of the depleted pump $I_p(L)$ can be much smaller than that of the erasure beam. The degree of compression is dictated by the beam-coupling constant of the photorefractive crystal. For a given coupling constant, it can also be controlled over a wide range by varying the beam splitting ratio. The absolute intensity level at which DRC occurs is determined by the total write-beam intensity I_0 . The theoretical result showing the output vs input intensities obtained by this scheme is given in Fig.2(d).

Theoretical and experimental results will be presented. Similarities and differences of these various schemes will be compared and contrasted.

REFERENCES:

- [1] H. K. Liu and L. J. Cheng, "Infrared predetection dynamic range compression via photorefractive crystals," *Appl. Opt.* **27**, 1006-1007 (1988).
- [2] I. McMichael, M. Khoshnevisan, and P. Beckwith, "Nonlinear optical ranging imager," in *Conference on Lasers and Electr-Optic Technical Digest Series 1988*, Vol. 7 (Optical Society of America, Washington, DC 1988) pp. 218.
- [3] Y. Shi, D. Psaltis, A. Marrakchi, and A.R. Tanguay, Jr. "Photorefractive incoherent-to-coherent optical converter," *Appl. Opt.* **22**, 3665-3667 (1983).

FIGURE CAPTION:

- Fig.1 Various schemes for real-time optical dynamic range compression using photorefractive two-beam coupling based on intensity-dependent gain due to: (a) dark-conductivity effect; (b) pump depletion; (c) intensity-dependent response time; (d) incoherent erasure.
- Fig.2 Theoretical results showing the output vs input intensities corresponding to the three schemes illustrated in Fig.1

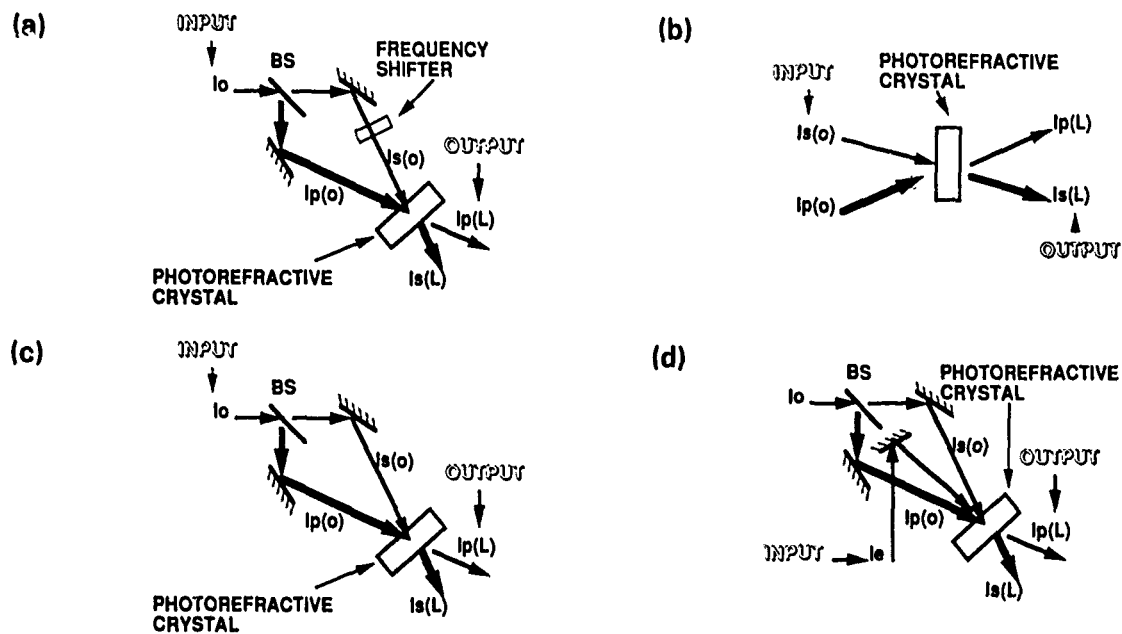


Fig. 1

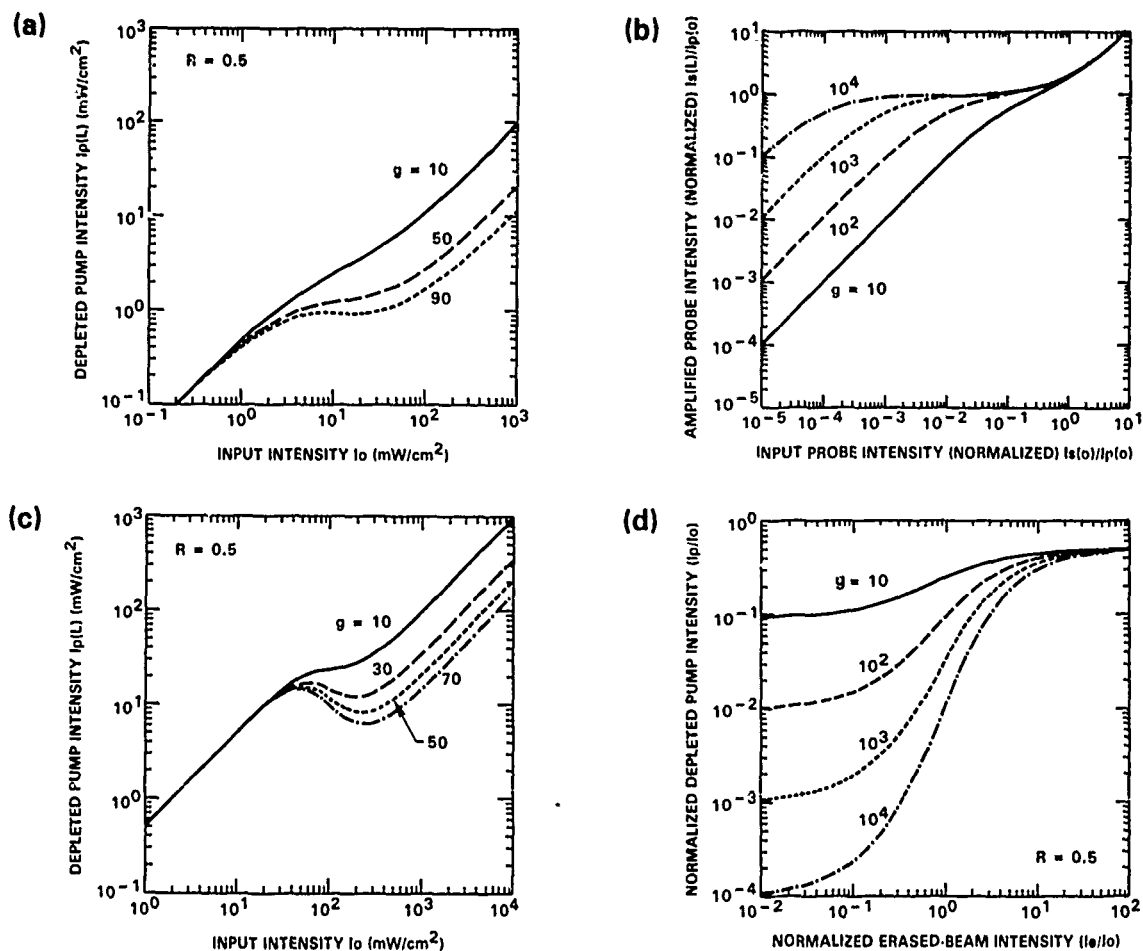


Fig. 2

Anisotropy of Second Harmonic Generation from Magnetized Surfaces

Ru-Pin Pan, H. D. Wei, and T. J. Watson Yang,
Dept. of Electrophysics, National Chiao Tung University
Hsinchu, Taiwan 30049, R.O.C.

In previous work,¹ we have discussed the feasibility of using second harmonic generation to study surface magnetism and suggested that one can detect the surface magnetization by analyzing the anisotropy of SH signals. In this work, we give a detailed discussion about the anisotropy change when a surface is magnetized.

Due to the change in surface symmetry, the surface optical second order susceptibility tensor will also change in symmetry when the surface becomes magnetized. Some of the vanishing tensor elements become nonzero. Although these new elements are larger than the detection limits, they are still smaller than those elements originally nonvanishing. It is not always possible to find an arrangement to probe a single element. However, by rotating the sample, changing the polarization of pumping beam or detecting a particular polarization of the signal, the effect of these new elements will manifest itself in the change of anisotropy of detected signals.

We will give the difference in anisotropy of SH signals from magnetized and nonmagnetized surface of a fcc crystal. The surface orientations and magnetization directions covered in this work are listed in Table 1. Our results include the polarization combinations for the incident and reflected SH beam (s,s), (s,p), (p,s) and (p,p) in each case. The first letter in the parenthesis is for the polarization of detected SH signals and the second letter is for the polarization of the pumping beam.

¹Ru-Pin Pan, H.D. Wei, and Y.R. Shen, Phys. Rev. B39, 1229(1989)

* This work was partially supported by the National Science Council, under Grant No. NSC77-0208-M009-04.

Table 1: The surface orientation and the direction of magnetization considered in this work.

Surface Orientation	Direction of \vec{M}
(111)	$[2\bar{1}1]$, $[111]$
(110)	$[110]$, $[001]$
(001)	$[100]$, $[001]$

Optical Second-Harmonic Generation at the Interface Between Silver Thin Film and LiNbO_3

T.Takano, Y.Inoue, K.Yano, T.Tokumaru and Y.Okada
Tokyo Research Laboratories, Sharp Corporation
273-1 Kashiwa, Kashiwa-Shi, Chiba, 277, Japan

It was reported that the enhanced electric field of the metal surface plasmon caused the considerable nonlinear electric polarization in quartz crystal and that the optical second-harmonic was brought about in close proximity to the metal surface when the phase-match condition was satisfied.⁽¹⁾

As the yield of the second-harmonic generation is proportional to the square of d-value, nonlinear coefficient of the crystal, the great improvement in the yield should be realized using a crystal with a greater optical nonlinearity instead of the quartz.

LiNbO_3 is one of popular optical nonlinear crystals. Its chemical and physical properties are well investigated and the nonlinear coefficient d_{33} is about two order larger than that of quartz. This is a great advantage for the experimental study, but the phase-matching can not be carried out by the method mentioned above because of its large optical anisotropy.

In this study, optical grade z-cut LiNbO_3 wafers of 1mm thickness were used as nonlinear crystal. Ag film was vacuum-evaporated on a polished surface of 5mm x 10mm LiNbO_3 sample piece. After AlN film was deposited on the Ag film by sputtering technique, Ag film was evaporated again. These thicknesses were 30nm, 160nm and 30nm respectively. This three-layer structure is the novel formation for the surface plasmon phase-matching.

The experimental arrangement is depicted in figure 1. Nd:YAG laser (1064nm) was used as a fundamental light source. Incident p-polarized fundamental light beam was totally reflected at the bottom of a GaP coupler prism. Surface plasmon which propagates at the interface between the lower Ag film and LiNbO_3 was excited at the particular incident angle where the frequencies and wavevectors of evanescent wave and plasmon are equal. This configuration is similar to Kretschmann configuration.⁽²⁾

Figure 2 shows the typical experimental results : the variations of the reflected fundamental light intensity and the resultant second-harmonic light intensity with increasing the incident angle from 0 to 5 degrees. These curves well agree with the theoretical curve shown in figure 3. However, the positional difference between the reflected light intensity minimum and the second-harmonic light intensity maximum in figure 2 had been theoretically expected,⁽³⁾ the experimental observation was first carried out. The second-harmonic light which was generated at the interface region of LiNbO_3 by the enhanced electric field of plasmon propagated in the direction that the plasmon and the harmonic were in the phase-matching condition. This phenomenon is Cherenkov radiation.⁽⁴⁾

It was also revealed theoretically that the yield of second-harmonic generation is proportional to the forth power of the forth power of the field enhancement magnitude, the ratio of electric field of plasmon to that of incident light. This is can be seen from the comparison of figure 2 to the calculated field enhancement in figure 3.

- (1) H.J.Simon, R.E.Beenner, and J.G.Rako Opt. Commun., 23, No.2 (1977) 4095. J.C.Quail, J.G.Roko, H.J.Simon and R.T.Deck Phys. Rev. Lett., 50, No.25, (1983) 1987 J.C.Quail and H.J.Simon J. Opt. Soc. Am. B Vol.1 No.2 (1984) 317.
- (2) E.Kretschmann Z. Physik, 241, (1971) 313.
- (3) E.F.Y.Kou, and T.Tamir Appl. Opt., 27, No.19 (1988).
- (4) P.K.Tien Appl. Phys. Lett., 14, (1970) 291.
T.Taniuchi CLEO'86 Tech. Digest, (1986) 230.

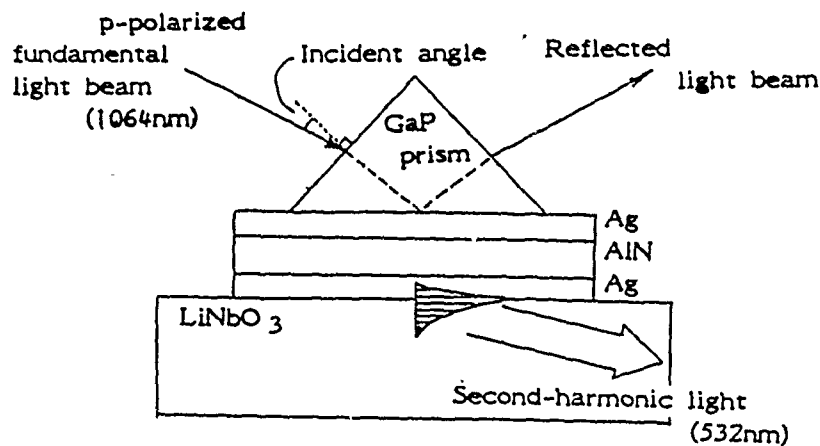


Fig.1 Experimental Configuration

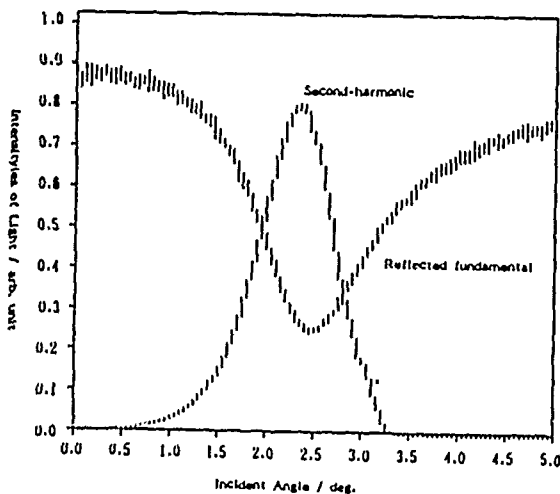


Fig.2 Experimental results ; reflected fundamental and Second-harmonic light intensities.

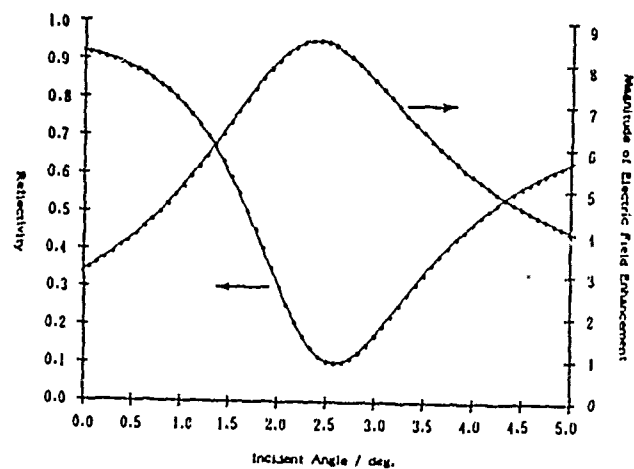


Fig.3 Theoretical curves of reflectivity (—) and magnitude of field enhancement (---).

Surface Magnetoplasmon-Polariton Solitons on Semiconductors: Voigt Geometry

T.P. Shen and D. Rogovin

Rockwell International Science Center
1049 Camino Dos Rios
Thousand Oaks, CA 91360
U.S.A.
(805) 373-4222

A.D. Boardman

Department of Physics
University of Salford
Salford M54WT
U.K.

SUMMARY

Nonlinear optical phenomena associated with surfaces or interfaces have attracted considerable attention recently.¹ Here we will investigate the effect of weak nonlinearity on surface magnetoplasmon-polariton (SMP). Specifically, we study the possible formation of SMP solitons on a n-type semiconductor surface in Voigt geometry.² The SMP soliton is a pulse envelope wave that has the nature of stationary wave propagation in the direction parallel to the surface. We will derive the evolution equation³ for this pulse envelope wave and examine its existence condition.³

The nonlinear effect on SMP to be discussed is resulting from the nonlinear interaction among the free carriers in the n-type semiconductor. A nonlinear phenomenological dielectric tensor is constructed by a simpler fluid approach.⁴ More precisely, we have adopted a quasi-hydrodynamic theory with damping. In the weakly nonlinear regime, we can perturbatively solve for the dielectric tensor at ω , which is given by

$$\vec{\epsilon}(\omega) = \vec{\epsilon}_L(\omega) + 4\pi\vec{\chi}^{(3)}(\omega) \vec{E}_1(\omega) \vec{E}_1^*(\omega) + \dots, \quad (1)$$

where $\vec{\epsilon}_L(\omega)$ is the linear dielectric tensor, $\vec{E}_1(\omega)$ is the linear electric field, and $\vec{\chi}^{(3)}(\omega)$ is the lowest-order nonlinear susceptibility at ω .

Because of the weakly nonlinear effect on the evolution of the SMP solitons, we can express the electric field of SMP soliton at ω_0 in the following form,³

$$\vec{E}(\vec{r}, t) = a(x, t) \vec{E}_L(z, \omega_0) e^{i(k_0 x - \omega_0 t)} + \text{c.c.}, \quad (2)$$

where $a(x, t)$ is the envelope function, and \vec{E}_L , k_0 and ω_0 are the electric field, wave number and frequency of SMP in the linear limit. The nonlinear dispersion relation^{3,5} of SMP soliton at ω_0 can be expanded as follows:

$$\omega = \omega_0 + \omega' (k - k_0) + \frac{1}{2} \omega'' (k - k_0)^2 + \Delta |a|^2 + \dots, \quad (3)$$

where ω' and ω'' are the group velocity and group dispersion of linear SMP, and Δ is the nonlinear frequency shift, which can be obtained by an application of Green's theorem,⁵ and is given by

$$\Delta = \frac{1}{2} \omega_0 N/D, \quad (4)$$

where

$$N = -4\pi \int_{-\infty}^0 dz \vec{E}_L^*(z, \omega_0) \vec{E}_L^*(z, \omega_0) \vec{\chi}^{(3)}(\omega_0) \vec{E}_L(z, \omega_0) \vec{E}_L(z, \omega_0), \quad (5a)$$

$$D = \int_{-\infty}^0 dz \vec{E}_L^*(z, \omega_0) [\vec{\epsilon}_L(\omega_0) + \frac{1}{2} \vec{\epsilon}_L'(\omega_0) \omega_0] \vec{E}_L(z, \omega_0). \quad (5b)$$

Based on Eq. (3), we can use either a more general Whitham method or a first principle derivation³ to obtain the evolution equation for the envelope function, which is given by

$$i \left[\frac{\partial a}{\partial t} + \omega' \frac{\partial a}{\partial x} \right] + \frac{1}{2} \omega'' \frac{\partial^2 a}{\partial x^2} = \Delta |a|^2 a. \quad (6)$$

The formation of bright SMP solitons requires the balance between the group dispersion (ω'') and the effective nonlinearity (Δ), which is described by the existence condition, viz., $\omega'' \Delta < 0$.

The frequency range over which the bright SMP soliton formation is possible will be discussed for a strongly doped n-type Insb in a DC magnetic field of few Telsa.

References

1. Feature issue on nonlinear guided-wave phenomena, JOSA B 5(2) (1988).
2. G.C. Aeres, A.D. Boardman, J. Phys. C. 11, 945 (1978).
3. A.D. Boardman, G.S. Cooper, A.A. Maradudin, T.P. Shen, Phys. Rev. B 34, 8273 (1986), A.D. Boardman, G.S. Cooper, JOSA B 5, 403 (1988).
4. G. Li, S.R. Seshadri, JOSA B 6, 1125 (1989).
5. A.P. Mayer, A.A. Maradudin, R. Garcia-Molina, A.D. Boardman, Opt. Comm. 72, 244 (1989).

WP27 Soliton Interaction and Spectral Laser Linewidth in Wavelength Multiplexing Transmission Systems,

T. Hauff, W. Heinlein, University of Kaiserslautern, D- 6750 Kaiserslautern,
P. O.Box 3049, Fed. Rep. of Germany

Introduction: All-optical transmission systems using solitons and wavelength division multiplexing (WDM) are proposed for long-distance communication systems /Mo/. For narrow-spaced channels, in WDM systems with periodically compensated loss, soliton interaction limits the maximum error-free transmission rate. For a bit error rate of 10^{-9} , an overall variance of time jitter less than 1.02 is necessary /Mo/. Here, new results on soliton interaction are presented paying account to practically attractive wide channel spacings, interaction-caused frequency and time shifts, and laser linewidth. A novel method using separation of the nonlinear Schroedinger - equation in frequency space is used.

Frequency shift: Fig. 1 shows a two-soliton-collision with a normalized channel spacing of $F = \pm 1$ ($=\Omega/2\pi$ in /Mo/). Fig. 2 shows the resulting normalized frequency shift versus normalized channel spacing of ± 1 to ± 30 . The frequency shift is approximately inversely proportional to the squared frequency difference between the channels, and therefore less than supposed in /Mo/.

Asymmetry of frequency shift: Fig. 3 and 4 shows the frequency shift after one collision as a function of fiber loss α . Note the asymmetry of this shift with respect to gain and loss. For this reason, a mean value of pulse arrival time jitter of about 10 ps per 2000 km system length occurs for the given data.

Time shift: Fig. 5 shows the time shift after one two-soliton collision as a function of channel spacing and fiber loss. With a proper choice of parameters, time shift can compensate for the asymmetry of frequency shift over long distances.

Influence of linewidth: Fig. 6 shows the influence of cw linewidth of a laser source on the variance of frequency shift in a fiber with 0.2 dB/km loss. For $F = \pm 1$, this variance is doubled for a cw linewidth of 1 MHz of the (external modulated) laser source.

Conclusion: This contribution gives new results on the influence of spectral linewidth and fiber loss and gain on soliton arrival time variance. Paying account to time shift and the asymmetry of frequency shift, transmission rates of 100,000 Gbit km/sec with only 5 channels are calculated with error rates less than 10^{-9} using standard fibers and a soliton FWHM of 20 ps.

Reference: L. Mollenauer et al., IEEE J. Quant. Electron., Vol. QE-22. No. 1, Jan. 1986

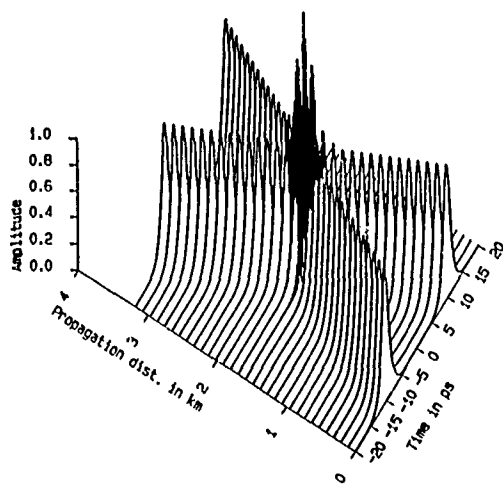


Fig. 1: Collision of two solitons with a soliton period of 13 km, $d = 17$ ps/km/nm, and $F = \pm 1$ corresponding to ± 0.077 THz

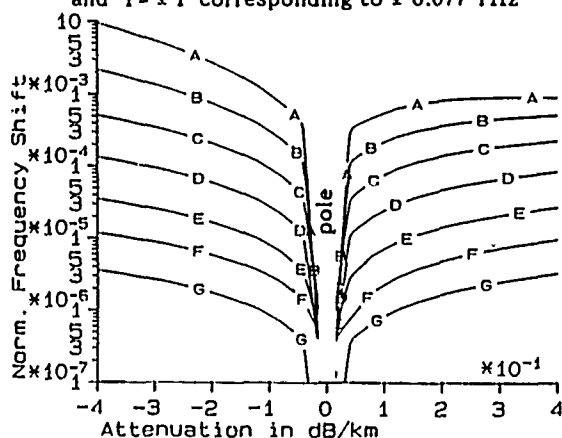


Fig. 3: Abs. values of norm. frequency shift after collision for $F = \pm 1$ to $F = \pm 30$ (comp. Fig. 2) vs. fiber loss

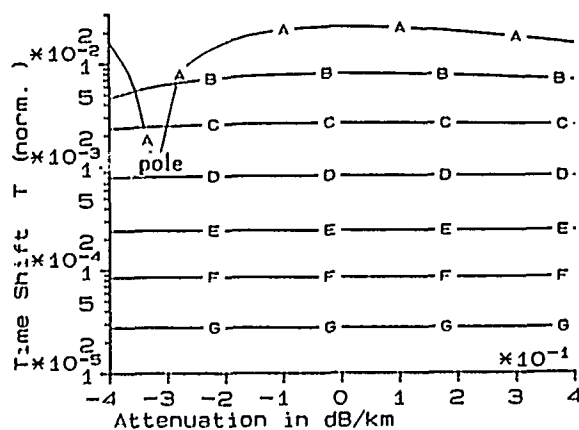


Fig. 5: Abs. values of norm. time shift after collision for $F = \pm 1$ to $F = \pm 30$ (comp. Fig. 2)

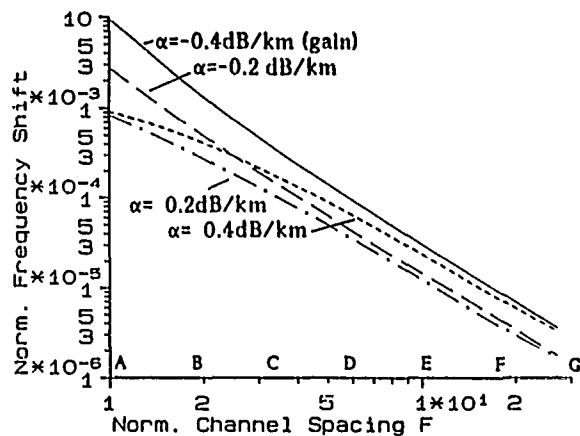


Fig. 2: Absolute values of norm. frequency shift for different channel spacings F

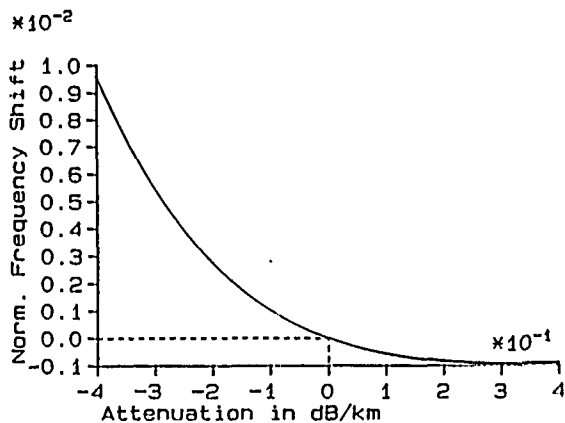


Fig. 4: Normalized frequency shift after collision for $F = \pm 1$ vs. fiber loss (linear scale)

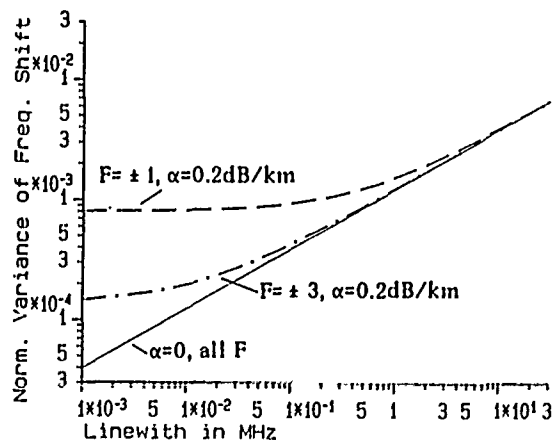


Fig. 6: Statistical influence of linewidth on frequency shift

Fundamental Dark Surface Waves at a Nonlinear Interface

Steven R. Skinner and David R. Andersen

Department of Electrical and Computer Engineering

The University of Iowa

Iowa City, IA 52242

In this work, we present analytic solutions obtained for the case of a TE fundamental dark surface wave (FDSW) propagating at the interface between two dissimilar defocussing Kerr media. Analytic expressions are derived in two dimensions and show the functional form of the surface wave and the range of independent and dependent parameters which will give FDSW solutions. The analytic solutions are in the form of eigenmodes of each of the respective nonlinear media [1], with propagation constants obtained by appropriate boundary conditions being applied at the interface. Analytic results indicate that it should be possible to observe propagation of the FDSW with currently available experimental apparatus and materials.

We have also obtained a stability criterion [2,3] for the FDSW which indicates that in order to have stable propagation of the dark surface wave, $\partial P_D / \partial k_z < 0$, where P_D is the dark power contained in the surface wave and k_z is the propagation constant for the bright background. To verify this stability criterion, the analytic solution was propagated numerically using a split-step algorithm. The computer results clearly show that for the stable branch of the FDSW effective wavenumber versus dark power curve, the dark wave propagates in a stationary fashion along the interface. Also, for the unstable branch of the curve ($\partial P_D / \partial k_z > 0$), the dark energy radiates away from the interface in the form of various unbound dark solitons and radiation. An example for each case (stable and unstable) is shown below in Fig. 1.

Novel applications of the results presented here are foreseen in the areas of nonlinear optical switching and communications.

Figure

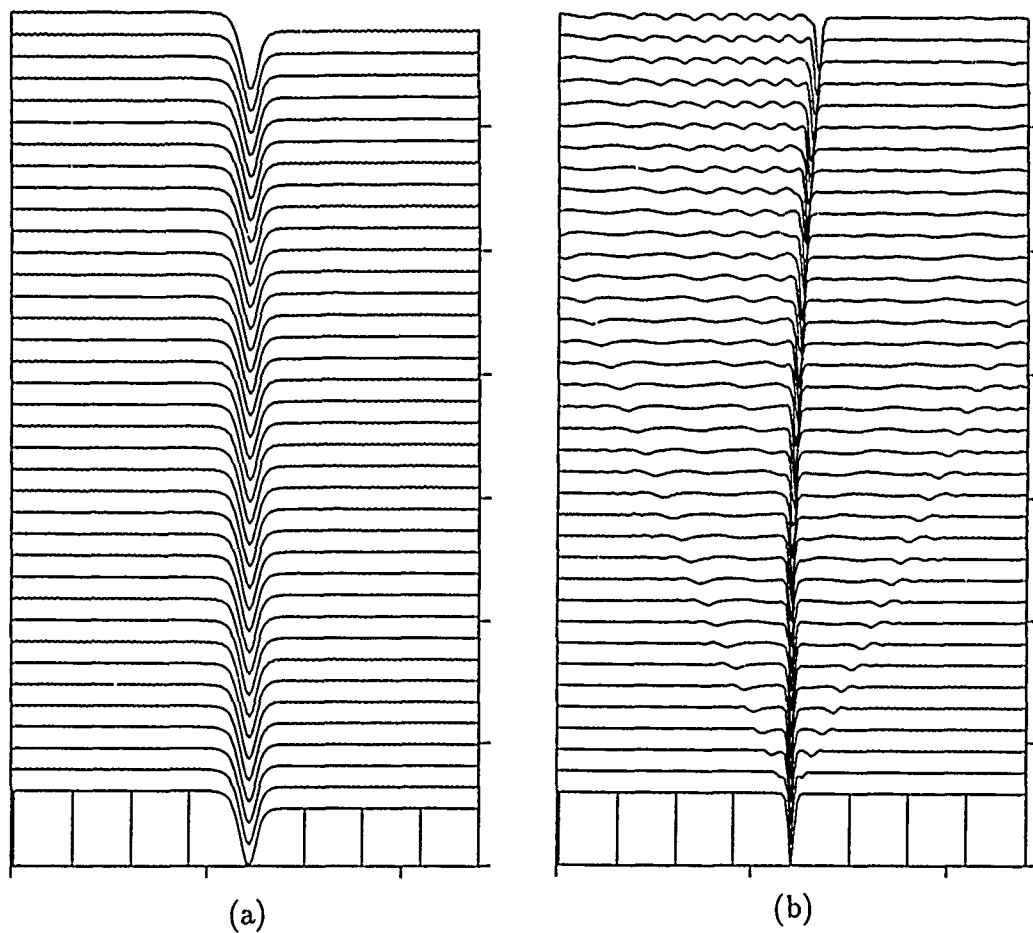


Fig. 1. Results of numerical simulation of the FDSW for (a) $\partial P_D / \partial k_z < 0$, corresponding to the stable branch of the effective wavenumber versus dark power curve, and (b) $\partial P_D / \partial k_z > 0$, corresponding to the unstable branch of the curve.

References

1. W. J. Tomlinson, *Opt. Lett.* 5, 323 (1980).
2. N. N. Akhmediev, V. I. Korneev, and Y. V. Kuzmenko, *Sov. Phys. JETP* 61, 62 (1985).
3. P. Varatharajah, A. B. Aceves, J. V. Moloney, and E. M. Wright, *J. Opt. Soc. Am. B* 7, 220 (1990).

Million Fold Enhancement of Surface Emitting Harmonic Generation in Semiconductor Waveguides

R. Normandin
Optoelectronic Devices
National Research Council
Ottawa, Ontario
Canada K1A 0R6
613-993-4449

F. Chatenoud and R.L. Williams
Solid State Optoelectronics Consortium
National Research Council
Ottawa, Ontario
Canada K1A 0R6

Several years ago Stegeman and Normandin predicted and demonstrated the nonlinear mixing of oppositely propagating guided waves. The resultant field was coupled to radiation modes and propagated in a direction perpendicular to the waveguide surface in the case of equal frequency fundamentals. Its application to picosecond signal processing, the creation of an all-optical transient digitizer and crude spectrometer ⁽¹⁾ demonstrated the potential usefulness of this interaction. Finally the nonlinear cross section was evaluated for a symmetric GaAs waveguide structure ⁽²⁾. Recent work has also apparently rediscovered this geometry and experimentally verified the GaAs calculations ⁽³⁾.

We previously demonstrated that the radiated harmonic field, in the geometry shown in Fig. 1, is strongly dependant on the exact shape of the field distribution of the guided fundamental and that by suitable modifications the overall interaction strength can be increased ⁽²⁾. Considering the case of a GaAs waveguide with $1.06\mu\text{m}$ light on a buffer layer made of AlGaAs (Fig. 1) interference effects in dipole contributions and strong absorption of the $0.53\mu\text{m}$ light by the GaAs will reduce the output intensity.

The option, presented here, is to use a combination of alternating nonlinear materials and changes in the refractive index to induce a phase coherence at the output plane. The nonlinear cross section, normalised to an interaction region of 1mm by 1cm, is given by $I(2\omega) = A^{nl} \cdot I^2$. A calculation for a normal GaAs guide compared with a superlattice of half period made of $\text{Al}_{0.8}\text{Ga}_{0.2}\text{As}$ and GaAs is shown in Fig. 2. The waveguide TE_0 cutoff point is around $0.2\mu\text{m}$. In the normal guide highly damped oscillations (by absorption) are visible as the guide thickness is increased. The superlattice geometry (SL) is clearly more efficient by up to 10^6 for large thicknesses. The cross section is calculated for a $1\mu\text{m}$ film as a function of the superlattice period in Fig. 3. The fundamental resonance is evident for $kx=1$. The resonance peak is fairly broad (only a few layers are present) making the fabrication non critical of materials parameters.

A waveguide of MBE grown GaAs ($0.6\mu\text{m}$ thick) on $1.6\mu\text{m}$ of $\text{Al}_{0.4}\text{Ga}_{0.6}\text{As}$ was compared with another made of a superlattice of alternating $0.06\mu\text{m}$ $\text{Al}_{0.4}\text{Ga}_{0.6}\text{As}$ /GaAs layers for a total thickness of $0.6\mu\text{m}$. The theory predicted an enhancement of approximately 1000. We observed a signal increase of over 800 in the geometry depicted in Fig. 1. Further experiments with $\text{Al}_{0.8}\text{Ga}_{0.2}\text{As}$ on

111 substrates are in progress. We will discuss the possibility of visible surface emitting diode laser geometries and efficient diode laser spectrometers in a fiber optics context using this work.

References.

1. "Integrated Optical Circuits and Components", Ed. L.D. Hutcheson, Dekker Inc., New York. Chap. 9 by Stegeman et al and many references therein.
2. P.J. Vella, R. Normandin and G.I. Stegeman, Appl. Phys. Lett 38,759(1981)
3. D. Vakhshoori, M.C. Wu and S. Wang, Appl. Phys. Lett 52, 422 (1988).

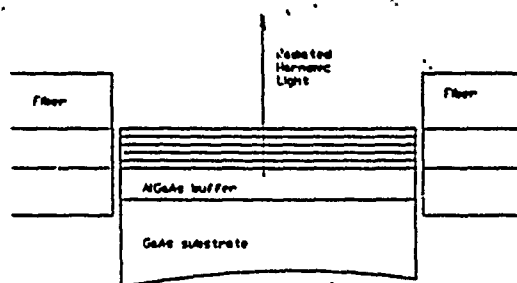


Figure 1.
Experimental geometry used for
nonlinear harmonic cross section
measurements.

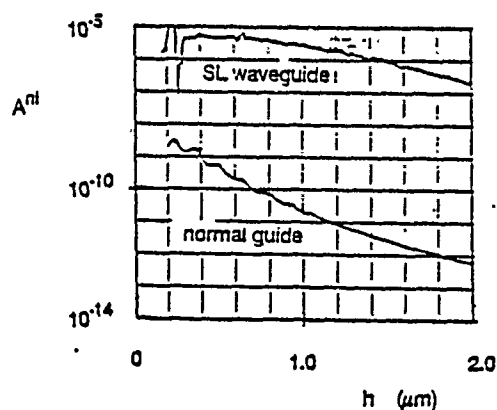


Figure 2.
Enhancement in harmonic signal (log scale)
as a function of waveguide thickness.

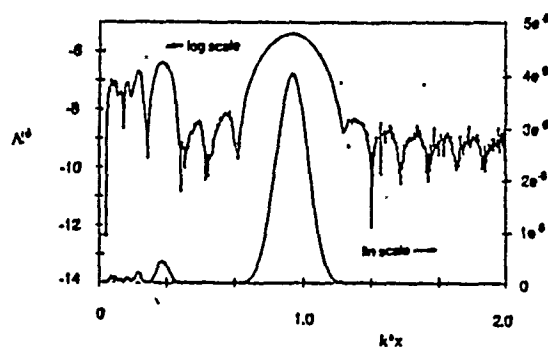


Figure 3.
Harmonic signal as a function of
the superlattice period. Same curve on
a linear and log scale.

Demonstration of Cascadability and Spectral Bistability In Bistable Diode Laser Amplifiers

Zeqi Pan, Tie-Nan Ding, and Mario Dagenais
Department of Electrical Engineering
and

Joint Program for Advanced Electronic Materials
University of Maryland
College Park, Maryland 20742

Summary

We report the demonstration of cascadability in bistable diode laser amplifiers operated below threshold. A schematic of the experimental set-up is shown in Figure 1. There it is shown that the optical input to the first bistable diode laser amplifier is modulated by a mechanical chopper at frequency Ω_1 . The output from the first bistable diode laser amplifier is then modulated at $\Omega_2 = 2\Omega_1$ using a second mechanical chopper. The light is thereafter used as the input to the second bistable device. When the input intensity to the second device is higher than a certain threshold, the output switches. These results are shown in Figure 2. For these experiments, each of the bistable diode laser amplifiers were carefully studied. Detailed bistability measurements at different bias currents and different cavity detunings were performed. It was found that both the bistability loop and the switching power gets larger as the detuning increases. The size of the hysteresis loop also increased as the laser was operated closer to threshold. In a two beam experiment, it was found that the switching power in the data beam can be as small as 25 nW. Gains larger than 1000 have been demonstrated, indicating the large fan-out capability of these devices. The turn-on and turn-off times in these bistable diode laser amplifiers was measured to be faster than 1 ns and detector limited. These bistable diode laser amplifiers are the most efficient optical devices that have yet been demonstrated and will find applications in photonic switching networks.

In a separate set of measurements performed on diode lasers operated above threshold, it was found that by injecting light slightly detuned from a cavity resonance, detuned itself 4 or 5 cavity modes away from the lasing mode, it was possible to quench the lasing mode of the laser. In these experiments, when monitoring the transmitted light at the lasing frequency, very large clockwise bistability loops were observed. This new type of bistability was called spectral bistability. Our results are shown in Figure 3. The contrast ratio between the on and off states was measured to be better than 40. This logic device appears particularly appropriate for implementing NOR and NAND logic operations. When monitoring the transmitted intensity at the wavelength of the injected light, normal counterclockwise hysteresis loops are obtained. This device will find applications in systems requiring wavelength switching or in optical self-routing networks.

Output From First Switch

Modulated Input to Second Switch

Output From Second Switch

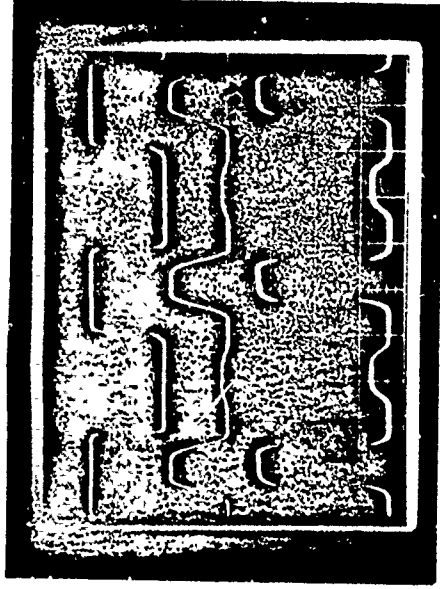


Figure 2. Demonstration of cascability in diode laser amplifiers

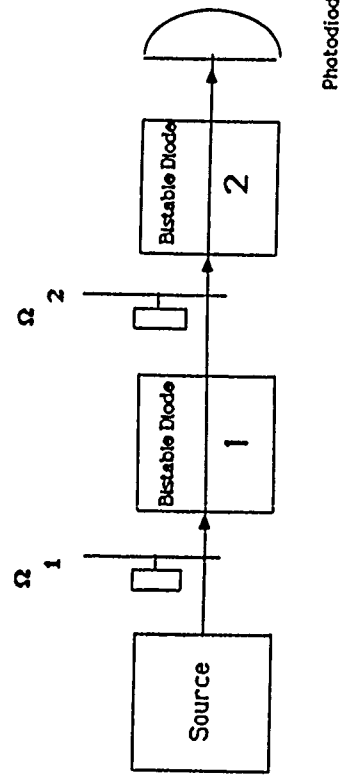


Figure 1. Experimental set-up for the cascability experiment

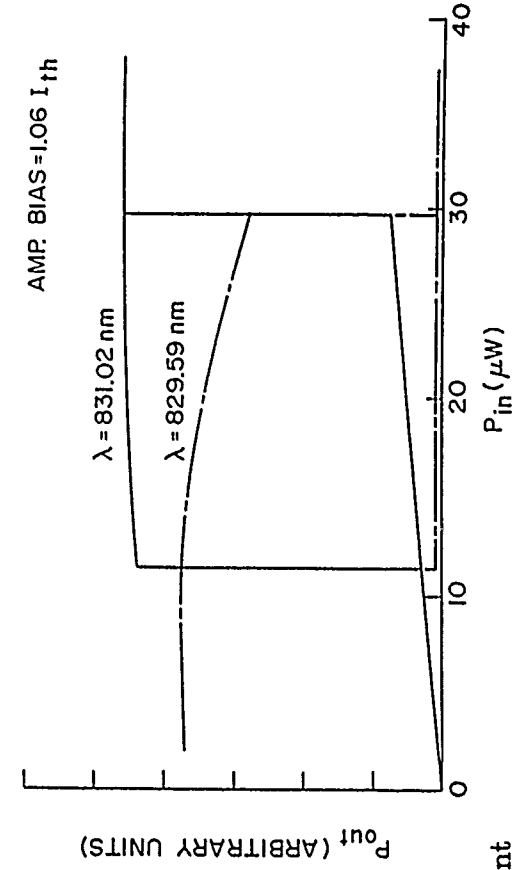


Figure 3. Demonstration of spectral bistability. $\lambda_{injection} = 831.02$ nm

WP31 **Optical Bistability and Switching by Nonlinear Waveguiding in Semiconductor Lasers and Laser Amplifiers**

John G. McInerney,* Li Yuan and Theodore C. Salvi

*Optoelectronic Device Physics Group
Center for High Technology Materials
University of New Mexico
Albuquerque, NM 87131, USA*

Daniel M Heffernan

*School of Physical Sciences
Dublin City University
Glasnevin, Dublin 9, Ireland*

SUMMARY

Bistable optical devices (BODs) are interesting for optical switching, limiting, memory, signal conditioning and logic [1]. Semiconductor-based BODs are especially promising because their large nonlinearities should permit development of compact, rugged and efficient systems. Here we concentrate on active semiconductor BODs and switches, that is those which have internal gain, such as injection lasers and amplifiers.

Semiconductor injection lasers are now used extensively as sources in optical communication and data storage, while superluminescent injection laser amplifiers are finding increasing use in fiber optics. These devices have intrinsic nonlinearities which, while undesirable for their usual applications, may well allow effective optical bistability and switching. In many cases these functions are limited by nanosecond carrier lifetimes [2]. Here we explore the phenomenology of nonlinear waveguiding, that is of modification of the index profile of a waveguide by the beam propagating therein, or by an external signal. We describe two systems in which we make use of nonlinear waveguiding to produce single-channel bistability or switching.

The first system consists of two weakly-guiding injection lasers or amplifiers longitudinally coupled in an external resonator. The system can operate in two modes: in the first, which is analogous to a combination of a source and saturable absorber, the switching transitions are limited by the spontaneous carrier lifetime. In the second mode of operation, the system acts as a combination of a source, self-focusing element and apertured retro-reflector. The latter mode allows photon-lifetime limited switching, which is potentially faster. An analytical model has been developed whose results agree well with experimental data. However, this system is complicated and is susceptible to slow self-pulsations in either mode of operation [3].

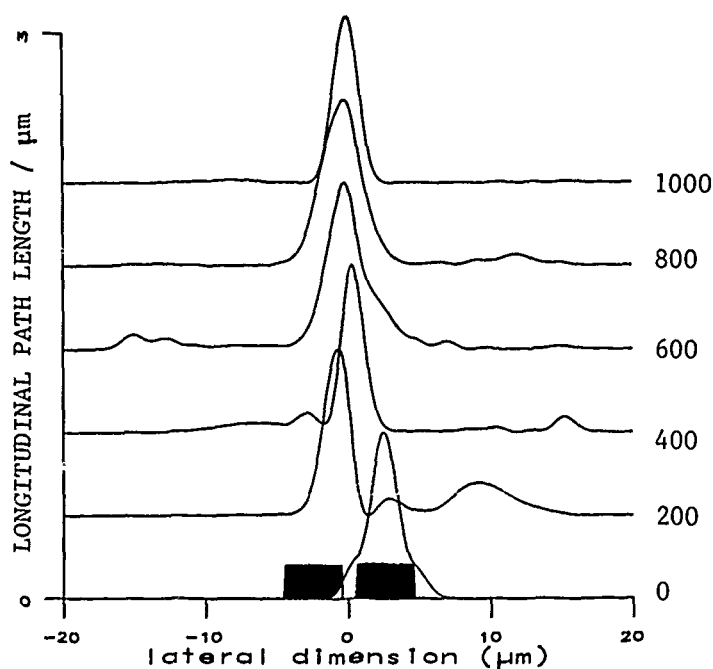
We then consider a second structure intended to overcome some of the limitations of longitudinally coupled systems. It consists of two laterally coupled active guides integrated monolithically on a semiconductor wafer. Theoretical results based on a numerical model indicate that an optical signal

can be injected into one of the guides and switched into the other by nonlinear guiding [4], as illustrated in Figure 1 for a gain-guided structure with two $3\text{ }\mu\text{m}$ stripes separated by $1\text{ }\mu\text{m}$. Index-guided devices have also been simulated. We shall assess the potential switching speeds and powers of such twin-stripe amplifier structures, and examine some experimental results, including those reported in the literature [5] concerning the conceptually similar twin-stripe injection laser. Diffusion-limited switching times of $\sim 10\text{ ps}$ should ultimately be possible.

REFERENCES

- 1 H M Gibbs, "Optical bistability - controlling light with light", Academic Press, New York, 1985.
- 2 J G McInerney and D M Heffernan, "Optical bistability in semiconductor injection lasers", IEE Proc. J - Optoelectronics 134, 41 (1987).
- 3 D M Heffernan, J McInerney, L Reekie and D J Bradley, "Bistability by induced waveguiding in coupled semiconductor lasers", IEEE J. Quantum Electron. QE-21, 1505 (1985).
- 4 T C Salvi, Y Li and J G McInerney, "Lateral mode bistability due to nonlinear waveguiding in semiconductor injection lasers", Proc. 1989 Annual Meeting of IEEE Lasers and Electro-Optics Society (LEOS '89), Orlando, FL, Oct. 1989, Paper OE13.6.
- 5 I H White and J E Carroll, "Optical bistability in twin-stripe lasers", IEE Proc. H - Microwaves, Antennas and Propagation 131, 309 (1984).

FIGURE 1: Propagation of light in a gain-guided laser amplifier, with closely coupled twin stripes indicated by the dark boxes. Complete right-to-left power switching requires $\sim 500\text{ }\mu\text{m}$.



**THURSDAY, JULY 19
ORAL PRESENTATIONS**

Nonlinear Optical Effects in GaAs/AlAs Type-II Heterostructures

G. R. Olbright, A. Owyong, and J. F. Klem

Sandia National Laboratories, Albuquerque, New Mexico, 87185†

SUMMARY

We report on femtosecond and quasi-steady state nonlinear spectroscopic studies of narrow-well Type-II GaAs/AlAs heterostructures. We observe a large intensity-dependent blue shift of the heavy-hole (HH) exciton absorption peak as well as a concomitant blue shift of the Γ -X indirect luminescence peak.¹ In addition, we describe femtosecond transmission measurements of this Type-II system in which an applied axial electric field has biased the levels into the region of an indirect/direct anti-crossing.² The femtosecond absorption spectra show intriguing transient energy shifts of the HH exciton. At high fields we report a transient red-shift while a transient blue shift is observed at low fields. These shifts are discussed in terms of the electric-field-dependent Γ -X splitting.

In Fig. 1a we show the potential-energy diagram of a GaAs/AlAs Type-II structure. The ~ 80 meV separation of the Γ and X levels requires a field of $\sim 27 \times 10^4$ V/cm to bring the levels into alignment. Figure 1b shows photoluminescence (PL) spectra of one of our samples (grown as a p-i-n photodiode) under flatband and high-field conditions. As expected,² a dramatic enhancement of the PL is observed at high fields. Corresponding absorption spectra in Fig. 2a show the presence of a field-induced red shift of the HH exciton produced by the quantum-confined Stark effect.

The absorption spectra shown in Figure 1c illustrate the nonlinear response of our Type-II heterostructure to 25 nsec duration excitation. Spectra are taken 40 nsec after pulsed excitation over a range of intensities corresponding to carrier densities to $5 \times 10^{11}/\text{cm}^2$. The distinctive blue shift and bleaching of the HH exciton along with negligible effects on the light-hole exciton may be understood in terms of phase-space filling effects in the optically generated dense heterogeneous Fermi gas¹ (spatially separated electron and hole plasmas). We also observe a pronounced blue shift in Γ -X luminescence spectra under these conditions. In this latter case, however, the shift is produced by the space-charge field resulting from the spatially separated electron and hole plasmas.³

In Figure 1d we show transient differential transmission spectra (DTS) taken at high fields using femtosecond pump/continuum-probe spectroscopy. These spectra reveal a pronounced transient red shift of the HH exciton. This red shift arises from modifications of the many-body plasma effects due to changes in the Γ -X splitting produced by varying the applied electric field. In contrast, at low fields, we observe a transient blue shift. In this latter case, the shift is evidence of the formation of electron/hole space-charge layers^{1,3} resulting from the subpicosecond transfer of electrons from the GaAs Γ point to the AlAs X point.⁴

In summary, we have observed striking features on the absorption and luminescence spectra of Type-II GaAs/AlAs superlattices due to the influences of electric field and carrier density on carrier-carrier interactions through the Γ -X splitting.

† Supported by the Department of Energy under contract No. DE-ACO4-76DP00789.

1. G. R. Olbright, W. S. Fu, A. Owyong, J. Klem, R. Binder, I. Galbraith, and S. W. Koch, Papers QWA2 and QWA3, 17th International Quantum Electronics Conference, Anaheim, June 21-25, 1990.
2. M.-H. Meynadier, R. E. Nahory, J. M. Worlock, M. C. Tamargo, J. L. de Miguel, and M. D. Sturge, Phys. Rev. Lett. **60**, 1338 (1988).
3. G. R. Olbright, J. Klem, A. Owyong, T. M. Brennan, R. Binder, and S. W. Koch, to be published J. Opt. Soc. Amer. B, July (1990)
4. J. Feldmann, R. Sattmann, E. O. Göbel, J. Kuhl, J. Hebling, K. Ploog, R. Muralidharan, P. Dawson, and C. T. Foxon, Phys. Rev. Lett. **62**, 1892 (1989).

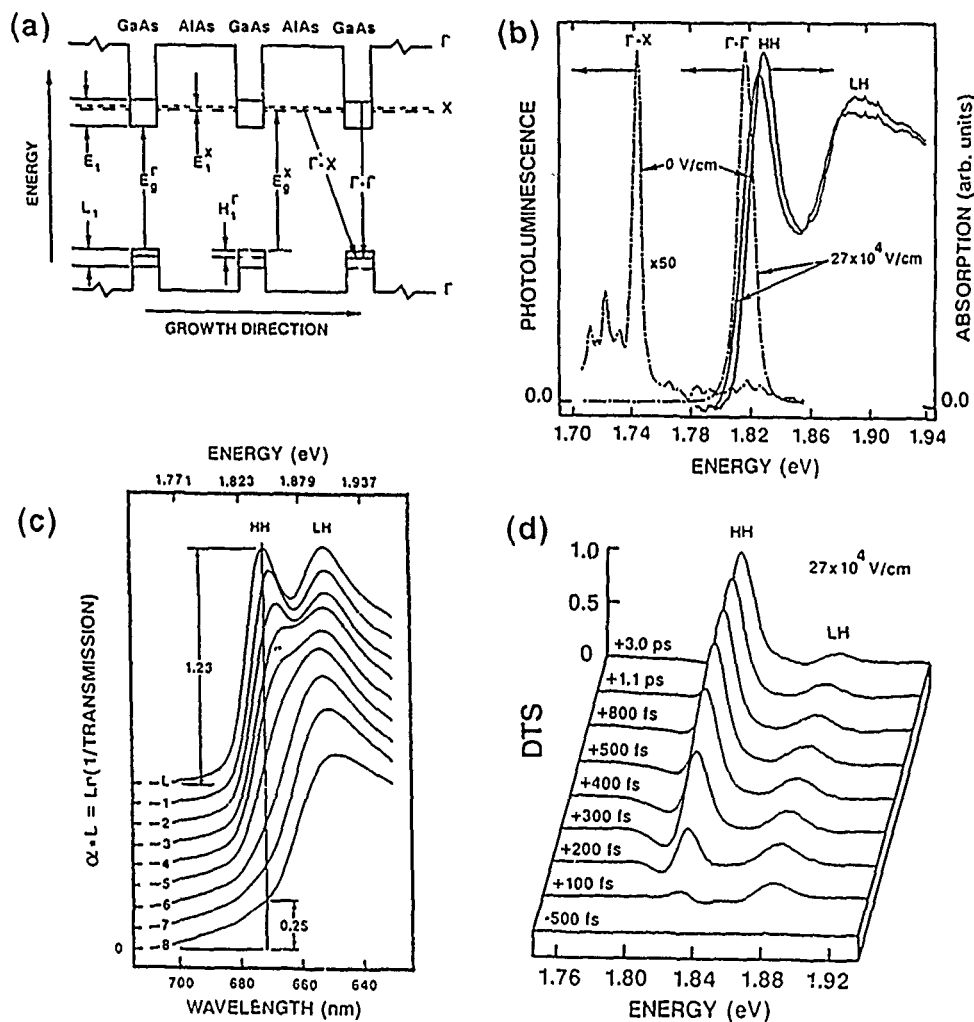


Fig. 1 (a) Crystal structure in the growth direction of a Type-II heterostructure for the flat-band case, where E_1^Γ and E_1^X are the direct- and indirect-bandgap energies, respectively. E_1^Γ , H_1^Γ , L_1^Γ and E_1^X are the quantum confinement energies of the direct electron, heavy-hole, light-hole, and indirect electron levels respectively. Both the direct, Γ - Γ , and indirect, Γ - X , recombination channels are shown with downward arrows; (b) Electric-field-dependent absorption and PL spectra for a p-i-n photodiode. The active region consists of 90 periods of GaAs(30Å)/AlAs(80Å), $I=1 \text{ W/cm}^2$; (c) Excitation-intensity-dependent absorption spectra taken on an undoped GaAs(29Å)/AlAs(90Å) superlattice. L =linear spectra, $I_{1-8} \approx 5, 8, 10, 12, 15, 25, 35, 45 \text{ kW/cm}^2$; (d) Transient differential transmission spectra. The pump energy used for (a)-(d) above is 1.96 eV and $T=15 \text{ K}$.

TH13 Two-Color, Ultrafast, Anisotropic Transient Grating Separation of Photorefractive, Bound-Electronic and Free-Carrier Grating Dynamics in Zincblende Semiconductors

A. L. Smirl, W. A. Schroeder, M. D. Dawson, T. S. Stark, and T. F. Boggess
Center for Laser Science and Engineering, University of Iowa, Iowa City, IA 52242

We describe a novel nondegenerate, polarization-sensitive, transient-grating technique, which we use to isolate, to probe the symmetry of, and to time resolve (with resolution < 5 -ps) the individual dynamics of several co-existing gratings written in GaAs:EL2 and CdTe:V. Specifically, we utilize optically-induced anisotropy to allow the first temporal resolution of the formation and decay of photorefractive gratings in these semiconductors on picosecond timescales. The measurements allow us to identify various contributions to the photorefractive effect, including the first direct evidence of a photorefractive grating arising from the Demmer field associated with free electron hole pairs. The technique also allows the instantaneous electronic and the cumulative free-carrier gratings (which normally obscure the weaker photorefractive grating) to be simultaneously monitored. Measurements were conducted with a unique, amplified, Styryl 13 dye laser system that was developed for these studies.

For these measurements, the gratings were written by two 1-psec pulses, at 960 nm with fluences of between $6 \mu\text{J}/\text{cm}^2$ and $3 \text{ mJ}/\text{cm}^2$. The writing beams were s-polarized and had equal fluences to eliminate transient energy transfer between the two beams. The pulses were produced by a Styryl 13 dye laser (synchronously pumped by the frequency-doubled, fiber-grating-compressed output of a mode-locked Nd:YAG laser) followed by a three-stage amplifier (which was pumped by the frequency-doubled output from a 10 Hz regenerative amplifier). The s-polarized "readout" beam was generated by Raman-shifting a fraction of the 960 nm radiation in benzene to produce a $1.06 \mu\text{m}$ pulse with a measured duration < 5 -ps. A frequency-shifted probe is necessary in the Bragg regime to allow separation of the diffracted signal from the transmitted pump beams. Furthermore, since backward readout configurations are limited in temporal resolution by the sample thickness, a forward traveling probe was used. The diffracted signal was measured as a function of time delay, pump fluence, and analyzer angle. The "photorefractive-cut" samples were oriented with the (100) crystallographic axis orthogonal to the grating wave vector, which for zincblende symmetry dictates that only the photorefractive grating will rotate the polarization of the diffracted probe. Consequently, the photorefractive contribution can be isolated from stronger free-carrier and electronic Kerr gratings by an analyzer oriented to transmit p-polarization.

The non-photorefractive signal, which was isolated by measuring the s-polarized component of the diffracted probe, exhibits three distinct features, all of which were independent of crystal orientation. An initial peak, which is symmetric about zero delay and has a third-order power law dependence, is associated with the instantaneous electronic index change (n_2). This peak is superposed on a broader feature arising from the accumulation of free electrons produced by the single-photon ionization of the midgap donors and from the accumulation and partial decay (by ambipolar diffusion) of an electron-hole grating produced by two-photon and step-wise (through midgap levels) two-photon absorption. The free carrier grating is prevented from decaying completely by the space-charge field associated with the ionized donors. This is manifested in a much weaker signal, that is observed to persist for delays greater than 100 ps.

The photorefractive signal, which was measured by detecting the p-polarized component of the diffracted probe, is also characterized by three distinct features. The grating exhibits an initial transient response (the origin of which is still under investigation) which has a rise time determined by the temporal integration of the probe pulse and a decay shorter than our temporal resolution. This is followed by a signal that is consistent with diffraction from a photorefractive grating associated with the space charge field between electron-hole pairs (i.e., the Demmer field), since it decays with a time constant determined by ambipolar diffusion. At longer delays we observe a weaker persistent signal associated with the space charge field between free electrons and ionized donors. We emphasize that no p-polarized signal was observed when the crystal was oriented with the (100) axis parallel to the grating wave vector.

Nonlinear Optical Effects in Visible-Band-Gap Semiconductors and Microcrystallites

F. Henneberger

Humboldt - Universität zu Berlin, Sektion Physik, Invalidenstr.110,1040 Berlin

Semiconducting II - VI compounds (CdS, CdSe, ZnSe, etc.) are materials that exhibit very large and fast optical nonlinearities in the vicinity of their fundamental absorption edge at room temperature [1]. Varying the compound or the composition one can use these semiconductors for nonlinear optical applications in the entire visible part of the spectrum.

The first part of the paper deals with the nonlinear optical response of bulk materials. The physical processes behind (exciton - screening, gap - shrinkage, bandfilling) are briefly discussed and compared with experimental data. The basic quantities (change of absorption and refraction per electron - hole pair per material unit volume) deduced by various experimental techniques are summarized and some low - power applications are demonstrated. The switching transients are studied by fs excite - and - probe and grating experiments.

The second part of the paper is addressed to the question, how the nonlinear response of these materials is changed in the situation of zero - dimensional quantum confinement. In specially prepared glasses II - VI microcrystallites were grown , the size of which is in the order or below the exciton bulk radius. By means of nonlinear absorption, hole - burning, and ps - luminescence experiments conclusions are drawn on the electronic structure of the dots, the homogeneous and (size - fluctuation induced) inhomogeneous line broadening, and the carrier kinetics. The data suggest further, that the nonlinearity is two - level - like, that is different to the bulk. Finally, electro - optical effects in II - VI quantum dots are discussed.

[1] F. Henneberger, J. Puls, H. Rossmann, U. Woggon, S. Freundt, A. Schülzgen, and Ch. Spiegelberg, Proc. 4th Internat. Conf. on II - VI Compounds, Berlin (West) 1989, J. Crystal Growth, in the press.

Degenerate Resonant Four Wave Mixing of Laser Radiation in a Plasma

C. Joshi

*Electrical Engineering Department, University of California, Los Angeles
Los Angeles, California 90024*

Although four wave mixing has been demonstrated in solids, liquids and gases using both resonant as well as non-resonant media, no conclusive demonstration of this phenomenon in plasmas has been reported. In plasmas there are two mechanisms that can excite standing density gratings necessary for degenerate four wave mixing (DFWM): the ponderomotive force resulting from the beating of each of the two pump waves with the probe wave and the thermal force resulting from localized collisional heating. In addition, there are two strong resonances in an unmagnetized plasma: the ion acoustic resonance and the Bohm-Gross resonance occurring close to the electron plasma frequency. Four wave mixing at these resonances is expected to yield higher probe beam reflectivities compared to the DFWM alone. The third order susceptibility χ_3 responsible for DFWM in a plasma is given by

$$\chi_3 \cong \frac{n_0/n_c^2}{8(4\pi)^2(T_e + T_i)} \left[1 + \sum \frac{n_0 v_e}{k_g^2 \kappa_e} \right].$$

The first term is the contribution to χ_3 due to ponderomotive force whereas the second term is the additional contribution to χ_3 due to collisional heating. Here v_e is the electron-ion collision frequency, κ_e is the electron thermal conductivity and k_g is the wavenumber of the plasma grating. When the electron mean free path becomes small compared to the grating wavelength, the thermal contribution to χ_3 can be significant. We will report experimental observation of such a collisionally dominated DFWM in a plasma using CO₂ laser light.

When the pump and the probe beat in the plasma at the ion acoustic frequency, the grating density fluctuations are enhanced by a factor $\left[\frac{\text{Re } \omega}{\text{Im } \omega} \right]$ compared to the DFWM case. Since this ratio is a function of the electron to ion temperature ratio, whereas the ion acoustic frequency is a function of $(ZT_e + 3T_i/M)^{1/2}$ we can obtain ion and electron temperatures. We have also observed this signal enhancement by beating the pump and the probe waves at the ion acoustic resonance in the plasma.

Finally, we shall present evidence of FWM at the electron plasma frequency resonance. A series of Stokes and anti-Stokes sidebands to the pump frequency are observed each separated by the electron plasma frequency.

Applications of DFWM and resonant four wave mixing in a plasma will be mentioned.

M. ORIA, M. CHEVROLIER, D. BLOCH, M. FICHET and M. DUCLOY

Laboratoire de Physique des Lasers,
Université PARIS-NORD,
Villetaneuse, France

In this talk, we review the properties of resonant atom-light interaction, close to interfaces between vapors and solid media (metal or dielectrics). These interaction processes are explored by monitoring the light reflected from the interface (reflection spectroscopy). This quantum optics at interfaces can be considered as quantum optics in 2 D-confined space, as light reflection originates in a wavelength-deep gas layer (open microcavity of transverse extension $\sim \lambda$).

Atom-light interaction processes are modified by the proximity of the surface in two ways :

(i) Atom-surface collisions abruptly interrupt the light interaction and destroy the induced dipole. The resulting transient behavior of atoms leaving the interface is responsible for the non-local character of the electric dipole polarization. In the case of normal incidence, the reflection signal gets predominantly sensitive to the atoms moving along the surface, which interact with light for long times without phase interruption. In this way, one simultaneously gets velocity selection and space confinement : this opens the way to studying velocity-selected, space-confined, resonant systems.

(ii) Another modification of the atom-light interaction comes from the long range atom-wall interaction forces : Van der Waals attractive potential shifts the atomic energy levels and open micro-cavity effects alter the spontaneous emission rate via vacuum fluctuation changes and self-reaction of the electric dipole image by the partially reflecting wall.

Experimental tests of the above properties have been performed on cesium vapor with diode lasers. Doppler-free reflection signals have been monitored at normal incidence, via frequency modulation of the laser beam. Spectral red shift of the Cs resonance line, induced by the atom-dielectric-wall Van der Waals interaction potential has been

demonstrated for the first time, as well as lineshape asymmetry which has been successfully compared with theoretical predictions.

Extension to non linear reflection spectroscopy has been performed: saturated absorption and dispersion spectroscopy in stationary evanescent waves, or inhomogeneous surface waves (surface plasmons), saturated reflection spectroscopy at normal incidence. Applications of these non linear optical phenomena to the analysis of adsorption/desorption processes will be discussed, along with the generalization to high-order non linear processes in intense inhomogeneous waves and the implication in compact diode laser frequency stabilization schemes.

Depletion, Diffraction and Partial Coherence in Non-Linear Optical Mixing

M. Nieto-Vesperinas and G. Lera
Instituto de Optica, C.S.I.C.
Serrano 121, 28006 Madrid, Spain

The coupled wave equations governing the wave-mixing effects in non-linear optics are usually addressed either by neglecting beam diffraction [1] (parametric approximation, PA) or by ignoring depletion effects [2-4]. It is, however useful to have theories that can deal with both aspects of the interaction.

A paraxial approximation (PXA) for optically isotropic media was initially established [5]. More recently, methods including depletion, non-paraxial diffraction and anisotropic propagation in uniaxial crystals have been developed both for difference-frequency (DF) and second harmonic (SH) generation [6,7]. The theory put forward considers, nevertheless, co-propagating beams only.

In addition, this model shows that the validity of the parametric approximation, as used in difference-frequency generation, is not sufficiently justified by the low conversion efficiency of the output beam, as usually stated, but also depends on the mutual conversion between the pumping waves. Thus, although the efficiency of the DF wave may be low due to its lower frequency, the conversion between the pumping beams (of larger frequencies) may still be large, thus making the PA inappropriate.

The same method can be applied to studying the influence of the spot size, frequency and state of polarization of the pumping beam in the SH wave. It shows that the effect of diffraction depends both on the efficiency of the process and the structure of the beam. On the other hand, the polarization of the angular components of the interacting beams also play a very important role.

The influence of the coherence properties in beam propagation has been noticed in some works on SH generation [8,9], and they predict a significant increase in the efficiency of the process under not complete coherence of the input beam. The method that we have developed also permits to incorporate partial coherence effects together with depletion effects. This permits to investigate the effect of the coherence radius on the efficiency, (which not always increases as coherence decreases, like predicted by the PA approximation). Also, the behavior of the statistics of the SH intensity can be studied by this theory [10].

The influence of the spatial structure and statistics of the pumping beams is also investigated in phase conjugation by four wave mixing [10]. This research shows that the reflectivity varies in the phase conjugator when the phase factor is not constant in the set of coupled equations governing the process. The mutual coherence function of the field generated can be in this way calculated from the mutual reflectivity of the mirror. This has been done for two well-known statistics of the partially coherent pumping beams. Also the analysis of the effects of diffraction reveals that it degrades the fidelity of the conjugation.

ACKNOWLEDGMENTS

Work supported by the Comision Interministerial de Ciencia y Tecnología under grant PB0278.

REFERENCES

1. J.A. Armstrong, N. Bloembergen, J. Ducuing and P.S. Persham, Phys. Rev. 127, 1918 (1962).
2. G.D. Boyd, A. Ashkin, J.M. Dzidic and D.A. Kleinman, Phys. Rev. 137 A, 1305 (1965).
3. G.D. Boyd and D.A. Kleinman, J. Appl. Phys. 39, 3597 (1968).
4. J.R. Morris and Y.R. Shen, Phys. Rev. 15, 1143 (1977).
5. S.C. Sheng and A.E. Siegman, Phys. Rev. 21, 599 (1980).
6. M. Nieto-Vesperinas and G. Lera, Opt. Comm. 69, 329 (1989); J. Opt. (Paris) 20, 169 (1989).
7. G. Lera and M. Nieto-Vesperinas, J. Mod. Opt. 8, 1121 (1989).
8. M.S. Zubairy and J.K. McIver, Phys. Rev. A 3, 856 (1985).
9. N.A. Ansary and M.S. Zubairy, Opt. Comm. 59, 390 (1986).
10. G. Lera and M. Nieto-Vesperinas, Opt. Comm. 73, 244 (1989).
11. G. Lera and M. Nieto-Vesperinas, Phys. Rev. A (May 1990).

Effects of Quantum Fluctuations on Raman Soliton Formation

J. L. Carlsten
Physics Department
Montana State University
Bozeman, MT 59717

Summary

Solitons in Stimulated Raman Scattering (SRS) were first observed in 1983 in CO_2 pumped para- H_2 .¹ Although their origin was not fully understood at the time, theoretical studies¹⁻⁶ indicated that a π phase shift in the Stokes beam could initiate the formation of the soliton. To test this conjecture, electro-optic π phase shifts were experimentally⁷ put into the Stokes beam to induce soliton formation, but surprisingly the height of the solitons was found to be highly variable.

Recent experiments⁹ on Raman scattering with visible lasers have shown that quantum fluctuations can lead to frequency variations within the gain narrowed Raman linewidth in a Raman generator. Based on Druhl's¹⁰ prediction that detuning will lead to soliton decay, it was then suggested⁹ that these frequency variations might explain the variation in soliton heights seen experimentally. Experiments performed recently¹¹ with visible lasers have measured the distribution of heights of solitons initiated by electro-optic π phase shifts and compared this distribution to the predictions of soliton decay due to detuning. The qualitative agreement suggests that the decay of solitons induced by electro-optic phase shifts is indeed related to frequency variations caused by quantum fluctuations.

Quantum fluctuations also play a role in the formation of spontaneous solitons in SRS. Englund and Bowden¹²⁻¹⁴ predicted that quantum noise can lead to a phase wave which can trigger the soliton formation just as the electro-optic π -phase shift did. Recently these spontaneous solitons have been observed¹⁵ and the statistics of the formation compared to the predictions of Englund and Bowden. While the experimental findings agree qualitatively with the predictions, differences are seen which may be due to finite time response of the detectors used which was not included in the theory. On the other hand the experimental delay time statistics appear to be close to that expected from theory, although the asymmetry in the distribution for both experiment and theory is not well understood.

Finally there have been several other experiments relevant to the formation of spontaneous Raman solitons. Midorikawa *et al.*¹⁶ have detected the π -phase shift using heterodyne phase detection in conjunction with observation of the Raman soliton. In addition Raymer, Li and Walmsley¹⁷ have studied temporal quantum fluctuations and have emphasized that the occasional formation of the second coherent mode can lead to the π -phase shift which causes the spontaneous soliton.

This work was supported by National Science Foundation Grant No. PHY-8900282.

References

1. K. Druhl, R.G. Wenzel, and J.L. Carlsten, Phys. Rev. Lett. 51, 1171 (1983).
2. K. Druhl, J.L. Carlsten, and R.G. Wenzel, J. Stat. Phys. 36, 615 (1985).
3. K. Druhl and G. Alsing, Physica 20D, 429 (1986).
4. H. Steudel, Opt. Commun. 57, 285 (1986).
5. D.J. Kaup, Physica 19D, 125 (1986).
6. J. R. Ackerhalt and P. W. Milonni, Phys. Rev. A33, 3185 (1986).
7. However, it should be noted that the soliton pulse, for a finite duration pump pulse, eventually will propagate to the back of the pump pulse and disappear. See C. R. Menyuk, Phys. Rev. Lett. 62, 2937 (1989).
8. R.G. Wenzel, J.L. Carlsten, and K.J. Druhl, J. Stat. Phys. 39, 621 (1985).
9. D.C. MacPherson, R.C. Swanson, and J.L. Carlsten, Phys. Rev. Lett. 61, 66 (1988).
10. M. Yousaf, K.J. Druhl, and S.A. Shakir, Physica 30D, 228 (1988).
11. D.C. MacPherson, R.C. Swanson, and J.L. Carlsten, Phys. Rev. A39, 6078 (1989).
12. J.C. Englund and C.M. Bowden, Phys. Rev. Lett. 57, 2661 (1986).
13. C.M. Bowden and J.C. Englund, Optics Comm. 67, 71 (1988).
14. J.C. Englund and C.M. Bowden, SPIE, Vol. 874, 218 (1988).
15. D. C. MacPherson, R. C. Swanson, and J. L. Carlsten, Phys. Rev. A40, 6745 (1989).
16. K. Midorikawa, H. Tashiro, Y. Akiyama, and M. Obara, Phys. Rev. A41, 562 (1990).
17. M.G. Raymer, Z.W. Li, and I.A. Walmsley, Phys. Rev. Lett. 63, 1586 (1989).

Sien Chi

Institute of Electro-Optical Engineering, National Chiao Tung University,
Hsinchu, Taiwan 30050, China

We review the soliton propagations in lossless fibers and in lossy fibers with Raman pumps.

In particular, we will discuss the interaction of optical solitons with a forward Raman pump wave, the optical solitons near zero-dispersion regime, and the Raman cross talk of the soliton collision.

If the relative group velocity between the pump wave and the soliton is sufficiently large, the depletion of the pump wave is uniform and the local interaction in time domain can be neglected. The relative group velocity between the backward pump wave and the soliton is large enough, but it is not generally true for the forward pump wave since it copropagates with the soliton. It is found that when the relative velocity is small and the soliton pulse width is short, the soliton frequency is shifted by the interaction. Near zero relative velocity the pulse shape is distorted, in addition to having a frequency shift.

The soliton propagation in a periodically Raman pumped fiber has been studied extensively. The stability of the soliton depends on the magnitude of the pulse energy. It is found that pulse shape distortion and velocity change are reduced near zero dispersion regime.

The cross talk induced by soliton collision with a Raman effect in a lossless fiber is discussed. There are frequency-shift enhancements for the two colliding solitons in addition to the energy transfer. The maximum rate-distance product limited by energy depletion is obtained for the soliton-based wavelength-division-multiplexing system.

The most fundamental nonlinear manifestations of nonlinear effects in light propagation occur when the matter is presented either by a single elementary particle (e. g. a single electron) or there is no matter at all (i. e. in vacuum), and when the nonlinearity is strictly due to relativistic (as in the case of a single electron) or QED (as in the case of vacuum) effects. These two fundamental phenomena could be observed at drastically different scales of the laser intensity: from 10^{-10} W/cm^2 in the former case to 10^{17} W/cm^2 in the latter case.

Due to the combination of a relativistic mass-effect, the Lorentz force, and the Doppler effect, a host of nonlinear interaction of light with a single cyclotron electron is possible. The first theoretically predicted [1] and experimentally observed [2] nonlinear effect with a single electron was the hysteretic (bistable) excitation of electron at the main resonance (i.e., when $\omega = \Omega$, where Ω is the cyclotron frequency and ω is the driving frequency), the hysteresis being attributed to a small relativistic change of an electron's mass. Other nonlinear optical effects [3,4] (due also to the Lorentz force and the Doppler effect) include multiphoton excitation of electron by a biharmonic laser pumping, having frequencies ω_1 and ω_2 such that $\omega_1 - \omega_2 = n\Omega$ ($n = 1, 2, \dots$) with $\omega_1, \omega_2 \gg \Omega$ (the so called cyclo-Raman excitation [3,4]), excitation of very high-order subharmonics [4,5] of the incident laser frequency ω such that $\omega = N\Omega$ ($N \gg 1$ being the integer), etc.

The power of laser light required to observe most of these effects is strikingly low (owing to a very low energy loss of a single electron via its synchrotron radiation) ranging from milliwatts to microwatts which allows one to use conventional cw lasers (e.g., He-Ne). All of these effects exhibit pronounced hysteresis attributed to the relativistic mass-effect. When the laser power increases, the cyclo-Raman multiphoton excitation [3,4] (with $\omega_1 - \omega_2 = n\Omega$) features allowed and prohibited excitation orbits. Using either subharmonic (with $N = 10^2 - 10^3$) or multiphoton excitation, an electron can be accelerated [4] to relativistic energies (e.g., 1 Mev and higher) in what amounts to a cw laser-driven accelerator with low required laser power (a few watts). High-order subharmonics can also provide coherent links between laser frequency standards in the optical range and molecular or atomic clocks in the microwave range [4,5].

The quantum theory of the hysteretic excitation (which is a common feature of nonlinear excitations in the system), shows that the upper (i.e., higher energy) branch of hysteretic curve predicted by the classical theory should slowly decay. However, when the driving frequency is swept sufficiently fast, the energy of quantum excitation as an increasing function of time, consists of "quantum stairs" each of which corresponds to the electron hopping abruptly from one state to the adjacent one.

In the absence of any matter, light may experience very weak nonlinear self-interaction via generation of virtual couples of particle+antiparticle (e. g. electron+positron), almost instant annihilation of which produces new photons that may have (in general) different frequencies and directions of propagation; the total energy and momentum of the field is conserved. This so-called photon-photon scattering [6] is one of the most fundamental QED mechanisms giving rise to nonlinear optical

effects in a vacuum; its experimental observation may provide a nonlinear optical test of QED. Previously proposed effects such as the birefringence of the refractive index for a probe field in a dc magnetic (or electric) field [7] or intense laser field [8], and multi-wave mixing processes [9], required too large intensities of optical field. The photon-photon scattering originates nonlinearity which for the fields much smaller than critical QED field ($H_{cr} \simeq 5 \times 10^{13} \text{ G}$), corresponds to a third-order nonlinearity of classical nonlinear optics, with a characteristic degeneracy, however: a single monochromatic plane wave does not exhibit any nonlinear effect. That degeneracy is broken if either (i) the wave is nonplanar or nonmonochromatic, or (ii) a strong static field is present. Both cases can result in birefringence of the refractive index for a probe field [8,9].

We have showed recently [10] that due to a broken symmetry, a dc magnetic field can also give rise to second-order nonlinear optical effects similar to those found in third-order nonlinear materials with an external dc field. In particular, we have demonstrated the feasibility of optical second harmonic generation (SHG) of the fundamental wave using available high-power laser systems [10]. Since only a second-order effect for the optical field is involved, the laser power required to observe SHG is much lower than in previously proposed effects [7-9]. The SHG photons will also be registered at a frequency different from the fundamental frequency injected into the system, which may result in higher sensitivity. Various aspects of new phenomenon including prospects for a possible experiment are discussed in the presentation by Y. J. Ding and this author at this conference. As one of examples, we consider a configuration with a pulsed magnetic field $H_0 \simeq 8 \times 10^6 \text{ G}$ with bore diameter $\simeq 3 \text{ cm}$ and a high power pulsed Nd:Glass laser with $\lambda_1 \sim 0.35 \mu\text{m}$ (NOVA), $\tau_p \sim 10^{-9} \text{ sec}$, providing the laser energy of 6-10 KJ/pulse in each of 10-12 beam lines. We show that in such a case the number of the SHG photons in each of the beams lines is $\simeq 4$, and if all the beam lines are used, the probability of observing them within a single laser pulse is $\simeq 1-10^{-4}$.

This research is supported by AFOSR.

- [1] A. E. Kaplan, Phys. Rev. Lett. **48**, 138 (1982).
- [2] G. Gabrielse, H. Dehmelt, and W. Kells, Phys. Rev. Lett. **54**, 537 (1985).
- [3] A. E. Kaplan, Phys. Rev. Lett. **56**, 456 (1986).
- [4] A. E. Kaplan and Y.J. Ding, IEEE J. Quant. Electr., **QE-24**, 1470 (1988).
- [5] D. J. Wineland, J. Appl. Phys. **50**, 2528 (1979); A. E. Kaplan, Opt. Lett. **12**, 489 (1987).
- [6] H. Euler, Ann. D. Phys. **26**, 398 (1936); W. Heisenberg and H. Euler, Zs. f. Phys. **28**, 714 (1936).
- [7] Z. Bialynicka-Birula and I. Bialynicki-Birula, Phys. Rev. D **2**, 2341 (1970); S. L. Adler, J. N. Bahcall, C. G. Callan, and M. N. Rosenbluth, Phys. Rev. Lett. **25**, 1061 (1970).
- [8] E. B. Aleksandrov, A. A. Ansol'm, and A. N. Moskalev, Sov. Phys. JETP **62**, 680 (1985).
- [9] R. L. Dewar, Phys. Rev. A **10**, 2107 (1974).
- [10] Y. J. Ding and A. E. Kaplan, Phys. Rev. Lett. **63**, 2725 (1989).

TH112 Nonlinear Faraday Rotation in Diluted Magnetic Semiconductors

R. Frey, J. Frey and C. Flytzanis
Laboratoire d'Optique Quantique du C.N.R.S.
Ecole Polytechnique
91128 Palaiseau CEDEX - France

Diluted magnetic semiconductors (DMS) [1] such as $\text{Cd}_{1-x}\text{Mn}_x\text{Te}$ exhibit extremely large Zeeman splittings and, consequently, giant Faraday rotations when such media are placed in static magnetic fields. For instance, polarization rotations larger than few thousand degrees are possible for magnetic fields smaller than one Tesla and interaction lengths of few millimeters.

Beyond these magnetic properties, the DMS alloys, as other semiconductors do, also show large optical nonlinearities whose origin is due to dipolar electric interactions. As a consequence, the Faraday rotation process may be strongly influenced by light intensity.

Linear Faraday rotation can be interpreted as a second-order nonlinear process, linear in optical electric field and static magnetic field. In such an analysis, the nonlinear polarization at frequency ω writes

$$P_{NL}^{(2)}(\omega) = \chi_{\equiv}^{(2)}(\omega, 0) E(\omega) H_S$$

where $E(\omega)$ and H_S are the optical and magnetic fields respectively and $\chi_{\equiv}^{(2)}(\omega, 0)$ is the magneto-electric second order nonlinear susceptibility. For high laser intensities a fourth order nonlinear polarization at frequency ω

$$P_{NL}^{(4)}(\omega) = \chi_{\equiv}^{(4)}(\omega, -\omega, \omega, 0) E(\omega) E^*(\omega) E(\omega) H_S$$

where $\chi_{\equiv}^{(4)}(\omega, -\omega, \omega, 0)$ is the magneto-electric fourth-order nonlinear susceptibility can be appreciable and induce a nonlinear Faraday rotation with an amplitude proportional to both magnetic field and optical intensity.

We will present experimental evidence and a detailed description of this nonlinear Faraday rotation process with particular emphasis on the physical origins of the nonlinearity, the impact of the medium symmetry, the role played by band-gap resonances, and the response time of the interaction. Some consequences and possible application related to this process will be also reviewed.

Reference

- (1) J.K. Furdyna, J. Appl.Phys., 64, R29 (1998)

Y. R. Shen

Department of Physics, University of California
Center for Advanced Materials, Lawrence Berkeley Laboratory
Berkeley, California 94720

Summary

Optical second harmonic generation (SHG) and infrared-visible sum-frequency generation (SFG) as surface probes have recently attracted a great deal of attention because of their seemingly unlimited possible applications to all areas of surface science. We review here the recent progress in this field.

We first discuss how surface-specific these techniques really are. This is important because the bulk contribution to the signal sets a limit to the sensitivity of such surface probes. We then give a number of examples to illustrate the power of the techniques. Most of them are chosen to show that SHG and SFG are unique in providing specific information about the particular surface or interfacial systems. The following problems will be discussed in some detail.

1. Measurements of molecular nonlinearities and the environmental effect on soluble and insoluble molecular monolayers at air/water interfaces.
2. Studies of molecular orientations of liquid surfaces.
3. Creation and detection of monolayer gratings on crystalline surfaces and measurements of anisotropic surface diffusion.

This work was supported by DOE under Contract No. DE-ACO3-76SF00098.

**THURSDAY, JULY 19
POSTER PRESENTATIONS**

Four Wave Mixing in Doped and Un-Doped KNSBN Crystals

Peng Wenji, Zhu Rong, She Weilong, Li Qinxing, and Yu zhenxin

Institute for Lasers and Spectroscopy, Zhongshan University
Guangzhou 510275, P. R. China

Chen Huan-Chu, Zhang Qing-Lun

The Institute of Crystal Materials, Shandong University, Jinan, PRC.

Xu. Yuhuan, Zhu De-Rui

Physics Department, Zhongshan University, Guangzhou, PRC.

Summary

Recently it has been found the photorefractive materials are some of the most sensitive materials for performing four-wave mixing and all kinds of the digital optical computing by using only a few milliwatt continuous laser beam. The photorefractive crystal KNSBN $[(K_{0.5}Na_{0.5})_{0.4}(Sr_{0.61}Ba_{0.39})_{0.8}Nb_6O_2]$, comparing with $BaTiO_3$, has the same or higher optical sensitivity and can be much more easily grown to produce doped and un-doped crystals of adequate size and optical quality for numerous applications. In this paper, we report the experimental results on the temporal responses and the reflectivity of the optical phase conjugation in the photorefractive crystal KNSBN.

We used the usual degenerated four-wave mixing experimental arrangement to generate the phase conjugate beam in doped and un-doped KNSBN with an Ar^+ -laser at 514.5nm. Two beams with the wave vectors k_1 and k_2 ($k_1 = k_2$) wrote a refractive index grating with wave vector $K = k_1 - k_2$. The angle between this two writing beams was about 8° . A reading beam with the wave vector $k_3 = -k_1$ Bragg-scattered off this grating to produce the phase-conjugate beam with the wave vector $k_4 = -k_2$. The phase-conjugate signal vs time was detected with a photomultiplier.

KNSBN belongs to the tetragonal tungsten bronze crystal structure. There are five kinds of empty sites among oxygen ions. And they can be filled with different kinds of metal ions with various contents or can be partially empty. Thus a number of different types of ferroelectric phase or different band gaps and absorption coefficients of the photorefractive crystals can be produced. So this kind of crystals can be chosen to generate the optical phase conjugate wave with different laser wavelength in a wide extent and to improve the reflectivity and response time of the optical phase conjugation by doping. We present the experimental data of the optical phase conjugation in home-made undoped and Ni, Cr, Co, Ce, Mn-doped KNSBN crystal, and show what kinds of ion-doped KNSBN are suitable to yield optical phase conjugate signal by Ar^+ -laser or He-Ne laser with a large reflectivity and fast response time.

The authors gratefully acknowledge the Support of National Science Fundation of China and K. C. Wong Education Fundation, Hong Kong.

THP2 Photorefractive Properties of CdTe:V at 1.5 μm

Mehrdad Ziari and William H. Steier

Department of Electrical Engineering, Center for Photonic Technology
University of Southern California, Los Angeles, CA 90089-0483
Telephone: (213)743-5640 or 743-3538 Fax: (213)746-8424

Afshin Partovi, James Millerd and Elsa Garmire

Department of Electrical Engineering, Center for Laser Studies
University of Southern California, Los Angeles, CA 90089-6418

Sudhir Trivedi

Brimrose Corporation of America
7720 Belair Road, Baltimore, MD 21236

Marvin Klein

Hughes Research Laboratories
3011 Malibu Canyon Road, Malibu, CA 90265

We have studied the photorefractive properties of CdTe:V at the wavelength of 1.5 μm which is of fundamental interest for optical fiber communications and signal processing¹. To the best of our knowledge, this is the first observation of photorefractivity at wavelengths longer than 1.3 μm . Cadmium telluride is a particularly interesting material since its figure of merit for photorefractive sensitivity n^3r/ϵ_r , being proportional to the linear electrooptic index change per absorbed photon, is one of the highest among inorganic bulk materials².

The semi-insulating crystal was grown using the modified Bridgman technique³ with a vanadium melt concentration of 10^{19} cm^{-3} . Bylsma and co-workers⁴ have previously identified vanadium as a proper dopant and reported on photorefractive beam coupling in CdTe:V at the wavelength of 1.06 μm . Our sample had an absorption tail extending to 1.8 μm which is believed to be due to vanadium doping. We have measured a dark resistivity of $1.3 \times 10^9 \Omega\text{cm}$.

The pump and the signal beams from a He-Ne laser operating at 1.523 μm were polarized along $\langle 110 \rangle$ crystallographic axis of the crystal and had intensities of 44.0 and 0.96 mW/cm^2 respectively. The grating wave vector was along the $\langle 001 \rangle$ direction. Figure 1 shows the beam-coupling gain as a function of grating spacing. The theoretical fit of Fig. 1 is for an effective trap density of $N_E = 5 \times 10^{15} \text{ cm}^{-3}$ and $\xi r_{41} = 4.45 \text{ pm/V}$ where r_{41} is the electrooptic coefficient and ξ is the electron-hole competition factor. We obtained a maximum gain of about 0.6 cm^{-1} . The absorption loss is about 2.0 cm^{-1} at this wavelength. The dependence of the normalized gain coefficient on the incident intensity is shown on Fig. 2. The normalized gain Γ/Γ_0 is expressed by

$$\frac{\Gamma}{\Gamma_0} = \frac{1}{1 + \frac{I}{I_d}}$$

where Γ_0 is the high intensity saturated gain coefficient and I_d is the dark equivalent irradiance⁵; the irradiance at which the photoconductivity equals the dark conductivity. The theoretical fit is for $I_d = 110 \mu\text{W}/\text{cm}^2$ which is consistent with the high resistivity of the sample. This value can be used to estimate the mobility lifetime product⁶ of $10^{-5} \text{ cm}^2/\text{V}$ for the sample.

A preliminary experiment using the moving grating enhancement technique resulted in a gain coefficient of 2.4 cm^{-1} which is comparable to the absorption loss ($\alpha \sim 2.0 \text{ cm}^{-1}$) of the sample. The measurements were made under an applied field of $11 \text{ kV}/\text{cm}$, a grating spacing of $10.7 \mu\text{m}$, and a beam ratio of 81:1. The optimization of these parameters is expected to result in a larger gain. We will present the measurements of the grating formation dynamics as well as moving grating under optimized conditions. The measurement of grating formation time will allow us to compare the photorefractive sensitivity of CdTe:V with other photorefractive materials.

1. A. Partovi et al, Photorefractive Materials, Effects and Devices II, Aussois, France, Post Deadline Technical Digest, PD2
2. A. M. Glass and J. Strait in *Photorefractive Materials and Their Applications I* (Springer-Verlag, Berlin, 1988) Ch. 8.
3. S. B. Trivedi and H. Wiedemeier, J. Electrochem. Soc. Sol. St. 134, 3199
4. R. B. Blysm, P. M. Bridenbaugh, D. H. Olson, and A. M. Glass, Appl. Phys. Lett. 51, 889 (1987)
5. L. J. Cheng and A. Partovi, Appl. Phys. Lett., 49, 1456 (1986)
6. G. C. Valley, H. Rajbenbach and H. J. Bardeleben, Appl. Phys. Lett., 56, 364 (1990)

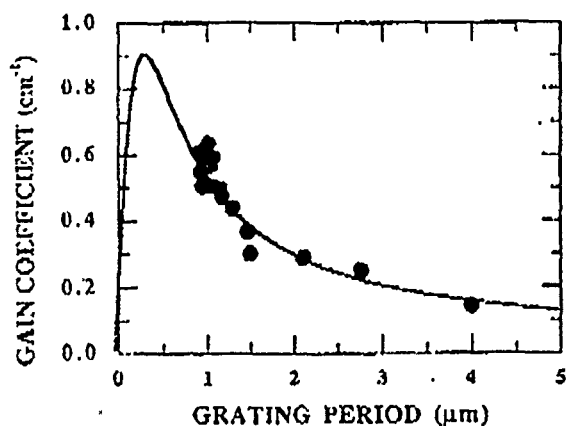


Figure 2. Beam coupling gain as a function of grating spacing.

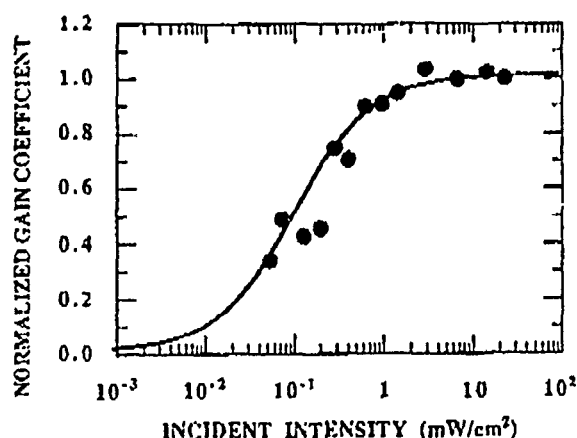


Figure 3. Normalized beam coupling gain coefficient as a function of incident intensity.

THP3 Electrooptic Properties of Lead Barium Niobate (PBN) Single Crystals

R. Guo, D. A. McHenry, A. S. Bhalla, and L. E. Cross
Materials Research Laboratory
The Pennsylvania State University, University Park, PA 16802

The lead barium niobate solid solution system, $\text{Pb}_{1-x}\text{Ba}_x\text{Nb}_2\text{O}_6$ (PBN[(1-x)%]), has drawn increasing interest mainly because of its unique properties as a tungsten bronze type ferroelectric relaxor with a morphotropic phase boundary (MPB) separating a tetragonal ferroelectric phase 4mm (with polarization dipole along [001]) and an orthorhombic ferroelectric phase m2m (with polarization dipole along [110]). Extraordinarily large dielectric, piezoelectric, and pyroelectric properties of morphotropic phase boundary PBN compositions have been reported. A morphotropic phase boundary has been shown to exist in the composition region near $1-x = 0.63^1$. Optical memory effects associated with a field-induced phase transition were also observed for the near-MPB composition single crystals^{1,2}.

In the present paper we report measurements of linear electrooptic coefficients and the temperature variation of the optical birefringence. Analysis of the above results were made in association with previously measured dielectric and pyroelectric properties. Electrooptic response of the PBN crystals to applied square wave voltage pulses were also studied.

Transparent optical quality single crystals of $\text{Pb}_{1-x}\text{Ba}_x\text{Nb}_2\text{O}_6$, where $1-x$ varies from 0.50 to 0.65, were grown by Czochralski technique. Transverse linear electrooptic coefficients were measured by using both a standard half wave voltage method and a Senarmont compensator method employing lock-in phase detection techniques. Measurements of temperature variation of optical birefringence, $\Delta n(T)$, were carried out by monitoring the transmitted intensity between crossed polarizers in the temperature range from room temperature up to $\sim 450^\circ\text{C}$ depending on the ferroelectric phase transition temperature of the corresponding sample.

References:

- ¹ R. Guo, A.S. Bhalla, C.A. Randall, Z.P. Chang and L.E. Cross, "Polarization Mechanisms of Morphotropic Phase Boundary Lead Barium Niobate (PBN) Compositions", *J. Appl. Phys.*, 67(3), 1453-1460 (1990)
- ² R. Guo, A.S. Bhalla and L.E. Cross, "Electric Field Induced Orthogonal Polarization Switching in Morphotropic Phase Boundary $\text{Pb}_{0.57}\text{Ba}_{0.43}\text{Nb}_2\text{O}_6$ (PBN57) Single Crystals", *Applied Optics* (to be published on Mar.1990 issue).

Growth of Single Crystal Fibers for Optical Applications

Joyce K. Yamamoto and Amar S. Bhalla
Materials Research Laboratory
Pennsylvania State University
University Park, PA 16802

Recently a modified float zone technique has been developed to grow single crystals in a fiber geometry. The technique, called the laser heated pedestal growth (LHPG) technique, employs a carbon dioxide ($10.6\mu\text{m}$) laser as the power source. Previous work has shown that this technique is capable of growing fibers ranging from $50\mu\text{m}$ to $1500\mu\text{m}$ in diameter and a variety of oxide compositions are possible.^{1,2} It is the aim of this project to demonstrate the feasibility of the LHPG technique to produce good quality, optically nonlinear oxide single crystal fibers.

The LHPG technique, as mentioned before, is powered by a 50 watt carbon dioxide laser. The circular beam is incident upon a coaxial conical mirrors, which converts the laser energy into an annular. The annular is then directed onto a parabolic mirror, which focuses the beam into a small spot. The hot zone is then defined by the focal point of the parabolic mirror and is characterized by a uniformly circular energy distribution. Crystal growth is accomplished by the feedrod and the seed crystal moving vertically along the parabolic axis. Details of the growth process and the effect of the growth parameters on the resulting crystal quality will be discussed.

The crystal compositions grown are all optically nonlinearly active, some more than others, but they also differ in their melting characteristics and melting temperatures. Different compositions in three structural systems were investigated; barium titanate (perovskite), strontium barium niobate (tungsten bronze) and lanthanum titanate (layered perovskite). Of these three groups the barium titanate and lanthanum titanate are congruently melting. The strontium barium niobate system is a solid solution system, therefore the melt and crystal composition will differ.

The crystals were grown at rates varying from 10mm/hr to 80mm/hr , and their diameters ranged from $300\text{-}600\mu\text{m}$. The crystals were clear and transparent, and no inclusions or voids were observed. The dielectric and pyroelectric properties were measured as a function of temperature to compare and evaluate the single crystal fibers. The paraelectric/ferroelectric transition temperatures of the barium titanate was 131°C indicating the high purity of the crystal. The transition temperatures of the strontium barium niobate for compositions varying in strontium content from 0.75, 0.61, and 0.50, were in good agreement with the literature. One important advantage the strontium barium niobate single crystal fibers had over the corresponding bulk grown crystals was the reproducible absence of compositional striations.

1. R.S. Feigelson, J.Cryst.Growth, **79**(1986)669-680.
2. J.K. Yamamoto, A.S. Bhalla, Mat.Res.Bull. **24**(1989)761-765.

THP5 Investigation of the Microscopic Parameters Governing the photorefractive effect in $\text{KTa}_{1-x}\text{Nb}_x\text{O}_3:\text{Cu},\text{V}$

Victor Leyva, Aharon Agranat, Amnon Yariv
128-95 Watson Lab
Department of Applied Physics
California Institute of Technology
Pasadena, Ca. 91125
(818)356-4413

We perform a microscopic analysis of the photorefractive effect in $\text{KTa}_{1-x}\text{Nb}_x\text{O}_3:\text{Cu},\text{V}$. We have independently measured all relevant parameters which enter into the Kukhtarev model of the photorefractive effect. Cu is found to be the partially filled donor level responsible for the photorefractive effect. The total Cu concentration was determined from electron microprobe analysis to be $1.8(10^{19})\text{cm}^{-3}$. A series of oxidation and reduction treatments were used to alter the concentration of Cu^{1+} and Cu^{2+} . The concentration of Cu in each valence state after each heat treatment was determined using the relative magnitudes of the Cu^{1+} charge transfer band and the Cu^{2+} crystal field transition. The electron photoexcitation cross section at 514nm was determined to be $9.08(10^{-20})\text{cm}^{-2}$. The ratio of the mobility to electron recombination rate was determined from photoconductivity measurements to be $6.20(10^8) \text{ 1/(v-cm)}$.

Oxidation and reduction treatments alter the photorefractive properties of metal oxide crystals by inducing changes in the valence state of dopant ions by altering the concentration of oxygen vacancies. The oxidation process is given by



where V_O represents an oxygen vacancy and O_2 an oxygen gas molecule. Charge neutrality is given by

$$4[\text{Cu}^{1+}] + 3[\text{Cu}^{2+}] + n = 2[\text{V}_\text{O}] + p \quad (2)$$

where n and p are the free electron and hole concentrations.

A mass action equation can be used to determine the concentration of the components of (1) in equilibrium

$$[\text{Cu}^{1+}][\text{V}_\text{O}]^{1/2}P_{\text{O}_2}^{1/4}/[\text{Cu}^{2+}] = K \exp(dH/kT) \quad (3)$$

where P_{O_2} is the partial pressure of oxygen, K is a constant, and dH is the change in enthalpy for the reaction. For each of the five heat treatments the temperature, P_{O_2} , $[\text{Cu}^{1+}]$, and $[\text{Cu}^{2+}]$ are known. By neglecting the free carrier concentration relation (2) can be used to determine V_O . Using (3) we are able to determine $dH=0.295\text{eV}$ and $K=2.83(10^{18})\text{atm}^{1/4}\text{cm}^{-3/2}$ (Fig. 1). dH is given by the band gap energy minus the energy below the conduction band of the Cu^{1+} level.

The above analysis allows us to determine the oxygen partial pressure and temperature necessary to control the Cu valence states (Fig. 2) and hence photorefractive properties of the KTN sample. We are thus able to vary and control the magnitude and response time for a given application. The theoretical and experimental dependence of these properties on heat treatments will be compared.

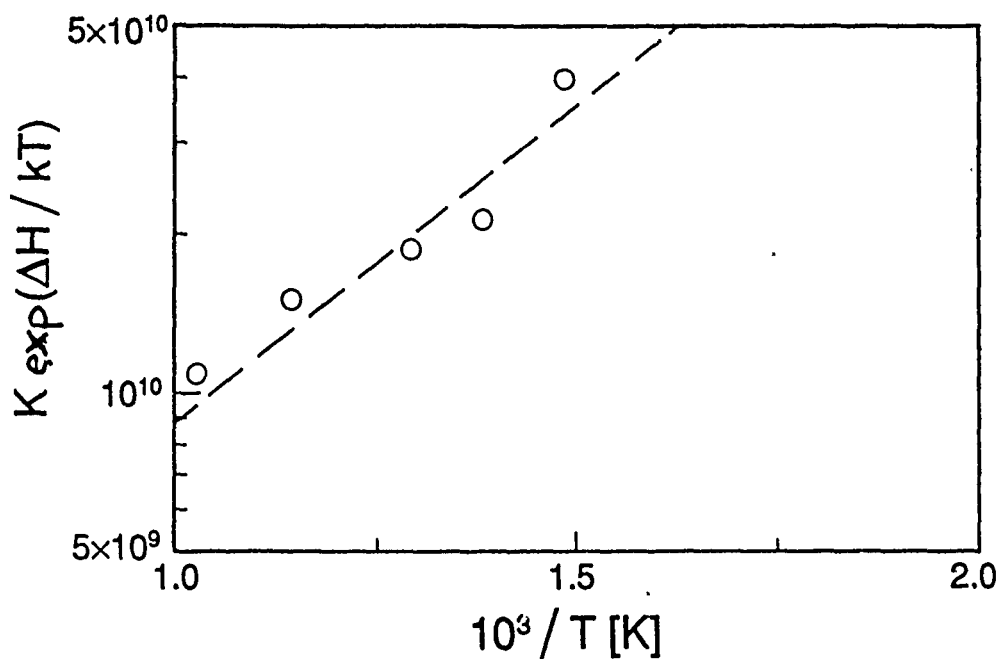


Fig. 1 Plot of the left hand side of the mass action equation (3) versus inverse processing temperature. Dashed line corresponds to $\Delta H = 0.295 \text{ eV}$ and $K = 2.83 \times 10^{18} \text{ atm}^{1/4} \text{ cm}^{-3/2}$.

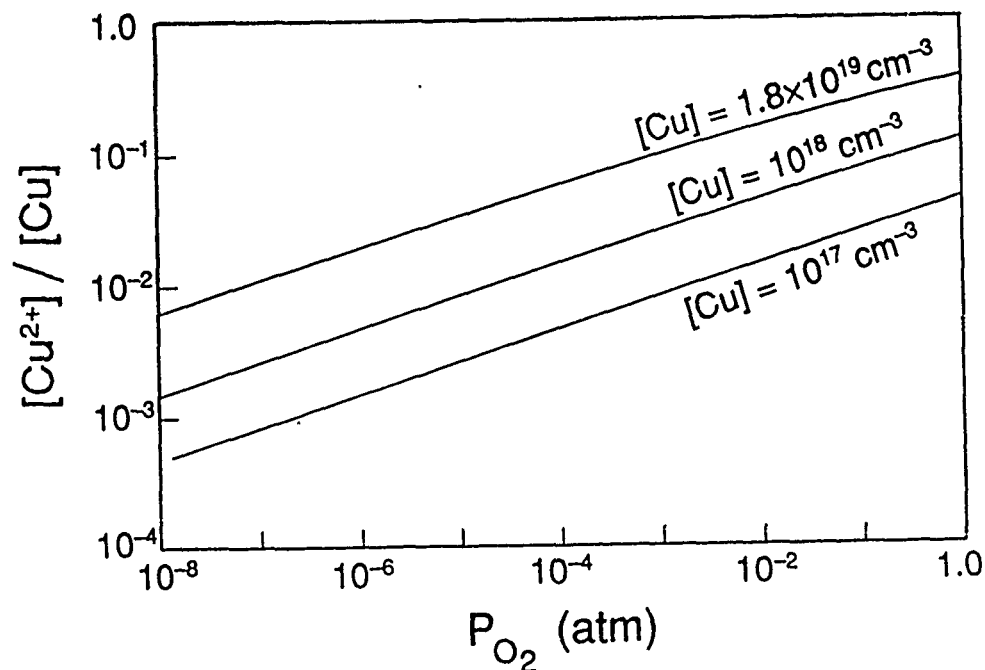


Fig. 2 Plots of the fraction of the Cu in the 2+ valence state versus partial pressure of oxygen for a 700C heat treatment. Plots for three doping levels are shown.

Direct Determination of the Electron Mobility in Photorefractive $\text{Bi}_{12}\text{SiO}_{20}$ by a Holographic Technique

J.P. Partanen, J.M.C. Jonathan[†], and R.W. Hellwarth, Departments of Physics and Electrical Engineering, University of Southern California, Los Angeles, CA 90089-0484.

[†]Permanent Affiliation: Institut d'Optique, Bat.503 BP 147, 91403 Orsay Cedex, France.

Purely electrical measurements of the carrier mobility in photorefractive insulating crystals have been inconsistent and difficult to interpret. The first holographic technique known to us gave an unambiguous value for the room-temperature mobility ($\sim 10^{-2} \text{ cm}^2/\text{Vs}$) for the photoexcited carriers (of unspecified charge sign) in three cubic, iron-doped $\text{Bi}_{12}\text{GeO}_{20}$ crystals.¹ Here we report the first holographic measurements of the electron mobility μ_e in nominally undoped n-type $\text{Bi}_{12}\text{SiO}_{20}$ (n-BSO). We use a more versatile technique that employs a static applied voltage V_0 rather than an alternating one.¹ After V_0 is applied to the dark-adapted sample, a 30 psc 532 nm pulse (of fluence between 0.1 and $5 \mu\text{J}/\text{cm}^2$) is split and used to form an intensity grating $I(x) \propto [1 + m \cos(kx)]$ parallel to the applied field. A density $n(x,t) = n_0(t) + \Re n_1(t) \exp(ikx)$ of photo-excited electrons is initially proportional to $I(x)$ and smaller than any saturation density. We assume the electrons then drift and diffuse while being re-trapped with rate constant τ_e^{-1} . The Coulomb field $[\Re E_1 \exp(ikx)]$ created by the displaced carriers creates a modulation of refractive index $\Re [(-\frac{1}{2} n^3 r E_1 \exp(ikx))]$. Here $n \equiv$ refractive index, $r \equiv$ effective electrooptic coefficient. A 633 nm beam ($\sim 10 \mu\text{W}$) Bragg-scatters from this index modulation to reveal its amplitude. Figure 1 shows a typical time behavior of the scattered intensity averaged over 50 pulses. The foregoing physical description gives immediately (in MKS)

$$E_1 = -en_1(0) (k_E + ik) (1 - e^{-\Gamma t}) / \epsilon D \quad (1)$$

Here e is the positive electron charge, ϵ is the static dielectric constant, and k_E equals $eE_0/k_B T$ where the applied static field E_0 is nearly V_0/d ($d \equiv$ sample width 5mm), k_B equals Boltzmann's constant and T is the sample temperature. The denominator D equals $K_e^2 - ikk_E + k^2$ where K_e^{-1} is the usual diffusion length $(k_B T \mu_e \tau_e / e)^{1/2}$. The complex decay coefficient Γ equals $D/(\tau_e K_e^2)$. Figure 1 fits well the absolute square of (1) after (1) is averaged over E_0 , which we observe by the electro-optic effect to vary in

space by $\sim \pm 50\%$ from $E_0 \sim V_0/d$. Here the data were taken on the n-BSO sample called SU1 in Ref.2 where it is described and characterized. The value of k chosen was about 0.4 times K_e as measured in Ref.2 ($K_e^{-1} = 5.8 \pm 2.3 \mu\text{m}$). For this case, $\Re\epsilon\Gamma \ll \Im\epsilon\Gamma$ so that for $k_E \gg K_e^2/k$ we predict from (1) that the time t_m at which the peak of the scattering occurs is $\pi/(k\mu_e E_0)$. This depends on no other material parameters but the mobility μ_e . A plot of t_m versus V_0^{-1} is shown in Fig.2 which bears out this prediction and allows us to estimate $\mu_e \pm 0.2 \text{ cm}^2/\text{Vs}$ with $\pm 10\%$ random error. We are currently reducing the larger systematic error introduced by spatial variations in E_0 inside the sample.

We have also measured the decay time of the dc photoconductivity in this sample to be $60 \pm 4 \mu\text{s}$. This, with the K_e given in Ref.2, gives $\mu_e = 0.22 \pm 0.05 \text{ cm}^2/\text{Vs}$, which is consistent with the above value. This value also predicts correctly the absolute value of the photocurrent that we observe after a pulse, if we assume unity quantum efficiency as was estimated in Ref.2.

This research was supported by the U.S. Air Force Office of Scientific Research under Contract #F49620-88-C-0027, and by the National Science Foundation under Grant #ECS-8821507.

References:

- ¹G. Pauliat, A. Villing, J.C. Launay, and G. Roosen, J.O.S.A. B (to be published).
- ²F.P. Strohkendl, P. Tayebati, and R.W. Hellwarth, J. Appl. Phys. 66, 6024 (1989).

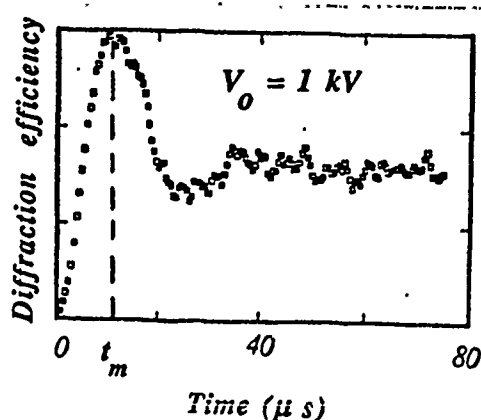


Figure 1: Time behaviour of the diffraction efficiency in n-BSO sample SU1 averaged over 50 laser pulses.

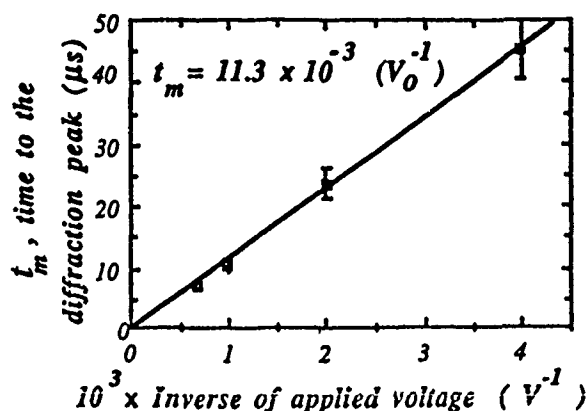


Figure 2: The rise time of the diffraction efficiency in n-BSO sample SU1, as a function of applied voltage.

M.S. Petrovic, A. Suchocki ², and R.C. Powell, *University Center for Laser Research, 413 Noble Research Center, Oklahoma State University, Stillwater, OK 74078, Tele. (405) 744-6575*; G.C. Valley, *Hughes Research Laboratories, 3011 Malibu Canyon Road, Malibu, CA 90265, Tele. (213) 317-5435*; G. Cantwell, J. Aldridge, *Eagle-Picher Research Laboratories, Specialty Materials Division, 200 Ninth Ave. , NE, Miami, OK 74354-3305, Tele. (918) 542-1801*.

Laser-induced gratings produced by two-photon absorption of picosecond pulses at 1.064 μm were used to examine the room temperature nonlinear optical responses of undoped CdTe crystals with different types of conductivity. We report what we believe to be the first observation of photorefractive two-beam coupling and transient energy transfer owing to space charge fields produced by electron-hole separation. Gains up to 2.5 cm^{-1} were obtained at fluences of 12 mJ cm^{-2} for 1.9 μm grating spacing. Good qualitative agreement is shown between the experimental results and theory. Scalar polarization rotation switching was also measured with on/off ratios of 6 at fluences of 56 mJ cm^{-2} . Pulse-probe degenerate four-wave mixing measurements of grating dynamics on subnanosecond time scales were used to measure the ambipolar diffusion coefficient of charge carriers in the crystals. The value of $D_a = 3.0\text{ cm}^2\text{ s}^{-1}$ which was obtained is in very good agreement with theoretical estimates. Free carrier lifetimes of 12 ns were measured. A long-lived contribution to the signal consistent with a trapped charge photorefractive effect was observed at large grating spacings for n-type conductivity, and is tentatively attributed to a larger trap density in this sample. The contribution of optical second harmonic generation (SHG) to the generation of free carriers in thick samples of CdTe was measured. We find the ratio of the number of photons generated by SHG to that generated by all two-photon absorption processes to be about 4%, demonstrating that the contribution of this mechanism to free carrier generation and therefore to the measurement of the two-photon absorption coefficient is not insignificant. Measurements of the relative scattering efficiencies of successive diffracted orders in the Raman-Nath regime allowed for calculation of the laser-induced change in the index of refraction, Δn , due to the creation of free carriers. The value of $\Delta n = 4 \times 10^{-4}$ which was obtained is in good agreement with theoretical estimates.

¹This work was supported by a DARPA grant, number MDA 972-89-K-001

²Permanent address: *Institute of Physics of Polish Academy of Sciences, Al. Lotników 32/46, 02-668 Warsaw, Poland*

Excitonic Nonlinearities in ZnSe/ZnS Multiple Quantum Wells

Chunfei Li and Yudong Liu

Department of Physics, Harbin Institute of Technology
Harbin 150006, P. R. CHINA

Dezhen Shen and Xiwu Fan

Changchun Institute of Physics, Academia Sinica
Changchun 130021, P. R. CHINA

SUMMARY

More attention should be paid on the excitonic nonlinearities of II-VI semiconductors such as ZnSe and its multiple quantum wells (MQWs)[1]-[2] because their big excitonic nonlinearities, visible wavelength operation, possibility of growing on the GaAs substrate for the potential use in nonlinear optical information processing. We present here the first study on excitonic optical nonlinearities of ZnSe/ZnS multiple quantum wells both experimentally and theoretically.

1. Exciton energy levels

For the purpose of determining exciton energy levels and identification of a MQWs structure, not a superlattice, we have calculated the exciton energy levels of ZnSe/ZnS MQWs structure for different barrier thickness according to the LCAO theory and Kronig-Penney model. We have also measured the photo luminescence and absorption spectra. The first exciton energy level is 2.85eV.

2. Excitonic nonlinearities

We have measured nonlinear absorption spectra in ZnSe/ZnS MQWs at low temperature. We observed obvious broadening of excitonic peak and excitonic state filling with the increase of light intensity. We have also calculated the nonlinear refractive index changes from the absorption changes based on Kramers-Kronig transformation, as shown in Fig. 1. The largest change of nonlinear refractive index is 0.012 and the corresponding n_2 is $7 \times 10^{-8} \text{cm}^2/\text{W}$. We attribute the nonlinear mechanisms to exciton broadening and phase space filling of exciton states.

3. Dynamic optical bistabilities(OB).

The typical character of excitonic broadening nonlinearity is that on the absorption spectrum, one can find absorption decrease near exciton peak and darkening on the two sides of the peak. Making use of this character, we have observed dispersive OBs at wavelengths near the exciton peak and increasing absorption OBs at wavelengths shorter and longer than the exciton peak wavelength, as shown in Fig. 2. The excitation pulse duration was 10 ns from dye laser pumped by N_2 laser.

REFERENCES

1. D. R. Andersen et al. Appl. Phys. Lett. 48(1986), 1559.
2. N. Peyghambarian et al. Appl. Phys. Lett. 52(1988), 182.

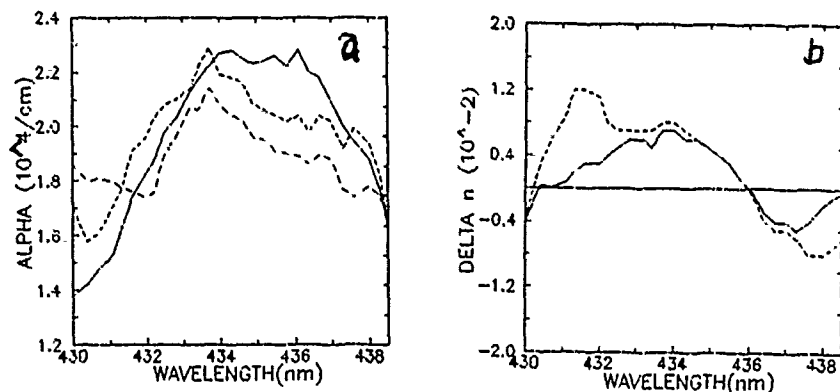


Fig. 1. Experimental absorption and nonlinear refractive index change spectra in ZnSe/ZnS MQWs at 77 K.

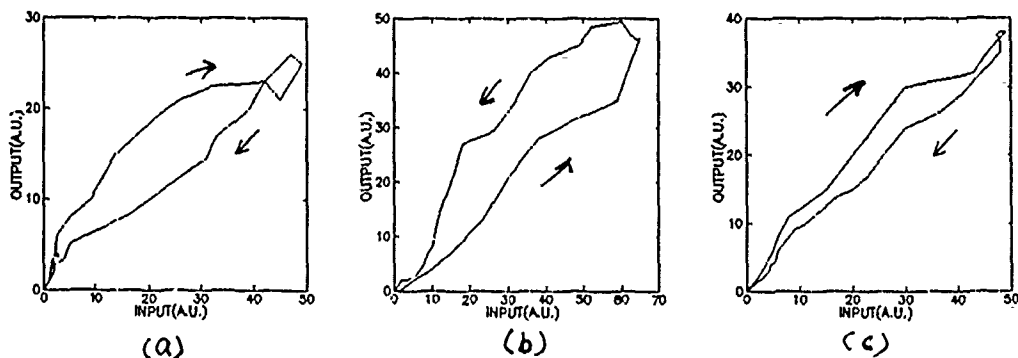


Fig.2. Experimental dynamic bistable loops of ZnSe/ZnS MQWs at 77 K at wavelengths (a) 432 nm, (b) 436 nm and (c) 438 nm.

Optical Nonlinearities of the Metal-Oxide Semiconductor Particles

Haosheng Fei, Jialong Zhao and Li Han

Department of Physics, Jilin University, Changchun 130023,
People's Republic of China.

Bingsuo Zhou, Liangzhi Xiao and Tiejin Li

Department of Chemistry, Jilin University, Changchun 130023,
People's Republic of China.

Small semiconductor microcrystallines have been received considerable attention recently as an interesting class of nonlinear optical materials. The commercial $\text{CdS}_x\text{Se}_{1-x}$ -doped glasses and metal colloids have been studied most extensively. Ying Wang et al [1] have discussed the nonlinear-optical properties of PbS and CdS clusters. The nonlinearities originate from the bleaching of the excitonic absorption owing to the presence of trapped carriers on the cluster surfaces. Here we report the measurements of third-order nonlinear susceptibilities of the metal-oxide semiconductor particles (Fe_2O_3 , Mn_2O_3 and Cr_2O_3) and show that the nonlinearities originate from the charge separation of laser-induced carriers in the coated particles.

The samples used in the experiments were prepared through colloidal chemical technique. The metal-oxide semiconductor particles were coated with a layer of surfactant molecules, such as sodium dodecyl benzene sulfonate (DBS) molecules and the other molecules, and embedded in an organic solvent. The physical properties of the coated particles were modified by surfactant molecules. Transmission electron micrographs show that the particles are spherical in shape with average diameter of 50-100 \AA and free of aggregates. The UV absorption curves of the samples are similar to that of the semiconductor-doped glasses.

The degenerate four wave mixing (DFWM) in the samples were performed using the SHG of a homemade Q-switched Nd:YAG laser. In

the experiments, we first ascertained that no signal was contributed by the solvent itself. Much higher optical nonlinearities and reflectivities in the coated particles were obtained. For example, the susceptibilities $X^{(3)}$ of the coated and uncoated particles for the same volume fraction of 10^{-6} are 3×10^{-9} and 1×10^{-10} esu respectively. The corresponding reflectivities are two orders of magnitude larger than that of the uncoated particles. For comparison, The $X^{(3)}$ of the semiconductor-doped glasses is 1×10^{-9} . The similar results are also found in the other samples.

On the other hand, the nanosecond power-dependent transmission experiments were performed with the SHG of Q-switched YAG laser. A strong beam was used as the excitation beam and a weak beam was used as the probe beam. Their relative intensity of two beams was 1000:1. Both beams overlapped on samples with an intersection angle of about 2° . The nonlinear absorption coefficient α_2 ($=\Delta\alpha/I$) to be $10^{-6} \text{ cm}^{-1}/\text{W}$. The saturation intensity is about $5 \text{ MW}/\text{cm}^2$ for the Fe_2O_3 particles that coated with DBS.

It should be emphasized that the enhancement of the optical nonlinearity in the metal-oxide semiconductor particles. The nonlinear optical properties of the coated particles were modified greatly by surfactant molecules due to the coupling interactions between the particles and surfactant molecules. The surface-coated molecular layer may be considered as an electric dipole layer. A separation of the electron and hole follows the excitation. Therefore, the charge separation results in large optical nonlinearities in the coated particles.

Reference

1. Y.Wang, N.Herron, W.Mahler and A.Suna, J.Opt.Soc.Am.B 6,808 (1989).

Temporal Behavior of the Optical Stark Effects on the Stacking Fault Exciton States in BiI_3

I. Akai, T. Karasawa and T. Komatsu

*Department of Physics, Faculty of Science, Osaka City University,
Sugimoto Sumiyoshi-ku, Osaka 558, Japan*

Summary

On a characteristic exciton system, we present the time-resolved optical Stark effect (OSE) with high spectral resolution. In layered crystal BiI_3 , several sharp absorption lines appear near the absorption edge.¹⁾ The lines have been attributed to the excitons having quasi-two-dimensional nature at a stacking fault (called stacking fault excitons, SFE's).²⁾ Figure 1(a) shows a typical absorption spectrum of BiI_3 . The sharp lines R, S and T are due to three transitions of the SFE states.³⁾ On this exciton system, large peak-shifts induced by the OSE appear under the excitation frequencies ($\hbar\omega$) of off- and on-resonance. The large dipole matrix element and the large nonlinear susceptibility of the SFE have been obtained.⁴⁾

Figures 1(b)-(d) show the $\hbar\omega$ dependence of peak-shift values. The time-integrated spectra are measured by a pump-and-probe method using a dye laser pumped by N_2 laser (the excitation density $\sim 1.5 \times 10^5 \text{ W/cm}^2$, the time-duration $\sim 4 \text{ nsec}$). The luminescence component from the dye cell is used as the probe-pulse. The two beam-paths are adjusted to coincide at the sample surface. Near all resonance, the peak-shifts of all lines resonantly enlarge, and the discontinuous jumps of peak-shifts occur. Such behavior of peak-shifts can be basically described by "multiple dressed exciton model" consisting of three exciton states and the ground state.⁵⁾ In the peak-shifts, systematic deviations from our simplified model exist. The peak-shifts of all absorption lines tend to blue-one for the higher energy excitation than

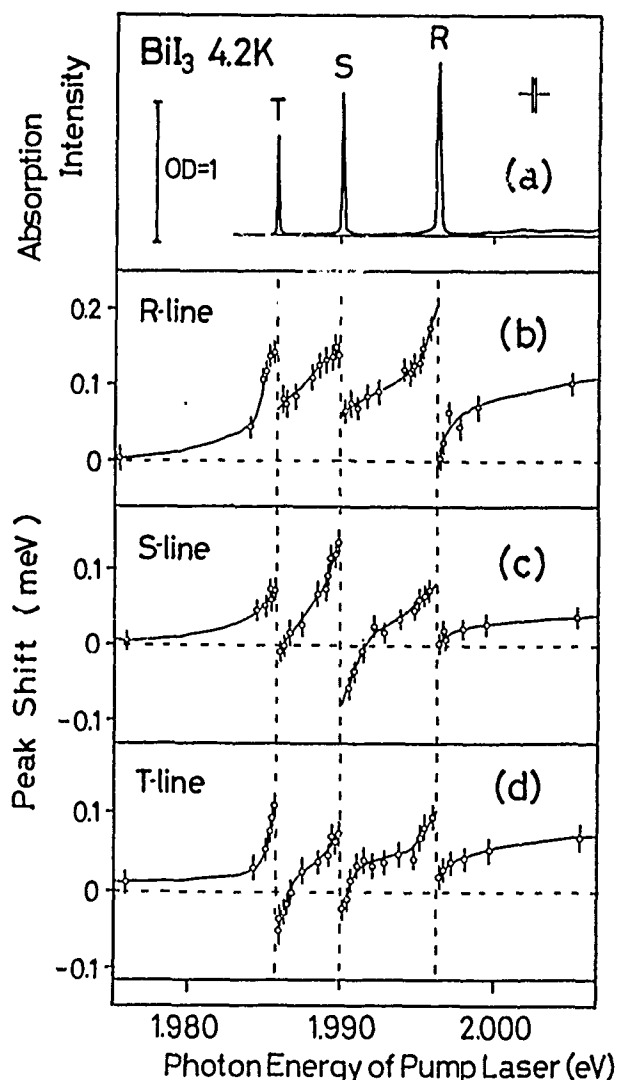


Fig. 1 (a) SFE absorption spectrum near the absorption edge in BiI_3 at 4.2K. R, S and T denote the absorption lines of SFE's; (b), (c) and (d) Excitation laser frequency ($\hbar\omega$) dependences of peak-shift values of R, S and T lines, respectively; vertical broken lines: the resonance energies of R, S and T excitons, respectively.

the T-resonance. Under this excitation condition, the real exciton creation is brought about. The additional nonlinear effect caused by the great number of excitons may obscure the optical Stark shifts (OSS). We measure the time-resolved spectra of OSE changing the time-delay Δt in the time resolution of ~ 250 psec with a streak camera. Figure 2 shows the absorption spectra of R-line for several Δt under the excitation of higher energy than T-resonance for $\Delta\hbar\omega = +0.76$ meV. R-line shifts to the red the very moment the pump-pulse starts up ($\Delta t = -2$ nsec). With increasing Δt , the red-shift changes to blue-one. The large blue-shift and the line broadening appear at 2 nsec after the peak of pump-pulse. The change of the peak-shift sign originates from the difference of the response-time between the OSS and the nonlinear shift due to the additional effect. The red-OSS should be induced by the coherent excitation in the ultrafast time domain. The delayed blue-shift is considered to be the nonlinear effect caused by the real exciton creation.

From the time-resolved measurement, the clear separation between the OSS and the additional nonlinear effect due to the real exciton creation is achieved for the first time.

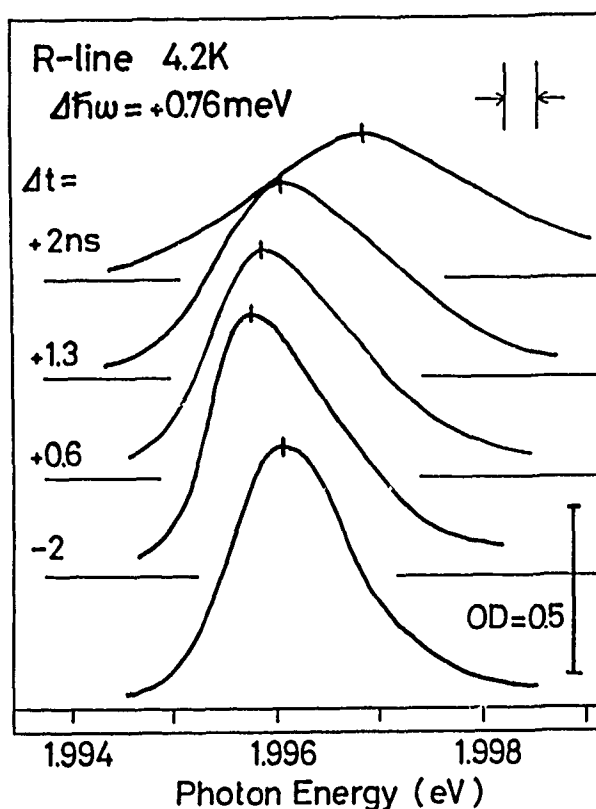


Fig. 2 Absorption spectra of the R-line for various time-delay; the lowest one: the absorption spectrum without laser excitation; Δt : the time-delay of the probe-pulse peak from the pump-pulse peak; $\Delta\hbar\omega$: the detuning parameter of the pump-laser from the T-resonance.

References

- 1) Y.Kaifu and T.Komatsu, J. Phys. Soc. Jpn **40**, 1377 (1976)
- 2) Y.Kaifu, J.Lumin. **42**, 61 (1988); K.Watanabe, T.Karasawa, T.Komatsu and Y.Kaifu, J. Phys. Soc. Jpn **55**, 897 (1986)
- 3) T.Komatsu, Y.Kaifu, S.Takeyama and N.Miura, Phys. Rev. Lett. **58**, 2259 (1987);
- 4) I.Akai, T.Karasawa, T.Komatsu and Y.Kaifu, phys. stat. sol. (b) **150**, 635 (1988);
- 5) I.Akai, T.Karasawa, T.Komatsu and Y.Kaifu, submitted to Phys. Rev. B

Nonlinear Optical Properties of Phenyl-Capped CdS Molecular Particle Doped Organic Polymer

Toshio Fukumi , Toru Sakaguchi, and Masaru Miya
Government Industrial Research Institute at Osaka
1-8-31 Midorigaoka, Ikeda-city, Osaka 563, Japan
Phone 0727-51-8351

Syozo Yanagida and Takashi Enokida
Faculty of Engineering, University of Osaka
2-1 Yamadaoka, Suita-city, Osaka 565, Japan
Phone 06-877-5111

Hiroto Mori and Hiroshi Fujita
Research Center for Ultra-high Voltage Electron Microscopy,
University of Osaka, 2-1 Yamadaoka, Suita-city, Osaka 565, Japan
Phone 06-877-5111

Degenerate four wave mixing (DFWM) along with optical spectral studies were performed on phenyl-capped CdS(Ph-CdS) molecular particle doped in poly-methyl metacrylate(PMMA) polymer.

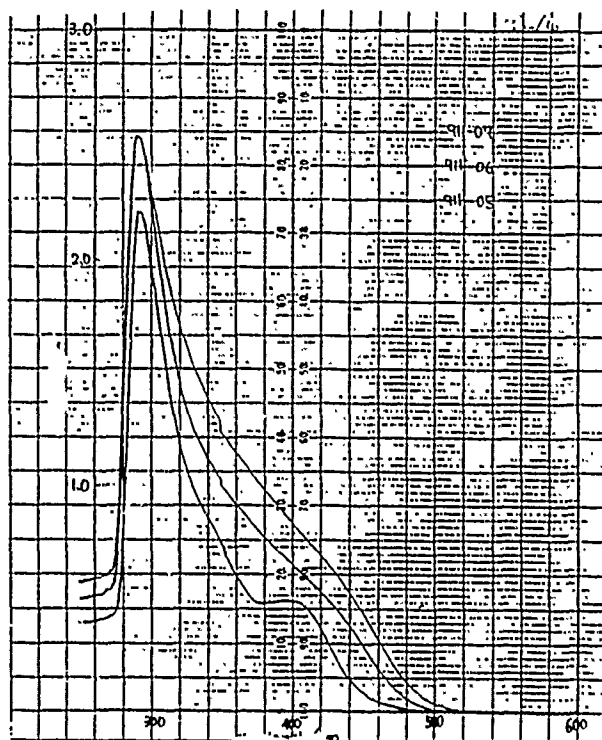
The sample was prepared by inverse micelle method. Ph-CdS was precipitated with bis(trimethylsilyl) sulfide in the inverse micelle, and then capped by Phenyl trimethylsilyl sulfide. Ph-CdS thus obtained was soluble in various organic solvents such as DMSO or pyridine. The polymer film was obtained by casting PMMA/Ph-CdS/pyridine solution.

The crystal structure of CdS particle was examined by an electron microscope, and was found to be cubic, whereas it has been known to be hexagonal in glasses. The sizes of particles were well controlled in the range from 10 to 50 angstrom depending on the precipitation conditions.

The optical excitation, absorption, and emission spectra were examined on the sample. In the excitation spectra, clear exciton band was resolved at the low energy side of spectra. In the absorption spectra, a shoulders were observed. In the emission spectra, the band edge structure was resolved at the high energy side of the peak from the trap level. These observations clearly indicate that there is quantum confinement effect in the examined sample.

The DFWM study was performed employing a 6 nano seconds laser pulse at 532 nm generated from frequency doubled Nd:YAG laser in the phase conjugation geometry. Carbon disulfide was used as a standard whose nonlinear susceptibility was determined in the present study to be 1.7×10^{-12} . We determined the third order

nonlinear susceptibility of our sample to be 2.9 E-10 esu , where the diameter of the particle was around 20 angstrom.



Absorption spectra of
Ph-CdS doped PMMA

Clockwise Bistable Photocurrent and Inverse Franz Keldysh Effect of Thin CdS Films

C. Bouchenaki, B. Ullrich, and J.P. Zielinger

Institut de Physique et Chimie des Matériaux de Strasbourg

Groupe d'Optique Nonlinéaire et d'Optoélectronique

5, rue de l'Université-67084 Strasbourg, France

In general optical bistability in transmission and/or photocurrent can be used for computing systems. Thus, it is of great interest to investigate systems having these bistable features. In our case we investigated thin ($2 - 10\mu m$) Cadmium Sulfide layers pointing out the thermal enhanced bistability. The layers are prepared using three different techniques: CSVT (Closed Space Vapor Transport, an epitaxial process) using Calcium Fluoride (111) as the substrate, evaporation and spray depositing on pyrex.

We observed nonlinearities and bistability in transmission and photocurrent for all our layers. So, we are able to present for the first time the nonlinearities and bistable features of CdS layers prepared by the CSVT method. In addition, the influences of the etching time of the CaF_2 substrate to the nonlinear properties and luminescence of the layers are also investigated. Furthermore, we want to mention here that we observed for the first time bistability in the photocurrent of an evaporated layer using the unfocused green $514.5nm$ argon laser line at room temperature.

In the context of the nonlinearities, the actual local temperature responsible for the bistability is discussed experimentally and theoretically. Furthermore, the run of the photocurrent as a function of the temperature is investigated to explain the direction of the bistable loop, because two directions of the loop are observed: clockwise (as observed by us¹) and anticlockwise (as observed by other groups²).

The influence from the onset and the steepness of the absorption edge to the bistability

are investigated by transmission measurements and additionally we discussed the surface quality of the different layers using the results of photocurrent and reflection measurements. The abnormal absorption behavior of the layers is very interesting. This might be caused by a memory effect presenting an inverse Franz-Keldysh effect which means that the sensitivity below the gap of the photocurrent spectra decreases on increasing the applied voltage.

As a conclusion, we present consistent informations of the bistable and optoelectronic features of thin CdS layers showing the possibilities and the boundaries of these sheets to use them in the near future for logic bistable functions which in turn are used for optical data processing.

¹ C. Bouchenaki, B. Ullrich, J.P. Zielinger, H. Nguyen Cong, and P. Chartier, Meeting of the Optical Society of America (OSA), Orlando 15-20th October 1989, to be published in the J.Opt.Soc.Am.B

² A. Witt, M. Wegener, C. Klingshirn, D. Gnass, and D. Jaeger, Appl.Phys.Lett.52, 342 (1988)

THP13 Preparation and Third-Order Optical Nonlinearities of CuCl Microcrystallite-Doped Glasses

N. Sugimoto, T. Manabe, S. Ito
Asahi Glass Co., Ltd. Advanced Glass R&D Center
Hazawa-cho 1150, Yokohama 221 Japan

T. Tokizaki, T. Kataoka, A. Nakamura
Department of Applied Physics, Nagoya University
Chikusa-ku, Nagoya 464-01 Japan

1. Introduction

There is increasing interest in the large optical nonlinearity of semiconductor-doped glasses due to the quantum confinement effects of an electron and hole or an exciton in microcrystallites¹⁾. Most of studies were done for color filter glasses doped with $\text{CdS}_x\text{Se}_{1-x}$ whose nonlinearity arises from the strongly confined electron and hole.

In this study, the preparation and the third-order optical nonlinearities $\chi^{(3)}$ of glasses doped with CuCl microcrystallites are investigated.

2. Experimental

Glasses with a CuCl microcrystallite phase were prepared with composition of $10\text{Na}_2\text{O} \cdot 52.5\text{B}_2\text{O}_3 \cdot 7.5\text{Al}_2\text{O}_3 \cdot 30\text{SiO}_2 \cdot x\text{CuCl} \cdot 0.5x\text{SnO}$ (mol ratio, $x=0.5\sim 1$) by a conventional melting method. Reagent grade of sodium carbonate, boric acid, aluminum hydroxide, silicon dioxide, cuprous chloride (CuCl) and stannous oxide (SnO) were used as the raw materials. The mixtures of raw materials were melted in a Pt crucible in a SiC furnace in air at 1300-1400°C for 2 hours. The melts were poured into stainless steel plate and pressed into plates about 2mm in thickness. A variety of heat treatments were performed to develop a various size of CuCl microcrystallites in glasses.

Transmission electron microscopy was performed on a Hitachi H-9000UHR at 300KV to observe crystallite sizes.

Third-order optical nonlinearities were measured by a degenerated four-wave mixing with two-beam configuration. We used an excimer laser pumped dye laser with a pulse duration of 20 ns, a spectral width of 0.2 cm^{-1} and a pulse energy of $\leq 30\text{ }\mu\text{J}$. Diffraction efficiency D_{eff} , defined as the intensity ratio of the signal beam I_s to the pump beam I_p (I_s/I_p) and absorption coefficient α were measured at the wavelength of the Z_3 exciton absorption peak.

3. Results and discussion

Figure 1 shows a transmission electron micrograph and a crystallite size distribution of the sample treated at 435°C for 30 min ($x=0.75$). The small particles are randomly distributed in the matrix glass. The average particle diameter is 40 Å with a standard deviation of the distribution equal to 6 Å. Changing the heat-treatment temperature and duration, we obtained the microcrystallites with diameters of 30~64 Å.

Optical absorption measurements at 77 K show that absorp-

tion peaks due to Z_3 and Z_{12} excitons of CuCl are shifted to the shorter wavelength sides compared to Z_3 and Z_{12} exciton energies of the bulk crystal. This result indicates that the translational motion of excitons is confined in the microcrystallite. The radiative lifetime of Z_3 excitons are found to be dependent on the crystallite volume confirming the giant oscillator strength due to the quantum confinement²⁾.

Figure 2 shows diffraction efficiency D_{eff} and absorption coefficient α as a function of diameters for the pump power density of $13\sim 36$ KW/cm². D_{eff} decreases with increase in the diameter; this result is due to increase in α . The $\chi^{(3)}$ values of samples with particles in diameters of $30\sim 64$ Å are estimated to be 3×10^{-9} to 1×10^{-6} esu. The larger the diameter, the larger the $\chi^{(3)}$ values are obtained.

4. Conclusions

We have prepared the glasses doped with CuCl microcrystallites and measured third-order optical nonlinearity. We have found that $\chi^{(3)}$ values are enhanced with increase in crystallite diameter.

A part of this work was supported by NEDO (New Energy and Industrial Technology Development Organization).

References

- 1) R. K. Jain and R. C. Lind, J. Opt. Soc. Am. 73, 647 (1983)
- 2) A. Nakamura, H. Yamada and T. Tokizaki, Phys. Rev. B40, 8585 (1989)

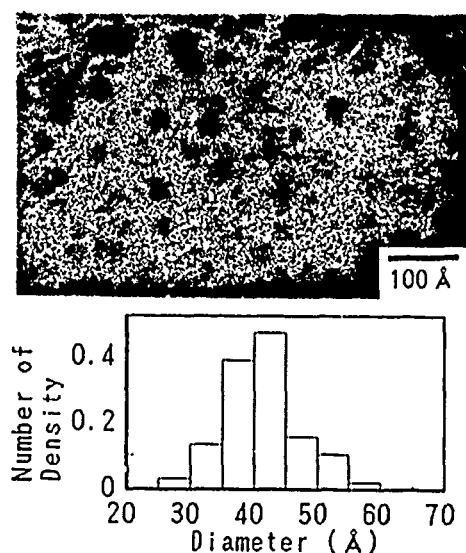


Fig.1 TEM micrograph and crystallite size distribution of sample treated at 435°C for 30 min.

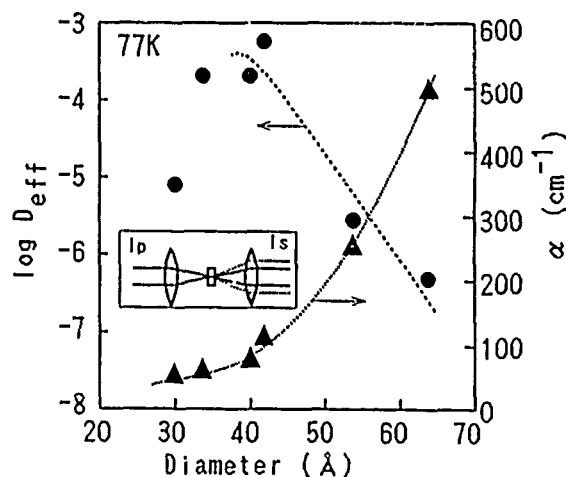


Fig.2 Diffraction efficiency and absorption coefficient as a function of diameter of microcrystallite.

THP14 Biexciton Phonon Interaction Studied by Two-Photon Polarization Spectroscopy

Makoto Kuwata-Gonokami, Jun Iwamatsu, Ryo Shimano
and Hidefumi Akiyama

Department of Applied Physics, Faculty of Engineering, The
University of Tokyo,
Hongo, Bunkyo-ku, Tokyo 113, Japan
tel. +81 3 812 2111 ext. 6836
fax. +81 3 816 7805

Line width of Γ 1 biexciton state of CuCl is measured under very weak excitation condition in the temperature range between 3.8K and 60K. To avoid the broadening of the line width due to higher order optical nonlinear effect, we used the two-photon polarization spectroscopy (TPPS)/1/ and kept the excitation power below $3\text{kw}/\text{cm}^2$. Because of the great sensitivity of this method, we could obtain the sufficient signal to noise ratio in such a weak excitation regime.

A dye laser pumped by an excimer laser is divided into two beams to make a circularly polarized pump beam and a linearly polarized probe beam. The dye laser line width is 0.024 meV. CuCl single crystals of the thickness between $5\mu\text{m}$ to $10\mu\text{m}$ are mounted in a He gas-flow-type cryostat. Figure 1 shows examples of TPPS spectra. At low temperature, the line width of the TPPS spectrum is very sharp and almost same as that of the dye laser. As we increase the temperature, the line width becomes broader. We plot the FWHM of TPPS signal as a function of temperature as shown in Fig.2. Below 30K the line width broadens gradually, almost linear to temperature but it starts broadening very rapidly above 40K.

We apply Toyozawa's theory of exciton phonon interaction into the analysis of the biexciton line width./2/ We found that single acoustic phonon absorption process determine the broadening of biexciton line width below 30K and LO phonon absorption process becomes important above 30K. The solid curve in Fig.2 shows the result of our fit. We obtain the value of deformation potential of biexcitons 1.04eV.

To evaluate the absolute value of true line width at low temperature limit, we analyze the line shape of TPPS signal including the effect of finite laser line width. From such analysis, it is possible to estimate the transverse relaxation constant Γ_{mg} from the experimentally obtained values of TPPS

line width and laser line width. In our experiments, TPPS line width is 0.0245meV at low temperature and the laser line width is 0.024meV. From these values, we get the value of $\Gamma_{mg} = 0.007\text{meV}$ which coincides with the relaxation constant calculated using the radiative life time of biexcitons, 50psec, measured by the luminescence decay time/3/. Thus at low temperature, the biexciton line width is determined by the radiative decay rate and there is no pure dephasing process.

references

1. M.Kuwata: J. Phys Soc. Jpn. 53 (1984) 4456.
2. T.Itoh, S.Watanabe and M.Ueta: J. Phys Soc. Jpn. 48 (1980) 542.
3. H.Akiyama, M.Kuwata-Gonokami, T.Kuga and M.Matsuoka: to be published.

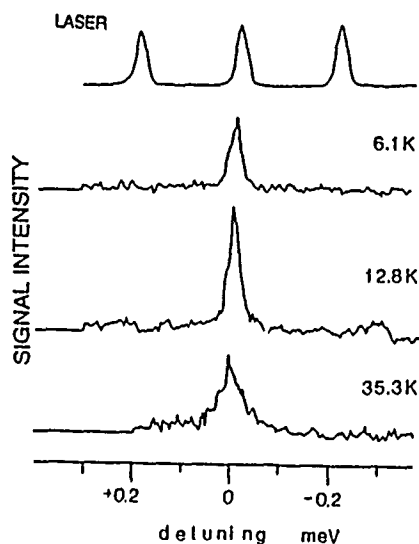


Fig.1
TPPS spectra at various temperature in CuCl.

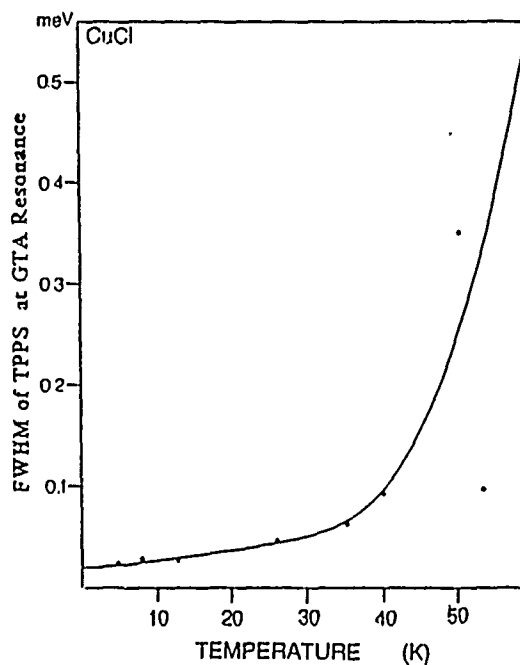


Fig.2
Plot of full width at half maximum of TPPS line versus temperature.

THP15 The Beam Propagation Method Applied to Nonlinear Optical Microstructures

I. Kim, P.J. Harshman, and T.K. Gustafson, University of California, Berkeley, CA

Summary

We have formulated expressions providing the number of terms (Y-G diagrams)¹ contributing to an n-th order susceptibility of a non-linear optical process. Obtaining an accurate count of these terms is important for diverse reasons:

- a) To accurately specify the number of terms needed to evaluate the nonlinear optical susceptibility either analytically or numerically,
- b) To help develop sequences of diagrammatic contributions which can be summed to provide analytical results for the strong interaction limit. An example is the two-level system for semiclassical and quantized fields,
- c) To treat two or more processes (terms) which could give rise to interference, resulting, for example, in extra resonances due to a lack of complete coherence,
- d) To generalize results from quantum electrodynamics to situations for which multiple photon interactions and zero point fluctuations associated with non-vacuum states need to be considered.

We shall discuss the number of possible diagrams in terms of three factors, which we call a permutation factor relating to the number of possible frequencies that can be assigned to each interaction vertex, a commutation factor relating to interaction vertex assignment on the two sides of the diagram, and a state factor relating to the number of diagrams generated from an enumeration of specific material state assignments between interaction vertices.

We will discuss the application of these results to several situations of interest including second harmonic generation, degenerate four-wave mixing, and resonant CARS (coherent anti-Stokes Raman scattering) in a four-level system.

The relevance of the present results to experimental results which have been obtained will be discussed along with future directions which need to be addressed including the summability of diagrams under specific approximations, the calculation of expectation values, and the nonperturbative representation of processes.

Reference

- ¹ T.K. Yee and T.K. Gustafson, Phys. Rev. **A18**, 1597 (1978).

THP16 Chirp and Self-Phase Modulation in Induced-Grating Autocorrelation Measurements of Ultrashort Pulses

Rick Trebino,** Carl C. Hayden,** Anthony M. Johnson,# and Alfred M. Levine†

While simple second-harmonic-generation autocorrelation techniques have been popular for measuring ultrashort pulse lengths, they do not provide the phase information that is crucial for a full understanding of the nonlinear-optical effects that can occur to pulses in ultrashort-pulse lasers and in optical fibers. *Interferometric* second-harmonic generation autocorrelation (ISHGA)¹ does provide phase information, but it is difficult to align and use. Here, we demonstrate theoretically and experimentally that *induced-grating* autocorrelation (IGA) techniques^{2,3} (or, equivalently, four-wave-mixing autocorrelation techniques) using slowly responding media yield the same phase information as ISHGA. IGA traces clearly display linear-chirp and self-phase-modulation (SPM) effects; linear chirp causes a narrowing of the trace, and SPM in the absence of group-velocity dispersion (GVD) causes easily recognized oscillations in the wings. These variations in the trace are the same as those that occur to the envelope of the high-frequency fringes in ISHGA traces, which are generally used to indicate the presence of the above two phase distortions. Conveniently, however, no high-frequency fringes occur in IGA methods. Other advantages of IGA methods include automatic phase-matching, single-wavelength operation, and applicability to most wavelength ranges (using a thermal grating simply requires an absorbing medium).

We also show that a wide range of four-wave-mixing autocorrelation and IGA arrangements (that is, three-beam induced grating,² two-beam coupling,³ phase conjugation, etc.) all yield *identical* theoretical results, specifically, the same two-dimensional integral of a fourth-order electric-field coherence function, which does not reduce to an intensity autocorrelation. In addition, we have performed numerical integrations, obtaining IGA and ISHGA traces for a variety of theoretical pulse distortions, including linear chirp, SPM, wave breaking, and phase and/or amplitude jitter. The table on the next page shows some of these traces. Note the close connection between IGA and ISHGA traces.

In addition, we have performed a wide range of two-beam-coupling experiments with ultrashort pulses <1 psec to 120 psec long at 1.06 μm and 532 nm from pulse trains of a cw mode-locked Nd:YAG laser. While any slowly responding nonlinear medium is appropriate for such measurements, we have used KNbO_3 , BaTiO_3 , and GaAs:Cr photo-refractive crystals, yielding simultaneous IGA and (non-interferometric) second-harmonic autocorrelations.³ We obtained varying amounts of chirp and SPM by using different wavelengths, different beam attenuations before propagation through a fiber, and different spacings between the pair of diffraction gratings in a fiber-grating compressor (or not using the gratings at all). The table also shows some of our experimental traces, illustrating the chirp-induced narrowing and SPM-induced oscillations in the wings.

Acknowledgements and References

We thank M. Klein and D. Rytz for providing the photo-refractive crystals.

1. J.-C. M. Diels, J.J. Fontaine, I.C. McMichael, and F. Simoni, Appl. Opt. 24, 1270 (1985).
2. R. Trebino, E.K. Gustafson, and A.E. Siegman, J. Opt. Soc. Am. B 3, 1295 (1986).
3. A.M. Johnson, A.M. Glass, W.M. Simpson, and D.H. Olson, CLEO '89.

** Combustion Research Facility, Sandia National Laboratories, Livermore, CA 94551.

AT&T Bell Laboratories, Holmdel, NJ 07733.

† The College of Staten Island, City University of New York, Staten Island, NY 10301.

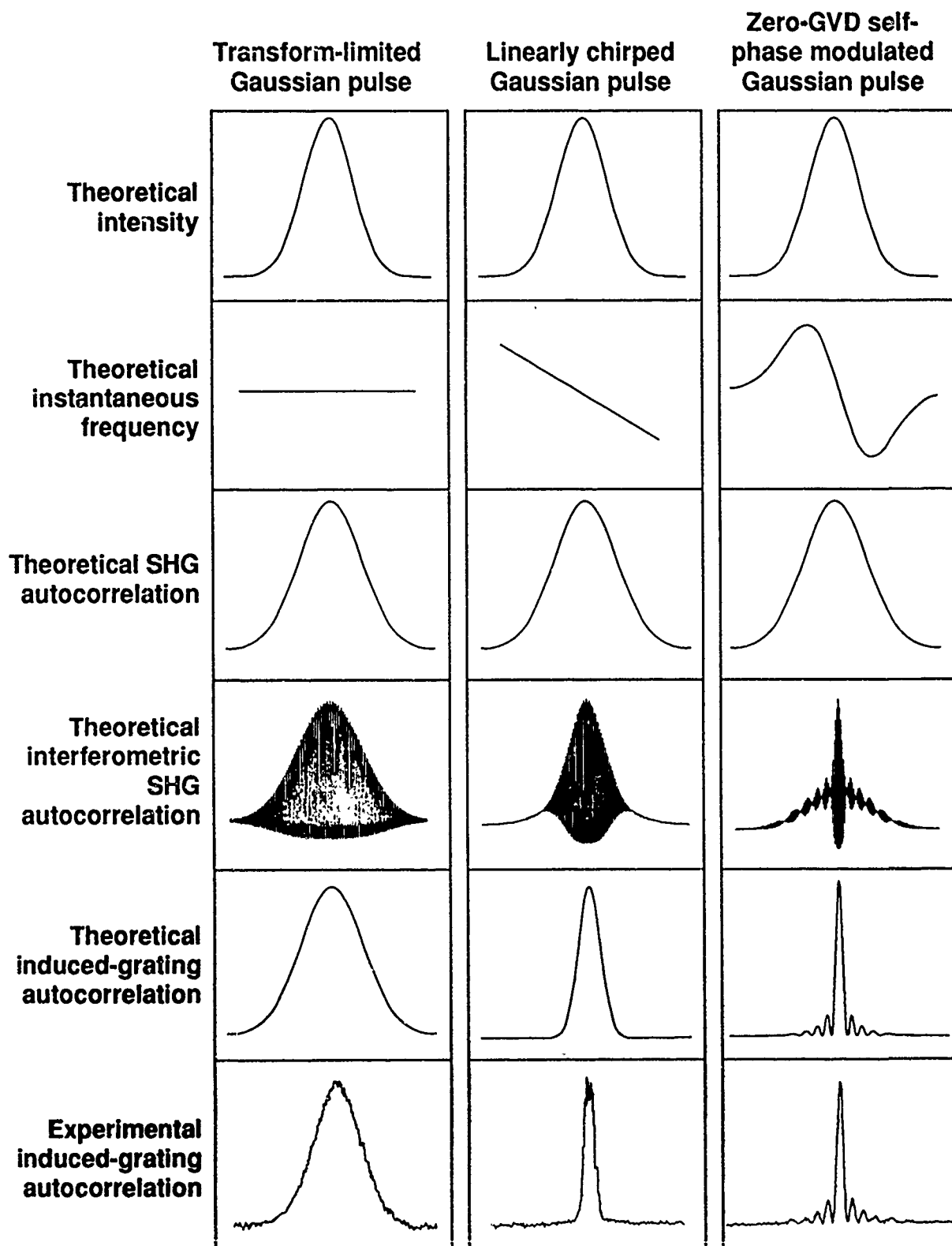


Table of autocorrelation traces. Induced-grating autocorrelation traces yield information similar to those of interferometric SHG autocorrelation, indicating the envelope of the latter's high-frequency fringes. Thus, chirp causes narrowing, and self-phase modulation yields narrowing and oscillations in the wings of the induced-grating autocorrelation trace. In these figures, the actual linearly chirped pulse yielded an SHG trace width of 121 psec and an induced-grating trace width of 1.7 psec, and so its induced-grating trace is shown with an expanded scale.

THP17 Phase Conjugate Interferometry for Thin Film Analysis

by Elaine R. Parshall and Mark Cronin-Golomb

Electro-Optics Technology Center
Tufts University
Medford, Massachusetts 02155
617-381-3136

A phase conjugate interferometer is used to measure the thickness (d) and complex index of refraction (n and k) of an absorbing thin film. This method is based on a interferometry technique developed by J. Shamir and P. Graff in 1975.¹ However, the phase conjugation process considerably improves the temporal stability and ease of alignment of the interferometer as discussed in a recent paper by Cronin-Golomb and Shamir.²

The interferometry technique of thin film analysis is based on the concept that absorption in the beamsplitter of an interferometer causes a relative phase change between the two exiting beams. Consequently, an absorbing film can be analyzed by placing it at the beamsplitter's position in a Michelson interferometer, as shown in Figure 1. By generating an additional phase difference with a translating mirror in one arm of the interferometer, the interfering beam intensities trace out an ellipse when the detector outputs are input to an X-Y plotter.

Self-pumped photorefractive barium titanate crystals which use four wave mixing to produce a phase conjugate reflection³ replace the conventional mirrors. The devices are self-aligning, making the interferometer easy to align and its operation very stable over time.

Using a method of thin film characteristic matrices where the reflectance and transmittance of a thin film are represented by⁴

$$r = -M_{12}/M_{11} \quad r' = M_{21}/M_{11} \quad t = 1/M_{11} \quad t' = |M|/M_{11},$$

the primes denoting light incident from the reverse direction of the unprimed quantities and M_{ij} being the elements of the characteristic matrix M , the detector outputs can be shown to be

$$I_1 = \alpha^2 + \beta^2 + 2\alpha\beta\cos\psi$$

$$I_2 = \gamma^2 + \delta^2 - 2\gamma\delta\cos[\psi - (\phi_{12} + \phi_{21})],$$

where

$$\alpha = qR_1|M|/m_{11}^2 \quad \beta = qm_{12}^2R_2/m_{11}^2$$

$$\gamma = m_{12}R_2|M|/m_{11}^2 \quad \delta = m_{21}R_1|M|/m_{11},$$

and where $M_{ij} = m_{ij}e^{i\phi}$, $R_j = |\rho_j|$, ρ_j being the complex reflectivity of each phase conjugate mirror (PCM), q is the relative efficiency of detectors one

and two of Figure 1, and ψ is a measure of the phase introduced by the translating mirror and each PCM.

By measuring the phase difference between the two sinusoids ($\phi_{12} + \phi_{21}$), and their relative intensities when each phase conjugate mirror is blocked in turn (α^2 , β^2 , γ^2 , δ^2), two independent parameters are obtained. The measured transmittance of the film ($T = n_3 \cos \theta_3 / m_{11}^2 n_1 \cos \theta_1$) gives a third parameter, m_{11}^2 , which together with the first two provide enough information to determine n , k , and d .

By this technique, a sample of vanadium pentoxide, V_2O_5 , was analyzed. A least squares minimization routine was used to fit the measured values of ($\phi_{12} + \phi_{21}$), $m_{12}m_{21}$, and m_{11}^2 to n , k , and d . The values for the optical constants are compared in Table 1 for ellipsometry versus interferometry measurements.

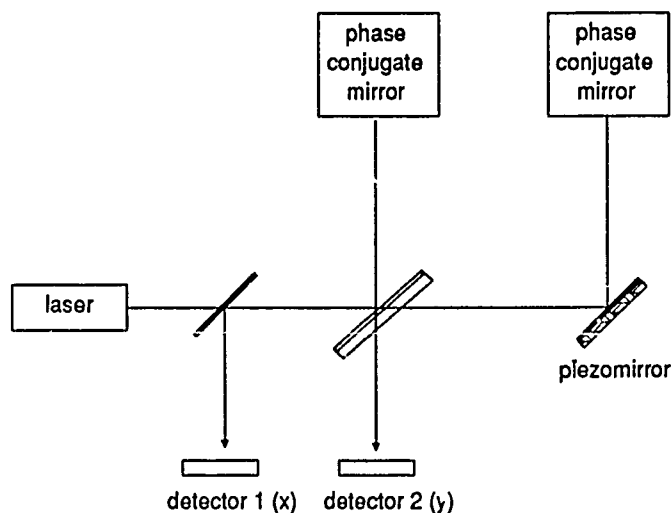
REFERENCES

1. J. Shamir and P. Graff, Appl. Opt., 14, 3053 (1975).
2. M. Cronin-Golomb and J. Shamir, Appl. Opt., 28, 5196 (1989).
3. J. Feinberg, Opt. Lett., 7, 486 (1982).
4. Pochi Yeh, Optical Waves in Layered Media, John Wiley and Sons, New York, (1988).

TABLE I: Comparison of ellipsometry and interferometry measurements of n , k , and d for V_2O_5 .

	n	k	d (nm)
Ellipsometry	2.0	0.1	82.5
Interferometry	2.1 ± 0.06	0.068 ± 0.004	79.0 ± 12

Figure 1: Phase conjugate interferometer for thin film analysis.



THP18 Coherence Effects in a Laser Phase-Locking Geometry

Mark T. Gruneisen, Edward D. Seeberger, and John F. Mileski
Quantum Optics Branch, The Weapons Laboratory
Kirtland Air Force Base, New Mexico 87117-6008

Summary

We present the results of an experimental study of the effects of laser coherence in a nonlinear coupling geometry. This geometry, which has been used to lock the frequencies and phases of separate laser oscillators,¹ combines the ring passive phase conjugate mirror² with incoherent beam coupling³ in photorefractive barium titanate. In practice, the two input beams that drive the nonlinear interaction are derived from separate lasers that are initially incoherent with respect to one another. The degree of coherence between the two input beams at the nonlinear medium will vary as the lasers lock phases. In addition, path-length considerations in the experimental set-up can strongly affect the fringe visibility within the nonlinear medium. In our experiments, the two input beams originate from a single, multilongitudinal-mode, helium-neon laser. The laser output is passed through a 50/50 beam splitter in order to generate the two input beams. The degree of coherence between the input beams at the crystal is varied through the use of both dynamic and static path-length delays.

In order to simulate the phase fluctuations that occur between two lasers that operate at the same frequency but are not phase locked, we make use of a dynamic path-length delay to vary the phase of one input field on a timescale much shorter than the response time of the barium titanate. If the magnitude of the delay is as large as one-half of an optical wavelength, we find that the interaction behaves as one would expect for two mutually incoherent input fields. That is, the input beams are diffracted into cones of light due to incoherent beam coupling.³ If however, the magnitude of the delay is decreased to much less than an optical wavelength, degenerate four-wave mixing occurs due to the coherent interaction of the counterpropagating fields of the passive ring with the second input field. During the transition from incoherent to coherent inputs, the cones of light collapse into phase conjugate spots.

The fringe visibility at the nonlinear medium can be severely degraded for an inappropriate choice of path-lengths within the phase-locking geometry. This results from the dephasing of the various longitudinal modes with propagation. We simulate this effect with a variable path-length delay. For the case in which the delay is comparable to the broadband coherence length (speed of light/total lasing bandwidth) of the laser, but less than the coherence length for a single longitudinal mode, we find that the individual lasing modes still interact coherently within the nonlinear medium even though the fringe contrast for the total optical field is

essentially zero. As a result, the interaction behaves as if the two input beams are mutually coherent and strong degenerate four-wave mixing is observed.

1. P.D. Hillman and M. Marciniak, WL/AROF, KAFB, NM.
2. M. Cronin-Golomb, B. Fischer, J.O. White, and A. Yariv, Appl. Phys. Lett. 42, 919 (1983).
3. D. Statman and B. Liby, J. Opt. Soc. Am. B 6, 1884 (1989).

THP20 Cross-Talk in Self-Pumped Photorefractive Phase Conjugation

F.C. Jai Gdz, P.R. Forman, and B.L. Mason

Los Alamos National Laboratory, MS-K639, Los Alamos NM, 87545

ABSTRACT:

We present data for Fourier-analyzed amplitudes of discrete frequency modulation components transferred between two multimode fibers configured as the signal arms of two Michelson interferometer pairs and sharing the same BaTiO₃ phase conjugation crystal.

SUMMARY:

In an attempt to use a single self-pumped BaTiO₃ phase conjugation crystal with several multimode fiber Michelson configuration interferometers deployed as independent temperature sensors we noticed some undesired cross-talk between them; i.e. some time correlated apparent temperature rises in interferometers not deliberately subjected to a temperature change when another channel was heated.

To investigate this cross-talk quantitatively we limited the inputs to only two interferometer pairs. The reference arms of the interferometers, as before, were wrapped around piezoelectric stretchers. Each was driven at a frequency, Ω , ~ 25 kHz, large compared to the signal frequencies of interest. This imparts a phase modulation to the light transmitted through the reference arms via the sinusoidal length modulation. The signal detected by a photodiode after return in both arms from the phase conjugator and recombination in the fourth port of the 50:50 input coupler can then be ex-

pressed with the well known expansions for $\cos(z \cos \Omega t)$ and $\sin(z \cos \Omega t)$ as an infinite series of Bessel functions:

$$I = 1 + \cos \phi [J_0(z) + 2 \sum_{k=1}^{\infty} (-)^k J_{2k}(z) \cos(2k\Omega t)] \\ + \sin \phi [2 \sum_{k=0}^{\infty} (-)^k J_{2k+1}(z) \cos((2k+1)\Omega t)]$$

where the reference beam phase modulation amplitude is given in radians of phase shift, z , and the desired signal from the sensing arm is ϕ . Electronic filtering of the signal at Ω and 2Ω then leads to $\cos \phi$ and $\sin \phi$, from which ϕ can be derived by repeatedly taking the arctan. (If successive data points do not differ by more than two quadrants, $\phi(t)$ can be followed through arbitrary multiples of 2π with standard techniques.)

By winding the fiber sections originally intended for temperature sensing also around piezoelectric cylinders as in the reference beams, but driven at much lower stretching frequencies, (400 and 500 Hz, respectively) we can Fourier analyze the signals of each interferometer and examine the frequency content of each.

The results are sensitively dependent on the exact configuration of the fiber inputs relative to the phase conjugation crystal and can vary from showing only the examined interferometer's own impressed signal frequency to an equal mix of both interferometers' impressed frequencies. Intermediate cases also exhibit small amplitude beat frequencies.

These observations can be accounted for by a model that allows for the phase conjugated return beams to vary from fully self-pumped phase conjugated to fully externally pumped phase conjugated.

The extent of the experimenter's control of the exact configurations will be discussed. This places limitations on the original multiple independent sensor concept, but opens new possibilities where cross-talk may be desirable. It also strongly suggests that the static two dimensional phase conjugate images attributed to the self-pumping mechanism may have considerable contributions from the more general external pumping mechanism.

THP21

Nonlinear Optics with an Argon Laser

J.D. Harvey
Department of Physics
University of Auckland
Private Bag
Auckland
New Zealand
Ph: 64-9-737932

Summary

Recently we have demonstrated^(1,2,3) that a mode locked cavity dumped argon laser system is capable of generating pulses considerably shorter than those available with a conventionally mode locked system. In conjunction with the reduced pulse width, the laser produces pulses with much higher (> 2 kW) peak powers than a simple mode locked system, whilst still operating at megahertz repetition rate. This repetition rate and the high stability of the system enable signal averaging techniques to be utilised in studies of nonlinear optical phenomena using this laser. Using this laser we have observed: frequency doubling in β barium borate crystals (BBO) stimulated Raman scattering in optical fibres (Figure 1), modulation instabilities in birefringent optical fibres and two photon absorption.

The strong stimulated Raman scattering has enabled the construction of a fibre Raman laser producing subpicosecond pulses at 527nm, whilst the study of the mechanism of production of the short pulses in the laser has led to interesting results concerning the coherent interaction of the beam with the atomic medium.^(3,4) The frequency doubling has generated a beam of short (~ 20 ps) pulses at 257nm wavelength and approximately 50W peak power.

The stability of this laser system is at least as good as that of a conventionally mode locked system, and we have been able to generate short pulses at all argon wavelengths except 488nm, where good mode locking has not been obtained due to the high gain of the amplifying medium.

References

1. J.D. Harvey, M.J. Proctor, C. Steed, (1988), *30ps cavity dumped pulses from an argon laser*, Appl.Phys. Lett. 52, 688-690.
2. J.D. Harvey, J. Dudley, R. Leonhardt, S. Carter and P.D. Drummond (1989), *The Generation of Mode-Locked Pi Pulses*, Quantum Optics V, Springer Proceedings, Vol. 41, 214-221, 1989.
3. J.D. Harvey, R. Leonhardt, S. Carter & P.D. Drummond, (1989), *Superfluorescent generation of Mode-Locked Pi pulses*, Phys.Rev., A40, 4789-4792, 1989.
4. J. Dudley, J.D. Harvey and R. Leonhardt, (1990), *Coherent Ringing in Pulses from a mode locked argon laser*. Accepted for publication in Optics Letters.

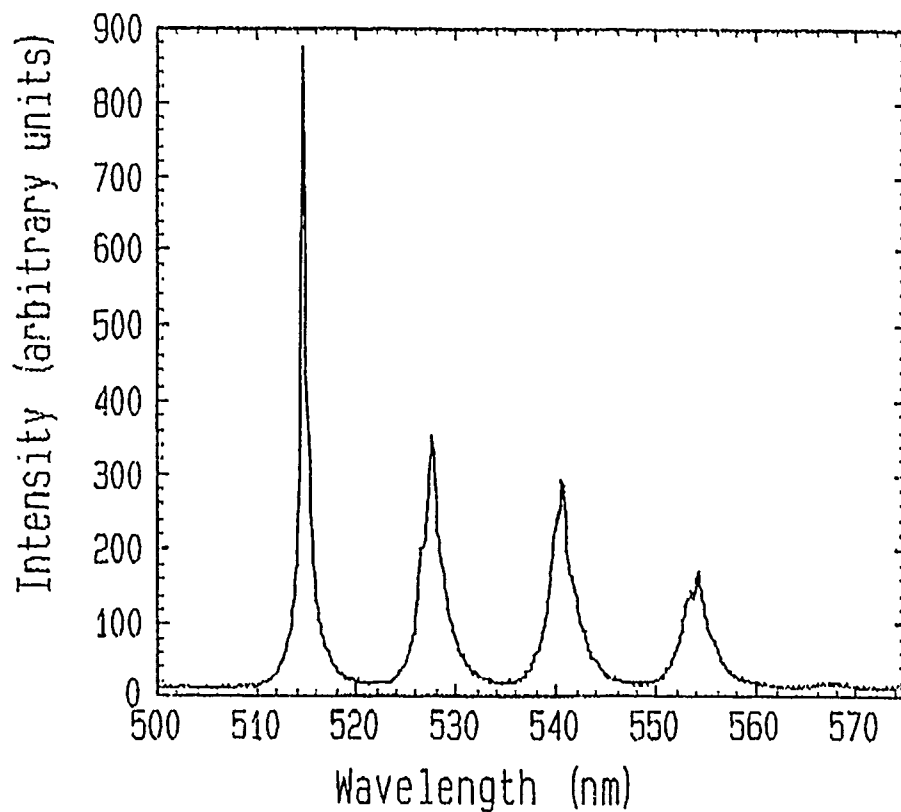


Figure Caption

Figure 1: Spectrum of pulse train exiting a 20m length of birefringent fused silica fibre pumped with pulses from the cavity dumped mode locked argon laser operating at 514.5nm. Peak power of the pulses ~2kW. Pulse repetition rate 3.8MHz. Peak power of pump pulses in the fibre ~500W. Pulse width 30ps. Up to 4th Stokes radiation can be detected.

THP22 Self-Pumped Optical Phase Conjugation In Cesium Vapor

C.J. Gaeta and J.F. Lam
Hughes Research Laboratories
3011 Malibu Canyon Road
Malibu, California 90265
U.S.A.
(213) 317 - 5760

Cesium vapor was used to demonstrate the first self-pumped optical phase conjugation process in the near-infrared in a resonant atomic system. Such a process has previously been demonstrated in a resonant two-level system in sodium vapor at visible wavelengths.¹ The use of cesium vapor makes it possible to operate at wavelengths in the range of operation of laser diodes making it a candidate phase conjugate mirror for use in a laser diode master oscillator/power amplifier (MOPA) system.

A glass cesium vapor cell was placed inside of an optical cavity formed by two mirrors arranged in approximately a concentric format. An incident cw probe beam from a Coherent 699 single frequency ring dye laser was directed into the cell at an angle of about 0.5° with respect to the resonator axis. Two-wave mixing gain² allowed the cavity mode to exceed oscillation threshold while internal four-wave mixing³ between the counterpropagating resonator optical fields and the incident beam produced a phase conjugate of the probe.

We will report on the behavior of this self-pumped process as experimental parameters such as probe frequency and intensity, as well as cesium number density, are varied. Prospects for the use of this atomic system as a phase conjugate mirror for a laser diode MOPA system will also be discussed. This work was supported by the Defense Advanced Research Projects Agency under contract N00014-87-C-0090.

Gaeta, et al, "Self-pumped optical phase conjugation in cesium vapor."

REFERENCES

1. C.J. Gaeta, J.F. Lam and R.C. Lind, Opt. Lett. 14, 245 (1989).
2. M.T. Gruneisen, K.R. MacDonald and R. Boyd, JOSA B 5, 123 (1988); G. Khitrova, P.R. Berman and M. Sargent III, JOSA B 5, 160 (1988).
3. R.L. Abrams and R.C. Lind, Opt. Lett. 2, 94 (1978); D.M. Bloom, P.F. Liao and N.P. Economou, Opt. Lett. 2, 58 (1978).

THP23 Dual-Port Optical Neural Network Using a Mutually Pumped Phase Conjugate Mirror

G.J. Dunning, Y. Owechko and B.H. Soffer

Hughes Research Laboratories
3011 Malibu Canyon Road
Malibu, California 90265
(213) 317-5544

We have demonstrated many features of an optical neural network which uses both spatial and angular selectivity of photorefractive holographic gratings to interconnect the neurons. A major advantage of this technique is that all neurons can be optically addressed simultaneously without the associate problems of crosstalk. This system has demonstrated homoassociations, heteroassociations, and interconnectivity between 1400 neurons. Devices based on this architecture have the potential of modeling networks with 10^5 neurons and 10^{10} interconnections.

The neurons are represented as a 2-D array of pixels on a spatial light modulator (SLM) with the activation level represented by the intensity (Figure 1). Each interconnection weight is stored as a set of photorefractive gratings in a mutually pumped phase conjugate mirror (MP-PCM). In this configuration there are two independently controlled input beams into the MP-PCM which mutually interact in a crystal of BaTiO_3 . The gratings produced by one beam are read by the second beam, producing two optical outputs. This allows the implementation of neural networks with simultaneous bottom-up and top-down interactions. The gratings are highly selective and only produce an output when both the angular orientations and positions of the input beams match those used during the recording process, which greatly reduces crosstalk.

We can implement learning algorithms by changing the interconnection weights coherently in real time with an electronic feedback loop consisting of a CCD detector, video frame grabber and computer-controlled SLM. The phase conjugate output from the crystal is monitored by Camera 1 and acquired by the frame grabber/image processor. The pattern is processed on a point by point basis electronically to generate an error signal. The signal is then displayed on the liquid crystal light valve SLM to adjust the weights between neurons.

In this talk we will present recent data on the system resolution, response time, cross-talk suppression, interconnectivity and our progress toward implementing supervised learning. This work is supported in part by Defense Advanced Research Projects Agency.

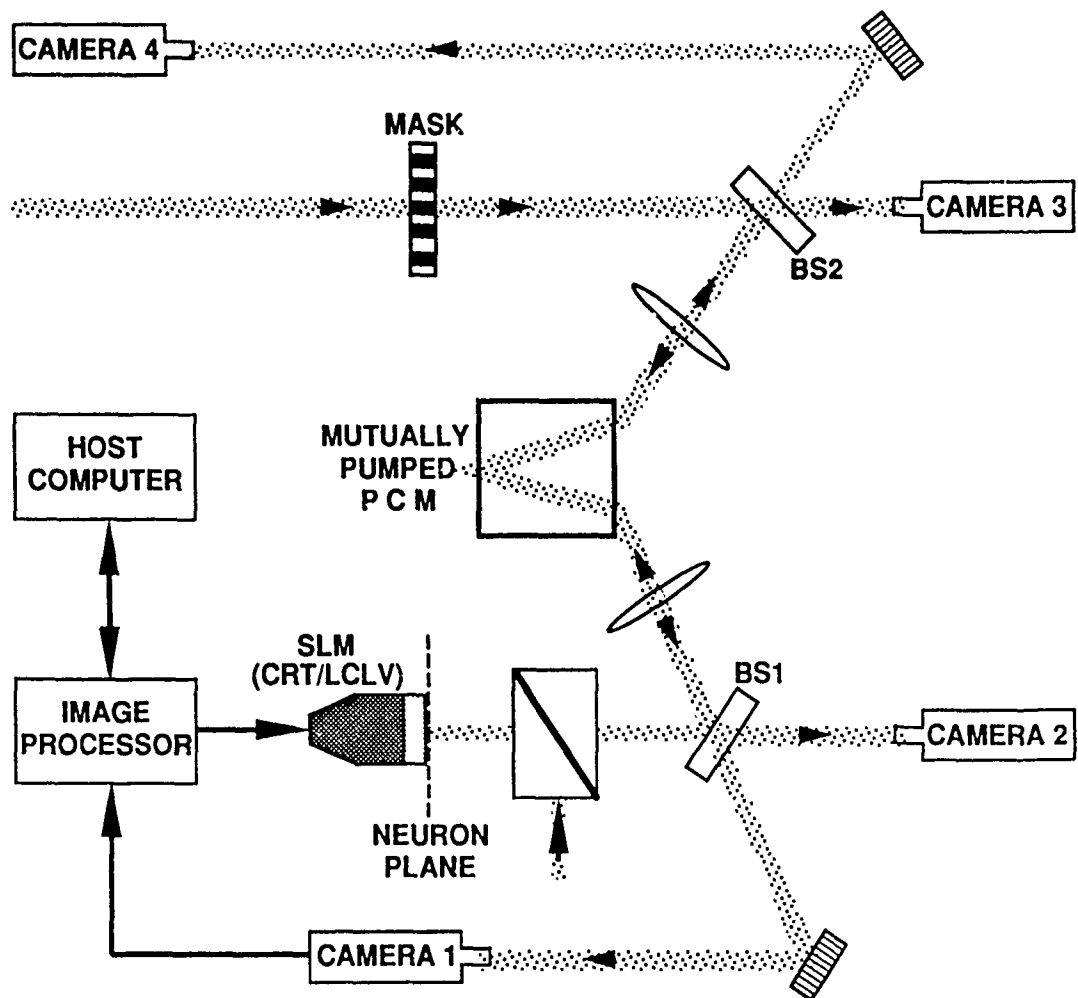


Figure 1. Architecture for mutually-pumped optical neural network.

A M Scott, K D Ridley, G Cook

Royal Signals and Radar Establishment
St Andrews Road, Malvern, Worcestershire WR14 3PS, UK

The direction of a laser beam may be steered either using a mechanically driven mirror or by other means such as acousto-optic or electro-optics deflectors. The problem with mechanically driven mirrors is that they are relatively slow and may consume substantial amounts of power. However acousto-optic deflectors can only handle low power beams because of their small aperture.

In this paper we describe a novel application of phase conjugation which makes it practical to steer laser beams without any mechanically moving parts [1]. A device such as an acousto-optic modulator can be used to steer a low power beam and this beam is then transmitted through a high reflectivity mirror (say 99%) to a high reflectivity phase conjugate mirror which may have a reflection co-efficient as high as 10^8 [2,3]. This will produce a conjugate beam which will be reflected by the high reflectivity mirror; and as the low power beam is pointed in a particular direction the direction of the higher power beam will also be controlled.

This approach has a number of advantages over an alternative approach, in which a low power steerable beam is amplified by a non-linear mechanism such as stimulated Brillouin scattering. In the amplification approach one has to generate a low divergence steerable beam and then transmit it without distortion through the amplifier, for all steering angles. When a high reflectivity phase conjugate mirror is used the problem can be split into two parts, firstly one of producing a low divergence steerable beam and then one of building a high reflectivity phase conjugate mirror which has a high fidelity. This is easier to achieve than coupling a beam through a high gain amplifier without distortion.

We describe the experiments in which the concept is demonstrated by using a mechanical mirror to produce the low power beam steering and Brillouin induced four wave mixing is used to produce the high reflectivity phase conjugation. Beam steering over a $2^\circ \times 2^\circ$ field of view has been achieved. Current experiments will also be described in which an acousto-optic modulator combined with a phase conjugate mirror produces high power beam steering without any mechanical moving parts. Finally an approach to achieving full two-dimensional beam steering will be described.

References:

- [1] A M Scott, British Patent Application No. 8909711 (1989)
- [2] N F Andreev, et al Soviet Physics JETP letters Vol. 32 625-629 (1981)
A M Scott, K D Ridley, IEEE Quantum Electron Vol 25 438-459 (1989)
- [3] K D Ridley, A M Scott 'High Reflectivity Phase Conjugation using Brillouin Preamplification' submitted to Optics Letters (1989)

THP25 Linear Stability of Photorefractive Phase Conjugation

G. Li, J. A. Tataronis, and B. E.A. Saleh
 University of Wisconsin-Madison
 Department of Electrical and Computer Engineering
 1415 Johnson Drive
 Madison, WI 53706-1691

The stability of photorefractive phase conjugation is an important issue in a variety of applications. Zozulya and Tikhonchuk¹ addressed the stability problem analytically and applied their results to specific nonlinear equilibrium states in various geometrical configurations. However, they limited their analysis to real wave amplitudes. Since phase information is crucial, it is important to determine the stability within the framework of complex amplitudes. The linear stability of such stationary states has been addressed *numerically* by Cronin-Golomb and Shaw². Here, we provide an analytical approach to the stability problem that leads to explicit solutions.

We consider photorefractive phase conjugators with only transmission gratings. The complex amplitudes of the forward pump, the backward pump, and the probe and conjugate signals are respectively A_f , A_b , A_p and A_c . From the four coupled first order differential equations that govern the spatial evolution of the wave amplitudes and the single first order equation describing the formation and evolution of the grating, we find that the ratio, $A_f/A_p^* \equiv \psi(z,t)$ satisfies a nonlinear integro-differential equation,

$$\tau \frac{\partial}{\partial t} \left[\int_0^z dz' \frac{2\psi^*}{|\psi|^2 + 1} \frac{\partial \psi}{\partial z'} - \ln \left(\frac{A_p^{*2}(z=0)}{d_1} \right) \right] \frac{\partial \psi}{\partial z} - \left(\tau \frac{\partial}{\partial t} + 1 \right) \frac{\partial \psi}{\partial z} = \frac{\gamma}{I_0} (\alpha \psi^2 + \beta \psi - \alpha^*), \quad (1)$$

where I_0 is the total intensity; τ is the material response time; γ is the photorefractive coupling coefficient; d_1 , α and β are spatially invariant quantities determined by boundary conditions. A similar equation for A_c/A_b^* can also be derived. We analyze Eq.(1) by perturbing about a time-invariant, equilibrium state, $\psi_0(z)$,

$$\psi_0(z) = \frac{D S_+ \exp(-\mu z) - S_-}{1 - D \exp(-\mu z)}, \quad (2)$$

where the constants D , S_+ , S_- and μ are related to α , β , γ , I_0 and the boundary conditions. Following the standard techniques of linear stability analysis, we find that $\psi_1(z, \omega)$, the complex Fourier transform of the perturbation about the equilibrium state, $\psi_0(z)$, is governed by a second order, ordinary differential equation with variable coefficients. Assuming a time dependence in the form, $\exp[i\omega t]$, the following equation governs $\psi_1(z, \omega)$,

$$2i\omega\tau \frac{\psi_1^*(\partial\psi_0/\partial z) - \psi_1(\partial\psi_0^*/\partial z)}{(|\psi_0|^2 + 1)^2} = \frac{\partial}{\partial z} \left[\frac{\gamma}{I_0} \frac{2\alpha\psi_0\psi_1 + \beta\psi_1}{\partial\psi_0/\partial z} - i\omega\tau \frac{2\psi_0^*\psi_1}{|\psi_0|^2 + 1} + (1 + i\omega\tau) \frac{\partial\psi_1/\partial z}{\partial\psi_0/\partial z} \right]. \quad (3)$$

Because of the mathematical structure of the equilibrium solution, we introduce a transformation of the independent variable in Eq. (3) from z to $\zeta \equiv \exp(\pm\mu z)$ for positive and negative coupling coefficients respectively. This coordinate transformation produces a second-order differential equation with variable coefficients that are finite polynomials in ζ . This feature of the equation suggests that ψ_1 be represented as a polynomial in ζ . The allowed values (poles) of complex ω and criteria for amplitude and phase stability appear after invoking homogeneous boundary conditions. The condition for instability is that the imaginary part of ω be negative. The computational effort involved in searching for the poles is expected to be less in the present approach than in purely numerical approaches.

With the present approach, the linear stability of some special conjugation geometries can be determined explicitly. One of such special cases is when the constant D is small for which ψ_1 can be approximated as

$$\psi_1 = B_1\zeta + B_2\zeta^{1/(1+i\omega)}. \quad (4)$$

We shall explore other special cases for which the linear stability can be determined analytically.

¹A. A. Zozulya and V. T. Tikhonchuk, Phys. Lett. A 135(8,9) 447-452 (1989).

²M. Cronin-Golomb and K. Shaw, XVI International Conference on Quantum Electronics Technical Digest (Tokyo), 132-133 (1988).

THP26 Optical and Structural Characterization of Semiconductor-Doped Glasses

L. Baldassarre^o, C. De Blasi⁺, V. Degiorgio^{*}, G. Fagherazzi^{oo}, M. Ferrara^o,
M. Lugarà^o, S. Pelli^{**}, and G. C. Righini^{**}

^o Physics Department, University of Bari, Italy

⁺ Department of Material Science, University of Lecce, Italy

^{*} Department of Electronics, University of Pavia, Italy

^{oo} Department of Physical Chemistry, University of Venice, Italy

^{**} IROE CNR, Firenze, Italy

Semiconductor-doped glasses (SDG) are attracting increasing attention due to their interesting nonlinear optical properties, combined with the advantage of a relatively simple technology of material processing, e.g. for producing guided-wave devices.

Commercial glass filters with $\text{CdSe}_x\text{S}_{1-x}$ microcrystallites, however, are certainly not optimized for this kind of applications, and experimental glasses are therefore being developed in several laboratories.

As a first step toward the optimization of SDG, a better knowledge of the optical and structural properties of the glasses already available is required. For that purpose, different techniques have been used and the results are discussed in the present paper. Measurements have been made on commercial Schott and Corning SDG filters, as well as on experimental glasses.

a) Optical properties

Spectroscopic methods, based on absorption, luminescence and Raman spectra, are used to investigate quantum effects due to electron, hole and exciton confinement. In particular, in experimental KS-19 glasses, luminescence spectra have been obtained using for the excitation a dye laser (Rhodamine 6G) pumped by a nitrogen laser ($h\nu = 3.68$ eV, $\tau = 5$ ns, $P(\text{peak}) = 100$ kW). Emission spectra obtained at different pump powers and at various temperatures, in a broad range, show the presence of: i) a luminescence band due to bulk exciton recombination, which is peculiar to the doping semiconductor; ii) a higher-energy band, due to exciton recombination in the microcrystallites: its energy location depends on the microcrystallites size. The latter band increases with the pump power more rapidly than the former band does and can be observed at temperatures up to 150 °K.

The measurement of the confinement energy, that is of the energy difference between the peaks of the two bands, allows one to have an estimate of the crystallite size; in

the KS-19 sample the estimated size is around 15 nm.

Tests are in progress for completing the optical characterization of optical waveguides produced in SDG by ion exchange; the effects of $\text{Cs}^+ - \text{K}^+$ exchange on absorption spectra will be discussed.

b) Structural properties

Transmission Electron Microscopy (TEM) and Transmission High Energy Electron Diffraction (THEED) have been used in order to study the morphology and the structure of the material. The specimen were chemically thinned and observed in a Philips EM 400T electron microscope, operating at 120 kV accelerating voltage. Crystallite "grains" have been observed in high-magnification TEM images and their sizes have been evaluated; for KS-19 sample there is a good agreement with the results obtained by luminescence measurements. Sharp and continuous rings have been evidenced in the THEED patterns, confirming that the grains have a rather polycrystalline structure.

The crystallite structure has been checked also by x-ray diffraction. Referring again to KS-19 sample, the angular diffraction scan shows two relatively broad peaks, corresponding to reflections from the (110) and (103) planes of the hexagonal structure. The derived crystallite sizes were: 5 nm normally to (110) and 8 nm normally to (103), so indicating a certain shape anisotropy. The selenium-to-sulfur mole fraction in the microcrystalline phase, as determined from x-ray diffraction data, is in agreement with the molar fraction as determined from optical spectrophotometric measurements. On the contrary, the molar fraction in the entire glass, as determined from microprobe analysis, is much smaller, indicating that large part of sulfur is not incorporated in the crystallites.

As an alternative, the crystallite size has been determined using an original approach, based on the small-angle neutron scattering technique; the measurements, at 10 Angstrom wavelength, have been carried out on different samples at the Institute Laue-Langevin in Grenoble, France.

A critical comparison of the various techniques and of the results obtained will be presented at the Conference.

We wish to express our acknowledgments to Dr. Zimin, USSR Academy of Sciences in Minsk, and to Dr. Grosskopf, IOT GmbH, for making available samples of experimental and commercial SDGs; thanks are due to Mr. M. Pucci, IEQ-CNR, for his technical assistance.

Part of this work has been supported by the CNR's Special Project on *Special Materials for Advanced Applications*.

THP27 New Phenomena on Laser-Induced Photorefractive Effect in $\text{LiNbO}_3:\text{Fe}$

New Phenomena on Laser-Induced Photorefractive Effect in $\text{LiNbO}_3:\text{Fe}$

Peng Wenji, Li Qingxing, and Yu Zhenxin

Institute for Lasers and Spectroscopy, Zhongshan University
Guangzhou 510275, P. R. China, Tel. 425563

Summary

In this paper, a new and regular oscillation phenomenon appeared in the two-beam coherent coupling in the photorefractive material ion-doped lithium niobate crystal is described.

Referring to Fig. 1, an argon-ion laser (488.0 nm) serves to pump the $\text{LiNbO}_3:\text{Fe}$ and the beam reflected from BS and M is used to probe the laser-induced Photorefractive effect in the crystal. This crystal is aligned so that its c-axis makes an angle of 45° with the polarizer P_1 which is perpendicular to the polarizer P_2 . As soon as the pump beam is unblocked, the probe signal is decreased greatly with a time constant of 5 seconds, just like switched off. And then a regular and permanent oscillation occurs (Fig. 2). the reduction and oscillation of the probed signal in the present of the pumped beam depend on the orientation of the crystal (c-axis) relative to the polarizer P_1 .

The mechanism of this permanent regular oscillation phenomenon will be discussed.

The authors gratefully acknowledge the Support of National Science Foundation of China and K. C. Wong Education Fundation, Hong Kong.

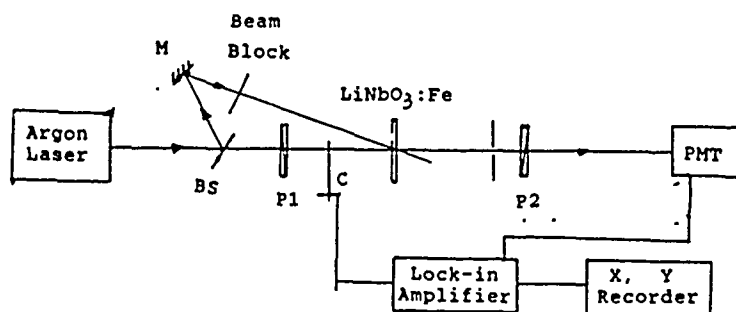


Fig. 1. Experimental arrangement for the Laser-Induced photorefractive effect. P1, P2 are polarizers; BS is a 10% beam splitter; C is a chopper; and PMT is a photomultiplier.

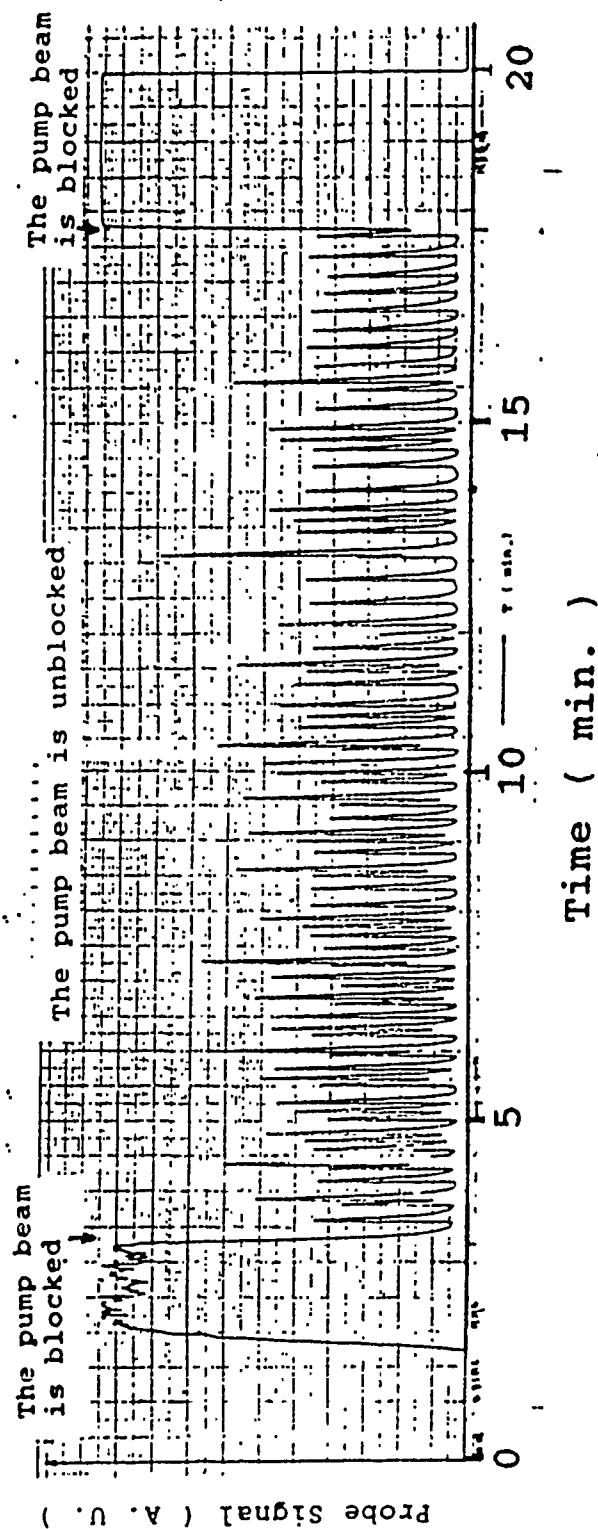


Fig. 2. Characteristics of the oscillation in the two-beam coherent coupling in $\text{LiNbO}_3:\text{Fe}$.

FRIDAY, JULY 20
ORAL PRESENTATIONS

Emmett N. Leith and Andre Cunha

Department of Electrical Engineering and Computer Science
University of Michigan, Ann Arbor, Mi. 48109-2122

Nonlinear methods have produced significant improvements in images formed under adverse conditions. In particular, phase conjugation, both double pass (object-bearing beam passing twice through the inhomogeneity) and single pass (object beam passing only once) have led to a capability of image formation through inhomogeneities. This process can be significantly enhanced by a combination of aperture and coherence reduction, leading to resolution beyond the classical limit, or superresolution. The basis for this second method is similar to phase conjugation in that an object bearing wave is mixed with a second beam at a detector. There are various differences, e.g., incoherent light is required, and a conjugation of the phase is not required. In the superresolution process, the object bearing wave behaves as if it had traversed the reference beam path, which is taken to be both aberration free and of significant size.

Using the superresolution method, we can improve on the two pass phase conjugation method, and we can effectively convert single pass phase conjugation into two pass phase conjugation, thereby gaining the full benefit of improved phase error compensation that the two pass method offers in comparison with the single pass method.

We have identified situations of image formation through inhomogeneities where the phase conjugation process, either one or two pass, completely fails, but the superresolution process by itself, without phase conjugation, gives perfect compensation. We also consider optimization, where a combination of the two processes is found to give better performance than either by itself.

We finally consider the possibility of obtaining resolution with small apertures for both paths, i.e., resolution through a pair of pinhole apertures with essentially no aperture at all in the system. Nonlinear effects combine to produce a system that sees a significant aperture where there is actually none.

A CO₂ Laser with a Nonlinear Mirror

N.R. Heckenberg, R. McDuff, and A.E. Smith
Physics Department
The University of Queensland
Qld 4072, Australia

A pulsed CO₂ laser has been operated using an InSb etalon as a cavity mirror. The nonlinear behaviour of the mirror causes significant modification of the pulse shape. Although a quasi-steady state analysis suggests the possibility of producing relatively square pulses (in time), experiment reveals strong transient ringing which a dynamic model reproduces and shows to be the result of quadrature oscillations in the cavity irradiance and etalon carrier density (and hence reflectivity).

The pulsed CO₂ laser is a single mode 2.7m cavity TEA/low pressure CW hybrid type with a 15mROC 85% reflector as output coupler and plane InSb etalon as second cavity mirror. Whole-beam output pulse shapes were measured using photon-drag monitors. The nonlinear behaviour of the etalon mirror had previously been characterized by extra-cavity measurements and shown to be satisfactorily explained by refractive index modifications due to the presence of photogenerated carriers which are produced by two photon absorption and lost by Auger recombination. [1,2] In this work diffusion can be neglected apart from its role in destroying refractive index gratings set up by standing waves.

The process is not a true χ_3 nonlinearity and is dominated by the characteristic decay time of the carriers which is typically of order 50ns. This turns out to be similar to the photon decay time in the laser cavity, leading to an instability, which is clearly exhibited in the output pulses (see fig.1) and the results [2] of numerical solutions of coupled rate equations for the discharge tube level populations, cavity irradiance (plane wave), and etalon photogenerated carrier density (fig.2).

Fig. 3 is an etalon reflectivity/cavity irradiance 'phase diagram' which compares the dynamical computer solution (full line) with the quasi-steady state solutions which would apply in the limit of slow (compared to 50ns) variations [3]. Under such conditions the operating point would be the intersection of the etalon reflectivity characteristic curve and the curve representing the increasing reflectivity required to maintain the laser at threshold in spite of saturation of the gain for the particular value of small signal gain pertaining. The diagram shows that quasi-steady conditions prevail in the tail of the pulse, and that because of the sharp drop in reflectivity around $1.3 \times 10^9 \text{ W/m}^2$, transients aside, a strong internal limiting process should act to stabilize the laser power in spite of temporal variation of laser small signal gain g .

Our calculations [3] also show that the transient ringing would be eliminated if the carrier lifetime were reduced to 1ns while retaining the same degree of nonlinearity, showing that square pulse production is still a possibility. It certainly should be with nonlinear materials exhibiting a true χ_3 response.

References

- (1) Wei Ji, A.K. Kar, J.G.H. Mathew and A.C. Walker, IEEE J Quantum Electron QE-22, 369-375 (1986).
- (2) R. McDuff and N.R. Heckenberg, "Laser Cavity with a Nonlinear Mirror" accepted for JOSA B.
- (3) N.R. Heckenberg, R. McDuff, and A.E. Smith, "Pulse Shaping in a Laser with an Irradiance Dependent Cavity Mirror", accepted for J. Mod. Opt.

Acknowledgements

The authors would like to thank Dr. A.C. Walker and the Physics Department, Heriot-Watt University for the etalon used, and DSTO for financial support.

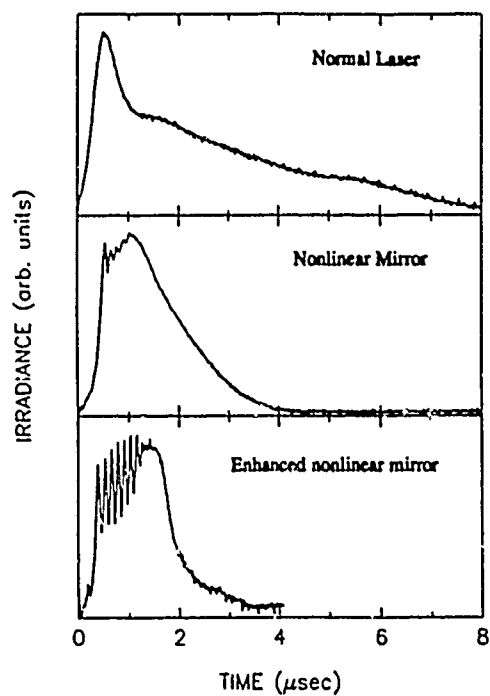


Figure 1. Experimental Pulse shapes

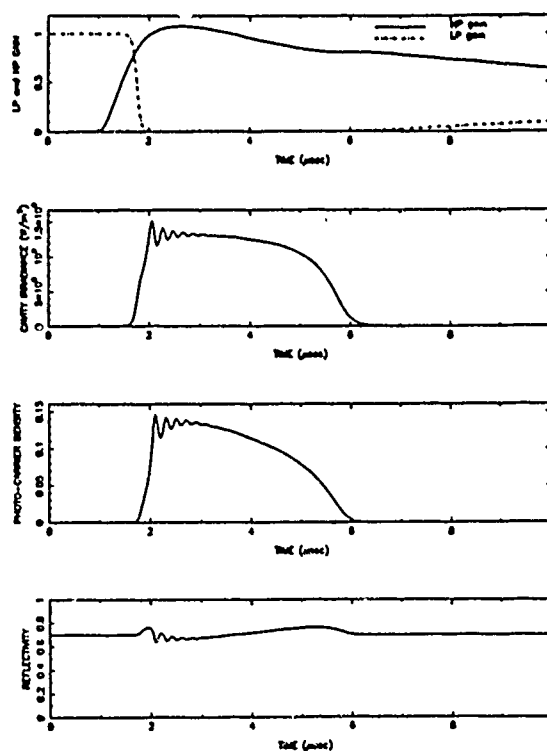


Figure 2. Computer Model Results (ref.3)

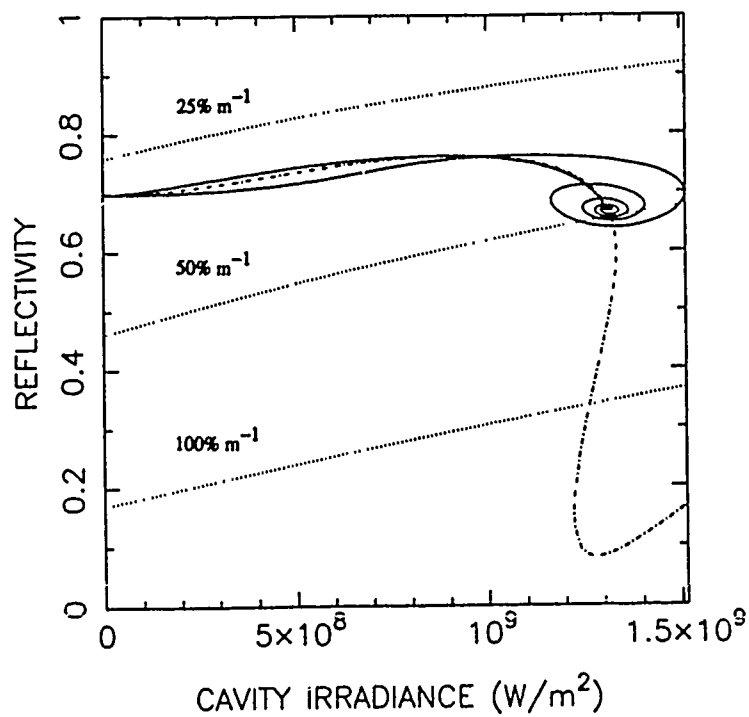


Figure 3. Operating Conditions

F15 WAVE MIXING IN THE PHOTOREFRACTIVE CRYSTALS

N. Kukhtarev, A. Volyar
Institute of Physics
Ukrainian Academy of Sciences
Prospect Nauki 26,252650 Kiev, USSR

Two-wave and four-wave mixing in the cubic and polar crystals is discussed. For cubic crystals influence of piezoelectricity and electrogyration in the dynamic hologram formation was investigated. It is show, that observed anomoly in the angular dependences of the 2-wave mixing in BSO and BTO crystals can be explained by influence of the piezoelectric effect.

In the polar crystal LiNbO_3 new configuration of phase conjugation was found which allow to produce polarization preserved PC with correction of an optical field after modal scrambling in a fiber.

M.D. Ewbank
 Rockwell International Science Center
 1049 Camino Dos Rios
 Thousand Oaks, CA 91360

SUMMARY

The demonstration of optical phase conjugation in photorefractive materials has been accomplished by numerous methods, including *i)* externally-pumped four-wave mixing,¹ *ii)* self-pumped (passive) phase conjugation,^{2,4} *iii)* stimulated backscattering,^{5,6} and *iv)* mutually-pumped phase conjugation.⁷⁻¹⁰ Stimulated backscattering and self-pumped phase conjugators have only a single incident beam. On the other hand, externally-pumped four-wave mixing has two auxiliary pumping beams in addition to the incident probe beam. Different still is the cross-conjugation of the two incident beams in mutually pumped phase conjugators. To use these conjugators in a given application, the compatibility between the processes generating the phase-conjugate wave(s) and the application must be considered. The distinguishing features of the different conjugators translate to advantages or disadvantages for certain applications.

Long-distance optical communication is a good example of an application which can benefit from phase conjugation (for aberration correction, self-tracking, etc.), but the coherence requirements favor self- and mutually-pumped phase conjugators over externally pumped four-wave mixing. Furthermore, the two independent laser transmitters can be readily accommodated by mutually-pumped phase conjugators, in contrast to self-pumped phase conjugators. Temporal signals transfer through the mutually-pumped phase conjugator having a modulation depth of 100% without any detectable cross-talk.

Pulsed lasers serve as temporally-modulated sources and are compatible with mutually-pumped phase conjugators in some unique ways. Incident pulses from two separate lasers onto a mutually-pumped phase conjugator are not required to be simultaneously present, but can be completely asynchronous, and the shared photorefractive holograms will still form. Since the temporal modulation of the two incident beams can be drastically different (e.g., nsec pulses and cw), useful laser-mode conversions can be performed.

Fiber-optic systems can also benefit from phase conjugation by nullifying modal scrambling, compensating thermal instabilities and maintaining fiber coupling alignment. When fiber lengths exceed laser coherence lengths, applicable phase conjugation techniques become restricted. As in optical communication, coherence is difficult to achieve in external pumping beams for four-wave mixing. Self-coherence in stimulated scattering or self-pumped phase conjugators and mutual incoherence in mutually-pumped phase conjugators make these conjugators more amenable with optical systems containing long fibers.

References

1. J. Feinberg and R.W. Hellwarth, *Opt. Lett.* **5**, 519 (1980).
2. J.O. White, M. Cronin-Golomb, B. Fischer and A. Yariv, *Appl. Phys. Lett.* **40**, 450 (1982).
3. J. Feinberg, *Opt. Lett.* **7**, 486 (1982).
4. M. Cronin-Golomb, B. Fischer, J.O. White and A. Yariv, *Appl. Phys.* **42**, 919 (1983).
5. T.Y. Chang and R.W. Hellwarth, *Opt. Lett.* **10**, 408 (1985).
6. R.A. Mullen, D.M. Pepper and G.C. Valley, *CLEO Tech. Dig.* **11**, 144 (1989).
7. S. Weiss, S. Sternklar and B. Fischer, *Opt. Lett.* **12**, 114 (1987).
8. R.W. Eason and A.M.C. Smout, *Opt. Lett.* **12**, 51 (1987).
9. M.D. Ewbank, *Opt. Lett.* **13**, 47 (1988).
10. P. Yeh, T.Y. Chang and M.D. Ewbank, *JOSA* **B5**, 1743 (1988).

Competitive and Cooperative Dynamics in Photorefractive Optical Systems

Dana Z. Anderson, Claus Benkert and Anno Hermanns
Department of Physics and Joint Institute for Laboratory Astrophysics
University of Colorado, Boulder, CO. 80309-0440 U.S.A.

Our purpose in this presentation is to discuss and demonstrate two multimode photorefractive systems. The first is a multimode ring oscillator with "winner-takes-all" dynamics. The oscillator has several (in our case five) possible stable steady state solutions. The state of the system can be switched with an injected signal. A slight modification of the resonator gives a system having no stable steady states; the modes of the system turn on then off in an ordered sequential pattern, looping continuously though the set of five modes. This is an optical manifestation of the "voter's paradox" in which a system of competing elements cannot come to a consensus.

The modes of a ring resonator having photorefractive gain can be qualitatively described by a set of Volterra-Lotka equations, which are the classic instance of a competitive system: The intensity I_j of mode j , for example, evolves as:¹

$$\dot{I}_j = I_j \left(a_j - \gamma_j - \beta_j I_j - \sum_{k \neq j} \theta_{jk} I_k \right), \quad (1)$$

where α is the gain and γ is the passive loss coefficient. The β_j 's are called the self-saturation coefficient while the θ_{jk} 's are the cross-saturation coefficients. We suppose that the modes have identical linear gains α and passive losses $\gamma < \alpha$. The key to designing the dynamics of the system is in controlling the values of the self- and cross- coupling coefficients. Setting all $\beta_j = \beta$ and $\theta_{jk} = \theta$, winner-takes all dynamics is established provided $\theta > \beta$. This condition is implemented by allowing the modes to interact via two-beam coupling. Fig. 1 shows a schematic of the ring oscillator, omitting lenses. Five multimode fibers define the modes of our system. The first photorefractive crystal on the left sits in the Fourier planes of two copies, the ring modes and a set of twins, of the image of the fiber outputs. The arrow shows the direction of energy coupling. Here, each mode's twin is able to derive energy from any of the other modes through two-beam coupling. This interaction alone induces $\theta = \beta > 0$. The second crystal lies in an image plane. Here, each mode is made to undergo coupling only with its twin—it gains energy from its twin. This reduces self-saturation, so that the combined pair of crystals gives $\theta > \beta$. The mode interaction is detailed in Fig. 2. The third crystal provides overall gain to all modes.

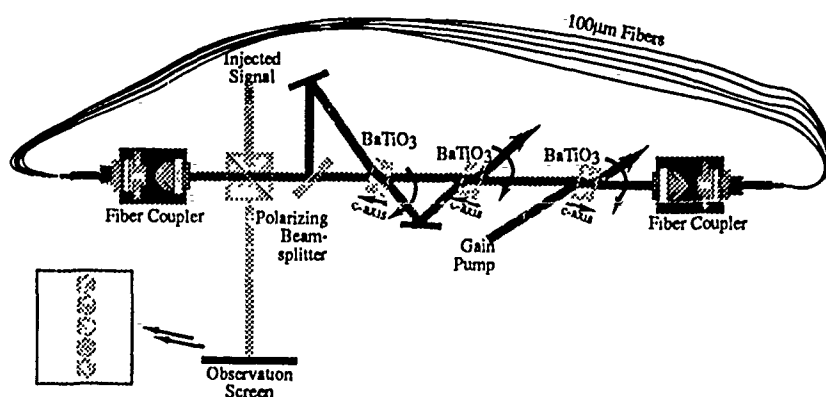


Figure 1. Schematic of photorefractive ring resonator. Five fibers define the modes of the ring. The beam coupling in the first two photorefractive crystals of barium titanate on the left determine the nature of the dynamics. The third crystal provides overall gain to the modes. The direction of energy coupling in the photorefractive crystals is shown by arrows.

The demonstration of this optical circuit is shown on video tape. Here we can merely describe the demonstration. With the gain present the ring oscillates in a single mode —on the observation screen only one fiber speckle pattern is observed. We show that any one of the five modes can be selected by injecting a gaussian beam in the direction of one of the desired mode. For convenience, we cheat a bit by injecting S-polarized light into the ring. Thus the coupling interactions for the injected signal take place after one round-trip in the ring.

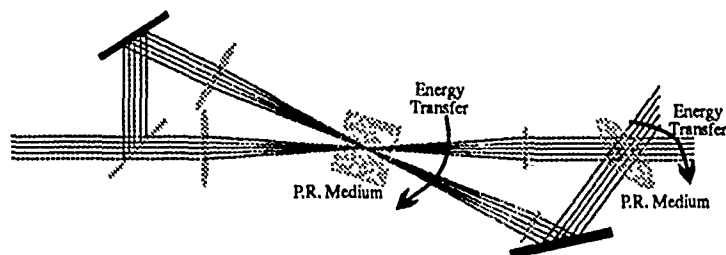


Figure 2. Schematic of mode interaction via two-beam coupling. The first photorefractive (P.R.) medium lies in the Fourier planes of the resonator modes and a set of "twins". The second medium lies in an image plane.

Voter's paradox dynamics is obtained by modifying the second coupling interaction, as shown in figure 3. Rather than simply couple a mode back to itself after the Fourier plane interaction, the mode is also coupled to its neighbor. This reduces $\theta_{j,j+1}$, in fact, it can cause it to become negative—in which circumstance a mode j cooperates with its neighbor, $j+1$. The last in the chain of twins is wrapped back to the first mode. The voter's paradox circuit is otherwise identical with the winner-takes-all. Again the behavior has been recorded on video tape. We force the system to start in the uppermost mode corresponding to figure 3 with an injected signal, or by blocking the path of the other four modes. Once the constrained system has reached steady-state the constraint is removed. The brightest output from the ring evolves successively from one mode to the next until the fifth one is reached. The fifth mode remains oscillating and is accompanied by a dimmer (by a factor of about 1/8) fourth mode.

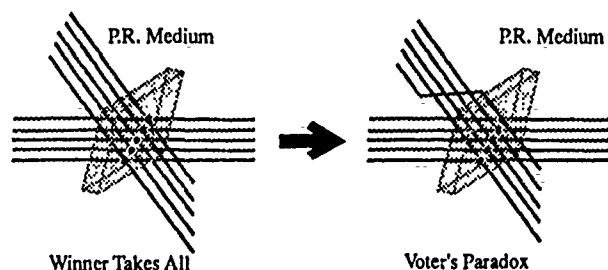


Figure 3. Modification of mode interaction to obtain Voter's Paradox dynamics. In the image plane, each twin is coupled to its neighboring mode. The last twin is wrapped back around to the first mode.

We gratefully acknowledge the support of the Office of Naval Research and the National Science Foundation's Engineering Research Center program through the Optoelectronic Computing Systems Center. Dana Z. Anderson is an Alfred P. Sloan Research Fellow.

1. D. Z. Anderson and R. Saxena, "Theory of multimode operation of a unidirectional ring oscillator having photorefractive gain: weak-field limit," JOSA B4, 164, (1987).

Internal and External Ring Cavity Self-Pumped Phase Conjugators and Their Dynamic Processes in Different Photorefractive Crystals

Zhang He-Yi and He Xue Hua
Physics Department, Peking University

Tang Sing Hai
Physics Department, National University of Singapore

SUMMARY

The exponential gain coefficient Γ of two wave coupling of $\text{KNbO}_3:\text{Fe}$ crystal was studied as a function of several external controlled parameters (such as the angle 2θ between two interaction beams and the angle β between the refractive index grating and c-axis of the crystal). The fitted calculated curve of Γ as a function of angle β agrees with the experimental data.

According to the data for Γ a new kind of passive self-pumped phase conjugator with external ring cavity was designed. The specially cut crystal allows the angle β to go from $40^\circ \sim 60^\circ$, which corresponds to the maximum gain. The p-polarized Ar^+ laser beam at $\lambda = 5145 \text{ \AA}$ with diameter 1 mm passes through a ring cavity formed by two mirrors. A retroreflected beam is thus generated by nonlinear processes. The maximum phase-conjugate reflectivity $R = 35\%$ was obtained.^[1]

A passive self-pumped phase conjugator with internal ring cavity using a specially cut $\text{KNbO}_3:\text{Fe}$ crystal was also designed.^[2] It is shown in Fig. 2. The self-pumped phase conjugate wave reflectivity is very high and $R \approx 70\% \sim 74.8\%$. The highest phase conjugate reflectivity is equal to $R = 74.8\%$ while the input laser power $P = 5 \text{ mW}$, the beam diameter $d \approx 0.3 \text{ mm}$. It is the highest value of R to our knowledge up to now.

The phase conjugate nature of the retroreflected beams both for external ring cavity and internal cavity phase conjugators has been confirmed. Similarly, passive self-pumped phase conjugator with external ring cavity made of BSKNN crystal was also investigated. The phase conjugate reflectivity is equal to 30%. When one of the cavity mirrors was vibrated a little bit the reflectivity increased to 40%. It is due to the increase of the two wave coupling gain Γ by the moving grating effect.

The specular reflectivity from the input surface of $\text{KNbO}_3:\text{Fe}$ crystal was observed to decrease with the building-up of the phase conjugate signal.

The dynamic processes of the creation and relaxation of the refractive index grating were also studied. Both the creation and relaxation processes are not single exponential curves. The relaxation process of the index grating is a fast decay followed by a slow decay. In some situations the oscillation of the phase conjugate wave was also observed and explained.

References

1. Zhang He-Yi et al, CLEO '89 Post deadline paper PD-6 (to be published).
2. Zhang He-Yi et al, To be published, APL.

Internal and External Ring Cavity Self-Pumped Phase Conjugators and Their Dynamic Processes in Different Photorefractive Crystals

Zhang He-Yi and He Xue Hua
Physics Department, Peking University

Tang Sing Hai
Physics Department, National University of Singapore

SUMMARY

The exponential gain coefficient Γ of two wave coupling of $\text{KNbO}_3:\text{Fe}$ crystal was studied as a function of several external controlled parameters (such as the angle 2θ between two interaction beams and the angle β between the refractive index grating and c-axis of the crystal). The fitted calculated curve of Γ as a function of angle β agrees with the experimental data.

According to the data for Γ a new kind of passive self-pumped phase conjugator with external ring cavity was designed. The specially cut crystal allows the angle β to go from $40^\circ \sim 60^\circ$, which corresponds to the maximum gain. The p-polarized Ar^+ laser beam at $\lambda = 5145 \text{ \AA}$ with diameter 1 mm passes through a ring cavity formed by two mirrors. A retroreflected beam is thus generated by nonlinear processes. The maximum phase-conjugate reflectivity $R = 35\%$ was obtained.^[1]

A passive self-pumped phase conjugator with internal ring cavity using a specially cut $\text{KNbO}_3:\text{Fe}$ crystal was also designed.^[2] It is shown in Fig. 2.

The self-pumped phase conjugate wave reflectivity is very high and $R \approx 70\% \sim 74.8\%$. The highest phase conjugate reflectivity is equal to $R = 74.8\%$ while the input laser power $P = 5 \text{ mW}$, the beam diameter $d \approx 0.3 \text{ mm}$. It is the highest value of R to our knowledge up to now.

The phase conjugate nature of the retroreflected beams both for external ring cavity and internal cavity phase conjugators has been confirmed. Similarly, passive self-pumped phase conjugator with external ring cavity made of BSKNN crystal was also investigated. The phase conjugate reflectivity is equal to 30%. When one of the cavity mirrors was vibrated a little bit the reflectivity increased to 40%. It is due to the increase of the two wave coupling gain Γ by the moving grating effect.

The specular reflectivity from the input surface of $\text{KNbO}_3:\text{Fe}$ crystal was observed to decrease with the building-up of the phase conjugate signal.

The dynamic processes of the creation and relaxation of the refractive index grating were also studied. Both the creation and relaxation processes are not single exponential curves. The relaxation process of the index grating is a fast decay followed by a slow decay. In some situations the oscillation of the phase conjugate wave was also observed and explained.

References

1. Zhang He-Yi et al, CLEO '89 Post deadline paper PD-6 (to be published).
2. Zhang He-Yi et al, To be published, APL.

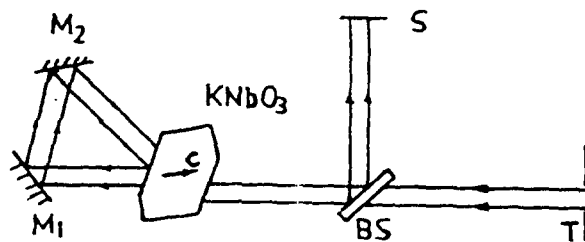


FIG.1 SELF-PUMPED PHASE CONJUGATOR WITH EXTERNAL RING CAVITY

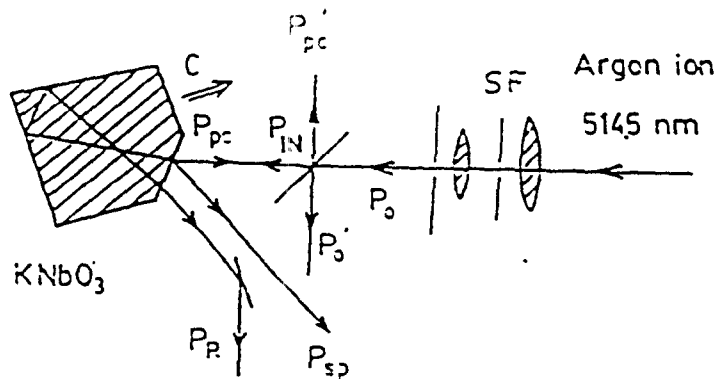


FIG.2 SELF-PUMPED PHASE CONJUGATOR WITH INTERNAL RING CAVITY

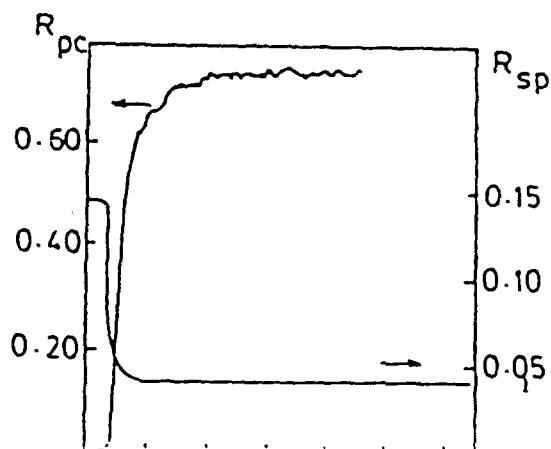


FIG.3 PHASE CONJUGATE REFLECTIVITY R_{pc} AND SPECULAR REFLECTIVITY AGAINST TIME

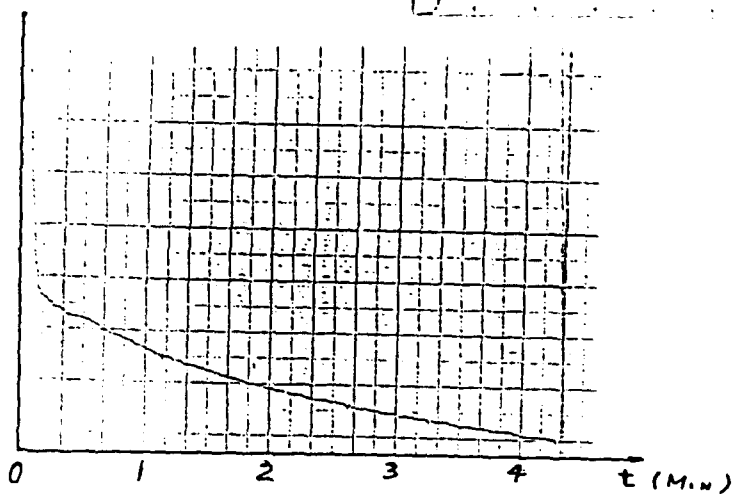


FIG.4 RELAXATION PROCESS OF INDEX GRATING OF A SELF-PUMPED PHASE CONJUGATOR

E.W. Van Stryland, D.J. Hagan, M. Sheik-bahae, D.C. Hutchings and M.J. Soileau

Center for Research in Electro-Optics and Lasers
 University of Central Florida
 Orlando, Florida 32816

Passive optical limiting results from irradiance-dependent nonlinear optical processes in materials. We review the mechanisms responsible for passive limiting using semiconductors.^{1,2} These devices utilize two-photon absorption (2PA) along with photogenerated carrier defocusing within the material to limit the output fluence and irradiance. We previously ignored the contribution from the bound electronic nonlinear refractive index n_2 .^{1,2} Recent measurements by us show that n_2 contributes significantly to the observed self-defocusing.³ It had previously been assumed that the electronic Kerr induced refraction (n_2) was positive. Using our newly developed Z-scan technique we observe (see Fig. 1) that n_2 changes sign from positive to negative at a wavelength somewhere between the 2PA and fundamental absorption edges.

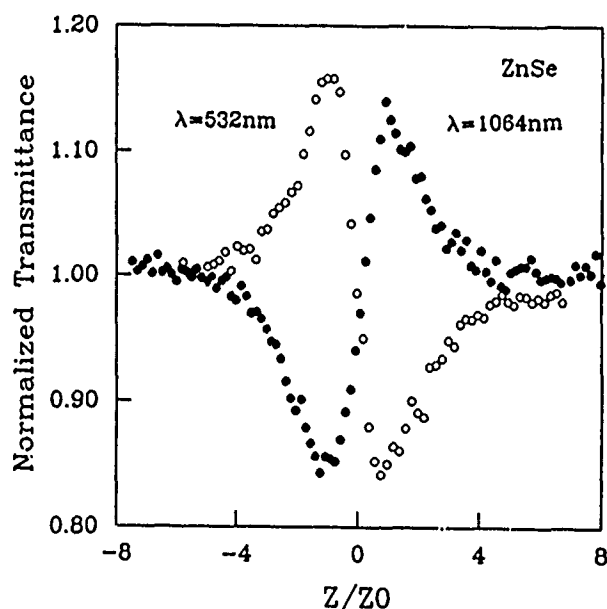


Fig. 1. Normalized transmittance versus sample position in units of $Z_0 = \pi \omega_0^2 / \lambda$ in a Z-scan experiment showing the sign change of n_2 from + at $1.06 \mu\text{m}$ to - at $0.53 \mu\text{m}$.

The sensitivity of this Z-scan technique has allowed us to make accurate measurements of the 2PA coefficient β , the free-carrier refraction coefficient σ , and n_2 for several semiconductors at different wavelengths. The equations governing these nonlinearities are; $dI/dz = -\beta I^2$ and $d\Phi/dz = k(n_2|E|^2/2 - \sigma N)$, where I is the irradiance, Φ the slowly varying phase of the field and N is the density of two-photon generated free carriers given by $dN/dt = \beta I^2 / 2\hbar\omega$.

We find that the wavelength dependence of σ is well described by simple band-blocking models⁴, and that β and n_2 are both well predicted by a simple two-parabolic-band model. In this model, β is calculated by second order perturbation theory from the transition probability. n_2 is then calculated via a Kramers-Kronig relation. More recently we have included the contributions of the electronic Raman and AC Stark effects to the nonlinear absorption spectrum for the Kramers-Kronig calculation of n_2 . Remarkably, this simple theory accurately predicts n_2 for dielectric materials as well as semiconductors for photon energies from far below the band-gap energy E_g , to within 3% of E_g .⁵ The sign change between the 2PA edge and 1PA edge is correctly predicted as seen in Fig. 2 which shows the dispersion of n_2 as a function of $\hbar\omega/E_g$.

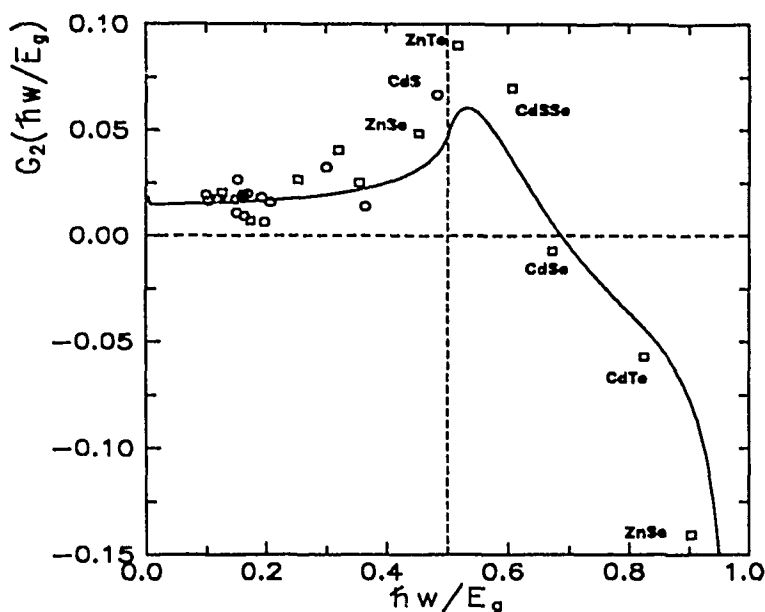


Fig. 2. A plot of $G_2(\hbar\omega/E_g)$, the dispersion of n_2 . Data are scaled by $n_0 E_g^4/K$, where n_0 is the linear index and K is a numerical constant.

We have used this combination of nonlinearities to build optical limiters for the visible based on ZnSe and ZnS.² These work exceedingly well for picosecond inputs where carrier absorption is negligible while carrier defocusing is still strong. The fluence limiting characteristics are seen in Fig. 3 which shows the spatial energy distribution of a $0.53 \mu\text{m}$ pulse ≈ 10 cm after transmission through a 3 mm thick polycrystalline sample of ZnSe. The solid line fit to the data uses $\beta=5.5$ cm/GW, $\sigma=0.8 \times 10^{-21}$ cm³ and $n_2 \approx -4 \times 10^{-11}$ esu, agreeing with the Z-scan results.

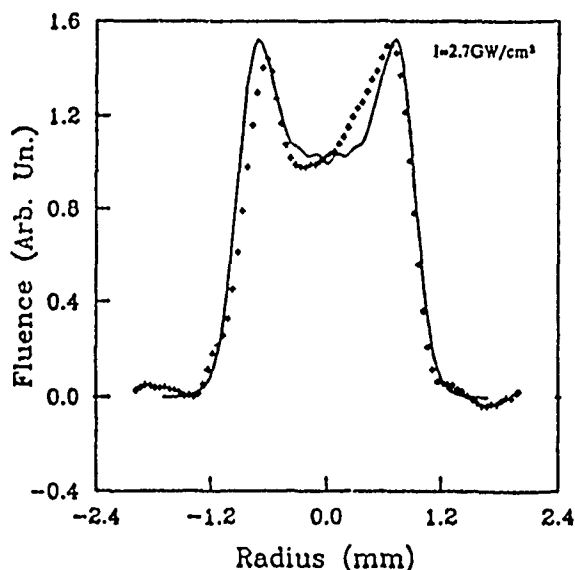


Fig. 3. The transmitted spatial energy distribution of a 30 ps $0.53 \mu\text{m}$ pulse after transmission and propagation through ZnSe as viewed on a vidicon. The solid line is the theoretical fit to the defocusing.

1. Van Stryland *et. al.*, Opt. Eng. 24, 613 (1985).
2. Van Stryland *et. al.*, J. Opt. Soc. Am. B5, 1980 (1988).
3. Sheik-bahae *et. al.*, IEEE J. Quantum Electron, April(1990).
4. Hagan *et.al.*, SPIE Vol 1105, (1989).
5. LaGasse *et. al.*, Appl. Phys Lett., 56, 417 (1990).

F111 Nonlinearities of Gallium Arsenide Doping Superlattices

M. S. Tobin, G. J. Simonis, J. D. Bruno

Harry Diamond Laboratories, 2800 Powder Mill Road, Adelphi, MD 20783

The doping superlattice (DSL) consists of alternating n- and p-doped layers that may have undoped (i-) layers in between. The unusual optoelectronic properties of these crystals include high sensitivity of the below-band-gap optical properties to low light intensities and very long recombination times of optically excited carriers.¹ We summarize results of several experiments done on gallium-arsenide (GaAs) doping superlattices at room temperature.

Optical phase and amplitude modulation of a 1.06- μm probe was obtained with a waveguide selectively-contacted² reversed-biased DSL sample. The waveguide structure consists of 10 periods of p-i-n-i layers of GaAs with thicknesses of 60, 50, 45, and 50 nm, respectively, plus an additional p-layer. The doping density of the p-type layer is $2 \times 10^{18} \text{ cm}^{-3}$ and that of the n-type layer is 10^{18} cm^{-3} . The incorporation of 1 μm of AlGaAs above and below the superlattice creates a 1.2-mm-long planar waveguide. A heterodyne interferometer was used for the measurements.³ Phase modulation in excess of 5π and power amplitude modulation of more than 30 dB have been achieved with above-band-gap excitation at milliwatt power levels.

Optical characterization was done over a broad spectral range using a tungsten lamp dispersed through a monochromator to serve as a low-intensity probe propagating normal to the layers. A helium-neon laser was the pump source. The results for a DSL grown to the same specifications as the waveguide sample, except for the exclusion of the AlGaAs layers, are shown here. Modulated transmission, modulated reflection, and absorption measurements are given in Fig. 1(a) to (c), respectively. These data were used to obtain changes in absorption as a function of pump intensity as indicated in Fig. 1(d).

We have also investigated the time response of a selectively contacted DSL following excitation with a cw laser or picosecond laser by monitoring the photovoltage decay across the n- and p-layers. Recombination times can be obtained ranging from a few hundred nanoseconds to fractions of a second, depending on the external circuit.⁴ The shorter time was capacitance limited for this relatively large-area device, whereas the longer time represents the intrinsic recombination time of the DSL.

Acknowledgements

The authors are grateful to G. Hasnain for use of the selectively contacted sample.

References

1. G. H. Döhler, "Doping Superlattices (*n-i-p-i Crystals*)," IEEE J. Quantum Electronics, QE-22, pp. 1682-1694, 1986.

2. G. H. Döhler, G. Hasnain, and J. N. Miller, "In Situ Grown-in Selective Contacts to *n-i-p-i* Doping Superlattice Crystals Using Molecular Beam Epitaxial Growth Through a Shadow Mask," Appl. Phys. Lett. **49**, pp. 704-706, 1986.
3. G. J. Simonis and K. G. Purchase, "Optical Generation, Distribution, and Control of Microwaves Using Laser Heterodyne," IEEE Microwave Theory and Tech. MTT-38, (to be published) May, 1990. G. J. Simonis, R. G. Hay, and K. G. Purchase, "Optical Control of Microwaves with III-V Semiconductor Optical Waveguides," SPIE **1217**, 1990.
4. M. S. Tobin, J. D. Bruno, and C. A. Pennise, "Relaxation of Optically Excited Gallium Arsenide Doping Superlattices," SPIE, **1177** pp. 149-154, 1989.

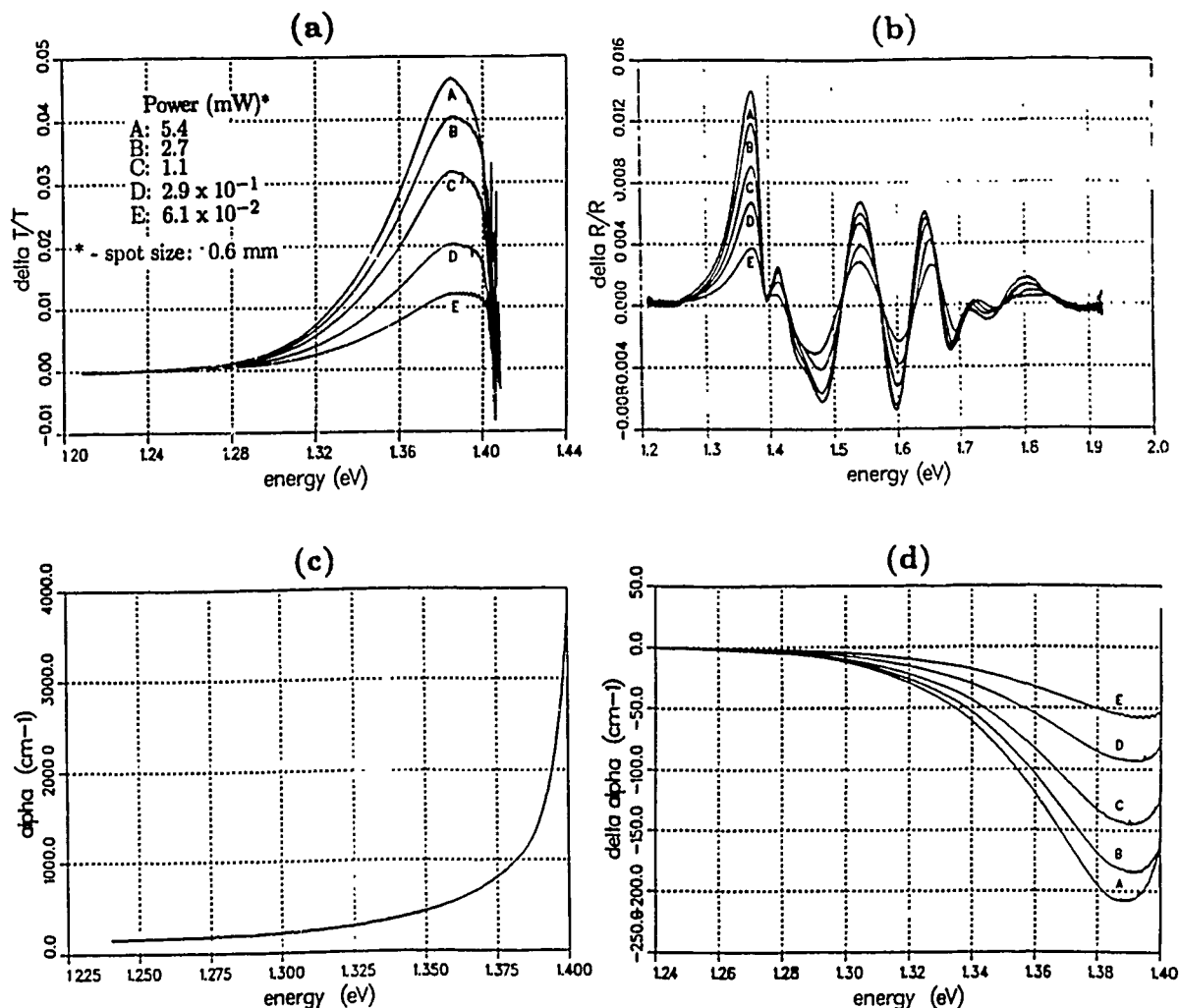


Figure 1: Optical Characterization of DSL. (a) modulated transmission (b) modulated reflection (c) absorption coefficient, and (d) nonlinear changes in absorption.

Elsa Garmire
National Center for the Integration of Photonic Technology
and
Center for Laser Studies
University of Southern California
Los Angeles CA 90089-1112

Improvements in the sensitivity of nonlinear materials can be made by utilizing the concepts of carrier transport [1]. These concepts may be applicable to bulk materials, or in depletion regions, and may be manifest either cw or in effects which are exclusively seen in the transient regime. This talk will outline some recent results in our laboratory. Emphasis will be on the following:

1. Enhanced Photorefractivity at the Band-edge in Semiconductors

By operating near the band-edge, we have demonstrated large photorefractive two-beam coupling gains in semi-insulating GaAs and InP. Using a moving grating in GaAs, 13 cm^{-1} net gain has been observed [2], and using temperature stabilization in InP, gains on the order of 20 cm^{-1} are expected [3]. This opens up for the first time the infrared regime with the possibility that semiconductors may be as useful here as BaTiO₃ has been in the visible in photorefractive applications.

2. Improved sensitivity in nonlinear switching devices using semiconductor depletion regions

We have demonstrated large and sensitive nonlinearities in hetero-nipi structures, incorporating both multiple quantum wells [4] and coupled quantum wells [5], as well as in single heterostructure Schottky barriers, using selective confinement of electrons over holes [6]. One important application is for spatial light modulators. The limitation of the materials reported to date is their contrast ratio. Techniques for increasing the contrast ratio while maintaining sensitivity will be discussed.

3. Band edge surface transient diffraction

As much as 25% self-diffraction of two intersecting pumps (and of a weak probe) in the Raman-Nath regime has been observed at the surface of n-GaAs:Te. The photo-induced gratings have been observed to decay away in less than 100 psec. The diffraction efficiency was nearly independent of sample thickness (40 μm and 350 μm) and careful investigation has shown that the diffraction arose primarily at the surface and was resonant just below the band edge. It is proposed that band-bending at the surface states causes increased absorption, resulting in a sheet of optically induced charge. The faster diffusion of electrons relative to holes allows a transient charge-separation to a distance of one diffusion length (1 μm). As a result, a space-charge field is formed, which can cause an index change, through the Franz-Keldysh effect. The resulting transient grating can cause the large observed diffraction. This new BEST effect offers potential for optical switching applications.

Finally, there will be a discussion of the relevant figures of merit required for any practical switching device. It will be shown that the carrier transport devices can have larger values of the index change per carrier density than the more traditional band-filling and phase-space filling nonlinearities.

The research described here was carried out in collaboration with a number of scientists, including Drs. Alan Kost and Fedor Karpushko (now at the Institute of Physics, Minsk, USSR) and students Afshin Partovi, James Millerd, Ching-Mei Yang and Nan Marie Jokerst. Collaborators at USC include Professor P. D. Dapkus and students H. C. Lee and A. Danner. Collaborators at Hughes include Marvin Klein, George Valley and Tom Hasenberg.

References

1. E. Garmire, N. M. Jokerst, A. Kost, A. Danner, P. D. Dapkus, J. Opt. Soc. Am. B6, 579 (1988)
2. A. Partovi, A. Kost, E. Garmire, G. Valley, M. Klein, Appl. Phys. Lett. March (1990)
3. A. Partovi, J. Millerd, E. Garmire, paper WP19 at this conference.
4. A. Kost, E. Garmire, H. C. Lee, P. D. Dapkus, Appl. Phys. Lett. 52, 637 (1988)
5. A. Kost, T. Hasenberg, E. Garmire, Proc. SPIE Conference on Superlattices (1990)
6. N. M. Jokerst, E. Garmire, Appl. Phys. Lett. 53, 897 (1988)

ST1 Nonlinear Optical Processes Using Electromagnetically Induced Transparency

S. E. Harris, J. E. Field, and A. Imamoglu

*Edward L. Ginzton Laboratory
Stanford University
Stanford, CA 94305*

Summary

It is well known by those practicing the techniques of nonlinear optics, that the power which may be generated in a frequency summing process, or the gain which may be obtained in a parametric process are determined by the interplay of the nonlinear and linear susceptibilities. In general, as an atomic transition to the ground state is approached, the nonlinear susceptibility is resonantly enhanced, but at the same time the media exhibits a rapidly increasing refractive index and becomes opaque.

In this paper we show how it is possible to create nonlinear media with resonantly enhanced nonlinear susceptibilities and at the same time to induce transparency and a zero in the contribution of the resonance transition to the refractive index. An energy level diagram for a prototype system is shown in Fig. (1). We apply a strong electromagnetic coupling field of frequency ω_c between a metastable state $|2\rangle$ and a lifetime broadened state $|3\rangle$, and generate the sum frequency $\omega_d = \omega_a + \omega_b + \omega_c$. We assume that $|1\rangle - |3\rangle$ is a resonance transition and that in the absence of ω_c , radiation at ω_d is strongly absorbed.

When the Rabi frequency of the coupling field exceeds the Doppler width of the $|1\rangle - |3\rangle$ transition, the media becomes transparent on line center. This transparency occurs because of the destructive interference of the split (Autler-Townes) components of the $|1\rangle - |3\rangle$ transition. Though one might expect that this interference would also negate the nonlinearity that causes the generation of ω_d , this is not so; because of a sign change in the dressed eigenvectors, for generated frequencies lying between the Autler-Townes components, there is a constructive rather than a destructive interference in the nonlinear susceptibility.

If one assumes that in the absence of applied fields that the nonlinear media is many absorption depths thick, then the nonlinear conversion efficiency, or parametric gain vary as $|\chi_D^{(3)}/\text{Im}\chi_D^{(1)}|^2$ where $\chi_D^{(1)}$ and $\chi_D^{(3)}$ are the dressed first and third order susceptibilities. Figure (2) shows this quantity as a function of the ratio of the Rabi frequency to the Doppler width of the transition. When Ω_{23} is small as compared to the Doppler width, the media remains opaque and one obtains the result of traditional (small field) nonlinear optics. As Ω_{23} approaches and exceeds the Doppler width the media becomes transparent. At the same time, as a result of increased Ω_{23} , the magnitude of $\chi_D^{(3)}$ is somewhat reduced. But $|\chi_D^{(3)}/\text{Im}\chi_D^{(1)}|^2$ increases over its small Ω_{23} value by the square of the ratio of the Doppler width to the decay or collisional width of state $|2\rangle$.

Atomic media in the visible or ultraviolet, at densities of 10^{16} atoms cm^{-3} become opaque at distances on the order of a wavelength. To attain several centimeters of transparency requires a Rabi frequency on the $|2\rangle - |3\rangle$ transition of ten to fifty times the resonance transition Doppler width. This requires power densities of several

MW/cm², metastability of state $|2\rangle$, and a sufficiently narrow coupling laser linewidth. For these conditions one finds an improvement in conversion efficiency and (four frequency) parametric gain, as compared to the traditional (small field) formulae of nonlinear optics, which often exceeds 10^4 . Nonlinear susceptibility-length products become comparable to those of second order (crystalline) media, and offer the possibility of improved nonlinear device operation over a wide range of the electromagnetic spectrum. In essence, one obtains a large, but very slow optical nonlinearity.

This technique also allows transparency of bands or continua, with possible application to fast switches.

ii) —————

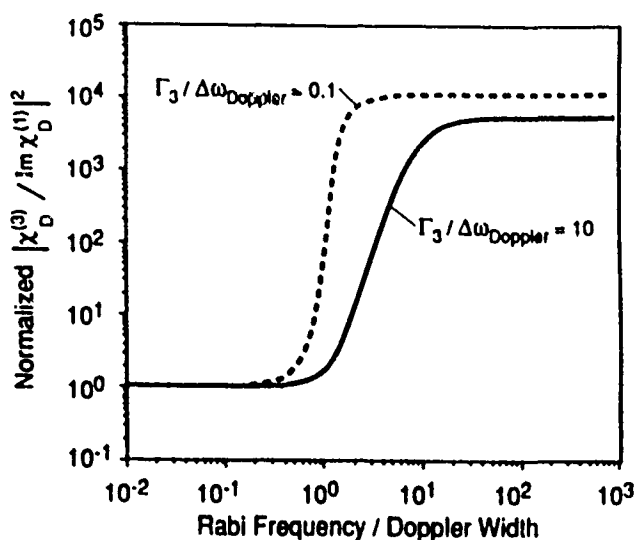
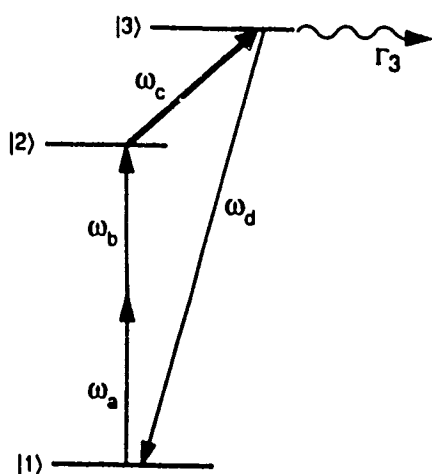


Fig. 1—Energy level diagram for the sum frequency process $\omega_d = \omega_a + \omega_b + \omega_c$. State $|3\rangle$ is lifetime broadened with a decay rate Γ_3 . When a strong field at frequency ω_c is tuned to line center of the $|2\rangle - |3\rangle$ transition, the media becomes transparent on the $|1\rangle - |3\rangle$ resonance transition. This allows much larger nonlinear $\chi^{(3)}L$ products than are normally possible.

Fig. 2— $2-|\chi_D^{(3)}/\text{Im}\chi_D^{(1)}|^2$ as a function of the ratio of the Rabi frequency Ω_{23} to the Doppler width of the resonance transition. Normalization is to the small Ω_{23} value of this ratio. Γ_2 and Γ_3 are the decay widths of states $|2\rangle$ and $|3\rangle$, respectively. For this figure we take $\Gamma_2 = 0.01\Delta\omega_{\text{Doppler}}$.

Kenneth C. Kulander and Bruce W. Shore
 Theoretical Atomic and Molecular Physics Group
 Lawrence Livermore National Laboratory, PO Box 808, L-438
 Livermore, California 94550

and
 Anne L'Huillier
 Service de Physique des Atomes et des Surfaces
 Centre d'Etudes Nucleaires de Saclay, F-91191 Gif-sur-Yvette Cedex, France

The production of short wavelength radiation has been the focus of considerable experimental and theoretical effort recently. One source is very high-order harmonic production observed when short-pulse, intense optical lasers are weakly focussed into a jet of rare gas atoms¹. As long as the confocal parameter of the laser focus was larger than the (propagation) distance through the gaseous medium, a spectrum of odd harmonics was observed in which many orders were of comparable intensity. In these experiments absolute conversion efficiencies for the harmonics were obtained as functions of gas pressure, peak laser intensity and geometry of the laser focus. On the strength of these results it is possible to project that coherent short-wavelength radiation with peak power far in excess of existing synchrotron sources can be achieved. Also, using a tunable, subpicosecond dye laser source, the wavelength of the harmonics can be varied continuously.

The strength of the harmonic emission depends on two factors. First, the exciting laser induces an oscillating dipole in each atom causing photoemission peaked at the odd harmonic frequencies on top of a broad, continuous background. Second, because of the differences between the indices of refraction in the medium for the pump and harmonic frequencies, the single-atom spectrum is altered as it propagates through the medium. The observed spectrum can be calculated only by including both of these effects.

We obtain the single atom spectrum using our method of direct solution of the time-dependent Schrödinger equation for the atom in a pulsed laser field.² We determine the time-dependent induced dipole from the time-dependent electronic wave function. From the Fourier transform of this dipole we obtain the emission spectrum. At the intensities of interest ($I > 10^{13}$ W/cm²) traditional perturbation techniques are invalid, requiring this explicit time-dependent approach which treats the laser electron and intra-atomic interactions on an equal footing. This induced-dipole is the source term for Maxwell's equations for the propagation of the harmonics through the macroscopic volume excited by the laser. Because of the non-perturbative nature of the atomic susceptibilities of these intensities, no trivial solution to Maxwell's equations exist, requiring numerical integration of these equations over the excited volume to provide the measured spectrum. The details of those calculations will be discussed and a comparison of these results to the existing experimental data will be made.

¹X. F. Li, A. L'Huillier, M. Ferray, L. A. Lompré, G. Mainfray, *Phys. Rev. A* **39**, 5751 (1989).

²K. C. Kulander and B. W. Shore, *Phys. Rev. Lett.* **62**, 524 (1989).

Herbert G. Winful
EECS Department
University of Michigan
Ann Arbor, MI 48109

In a recent paper, Levenson and coworkers have shown that spontaneous emission into higher transverse cavity modes forces the centroid of a single transverse mode laser beam to fluctuate in position⁽¹⁾. This stochastic position noise means that it is literally impossible for a laser beam to "go straight." In this paper, we show that a breakdown of phase-locking in an array of coupled single mode lasers can lead to random fluctuations of the far field beam position even in the absence of stochastic noise sources. The fluctuations in this case are a manifestation of deterministic spatio-temporal chaos and are due to a loss of synchronization between coupled lasers and the non-instantaneous population dynamics.

The model considered here is that of an array of waveguide lasers with evanescent wave coupling. In the absence of coupling each laser operates in a single longitudinal and transverse mode, assumed same for all the lasers. For the particular case of coupled semiconductor lasers, the evolution of the mode amplitude (E_j) and population (N_j) in the j^{th} laser is described by the equations⁽²⁾

$$\dot{E}_j = \frac{1}{2} \left[G(N_j) - 1/\tau_p \right] (1 - i\alpha) E_j + iK [E_{j+1} + E_{j-1}],$$

$$\dot{N}_j = P - N_j/\tau_s - G(N_j) |E_j|^2,$$

where G is the gain, τ_p is the photon lifetime, τ_s is the lifetime of the active population, P is the pump rate and K is the coupling coefficient between adjacent lasers. The parameter α is the linewidth enhancement factor whose value is in the range 1-5 for semiconductor lasers and is equal to zero for most other lasers. Note that the above equations are completely deterministic and do not involve any noise sources.

A stability analysis of the above equations has shown that over a wide range of coupling strengths this system is unstable and exhibits sustained oscillations in the field amplitudes, phases, and the population inversion⁽²⁾. For two coupled lasers, amplitude-phase coupling due to the parameter α plays an important role in the instability. For three or more coupled lasers, the instability is possible even when α is zero. Supermode competition driven by the population dynamics is the key mechanism in that case.

The far field beam profile is the spatial Fourier transform of the near field amplitude and phase distribution. Phase fluctuations in the near field are transformed into beam displacements in the far field. Figure 1 shows a computer simulation of the dynamic evolution of the far field of two coupled semiconductor lasers based on the coupled-mode equations.

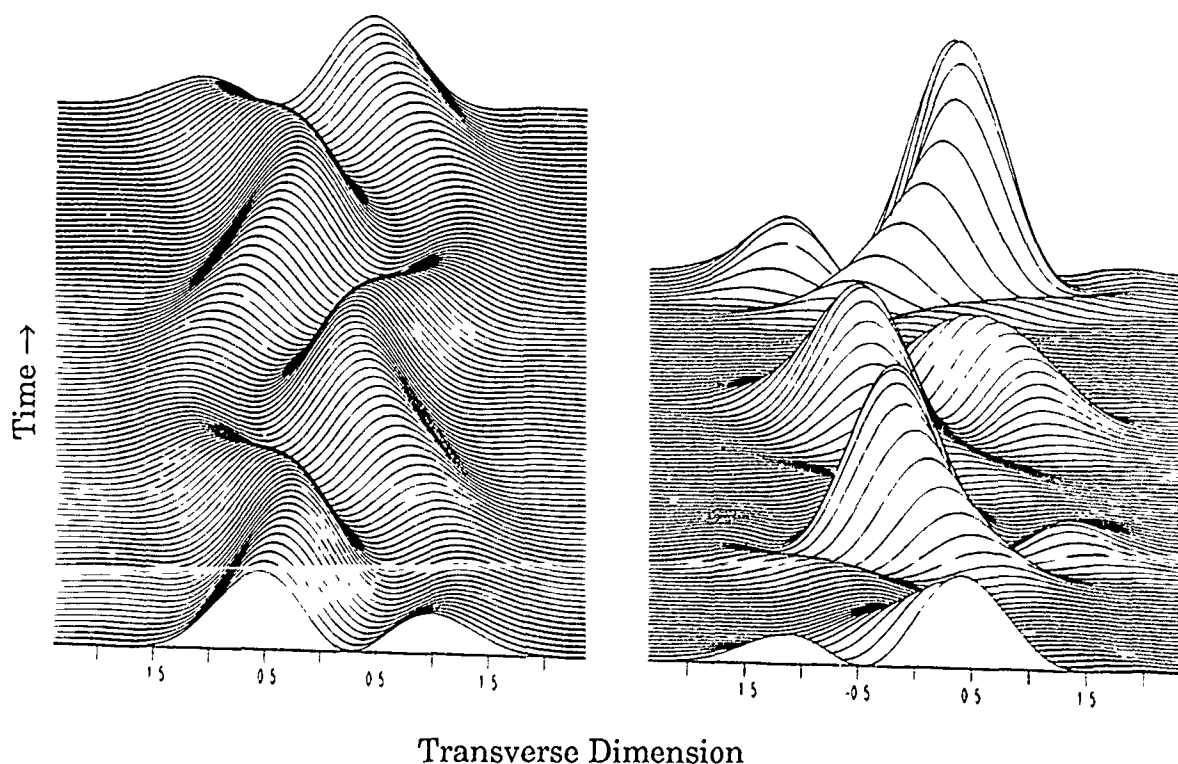
In Fig. 1a, the coupling strength K is chosen such that the pulsations are periodic, while in Fig. 1b a larger value of K is used, which makes the pulsations chaotic. The far field beam position is seen to wander erratically in time with a characteristic frequency of order several gigahertz (for typical semiconductor laser arrays). Recent measurements made with high speed streak cameras show some evidence of this deterministic far field beam steering.

- (1) M. D. Levenson, W. H. Richardson, and S. H. Perlmutter, *Opt. Lett.* **14**, 779 (1989).
- (2) H. G. Winful and S. S. Wang, *Appl. Phys. Lett.* **53**, 1894 (1988).

Fig. 1 Temporal Evolution of Far Field Intensity Profiles

(a) Periodic

(b) Chaotic



ST4 Organic Nonlinear Optical Materials and Their Device Applications

by Donald M. Burland, Steven Ducharme, William W. Fleming, Robert D.
Miller, W.E. Moerner, William P. Risk, Robert J. Twieg,
and Ceolla A. Walsh

IBM Almaden Research Center
Dept K95/801
650 Harry Road
San Jose, CA 95120
(408) 927-1501

SUMMARY

Advanced opto-electronics technology requires nonlinear optical (NLO) materials for frequency shifting, modulation, and switching. Organic NLO materials have intrinsic figures of merit that in many cases exceed the incumbent materials of choice, inorganic crystals such as lithium niobate, for these applications. In this paper we review the prospects for practical utilization of organic NLO materials and report results on the synthesis and characterization of several families of nonlinear molecular chromophores, on intracavity second harmonic generation using an organic crystal, and on high frequency electrooptic modulation using organic crystals and poled polymers.

Our work with nonlinear chromophores has included the synthesis and molecular hyperpolarizability β measurement of a variety of nitroaniline, benzene, and nitropyridine derivatives with the aim of understanding the effect of combinations of aromatic ring type and substituents on β . The electric field induced second harmonic (EFISH) technique was utilized at fundamental wavelengths of 1.064 μm and 1.907 μm to measure hyperpolarizabilities relative to a MNA standard. The nitropyridine deriva-

tives were found to have generally lower β values than the nitroanilines and the correlation of β with energy gap and solvatochromic data was found to be in agreement with the predictions of the 2-level model. Currently, we are extending this work and also using solvatochromism to study more novel chromophore types, including donor-acceptor substituted silanes and molecules with large ground state but zero excited state dipole moments.

In a recent set of experiments with crystals of the organic nonlinear material DAN (4-(N,N-dimethylamino)-3-acetamidonitrobenzene), we have succeeded in CW intracavity doubling of an optically pumped Nd:YAG laser. This represents the first CW intracavity application of an organic NLO material and demonstrates that laser grade optical quality can be achieved with organic NLO crystals. Quasi-CW operation was achieved with crystal samples immersed in index matching fluid in an antireflection coated cuvette. This technique permits rapid surveying of crystal samples obtained directly from solution growth without polishing or antireflection coating them. Up to 0.56mW peak power of 532nm light was generated from 2.3W of circulating intracavity 1064nm peak power using 0.5W of 810nm pump. True CW operation was achieved using antireflection coated DAN crystals and work is in progress to optimize these coatings further. Reflection losses of less than 0.25% per surface at the phase matching angle of incidence have already been achieved.

In another set of experiments aimed at demonstrating high frequency electrooptic phase modulation with organic NLO materials, we have tested several candidate crystals in a specially designed test fixture that incorporates a stripline electrode structure to produce a transverse traveling wave electrical field. The electrical response of the stripline structure was tested and found to be flat at least up to 3 GHz. A single frequency laser beam was directed through the crystal and a high finesse scanning etalon was used to directly detect the optical power in the resulting FM sidebands. Using a crystal of MNMA (2-Me-4-nitro-N-methylaniline), a modulation index of $M = .014$ was achieved at a drive frequency of 400 MHz. This represents the first demonstration of high speed electrooptic phase modulation in an organic crystal. Experiments are now in progress to test organic NLO crystals at drive frequencies up to 10 GHz and also to fabricate waveguide phase modulators using poled polymers.

AUTHOR INDEX

A

Abbate, C. 149
 Adams, M.J. 49
 Agarwal, G.S. 13
 Agranat, A. 259
 Akai, I. 268
 Akhmediev, N.N. 24
 Akiyama, H. 276
 Aldridge, J. 263
 Andersen, D.R. 36,226
 Anderson, D.Z. 307
 Antonetti, A. 160
 Aron, K.P. 111
 Assanto, G. 166
 Au, L.B. 6

B

Bachor, H.A. 32,103
 Baldassarre, L. 296
 Baldwin, K.G.H. 32
 Ballagh, R.J. 17
 Banerjee, P.P. 96,187,190
 Barker, R.C. 208
 Barnes, N.P. 136
 Bashaw, M.C. 208
 Beekman, D. 55
 Benkert, C. 307
 Bhalla, A.S. 257,258
 Birnbaum, M. 93
 Bjorklund, G. 206
 Bloch, D. 241
 Block, K.L. 183
 Bloembergen, N. 87
 Blok, V.R. 18
 Blum, O. 191
 Boardman, A.D. 222
 Boggess, T.F. 238
 Bosenberg, W.R. 137
 Bouchenaki, C. 272
 Browne, P. 95
 Bruno, J.D. 313
 Burland, D.M. 26,322
 Byer, R.L. 34,

C

Cai, Y.M. 73
 Cantwell, G. 263
 Capasso, F. 119
 Cardimona, D.A. 16,130
 Carlsten, J.L. 245
 Chambers, D.H. 97

Chang, W.S.C. 111
 Chantenoud, F. 228
 Chapple, P.B. 32
 Chatterjee, M.R. 190
 Chauchard, E. 55
 Chen, H.-C. 254
 Chevrollier, M. 241
 Chi, S. 247
 Chiou, A. 217
 Cho, K. 193
 Cipparrone, G. 77
 Clark III, W.W. 155
 Clayton, C. 128
 Coldren, L.A. 117
 Collett, M.J. 3
 Combescot, M. 161
 Conner, P. 143
 Cook, G. 293
 Corvo, A. 128
 Coulter, D.R. 61
 Cronin-Golomb, M. 281
 Cross, L.E. 257
 Cunha, A. 302

D

Dagenais, M. 230
 Dawson, M.D. 238
 DeBlasi, C. 296
 Degiorgio, V. 296
 Ding, T.-N. 230
 Ding, Y. J. 22
 Dixit, S. 97,99
 Doroski, D. 147
 Dreier, T. 194
 Droopad, R. 115
 Dube, R.R. 208
 Duca, D. 77
 Ducloy, M. 241
 Ducharme, S. 322
 Dunning, G.J. 291

E

Eason, R.W. 216
 Eichler, H.J. 6
 Ehrlich, J.E. 166
 Eliseev, V.V. 132
 Ema, K. 210
 Enokida, T. 270
 Enok, T. 34
 Ewart, P. 72

Ewbank, M.D. 306

F

Fa, O. 174
 Fagherazzi, G. 296
 Falk, J. 55
 Fan, X. 264
 Farrow, R.L. 194
 Fayet, P. 28
 Fei, H. 266
 Feinberg, J. 152
 Ferrara, M. 296
 Fichet, M. 241
 Field, J.E. 317
 Fischer, B. 157
 Fisher, M.A. 49
 Fleming, W.W. 322
 Flom, S.R. 37
 Flytzanis, C. 250
 Forman, P.R. 285
 Forrest, S.R. 59
 Frazier, C.C. 55
 Frey, J. 250
 Frey, R. 250
 Fujita, H. 270
 Fukumi, T. 270

G

Gaeta, C.J. 290
 Galameau, L.M. 37
 Gang, L. 20
 Garnire, E. 93,122,212, 255,315
 Garito, A.F. 73
 Gavrielides, A. 128
 Gerber, D.S. 115
 Grave, I. 113
 Gregor, E. 90
 Grimes, C.A. 92
 Grischowsky, D. 11
 Gruneisen, M.T. 283
 Grynberg, G. 28,70
 Gu, X. 21
 Guha, S. 55,143
 Guo, R. 257
 Gustafson, T.K. 191,214,278

H

Hadley, G.R. 30
 Haga, H. 196
 Hagan, D.J. 61,311

Hai, T.S. 309
 Han, L. 266
 Hanamura, E. 158
 Hansen, G.A. 111
 Harris, S.E. 317
 Harshman, P.J. 278
 Harvey, J.D. 288
 Hasenberg, T. 122
 Hashizume, N. 198
 Hauff, T. 224
 Hayden, C.C. 279
 Heckenberg, N.R. 303
 Heffernan, D.M. 232
 Heflin, N.Q. 73
 Heinlein, W. 224
 Hellwarth, R.W. 261
 Henneberger, F. 239
 Hermann, M.R. 97,99
 Hermanns, A. 307
 He-Y., Z. 309
 Higgins, B.G. 202
 Hixon, E.L. 92
 Hong, B.J. 51
 Hosomi, T. 5
 Hua, H.X. 55,309
 Huang, L. 134
 Huguley, C.A. 128
 Huilin, D. 160
 Hutchings, D.C. 311

I

Imamoglu, A. 317
 Inoue, Y. 220
 Ishihara, H. 193
 Ito, R. 105,198
 Ito, S. 274
 Iwamatsu, J. 276
 Izutsu, M. 63

J

Jahoda, F.C. 285
 James, S.W. 216
 Jiang, M. 121
 Joffe, M. 160
 Johnson, A.M. 279
 Johnson, D.A. 115
 Johnson, K.M. 147
 Jonathan, J.M.C. 261
 Joshi, C. 240
 Jungbauer, D. 206

K

Kang, K. 55
 Kao, Y.H. 188
 Kaplan, A.E. 22,36,248
 Karasawa, T. 268
 Karr, T.J. 97,99
 Kataoka, T. 274
 Katogi, S. 5
 Kawaguchi, H. 79
 Kelley, P.L. 191
 Khoo, I.C. 77,78,145
 Khundkar, L.R. 61
 Khurgin, J. 109
 Kim, I. 191,278
 Klein, M. 57,255
 Klem, J.F. 236
 Knoesen, A. 202
 Kobayashi, T. 75
 Komatsu, T. 268
 Kondo, T. 198
 Korpel, A. 187
 Kost, A. 122
 Kowel, S.T. 202
 Krochik, G.M. 18
 Kukhtarev, N. 305
 Kulander, K.C. 319
 Kuszelewicz, R. 83
 Kuwata-Gonokami, M. 276
 Kuze, N. 113

L

Laferriere, P.A. 130
 Lam, J.F. 59,290
 Lambropoulos, P. 32
 Lane, A.S. 3
 Lane, R. 137
 Lapp, J.C. 45
 Law, K.K. 117
 Leith, E.N. 302
 Lera, G. 243
 Levenson, M. 162
 Levien, R.B. 3
 Levine, A.M. 279
 Leyva, V. 259
 L'Huillier, A. 319
 Li, C. 264
 Li, G. 134
 Li, Q. 254,294,298
 Li, T. 266
 Liebman, A. 126
 Lindquist, R.G. 145

Liu, J. 147
 Liu, Y. 264
 Lo, S.K. 37
 LoPresti, P. 145
 Lotshaw, W.T. 170
 Lucht, R.P. 185
 Lugara, M. 296
 Luther-Davies, B. 126
 Lytel, R.S. 111

M

Ma, T.P. 208
 MacCormack, S. 216
 Macdonald, R. 6
 Mace, D.A.H. 49
 Maddever, A. 126
 Maddalena, P. 149
 Malik, R.J. 119
 Manabe, T. 274
 Mansfield, R.J. 145
 Maracas, G.N. 115
 Masaki, A. 10
 Marrucci, L. 149
 Mason, B.L. 285
 Matsuda, H. 10
 Mayers, A. 215
 McCahon, S.W. 57
 McClelland, D.E. 103
 McCord, A.W. 96
 McDuff, R. 303
 McHenry, D.A. 257
 McInerney, J.G. 232
 McMichael, I. 14
 McMorrow, D. 170
 Meijer, E.W. 65,204
 Merz, J.L. 117
 Michael, R.R. 145
 Migus, A. 160
 Milburn, G.J. 172
 Mileski, J.F. 283
 Miller, D.A.B. 85
 Miller, R.D. 26,34,322
 Millerd, J.E. 93,212,255
 Mishra, R.M. 187
 Miya, M. 270
 Miyata, S. 5
 Miyoshi, S. 198
 Moerner, W.E. 322
 Mordaunt, D.W. 90
 Mori, H. 270
 Morita, R. 105,198
 Morita, T. 202

Mroczkowski, S. 208
Mullen, R.A. 153
Murata, H. 63

N

Nakanishi, H. 10
Nakamura, A. 274
Nayar, B.K. 47
Neurgaonkar, R. 214
Newhouse, M.A. 45
Nguyen, K. 214
Nieto-Vesperinas, M. 243
Nijhuis, S. 204
Niki, S. 111
Noda, S. 124
Normandin, R. 228

O

Ogasawara, N. 105,198
Ohbayashi, Y. 139
Ohsugi, M. 10
Okada, S. 10
Okada, Y. 220
Olbright, G.R. 236
Oria, M. 241
Osborne, R. 40
Osborne, Z. 101
Oudar, J.L. 83
Owechko, Y. 291
Owyong, A. 236

P

Pan, R. 219
Pan, Z. 230
Park, S.H. 55
Parshall, E.R. 281
Partanen, J.P. 261
Partovi, A. 212,255
Pegg, D.T. 2
Pelli, S. 296
Pelouch, W.S. 137
Peng, W. 107,254,298
Pepper, D.M. 153
Perry, J.W. 61
Petrovic, M.S. 263
Porter, P. 55
Powell, R.C. 263
Puechner, R.A. 115

Q

Qian, S. 107

R

Rahn, L. 185
Rakestraw, D.J. 194
Rajan, S. 215
Ralph, S.E. 119
Reck, B. 206
Redus, K.S. 183
Remillard, J.T. 121
Ridley, K.D. 293
Righini, G.C. 296
Rikken, G.L.J.A. 65,204
Risk, W.P. 322
Robinson, M.G. 147
Rogers, D.J. 37
Rogovin, D. 222

S

Sa'ar, A. 113
Sakaguchi, T. 270
Salamo, G.J. 155
Saleh, B.E.A. 294
Salvi, T.C. 232
Santamato, B. 149
Sasaki, A. 124
Savage, C.M. 20
Schellenberg, F.M. 34
Schiek, R. 43
Schroeder, W.A. 238
Schumacher, K.L. 153
Scott, A.M. 293
Seeberger, E.D. 283
Seppen, C.J.E. 204
Sfez, B. 83
Shapiro, J.H. 30
Sharma, M.P. 16
Sharp, E. 155
Shelk-Bahae, M. 311
She, W. 254
Shen, D. 264
Shen, T.P. 222
Shen, Y.R. 149,251
Shepard, S.R. 30
Shevy, Y. 19
Shi, W.Q. 93
Shimano, R. 276

Shimizu, F. 210
Shixiong, Q. 18
Shore, B.W. 319
Shu, Y. 18
Simoni, F. 77
Simonis, G.J. 313
Singh, J. 49
Skinner, S.R. 226
Smirl, A.L. 238
Smith, A. 303
Soffer, B.H. 291
Soileau, M.J. 311
Solymar, L. 6
Spiro, M. 28
Stark, T.S. 238
Steel, D.G. 121
Stegeman, G.I. 101,166
Steier, W.H. 255
Strahm, K.V. 90
Suchocki, A. 263
Sueta, T. 63
Sugimoto, N. 274
Suzuki, H. 139
Swalen, J.D. 206
Swartzlander, G.A. 36
Szabo, A. 14

T

Tabiryan, N.V. 78
Takahashi, M. 139
Takano, T. 220
Takaragi, S. 10
Tang, C.L. 137
Tangonan, G.L. 59
Taran, J.P. 191
Tataronis, J.A. 294
ten Hoeve, W. 65
Thienpont, H. 65
Ticknor, A.J. 200
Tikhonchuk, V.T. 132
Tobin, M.S. 313
Tokizaki, T. 274
Tokumaru, T. 220
Torruellas, W.E. 101
Trebino, R. 185,279
Trillo, S. 53
Trivedi, S. 255
Tutt, L.W. 57
Twieg, R.J. 206,322

U

Uemura, T. 124
Ukachia, T. 137
Ullrich, B. 272
Umegaki, S. 105,198
Umeton, C. 77

V

Valley, G.C. 263
Valley, J.F. 200
VanEck, T.E. 111
Vanherzeele, H. 47
VanStryland, E.W. 61,311
Verkerk, P. 28
Vickers, D. 153
Volyar, A. 305

W

Wabnitz, S. 53
Walba, D. 147
Walls, D.F. 3
Walsh, C. 26,322
Wang, C.S. 188
Wang, H. 121
Wang, J.C. 103
Wang, N.Q. 73
Webb, R.P. 81
Wei, H.D. 219

Wei, T.H. 61
Weidman, D.L. 45
Weller-Brophy, L.A. 101
Wetterer, C.J. 130
Wider, H.H. 111
Williams, R.L. 228
Willson, C.G. 206
Winful, H.G. 320
Wong, N.C. 30
Wood, G.L. 155
Wu, S. 215
Wynberg, H. 65

X

Xiao, L. 266
Xu, G.F. 93
Xu, Y. 254

Y

Yamamoto, H. 5
Yamamoto, J.K. 258
Yamamoto, S. 196
Yan, R.H. 117
Yanagida, S. 270
Yang, C.C. 51
Yang, T.J. 219
Yano, K. 220

Yao, J.Q. 93
Yao, Y.-C. 134
Yariv, A. 113,259
Ye, P. 164
Yee, S. 214
Yeh, P. 141
Yin, B.-L. 134
Yoon, D.Y. 206
Yoshizawa, M. 75
Yu, F.T.S. 215
Yu, Z. 107,254,298
Yuan, L. 232
Yuan, S. 107

Z

Zanoni, R. 101
Zelinski, B.J.J. 101
Zhao, J. 32,266
Zhang, J. 32
Zhang, Q.L. 254
Zhou, B. 266
Zhu, D.-R. 254
Zhu, Q. 95
Zhu, R. 254
Ziari, M. 255
Zielinger, J.P. 272
Zozulya, A.A. 132
Zylberajch, S. 28

ATCH A

AFOSR-90-0197

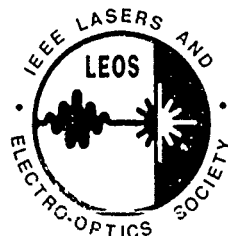
NLO'90

NONLINEAR OPTICS

Materials, Phenomena and Devices

POST DEADLINE PAPERS

Stouffer Waiohai Beach
Kauai, Hawaii
July 16-20, 1990



Sponsored by
IEEE Lasers and Electro-Optics Society
in Cooperation with
the Optical Society of America

NONLINEAR OPTICS CONFERENCE
July 16-20, 1990

POST DEADLINE PAPERS

MONDAY, JULY 16

- PD1 Large Third-Order Optical Nonlinearities of
Phthalocyanines, Bisphthalocyanines, and Metal Complexes of
o-Aminobenzenethiol, J.R. Lindle, J.S. Shirk, F.J.
Bartoli, Z.H. Kakafi, A.W. Snow, E. Boyle and O.K. Kim
- PD2 Theory of Cherenkov Radiation Type Second Harmonic
Generation Optical Waveguides, X. Wang, C. Liao and S.
Liu
- PD3 Second Harmonic Generation and Laser Induced DC
Polarization in Ferroelectric
Vinylidene-Fluoride/Trifluoro-ethylene Copolymer
Films: New Optical Reading and Electro-Optical Writing
Methods for the Nonvolatile Ferroelectric Memory
H. Gamo, D. Zhang, J. Zhao, A. Kojima

WEDNESDAY, JULY 18

- PD4 Observation of the Fundamental Dark Spatial Soliton
S. Skinner, G. Allan, D. Andersen and A. Smirl
- PD5 Second Harmonic Generation in Atomic Hydrogen Induced by
a D.C. Field, K. Hakuta, L. Marmet, and B.P. Stoicheff
- PD6 Self-Focusing Effects in the Near Field of a Thin
Nonlinear Medium, J.A. Hermann and P.B. Chapple

Large Third-Order Optical Nonlinearities of Phthalocyanines, Bisphthalocyanines, and Metal Complexes of o-Aminobenzenethiol

J. R. Lindle, J. S. Shirk, F. J. Bartoli, Z. H. Kafafi,
A. W. Snow, M. E. Boyle, and O-K. Kim
Naval Research Laboratory
Washington, DC 20375

The third-order nonlinear susceptibility of metal-substituted phthalocyanines (Pc), bisphthalocyanines (Pc₂) and transition metal complexes of o-aminobenzenethiol (ABT) have been measured at 1.06 μm using degenerate four-wave mixing techniques. The results show that all three of these metallo-organics exhibit large, non-resonant, third-order nonlinearities.

The third-order susceptibilities of CoPc, NiPc, CuPc, ZnPc, PdPc, PtPc and H₂Pc have been measured. The susceptibility was enhanced by metal substitution and varied substantially with metal substitution ranging from 2 to 45 times larger than metal-free Pc. Measurements were also performed on a series of peripherally substituted Ni phthalocyanines. The results show that peripheral substitution also effects the nonlinear optical properties. PtPc had the largest third-order susceptibility of the mono-phthalocyanines ($\chi_{xxxx}^{(3)} = 2 \times 10^{-10} \text{esu}$).

The interaction of the two Pc rings in the bis-Pc's gives rise to a ring-to-ring charge transfer transition in the near IR whose frequency depends on the size of the substituted metal. A systematic study was undertaken to determine the contribution of this charge transfer band to the optical nonlinearity. The third order susceptibilities of NdPc₂, GdPc₂, LuPc₂, EuPc₂, YPc₂, YbPc₂, ScPc₂, and their anions have been measured. The results show that, although the charge transfer band does contribute to the nonlinear properties of the bis-Pc, the charge transfer mechanism is not the dominate mechanism producing the large optical nonlinearity. ScPc₂ exhibited the largest nonlinearity ($\chi_{xxxx}^{(3)} = 1.7 \times 10^{-9} \text{esu}$).

Temporal studies on the mono- and bis-phthalocyanines show that the nonlinear response is faster than the optical pulsewidth (35 pS).

Measurements of the third-order susceptibility of a new class of organometallics, namely Co and Ni complexes of ABT, show that the nonlinear optical properties of ABT's are significantly enhanced by metal substitution. Ni(ABT)₂ exhibited the largest third-order nonlinearity ($\chi_{xxxx}^{(3)} = 2.3 \times 10^{-9} \text{esu}$).

Theory of Cherenkov Radiation Type Second Harmonic Generation in Optical Waveguides

Xiaodong Wang Changjun Liao Songhao Liu

South China Institute of Quantum Electronics,
South China Normal University, Guangzhou, 510631, P.R.China

Summary

Second Harmonic Generation (SHG) in nonlinear optical waveguides is very attractive because of the long interaction distance and the existence of multiple modes with different values of the effective index which facilitates phase matching. A number of experimental investigations and theoretical analyses have been carried out for years. However, the preceding theories only dealt with the guided-guided type SHG, i.e., both of the fundamental and the second harmonic are the guided modes. The case of a radiated-mode second harmonic generated by a guided-mode fundamental, that is usually called Cherenkov radiation type SHG, is either neglected or regarded as a useless loss. In this paper we will for the first time to our knowledge analyze theoretically this Cherenkov radiation type SHG by a ray approach.

Our approach is to determine the condition under which Cherenkov radiation type SHG will occur and to calculate multiple transmissions of the second harmonic, then to obtain the total amplitude of electric field, by finding the total electromagnetic fields which satisfy both Maxwell's equations for a nonlinear medium and the boundary conditions. For specificity the fundamental is assumed to be a TE guided-mode with the effective index $(\omega/c) k_{1x}(\omega)$. Referring to Fig.1 (a) and Fig.1 (b), we deduce that when

$$(\omega/c) k_{1x}(\omega) - n_0(\omega) < n_0(2\omega) - n_0(\omega)$$

Theory of Cherenkov Radiation Type SHG in Optical Waveguides

X.Wang C.Liao S.Liu

is satisfied, the second harmonic will radiate from medium n_0 . Its total amplitude of electric field is finally given by

$$\varepsilon_0(x) = \frac{\chi_{322} \varepsilon_1^2(\omega) t_{11}}{D \cos \theta_2} \left[\left(\frac{e^{i\delta} J_\delta}{1 - r_{11} e^{i\delta}} + c \right) x - \frac{D r_{11} e^{i2\delta} J_\delta}{(1 - r_{11} e^{i\delta})^2} \left(1 - r_{11}^{\frac{x}{D}} e^{i\frac{\delta}{D} x} \right) \right]$$

where

$$J_\delta = \frac{1}{2} [(1 - r_{11}) \alpha_{10} - i(1 + r_{11}) \beta_{10}] + (-1)^m e^{-i\frac{\delta}{2}} [\alpha_{12} \sin \varphi_{12}(2\omega) - \beta_{12} \cos \varphi_{12}(2\omega)]$$

$$C = -\frac{1}{2} (\alpha_{10} + i\beta_{10})$$

with

$$\alpha_{11} = \frac{8\pi \sin \theta_1 \cos \theta_2}{\varepsilon_1(2\omega) - \varepsilon_1(\omega)} \cdot \frac{n_1(\omega)}{n_1(2\omega)} \left[\cos 2\varphi_{11}(\omega) + \frac{\varepsilon_1(2\omega) - \varepsilon_1(\omega)}{\varepsilon_1(2\omega) \cos^2 \theta_2} \right]$$

$$\beta_{11} = \frac{8\pi \sin \theta_1}{\varepsilon_1(2\omega) - \varepsilon_1(\omega)} \cdot \frac{\varepsilon_1(\omega)}{\varepsilon_1(2\omega)} \cos \theta_1 \sin 2\varphi_{11}(\omega)$$

and $D = 2(Z_h + W) \tan \theta_2$

Z_h : Goos-Haenchen shift at the interface of media n_1 and n_2

r_{11} , t_{11} : reflection and transmission coefficients at the interface of media n_0 and n_1

Note that $\delta = 2k_{1z}(2\omega)W - 2\varphi_{12}(2\omega) - 2m\pi$

where m is an integer and $|\delta| < 2\pi$

Theory of Cherenkov Radiation Type SHG in Optical Waveguides

X.Wang C.Liao S.Liu

In summary, we have studied Cherenkov radiation type SHG in thin film nonlinear waveguides. It is found that material dispersion of the cladding layer with larger index is more decisive than other parameters of the waveguide for this type SHG. For $\delta = 0$, which we call phase matching, the amplitude of this SHG is proportional to the propagation distance. The approach used here is easy to extend to other cases such as a fundamental of TM guided-mode or different thin films with other nonlinear susceptibility tensor element χ_{ijk} .

References:

1. E.M.Conwell, IEEE J.Quantum Electron., QE-9, 867 (1973)
2. V.C.Y.So, R.No Mandin, G.I.Stegeman, J. Opt. Soc. Am. , 69, 1166 (1979)

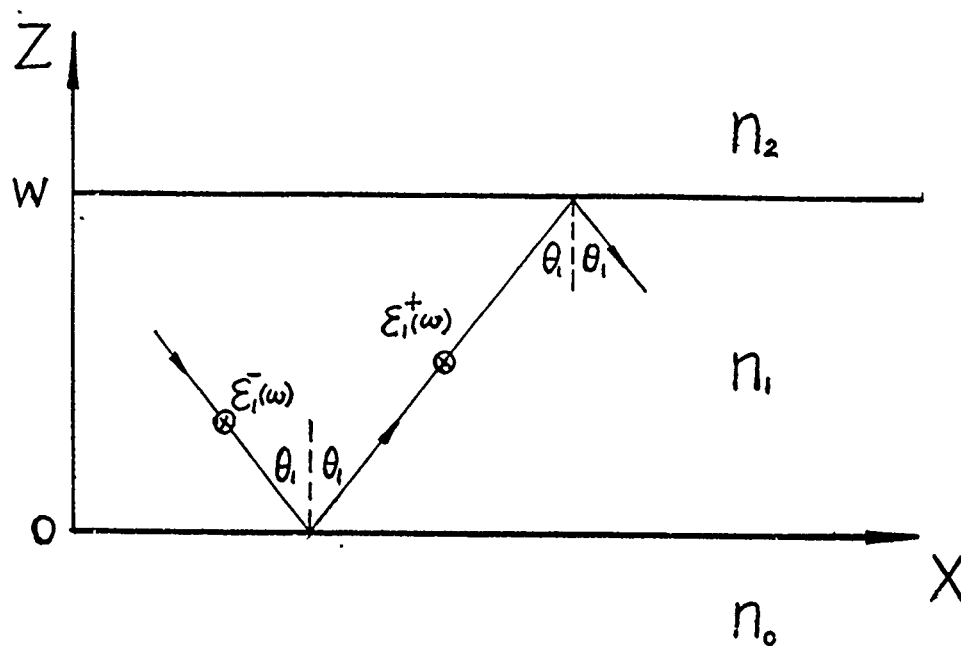


Fig. 1 (a)

Fig.1 (a) The waveguide configuration and coordinate system. The only nonlinear polarization is χ_{322} in medium n_1 .

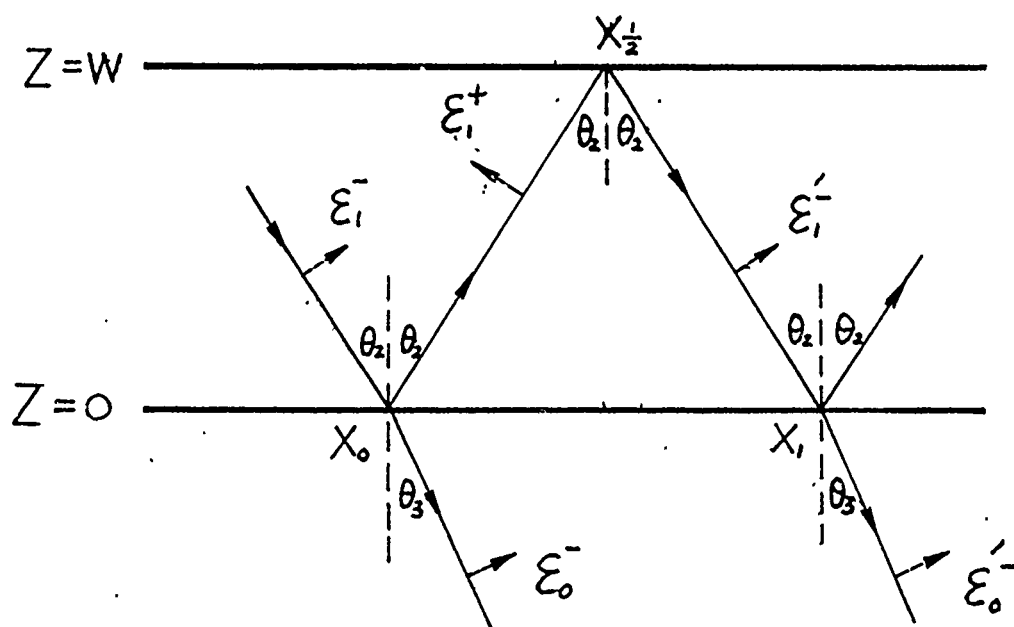


Fig. 1 (b)

Fig.1 (b) Schematic diagram of Cherenkov radiation type SHG when $n_1(2\omega) > n_0(2\omega) > n_2(2\omega)$, using a ray approach.

SECOND HARMONIC GENERATION AND LASER INDUCED DC POLARIZATION IN FERROELECTRIC VINYLIDENE-FLUORIDE/TRIFLUORO-ETHYLENE COPOLYMER FILMS: NEW OPTICAL READING AND ELECTRO-OPTICAL WRITING METHODS FOR THE NONVOLATILE FERROELECTRIC MEMORY

Hideya Gamo, Dapeng Zhang, and Ji Zhao

University of California, Irvine

Department of Electrical and Computer Engineering

Irvine, California 92717

and

Akio Kojima

Ricoh Research and Development Center

4686 Nippacho

Yokohama 223, Japan

With the objective of developing new optical/electro-optical methods for reading and writing nonvolatile ferroelectric memory, we investigated the second harmonic generation (SHG) and the DC polarization current associated with SHG in vinylidene fluoride/trifluoro-ethylene (VDF/TrFE) copolymer thin-films. The sample consists of VDF(65)/TrFE(35) copolymer film of thickness $4\mu\text{m}$ on the transparent electrode, Indium Tin Oxide (ITO) on the glass substrate, and the other side of VDF/TrFE film has another transparent electrode In_2O_3 . By applying DC voltage larger than 200V between two electrodes, we can pole the VDF/TrFE film. By varying voltage across the transparent electrodes we observe typical D-E hysteresis curve.

When the linearly polarized Q-switched Nd-YAG laser beam (wavelength $1.06\mu\text{m}$, pulse width 200ns, and repetition rate 1 kHz) is obliquely incident on the poled sample mentioned above and the electric vector of the incident beam is on the plane of incidence (p-wave, or TM wave), the SHG is maximum when its incident angle is 50° . When we apply the reversed voltage just enough to depolarize the ferroelectric VDF/TrFE copolymer film, the SHG disappears. When the poling field increases, the dielectric polarization of the film develops slowly and gradually saturates; then when the poling field is reduced to zero, the residual polarization remains. Therefore, SHG can be used for reading the polarized and unpolarized states of copolymer films in real time.

While the Q-switched Nd-YAG laser is generating the second harmonic, we also observe the DC polarization current pulse between the electrodes. When the sample is depolarized by applying some reverse voltage both SHG and DC current pulse disappear. However, when we increase the reverse voltage, both the SHG and DC current pulse reappear but the sign of the DC pulse is reversed. It should be noted that the direction of the laser induced pulse voltage V_d generated in the poled medium is opposite to the existing polarization. With the assistance of the reverse bias voltage V_b smaller than but close to the coercive voltage V_c , the sum of V_b and V_d can exceed V_c . Hence, the polarization of VDF/TrFE copolymer film will disappear. Consequently, the SHG is non-existent. While the reverse bias voltage slightly less than the coercive field is present across the film, the region exposed to the Nd-YAG laser beam is depolarized and SHG no longer appears. Thus, the spatial hole burning results within the poled media. This polarization hole burning process will be completed within about 500 nanoseconds. This is our method of electro-optical writing process for nonvolatile memory.

The DC current pulse associated with SHG may be relevant to the so-called "optical rectification" in ferroelectric thin-films, which is the DC component generated within nonlinear polarization in orthorhombic crystal of class mm2: $P_x(2\omega) = 2d_{15}E_z(\omega)E_x(\omega)$, $P_y(2\omega) = 2d_{24}E_y(\omega)E_z(\omega)$, and $P_z(2\omega) = d_{31}E_x(\omega)^2 + d_{32}E_y(\omega)^2 + d_{33}E_z(\omega)^2$, where the poling direction is chosen as z-axis. There exists a 100 ns delay between the SHG and DC current pulse, and the width of polarization current pulse is 400 ns, wider than the incident laser pulse width 200 ns.

Recently, M. Daté et al. in Japan proposed optoferroelectric memory utilizing the VDF/TrFE copolymer thin film including a dye and its sub-Curie point writing under the electrostatic field and pyroelectric detection of polarization states.¹ Compared to this scheme, our optical memory based on the SHG and laser induced DC current pulse assisted with electric field has the following advantages: the reading by SHG is solely optical and is very fast, and the writing by the laser induced DC polarization current with electrostatic field does not require any heating. Hence, overwriting can be achieved without any additional delay caused by heating in the other method. The SHG in VDF/TrFE copolymer films was originally detected by H. Sato and H. Gamo, one of co-authors of this paper.²

1. M. Daté, T. Furukawa, T. Yamaguchi, and A. Kojima, *IEEE Trans. Elect. Insul.*, **24**, pp. 537-540 (1989).
2. H. Sato and H. Gamo, *Japanese Journal of Applied Physics, Letters*, **25**, pp. L990-992 (1986).

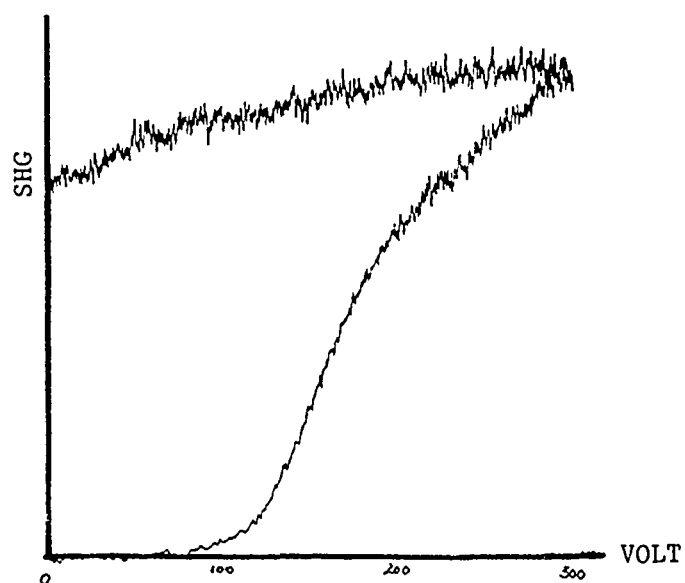


Fig. 1 The SHG vs. bias voltage in VDF/TrFE copolymer film.

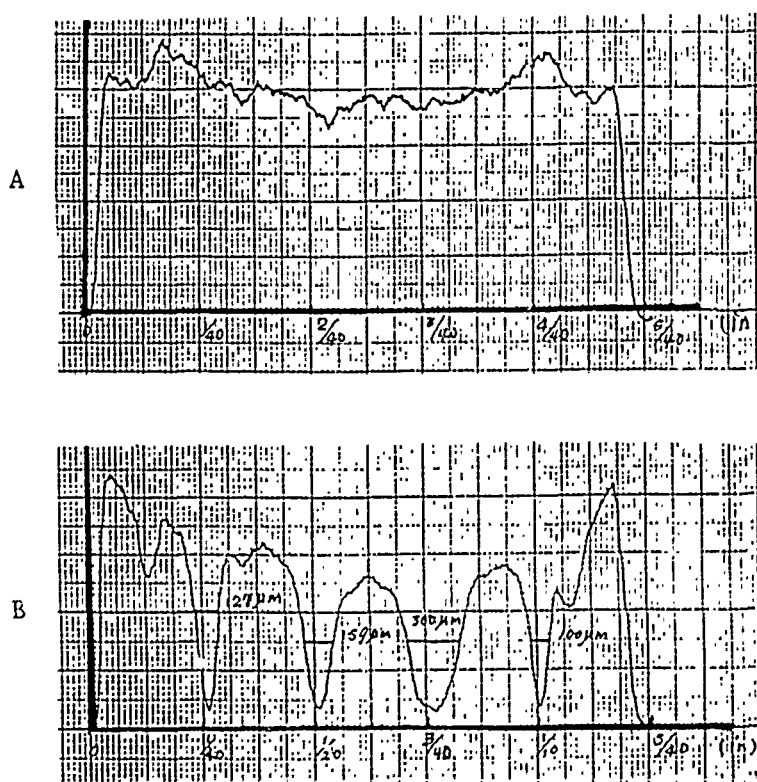


Fig. 2A The SHG in a uniformly poled VDF/TrFE copolymer film.

Fig. 2B The SHG in the film where the polarization hole burning was generated by the Nd-YAG laser pulse under the electrostatic field.

Observation of the Fundamental Dark Spatial Soliton

Steven R. Skinner, Graham R. Allan, David R. Andersen, and Arthur L. Smirl

Center for Laser Science and Engineering
Department of Electrical and Computer Engineering
The University of Iowa
Iowa City, IA 52242 USA

In this work, we report the first observation of the *fundamental* dark spatial soliton (FDSS). The FDSS is characterized by a zero intensity minimum and an abrupt π phase shift at that minimum. The FDSS can be generated in defocussing bulk material by introducing a π phase shift in the spatial profile of an incident optical beam.

Our experimental setup consists of the focussed output of a frequency doubled 30 ps Nd:YAG laser, of near Gaussian temporal and spatial profile, illuminating a single-crystal ZnSe sample (a material with an instantaneous defocussing nonlinear refractive index component at $\lambda = 532$ nm). Half of the incident Gaussian pulse was passed through a 150 μm thick glass platelet positioned directly in front of the sample. The platelet was rotated to provide a variable phase shift between the two transverse spatial halves of the pulse. The near field profile at the rear face of the sample was then imaged onto the entrance slit of a streak camera which recorded the temporal evolution of the diffraction pattern in the plane perpendicular to the edge of the glass platelet. The temporal center of the pulse, recorded by the streak camera, is shown in Figs. 1(a and c) for phase shifts between the two sides of the pulse of 0 and π respectively. Figs. 1(b and d) are photographically recorded interferograms formed by interfering the image of the near field profile at the rear face of the sample with a reference beam, again for transverse phase shifts of 0 and π respectively. For the even initial condition (0 phase shift), a pair of dark spatial solitons which possess kink-antikink symmetry are observed propagating at a non-zero angle with respect to the propagation axis of the incident pulse. Across each of the dark structures, a phase shift of less than π can be noted in the interferogram. For the odd initial condition (π phase shift), a single, fundamental, dark spatial soliton is observed. This soliton maintains its π phase shift and propagates parallel to the propagation axis of the incident optical pulse.

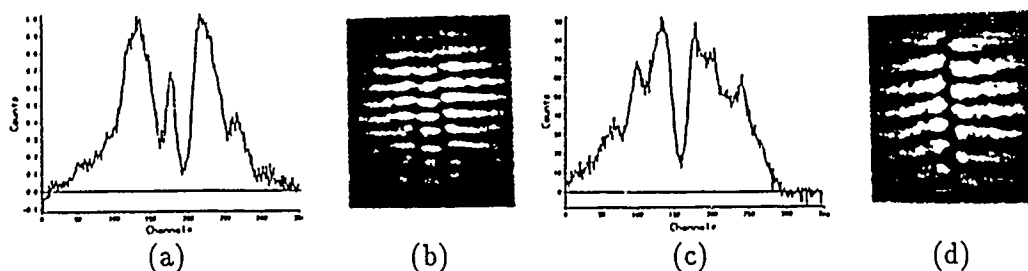


Fig. 1. Experimental results for bulk ZnSe at $\lambda = 532$ nm, depicting the temporal center of the output field and the corresponding interferogram with: (a) and (b) even initial condition; (c) and (d) odd initial condition.

This work was supported by NSF and DARPA.

SECOND-HARMONIC GENERATION IN ATOMIC HYDROGEN INDUCED BY A D.C. FIELD

K. Hakuta¹, L. Marmet, and B.P. Stoicheff
Ontario Laser and Lightwave Research Centre,
and Department of Physics, University of Toronto
Toronto, Ontario M5S 1A7, Canada

Recently, Harris, Field and Imamoglu² have proposed a method for obtaining high conversion efficiency in four-wave frequency mixing by the application of a strong-coupling field between metastable and upper states to resonantly enhance the nonlinear susceptibility of the medium, and at the same time to induce transparency. In the present paper, we show theoretically and experimentally that the same characteristics may be realized with D.C. electric-field-induced second-harmonic generation in atomic hydrogen for the $n=2 \rightarrow 1$ transition at 121.6 nm.

Experiments with a cw atomic beam were carried out using a pulsed dye laser tuned to 243 nm for two-photon excitation of the $n=2-1$ transition. The laser beam was focused about 1 mm below the H-source nozzle, where the H-atom density was estimated to be $\sim 5 \times 10^{13} \text{cm}^{-3}$. Measurements of SHG at ~ 122 nm and ion current (corresponding to photon absorption) were made at various D.C. fields up to 12 kV/cm, and the tuning characteristics at two different fields are shown in Fig.1. At the higher field, it is seen that while the SH signal at the centre of the Stark-split components decreases to about half the peak value, the ion current becomes almost zero. This observation is a clear demonstration of the prediction by Harris et al², and suggests the possibility of obtaining high conversion efficiency in generating Lyman- α radiation.

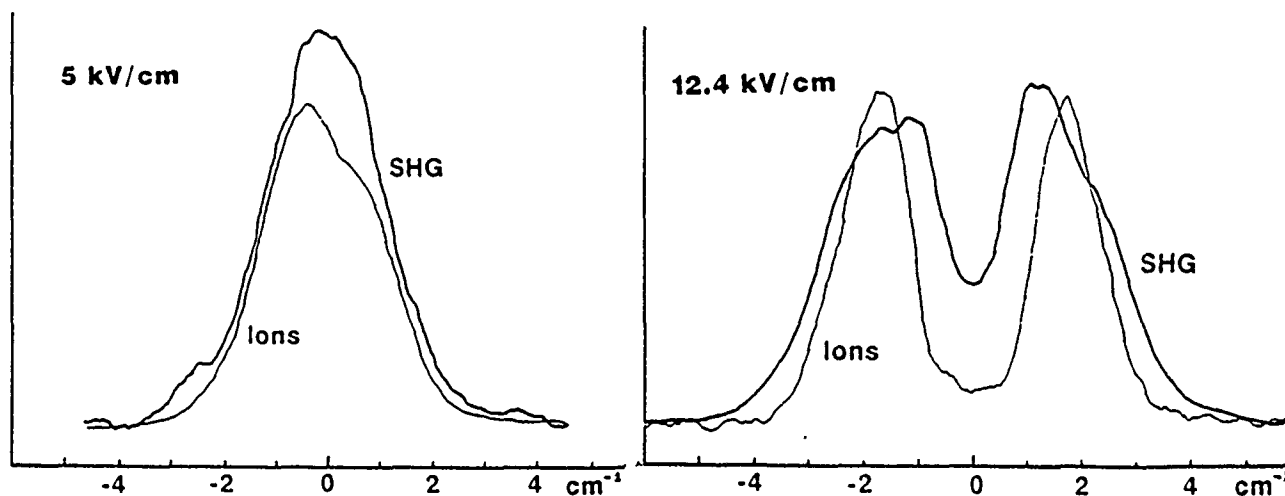


Fig.1. Tuning characteristics of second harmonic generation at 121.6 nm and of ions.

- ¹ Visiting scientist, University of Toronto, 1988-89, Permanent address: Department of Applied Physics and Chemistry, and Institute of Laser Science, University of Electro-Communications, Tokyo 182, Japan.
- ² S.E. Harris, J.E. Field, and A. Imamoglu, Phys. Rev. Lett. 64, 1107 (1990).

SELF-FOCUSING EFFECTS IN THE NEAR FIELD OF A THIN NONLINEAR MEDIUM

J.A. Hermann and P.B. Chapple
 DSTO Surveillance Research Laboratory
 Box 1650, Salisbury, South Australia 5108

Novel phenomena can occur in the near field of a thin nonlinearly refracting medium placed at the waist of a focused laser beam. In our model of these effects a cw gaussian beam interacts with a Kerr medium, however time-dependent behaviour can be easily incorporated if required.

SUMMARY

The theory of the interaction of a laser beam with a thin Kerr-type medium predicts interesting new behaviour. Device applications can be envisaged when the beam is focused by a lens and the medium is placed at the waist. With an axisymmetric gaussian beam, external self-focusing is manifested in the near field as an axial shift in the position of the irradiance maximum. If a second lens is introduced in the far field, then the irradiance profile near the image plane of the thin medium is found to be compressed, compared with the linear profile. Correspondingly, the normalised axial transmission (ratio of the nonlinear to the linear transmitted irradiances) exhibits a dispersion-shaped profile, centred on the image plane. The wave optics description of this two-lens system allows a simple correspondence to be found between nonlinear effects appearing in the object space (surrounding the thin Kerr sample) and in the image space (surrounding the image plane of the sample). The situation in the object space can be described, for an incident beam convergent from the left, in terms of a real field profile to the right of the sample and a virtual field profile to the left of the sample. The irradiance distribution of the virtual field is equivalent to that of a real field produced when (all else being identical) the direction of propagation and the sign of n_2 are both reversed. The field profiles on each side of the image plane, by contrast, are both real. For self-focusing media, our calculations of transverse profiles in the image space indicate that the beam is compressed on the right-hand side of the image plane, and is expanded into diffraction rings on the left-hand side, relative to the linear profile. With defocusing media, the relative positions of these features on the optic axis are reversed, as n_2 possesses the opposite sign. Useful applications of these effects include optical power-limiting devices and z-scan techniques for measuring n_2 .

Beam irradiance in the image space, as a function of the scaled distance along the optic axis, showing focal shift and compression. The nonlinear optical phase shift at the sample, located midway between the lenses, has the value 1. The separation of the lenses is twice the focal length of the first lens.

a: linear profile; b: 1st nonlinear order; c: 2nd nonlinear order

